AN INVESTIGATION INTO THE MECHANISMS OF TIME DEPENDENT DEFORMATION OF HARD ROCKS

By

Karsten Drescher

Submitted in fulfilment of the requirements for the degree of

Master of Science

In the Faculty of Engineering

University of Pretoria

Study Leader: Prof Mathew Handley

November 2002

ABSTRACT

The testing undertaken for this dissertation is intended to help quantify the various time-dependant deformation processes around typical deep level hard rock tabular excavations. Three mechanisms were investigated and two different hard rock types, Ventersdorp Lava and Elsburg Quartzite were used. Uniaxial compression creep studies were done as the first part of the study followed by shear creep studies on discontinuities where crushed lava and crushed quartzite as well as a natural gouge were used as infilling. An important conclusion made is that the relationship between grain size and infilling thickness is more important than previously might have been assumed. The last part of the study consisted of triaxial post-failure relaxation tests. As far as could be determined, this is the first time triaxial post-failure tests were attempted, particularly on typical South African hard rocks. An important finding of this study is that during compression creep as well as during triaxial post-failure relaxation the amount of energy dissipated for the lava is significantly less than for quartzite. For mines operating at great depth (more than 2000m) the implication is that the rock material might relax much more slowly than might have been assumed and this means that after failure the rock mass continues to store large amounts of strain energy. This study provides the first data available for energy change calculations in fractured rock masses. Three mechanisms of time-dependant deformation were quantified providing valuable data for numerical investigations.

ACKNOWLEDGEMENTS

This research was conducted as part of the Experimental Investigation of Fundamental Processes in Mining Induced Fracturing and Rock Instability project of the Rock Engineering Programme, CSIR Division of Mining Technology, South Africa. The project was funded by the Safety in Mines Research Advisory Committee (SIMRAC), whose support is gratefully acknowledged.

The following individuals are herein also acknowledged for their valuable contributions:

Dr. Francois Malan for acting as co-promoter. He is the person who awakened my interest in time-dependant studies. I would like to thank him for his encouragement. His positive attitude to life in general will always be an inspiration to me.

Prof. Mathew Handley for his role as promoter and the valuable discussions.

Dr. Güner Gurtunca, Director of Miningtek, who created opportunities for post graduate studies.

Dr Ewan Sellers for his leadership and the many valuable discussions.

Mr Uli Vogler, whose passion for rock mechanics, is inspiring. The first time-dependant tests that I conducted were done under his leadership.

Mr Mark Grave for the assistance with the particle size analysis.

My wife and my parents for their encouragement.

TABLE OF CONTENTS

LIST OF TABLES

LIST OF FIGURES

Chapter 1

1 Introduction

1.1 Introduction

Closure measurements in South African mines show definite time-dependant behaviour (Malan, 1998: 76). Time dependant deformation in hard rocks consists of at least three components: (1) compression creep of the intact rock, (2) shear creep on discontinuities and (3) post-failure relaxation of rock material (Malan and Drescher, 2000: 909). Understanding the mechanisms of time-dependant behaviour of hard rocks will be of great importance when a decision on the optimum mining rate for the deep mines is made. Furthermore, the occurrence of rock bursts can be linked to the time-dependant behaviour of hard rocks.

1.2 Background

Time dependant behaviour in rocks is best known for the weaker types of rock such as rock salt and potash (Latjai & Duncan, 1988: 227). In these weaker rocks significant creep is often observed, even in shallow mines were the overburden stress is often close to the uniaxial compressive strength of the material. Creep in intact hard rocks tends to be significantly less than in the weaker rocks and is therefore often completely ignored. Underground observations however show the existence of time-dependant behaviour and thus it must be investigated in the laboratory.

1.3 The state of existing knowledge

Several uniaxial compression creep experiments appear in the literature, such as Price (1964) or Singh (1975). A detailed literature survey is given in Chapter 2. However, most of the studies carried out were done using material that, especially in the context of the South African goldmines, can be regarded as relatively weak and soft materials such as shale (with a strength of < 50 MPa) and sandstone (50-100 MPa). Even marble which is a fairly hard rock (100-150 MPa) is relatively soft compared to Witwatersrand quartzite (100 to 250 MPa) or Ventersdorp Lava (400 to 600 MPa), which are encountered in the deep mines. Most of the studies on uniaxial compression creep report only the strain-time data for the axial deformation and do not mention the lateral deformation.

In terms of creep testing on discontinuities far less information is found in the literature (See Chapter 3 for details). Cylindrical test specimens containing a discontinuity were tested in triaxial compression (Wawersik, 1974: 361). In tests conducted on Westerly granite, the discontinuity was inclined at 30° relative to the direction of the principal stress. Amadei (1979) proposed a hypothesis that the shear creep of a joint would be governed by the ratio of applied shear stress to peak shear strength. Schwartz and Kolluru (1984: 333) did some studies using a synthetic rock material (consisting of a gypsum plaster mix) to test the hypothesis of Amadei. Bowden and Curran (1984: 321) performed tests on artificial discontinuities prepared from shale. Malan (1998:153) and Malan, Drescher and Vogler (1998:475) did more elaborate work on shear creep of discontinuities, which are commonly encountered in typical South-African deep mines. Shear creep experiments were done on natural joints with natural gouge and artificial joints with artificial gouge (crushed rock).

As far as the relaxation of failed rock is concerned, studies are limited to the relaxation of failed rock under uniaxial compression. There is almost no evidence that triaxial post-failure relaxation studies have ever been carried out.

Uniaxial compression creep for weaker rock types is very well covered in the literature, but the amount of data available for typical South African hard rocks

is limited. The data available for South African hard rocks consists only of axial deformation measurements. Generally lateral deformation measurements during creep testing are lacking. Some work has been done on the time-dependant behaviour of discontinuities but the amount of data is still limited. No data (not only South African hard rocks) is available for the post failure relaxation of rocks under triaxial conditions.

1.4 Problem Statement

Much is known about the time dependant behaviour of intact rock in potash, rocksalt and other softer rock types. The objectives of this study are to determine the time-dependent behaviour of Elsburg Quartzite and Ventersdorp Lava (typical South African hard rocks) and then compare the results by:

- Obtaining more strain-time data (axial and lateral strain) under uniaxial compression.
- Gaining more insight into the time-dependant behaviour of discontinuities by performing direct shear creep tests using crushed rock as well as natural gouge as infilling.
- Studying the axial stress relaxation of failed rock under triaxial compression.

1.5 Motivation

Mining induced seismic events (e.g. rock burst) sometimes seem to be the result of rheological processes in the rock mass because they do not always occur immediately after the blast. Instead many (about 50%) occur during the shift, many hours after the blast. Malan (1998: 76-108) has shown that closure in stopes continues to take place long after the blast. Malan also states that the time dependent closure behaviour is linked to time-dependant failure processes. The testing undertaken for this dissertation is intended to help quantify the various time-dependant deformation processes around typical deep level hard rock tabular excavations. Armed with better laboratory data, numerical modelling will be able to further investigate rheological processes in highly stressed hard rock masses.

A better understanding of the time dependant behaviour of hard rocks at great depth could thus lead to a better understanding of the seismic events. Together with advances in numerical modelling, this should make the mines at great depth a safer working place.

Chapter 2

2 Compression Creep

2.1 Introduction

Compression creep or the time dependent deformation of rock under constant loading is usually associated with weaker rocks such as sandstone, mudstones, and limestone or with salt. It is also referred to as squeezing. Barla (1995: 45) defines squeezing as:

"Squeezing of rock is the time-dependant large deformation, which occurs around the excavation, and is essentially associated with creep caused by exceeding a limiting shear stress. Deformation may terminate during construction or continue over a long time period."

Dusseault and Fordham (1993: 133) state that hard rock usually does not show significant steady state creep under engineering conditions. Closure measurements in tabular stopes in deep South African gold mines show time-dependant deformation (Malan, 1998: 76). This study aims at comparing the time-dependent deformation of two hard rock types, often found in South African deep mines. Temperature below 100°C does not influence the creep behaviour of hard rock significantly (Dusseault and Fordham, 1993: 145). The temperatures encountered in the South African deep level mines are lower than 100°C; therefore, this study concentrates on low temperature creep behaviour.

2.2 Analysis of existing data

A typical strain-time graph showing primary, secondary and tertiary creep phases, is shown in Figure 2.2.1 (Lama and Vutukuri, 1978: 237). If load is applied to rock (for this study, uniaxial compression) the specimen will show an immediate elastic response followed by the primary creep phase during which the deformation or strain decreases with time. If the stress is released during the primary creep phase the specimen would recover elastically and there would be no permanent deformation.

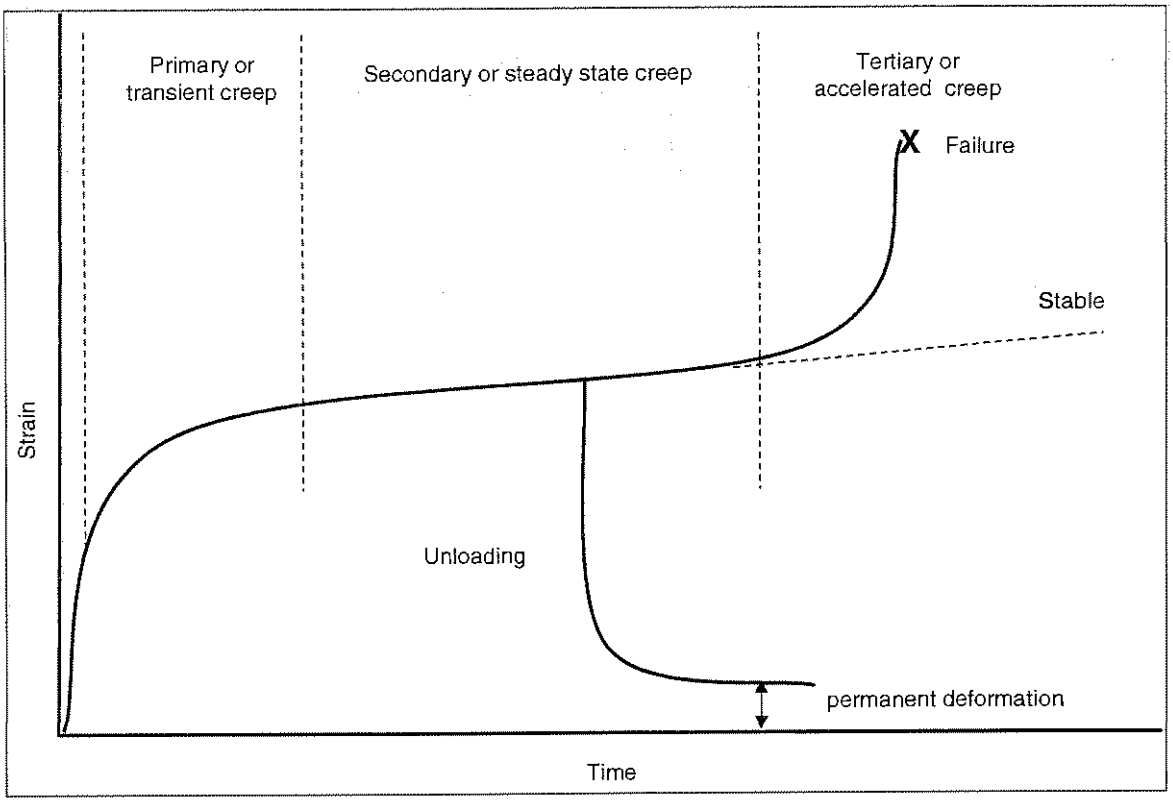

Figure 2.2.1 Strain-time curve (after Lama and Vutukuri, 1978)

If the stress persists past the primary creep phase, secondary creep sets in where the strain-rate is almost constant. If the stress is released during this phase, the specimen would only recover partially and show some permanent deformation.

If the rock is not de-stressed after the secondary creep phase and the stress is high enough, the strain rate increases: this is the tertiary creep phase. If the stress is high enough to cause failure, the tertiary creep phase is relatively short and the specimen becomes unstable. If the stress is not high enough, the strain

rate would gradually decrease with time and the specimen would become stable.

It appears that the CSIR produced the earliest available data on South African hard rocks i.e. quartzite; see (CSIR, 1963:4). Some of the results are shown in Figure 2.2.2.

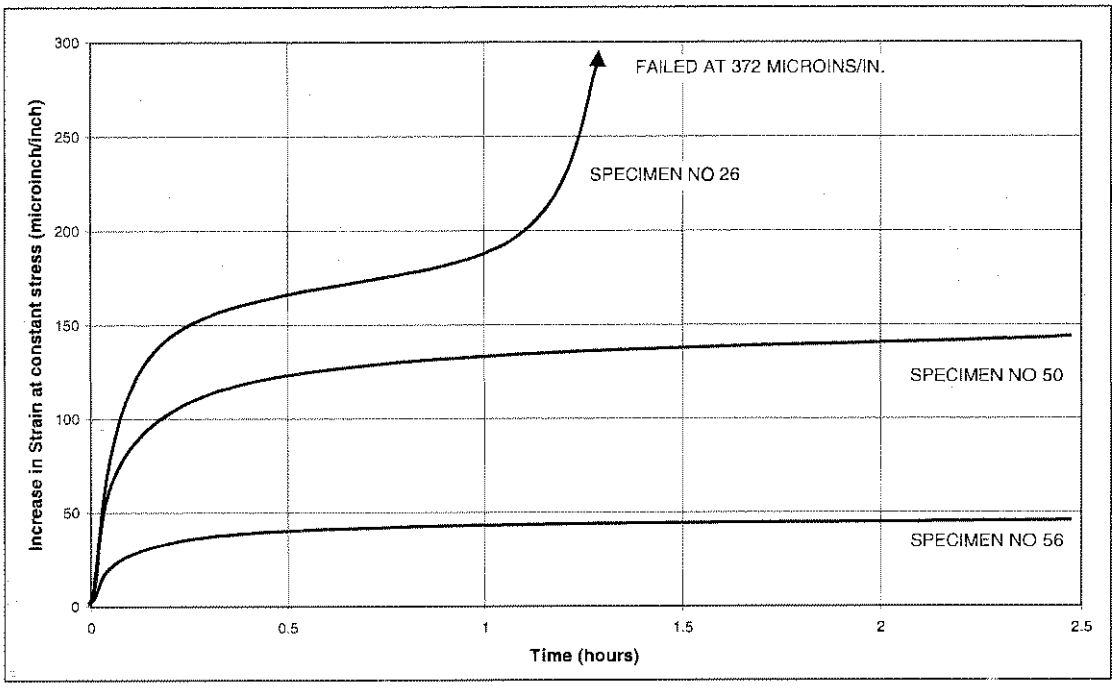

Figure 2.2.2 Creep curves for quartzite (after CSIR, 1963)

The results of the three specimens shown in the Figure 2.2.2 were obtained by applying different loads to the three specimens respectively. For specimens 50 and 56, the induced stress was not high enough to cause tertiary creep and the specimens are stable. For specimens 26, the induced stress was high enough to cause tertiary creep; the specimen became unstable and failed within approximately 1.3 hours.

A summary of uniaxial compression creep tests on different rock types found in the literature is given In Table 2.2.1. On order to compare the results, the data has been classified in terms of rock strength. The classification is according to Deere and Miller (1965) and are listed in Table 2.2.2.

Table 2.2.1 Summary of compression creep studies

Rock Type	UCS (MPa)	Strength Class	Reference
Quartzite (Hartebeest-fontein Mine)	193	High Strength	CSIR (1963:4)
Markham Sandstone	N/a	N/a	Price (1964:288)
Wolstanton Calcareous Siltstone	N/a	N/a	Price (1964:288)
Warsop Nodular, Muddy Limestone	N/a	N/a	Price (1964:294)
Norite	270	Very High Strength	Bieniawski (1967: 428)
Dolerite	345	Very High Strength	Wiid (1966:21)
Carrara Marble	193	High Strength	Cruden (1971: 136)
Westerly Granite	282	Very High Strength	Wawersik (1973:97)
Nugget Sandstone	282	Very High Strength	
Tennessee Marble	117	High Strength	
Appin Colliery Shale	17*	Very Low Strength	Singh (1975:274)
Sicilian Marble	83*	Medium Strength	Singh (1975:274)
Oil Shale	N/a	N/a	Chong, Smith and Khaliki (1978)
Ormonde Siltstone	68.9	Medium Strength	Lama and Vutukuri (1978:245)
Lea Hall Sandstone	47.6	Low Strength	
Hucknall Shale	58.7	Medium Strength	
Portland Limestone	85.0	Medium Strength	
Indiana Limestone	48-75	Low to Medium Strength	Lama and Vutukuri (1978:247)
Tennessee Sandstone	124-138	High Strength	
Barre Granite	200-214	Very high strength	
Neogene Slty Mudstone	2.7	Very Low Strength	Ohtsuki, Nishi, Okamoto and Tanaka (1981:119)
Gypsum Plaster Mix (synthetic rock material)	26.5	Low Strength	Schwartz & Kolluru (1984: 334)

Table 2.2.1 Summary of compression creep studies (continued)

Lac du Bonnet Granite	225	Very High Strength	Latjai, Schmidke and Bielus (1987:249)
Potash	17	Very Low Strength	Latjai and Duncan (1988:277)
Argillaceous Footwall Quartzite (Strong coarse, Lorraine Gold Mine)	98.9	Medium Strength	Vogler (1990)
Argillaceous Footwall Quartzite (Strong fine, Lorraine Gold Mine)	101.6	High Strength	Vogler (1990)
Argillaceous Footwall Quartzite (weak, Lorraine Gold Mine)	38.1	Low Strength	Vogler (1990)
Ventersdorp Lava (Western Deep Levels)	436	Out of Range > 400 MPa	Vogler and Drescher (1997)
Pietra Leccese Chalk	24	Very low strength	Maranini & Brignoli (1999: 129)
Quartzite (Stilfontein & Strathmore formations)	167-180	High Strength	Bosman, Malan and Drescher (2000: 58)
Marble	120	High Strength	Yongsheng and Caichu (2000: 468)
Red Sandstone	60	Medium Strength	
Sandstone	12	Very low strength	
Claystone	5	Out of Range: < 10 MPa	

*Failure strength during creep test. The conventional UCS tests may produce higher strength values than these.

Table 2.2.2 Strength Classification (after Deere and Miller)

Strength, UCS (MPa)	Classification
10-24	E – Very low strength
25-50	D – Low Strength
51-100	C – Medium Strength
101-200	B – High Strength
201-400	A – Very high Strength

Only a few of the rock types given in Table 2.2.1 are of importance in the South African deep mines, i.e. Quartzite and the very hard Ventersdorp Lava. The Ventersdorp Contact Reef (VCR) is one if several major gold bearing reefs in South Africa. The VCR is underlain by quartzite, and overlain by Ventersdorp Lava. As the VCR is undulating, mining operations often extend into either the quartzite (footwall) or the lava (hanging wall).

If a compression creep test is performed at constant temperature, the steady-state strain rate (axial strain) is given by a widely used steady-state creep law:

$$\dot{\varepsilon}_{SS} = A'\sigma^{n} \qquad [2.1]$$

where σ is the applied axial stress (Malan, 1998: 35). The exponent n and the coefficient A' can be determined from a least squares fitting procedure on a graph of log (strain rate) vs log (stress). The values for n and log (A') for some rock types are given in Table 2.2.1 (after Malan, 1998: 35).

Table 2.2.3 Calibration values for the steady-state creep law (after Malan, 1998)

Rock	Maximum Strain x 10^{-3}	Maximum Stress MPa	Exponent n	Coefficient Log (A')
Ventersdorp Lava (Western Deep Levels Mine)	4.7	366	4.3	-46.8
Quartzite (Western Deep Levels Mine)	2.6	193	4.4	-19.8
Argillaceous Quartzite (Hartebeestfontein Mine)	2.3	143	4.8	-20.2
Argillaceous Quartzite (Lorraine Mine)	1.9	107	9.1	-83.2
Granite	1.0	345	3.3	Unknown
Shale	3.0	9.7	2.7	Unknown

2.3 Experimental Procedure

Ventersdorp Lava and Elsburg Quartzite are two of the rock types encountered in South African mines. With a strength of over 400 MPa, Ventersdorp Lava is one of the hardest rocks known, and more than twice as strong as most of the Elsburg Quartzite. This study concentrates on the different creep behaviour of Elsburg Quartzite and Ventersdorp Lava. The test results for the Ventersdorp Lava were obtained by Vogler and Drescher (1997) and are still available for evaluation purposes. Under the guidance of Vogler, the author conducted these tests.

2.3.1 Geological description

A full petrographic report on the rock types selected is given in Appendix A.

The Ventersdorp Lava specimens originated from the Western Deep Levels Mine where they occur in the Alberton formation. The lava can be described as fine to medium grained meta-tholeiite (metamorphosed andesite/basalt, Appendix A, sample 2056-158).

The Quartzite blocks were collected at the reservoir near Risana and belong to the Elsburg formation. The quartzite can be described as a meta-quartzite (metamorphosed quartz-wacke, Appendix A, sample 2056-159)

2.3.2 Specimen preparation

Specimens were drilled out of Elsburg quartzite blocks. They have a diameter of 20±0.5mm and a length of 60±1mm, resulting in a height to diameter ratio of approximately 3:1. The end-surfaces are ground flat according to ISRM (1979) specifications.

For strain measurements, two rosettes with two perpendicular orientated strain gauges each are fitted to the specimen, giving two axial and two lateral strain readings, which are all monitored independently.

2.3.3 Testing equipment

The specimens are tested in the CSIR creep-testing machine, originally used by Bieniawski (1967: 428). The data acquisition has been modified and involves a data logger and a computer. The system is fitted with an uninterruptible power supply unit. The machine is housed in a special climate controlled laboratory, where the temperature is kept constant at 20±0.5°C and the relative humidity is maintained at 50±2%. This is done to eliminate any effect temperature and moisture fluctuation might have on either the specimen or the equipment. A photograph of the testing machine is shown in Figure 2.3.1.

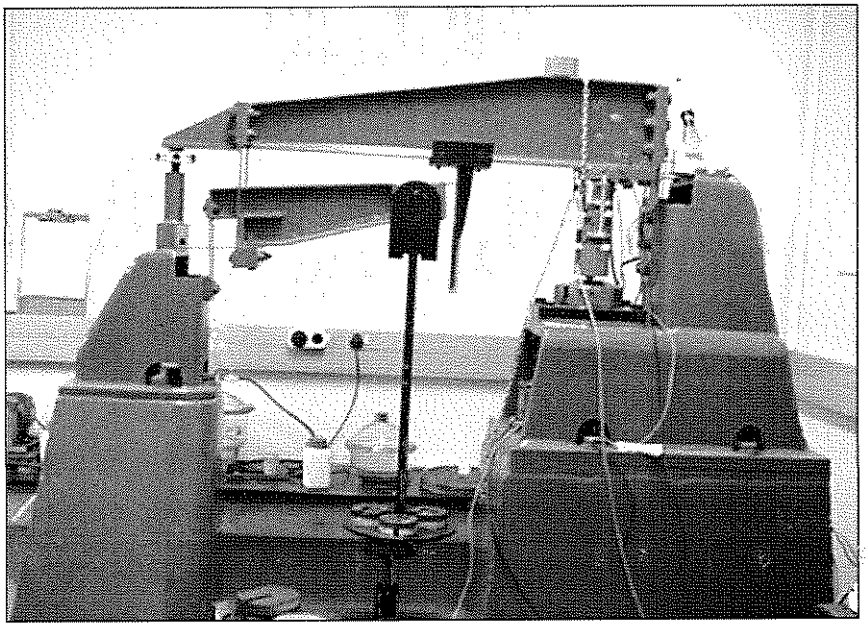

Figure 2.3.1 CSIR compression creep apparatus

Specimens are loaded mechanically by weights, which ensure a constant load. The principle of operation is shown in Figure 2.3.2. The loading mechanism consists of two cantilever beams each with a 7:1 loading ratio, which gives an overall loading ratio of 49:1.

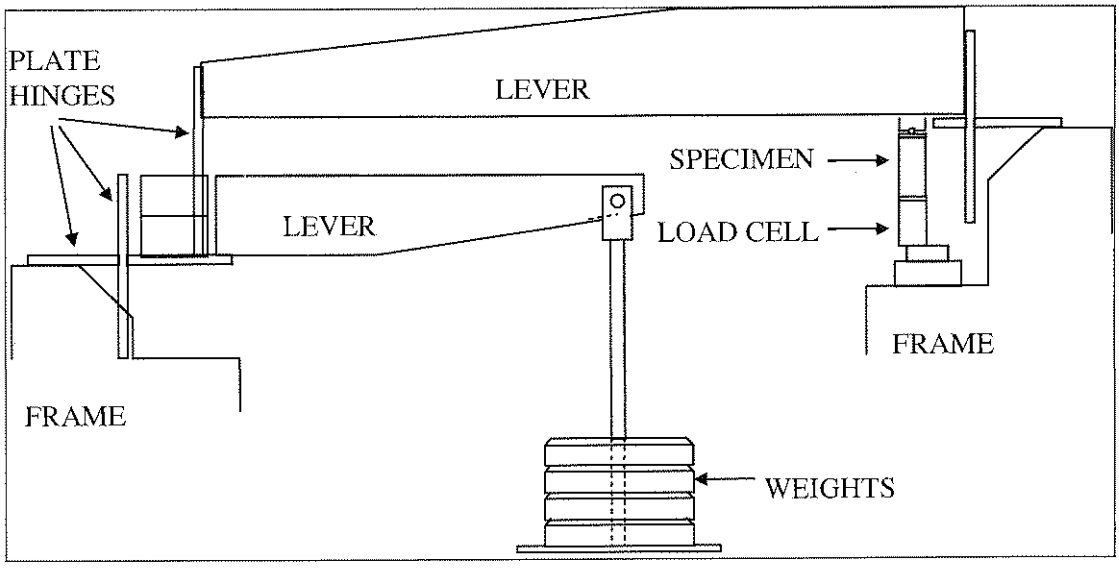

Figure 2.3.2 Principal of operation

The specimen set-up is as shown in Figure 2.3.3. LVDT's (Linear Voltage Differential Transformer) are used alongside the axial strain gauges to measure axial strain. This is done to confirm that the axial strain (especially creep strain) measured by the strain gauges is in fact the deformation of the rock and not the time dependant behaviour of the strain gauges. The strain gauge readings are usually more accurate than the LVDT readings, and are thus used for evaluation. The LVDT's are also used as a trigger for the data logging. Data points are typically taken every 2 hours during the secondary creep phase. The data logger will be triggered (by the LVDT's, in 20 microstrain increments) to take readings more often if the strain rate accelerates suddenly. Hence tertiary creep can also be captured by the system just before the specimen fails.

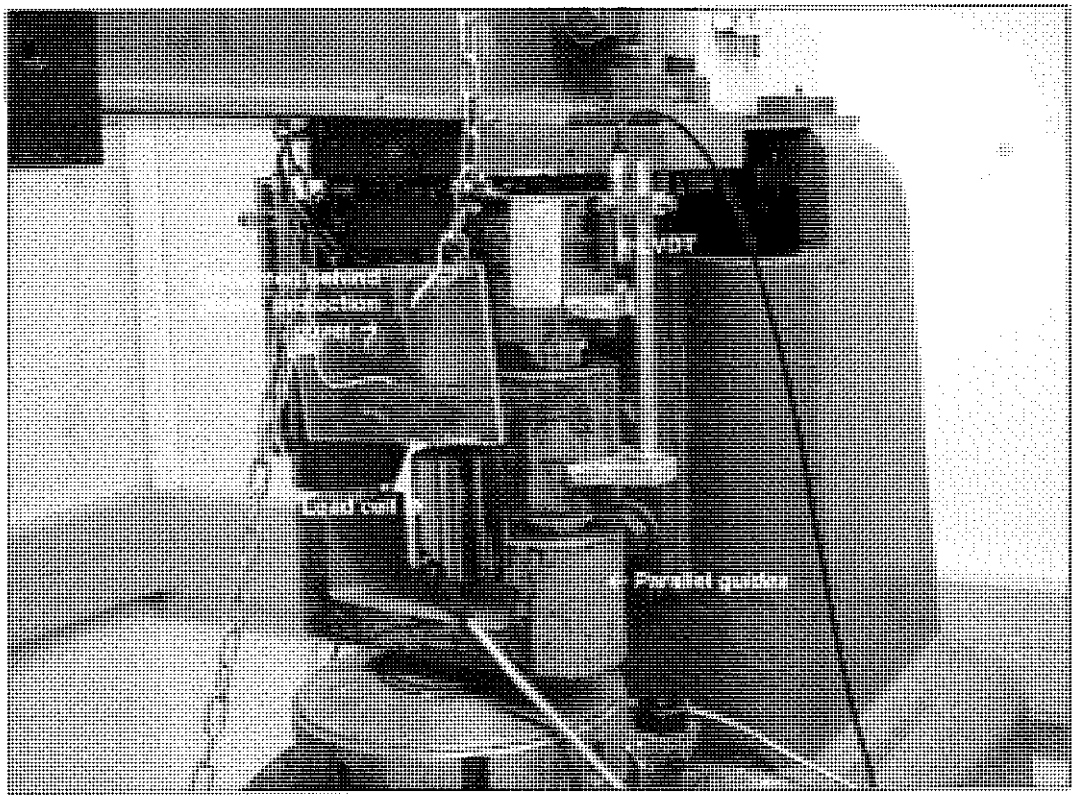

Figure 2.3.3 Close-up look of the testing configuration

Figure 2.3.4 A tested specimen (quartzite)

Figure 2.3.4 shows a photograph of a quartzite specimen that failed during a creep test. The failure plane is clearly visible as well as the strain gauges fitted in the axial and lateral directions.

2.3.4 Testing method

Prior to testing, the specimens are stored in the climate-controlled laboratory for a minimum of 14 days. There are two methods of creep testing:

a) Specimens are loaded to a predefined stress level which may be the stress level encountered in a mine or it may be a stress level which is a certain percentage of the uniaxial strength. Strain gauges and LVDT's monitor the creep strain while the specimen is kept under constant stress until failure. As the strength of rock material can be quite variable, the time to failure could vary between a few days and a few weeks. Sometimes, the specimens never fail.

b) Specimens are loaded stepwise; starting at a relatively low value, (e.g. 60% of the UCS value) and increasing the load after predefined time intervals

(e.g. 48 hr). With this method, more information about the creep behaviour of a certain rock type can be obtained from one specimen.

During this study all specimens were tested using the second method, aiming to use stress levels of 70%, 80%, 85%, 90%, 95% and 100% of the anticipated failure stress. If the specimen does not fail within 48 hr of the last load increment, further loading is applied in increments of 5% every 48 hrs. The 48 hr interval is selected for this study because it is relevant to the underground mining situation where a face could stand for 48 hours during a weekend.

The testing programme is as follows: Four test results which were done by Vogler and Drescher (1997) were selected and six uniaxial creep tests were done on Elsburg quartzite specimens of which two were unsuccessful as the specimens failed prematurely on previously unseen weaknesses. Additionally, standard uniaxial compressive strength tests with strain gauge measurements (UCM tests) for both the Ventersdorp Lava and the Elsburg Quartzite were done.

2.4 Experimental Results

2.4.1 Ventersdorp Lava

A summary of the test results on Ventersdorp Lava is given in Table 2.4.1.

Table 2.4.1 Summary of test results

Specimen No 1640 -	Creep Strength (MPa)	Nosepoint Stress (MPa)	Nosepoint as % Strength	Axial Strain at Failure x 10^{-6}	Modulus Loading (GPa)	Modulus Unloading (GPa)	Damage Index
CRP-23	363.7	328.2	90.3	4645	84.7	96.8	0.88
CRP-53	435.4	397.4	91.3	5135	92.8	101.2	0.92
CRP-55	398.7	361.9	90.8	4039	93.8	109.5	0.86
CRP-63	402.2	330.3	82.1	4582	89.1	101.8	0.88

The nosepoint is defined by Bieniawski (1967: 428) as the point of maximum volumetric strain, which is the onset of unstable fracture propagation. The axial

strain (ε_a) and lateral strain (ε_l) are plotted as positive quantities. Hence the volumetric strain is given by:

$$\varepsilon_v = |\varepsilon_a| - |2\varepsilon_l| \qquad [2.2]$$

The modulus values (elastic constant) during loading and unloading were determined for the first loading-creep-unloading cycle as shown in Figure 2.4.1.

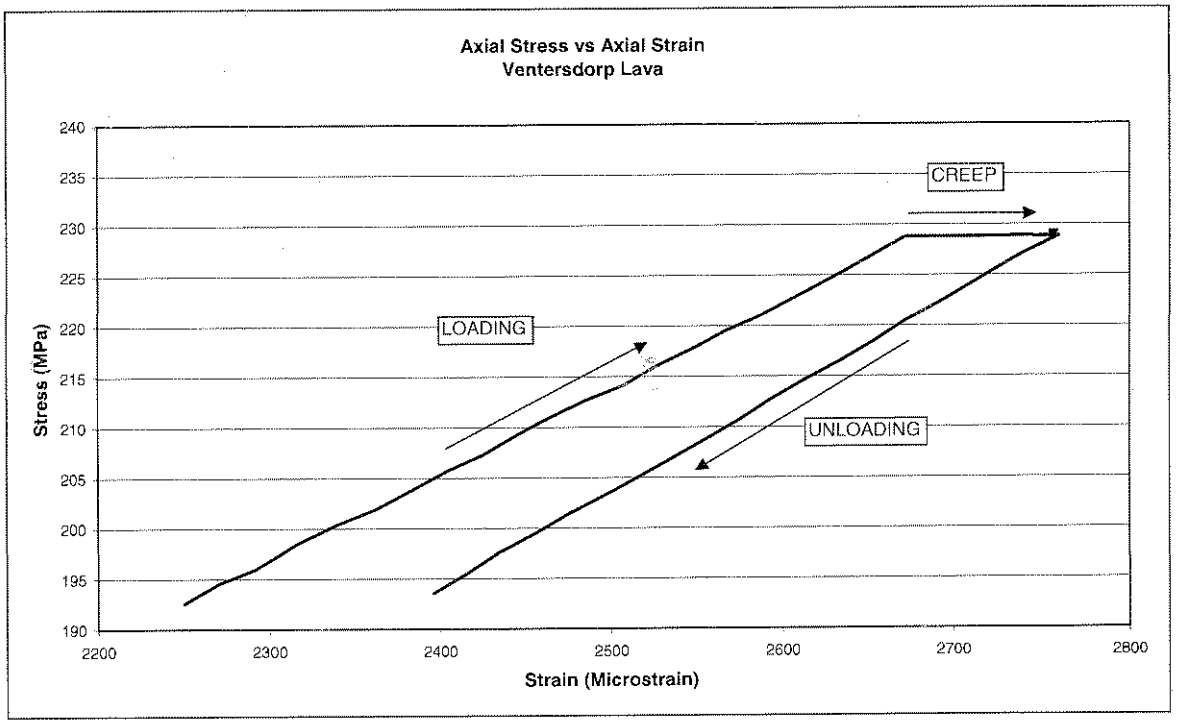

Figure 2.4.1 Modulus during loading and unloading

It is important to note that the loading and unloading modulus values are calculated over only ± 12% of the full stress-strain curve. The unloading modulus can thus be regarded as the intrinsic modulus of the material while the loading modulus is the modulus of the specimens, which might include small micro cracks. The ratio between the loading and unloading modulus is therefore a measure of the damage done to the specimen. Although the loading modulus and unloading modulus values for the different specimens differ slightly, the ratio between the respective loading and unloading modulus values appear to be very constant.

A typical complete strain-time curve for a Ventersdorp Lava specimen is shown in Figure 2.4.2. The time interval for the load increments on the lava was 72 hours. The lava test results showed that very little creep strain occurs between 48 hours and 72 hours. It was therefore decided to perform the tests on Elsburg Quartzite using 48 hr time intervals for reasons discussed above. The evaluation for the tests on lava was done for the first 48 hours to be able to compare the results of the lava to the results of the quartzite.

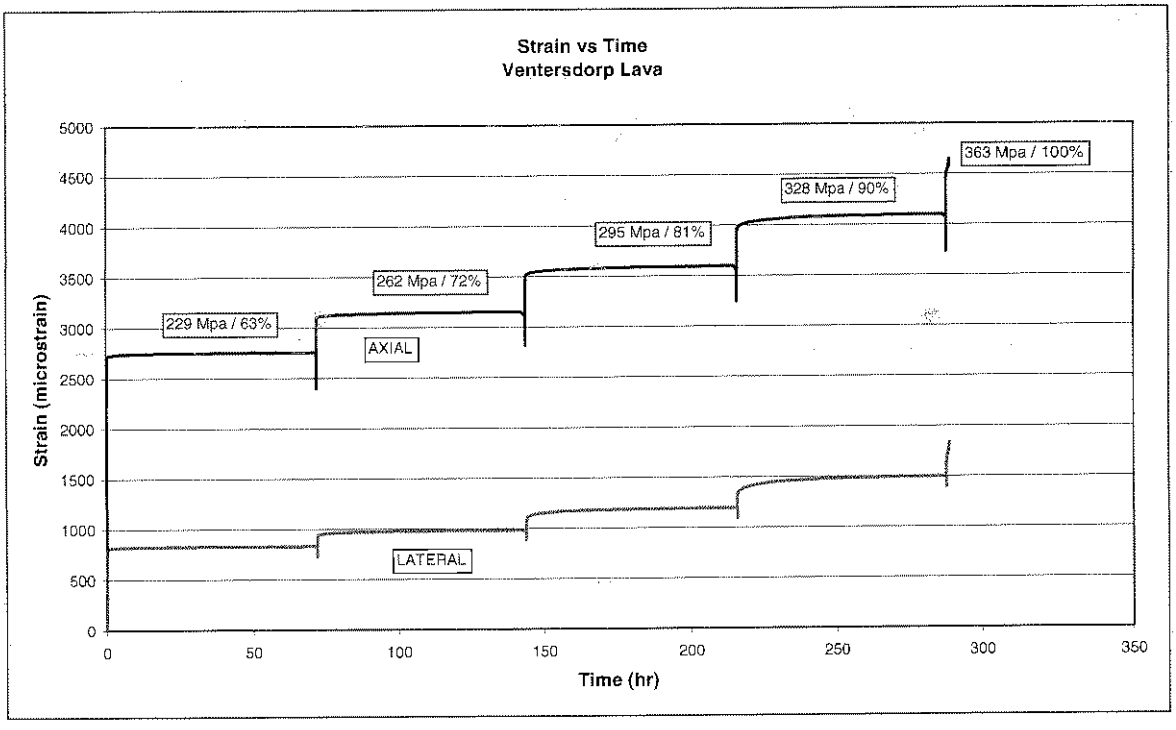

Figure 2.4.2 Strain-time curve for Ventersdorp Lava

Note that each creep stage is followed by an unloading cycle before the load is increased to the following increment. The unloading and loading was done by using a scissor jack to lift the weights gradually, followed by adding an extra weight and lowering the weights again gradually. As weights were not always just added but also exchanged, this procedure was followed to prevent sudden decreases or increases in the load. The figures below are representative examples of the results. The full results are given in Appendix B.

Typical strain-time curves for the last three stages prior to failure are given in Figures 2.4.3 (axial strain) and 2.4.4 (lateral strain). The strain-time (axial and

lateral strain) curves for the final creep cycle (during which failure occurs) are shown in Figure 2.4.5.

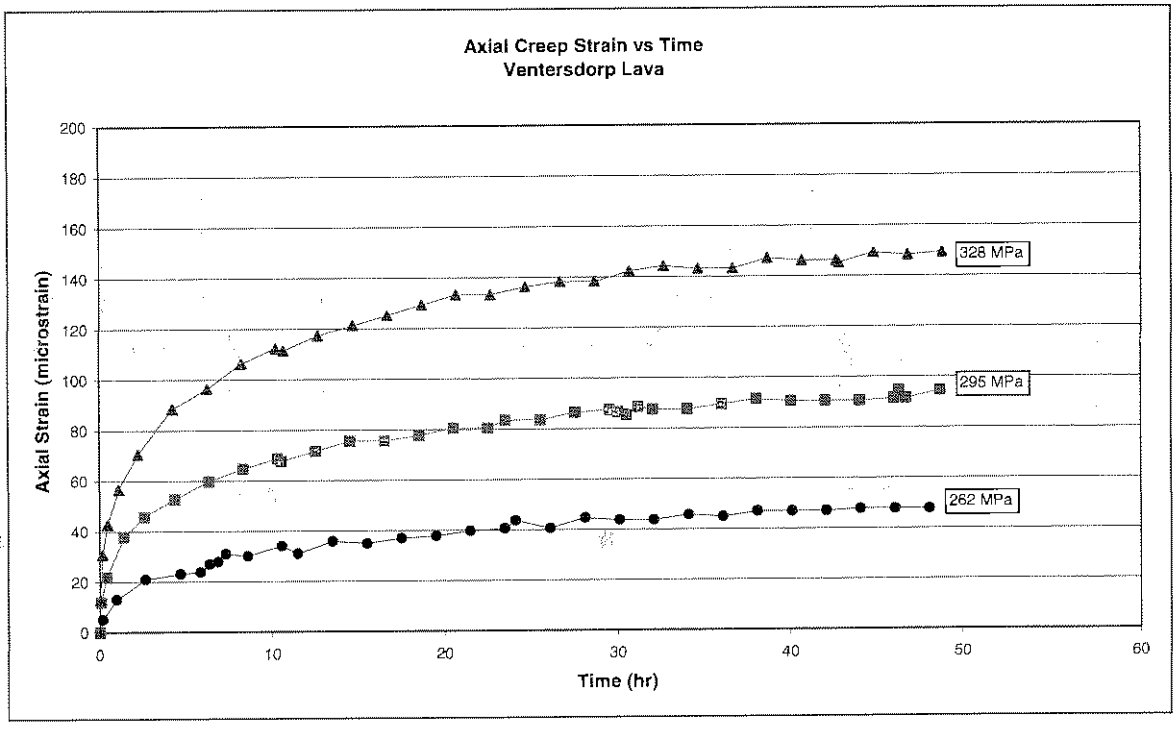

Figure 2.4.3 Axial strain-time curves for Ventersdorp Lava

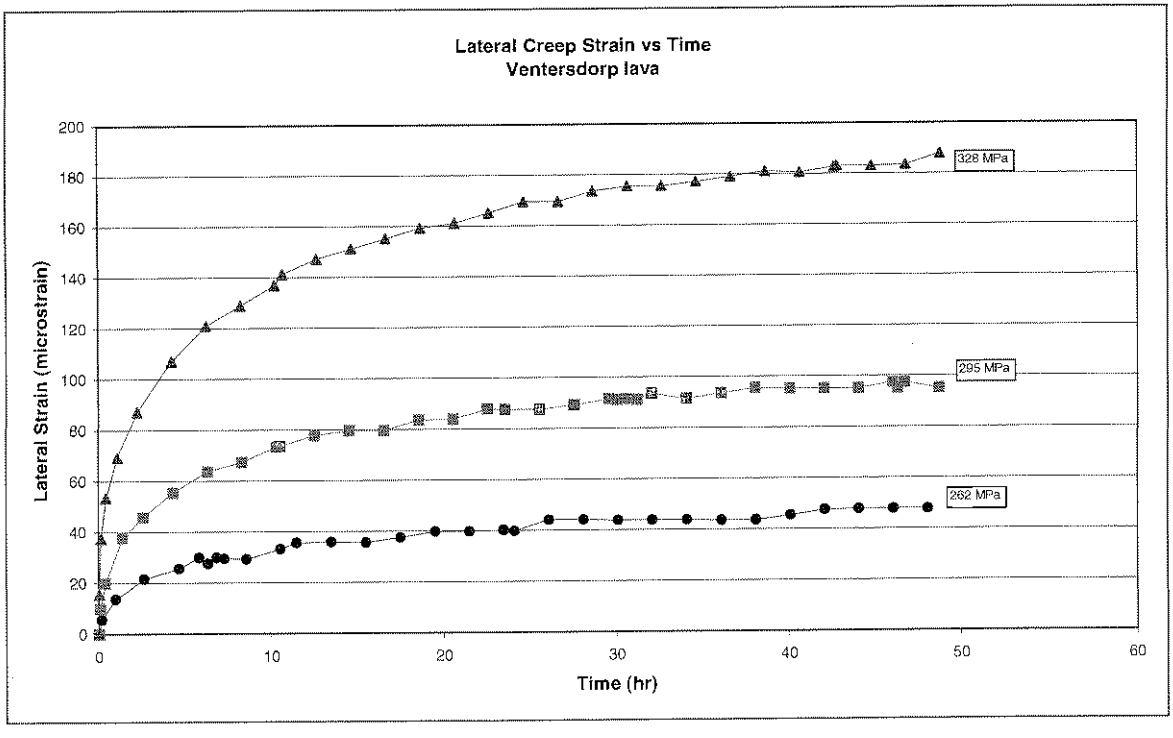

Figure 2.4.4 Lateral creep strain-time curve for Ventersdorp Lava

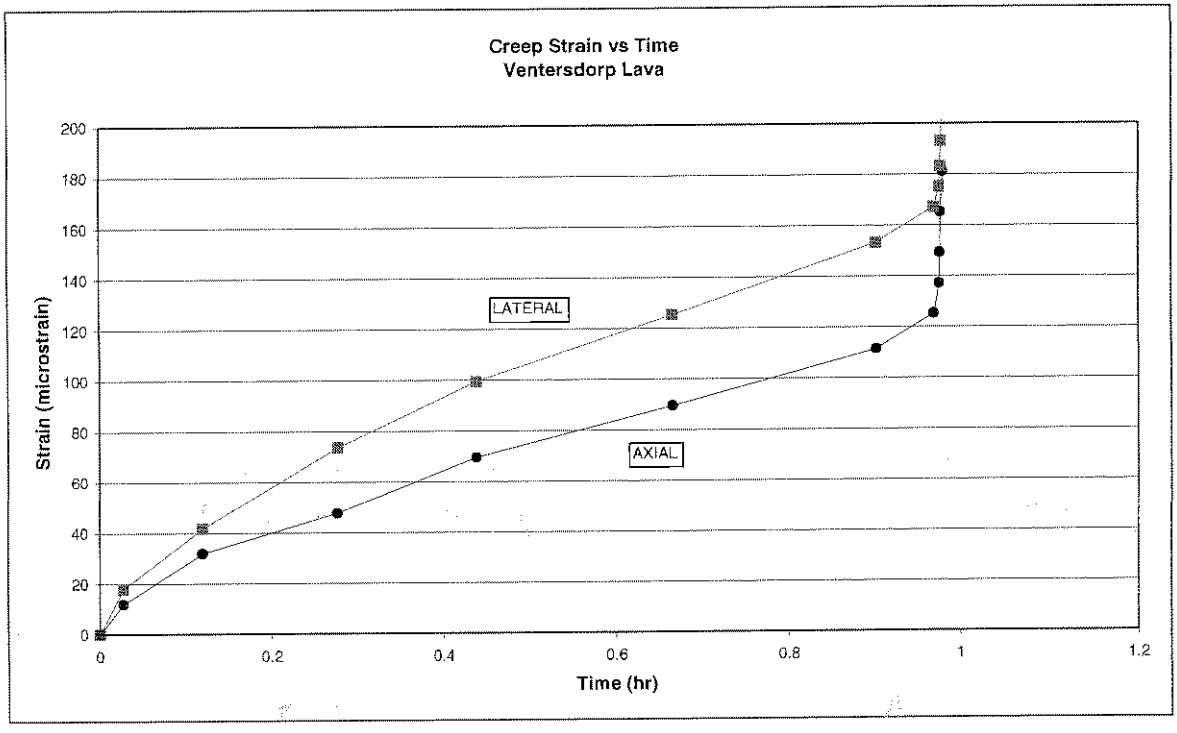

Figure 2.4.5 Final creep cycle for Ventersdorp Lava

When studying Figures 2.4.3, 2.4.4 and 2.4.5 it can be seen that during the later creep cycles (at 295 MPa an onwards) the lateral creep strain is higher than the axial creep strain. This is similar to the results obtained by Singh (1975: 273) on Sicilian Marble. The ratio of lateral creep strain to axial creep strain in the Sicilian Marble is much higher than for the lava. The increasing lateral creep strain can be attributed to progressive damage to the test specimen resulting in more fractures forming. Fractures form in the direction of the axial load and will lead to lateral dilation.

Calibration values for the steady-state creep law (see equation 2.1) for axial creep rate were determined by a log creep rate-log axial stress curve. It is assumed that the steady-state creep law is also valid for the lateral creep rate. The curve is shown in Figure 2.5.6 and the determined calibration values in Table 2.5.2.

Table 2.4.2 Calibration values for the steady-state creep law, Ventersdorp Lava

Spec No 1640-	% Strength	Axial Creep rate (strain/s)	Lateral Creep rate (strain/s)	Axial 'n'	Axial log(A')	Lat. 'n'	Lateral log(A')
CRP-23	90	2.03E-10	2.67E-10	3.15	-36.5	5.06	-52.7
CRP-53	91	3.14E-10	3.33E-10	4.24	-46.1	5.08	-53.3
CRP-55	91	1.06E-10	1.44E-10	6.90	-68.6	5.33	-55.5
CRP-63	91	3.36E-10	4.83E-10	7.96	-77.7	5.98	-60.6

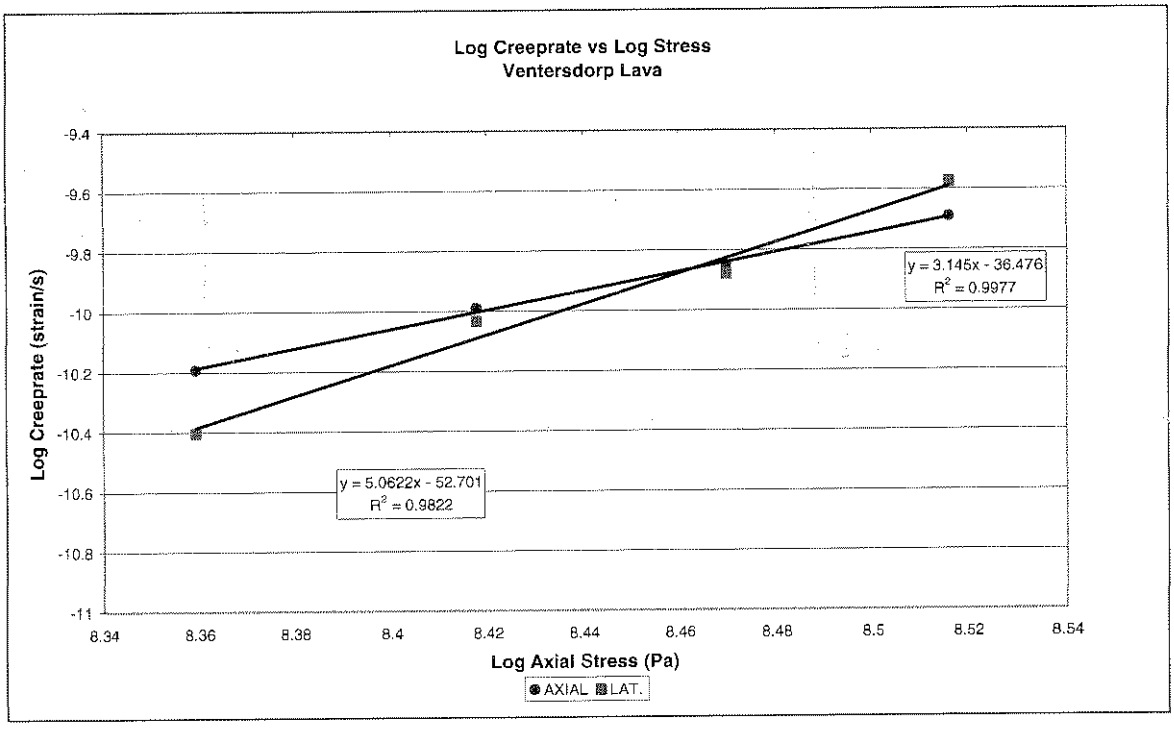

Figure 2.4.6 Log creep rate vs log Stress

2.4.2 Elsburg Quartzite

The tests results are summarised in Table 2.4.3. Similar to the Ventersdorp Lava results, calibration values for the steady-state creep law were calculated for the axial and lateral creep rates. The values are given in Table 2.4.4.

Table 2.4.3 Summary test results for Elsburg quartzite

Specimen No 2056-	Creep Strength (MPa)	Nosepoint Stress (MPa)	Nosepoint as % Strength	Axial Strain at Failure $x10^{-6}$	Modulus Loading (GPa)	Modulus Unloading (GPa)	Damage Index
CRP-116	117.6	91.0	77.4	3055	39.5	76.5	0.52
CRP-117	114.1	91.9	80.5	3642	40.7	75.2	0.54
CRP-118	112.6	91.0	80.9	4142	39.7	73.9	0.54
CRP-121	135.2	105.9	78.3	3267	51.0	79.7	0.64

As mentioned above, the modulus values during loading and unloading were determined for the first loading-creep-unloading cycle The damage index is the ratio between the loading and unloading modulus.

Table 2.4.4 Calibration values for the steady-state creep law, Elsburg quartzite

Spec No 2056 -	% Strength	Axial Creep rate (strain/s)	Lateral Creep rate (strain/s)	Axial 'n'	Axial log(A')	Lat. 'n'	Lateral log(A')
CRP-116	89	1.83E-10	2.75E-10	2.14	-27.0	4.06	-35.2
CRP-117	93	2.39E-10	4.47E-10	3.70	-39.3	13.30	-108.7
CRP-118	91	2.72E-10	3.53E-10	5.76	-55.5	10.55	-86.6
CRP-121	93	4.69E-10	9.83E-10	4.40	-45.1	6.30	-53.0

A typical complete strain-time curve for Elsburg Quartzite is shown in Figure 2.4.7. Typical incremental strain-time (axial and lateral) curves for the creep cycles preceding the final cycle are shown in Figures 2.4.8 and 2.4.9. The strain-time curve for the final creep cycle is shown in Figure 2.4.10. Similar to the Ventersdorp Lava the lateral creep strain for the quartzite increases more than the axial creep strain, as the load approaches the failure load.

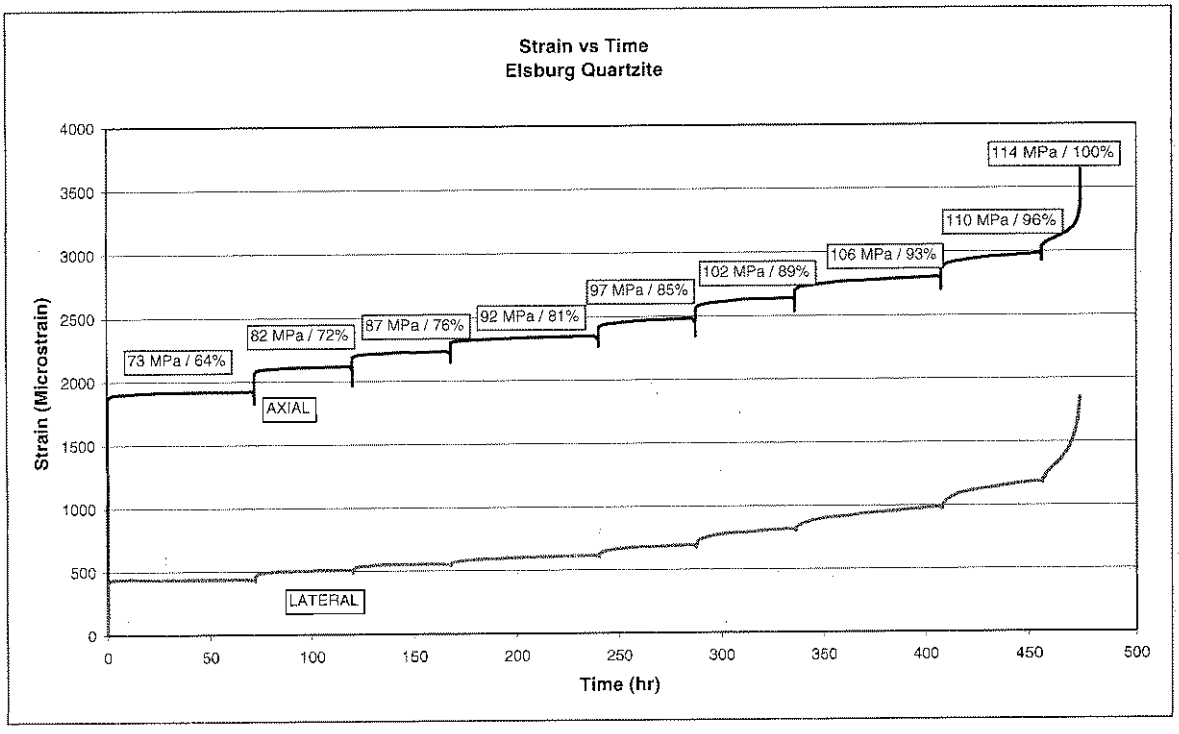

Figure 2.4.7 Strain-time curve for Elsburg Quartzite

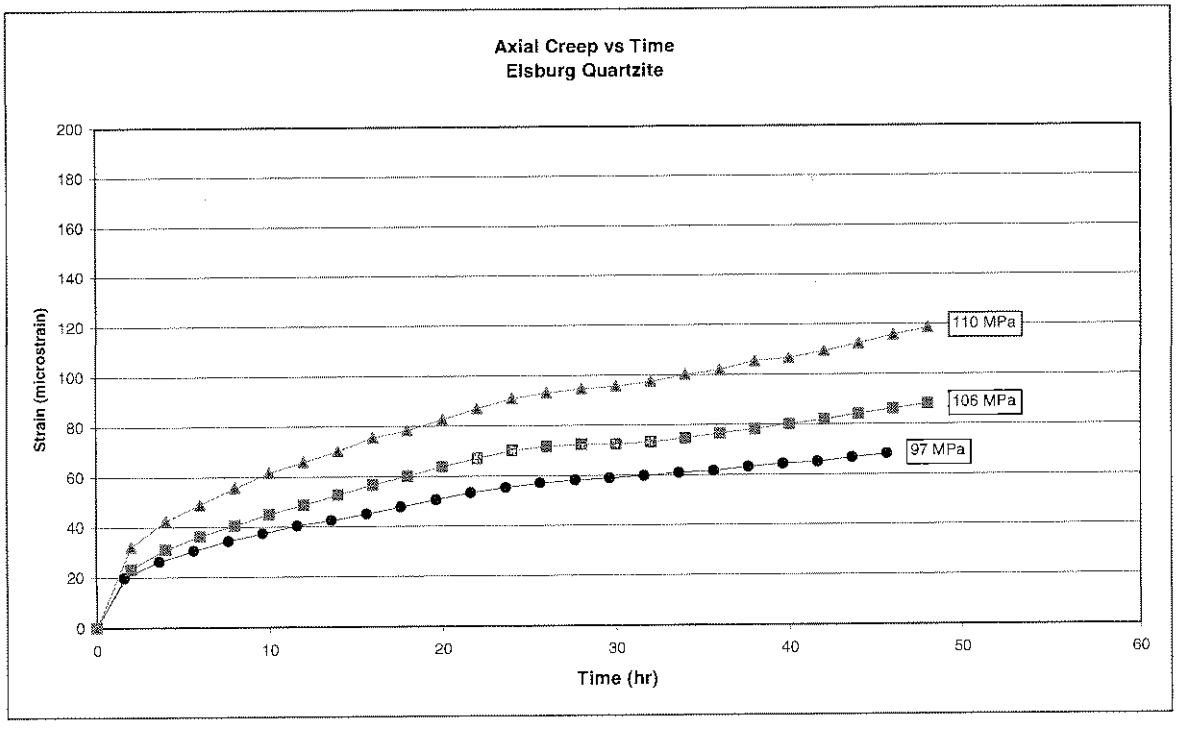

Figure 2.4.8 Axial strain-time curves for Elsburg Quartzite

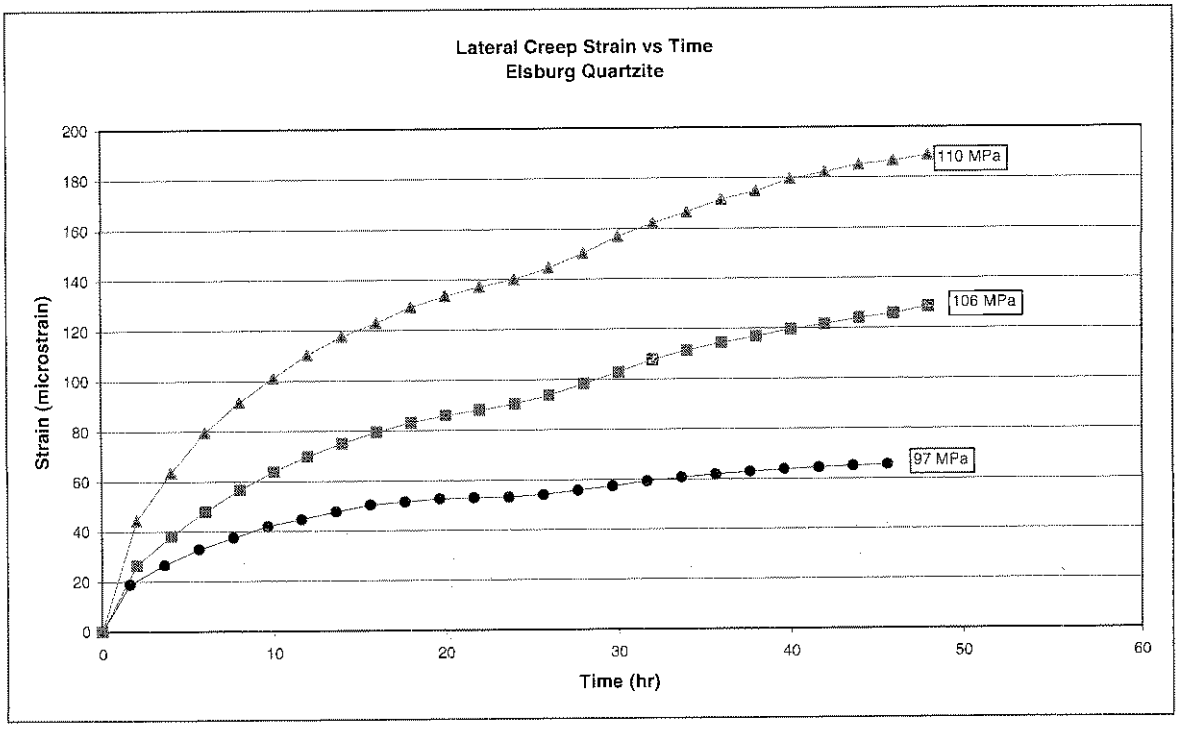

Figure 2.4.9 Lateral strain-time curves for Elsburg Quartzite

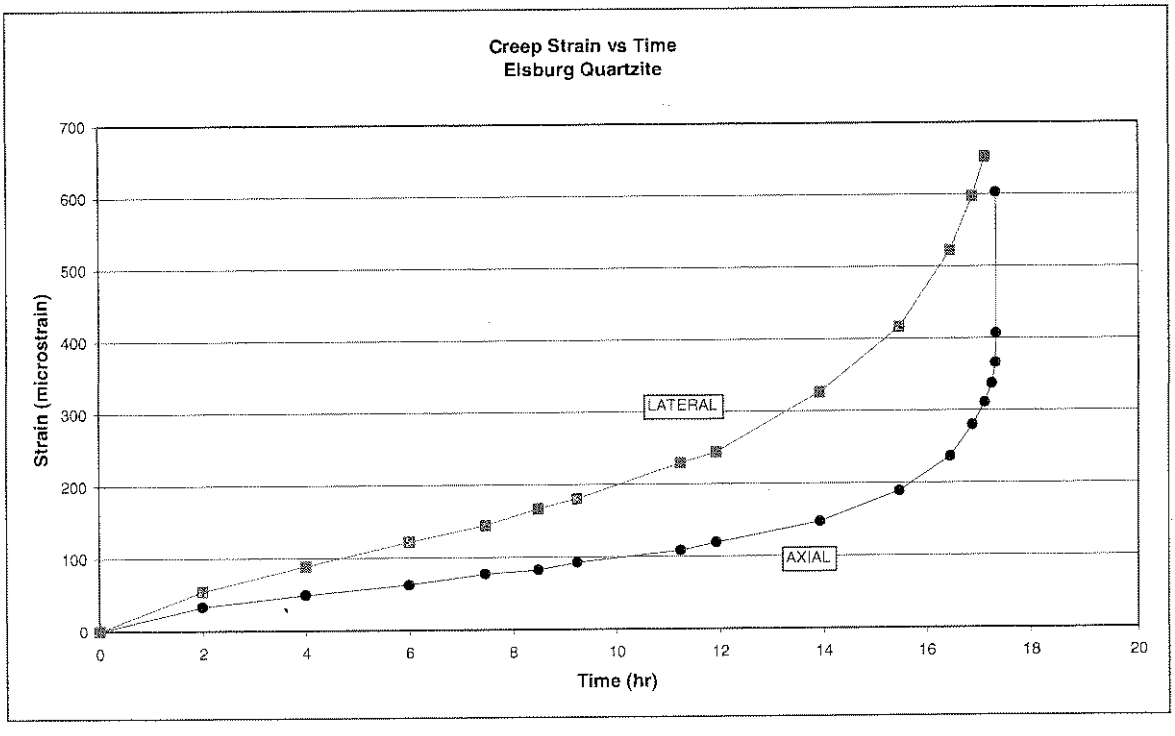

Figure 2.4.10 Final strain-time curve for Elsburg Quartzite

2.4.3 Discussion

Although the Ventersdorp Lava is much stronger than the Elsburg Quartzite, it appears as if the axial and lateral creep rates of both types of rock at approximately 90% of the failure load are of the same order of magnitude. Figure 2.4.11 shows the axial and lateral creep rates (strain/s) of the lava and the quartzite at different axial stress levels. If the axial stresses are normalised, by dividing the applied stress by the failure stress, as shown in Figure 2.4.12 it appears as if the ratio between applied stress and ultimate strength determines the creep rate rather than the absolute applied stress.

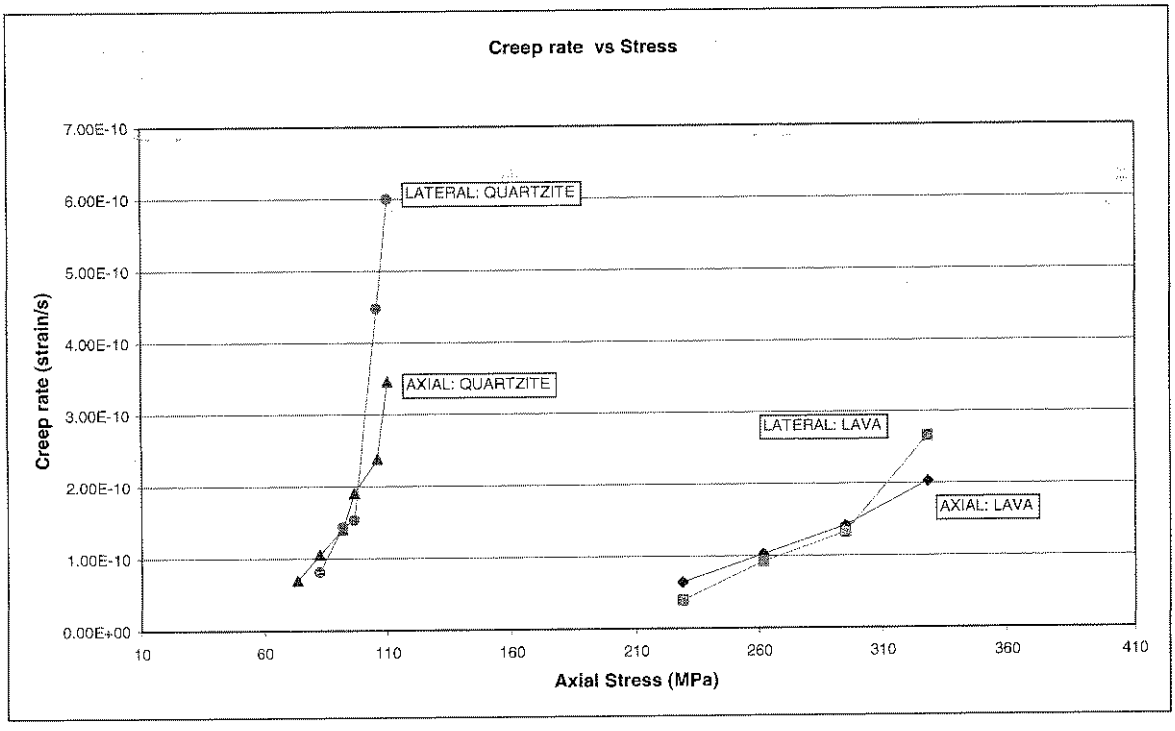

Figure 2.4.11 Creep rate vs axial stress

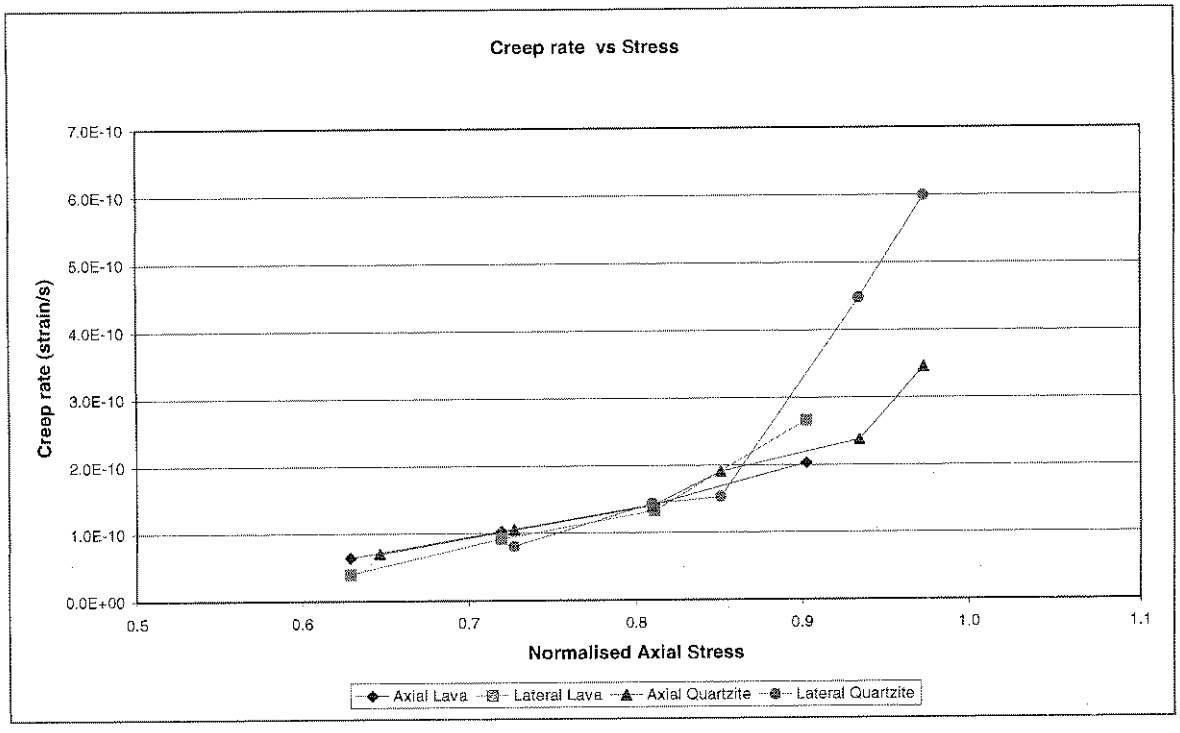

Figure 2.4.12 Creep rate vs normalised axial stress

To evaluate the creep rates that could be expected in the intact rock surrounding a stope at a depth of 4000m it is necessary to extrapolate the measured values.

Using the averages for the values in Table 2.4.2 and extrapolating downwards, estimated values of the axial and lateral creep rates of lava were determined at a stress level of 100 MPa, which is comparable to a mining depth of approximately 4000m. The average of the values in Table 2.4.3 were used to estimate the axial and lateral creep rates of the quartzite. The estimated values are given in Table 2.4.5

Table 2.4.5 Estimated creep rates

Applied Stress MPa	Axial creep Rate lava (strain/s)	Lateral creep Rate lava (strain/s)	Axial creep Rate quartzite (strain/s)	Lateral creep rate quartzite (strain/s)
100	1.88E-13	3.16E-13	1.88E-10	2.74E-10

As can be seen from Table 2.4.5 the axial and lateral creep rates of the quartzite at the applied stress of 100 MPa are three orders of magnitude greater than the respective creep rate for lava. This is because an absolute stress state

is being considered and at 100 MPa the quartzite is at approximately 90% of its ultimate strength whereas the lava is at approximately 25% of its ultimate strength.

In addition, the following observation are made:

- For the lava, most specimens reach the "nosepoint" at approximately at 90% of the failure strength while the quartzite specimens reach the nosepoint at ± 80% of the failure strength, indicating that in the quartzite the onset of unstable fracture propagation occurs at a lower applied stress / strength ratio.
- Very hard and brittle rocks, if subjected to sufficient stress, show creep behaviour.
- For lava and quartzite, the amount of creep strain as well as the creep rate is proportional to the applied stress / strength ratio.
- The ratio between the loading modulus and unloading modulus for the quartzite is significantly lower than for the lava indicating that the damage done to the quartzite specimen is greater than the damage done to the lava specimen.
- The average creep strength for both the quartzite and the lava are lower than the respective uniaxial compressive strength (Appendix B, Figure B2).
- Although the modulus values for the lava are higher than those of the quartzite specimens, the maximum strain at failure of the lava is higher than that of the quartzite.

The amount of specific energy the specimens were subjected to and the amount of specific energy that was dissipated during the creep time periods were calculated using the following:

$$w = \frac{1}{2}(\sigma_{11}\varepsilon_{11} + \sigma_{22}\varepsilon_{22} + \sigma_{33}\varepsilon_{33}) \qquad [2.3]$$

Under uniaxial compression σ_{22} and σ_{33} are zero, thus the specific energy is calculated using only the axial stress and axial strain ($\sigma_{11}\varepsilon_{11}$). The dissipated energy is calculated during each creep cycle (constant axial stress) followed by adding them all up. The specific energy calculation for lava and quartzite are given in Table 2.4.6. The percentage strength values correlate to the values in Table 2.4.2 and 2.4.4 respectively.

Table 2.4.6 Specific energy calculations for lava and quartzite

Spec No	% Strength	Energy Dissipation (kJ/m^3)	Total Energy at % Strength (kJ/m^3)	Percentage Energy Dissipation
Lava				
1640-23	90	64.0	671.3	9.5
1640-53	91	91.8	922.7	10.0
1640-55	91	48.5	728.8	6.7
1640-63	91	102.3	799.8	12.8
Quartzite				
2056-116	89	23.4	137.1	17.1
2056-117	93	27.1	147.8	18.4
2056-118	91	26.0	143.3	18.1
2056-121	93	29.0	163.9	17.7

The percentage energy dissipation for the quartzite is significantly higher than for the lava, showing that the quartzite is relatively more "plastic" than the lava. Also, this shows why rockbursts in lava are perceived to be more energetic and violent than rockbursts in quartzite. Lavas store up to 90% of the energy as elastic energy and dissipate only 10% in plastic deformation; while in quartzite up to 20% of the energy is dissipated by plastic deformation and 80% is stored as elastic energy. In lava, there is thus more energy available for violent deformation or failure.

Chapter 3

3 Shear Creep on discontinuities

3.1 Analysis of existing data

In some of the earlier studies aimed at determining the time-dependant behaviour of rock joints, cylindrical tests specimens containing a discontinuity were tested in triaxial compression. In tests conducted on Westerly granite (Wawersik, 1974: 361) the discontinuity was inclined at 30° relative to the direction of the principal stress. For unfilled rock joints Wawersik made the following conclusions: (1)The instantaneous response (primary creep phase) of the rock joint exceeds the time dependant response (secondary creep phase) by orders of magnitude and (2) For all practical purposes the unfilled rock joints are inactive regardless of the amount of water present.

Crawford & Curran (1980: 597) used numerical modelling to investigate the *in situ* time-dependant behaviour of a rock mass. The most important conclusion they made is that joint creep was only important when the joint surfaces were relatively free to move. Crawford & Curran (1981: 293) later did studies that concentrated on the rate-dependant behaviour of rock joints and these do not give any information of time-dependant shear displacements of joints at constant normal stresses.

Amadei (1979) hypothesised that the shear creep of a joint would be governed by the ratio of applied shear stress to peak shear strength. Schwartz and Kolluru (1984: 333) did some studies using a synthetic rock material (consisting

of a gypsum plaster mix) to test the hypothesis of Amadei. Uniaxial creep tests with clean unfilled joints, at different angles in relation to the axial loading direction, were done to investigate the influence of different stress levels on the creep of unfilled rock joints. They found that at small inclinations, the amount of joint creep is proportional to the inclination. However, the increasing joint creep peaks at between 15° and 20°. At inclinations of larger than 20°, the amount of joint creep would decrease again. They concluded that creep of a discontinuity depends on the applied shear stress to peak shear strength ratio as well as the absolute normal and shear stresses on the discontinuity.

Bowden and Curran (1984: 321) performed tests on artificial discontinuities prepared from shale. Two types of tests were performed: (1) Sheared and unsheared joints were loaded and unloaded vertically (2) Under a constant normal stress, different shear stresses were applied to a joint. They made the following conclusions: (1) For sheared joints the plastic component of normal joint deformations is very small or non-existent and (2) There is a non-linear relationship between the ratio of applied shear stress to peak shear strength and the creep rate. For small shear stress ratios they found that the creep rate is small and did not consider it to be significant as a source of long-term displacements. For large shear stress ratios (especially those greater than 0.9) the time dependant displacements along joints were considered to be significant. Bowden and Curran suggested that they should be taken into account when designing excavations in shale.

Malan (1998:153) and Malan, Drescher and Vogler (1998:475) did more elaborate work on shear creep of discontinuities in rocks from deep South-African gold mines. Shear creep experiments were done on natural joints with natural gouge and artificial joints with artificial gouge (crushed rock). Creep of discontinuities was divided into two classes: (i) creep of discontinuities with gouge infilling and (ii) creep of discontinuities with matching surfaces and no infilling. It was concluded that the creep of the latter class on a laboratory scale appears to be rather insignificant. Thus it is the infilling that allowed the observed creep. For rock joints that contain gouge infilling, the following conclusions were made:

- For a discontinuity under normal stress an applied shear stress (smaller than the peak shear strength) results in primary and secondary creep behaviour
- With greater shear stress / shear strength ratios instantaneous response noted during the primary creep phase became increasingly prominent.
- With greater shear stress / shear strength ratios, the creep rate increases in the secondary creep phase.
- The amount of creep is dependent on the shear stress / shear strength ratio as well as the absolute shear and normal stresses.
- Creep normal to the discontinuity was recorded and reduces the gouge thickness with time. Furthermore, with increasing shear stress at constant normal stress further normal creep was observed.
- The creep rate is directly proportional to the gouge thickness – the thicker the gouge infilling the higher the creep rate.

According to Malan (1998: 166) and Malan, Drescher and Vogler (1998: 476), the secondary or steady state creep rate is given by the following equation:

$$\dot{D}_{SS} = A\left(\frac{\tau}{\tau_s}\right)^n \qquad [3.1]$$

Where D_{SS} is the shear deformation rate of the secondary creep phase, τ is the applied shear stress and τ_s is the peak (Coulomb) shear strength. The parameters A and n can be obtained from a least squares fitting procedure on a graph of log (D_{SS}) versus log (τ/τ_s). Figure 3.1.1 shows the recalculation of the first artificial gouge tests in table 3.1.1. A mathematical error was found in the log (τ/τ_s) data presented by Malan, Drescher and Vogler (1998: 476) and this affects the value of log (A). Table 3.1.1 shows the results of a recalculation of the data.

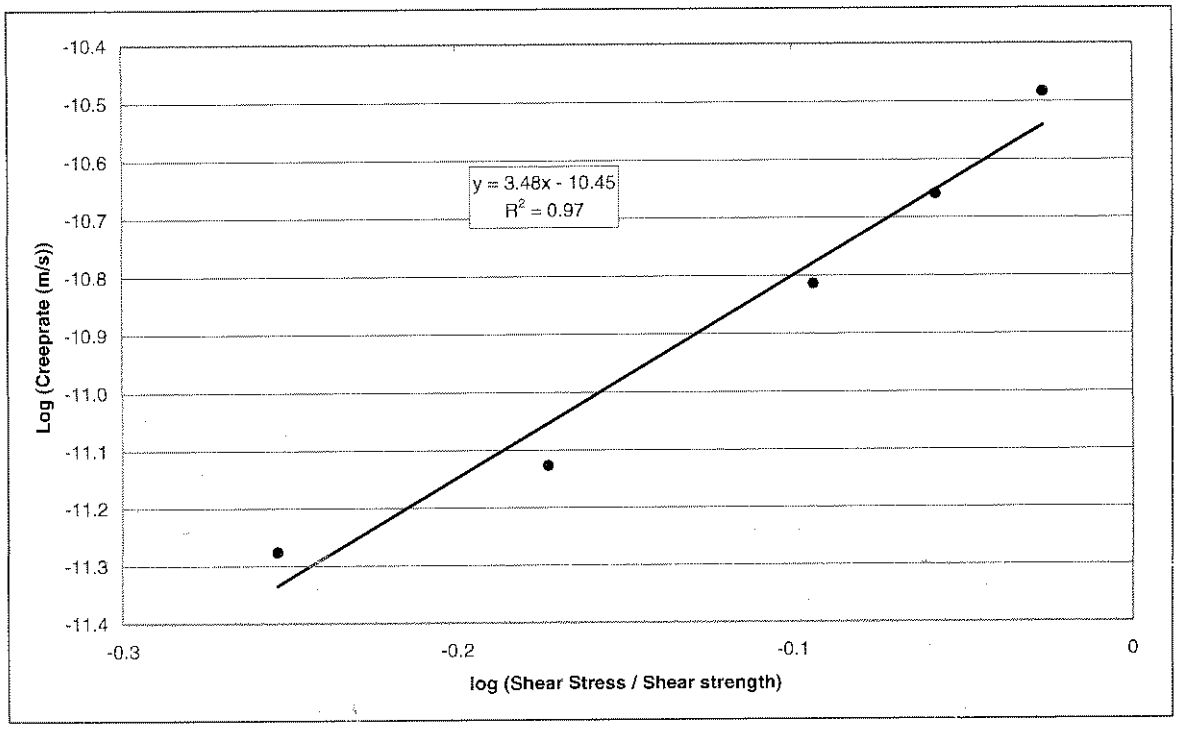

Figure 3.1.1 Artificial gouge, thickness 2mm, normal stress 0.5 MPa

Table 3.1.1 Recalculated calibration values for the power law in equation 3.1

Test No	Gouge Type	Thickness (mm)	Humidity (%)	Normal Stress	n	Log A
1	Artificial	2	50	0.5	3.5	-10.5
2	Artificial	2	50	1	2.3	-10.0
3	Artificial	2	50	1.5	2.9	-9.7
4	Natural	2	100	1	2.4	-9.7

3.2 Experimental Procedure

For the purpose of this study it was decided to use artificial joints because the aim was to study specifically the behaviour of different types of infilling. These comprise of an infilling material placed between two specially prepared quartzite blocks. Three different infillings were used: Two artificial infillings made from crushed Elsburg quartzite and crushed Ventersdorp lava and one natural gouge collected at Hartebeestfontein Gold Mine.

3.2.1 Geological Description

The Elsburg quartzite that was crushed for one of the artificial infillings is the same material used for the compression creep tests. The geological description is given in section 2.3.1 and in Appendix A.

The Ventersdorp Lava that was crushed for the second artificial infilling also originates from the Alberton formation but was collected at the Hippo quarry, south of Meredale. The rock is described as a fine-grained meta-tholeiite. A full petrographic description is given in Appendix A, sample 2056-160.

The natural gouge was collected from a fault between the hangingwall and sidewall and originates from the Stilfontein formation of the Johannesburg subgroup (Bosman, Malan and Drescher, 2000,56-57).

3.2.2 Specimen Preparation

A test specimen would comprise of one of the infilling materials between two rectangular quartzite blocks. The blocks were cut to the dimension of 95±1mm x 55±1 mm. The two shear surfaces were ground to ISRM (1979) specifications for uniaxial compression tests. All three materials used as infilling, were sieved to a particle size of smaller than 0.5mm

3.2.3 Testing Equipment

The testing equipment is shown in Figure 3.2.1 and is described in detail by Vogler, Malan & Drescher (1998: 230). For this study two of the described testing machines were used: one capable of performing tests wet and dry, the

other for dry testing only. The tests are performed in a climatically controlled laboratory with a temperature of 20±0.5°C and a relative humidity of 50±2%.

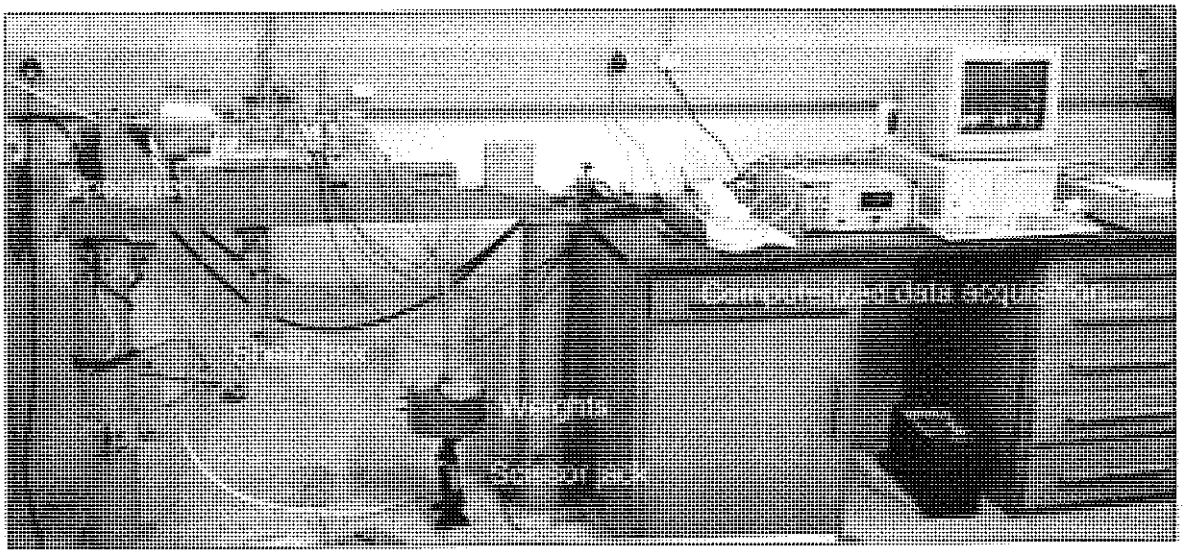

Figure 3.2.1 Shear creep testing apparatus

For this study modifications were made to the air pressure control of the testing machines. The testing machines were originally fitted with manually adjustable valves. These valves are of the diaphragm type that constantly leak air. Each of these valves was replaced by a set of solenoid and flow-control valves controlled by computer (Figure 3.2.2). The data acquisition software was updated to control the solenoid valves and keep the air pressure constant. The modified system would also allow automatic adjustment of the air pressure level after a given time interval, which is very useful if an adjustment has to be made overnight or during a weekend.

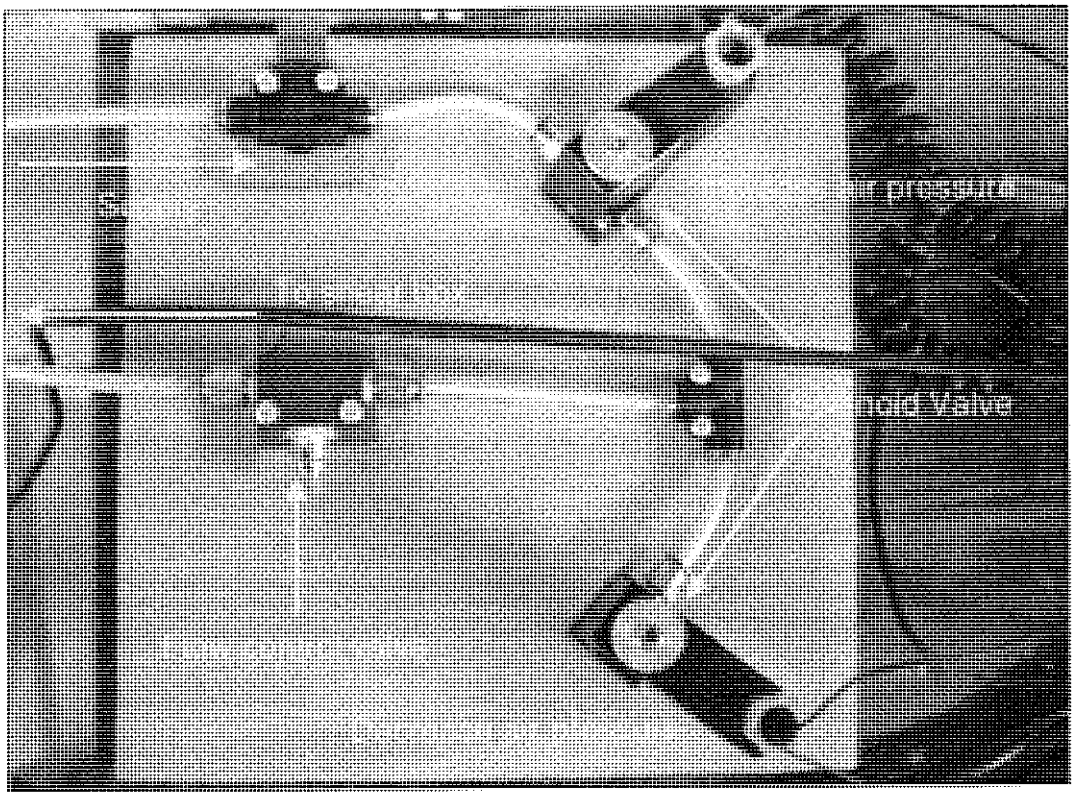

Figure 3.2.2 Air pressure controls

Figure 3.2.3 shows a close-up picture of a specimen, which is set-up for testing. Furthermore, the normal and shear load directions are indicated. One set of LVDT's is shown in the photograph. An identical set of LVDT's is installed on the opposite side of the specimen. The average readings of both sets of LVDT's are used during evaluation.

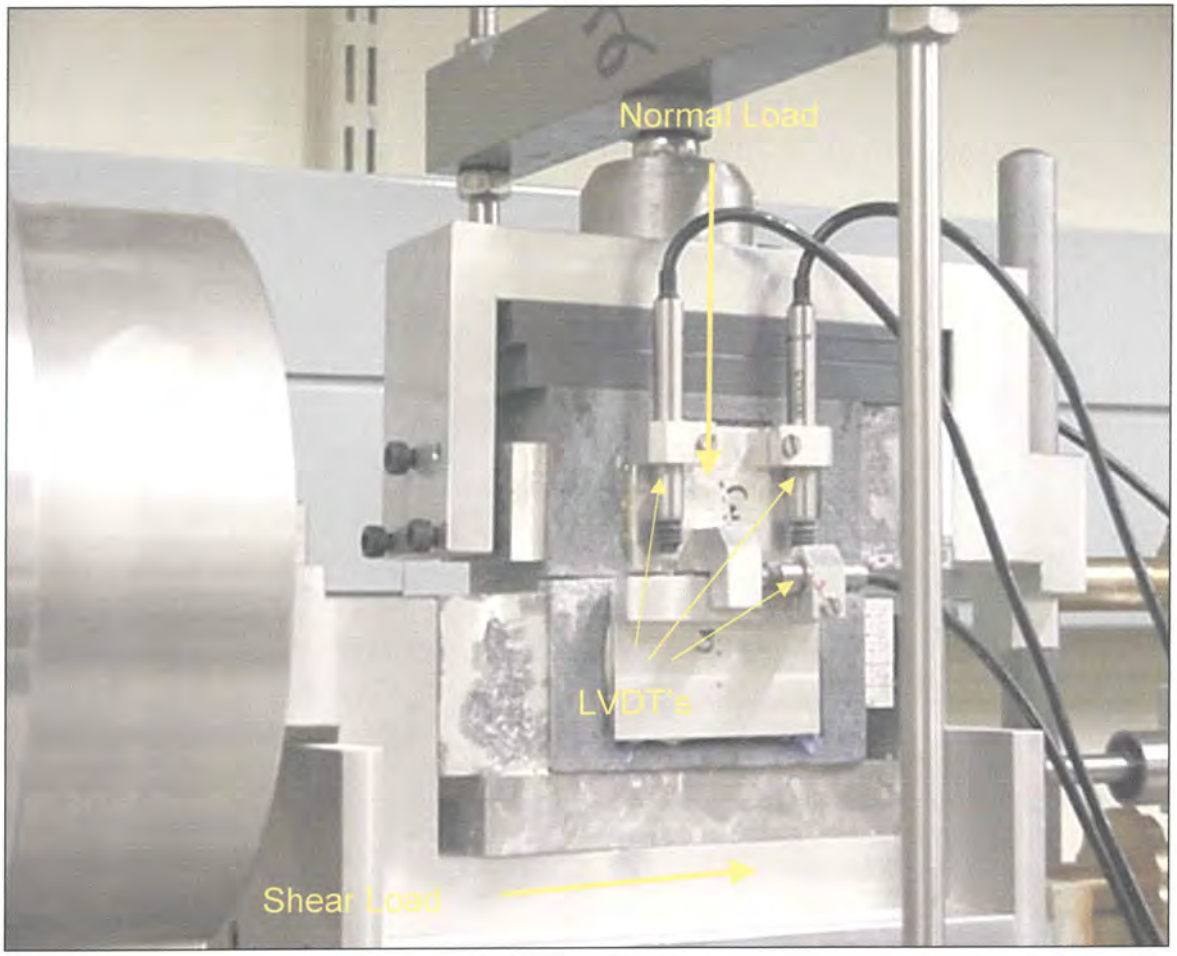

Figure 3.2.3 Testing configuration

3.2.4 Testing Procedure

The shear surfaces of the quartzite blocks are cleaned with Acetone before any given test. The infilling is placed on the lower shear surface and levelled to a given thickness (for this study 0.5, 1 or 2mm). The upper block is then placed on the infilling. The arms and weight hanger are placed on top, giving a slight normal preload. The weights are put on the weight hanger but kept up with a scissor jack (see Figure 3.2.1). The LVDT's are brought to the starting positions and the data acquisition is started. Finally, the weights are slowly lowered and the initial normal compression of the infilling is measured. By pressing one of the function keys on the computer keyboard, the air pressure is brought to the first preset air pressure level and the computer then controls the remainder of the test.

For the purpose of this study, tests were conducted at two humidity conditions: Firstly at the air relative humidity of the climate controlled lab (50% ± 2%, referred to as dry) and secondly, water saturated (relative humidity of 100%, referred to as wet), i.e. the infilling material is mixed with water beforehand and kept saturated during the test.

The time interval between the different air pressure (shear stress) levels is set at 48 hours. The shear stress levels of approximately 70%, 80%, 85%, 90%, 95% and 100% of the anticipated failure strength are then applied sequentially.

3.3 Experimental Results

Particle size distributions for all three materials were done by a Fritsch Particle Sizer Analysette 22 and the results are shown in Figures 3.3.1, 3.3.2 and 3.3.3.

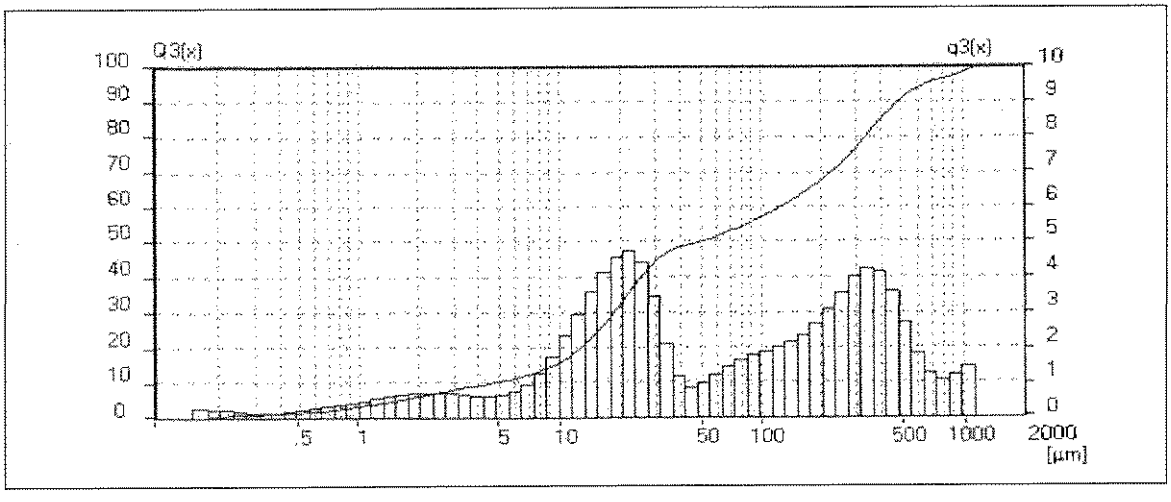

Figure 3.3.1 Particle size distribution for crushed quartzite

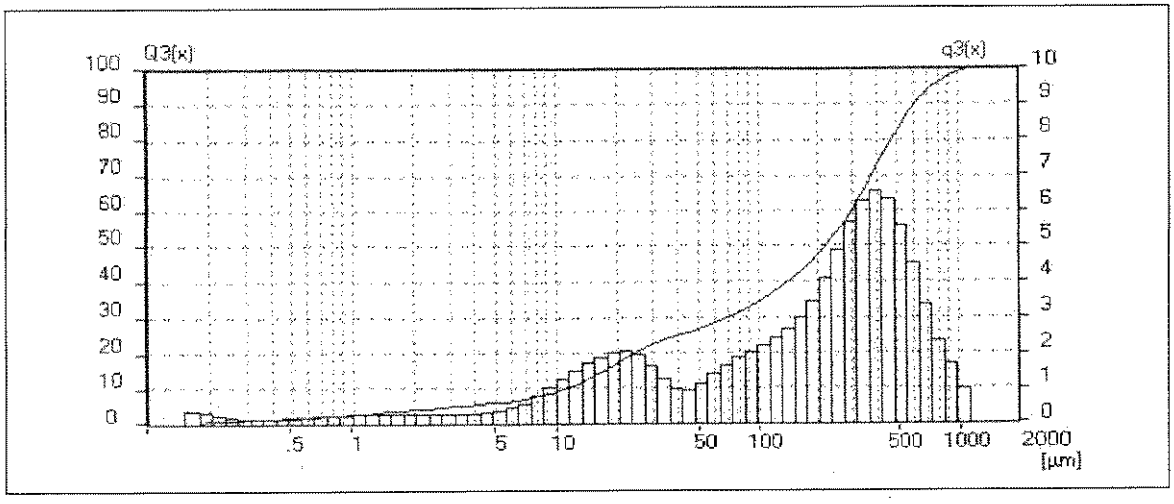

Figure 3.3.2 Particle size distribution for the crushed lava

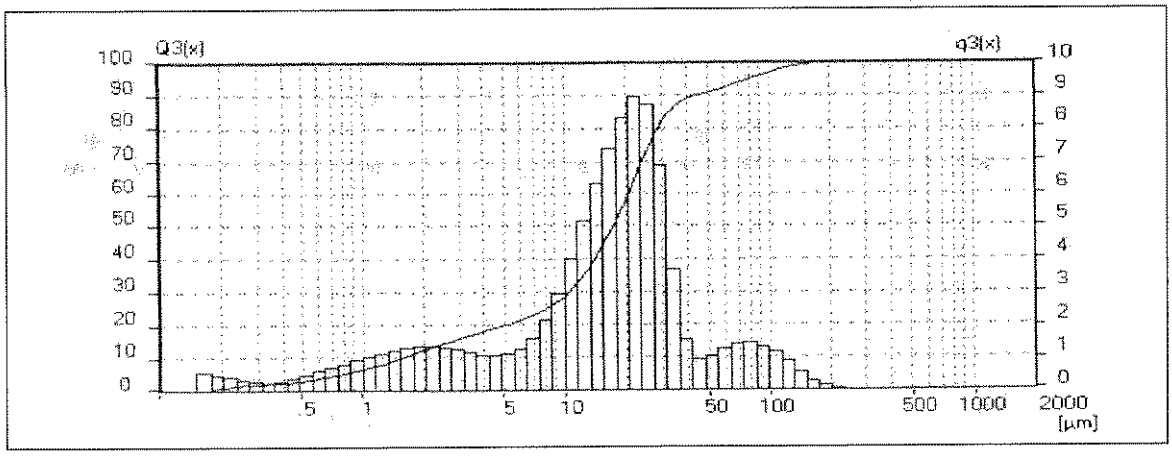

Figure 3.3.3 Particle size distribution for the natural gouge

The histograms represent the number of points in any given size range while the line indicates the cumulative size distribution.

In order to obtain some initial values of the peak friction angles, shear tests were conducted in the shearbox. The specimens consisted of saw-cut joint with lapped surfaces. Each of the three materials in turn was used as infilling with a thickness of approximately 1 mm. The tests were conducted in the air-dry condition. The results are given in Table 3.3.1 and shown in Figure 3.3.4.

Table 3.3.1 Shear test results

Specimen No	Description	Friction Angle
2056-151	Crushed Elsburg Quartzite	27.8°
2056-152	Crushed Ventersdorp Lava	31.3°
2056-153	Natural Gouge	16.7°

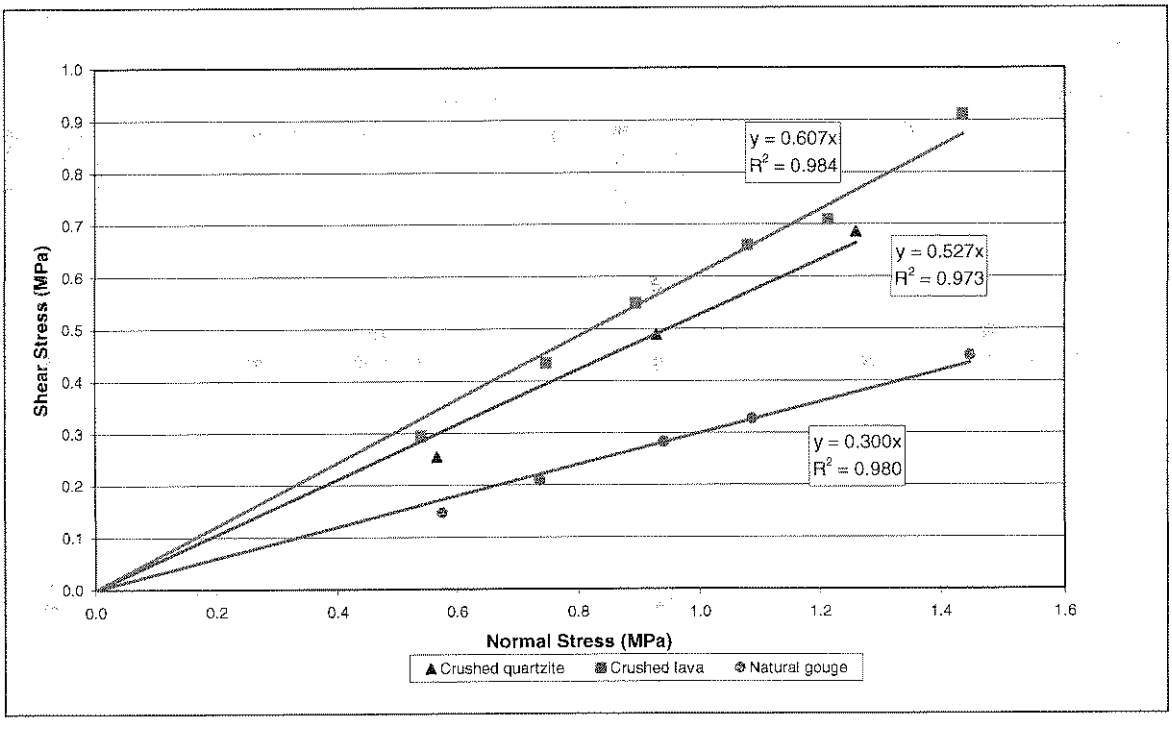

Figure 3.3.4 Shear stress – normal stress results for the three types of infilling

The standard shearbox tests on the different material showed that the natural gouge tends to have a much lower friction angle than the two crushed rock types, i.e. quartzite and lava. Furthermore, the crushed lava showed a slightly higher friction angle than the crushed quartzite.

The test results are summarised in Table 3.3.2. All the tests results are given in Appendix C. A typical complete displacement-time curve is shown in Figure 3.3.5. The increasingly normal displacement indicates compaction of the material during testing. Malan, Drescher and Vogler (1998: 476) did the tests at normal stresses of 0.5, 1.0 and 1.5 MPa, were 1.5 MPa is very close to the capacity of the machine. It was decided to perform the tests at a normal stress

of between 0.5 and 1 MPa, thus all tests were done at a normal stress of 0.65 MPa. Furthermore, 0.65 MPa is practically easy obtainable as 30kg of weights are required.

Table 3.3.2 Summary of the test results

Spec. No 2056-	Thickness (mm)	τ/τ_s (%)	Humidity (%)	Peak Friction angle (°)	Shear Creep rate (mm/hr)	n	Log A
Crushed Elsburg Quartzite							
CPS-143	0.5	92	50	19.5	1.53E-04	4.46	-10.19
CPS-144	1	90	50	29.6	1.50E-04	3.54	-10.32
CPS-145	2	91	50	28.2	1.60E-04	2.54	-10.27
CPS-146	1	89	100	28.5	4.42E-04	3.78	-9.82
Crushed Ventersdorp Lava							
CPS-162	0.5	92	50	23.1	1.21E-04	2.89	-10.35
CPS-148	1	90	50	30.5	6.15E-05	5.33	-10.41
CPS-149	2	89	50	30.7	4.60E-05	3.82	-10.70
CPS-150	1	90	100	31.9	2.86E-04	3.58	-9.97
Natural Gouge							
CPS-239	0.5	94	50	17.5	2.41E-05	0.38*	-11.64*
CPS-238	1	91	50	20.3	5.69E-05	1.84	-10.66
CPS-240	2	89	50	20.8	5.81E-05	7.24	-10.44
CPS-241	1	89	100	18.5	8.75E-05	3.89	-10.47

*Only two data points

All the previous work done by the various authors on the creep behaviour of discontinuities, show that there are definite primary and secondary creep phases. During this study it was expected to obtain a displacement-time curve that shows all three creep phases, which are shown in Figure 3.3.6.

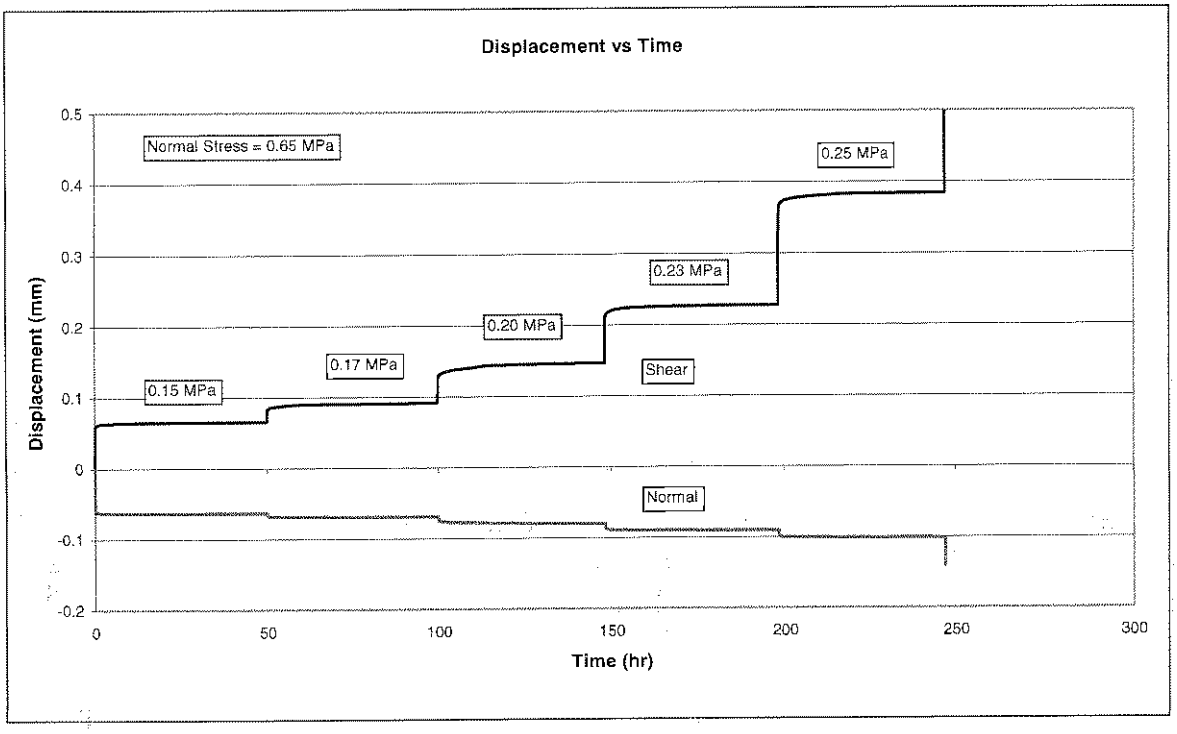

Figure 3.3.5 Complete displacement-time curve

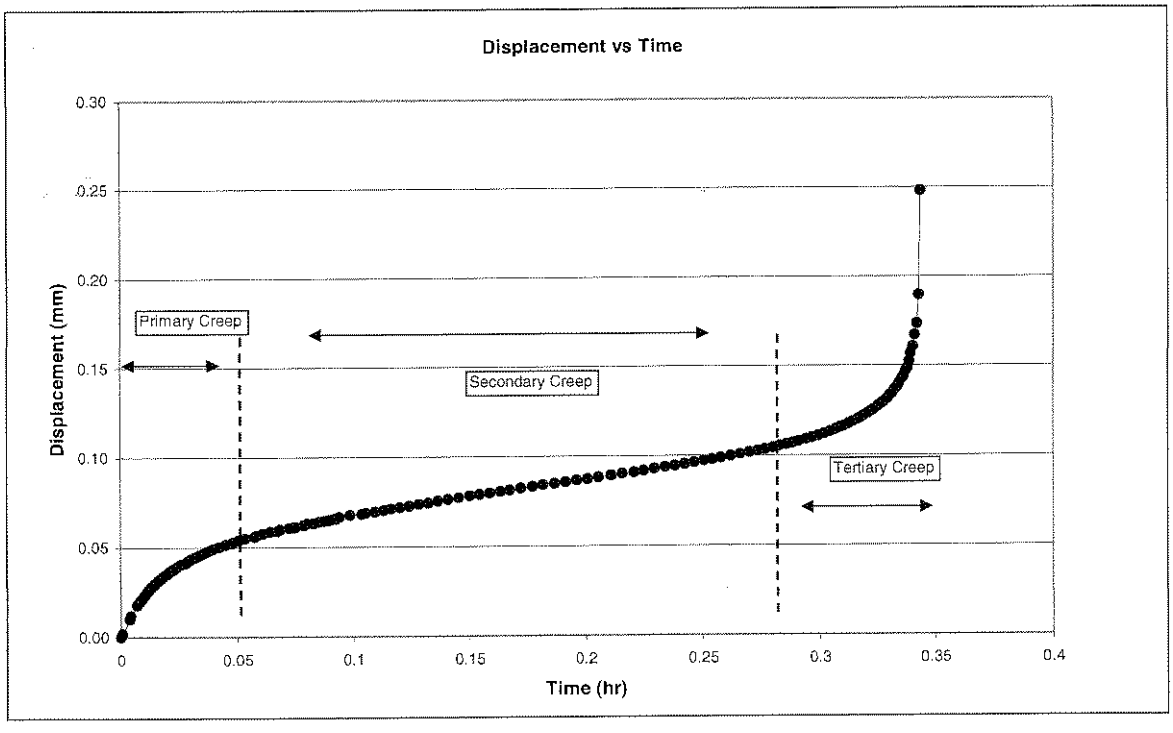

Figure 3.3.6 Shear displacement-Time curve with all three creep phases

It proved to be rather difficult to obtain a curve showing all three creep phases (Figure 3.3.6). This one was obtained from specimen 2056-CPS-238 which provided the data for Figure 3.3.6. When the applied shear stress / peak shear

stress ratio (τ/τ_s) is too small, only primary and secondary creep phases occur. This is typical for low τ/τ_s ratios. If on the other hand the ratio is too high and the specimen approaches too close to the point of failure, the creep curve for that specific cycle consists of a small portion of the secondary creep phase followed by the tertiary creep phase.

Furthermore it is noteworthy that the typical time period for creep cycles was 48 hours, but that the curve shown in Figure 3.3.6 was obtained within 20 minutes after adjustment of the shear stress level. Thus, the three creep phases are the real response of the gouge material. Obtaining such a curve will depend on the applied stress level as well as the time allowed to reach failure.

During the study it was also observed that the amount of creep displacement during the different cycles as well as the shear creep rate is dependant on the τ/τ_s ratio (applied shear stress / peak shear strength). This is shown in Figure 3.3.7 where the τ/τ_s ratios are given as a percentage. With the normal stress of 0.65 MPa and an ultimate friction angle of 23.1°, the applied shear stress at 83% of the shear strength is 0.23 MPa. The cumulative displacement - τ/τ_s ratio curve is shown in Figure 3.3.8 and the shear creep rate - τ/τ_s ratio curve is shown in Figure 3.3.9.

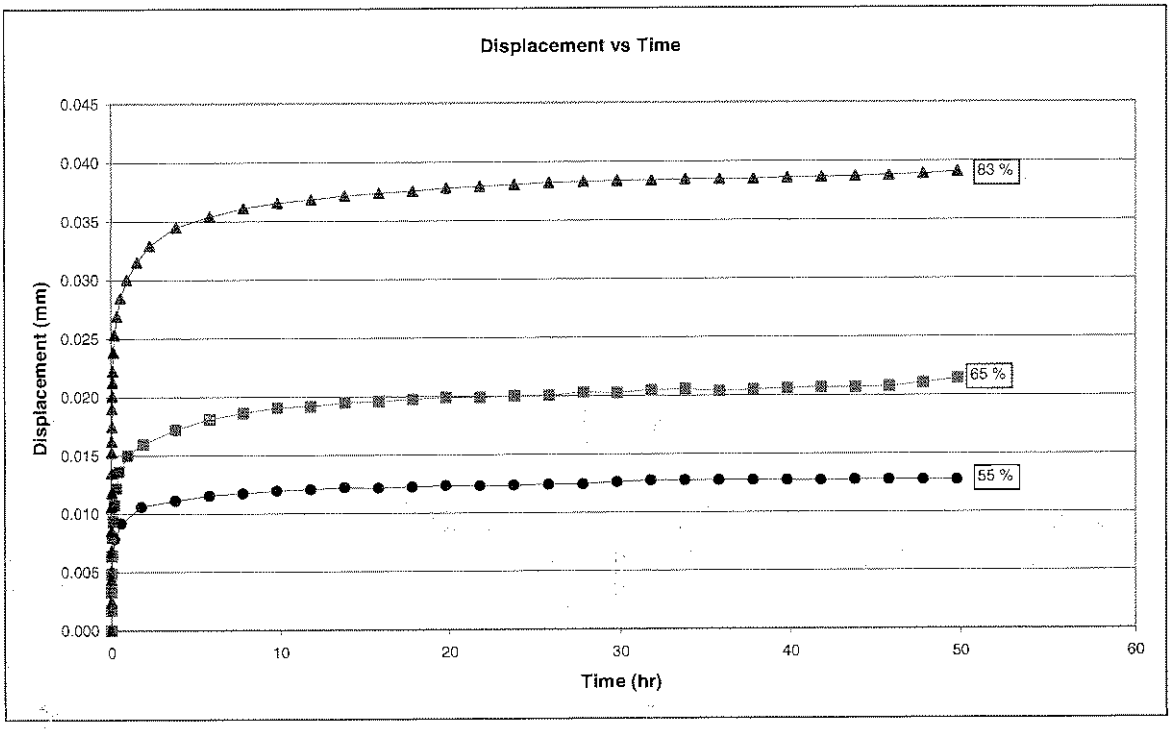

Figure 3.3.7 Shear displacement-time curves at different - τ/τ_s ratios

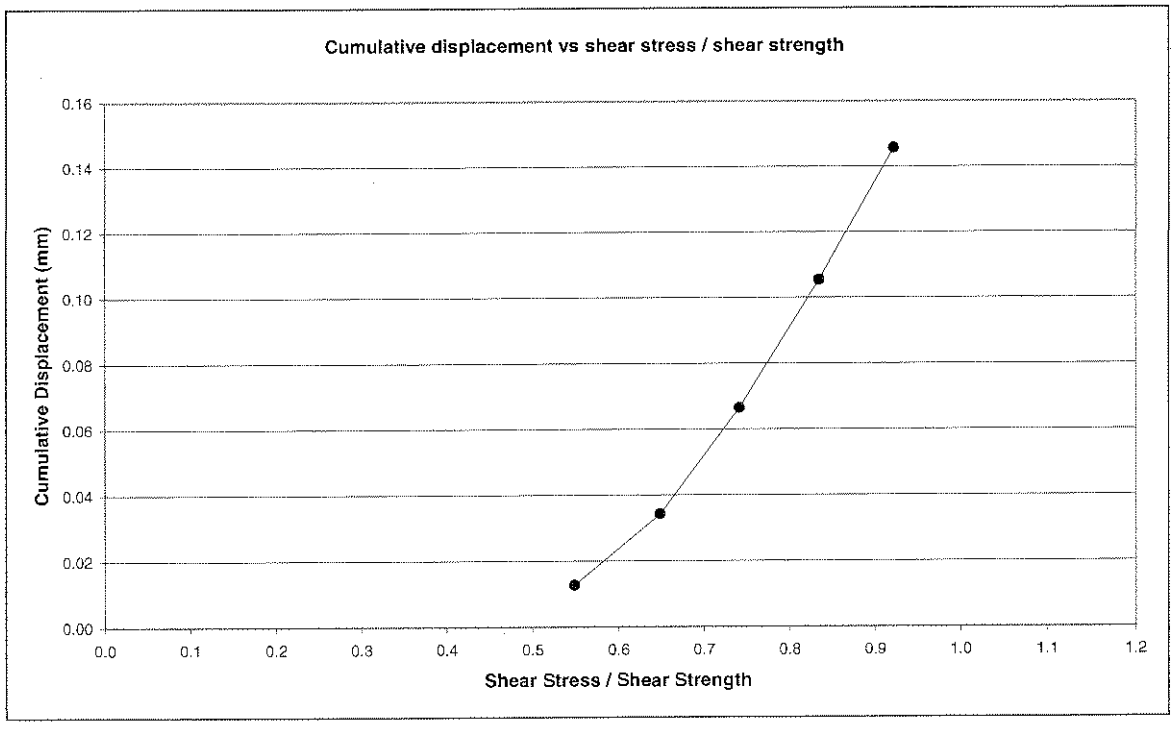

Figure 3.3.8 Cumulative shear displacement -τ/τ_s ratio curve

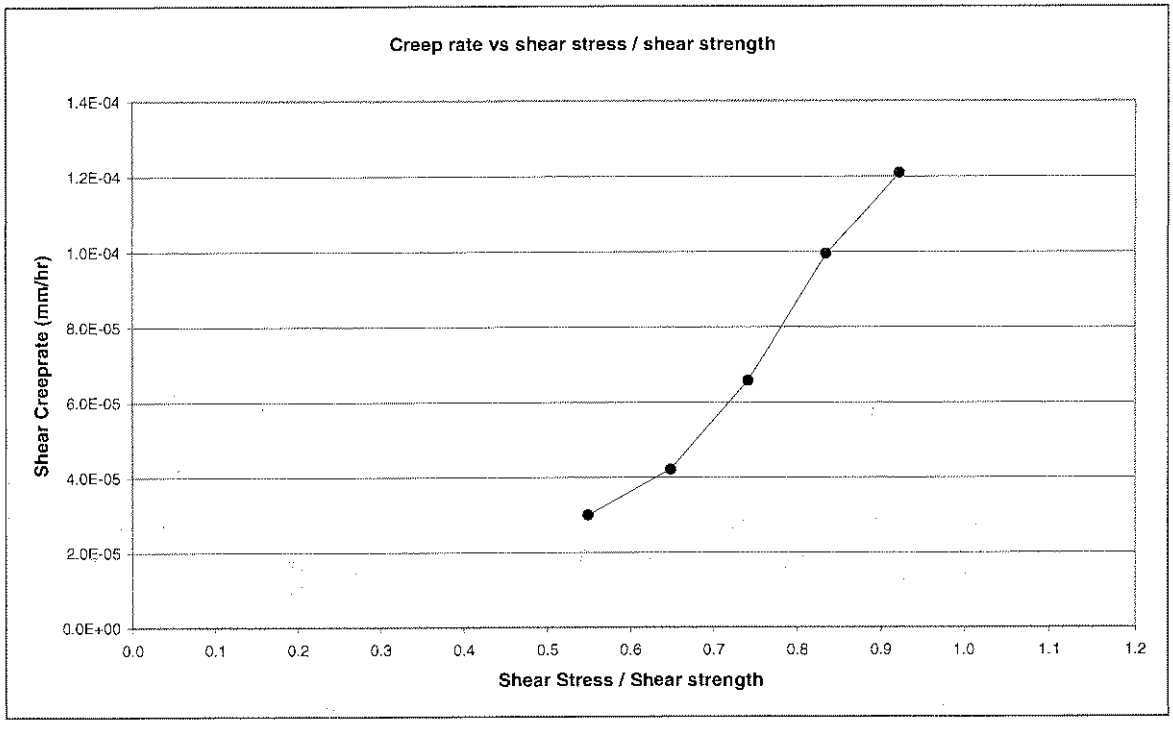

Figure 3.3.9 Shear creep rate-τ/τ_s ratio curve

These results confirm the hypothesis of Amadei (1979) and are similar to the results obtained by Schwartz and Kolluru (1984), and Bowden and Curran (1984), i.e. that the creep rate is proportional to the τ/τ_s ratio. Furthermore, the study confirms the results obtained by Malan (1998), i.e. that the moisture content has a significant influence on the creep rate. The results also extend the knowledge of creep behaviour of discontinuities in regard to the existence of the tertiary creep phase.

The results of the shear creep tests are shown in Figures 3.3.10, 3.3.11 and 3.3.12 for the crushed quartzite, crushed lava and natural gouge respectively. In the figures, "dry" indicates the standard humidity of the climate control laboratory, which is at 50% ± 2, while "wet" indicates that the sample was mixed with water and kept saturated during the test. The percentages given in the figures indicate the τ/τ_s ratios. The curves, for those ratios where the applied shear stress is close to the shear strength, were selected as these generally show the most prominent creep behaviour.

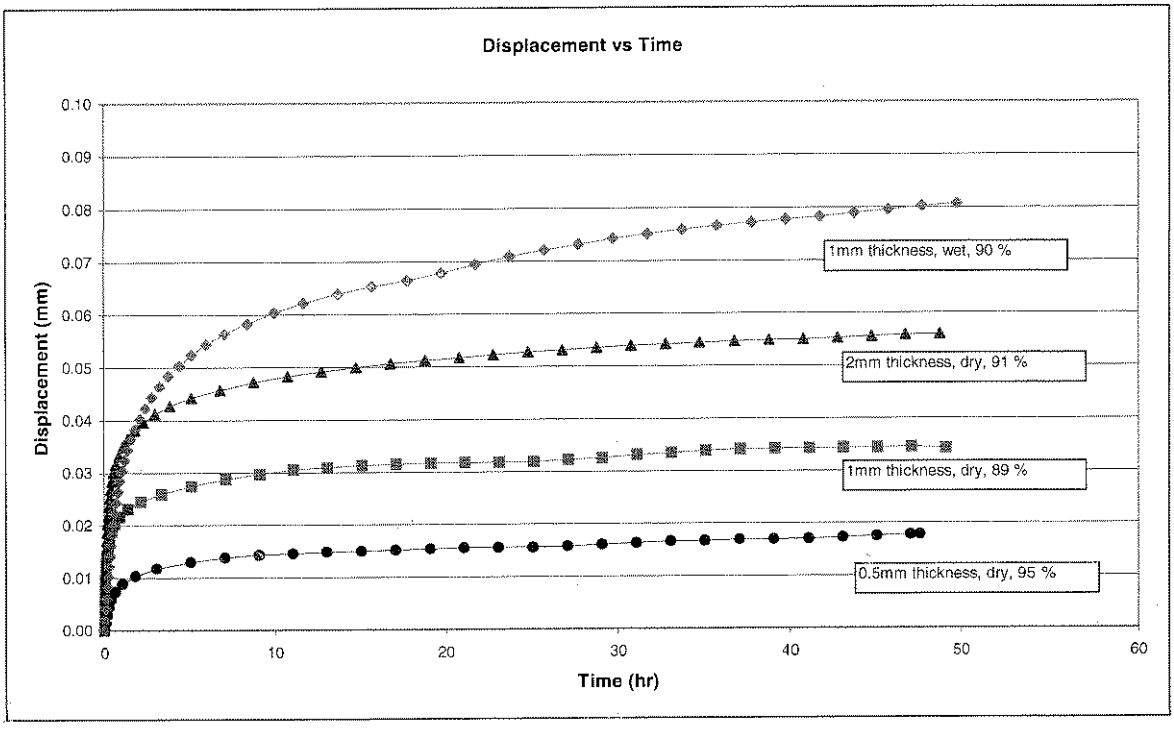

Figure 3.3.10 Shear displacement-time curves for crushed quartzite

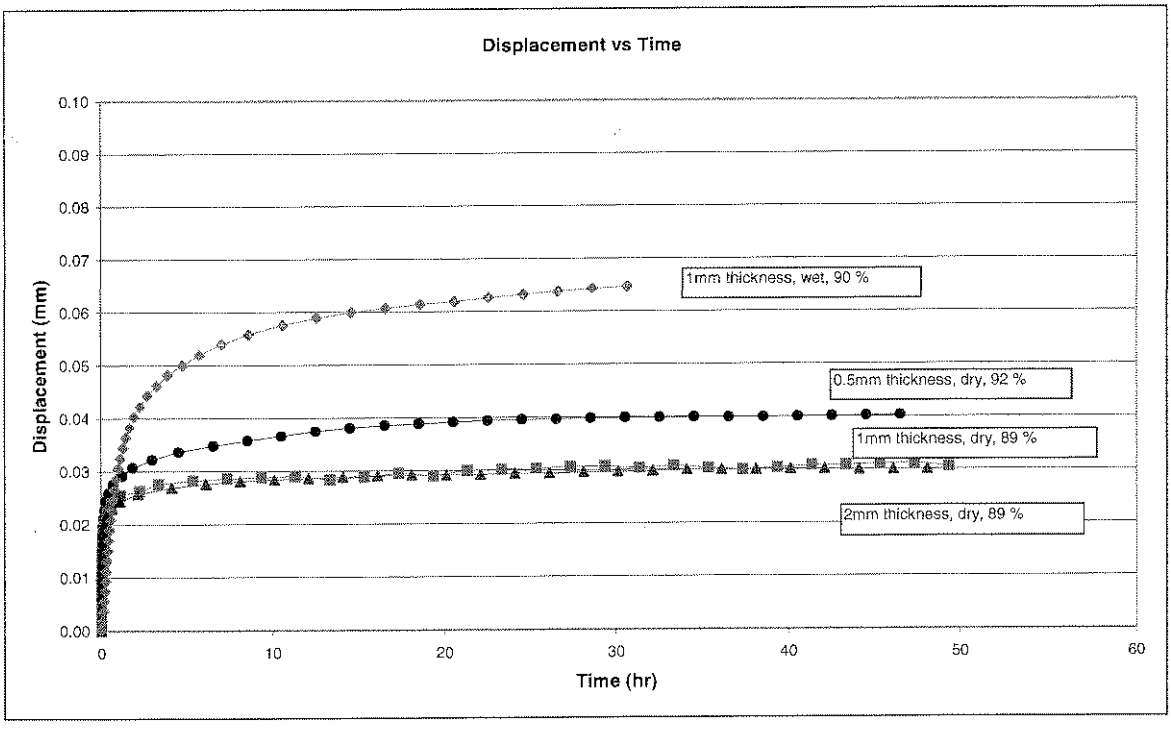

Figure 3.3.11 Shear displacement-time curves for crushed lava

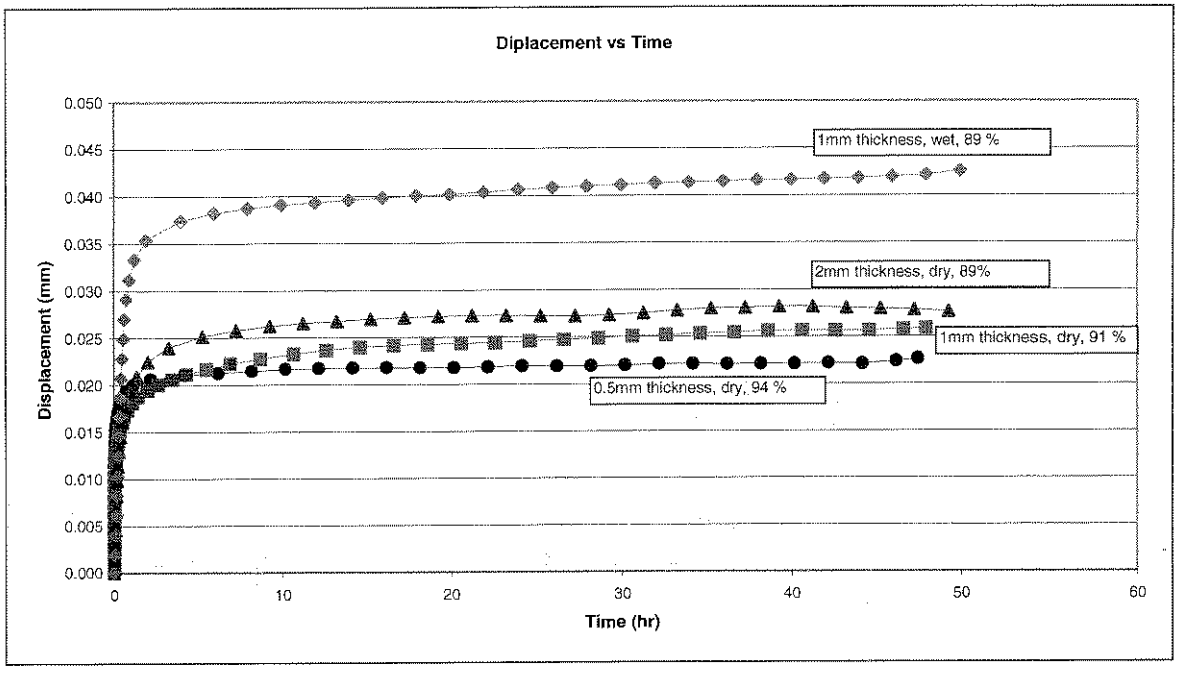

Figure 3.3.12 Shear displacement-time curves for natural gouge

3.4 Discussion

Considering figures 3.3.1, 3.3.2 and 3.3.3, the following observations are made:

- The crushed quartzite consists mainly (±30%) of material with a particle size of between 20 and 40 micron as well as between 200 and 500 micron.
- The crushed lava consists mainly (±60%) of material with a particle size of between 300 and 600 micron
- The natural gouge consists mainly (±80%) of material with a particle size of between 10 and 40 micron.
- Although all three materials were sieved with a 500-micron sieve, the particle size distribution shows material between 500 and 1000 micron for the quartzite and the lava. This indicates that some of the grains might have an elongated shape.
- The abovementioned shows that although all three materials were sieved with a 500-micron sieve, the grain size distribution varies for all three materials.

Considering Table 3.3.2 the following observations are made:

- At the same applied normal stress the peak shear strength for the natural gouge is much lower than that of the crushed quartzite and crushed lava.
- Primary, secondary and tertiary creep phases were observed
- The creep rate is dependent on the τ/τ_s ratio: a higher ratio leads to a higher creep rate as well as to a larger displacement in a given time period.
- The creep rate is significantly influenced by the moisture content: more moisture leads to higher creep rates as well as larger displacements in a given time period.
- There is a tendency that thicker infillings lead to higher creep rates: For the crushed quartzite and the natural gouge this is shown clearly in Figures 3.3.10 and 3.3.12 respectively. For the crushed lava this is not clear as can be seen in Figure 3.3.11.
- The ratio of grain size to infilling thickness as well as the grain size distribution might have an influence on the peak shear strength.

In order to compare the three types of infilling, the creep rates were estimated for all three types of infilling with a thickness of 1mm (dry). At a normal stress of 0.65 MPa, and a given applied shear stress the estimated values for the resulting shear creep rates are given in Table 3.4.1

Table 3.4.1 Calculated shear creep rates at the same normal and shear stresses (1mm dry)

Applied Shear Stress MPa	Shear creep Rate: natural gouge (mm/hr)	Shear creep Rate: crushed quartzite (mm/hr)	Shear creep Rate: crushed lava (mm/hr)
0.22	5.69E-05	2.73E-05	6.45E-06

Table 3.3.2 shows that the peak friction angles for 0.5mm layers of crushed quartzite and crushed lava, are much lower than those of 1mm and 2mm thickness. As the particle size of 0.5mm is very close to the thickness of the infilling, it appears that the mechanism of displacement for these may differ to that in tests were the thickness of the infilling is significantly larger than the particle size. The peak friction angle for the natural gouge is relatively constant, and therefore appear to be independent of the gouge thickness. Most of the particles in the natural gouge are however significantly smaller than the smallest thickness of 0.5mm.

If the normal force is not high enough to crush the individual grains, two types of shear creep mechanism are proposed below:

Single layer mechanism

In this mechanism, there is one layer of grains between the two sides of the discontinuity, which would just roll over each other. An analogy to this mechanism is a ball bearing or a roller bearing, especially when the sides of the discontinuity are without any asperities. The grains act similarly to the steel rollers in a roller bearing. This mechanism could explain the lower friction angles of the quartzite and lava at a thickness of 0.5mm. Since the major particle size for the natural gouge is much smaller, this mechanism is not applicable to the natural gouge if the infilling thickness is 0.5mm. A simplified illustration of this mechanism is shown in Figure 3.4.1.

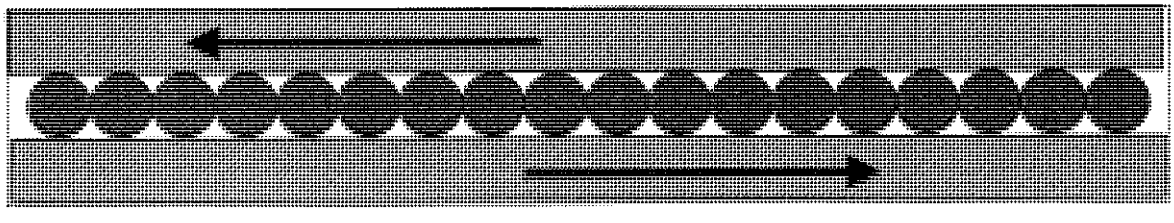

Figure 3.4.1 Simplified one layer mechanism

Composite layer mechanism

For this mechanism, considerable compaction of the material occurs during any movement of the two halves of the discontinuity. The material would be packed tighter increasing the friction between the grains, which would lead to an overall greater resistance and bigger friction angle values

A simplified illustration of this mechanism is shown in Figure 3.4.2.

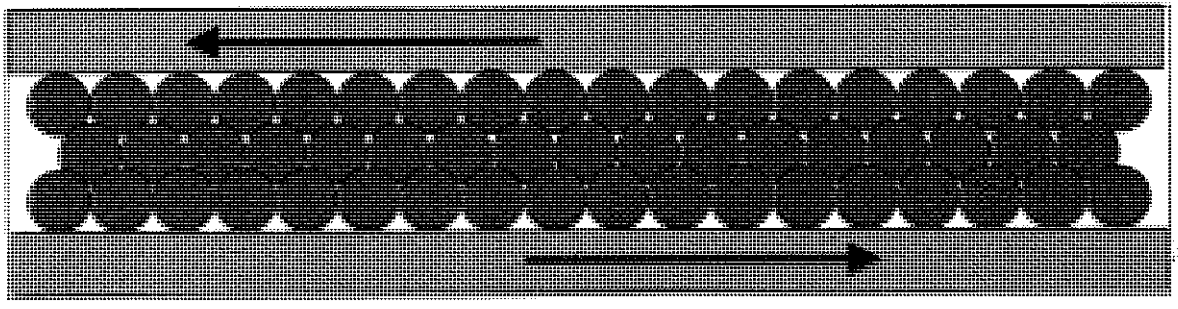

Figure 3.4.2 Simplified composite layer mechanism

An attempt was made to calculate the shear energy dissipation during the shear creep tests. The energy calculations were done as follows:

$$w = \frac{1}{2}(\tau d) \qquad \textbf{[3.2]}$$

where τ is the shear stress and d is the shear displacement in mm. The calculated values are given in Table 3.4.2. Note that the energy is calculated as kJ/m^2.

Table 3.4.2 Energy calculation for three types of infilling

Spec. No 2056-	Thickness (mm)	τ/τ_s (%)	Humidity (%)	Shear Energy Dissipation (kJ/m^2)	Total Shear Energy at τ/τ_s (kJ/m^2)	Percentage Shear Energy Dissipation
Crushed Elsburg Quartzite						
CPS-143	0.5	92	50	0.0036	0.0076	47.4
CPS-144	1	90	50	0.018	0.025	71.7
CPS-145	2	91	50	0.016	0.041	37.7
CPS-146	1	89	100	0.034	0.043	81.1
Crushed Ventersdorp Lava						
CPS-162	0.5	92	50	0.019	0.049	37.9
CPS-148	1	90	50	0.019	0.038	55.2
CPS-149	2	89	50	0.016	0.029	55.2
CPS-150	1	90	100	0.033	0.050	66.6
Natural Gouge						
CPS-239	0.5	94	50	0.0028	0.0056	50.0
CPS-238	1	91	50	0.0086	0.016	54.6
CPS-240	2	89	50	0.014	0.021	67.5
CPS-241	1	89	100	0.014	0.019	72.8

The energy calculations show that for all three types of infilling the percentage energy dissipation is the highest for the tests done under the saturated condition, confirming that the moisture content of the infilling has a significant influence on the shear creep behaviour.

Chapter 4

4 Post Failure Relaxation

4.1 Analysis of existing Data

Some of the earliest work on the behaviour of rock in the post failure state was done by Bieniawski (1970: 126) who investigated the time-dependant behaviour of fractured sandstone under uniaxial compression. The specimens had a height to diameter ratio of 0.5, i.e. the specimens were very squat relative to the ISRM (1979) specifications. The strength of these squat specimens was ±95 MPa. The following scenarios were studied (1) Increasing stress at a constant strain rate, (2) increasing stress at changing strain rates and (3) constant load applied to failed rock. Bieniawski made one important conclusion concerning the behaviour of failed rock: A decrease in strain rate would result in flatter pre- and post failure slopes of the stress-strain curve, i.e. lower peak strength and modulus as well as more stable post-failure behaviour.

Hudson and Brown (1973: 29) investigated the load relaxation of failed rock when the axial deformation was kept constant after the failure of a specimen. Cherokee marble (strength = 55 to 62 MPa) specimens were used and, contrary to Bieniawski's specimens, the height to diameter ratio was 2:1. They regarded the application of constant load to a failed specimen to result in further rapid failures. Uniaxial compressive strength tests at different strain rates were done and they made similar conclusions for marble as Bieniawski did for sandstone, i.e. that increasing strain rates lead to higher strength and steeper pre- and post-failure slopes of the stress-strain curve. Hudson and Brown (1973)

determined load relaxation graphs for failed marble, using a relaxation time period of 600 seconds.

Peng (1973: 237) carried out similar studies on Arkose sandstone (82 MPa), Tennesse marble (40 MPa), Berea sandstone (45 MPa) and Charcoal granite (190 MPa). The numbers in brackets are the strength values calculated from the given load-deformation curves. The strength value of 40 MPa for marble appears to be low. His attempts on the Charcoal granite were unsuccessful, since the fracture process of the granite was so rapid that the testing machine failed to follow it.

All the above mentioned rock types (except the granite) have relatively low strength values when compared to some of the hard rocks (strength between 150 and 400 MPa) found in South African deep level mines. There is no evidence in the literature of attempts to do relaxation tests on South African hard rocks. Apart from Malan and Drescher (2000: 911) it appears as if relaxation measurements during post-failure triaxial compressive strength tests have not been attempted previously.

4.2 Experimental Procedure

4.2.1 Geological description

The quartzite and lave specimens prepared for the post-failure relaxation tests were drilled from the same samples described in section 3.2.1.

4.2.2 Specimen Preparation

Rock cores were drilled out of blocks of the selected rock types, i.e. Ventersdorp Lava and Elsburg Quartzite. Specimens with a diameter of 42mm

and a length of 84mm were prepared, giving a height to diameter ratio of 2:1. The end surfaces were ground to ISRM (1979) specifications.

4.2.3 Testing Equipment

The testing machine used for these tests is a MTS, Model 850 uniaxial and triaxial rock-testing machine. The machine appears in Figure 4.2.1 with the triaxial cell. The open cell with a mounted test specimen is shown in Figure 4.2.2. In the triaxial configuration, an in-vessel load cell measures the true axial load. The machine is fitted with two fast-response servo-valves: one controlling the axial ram, the other controls the intensifier, which provides the confinement. The machine has a digital-closed-loop control system and is controlled from a computer using the MTS Teststar II control system (MTS, 1996). Special Teflon shrink-sleeve jackets (MTS specification) are used during triaxial tests to prevent contact between the confining medium (oil) and the specimen while at the same time allowing axial and circumferential strain measurements.

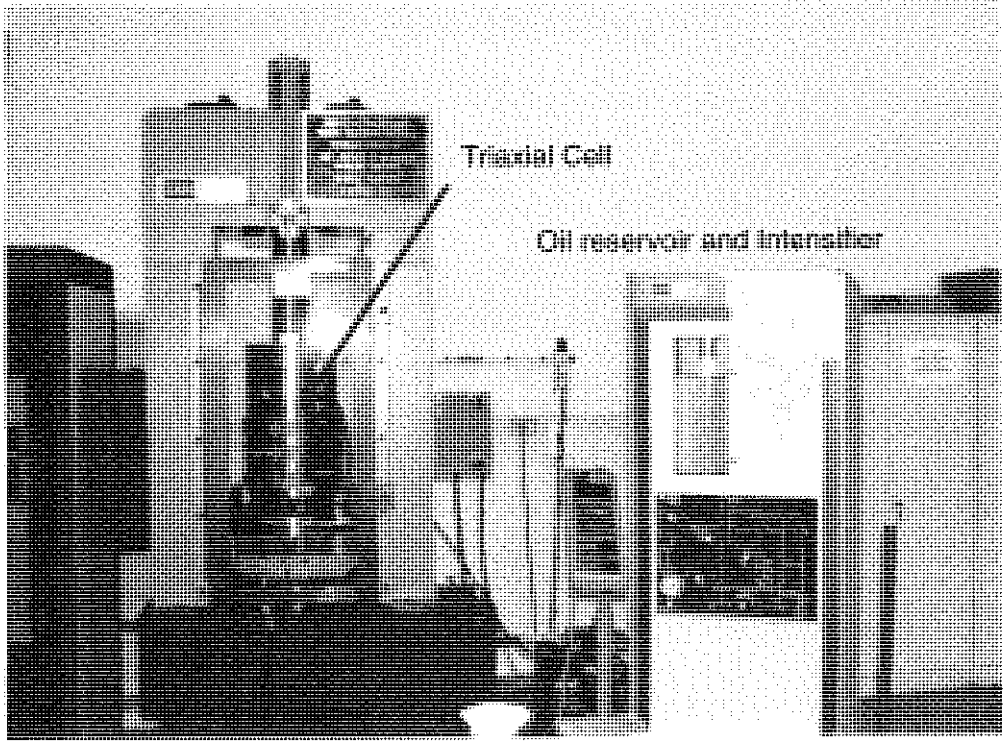

Figure 4.2.1 MTS rock testing machine

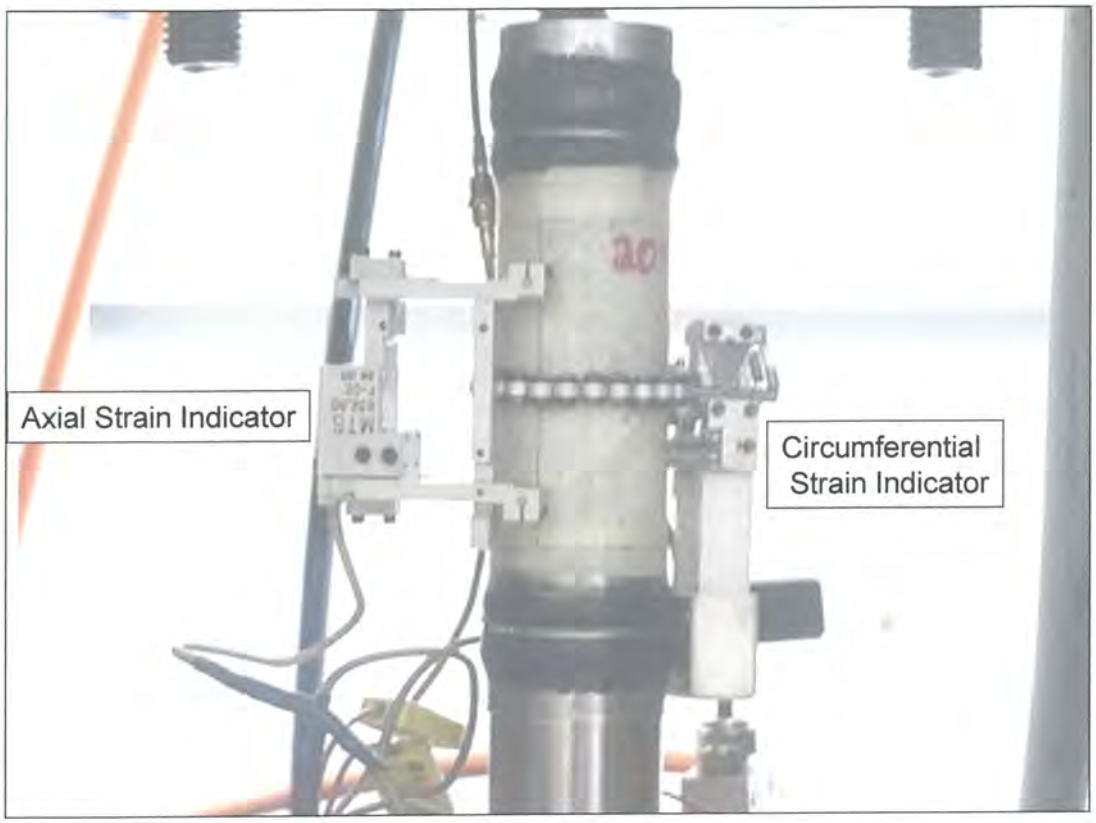

Figure 4.2.2 Mounted specimen with axial and circumferential strain indicators

4.2.4 Testing Method

For this study is was decided to perform the tests at a confining pressure of 40 MPa because this represents the confinement of rock approximately 3200m below surface in deep level mines in South Africa. Special Teststar II procedures for these types of test were compiled and are given in Appendix E.

After fitting the endpieces and jacket to the specimens, the axial and circumferential strain indicators are fixed to the specimen. The triaxial cell is closed, a small axial preload of ± 2 kN is applied, and the cell is pumped full of oil. At the start of the test, the axial and confining stresses are increased simultaneously, in true hydrostatic conditions.

When the confinement level of 40 MPa is reached, the confinement is kept constant. The axial loading switches over to circumferential strain control.

Using the circumferential signal as a feedback signal in the digital closed-loop, the circumferential strain rate is set at 0.01mm/min.

When the pre-determined post-failure load-level is reached, the machine is switched to the "relaxation" control mode, during which the axial ram position as well as the confinement are kept constant (within 0.02%) for a period of 24 hours. The load, time and circumferential strain data is logged during the test.

For some later tests, this testing method was extended to perform multiple relaxation steps in a single test, in which the aim was to obtain up to three post failure relaxation steps. One of these tests would take four days to complete.

4.2.5 Determining the relaxation period

When Hudson and Brown (1973) did their post-failure relaxation tests on Cherokee marble with a uniaxial strength of between 55 MPa and 62 MPa, they used relaxation periods of 600 seconds. The relaxation curves they obtained have an exponential decay shape with the curves flattening within the 600 second time period. It was expected that harder rock confined at 40 MPa would have a longer relaxation time, thus a hold time of 7200 second (2 hours) was applied. The post-failure relaxation test result is shown in Figure 4.2.3, in which it is clear that the hold time was not nearly long enough. The effect of rock strength and confinement is thus even more than expected and the relaxation time period for the tests to follow was increased to 24 hours.

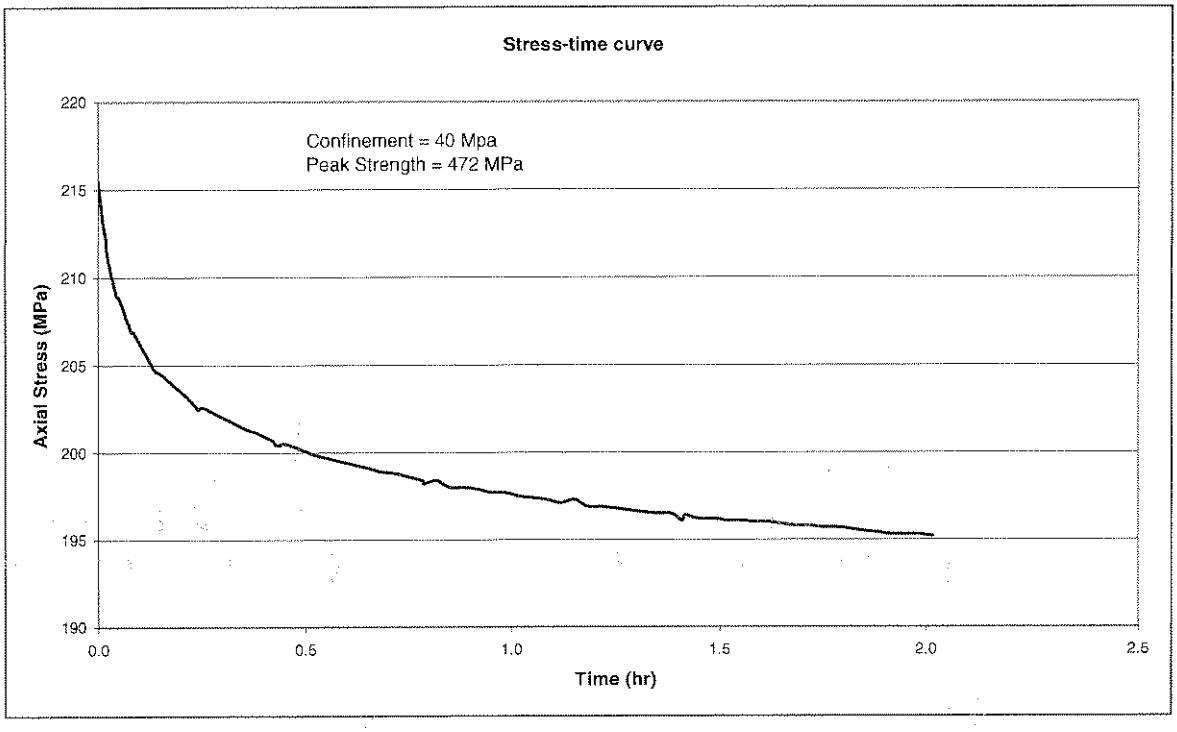

Figure 4.2.3 Post failure relaxation curve for quartzite with a relaxation period of 2 hr.

4.3 Experimental Results

Several attempts were made to obtain post-failure relaxation curves for Ventersdorp Lava with a triaxial strength (at a confinement of 40 MPa) of up to two times as high as that of the Elsburg quartzite. The result of one of the successful attempts is shown In Figure 4.3.2.

A typical stress-strain curve (obtained during triaxial testing) for Ventersdorp Lava is shown in Figures 4.3.1. The modulus and Poisson's ratio values were calculated using the tangent method at 50% of the peak strength. All the test results are given in Appendix D.

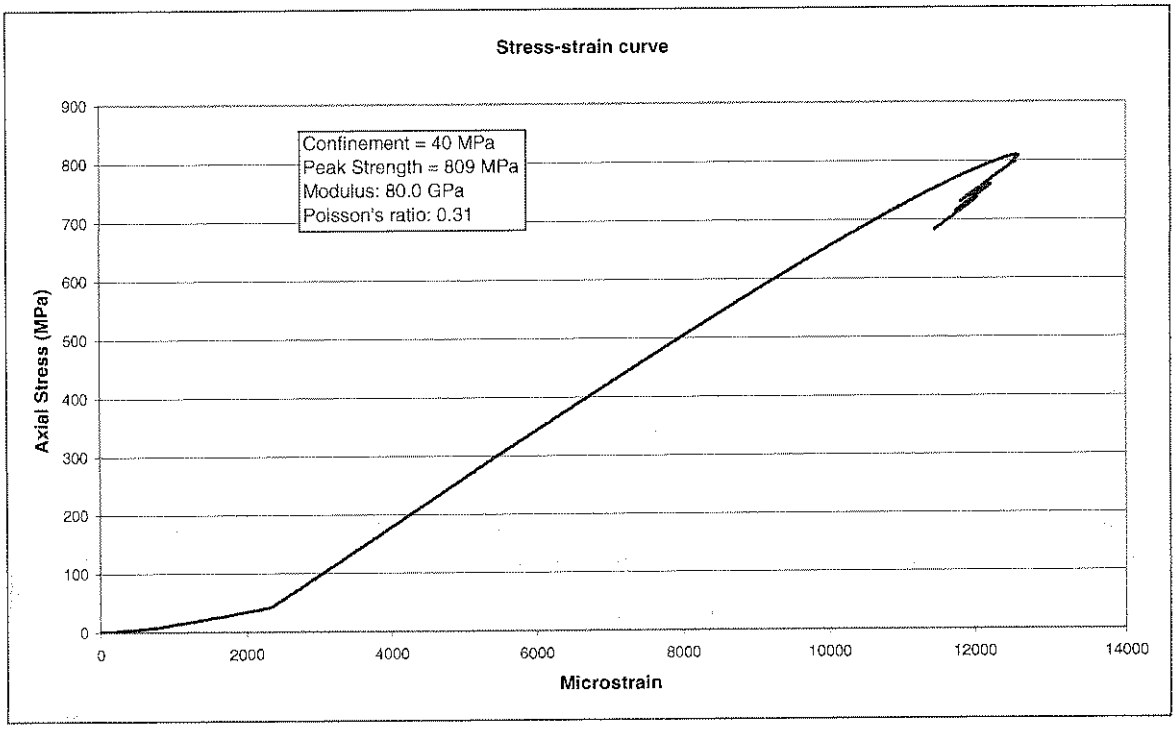

Figure 4.3.1 Axial stress-strain curve for lava

The stress-time curve typical for lava is shown in Figure 4.3.2, which show the post failure stress relaxation. The indicated relaxation rate was determined in the period between 10 and 24 hrs.

During the post-failure relaxation period, the circumferential strain was measured. A typical circumferential strain-time curve for the lava is shown in Figure 4.3.3. The indicated circumferential strain rate was determined in the period between 10 and 24 hrs.

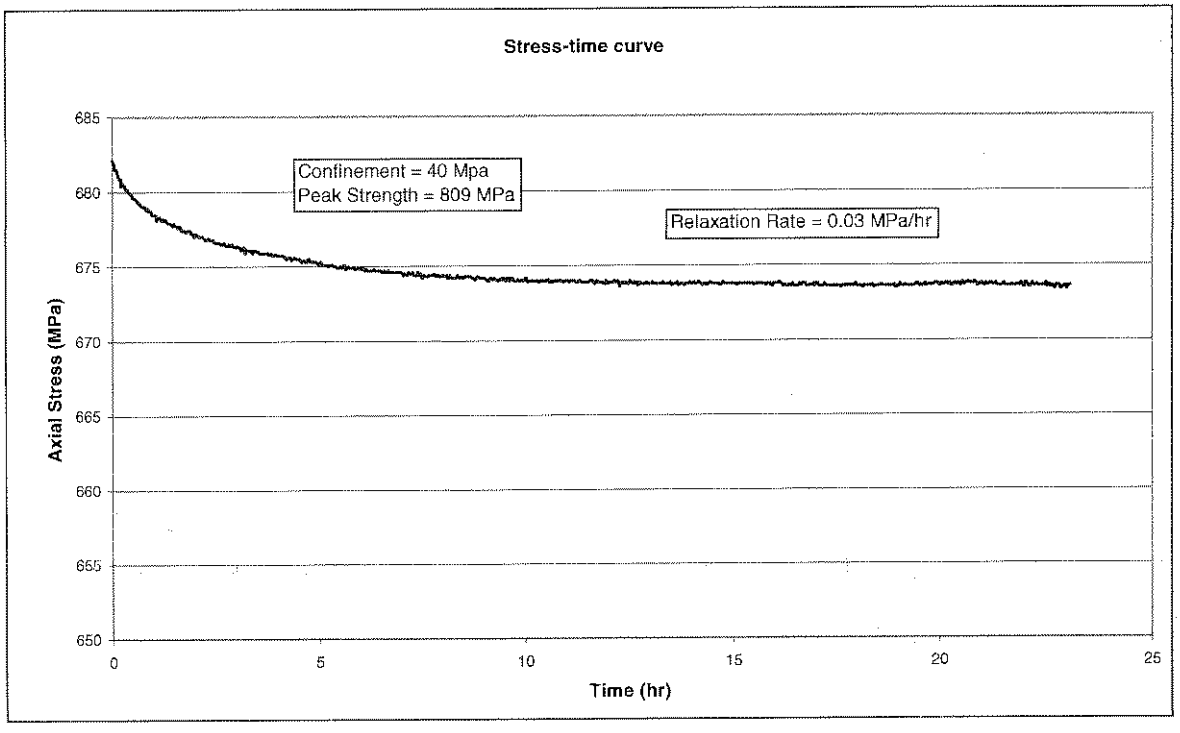

Figure 4.3.2 Stress-time curve for lava

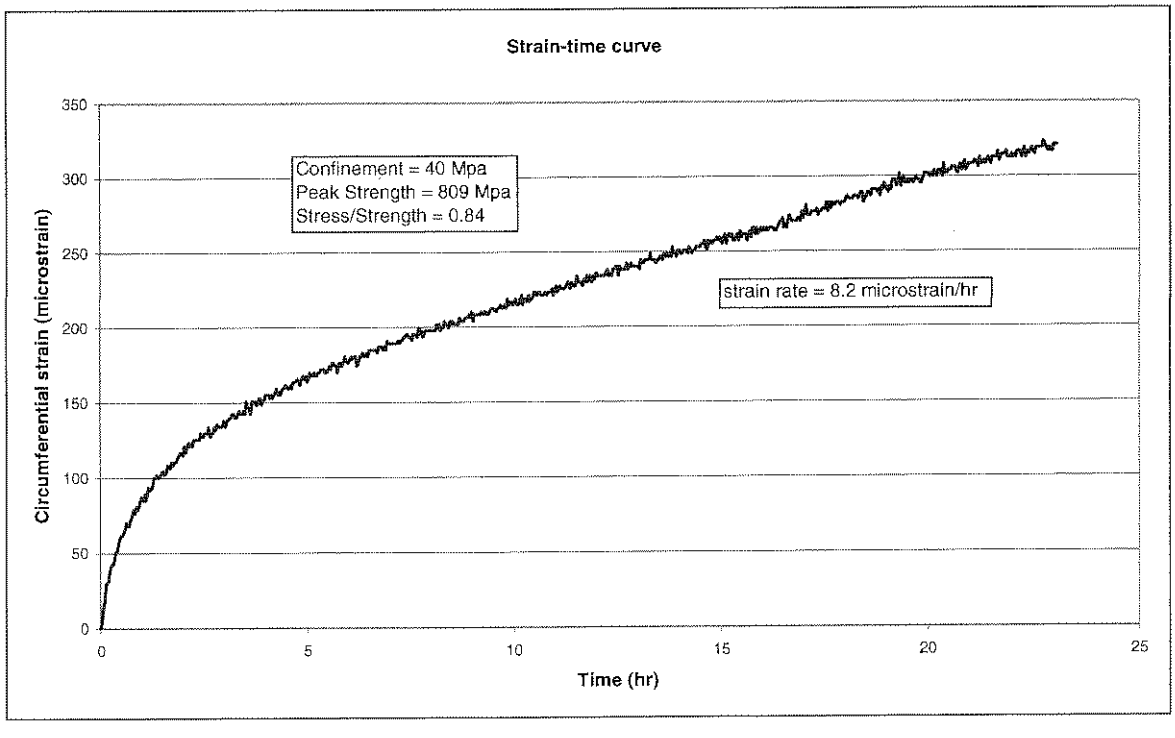

Figure 4.3.3 Circumferential strain-time curve for lava

A typical stress-strain curve for the Elsburg quartzite is shown in Figure 4.3.4.

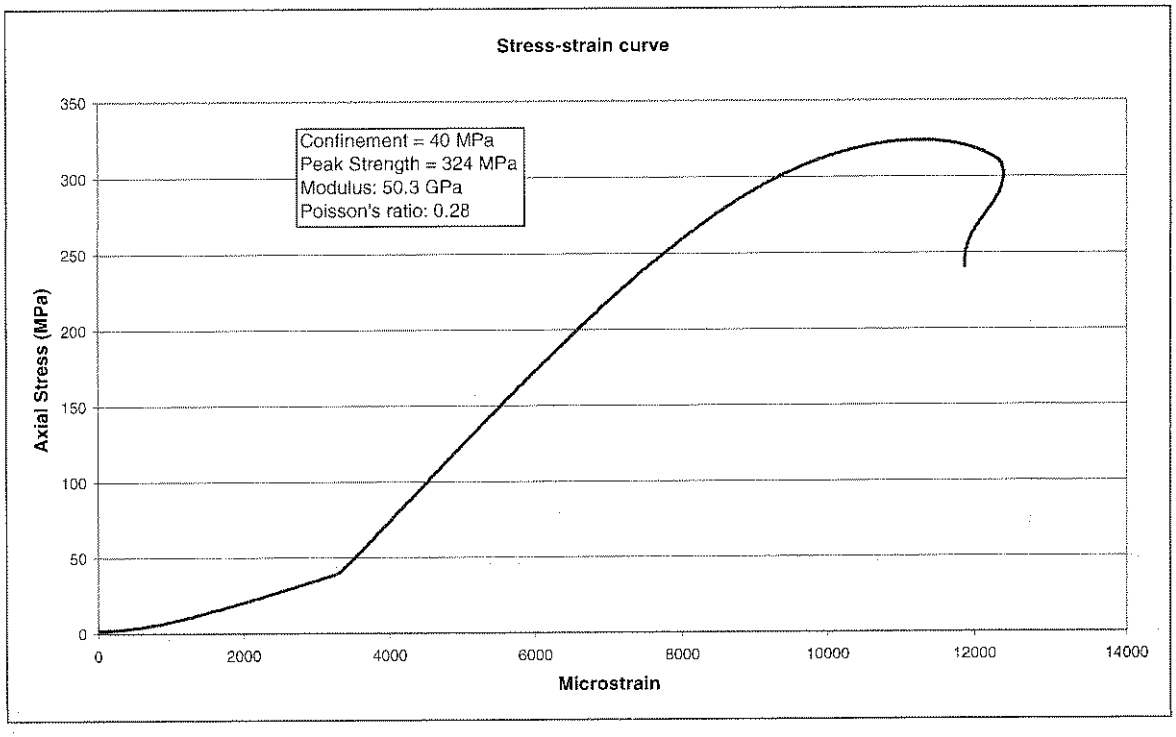

Figure 4.3.4 Axial Stress-strain curve for quartzite

A typical stress-time curve for quartzite is shown in Figure 4.3.5, which show the post failure stress relaxation. The indicated relaxation rate was determined in the period between 10 and 24 hrs.

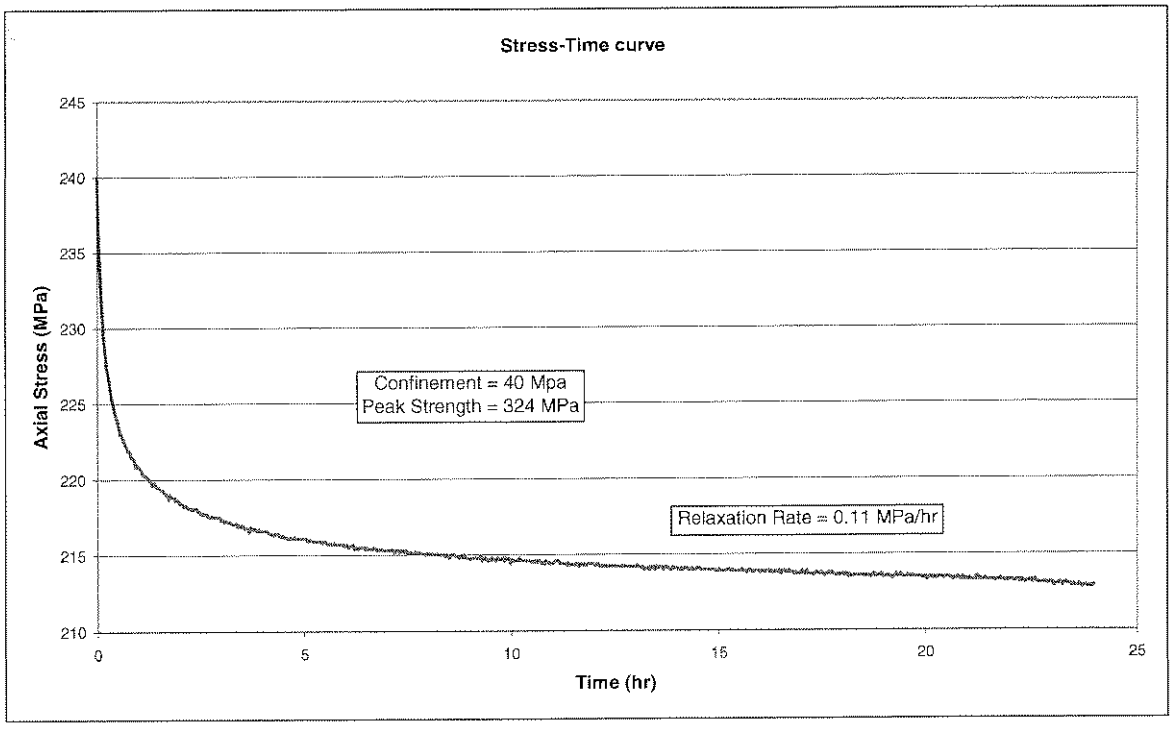

Figure 4.3.5 Stress-time curve for quartzite

During the post-failure relaxation period, the circumferential strain was measured. The circumferential strain-time curve typical for the quartzite is shown in Figure 4.3.6. The indicated circumferential strain rate was determined in the period between 10 and 24 hrs.

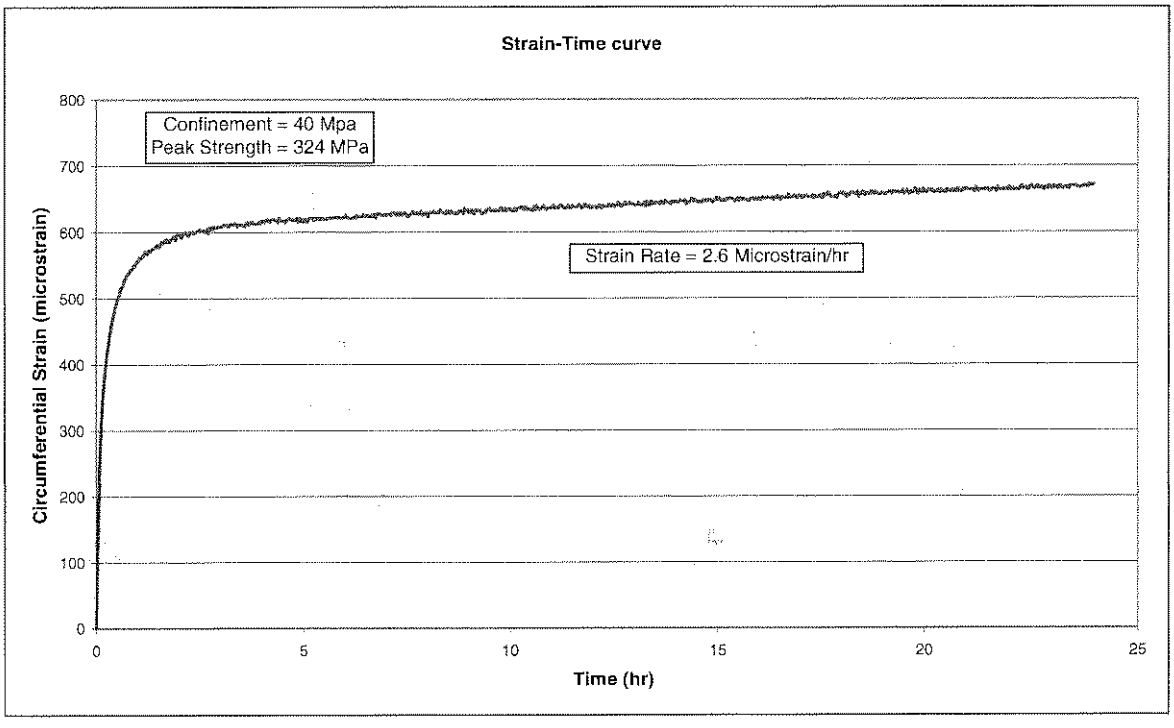

Figure 4.3.6 Circumferential strain-time curve for quartzite

One of the objectives of this study is to investigate the triaxial post-failure relaxation of one material with the post-failure starting point at different σ/σ_C (stress divided by peak strength) values. This proved to be more difficult than anticipated. It was observed that if the post-failure starting point is too close to the peak strength, the specimen would be stable for up to 2 hours after which it would fail violently. If the post-failure point is too close to the residual strength value, the post-failure stress relaxation becomes very small.

The post-failure relaxation results for three different specimens of the same material (quartzite), starting the relaxation at different σ/σ_C post failure points, is shown in Figure 4.3.7. These initial results indicate that there appears to be a relationship between the post failure σ/σ_C ratio and the relaxation rates: The test with the lower post failure σ/σ_C starting point showed a higher relaxation rate. This is contrary to expectations. The difference in the relaxation rates are

however fairly small and it might not be significant and could be due to the variability of the material. Note that the test with the lowest post failure σ/σ_C starting point has the highest strength. The relaxation rates were calculated for the period between 10 and 24 hours, as the relaxation appears to stabilise after 5 to10 hours.

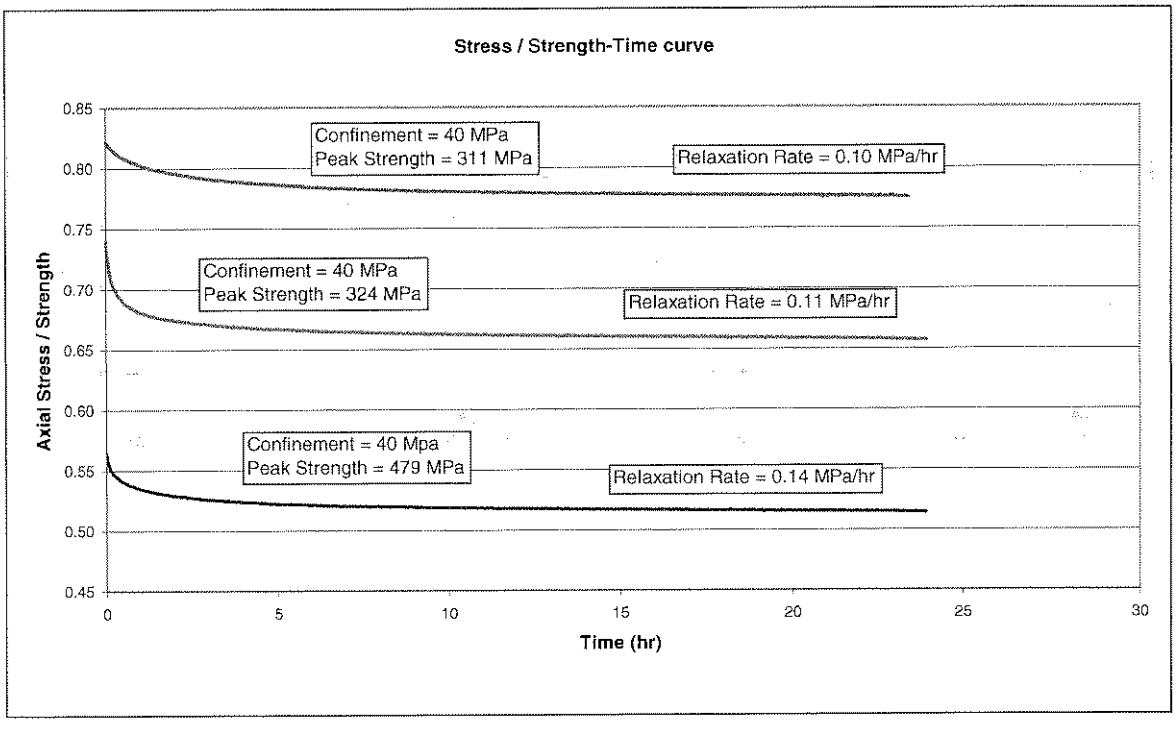

Figure 4.3.7 Post failure relaxation for quartzite at different σ/σ_C post failure starting points

As mentioned above and shown in Figure 4.3.7 tests were done using different specimens of the same rock type and starting the post-failure relaxation at different σ/σ_C ratios. It was decided to take the investigation a step further by aiming to obtain at least three different relaxation curves for a single specimen. This rules out material variability among different specimens. The modified Teststar II procedures are given in Appendix E. The modified procedures for multiple relaxation steps require the testing machine to run for four days continuously.

Various attempts were made using quartzite specimens and the result of a successful attempt is shown in Figure 4.3.8.

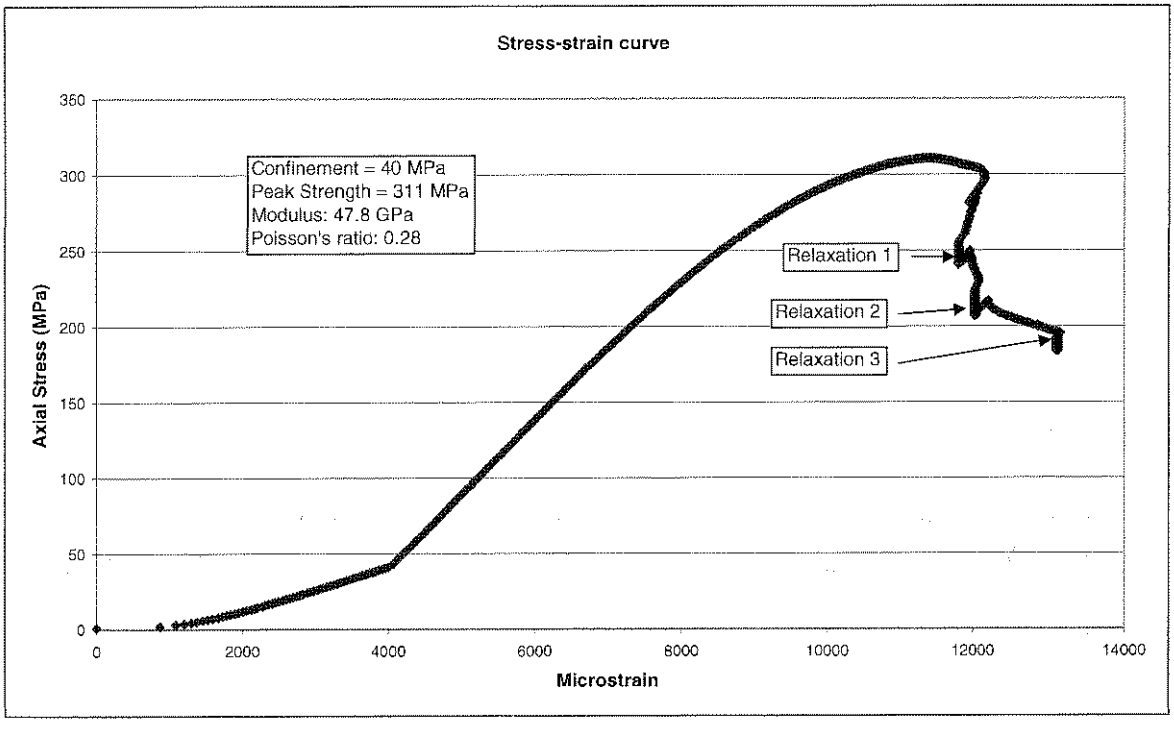

Figure 4.3.8 Stress-strain curve for the multiple step relaxation test for quartzite

The three post failure relaxation curves are shown in Figure 4.3.9. Contrary to the results shown in Figure 4.3.7, the stress relaxation rate is lower at smaller σ/σ_C post failure starting points. The differences are however small.

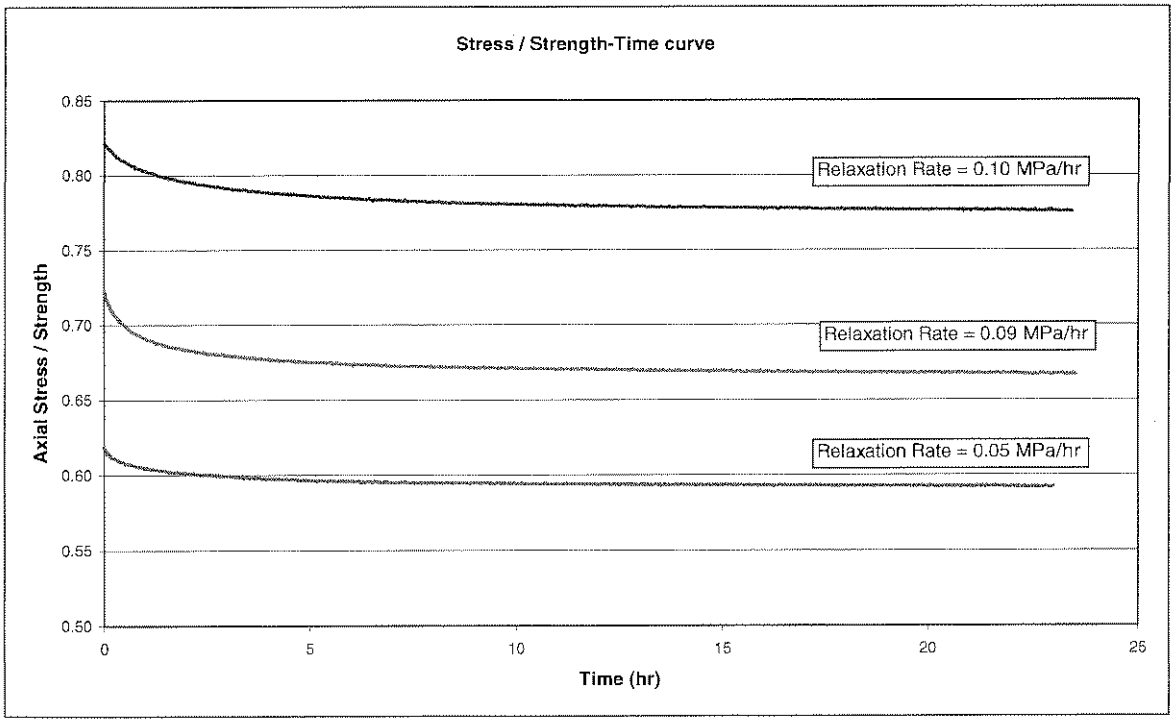

Figure 4.3.9 Axial stress /strength-time curves for multiple post failure relaxation steps of the same quartzite specimen

The circumferential strain-time curves for a post failure test with multiple relaxation steps on quartzite are shown in Figure 4.3.10. The indicated strain rates were determined in the period between 10 and 24 hrs. At a lower σ/σ_C ratio, the amount of circumferential strain during the relaxation period is lower. The strain rate is also lower at a lower σ/σ_C ratio.

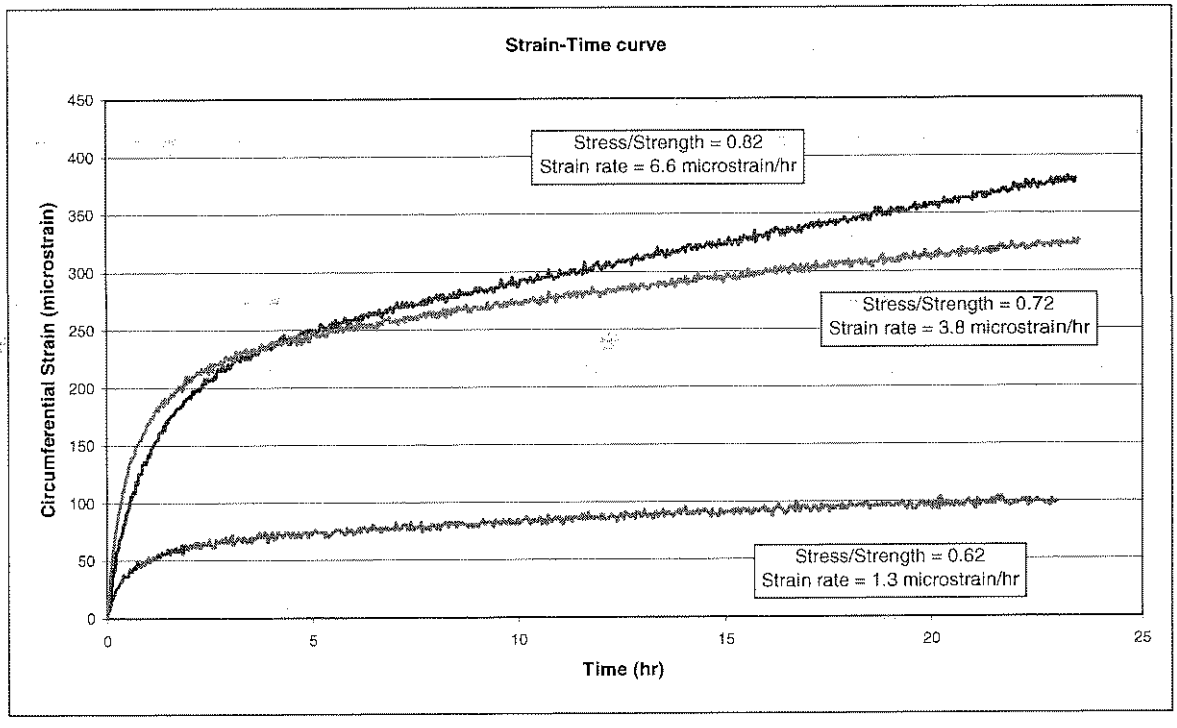

Figure 4.3.10 Circumferential strain-time curves for a multiple relaxation test on quartzite

To compare the relaxation behaviour of Elsburg Quartzite and Ventersdorp Lava, the σ/σ_C ratio (normalised stress) was plotted against time as shown in Figure 4.3.11. The results of a quartzite and lava specimen with similar post failure σ/σ_C starting points were selected. As can be seen in Figure 4.3.6 the stress relaxation for the quartzite is more than three times that for the lava, which is significant.

Calculating the stress drop during the relaxation period as a percentage of the stress at the start of the relaxation period, it was found that quartzite shows a stress relaxation of 5.7% and lava only shows 1.2 %. In terms of absolute

stress the relaxation for the quartzite and lava amounts to 14.5 MPa and 8.5 MPa respectively.

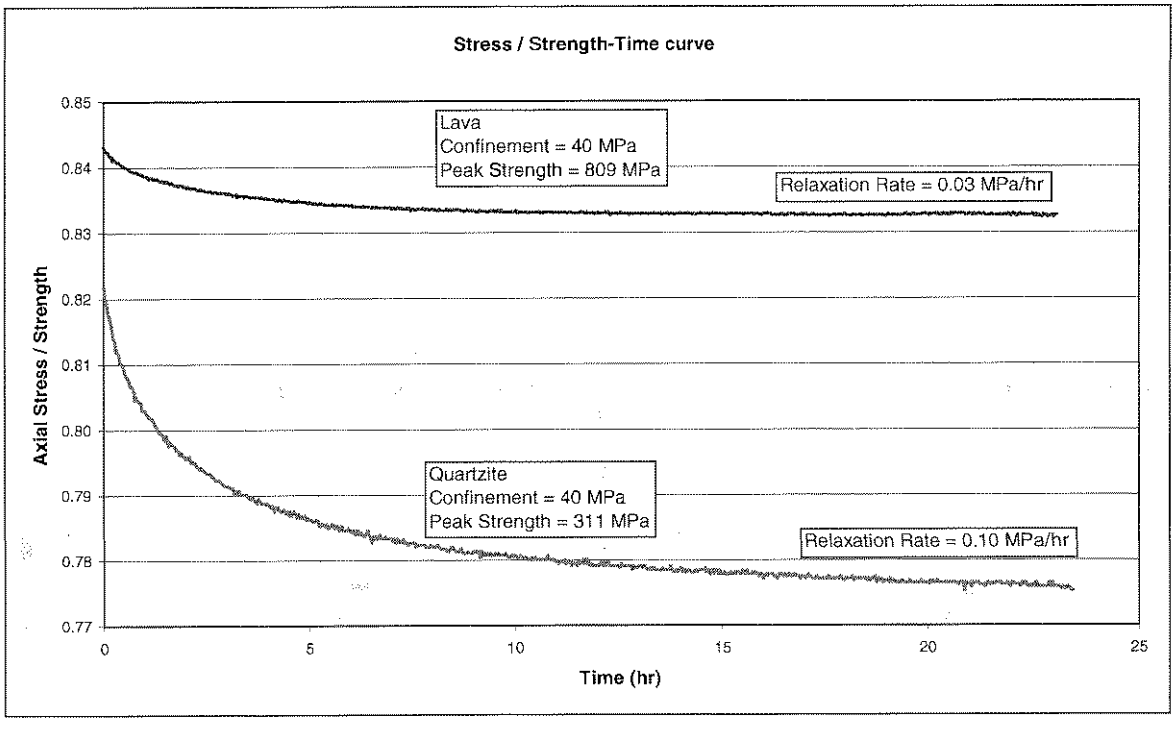

Figure 4.3.11 Stress/Strength-time curves for quartzite and lava

Photographs of a quartzite and a lava specimen are shown in Figures 4.3.7 and 4.3.8 respectively. The quartzite specimen exhibits a much more developed fracture pattern with fractures in two directions, while the lava specimen has only a few cracks.

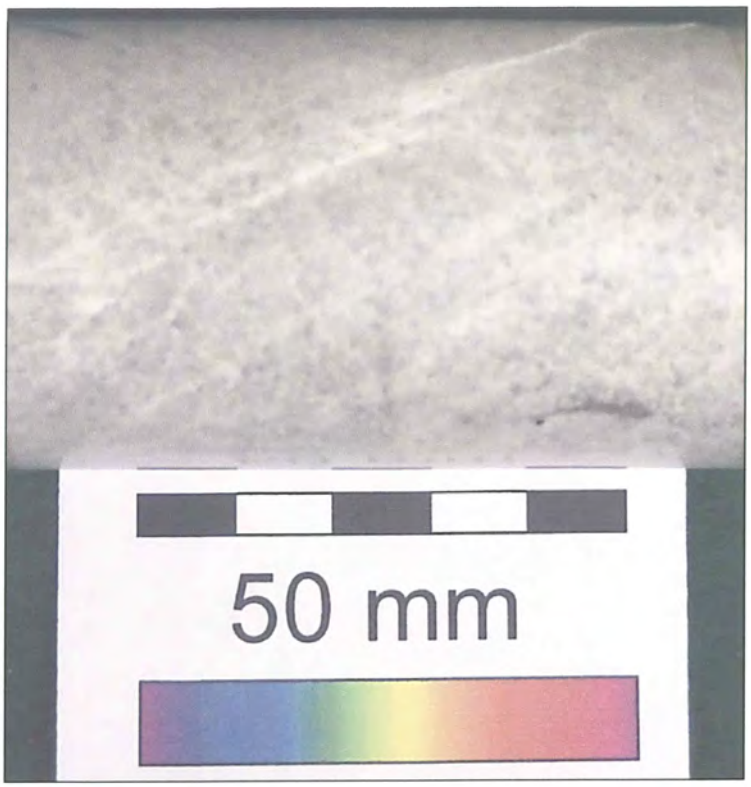

Figure 4.3.12 Tested quartzite specimen, showing fracture damage

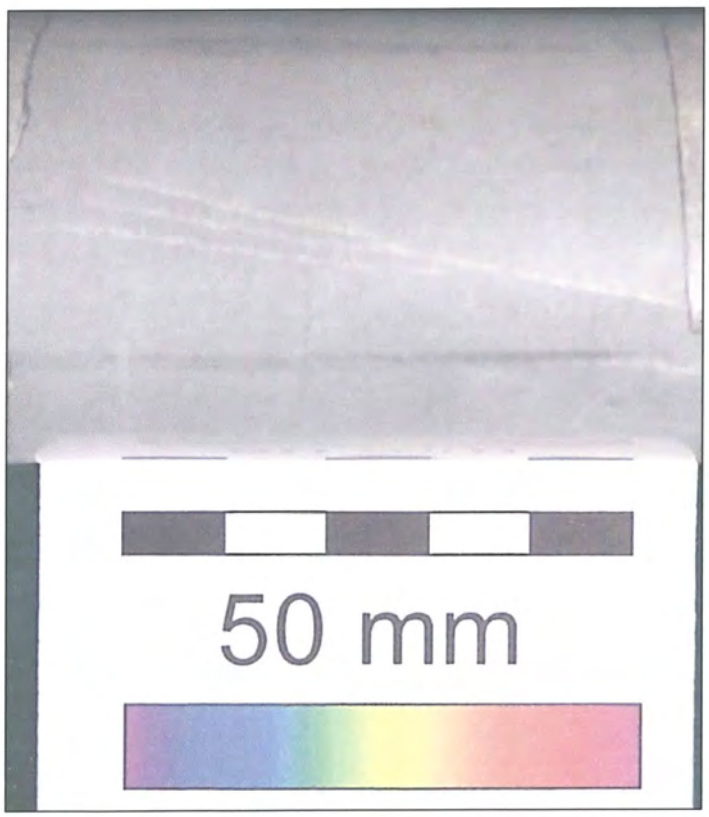

Figure 4.3.13 Tested lava specimen, showing only a few fractures.

The circumferential strain-time curves for lava and quartzite which have similar σ/σ_C post failure starting points are shown in Figure 4.3.14. Although the circumferential strain rate for both the lava and quartzite specimens is very similar, the amount of circumferential strain for the quartzite is significantly larger than for the lava.

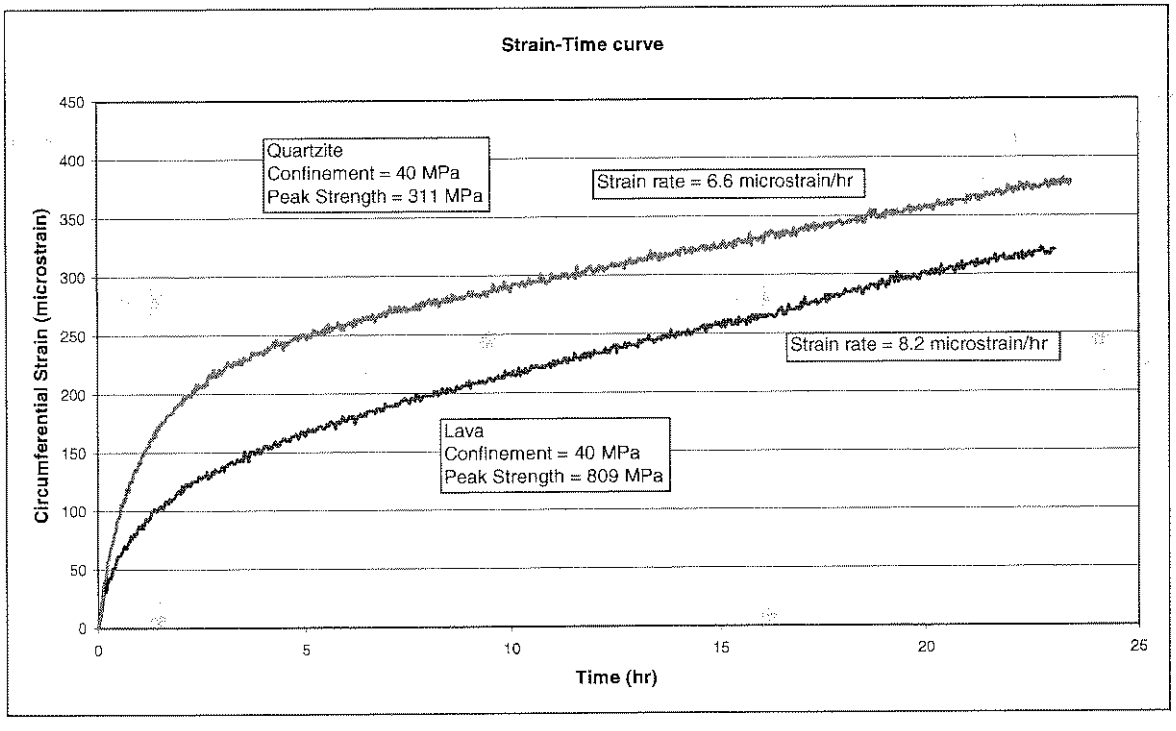

Figure 4.3.14 Comparative circumferential strain-time curves for lava and quartzite

Summaries of the test data of the successful tests appear in Table 4.3.1.

Table 4.3.1 Summary of test results

Specimen No	Peak Strength (MPa)	σ/σ_c starting point	Relaxation rate (MPa/hr)	Circumferential strain rate (microstrain/hr)
Elsburg Quartzite				
2056-105	324	0.56	0.14	6.7
2056-106	479	0.74	0.11	2.6
2056-157-1	311	0.82	0.10	6.6
2056-157-2	311	0.72	0.09	3.8
2056-157-3	311	0.62	0.05	1.3
Ventersdorp Lava				
2056-123	809	0.84	0.03	8.2

4.4 Discussion

Studying the results above, the following observations are made:

- Under a fairly high confinement the post failure relaxation periods for quartzite and lava are orders of magnitude larger than the relaxation periods for marble under uniaxial post-failure conditions.
- The more coarse-grained quartzite specimens show a well-developed fracture pattern after testing, while the extremely fine-grained lava specimens only show a few cracks.
- At a confinement of 40 MPa, the triaxial peak strength of lava is more than twice that of the quartzite
- The stress/strength-time curve appears to have definite primary and secondary relaxation phases as shown in Figure 4.4.1. The non-linear portion of the graph defines the primary phase while the linear portion of the graph defines the secondary phase.
- Similar to the post-failure stress-relaxation curves the circumferential strain-time curves appear to have a primary and secondary phase as shown on Figure 4.4.2.

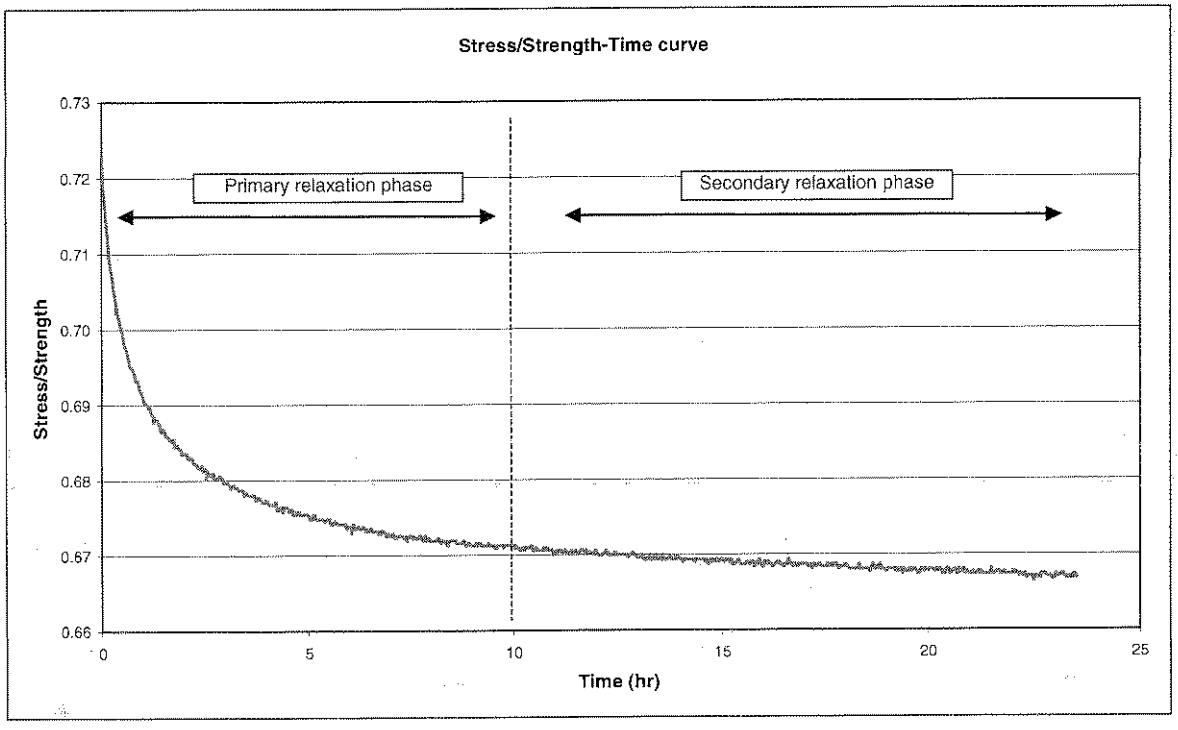

Figure 4.4.1 Stress/strength-time curve

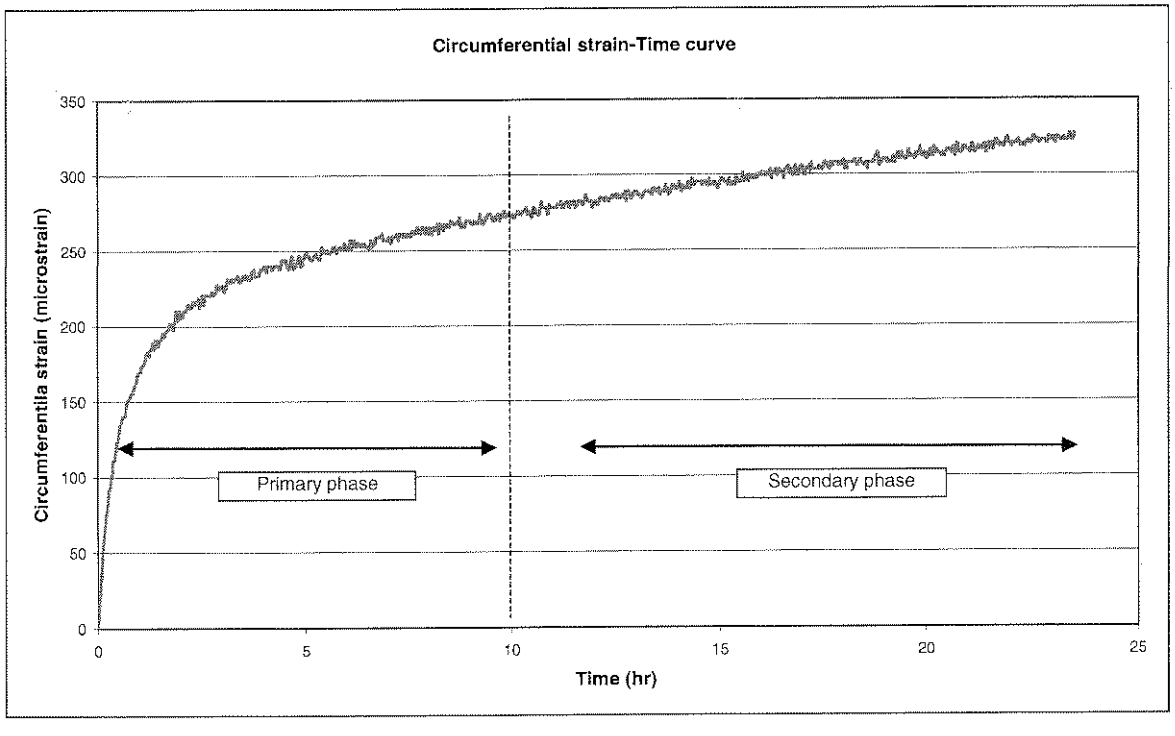

Figure 4.4.2 Circumferential strain-time curve

- Unsuccessful post failure relaxation tests, during which the specimens failed during the relaxation phase, were observed several times at very

high σ/σ_C post failure ratios (0.95) and once at a fairly low ratio (0.53) as shown in Figure 4.4.3.

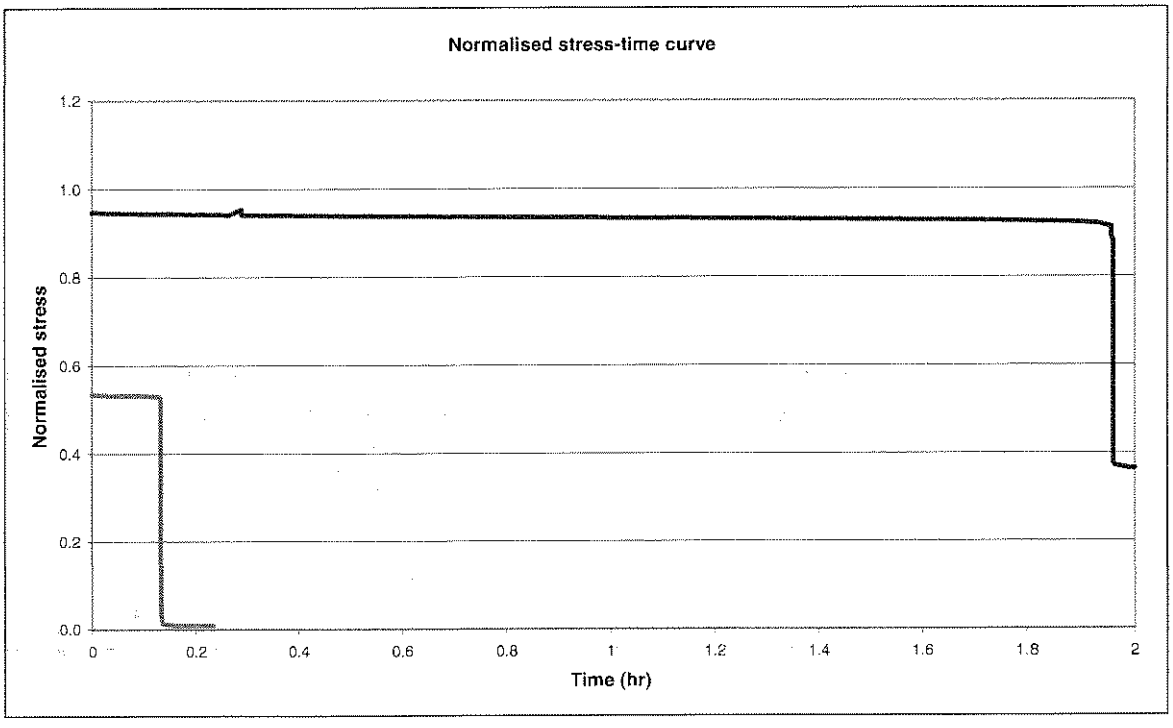

Figure 4.4.3 Stress/Strength-time curve for two unsuccessful tests

- At similar σ/σ_C ratios in the post-failure region, relaxation tests on lava and quartzite show the following with regard to the circumferential strain measured during the relaxation period:
  - The immediate response, i.e. the amount of primary circumferential strain of the quartzite is more than that of the lava (see Figure 4.3.14)
  - The circumferential strain rate of the lava in the secondary relaxation phase is higher than that of the quartzite
- Contrary to individual post failure relaxation tests at different σ/σ_C ratios, the relaxation rate for the post failure test with multiple relaxation steps is smaller at lower σ/σ_C ratios.
- At similar σ/σ_C ratios in the post failure region, quartzite shows significantly more stress relaxation than lava for a given time period.

- The stress relaxation rate is higher for the quartzite than the lava.

Interpreting the tests results further, the question arises on how much energy was dissipated during the relaxation process. The specific energy calculations were made using the following:

$$w = \frac{1}{2}(\sigma_{11}\varepsilon_{11} + \sigma_{22}\varepsilon_{22} + \sigma_{33}\varepsilon_{33}) \quad \textbf{[4.1]}$$

The following observations are made:

- During the relaxation process the axial deformation is kept constant which means that the specific energy dissipation is expressed in the circumferential strain during relaxation.
- The specific energy dissipation for lava and quartzite (the multiple relaxation step) were calculated and are similar as given in Table 4.4.1 and shown in Figure 4.4.4.
- Although the absolute specific energy dissipation values for lava and quartzite are similar, the total energy before relaxation is significantly more in the lava than in the quartzite.
- Hence at similar σ/σ_C post failure ratios, the percentage specific energy dissipation for the lava is much lower than for the quartzite

Table 4.4.1 Specific energy calculation for quartzite and lava

Specimen No	Peak Strength (MPa)	σ/σ_C starting point	Energy dissipation (kJ/m^3)	Energy at start of relaxation (kJ/m^3)	Percentage Energy dissipation
Elsburg Quartzite					
2056-157-1	311	0.82	15.2	1704	0.89
2056-157-2	311	0.72	13.1	1689	0.77
2056-157-3	311	0.62	3.9	1676	0.23
Ventersdorp Lava					
2056-123	809	0.84	12.8	3834	0.33

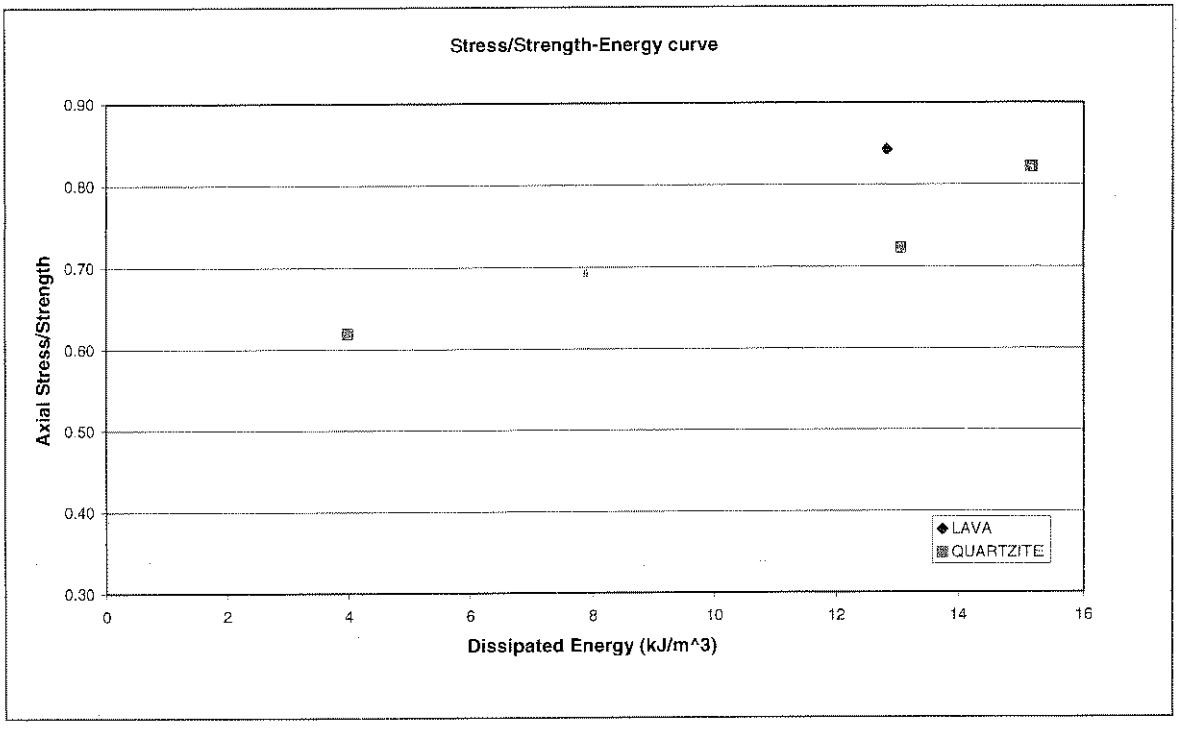

Figure 4.4.4 Stress/Strength-Energy curve for lava and quartzite

Chapter 5

5 Conclusions and Recommendations

5.1 Conclusions

Typical South African hard rocks were subjected to uniaxial and triaxial compression and their time-dependent response was studied. Creep parameters suitable for use in numerical investigations have been determined for hard rocks from the South African gold mines. It has been shown that if hard rocks are subjected to sufficient uniaxial compressive stress they do exhibit well-defined time-dependent behaviour. Significantly, quartzite and lava show similar axial and lateral creep rates at similar σ/σ_C ratios. However, for a given stress level close to the peak stress of quartzite, the axial and lateral creep rates of the quartzite are orders of magnitude greater than the axial and lateral creep rates of the lava at an equivalent stress level.

Energy calculations for the compression creep tests show that for lava ± 10% of the total applied energy is dissipated during the creep cycles while for quartzite ± 18% of the total applied energy is dissipated. During shear creep tests on discontinuities with infilling, the energy dissipation for dry infilling varies between ±40% and ± 70% for the different infilling materials. For saturated infilling the energy dissipation for the different infilling materials varies between ±65% and ±80%. For all three infilling materials the energy dissipation is more when the infilling is saturated. During triaxial post failure relaxation tests, at a σ/σ_C ratio of ±80% the energy dissipation for quartzite is ±0.90% compared to the lava where it is ± 0.3%.

It is furthermore noteworthy that although the strength of lava is more than twice as high as that of the quartzite the strain at failure of the lava is more than that of the quartzite. It is also evident from the results that the onset of unstable fracture propagation for lava occurs at a higher σ/σ_C ratio than for the quartzite.

When studying the deformation modulus during loading and unloading, the indication is that the quartzite shows more material damage then the lava. Energy calculations show that the percentage energy dissipation for the quartzite is significantly more than for the lava and this is a consequence of damage. This also shows that in lava there is more energy available for violent failure than in quartzite. Hence rockbursts in lava are perceived to be more violent than rockbursts in quartzite.

For a discontinuity that contains an infilling and is subjected to a normal stress, the application of a constant shear stress will lead to shear deformations that exhibit primary, secondary and tertiary creep phases. It was also determined that higher τ/τ_s ratios lead to higher shear creep rates. There appears to be a tendency that the thicker infillings lead to higher creep rates. The experimental results show that the peak shear strength of the natural gouge is significantly less than that of the crushed quartzite and crushed lava.

Furthermore, it is evident that for all three joint infill materials, the moisture content has an influence on the amount of time-dependent shear displacement as well as the shear creep rate. More experiments are needed to determine this exactly. The test results show that the shear creep mechanism is governed by the ratio between the thickness of the infilling and the grain size distribution of the infilling.

Triaxial post failure relaxation tests were done using a confinement of 40 MPa. The first conclusion is that the post failure relaxation time periods for hard rocks under a fairly high confinement are orders of magnitude greater than the relaxation periods for softer rocks under uniaxial compression conditions. For

mines, operating at great depth (more than 2000m) the implication is that the rock material might relax much more slowly than might have been assumed and this means that after failure the rock mass continues to store large amounts of strain energy.

Comparing the behaviour of quartzite and lava, the test results show that during a relaxation period of 24 hours the total stress relaxation for the failed quartzite is approximately twice that of the failed lava. The relaxation rate in the secondary relaxation phase for the quartzite is more than three times higher than for the lava.

The relationship, between the relaxation rates and the σ/σ_C ratios for individual tests, is different to the relationship between relaxation rates of the relaxation test with multiple steps and the σ/σ_C ratios: the results are not conclusive. The quartzite shows a well-developed fracture pattern while the lava shows only a couple of cracks, i.e. the damage to the lava is significantly less than the damage to the quartzite. The photographs of the tested specimens show clearly more damage in the quartzite than in the lava.

The circumferential strain measurements associated with the post-failure relaxation show that the amount of circumferential strain for quartzite is more than for the lava (larger immediate response) while the strain rate during the 10 to 24 hr period is higher for lava than for quartzite.

Energy calculations show that for similar σ/σ_C ratios (post-failure) the percentage energy dissipation is significantly more for the quartzite than for the lava.

5.2 Application of the test results to the stope fracture model

A stope fracture model, after Gay and Jager (1986: 759) is given in Figure 5.21.

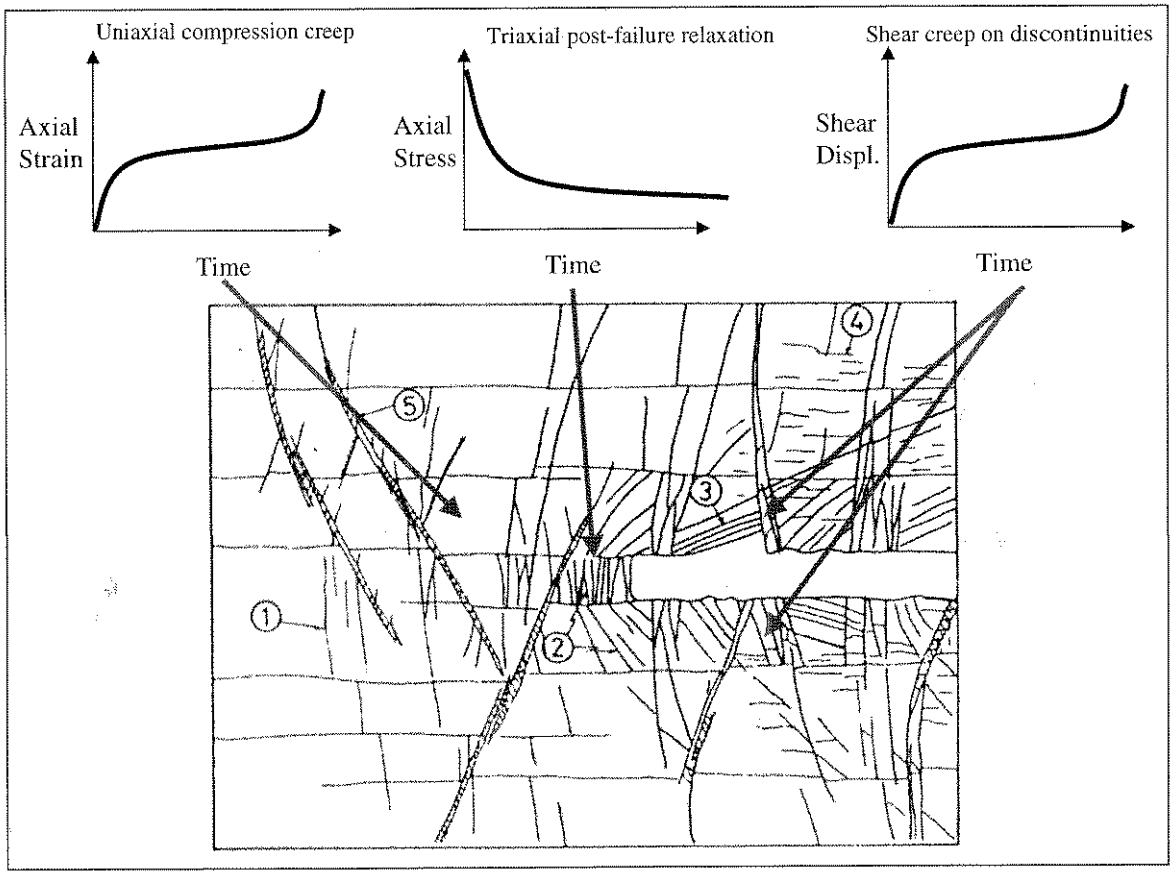

Figure 5.2.1 Application of the tests results to the stope fracture model

Gay and Jager (1986: 759) identified five types of fractures and described them in detail. The descriptions are summarised as follows:

Types ① to ④ are extensions fractures:

Type ①: This first set of fractures form some meters ahead of the stope face and are chronologically the first extension fractures that form.

Type ②: These fractures are the most common and form later in solid blocks left unfractured by type ①. They occur mostly within 1m of the stope face.

Type ③: These fractures form almost at the same time as type ② and occur in the strata immediately above and below the stope.

Type ④: These fractures form approximately in the plane of bedding, are irregular in outline and cut across short distances between bedding horizons.

Type ⑤: These are shear fractures and often occur in a spacing of between 1m and 3m. They are mining induced normal faults on which displacements of up to 200mm occur.

The time-dependant response of a stope at great depth is represented by the following tests:

- The time-dependent deformation of the intact rock ahead of the face can be approximated by the results of the uniaxial compression creep tests.
- The stress-relaxation of the failed rock just ahead of the face. The mining rate can play an important role here: If the mining rate is faster than the relaxation of the failed rock the stress just ahead of the face increases. During the triaxial post-failure relaxation tests, it was noted that the specimens appear to be very unstable in the post-failure region if the post-failure stress level is close to the failure strength. If the mining rate is such that the stress ahead of the face moves into the unstable post-failure stress region, there is a good possibility that a rock burst can occur.
- The time dependent shear displacement on discontinuities surrounding the stope. Input data for these is obtained from shear creep tests on discontinuities. Other important factors are the frequency of the discontinuities, their orientation, presence and type of infilling as well as the moisture content of these.

All these processes have now been quantified by the tests described and provide the first data available for energy change calculations in fractured rock masses.

5.3 Recommendations

It is recommended to develop numerical models for the conceptual model mentioned above. The numerical models would be of significant assistance in understanding the time-dependant behaviour of hard rocks and could possibly be used to estimate or predict the underground time-dependant deformation

(e.g. closure of stopes). There are currently no models available that are able to simulate all three mechanisms simultaneously.

Although this study increased the knowledge of the time-dependent behaviour of discontinuities, it is recommended to do some further tests on more different natural infillings. The natural infilling material is however quite difficult to obtain. A limiting factor during this study was the normal loading capacity of the shear creep apparatus. It is recommended to investigate shear creep behaviour of discontinuities at much higher normal stresses.

As far as triaxial post-failure testing is concerned, some more multiple post-failure relaxation tests on different materials would broaden the knowledge. Performing tests at different confinements would also lead to a better understanding of the triaxial post-failure relaxation behaviour.

During this study an attempt was made to look at the amount of energy dissipated during three different mechanisms of time dependant behaviour of hard rock.

A better understanding of the time-dependent behaviour of the hard rocks could have a major influence on the safety of the deep mines in South Africa.

6 References

BIENIAWSKI, Z.T. 1970. Time-dependant behaviour of fractured rock. CSIR internal report, report no MEG 869.

BIENIWASKI, Z. T. 1970. Time-dependant behaviour of fractured rock. Rock Mechanics, Springer-Verlag, 2:123-137.

BOSMAN J.D., MALAN, D.F., DRESCHER K. 2000. Time-dependant tunnel deformation at Hartebeestfontein Mine. Proceedings of the AITES-ITA 2000 World Tunnel Congress, SAIMM, Durban: 55-62.

BOWDEN R.K , CURRAN, J.H. 1984. Time-dependant behaviour of joints in shale. In: Proc. 25th Symp. Rock Mech. edited by C. H. Dowding & M. M. Singh: 320-327.

CHONG, K.P., SMITH, J.W., KHALIKI, B.A. 1978. Creep and relaxation of oil shale. In: Proceedings of the 19th U.S. Rock Mechanics Symposium: 414-418.

CRAWFORD, A.M., CURRAN, J.H. 1981. Rate-dependant behaviour of rock joints. Black quartz syenite. In: Proceedings of the International Symposium on Weak Rock, Tokyo: 291-296.

CRUDEN D.M. 1971. Single-increment creep experiments on rock under uniaxial compression. Int. J. Rock Mech. Mining Sci., Pergamon Press, 8:127-142.

CSIR, NATIONAL MECHANICAL RESEARCH INSTITUTE 1963. Report on the non-elastic properties of rock from borehole number 3034 from Hartebeestfontein Goldmine. CSIR Contract Report, C MEG/563.

DEERE, D.U., MILLER, R.P. . Engineering Classification and index properties for intact rock: US Air Force System Command, Air Force Weapons Lab.. Tech Rep. AEWL-TR-65-116, Kirtland Air Force Base, New Mexico.

DUSSEAULT, M.B., FORDHAM, C.J. 1993. Time-dependant behaviour of rocks.. In: Comprehensive Rock Engineering, edited by J. A. HUDSON, Pergamon Press, 3: 119-149.

GAY, N.C. & JAGER, A.J. 1986. The influence of geological features on problems of rock mechanics in Witwatersrand mines. In: Mineral Deposits of Southern Africa Vol I&II edited by C.R. ANHAEUSSER & S. MASKE, Geological Society of South Africa, Johannesburg, 753-772.

HUDSON, J.A. & BROWN, E.T. 1973. Studying the time-dependant effects in failed rock. In: Proc. Fourteenth Symposium on Rock Mechanics edited by H.R. HARDY & R. STEFANKO, American Society of Civil Engineers, New York: 25-34.

ISRM, COMMISSION ON STANDARDISATION OF LABORATORY AND FIELD TESTS. 1979. Suggested methods for determining the uniaxial compressive strength and deformability of rock materials. Int. J. Rock Mech. Min. Sci. & Geomech. Abstr. 16: 135-140.

LAMA, R.D. & VUTUKURI, V.S. 1978. Handbook on Mechanical properties of rocks. Trans Tech Publications, Clausthal, Germany, III: 209-323.

LATJAI, E.Z., DUNCAN, E. J. S. 1988. The mechanism of deformation and fracture in potash rock. Can. Geotech. J., 25: 262-278.

MALAN D.F. 1998. An investigation into the identification and modelling of time-dependant behaviour of deep level excavations in hard rock. PhD thesis, University of the Witwatersrand, Johannesburg.

MALAN D.F. 2000. Personal communication.

MALAN, D.F. & DRESCHER K 2000. Modelling the post-failure relaxation behaviour of hard rock. In: Proc. of the fourth North American Rock Mechanics Symposium, edited by J. GIRARD, M. LIEBMAN, C. BREEDS & T. DOE, Balkema, Rotterdam: 909-917.

MALAN, D.F., DRESCHER, K. & VOGLER, U.W. 1998. Shear creep of discontinuities in hard rock surrounding deep excavations. In: Proc. Mechanics of faulted and jointed rock, MJFR-3, edited by H.P. ROSSMANITH, Balkema, Rotterdam: 473-478.

MARANINI, E. & BRIGNOLI, M. 1999. Creep behaviour of a weak rock: experimental characterization. Int. J. Rock Mech. & Min. Sci., 36, :127-138.
MTS, 1996. Teststar II Control System, 790.10 Testware-Sx, Release 4.0A

OHTSUKI, H., NISHI, K., OKAMOTO, T., TANAKA, S. 1981. Time-dependent characteristics of strength and deformation of a mudstone. In: Proceedings of the International Symposium on Weak Rock, Tokyo, :119-124.

PENG S.S 1973. Time-dependent aspects of rock behaviour as measured by a servo controlled hydraulic testing machine. International Journal of Rock Mechanics and Mining Sciences, Pergamon Press, 10: 235-246.

PRICE N.J. 1964. A Study of the time-strain behaviour of coal-measure rocks. Int. J. Rock Mech. Mining Sci., Pergamon Press, 1: 277-303.

SCHWARTZ, C.W. & KOLLURU, S. 1984. The influence of stress level on the creep of unfilled rock joints. In: Proc. 25th Symp. Rock Mech. edited by C. H. DOWDING & M. M. SINGH: 333-340.

SELLERS, E.J. 2001. Personal communication.

SINGH, D.P. 1975. A study of creep of rocks. Int. J. Rock Mech. Min. Sci. & Geomech. Abstr., 12: 271-276.

VOGLER U.W. 2000. Personal communications.

VOGLER, U.W. 1990. Creep tests on argillaceous footwall quartzite. CSIR Report, EMA-C 9052.

VOGLER, U.W. & DRESCHER, K. (1997). Determination of creep properties of lava rock from Western Deep Levels. CSIR Internal Report RE 1/97.

VOGLER, U.W., MALAN, D.F., DRESCHER, K. 1998. Development of shear testing equipment to investigate the creep of discontinuities in hard rock. In: Proc. Mechanics of faulted and jointed rock, MJFR-3 edited by H.P. ROSSMANITH, Balkema, Rotterdam: 229-234.

WAWERSIK W.R. 1974. Time--dependant behaviour of rock in compression. In: Proceedings of the third Int. Soc. Rock Mech. Congress, Denver: 357-363.

WAWERSIK, W. R. 1973. Time Dependant rock behavior in uniaxial compression. In: Proc. Fourteenth Symposium on Rock Mechanics, edited by H.R. HARDY & R. STEFANKO, American Society of Civil Engineers, New York: 85-106.

WIID, B.L. 1966. The time-dependent behaviour of rock: considerations with regard to a research programme. CSIR Report, Pretoria, MEG 514.

YONGSHENG L. & CAICHU X. 2000. Time-dependant tests on intact rocks in uniaxial compression. International Journal of Rock Mechanics and Mining Sciences, Pergamon, 37: 467-475.

Appendix A

Petrographic descriptions of samples

UNIVERSITEIT VAN PRETORIA
UNIVERSITY OF PRETORIA
YUNIBESITHI YA PRETORIA

PETROGRAPHIC LABORATORY REPORT

COUNCIL FOR GEOSCIENCE

1. Introduction

Three borehole core samples and one hand specimen were submitted for petrographic evaluation on 11 May 2001.

2. Description

Sample no.: 2056-158

Rock type: Medium-grained meta-tholeiite (metamrphosed andesite/ basalt)

Macroscopic description: The sample consists of 3cm diameter drill core of fine to medium-grained, greenish-grey rock with dark spots. The rock is unfractured, solid-looking and has moderate absorbency.

Mineral assemblage: Plagioclase (40%), Chlorite (28%), Actinolite (16%), Quartz (8%), Epidote (3%), Sphene (2%), Calcite (1%), Zeolite (1%)

Texture: Intergranular and intersertal

Grain size: Fine to medium-grained
Plagioclase (0.22-0.0.30mm), micro-porphyres (1,25mm)
Amphibole (0.16- 0.26mm)
Epidote (0.14mm)

Observations: A phantom intergranular texture typical of andesitic/ basaltic rock is still visible in the manner plagioclase and mafic minerals are arranged. Plagioclase is still mostly lath-shaped and locally micro-phenocrysts occur, but is also moderately altered to sericite, epidote, calcite and chlorite. Actinolite is xenoblastic and fibrous and crosscuts original mineral boundaries. Chlorite is largely pseudomorphous after interstitial glass and often infills former amygdales (Figure 1) along with epidote. It also seems to partially occupy intergranular sites after pyroxene together with fibrous actinolite. Quartz is xenoblastic and fine-grained. Opaque minerals are xenoblastic to needle-like and moderately altered to sphene.

Comments: The rock has no deleterious minerals. The texture of the rock is felted (random). The interlocking grains will impart a high mechanical durability (toughness) despite minerals not being excessively hard. Good durability to be expected.

Figure 1: Photomicrograph of a medium-grained meta-tholeiite with phantom intergranular texture and relict amygdales containing chlorite (black) and epidote.

Sample no.: 2056-159

Rock type: Meta-quartzite (metamorphosed quartz-wacke)

Macroscopic description: The sample, in the form of a 5cm diameter drill core, consists of a light green rock containing medium-sized grains set in a light beige matrix. The rock is unfractured, solid-looking and has moderate absorbency.

Mineral assemblage: Quartz (84%), Mica (15%), Chert (1%), Opaque minerals (<1%)

Texture: Weakly schistose and stylolitic

Grain size: Fine to medium-grained (0.24- 1.52 mm)

Observations: The rock appears to have been a fine-grained, poorly sorted quartz-wacke with subangular quartz and chert grains set in an argillaceous matrix (15%) which has since been altered to mica (sericite) through low grade greenschist metamorphism. Quartz grains are corroded, slightly strained and locally form stylolites (pressure solution indentations). The grains also appear slightly recrystalised in places probably due to strain. Mica is xenomorphic and shows a weak schistosity, especially in the pressure shadows of larger quartz grains where it is co-precipitated with very fine-grained quartz (Figure 2). Opaque minerals are xenomorphic and occur in the matrix.

Comments: Depending on the application the high (15%) mica content may be considered deleterious to the mechanical durability of the rock. Quartz is noticeably strained and may thus produce soluble silica for reaction with cement. If these factors are not applicable to the intended application, good durability can be expected.

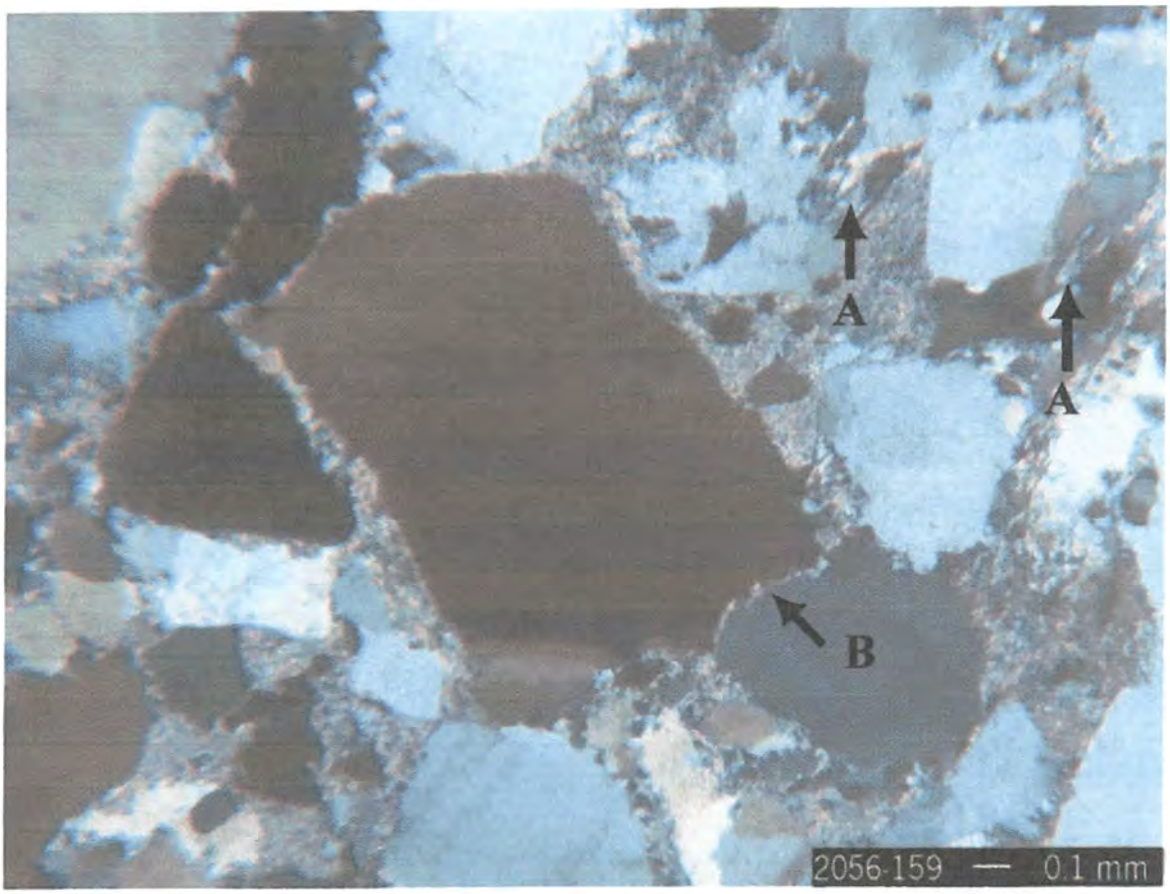

Figure 2: Photomicrograph of quartz grains set in a micaceous matrix. Note new schistose quartz-mica intergrowths (A) and stylolitic indentations of the larger grain along its lower edge (B). Lower left corner of large quartz grain also shows extreme undulose extinction.

Sample no.: 2056-160

Rock type: Fine-grained meta-tholeiite

Macroscopic description: Fine-grained, dark green-grey rock with white flecks and rounded (0.5 cm sized) amygdales filled with white and translucent minerals. Joints occur locally with a spacing of 1cm and are infilled with a white mineral.

Mineral assemblage: Plagioclase (57%), Epidote (15%), Amphibole (15%), Chlorite (7%), Sphene (4%), Quartz (2%), Opaque minerals (<1%), Calcite (<1%)

Texture: Felted (interlocking mineral grains)

Grain size: Fine-grained
Plagioclase (0.08-0.16mm)
Amphibole (0.08mm)

Observations: The original intergranular texture of a fine-grained basalt is preserved despite the greenschist metamorphic overprinting. Plagioclase is still lath-shaped but moderately altered to chlorite, epidote and calcite. Amphibole is acicular and crosscuts most minerals. Quartz is anhedral and occurs as recrystallised subgrains. Chlorite occurs mostly in intersertal areas. Opaque minerals are xenomorphic to needle-like and altered to sphene. Hairline fractures crosscut the sample and have been annealed by sphene.

Comments: The sample has no deleterious mineral content. Hairline fractures are annealed. The low deleterious mineral content and the felted texture of the rock should yield good durability.

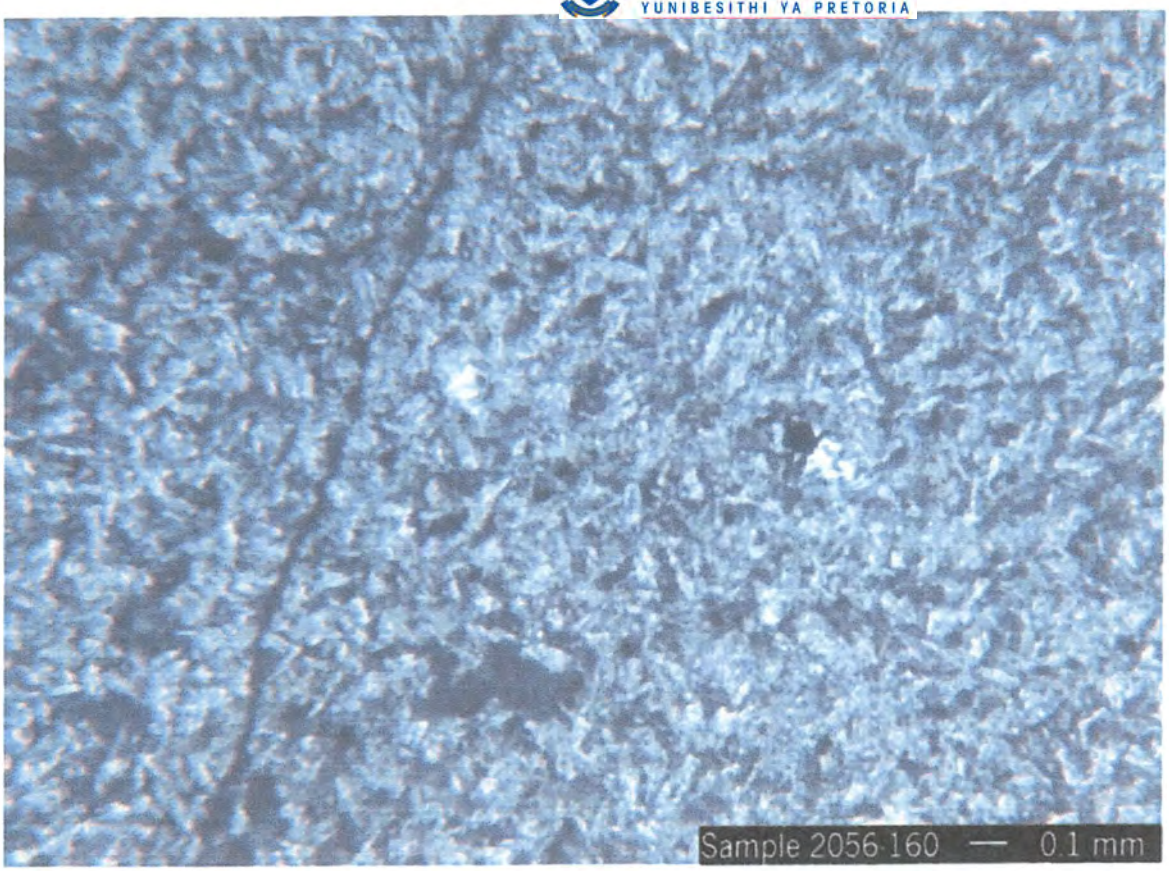

Figure 3: Photomicrograph of a fine-grained meta-tholeiitic rock (greenschist) with felted texture and sphene annealed micro-fractures.

Appendix B

Results of uniaxial compression creep tests

TABLE : B1

SUMMARY OF TEST RESULTS

CSIR

SPECIMEN PARTICULARS		SPECIMEN TEST RESULTS								
CSIR Specimen No	Rock Type	Strain at Failure ($\times 10^{-6}$)	Strength (UCS) (MPa)	Tangent @ 50% UCS				Modulus Ratio	Modulus Ratio unloading	Notes
				Poisson's Ratio	Deformation Modulus	Poisson's Ratio unloading	Deformation Modulus unloading			
1640-UCM-22	Lava	5093	396.0	0.301	82.0	n/a	n/a	207	n/a	
1640-UCM-52		5665	465.0	0.313	88.3	n/a	n/a	190	n/a	
1640-UCM-54		5485	458.2	0.305	88.6	n/a	n/a	193	n/a	
1640-UCM-62		5463	429.6	0.314	88.5	n/a	n/a	206	n/a	
1640-CRP-23	Lava	4645	363.7	0.361	84.7	0.279	96.8	233	266	
1640-CRP-53		5135	435.4	0.329	92.8	0.291	101.2	213	232	
1640-CRP-55		4039	398.7	0.338	93.8	0.274	109.5	235	275	
1640-CRP-63		4582	402.2	0.346	89.1	0.266	101.8	222	253	
2056-UCM-119	Quartzite	3600	170.6	0.247	50.1	n/a	n/a	294	n/a	
2056-UCM-120		2950	142.9	0.200	48.2	n/a	n/a	337	n/a	
2056-UCM-122		3000	125.9	0.277	43.5	n/a	n/a	346	n/a	
2056-CRP-116	Quartzite	3055	117.6	0.342	39.5	0.160	76.5	336	650	
2056-CRP-117		3642	114.1	0.366	40.7	0.129	75.2	357	659	
2056-CRP-118		4142	112.6	0.356	39.7	0.123	73.9	353	656	
2056-CRP-121		3267	135.2	0.347	51.0	0.157	79.7	377	589	

UNIVERSITEIT VAN PRETORIA
UNIVERSITY OF PRETORIA
YUNIBESITHI YA PRETORIA

Revision 0

FIGURE B1: TANGENT MODULUS vs UNIAXIAL COMPRESSIVE STRENGTH

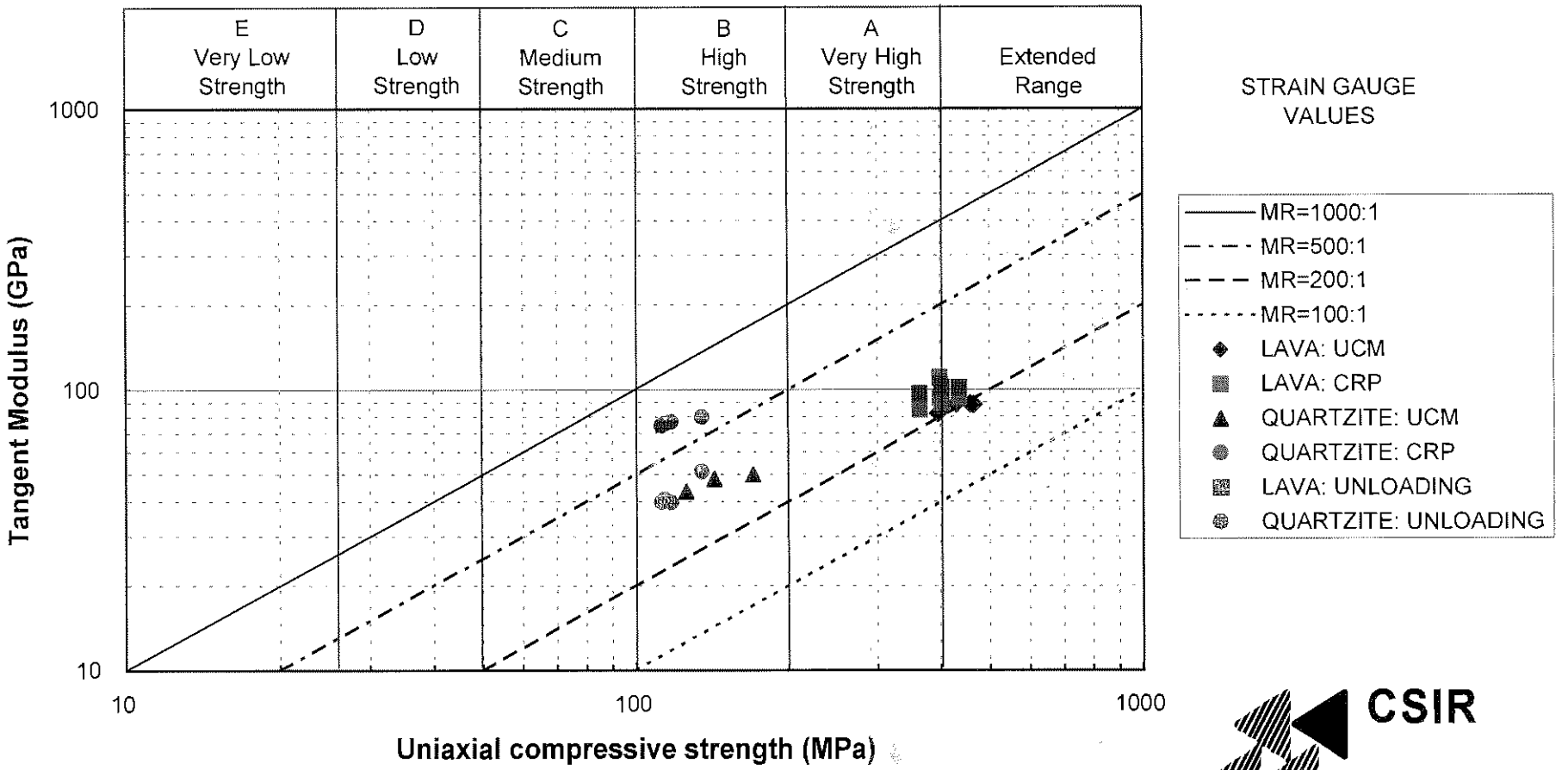

MODIFIED AFTER DEERE AND MILLER

CSIR

Revision 0

FIGURE B2: UNIAXIAL COMPRESSIVE STRENGTH vs UNIAXIAL CREEP STRENGTH

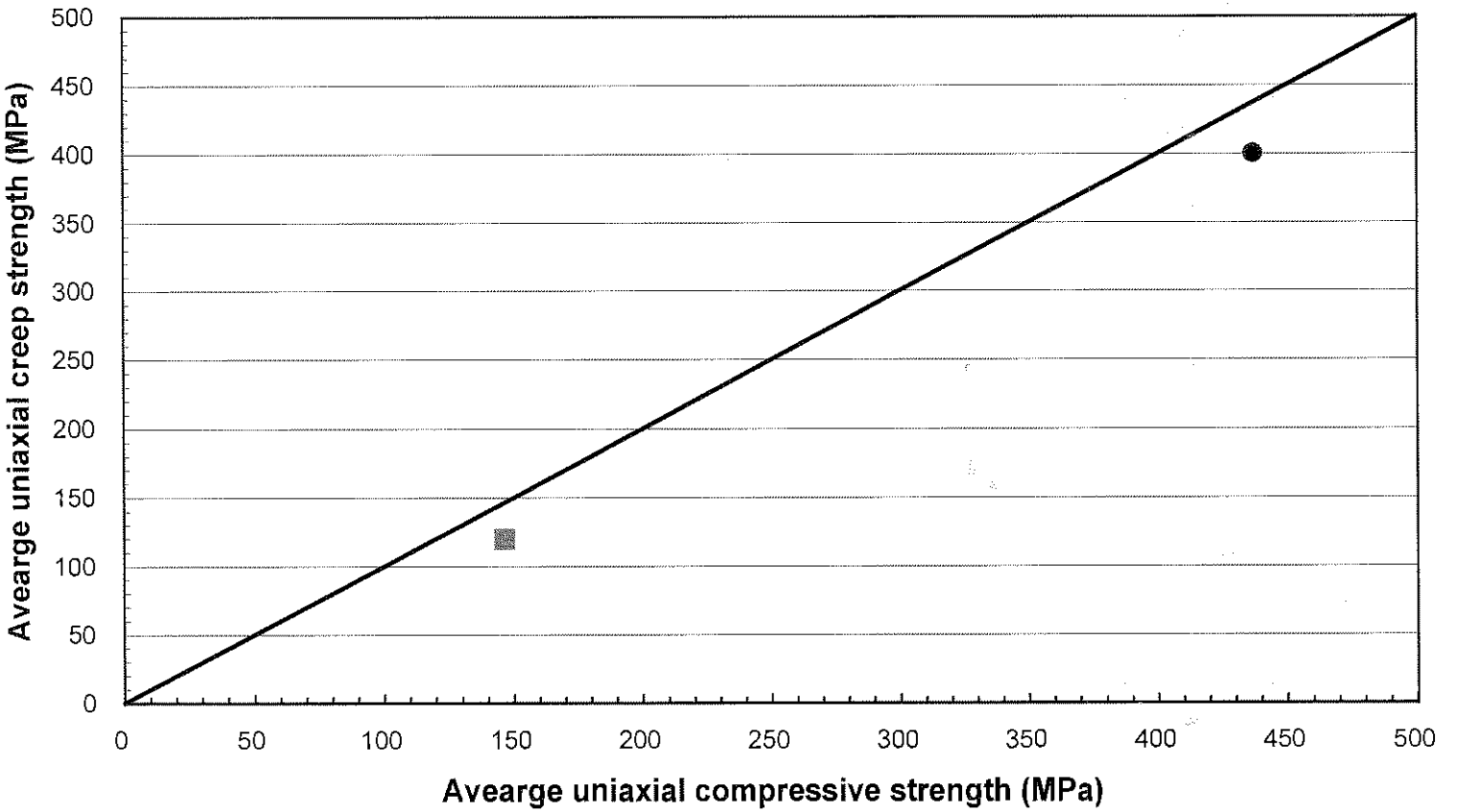

MODIFIED AFTER DEERE AND MILLER

CSIR

Revision 0

UNIVERSITEIT VAN PRETORIA
UNIVERSITY OF PRETORIA
YUNIBESITHI YA PRETORIA

)MECHANICS
3ORATORY

UNIAXIAL COMPRESSION TEST

WITH DEFORMABILITY MEASUREMENTS BY MEANS OF STRAIN GAUGES
STRAIN GAUGE: (A+B) / 2

CSIR MININGTEK

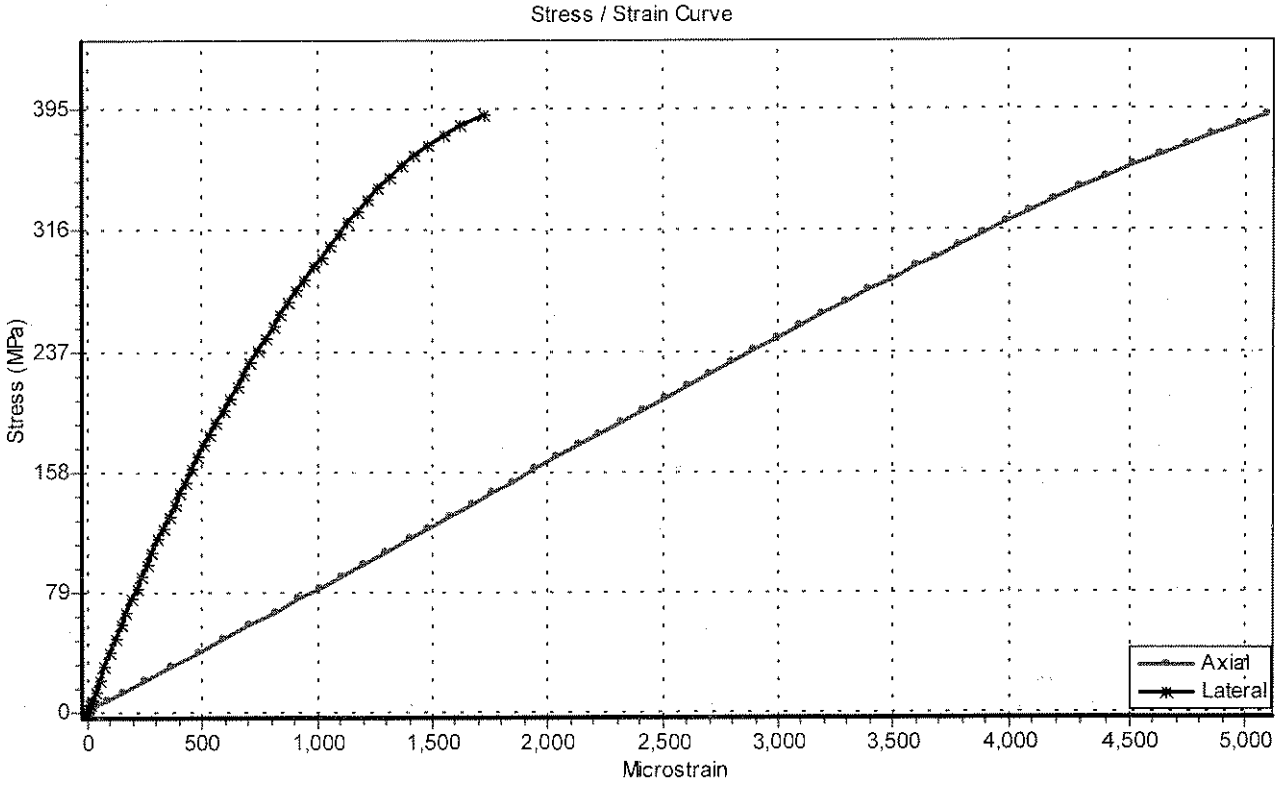

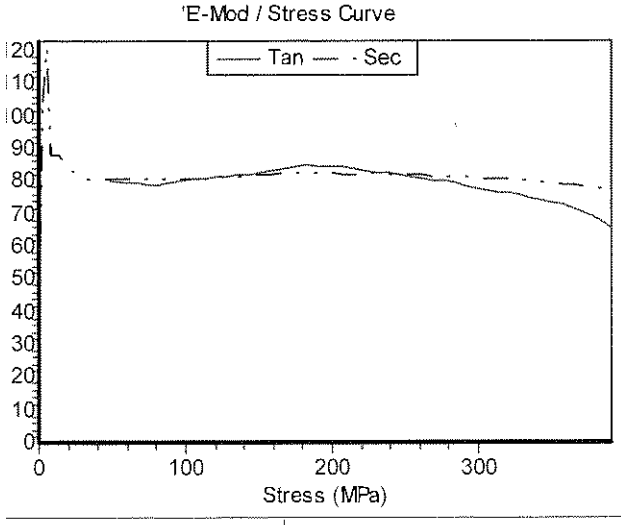

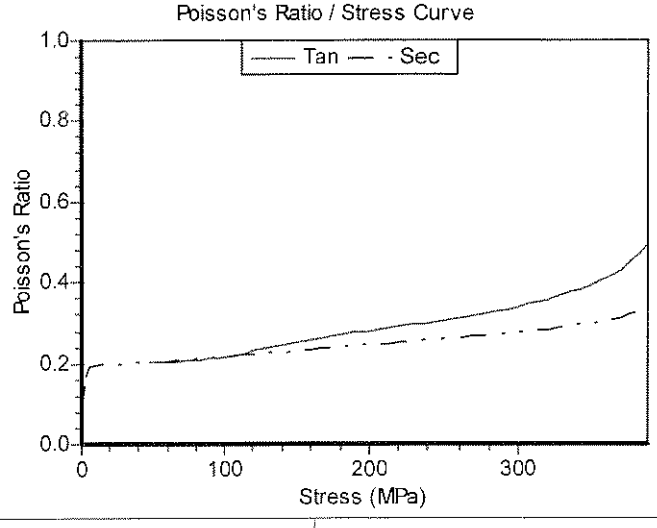

'E'-Mod @ 30% UCS	'E'-Mod @ 50% UCS	Poisson's Ratio @ 30% UCS	Poisson's Ratio @ 50% UCS
83.9 GPa	**82.0 GPa**	Tan: 0.262	**0.301**
81.0 GPa	82.3 GPa	Sec: 0.221	0.243

lod Ratio: Tan @ 50% UCS:	UCS (MPa):	Toughness Index:	
207	396	Farmer (MPa): 0.9559	CSIR (MPa): 1.0450

TEST DETAILS

Date: 1994-12-09
Time: 10:58:01
Test Machine: Amsler
Range (kN): 1000
Falure Load (kN): 297
Tester: KD
Client: MININGTEK

SPECIMEN DETAILS

Rock Type: LAVA
CSIR Number: 1640-UCM-22
Diameter (mm): 31
Length (mm): 80
Mass (g): 172
Density (kg/m^3) 2866
Deg. of Sat.: LAB DRY

)MECHANICS
BORATORY

UNIAXIAL COMPRESSION TEST

WITH DEFORMABILITY MEASUREMENTS BY MEANS OF STRAIN GAUGES

STRAIN GAUGE: (A+B) / 2

CSIR MININGTEK

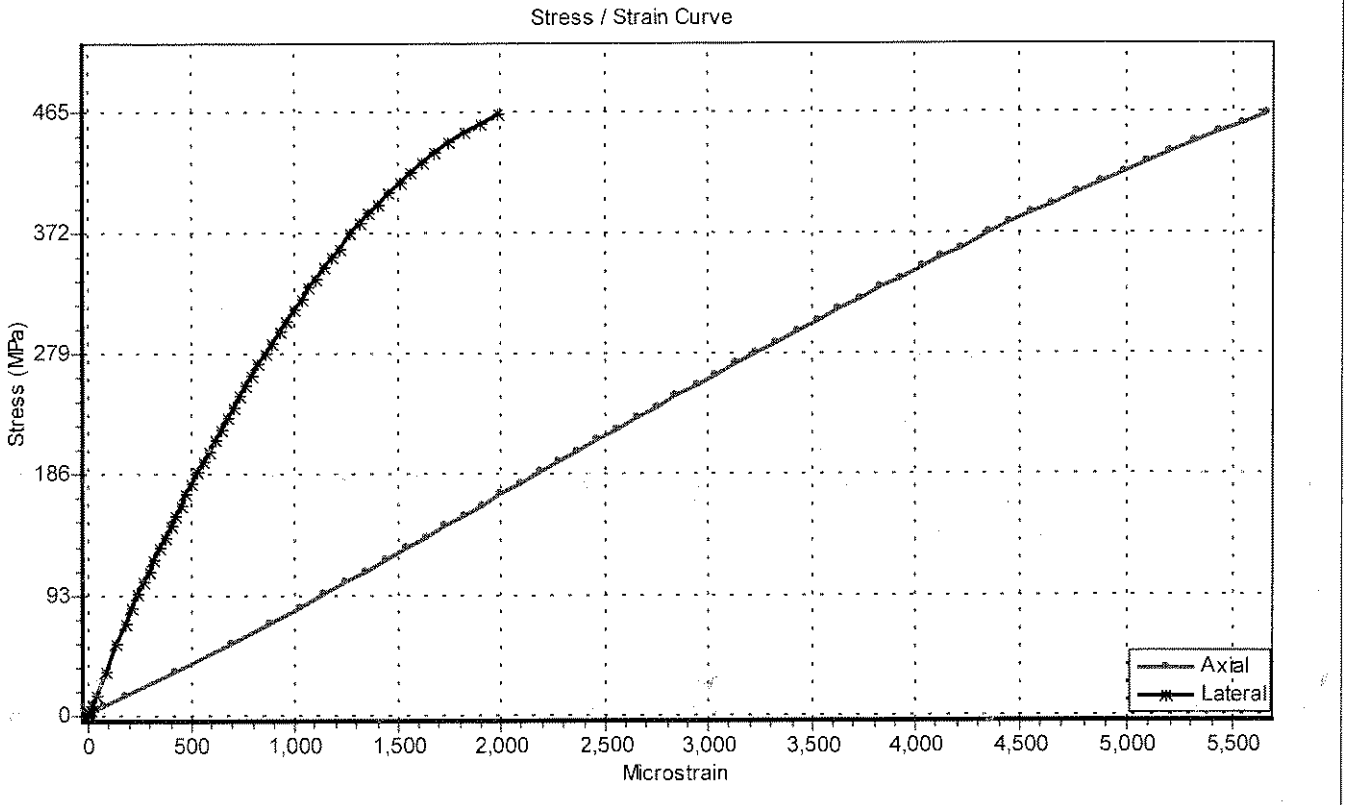

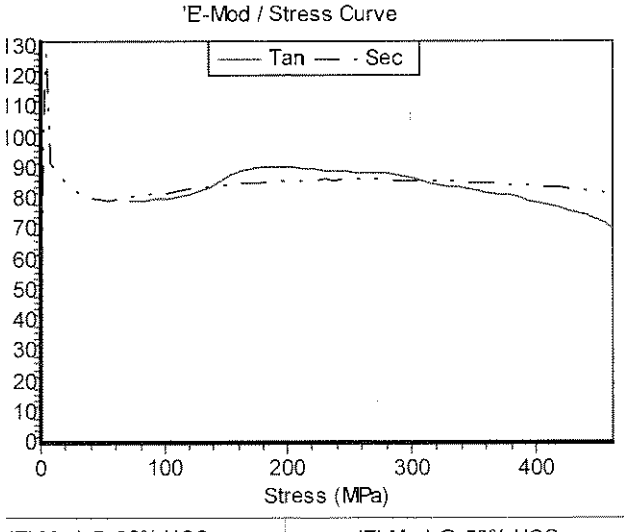

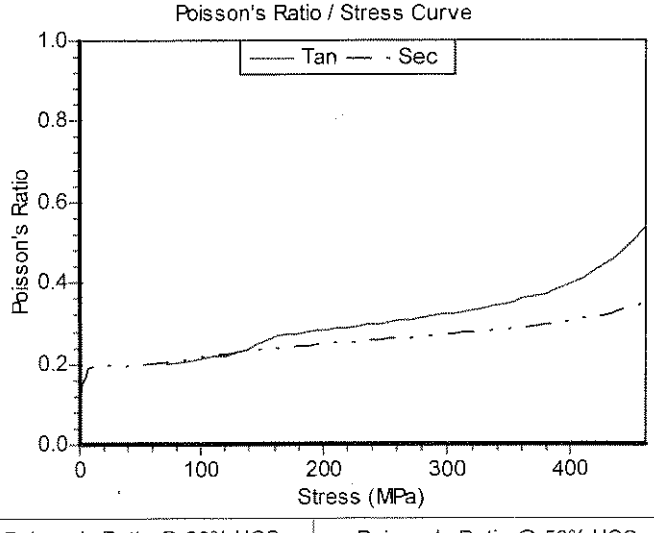

'E'-Mod @ 30% UCS	'E'-Mod @ 50% UCS	Poisson's Ratio @ 30% UCS	Poisson's Ratio @ 50% UCS
91.3 GPa	**88.3 GPa**	Tan: 0.279	**0.313**
84.2 GPa	86.6 GPa	Sec: 0.231	0.254

lod Ratio: Tan @ 50% UCS:	UCS (MPa):	Toughness Index:	
190	465	Farmer (MPa): 1.2240	CSIR (MPa): 1.3590

TEST DETAILS

Date: 1994-12-09
Time: 12:06:33
Test Machine: Amsler
Range (kN): 1000
Failure Load (kN): 342
Tester: KD
Client: MININGTEK

SPECIMEN DETAILS

Rock Type: LAVA
CSIR Number: 1640-UCM-52
Diameter (mm): 31
Length (mm): 80
Mass (g): 172
Density (kg/m^3): 2921
Deg. of Sat.: LAB DRY

ımmary sheet: 1640-UCM-52

2001-08-27 10:09:06

)MECHANICS
BORATORY

UNIAXIAL COMPRESSION TEST

WITH DEFORMABILITY MEASUREMENTS BY MEANS OF STRAIN GAUGES
STRAIN GAUGE: (A+B) / 2

CSIR MININGTEK

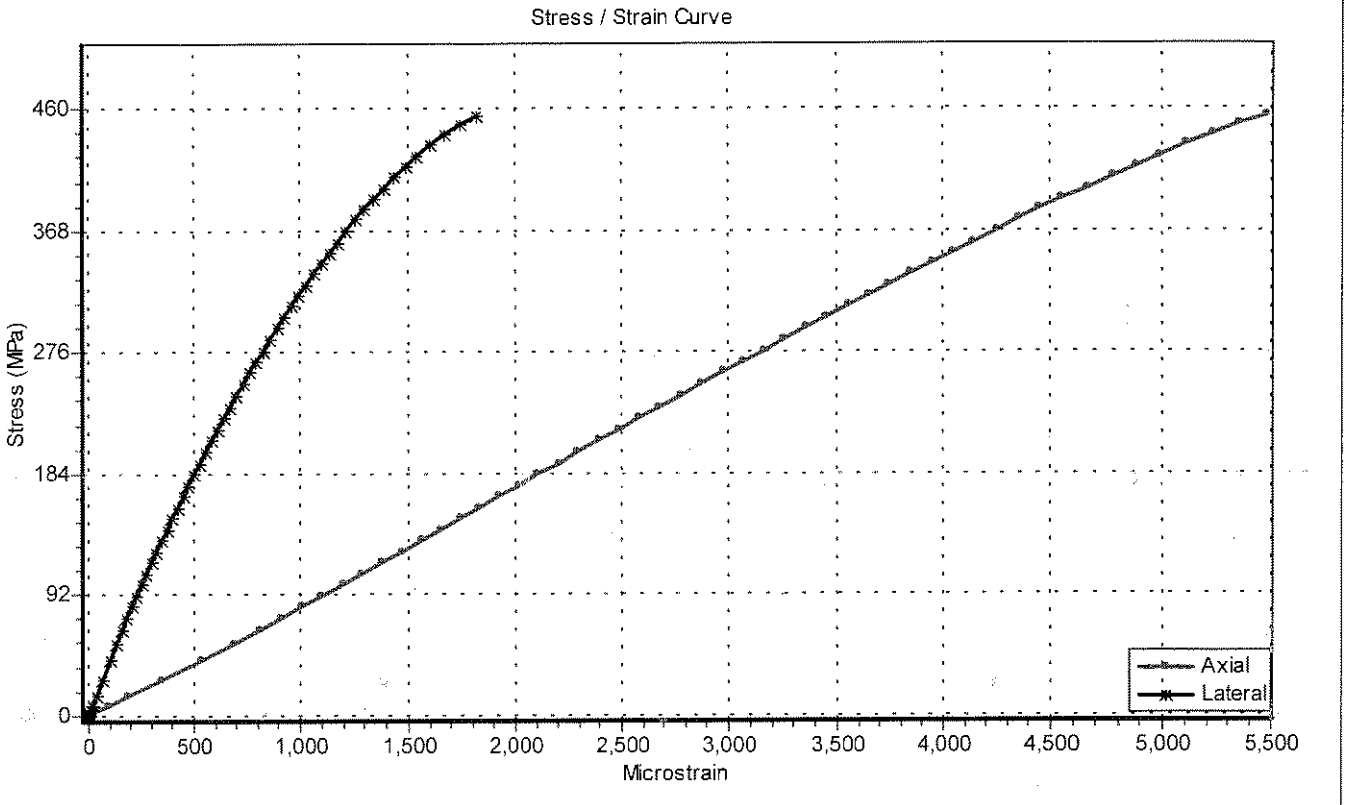

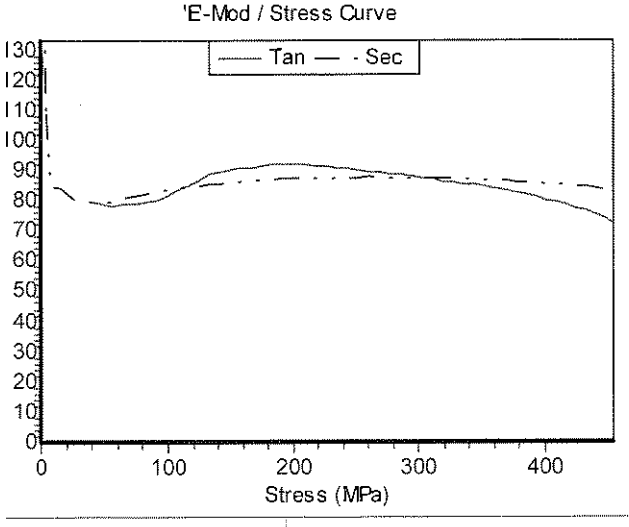

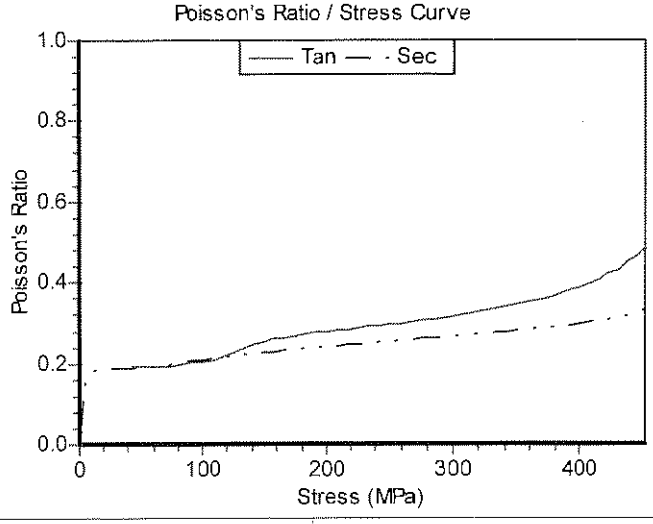

'E'-Mod @ 30% UCS	'E'-Mod @ 50% UCS	Poisson's Ratio @ 30% UCS	Poisson's Ratio @ 50% UCS
91.8 GPa	**88.6 GPa**	Tan: 0.274	**0.305**
85.3 GPa	87.5 GPa	Sec: 0.222	0.248
lod Ratio: Tan @ 50% UCS:	UCS (MPa):	Toughness Index:	
193	458.2	Farmer (MPa): 1.1850	CSIR (MPa): 1.2920

TEST DETAILS

Date: 1994-12-09
Time: 12:26:28
Test Machine: Amsler
Range (kN): 1000
Falure Load (kN): 337
Tester: KD
Client: MININGTEK

SPECIMEN DETAILS

Rock Type: LAVA
CSIR Number: 1640-UCM-54
Diameter (mm): 31
Length (mm): 80
Mass (g): 172
Density (kg/m^3): 2920
Deg. of Sat.: LAB DRY

)MECHANICS
3ORATORY

UNIAXIAL COMPRESSION TEST

WITH DEFORMABILITY MEASUREMENTS BY MEANS OF STRAIN GAUGES

STRAIN GAUGE: (A+B) / 2

CSIR MININGTEK

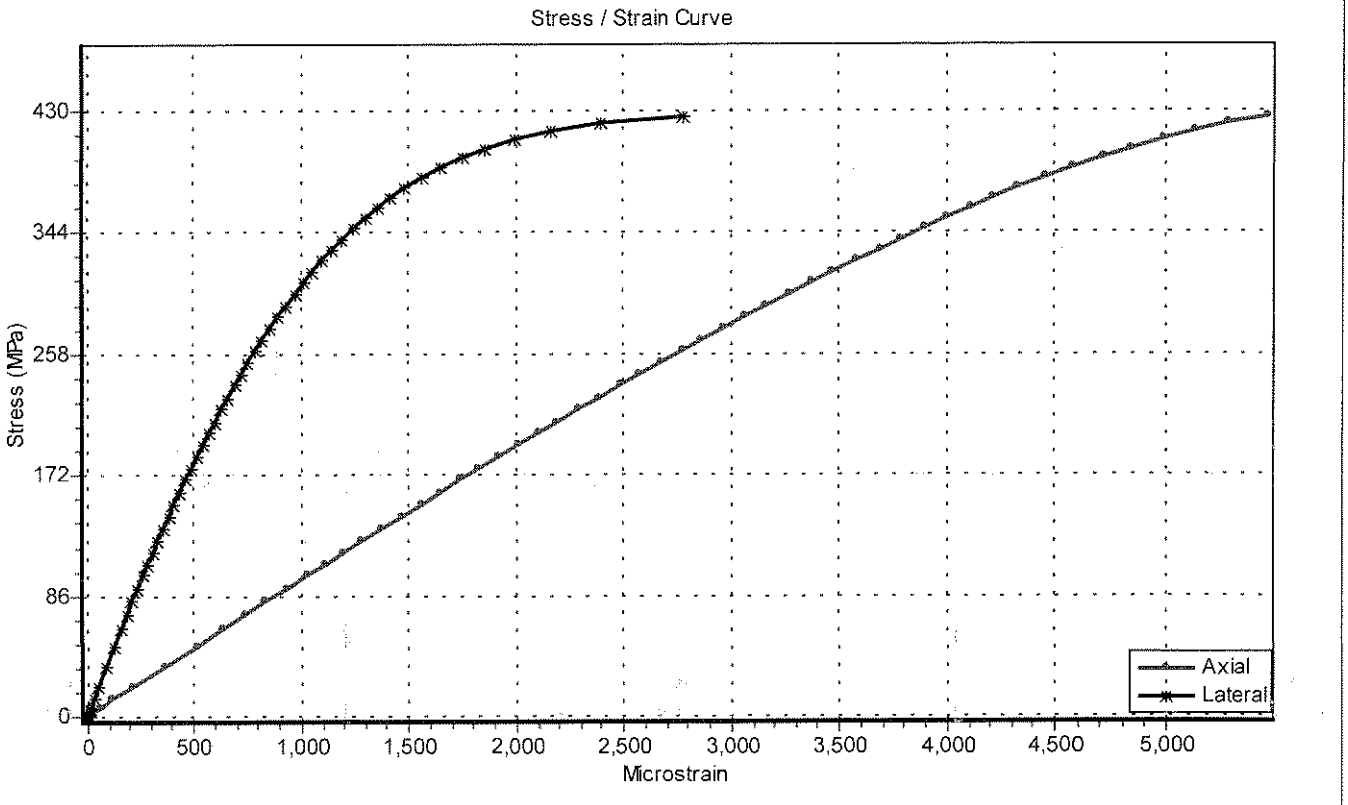

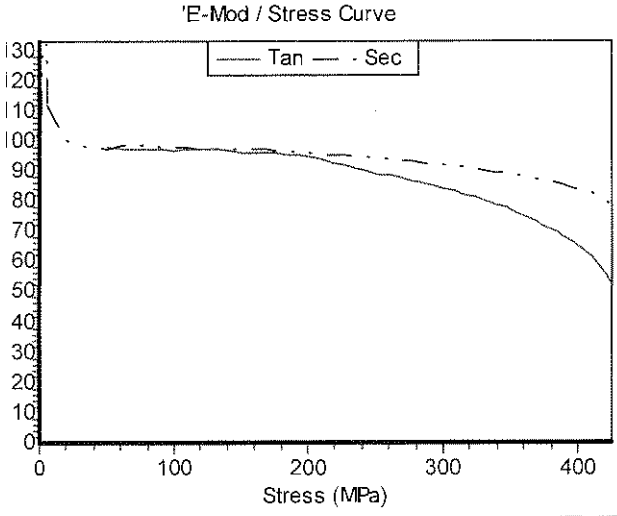

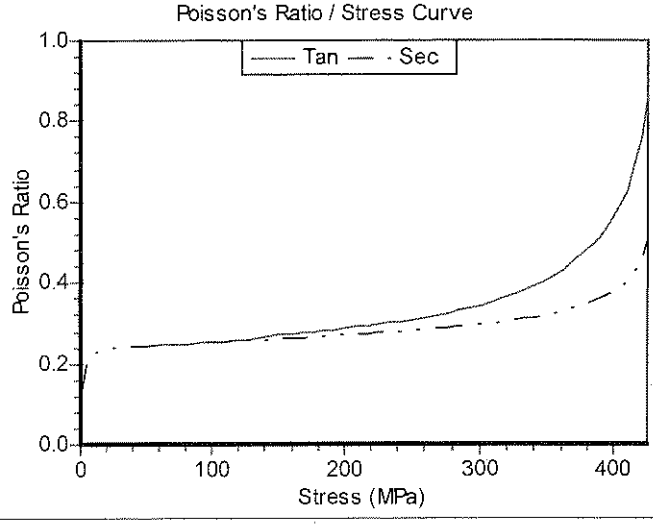

'E'-Mod @ 30% UCS	'E'-Mod @ 50% UCS	Poisson's Ratio @ 30% UCS	Poisson's Ratio @ 50% UCS
96.2 GPa	**88.5 GPa**	Tan: 0.279	**0.314**
97.5 GPa	95.6 GPa	Sec: 0.257	0.271

lod Ratio: Tan @ 50% UCS:	UCS (MPa):	Toughness Index:	
206	429.6	Farmer (MPa): 1.0430	CSIR (MPa): 1.3280

TEST DETAILS

Date: 1994-12-09
Time: 12:46:30
Test Machine: Amsler
Range (kN): 1000
Falure Load (kN): 318
Tester: KD
Client: MININGTEK

SPECIMEN DETAILS

Rock Type: LAVA
CSIR Number: 1640-UCM-62
Diameter (mm): 31
Length (mm): 80
Mass (g): 175
Density (kg/m^3): 2934
Deg. of Sat.: LAB DRY

ımmary sheet: 1640-UCM-62

2001-08-27 10:10:15

OMECHANICS
BORATORY

UNIAXIAL COMPRESSION TEST

WITH DEFORMABILITY MEASUREMENTS BY MEANS OF STRAIN GAUGES

STRAIN GAUGE: (A+B) / 2

CSIR MININGTEK

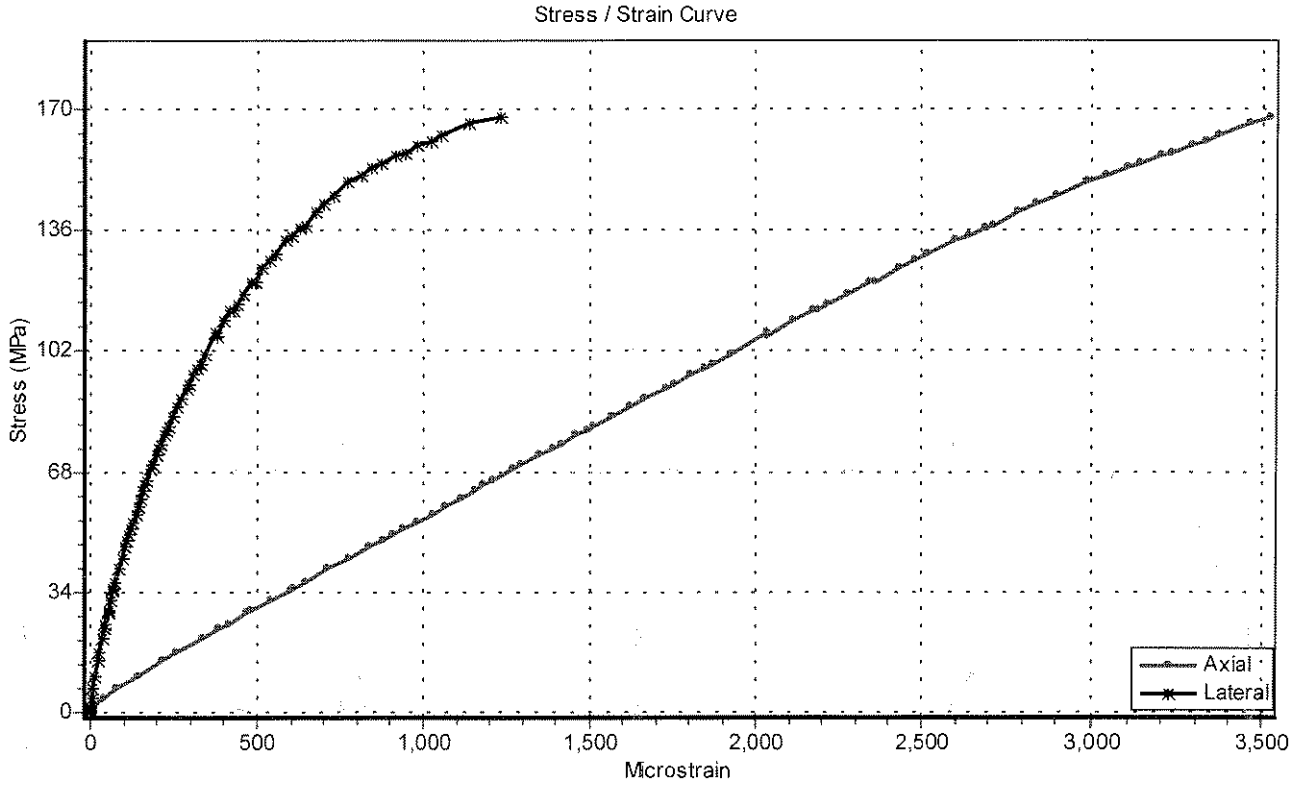

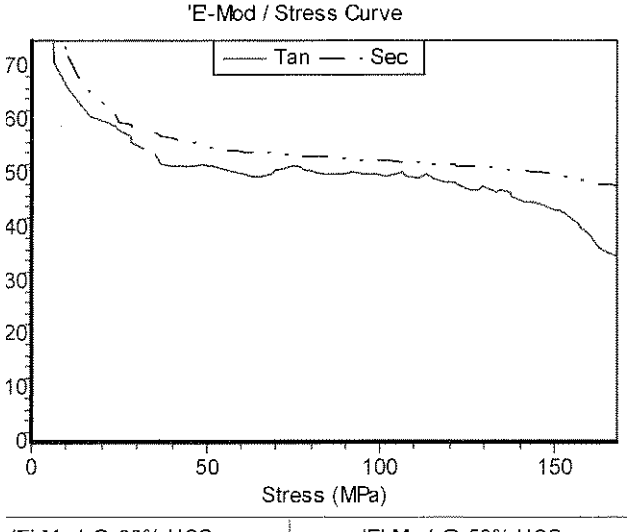

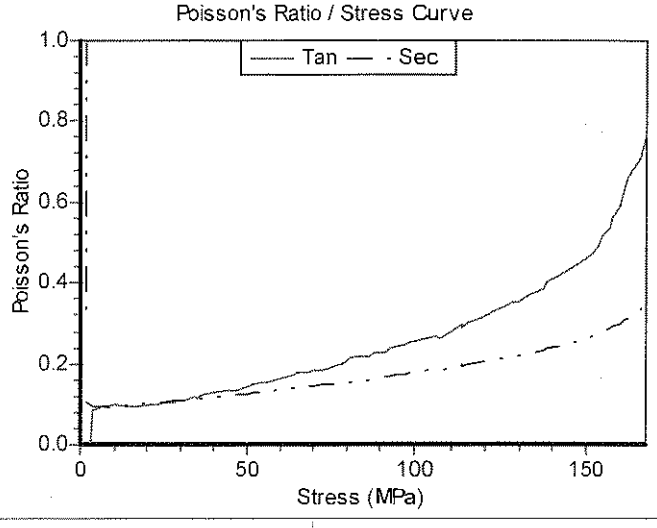

'E'-Mod @ 30% UCS	'E'-Mod @ 50% UCS	Poisson's Ratio @ 30% UCS	Poisson's Ratio @ 50% UCS
49.8 GPa	**50.1 GPa**	Tan: 0.171	**0.247**
55.4 GPa	53.3 GPa	Sec: 0.126	0.157

lod Ratio: Tan @ 50% UCS:	UCS (MPa):	Toughness Index:	
294	170.6	Farmer (MPa): 0.2905	CSIR (MPa): 0.3207

TEST DETAILS

Date: 2001-07-16
Time: 15:27:17
Test Machine: Amsler
Range (kN): 100
Falure Load (kN): 52
Tester: JD
Client: RE

SPECIMEN DETAILS

Rock Type: QUARTZITE
CSIR Number: 2056-UCM-119
Diameter (mm): 20
Length (mm): 59
Mass (g): 48
Density (kg/m^3): 2662
Deg. of Sat.: LAB DRY

ummary sheet: 2056-UCM-119

2001-08-27 09:58:03

MECHANICS
ORATORY

UNIAXIAL COMPRESSION TEST

WITH DEFORMABILITY MEASUREMENTS BY MEANS OF STRAIN GAUGES

STRAIN GAUGE: (A+B) / 2

CSIR MININGTEK

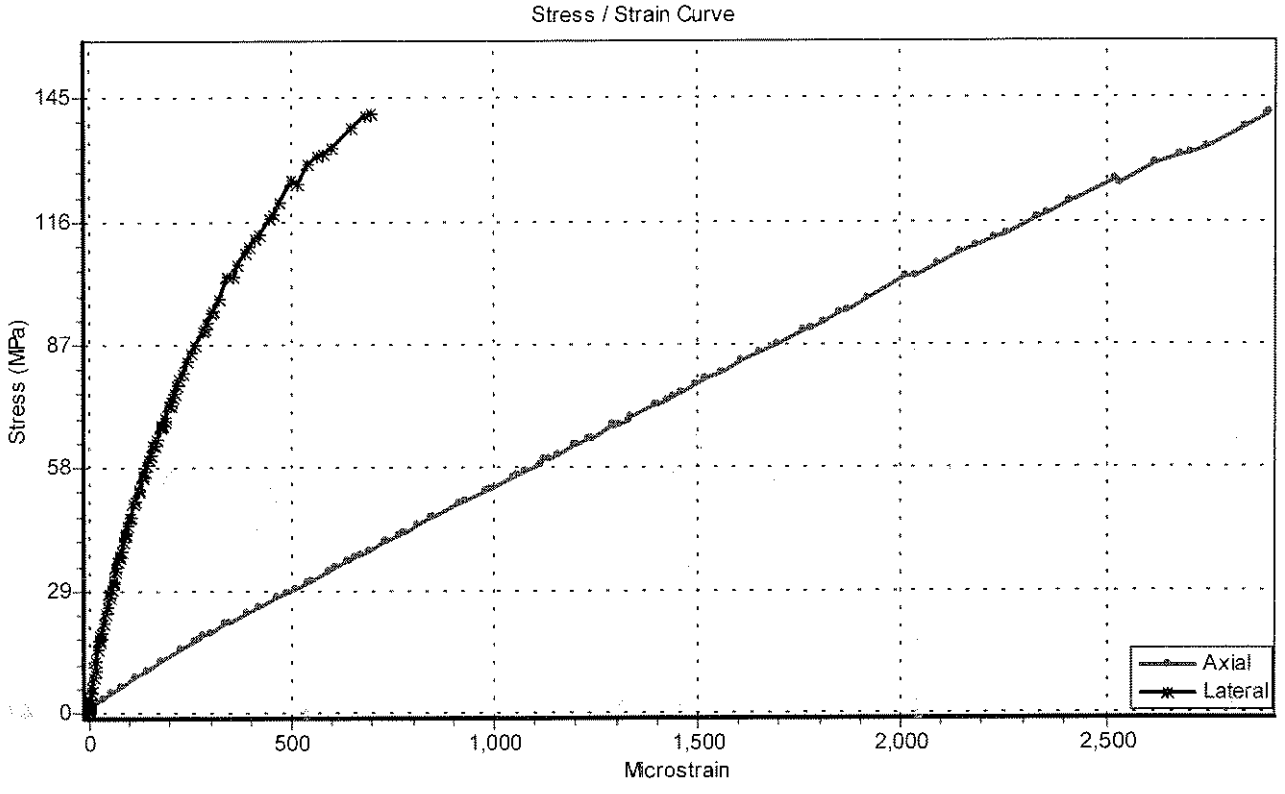

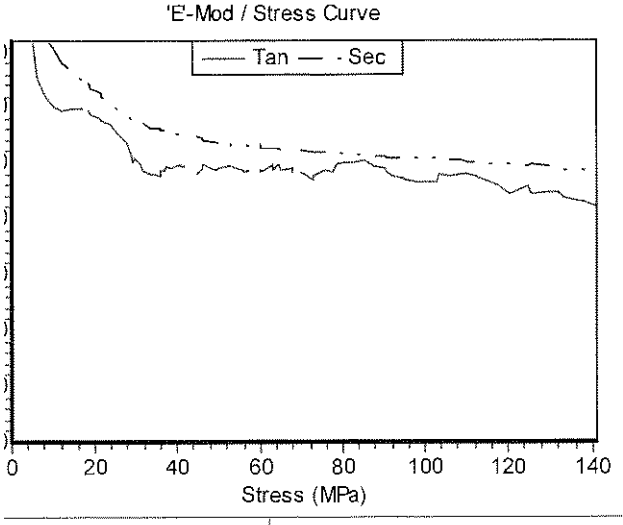

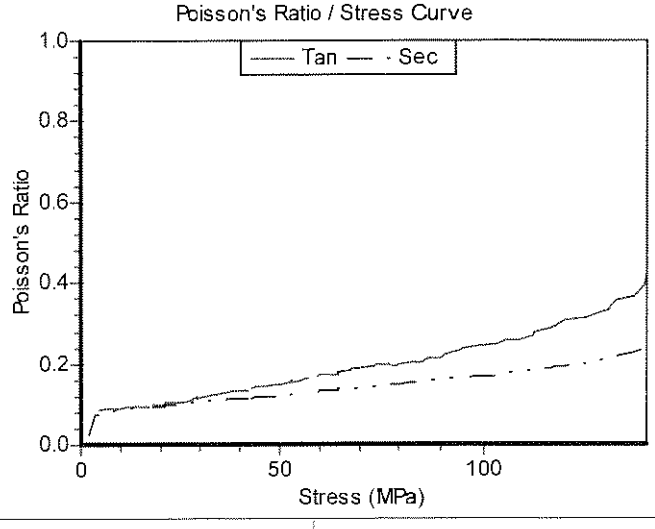

E'-Mod @ 30% UCS	'E'-Mod @ 50% UCS	Poisson's Ratio @ 30% UCS	Poisson's Ratio @ 50% UCS
48.6 GPa	**48.2 GPa**	Tan: 0.149	**0.200**
54.3 GPa	51.8 GPa	Sec: 0.117	0.141

d Ratio: Tan @ 50% UCS:	UCS (MPa):	Toughness Index:	
337	142.9	Farmer (MPa): 0.2119	CSIR (MPa): 0.2143

TEST DETAILS

Date: 2001-07-16
Time: 14:21:30
Test Machine: Amsler
Range (kN): 100
Falure Load (kN): 44
Tester: JD
Client: RE

SPECIMEN DETAILS

Rock Type: QUARTZITE
CSIR Number: 2056-UCM-120
Diameter (mm): 20
Length (mm): 59
Mass (g): 48
Density (kg/m^3): 2658
Deg. of Sat.: LAB DRY

nmary sheet: 2056-UCM-120

2001-08-27 09:59:12

)MECHANICS
BORATORY

UNIAXIAL COMPRESSION TEST

WITH DEFORMABILITY MEASUREMENTS BY MEANS OF STRAIN GAUGES

STRAIN GAUGE: (A+B) / 2

CSIR MININGTEK

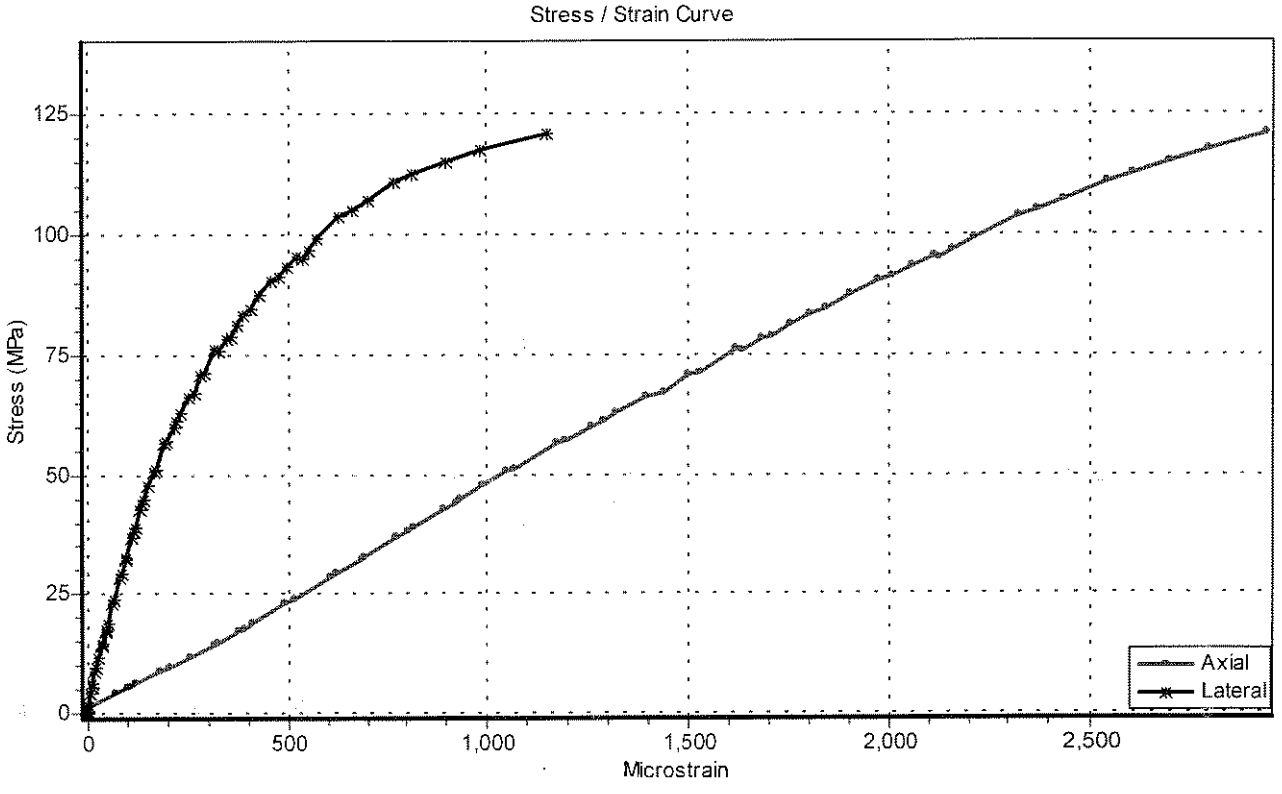

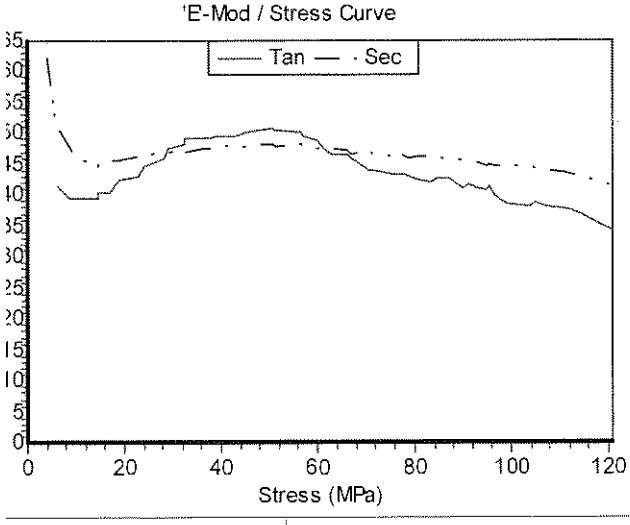

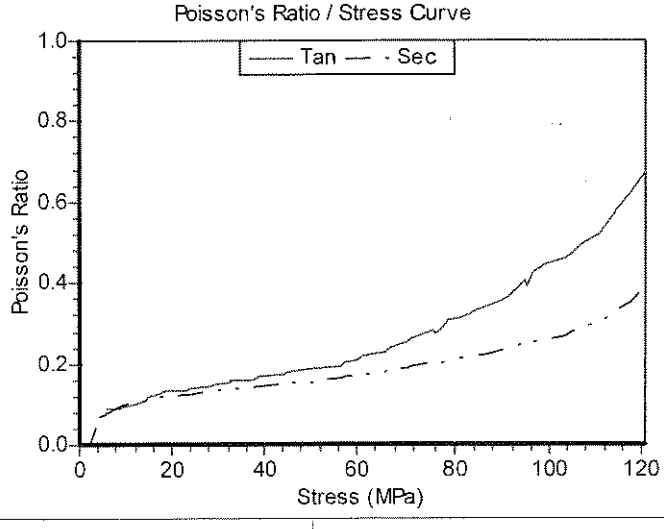

'E'-Mod @ 30% UCS	'E'-Mod @ 50% UCS	Poisson's Ratio @ 30% UCS	Poisson's Ratio @ 50% UCS
51.4 GPa	**43.5 GPa**	Tan: 0.179	**0.277**
47.6 GPa	47.6 GPa	Sec: 0.141	0.174

lod Ratio: Tan @ 50% UCS:	UCS (MPa):	Toughness Index:	
346	125.9	Farmer (MPa): 0.1822	CSIR (MPa): 0.1937

TEST DETAILS

Date: 2001-07-17
Time: 08:51:41
Test Machine: Amsler
Range (kN): 100
Falure Load (kN): 38
Tester: JD
Client: RE

SPECIMEN DETAILS

Rock Type: QUARTZITE
CSIR Number: 2056-UCM-122
Diameter (mm): 20
Length (mm): 59
Mass (g): 47
Density (kg/m^3) 2652
Deg. of Sat.: LAB DRY

ummary sheet: 2056-UCM-122

2001-08-27 10:01:07

XIAL STRAIN GAUGES
ATERAL STRAIN GAUGES

UNIVERSITEIT VAN PRETORIA
UNIVERSITY OF PRETORIA
YUNIBESITHI YA PRETORIA

Ventersdorp Lava

Axial Stress vs Strain
1640-23

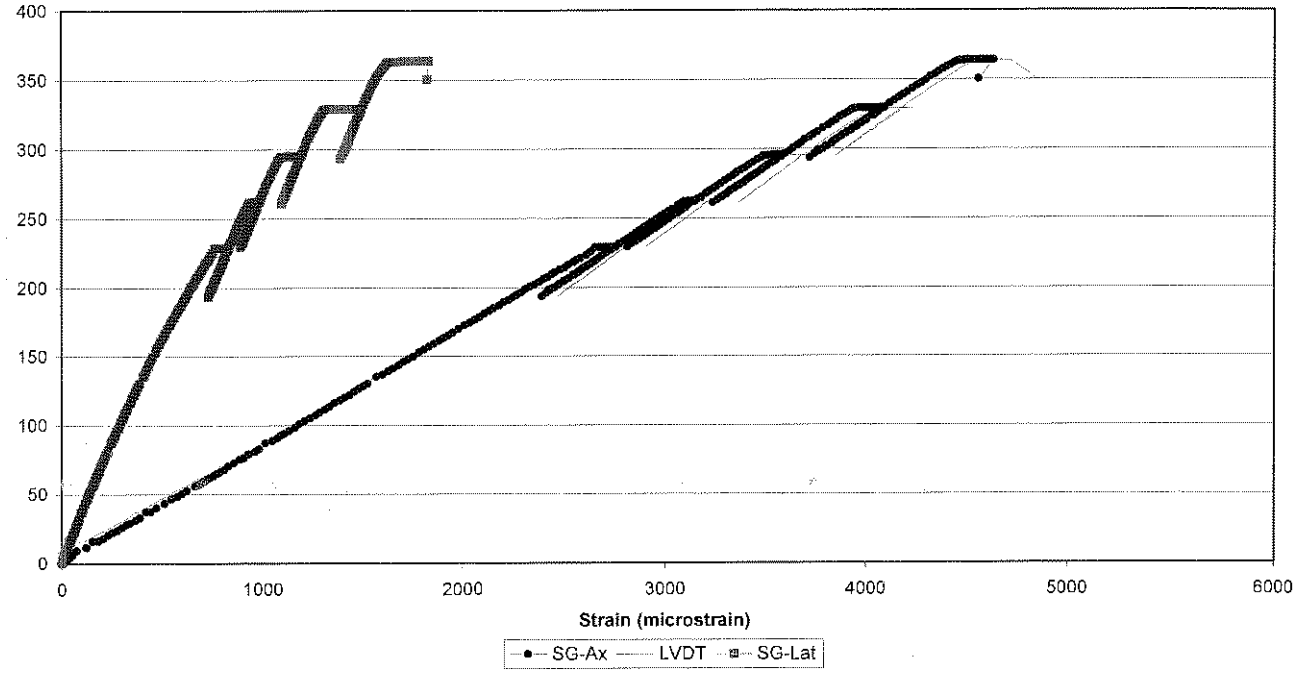

Strain vs Time
1640-23

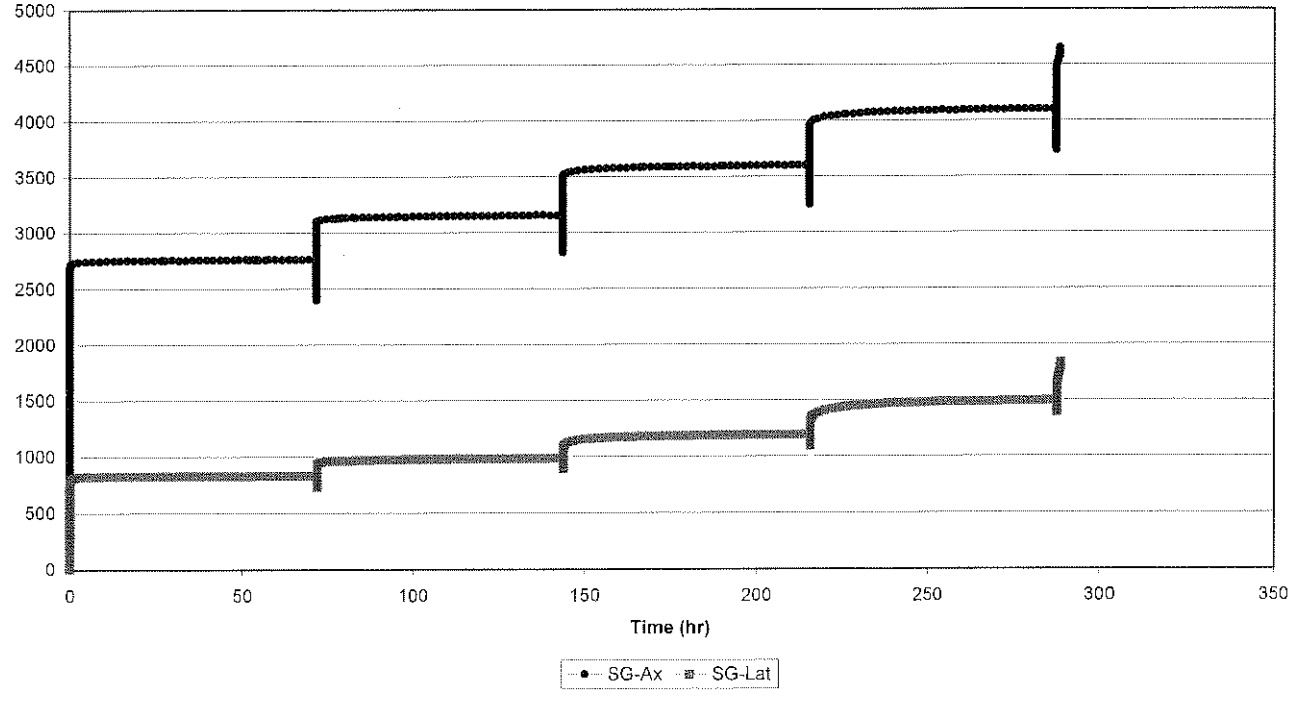

Ventersdorp Lava

Strain vs Time
1640-23 Cycle 1

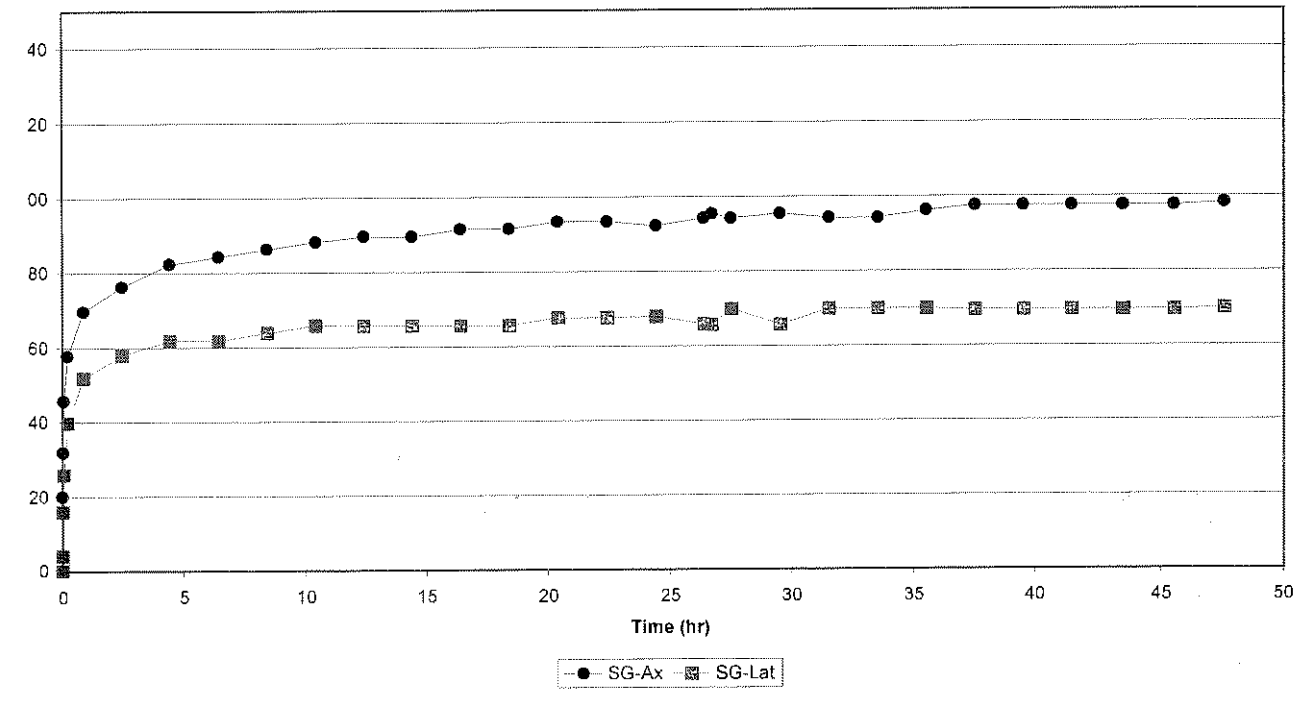

Strain vs Time
1640-23 Cycle 2

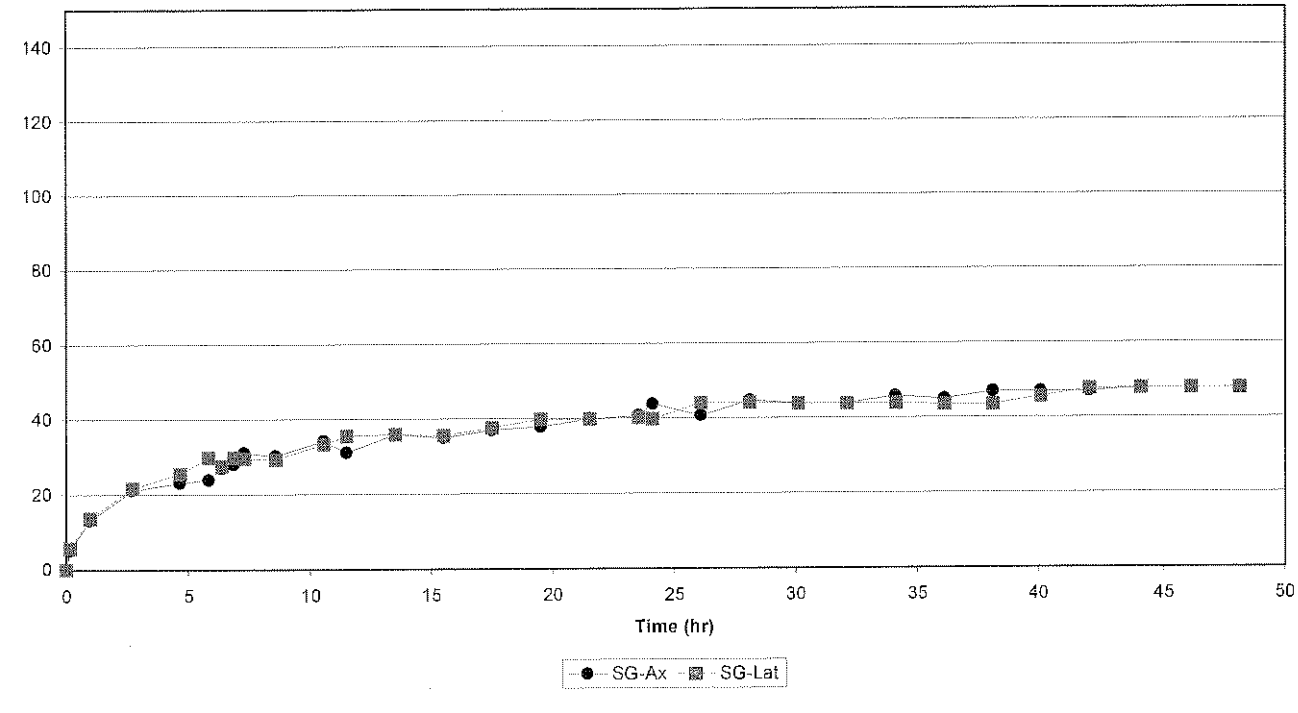

Ventersdorp Lava

Strain vs Time
1640-23 Cycle 3

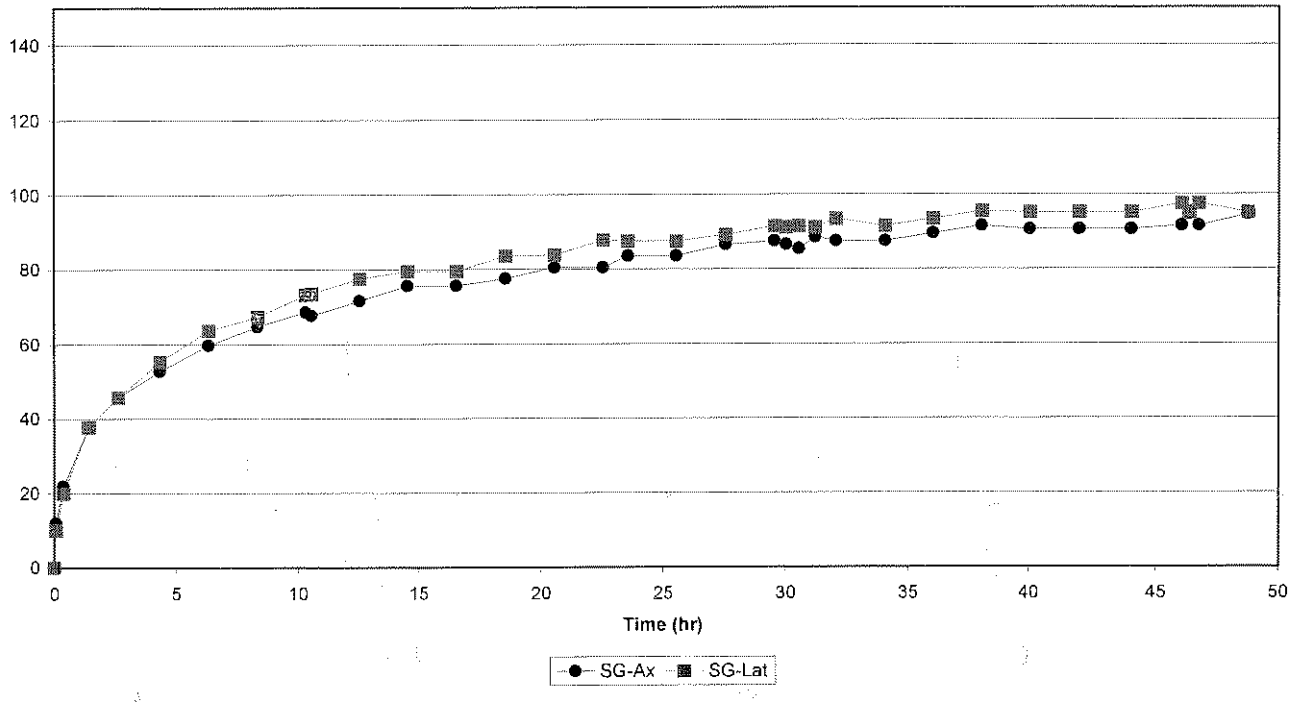

Strain vs Time
1640-23 Cycle 4

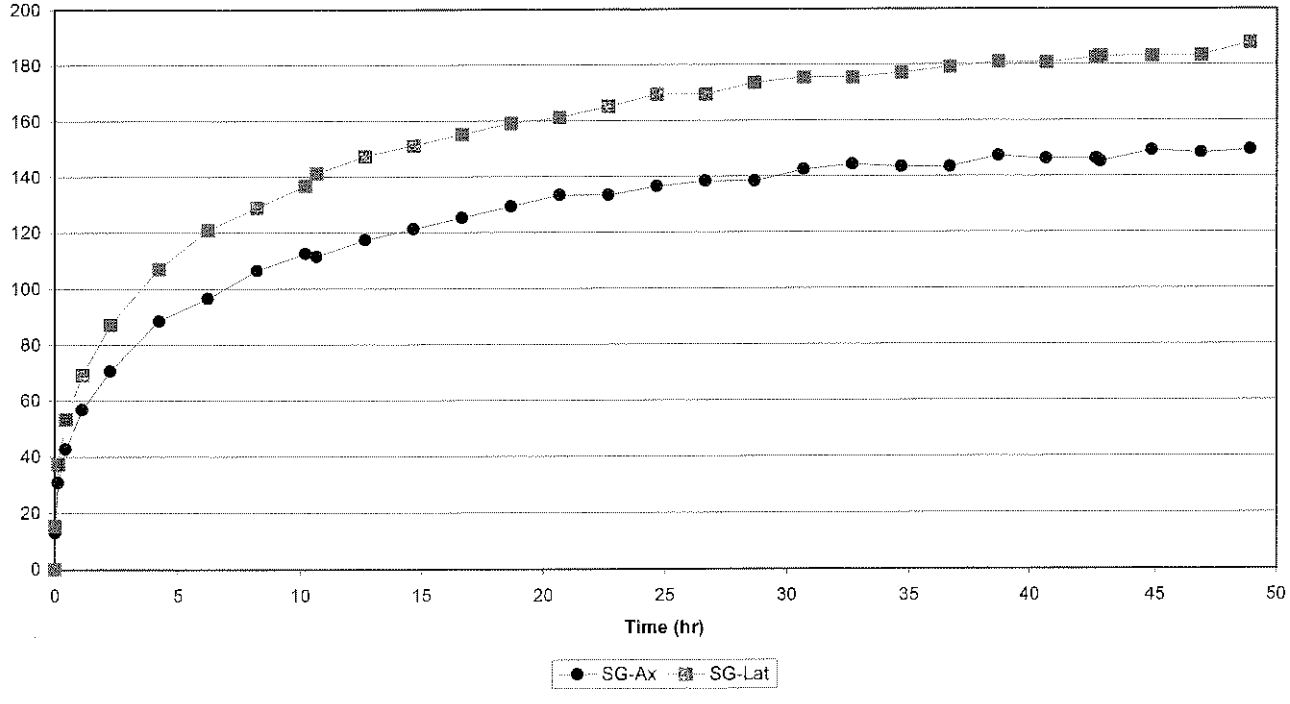

Ventersdorp Lava

Strain vs Time
1640-23 Cycle 4

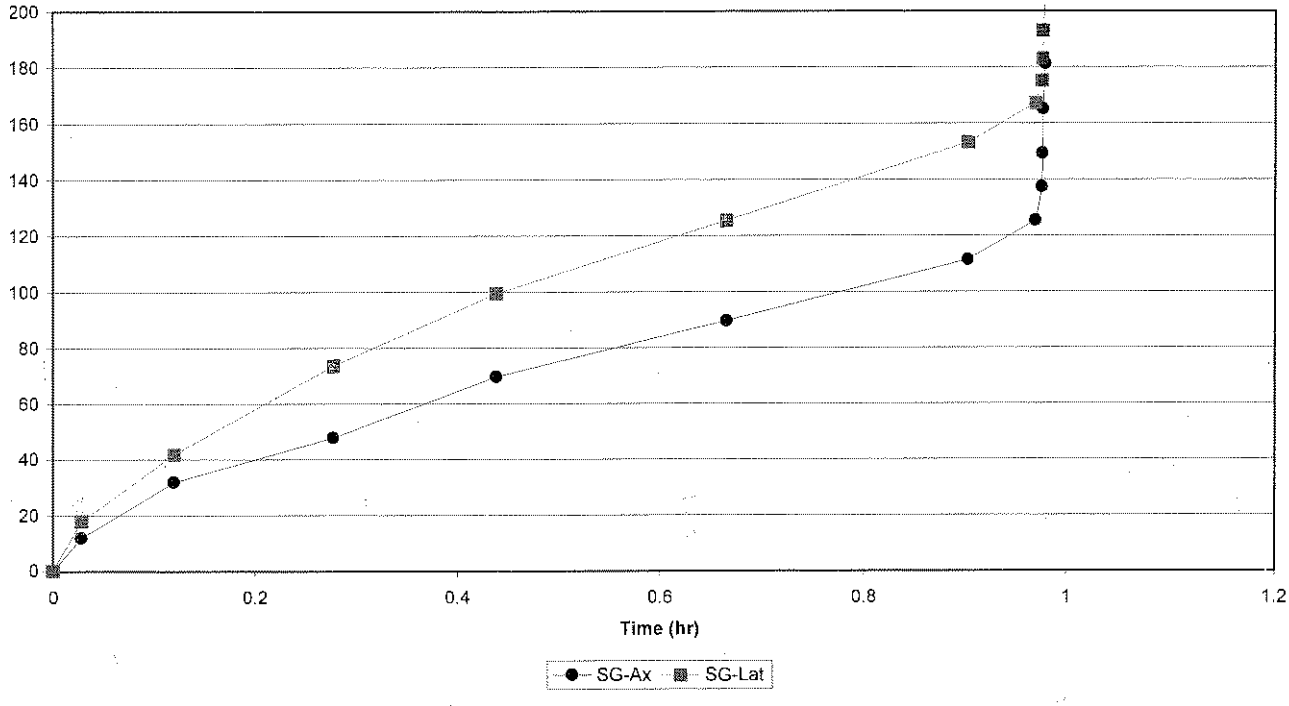

Cumulative Strain vs Stress
1640-23

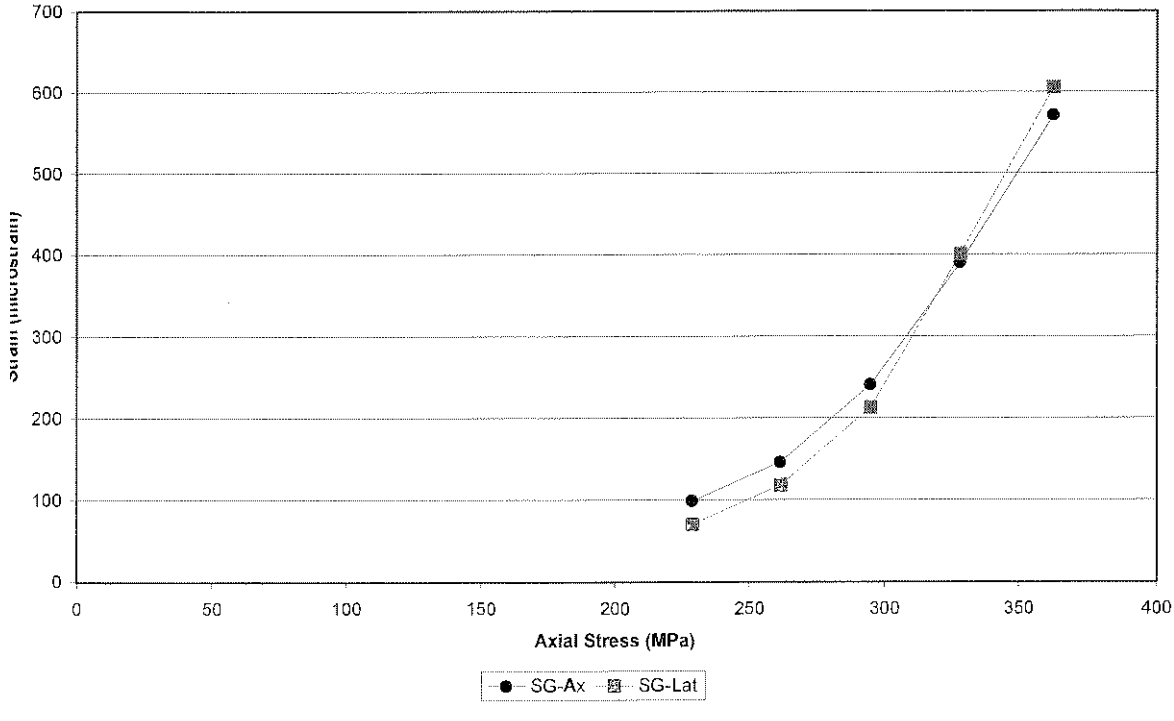

Ventersdorp Lava

Creep rate vs Stress
1640-23

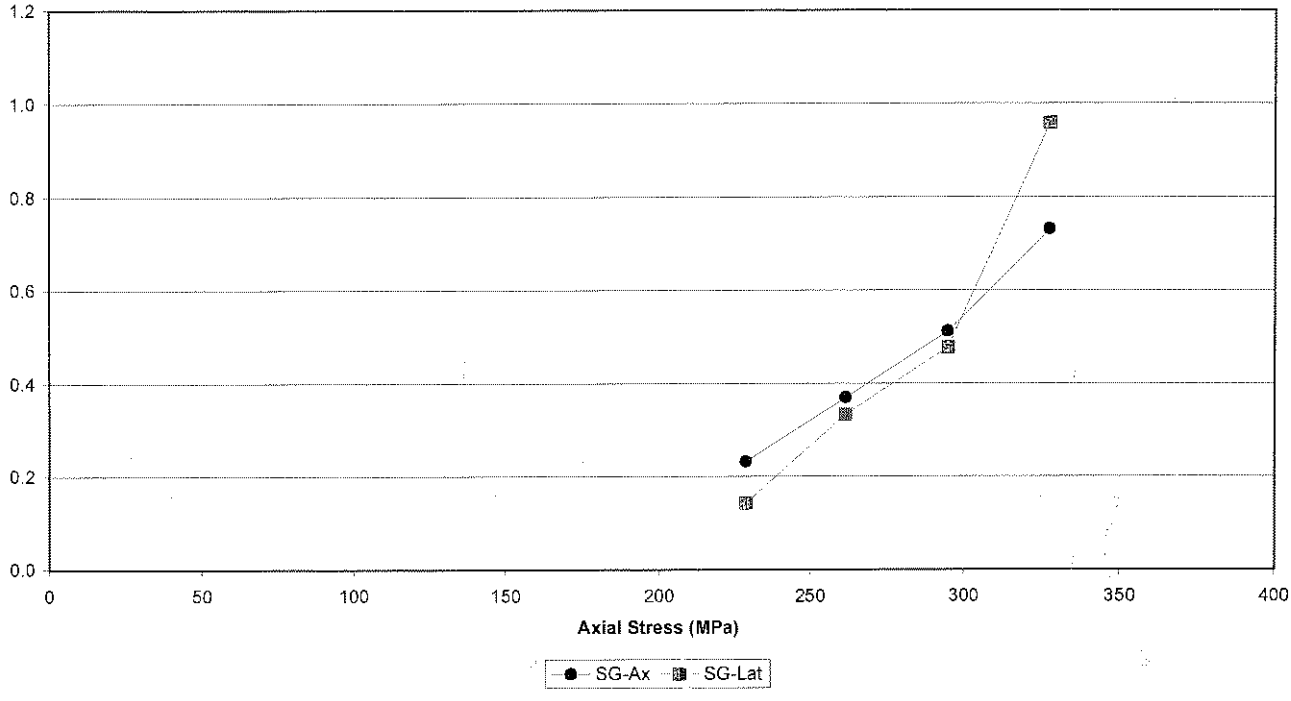

Log Creeprate vs Log Stress
1640-23

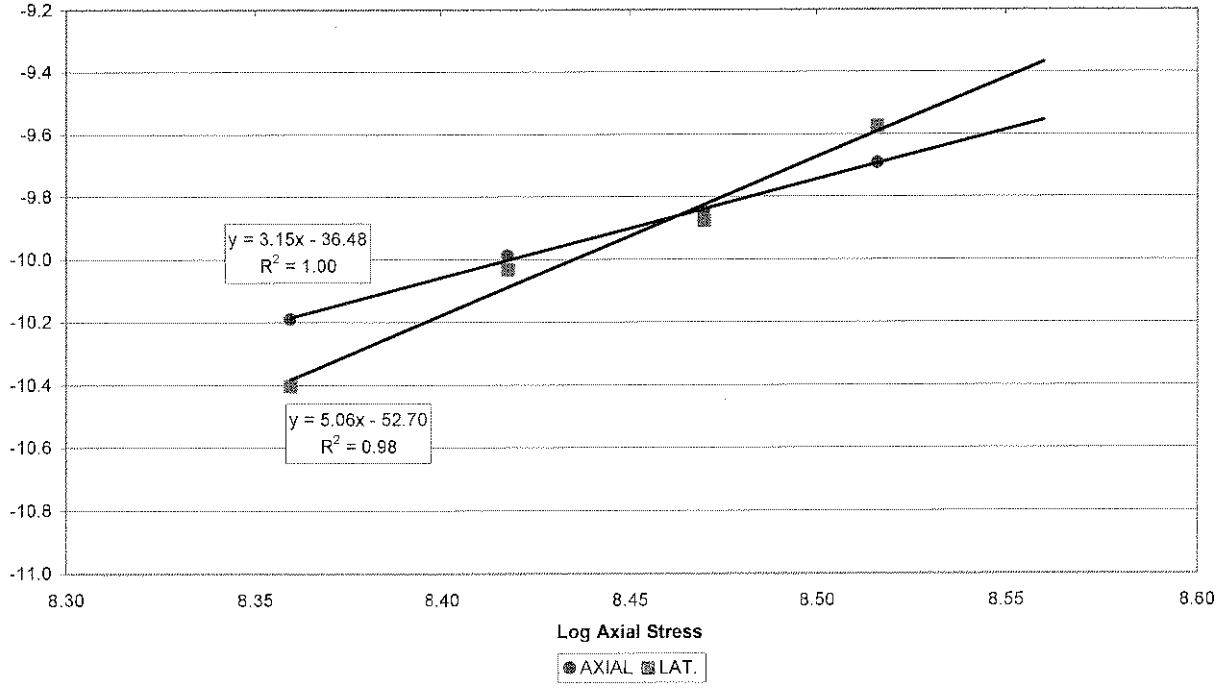

Ventersdorp Lava

Axial Stress vs Strain
1640-53

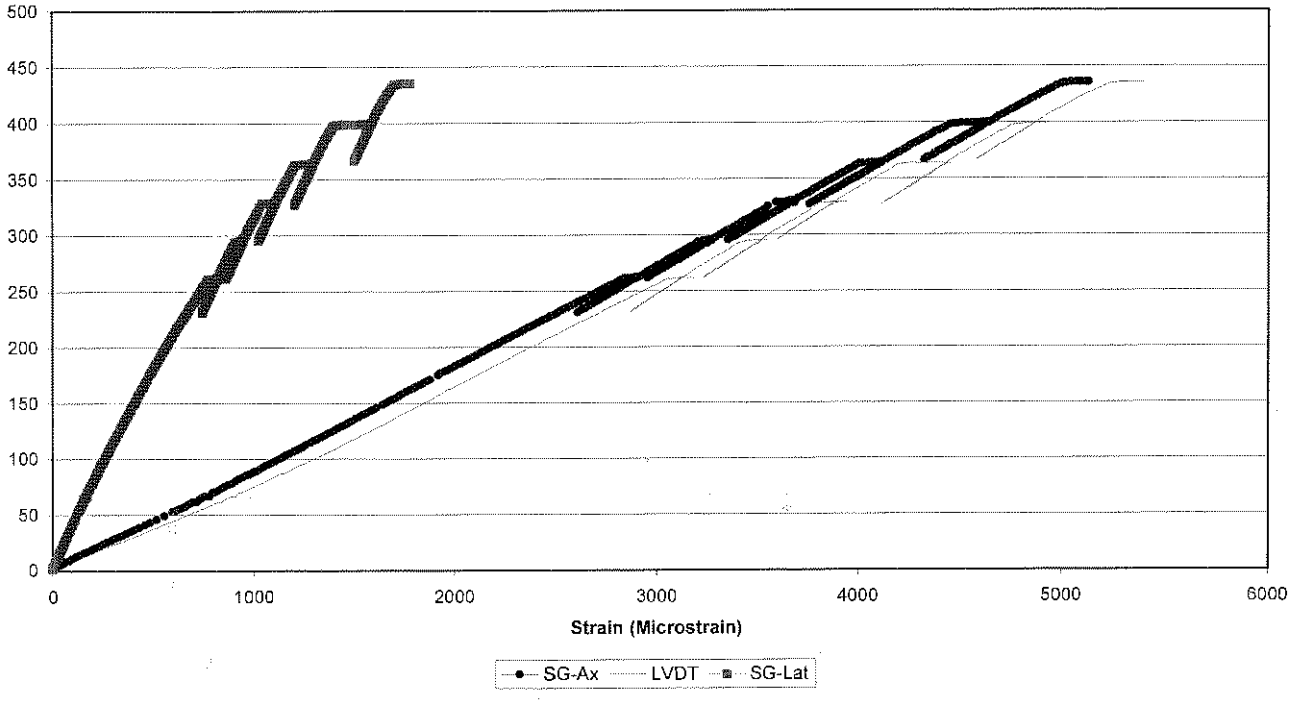

Strain vs Time
1640-53

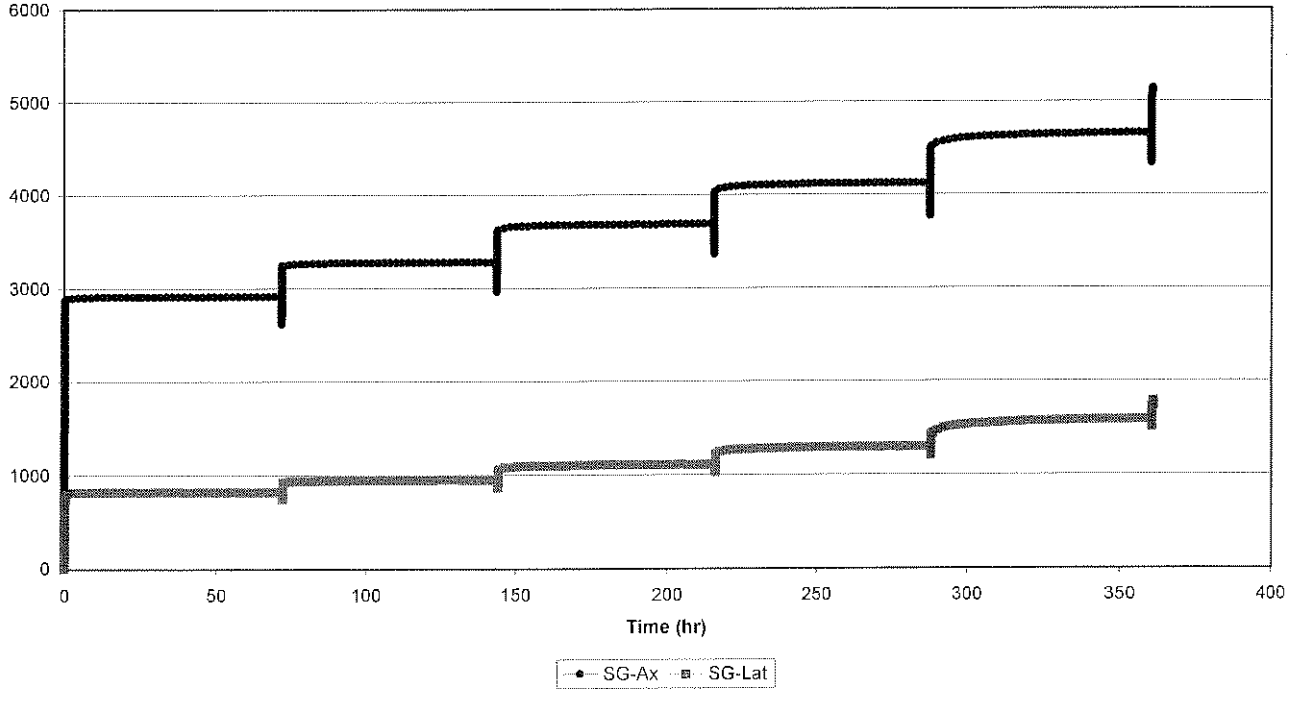

Ventersdorp Lava

Strain vs Time
1640-53 Cycle 1

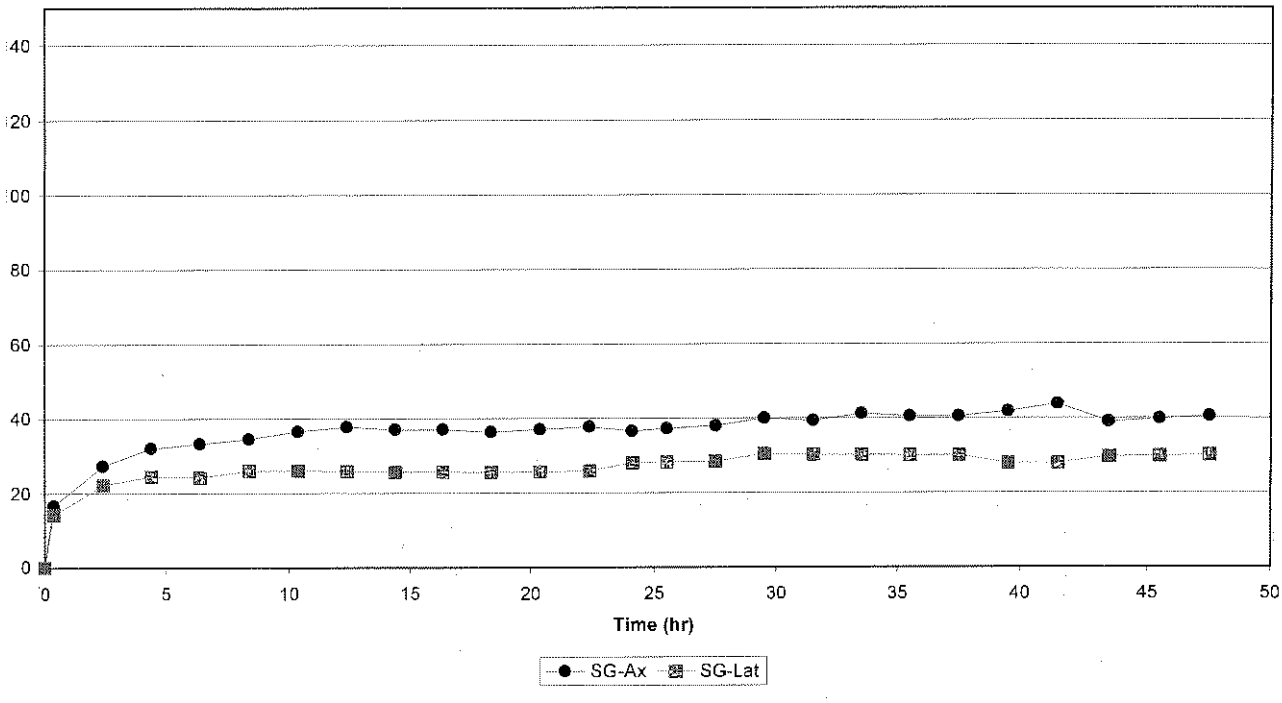

Strain vs Time
1640-53 Cycle 2

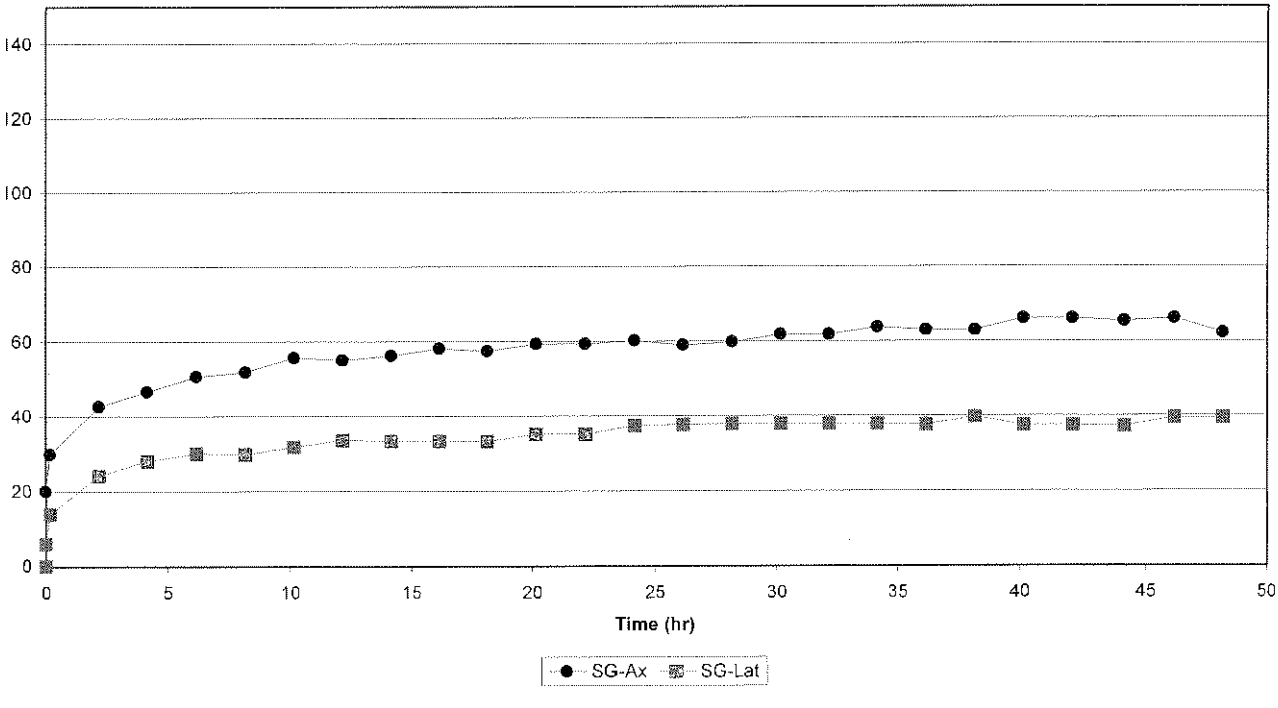

Ventersdorp Lava

Strain vs Time
1640-53 Cycle 3

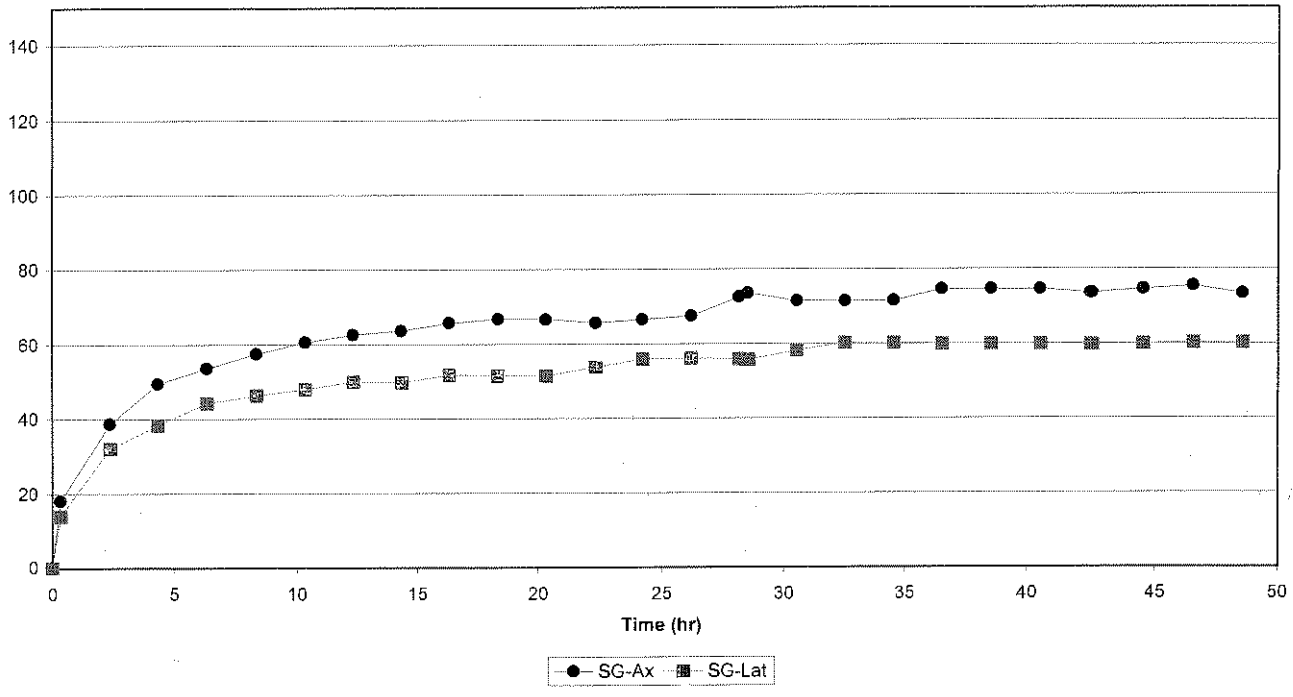

Strain vs Time
1640-53 Cycle 4

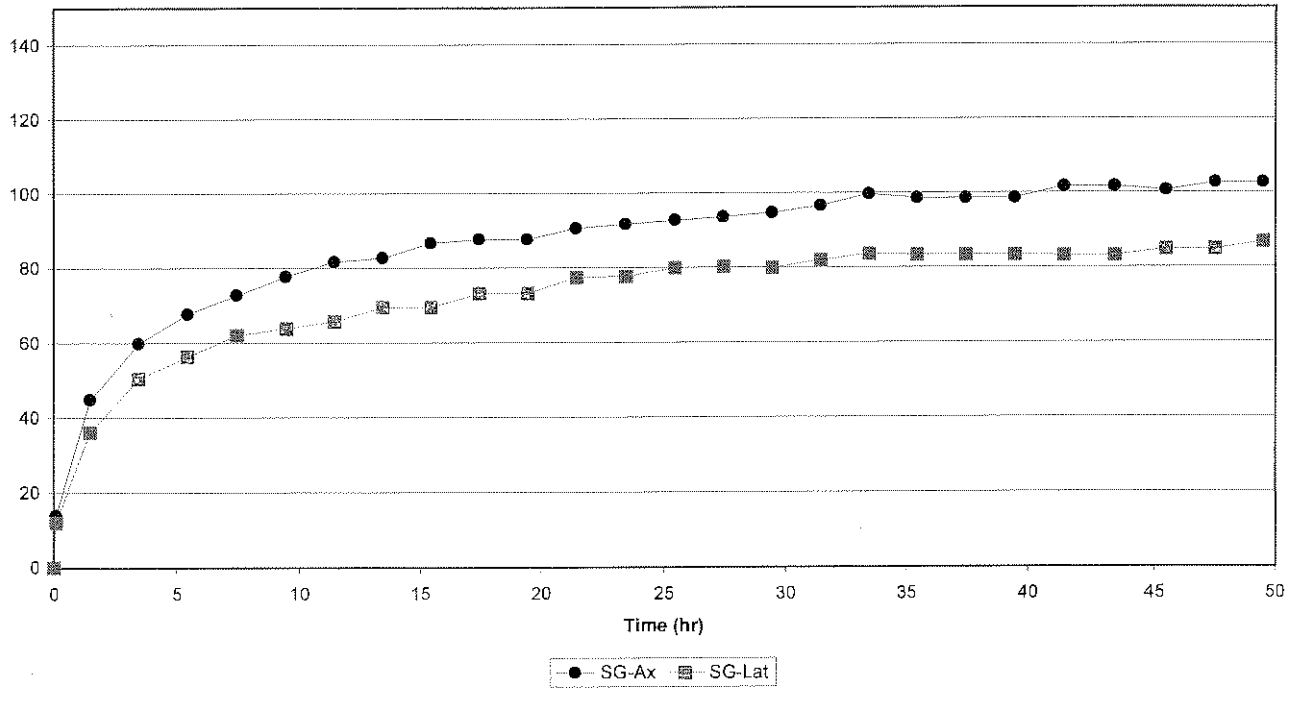

Ventersdorp Lava

Strain vs Time
1640-53 Cycle 5

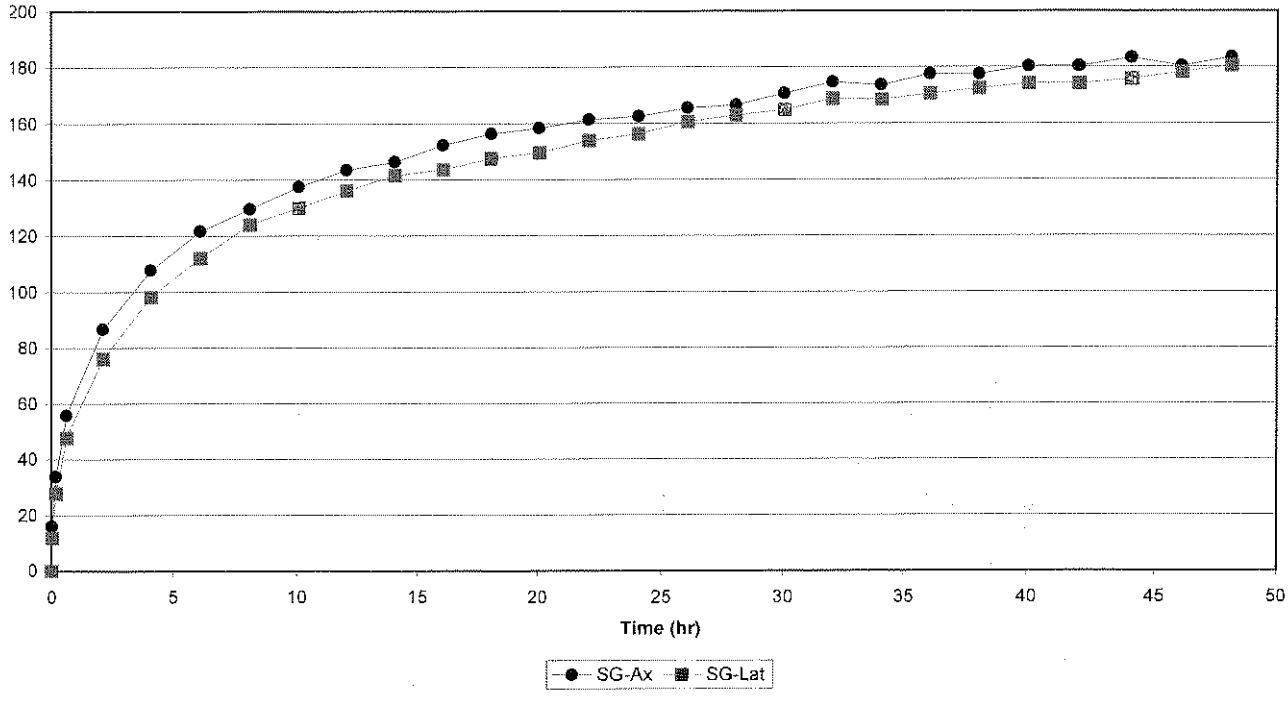

Strain vs Time
1640-53 Cycle 6

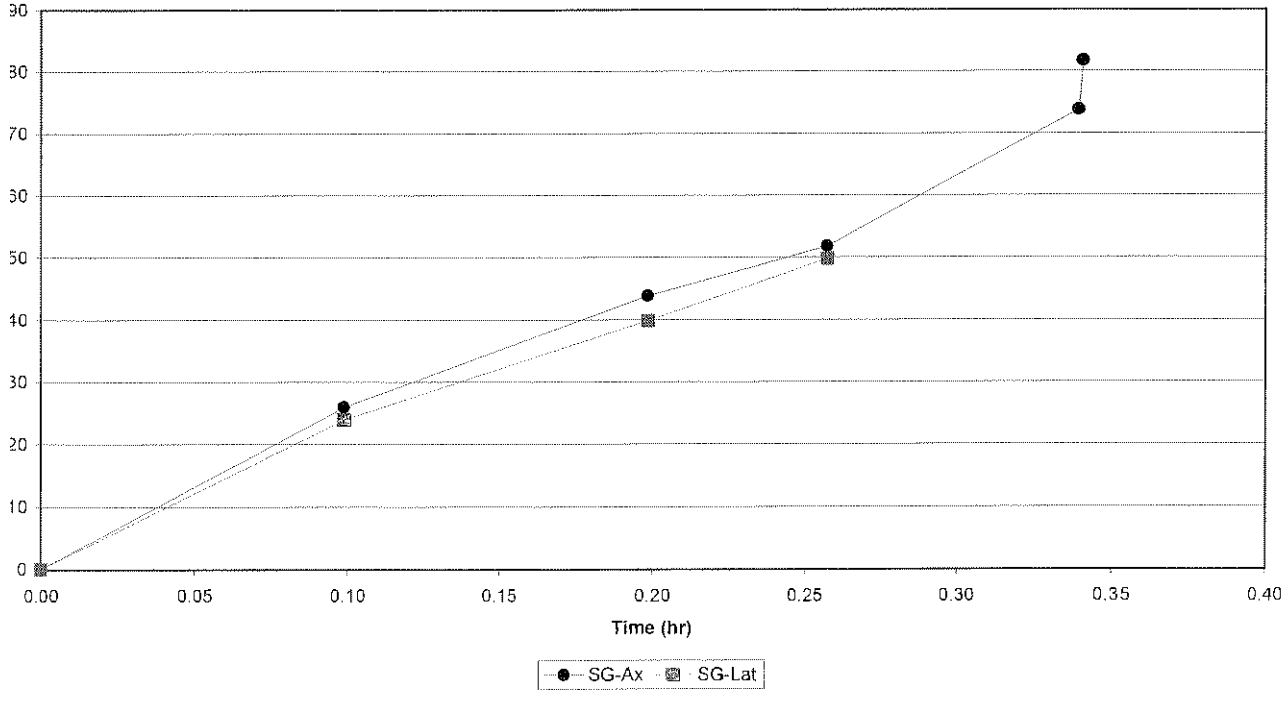

Ventersdorp Lava

Cumulative Strain vs Stress
1640-53

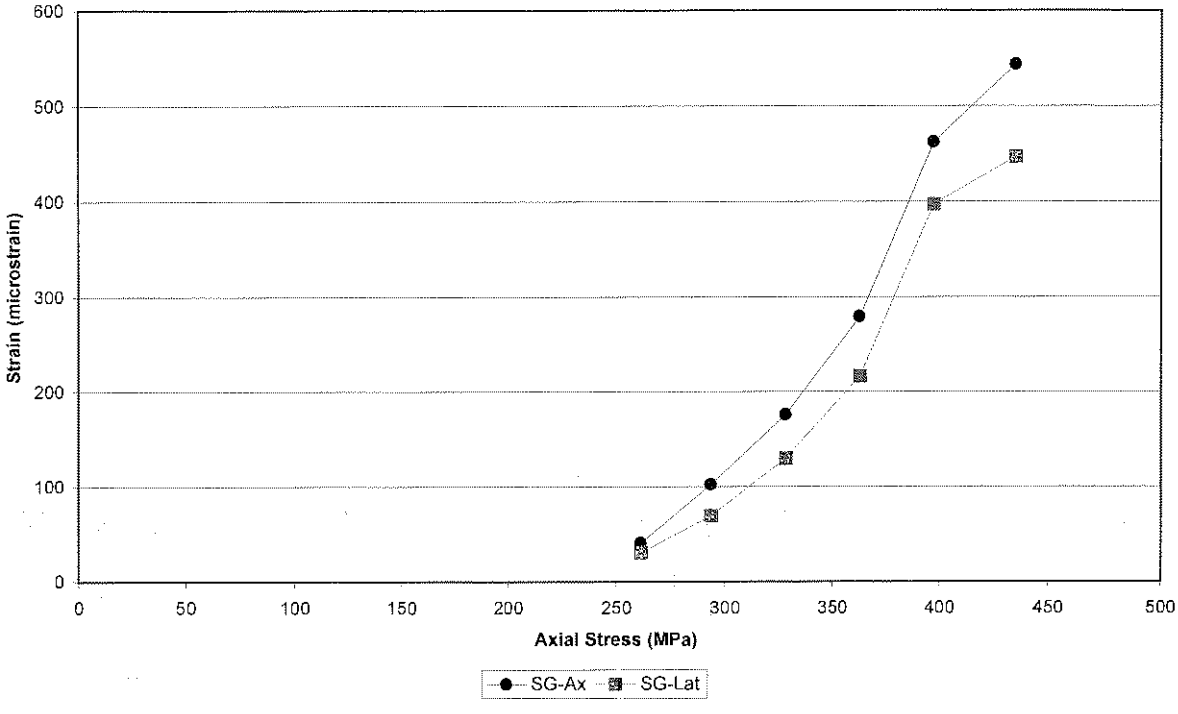

Creep rate vs Stress
1640-53

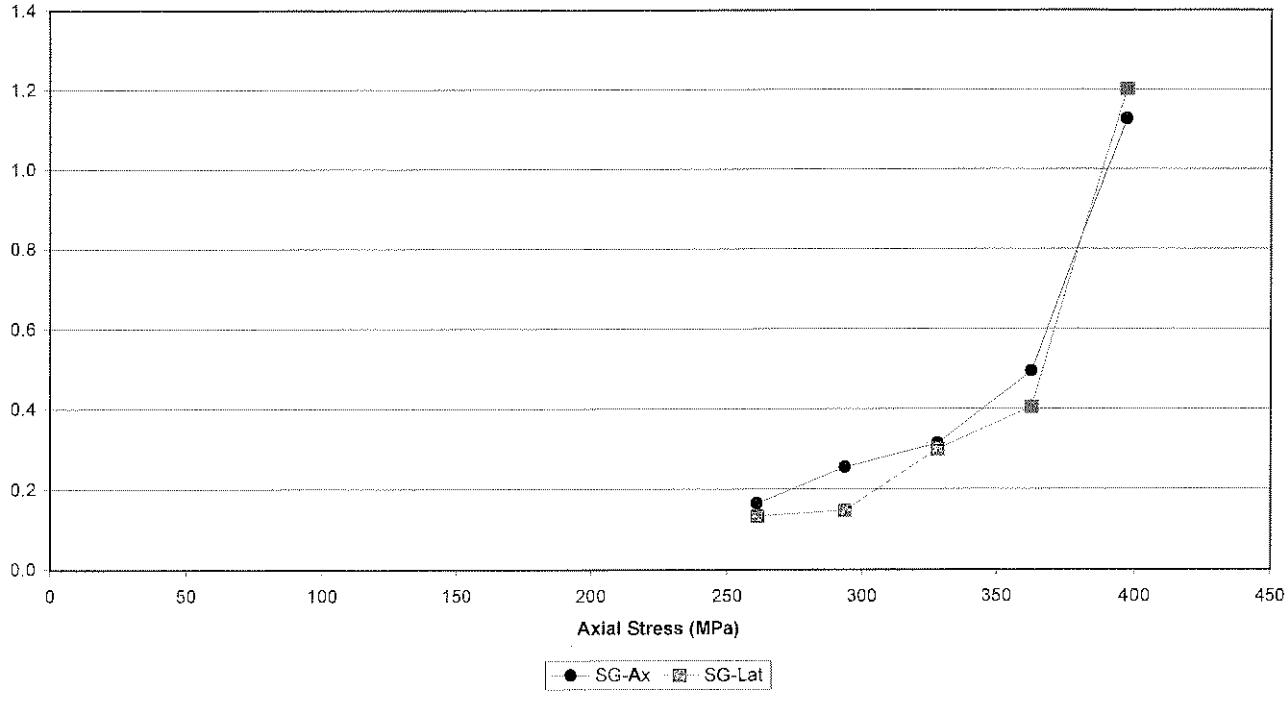

Ventersdorp Lava

Log Creeprate vs Log Stress
1640-53

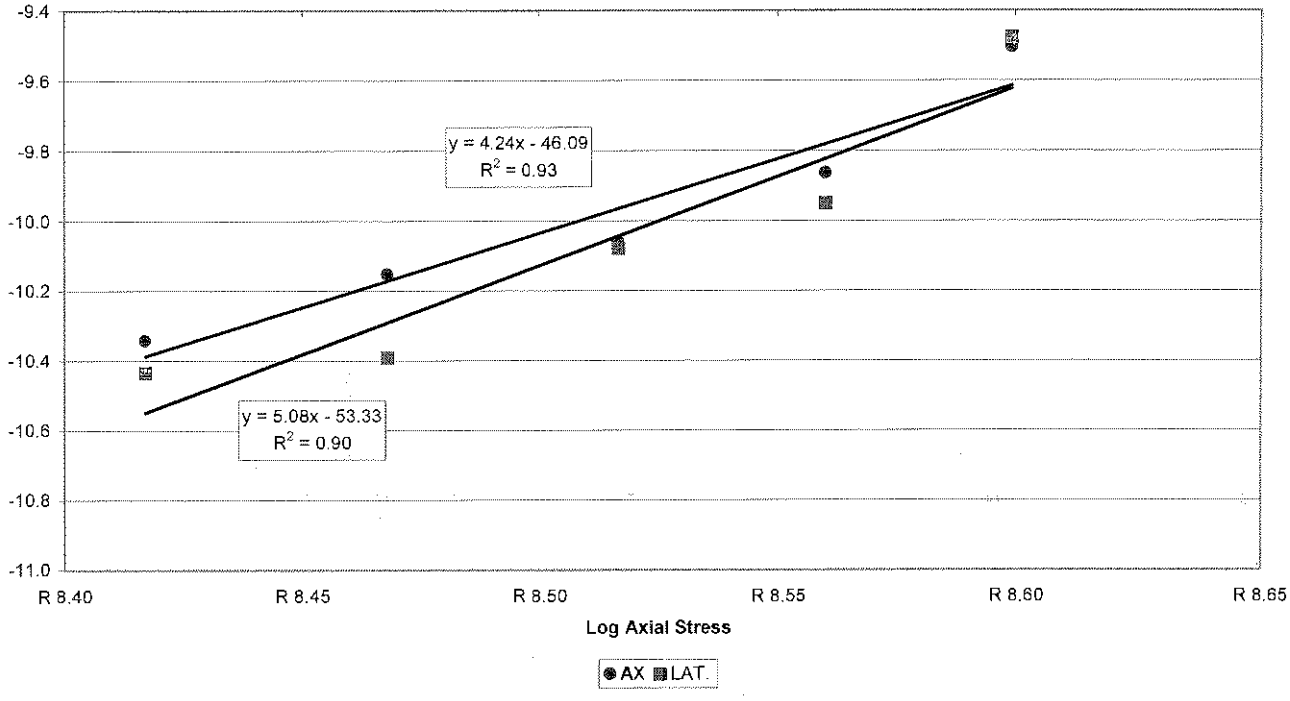

Ventersdorp Lava

Axial Stress vs Strain
1640-55

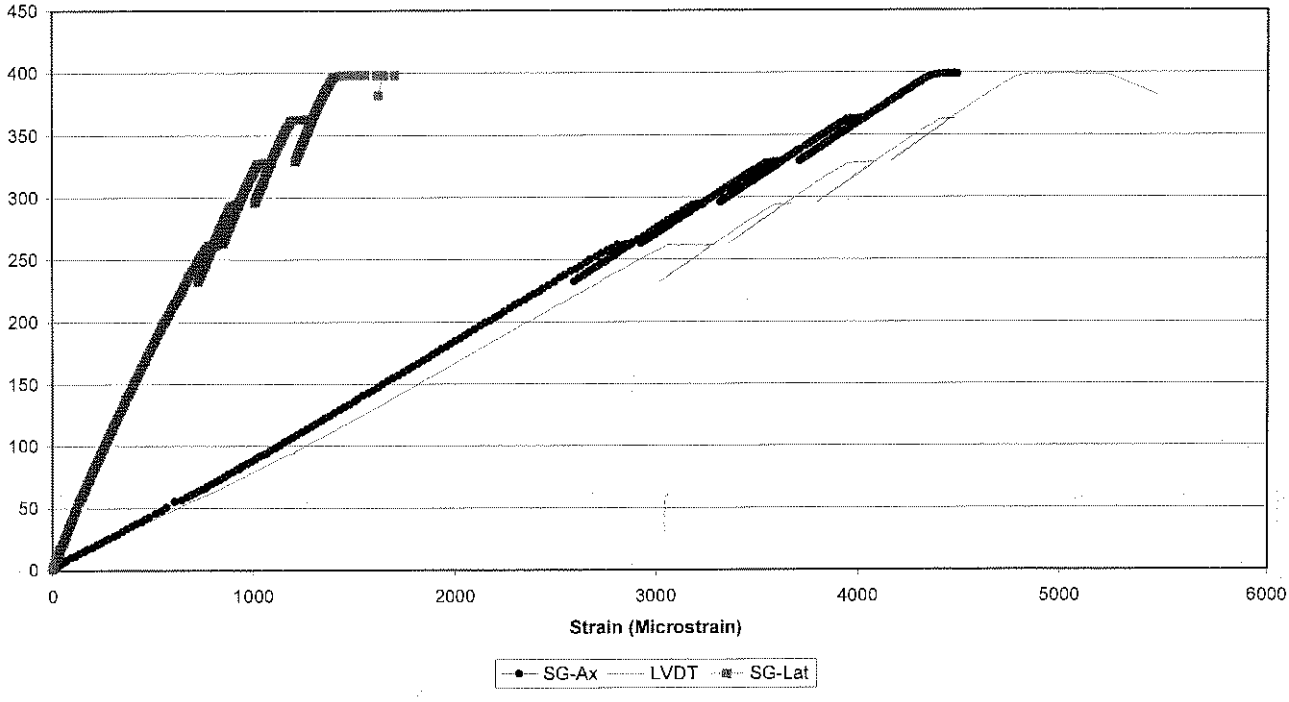

Strain vs Time
1640-55

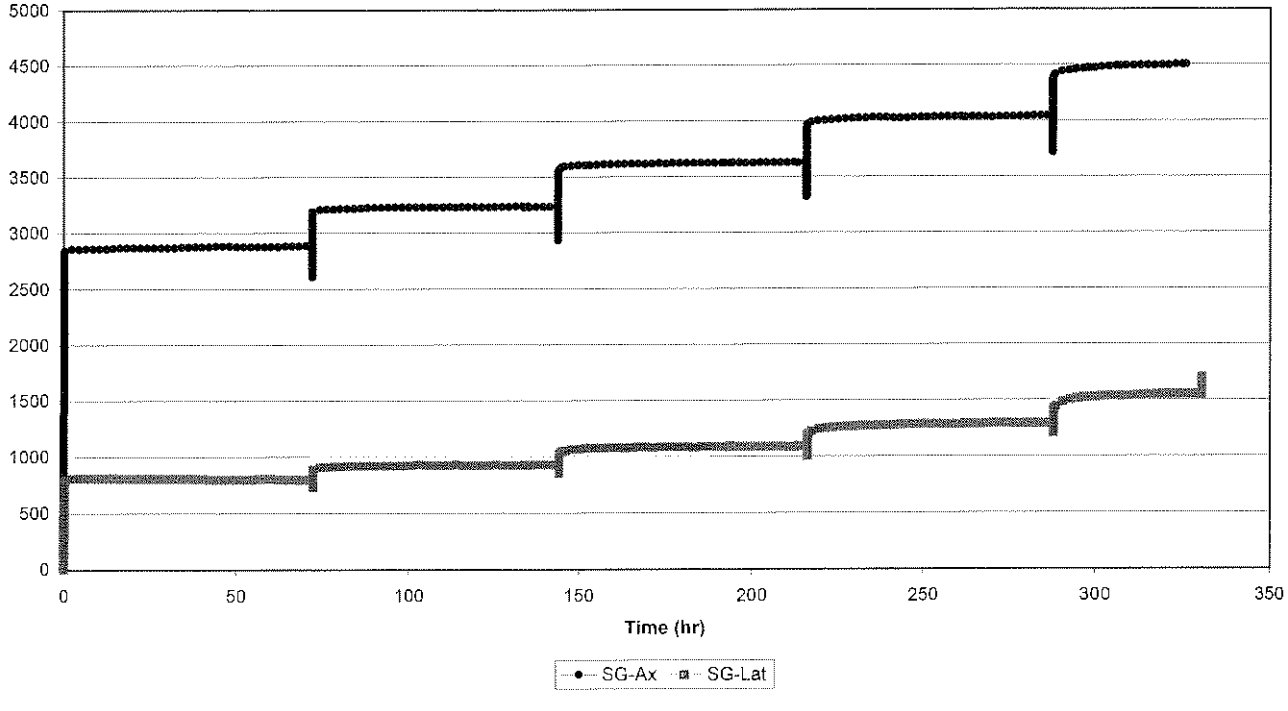

Ventersdorp Lava

Strain vs Time
1640-55 Cycle 1

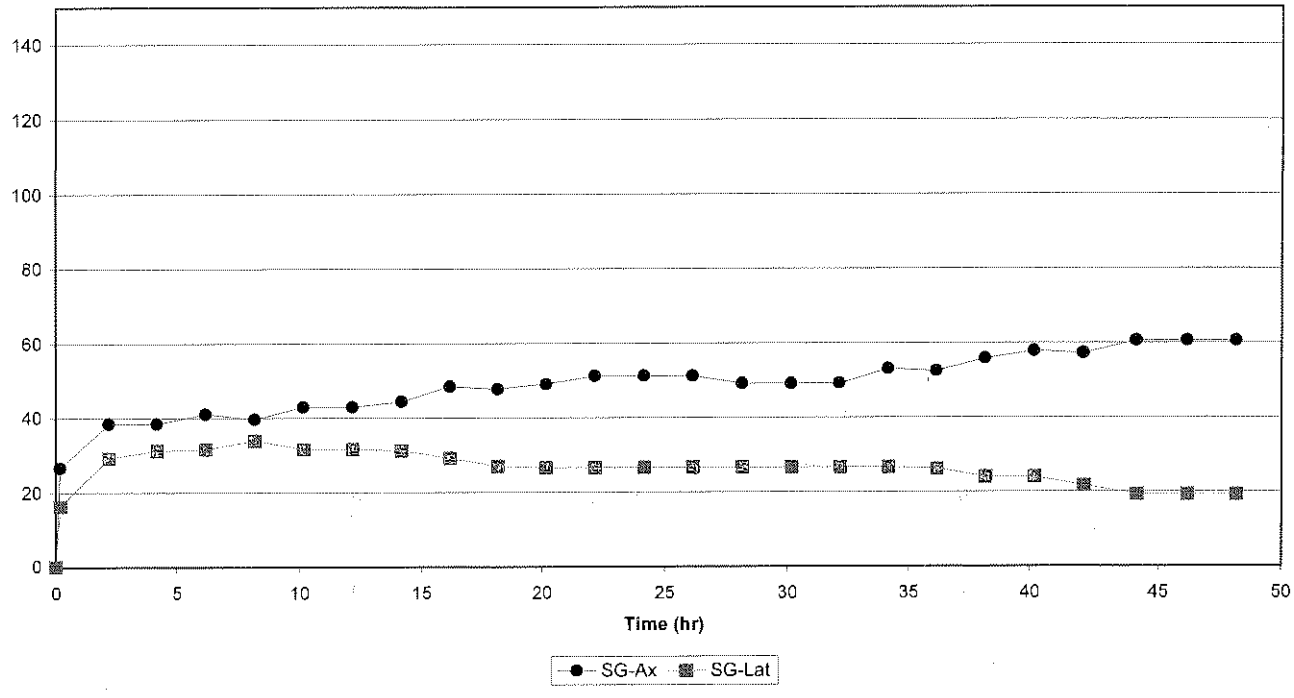

Strain vs Time
1640-55 Cycle 2

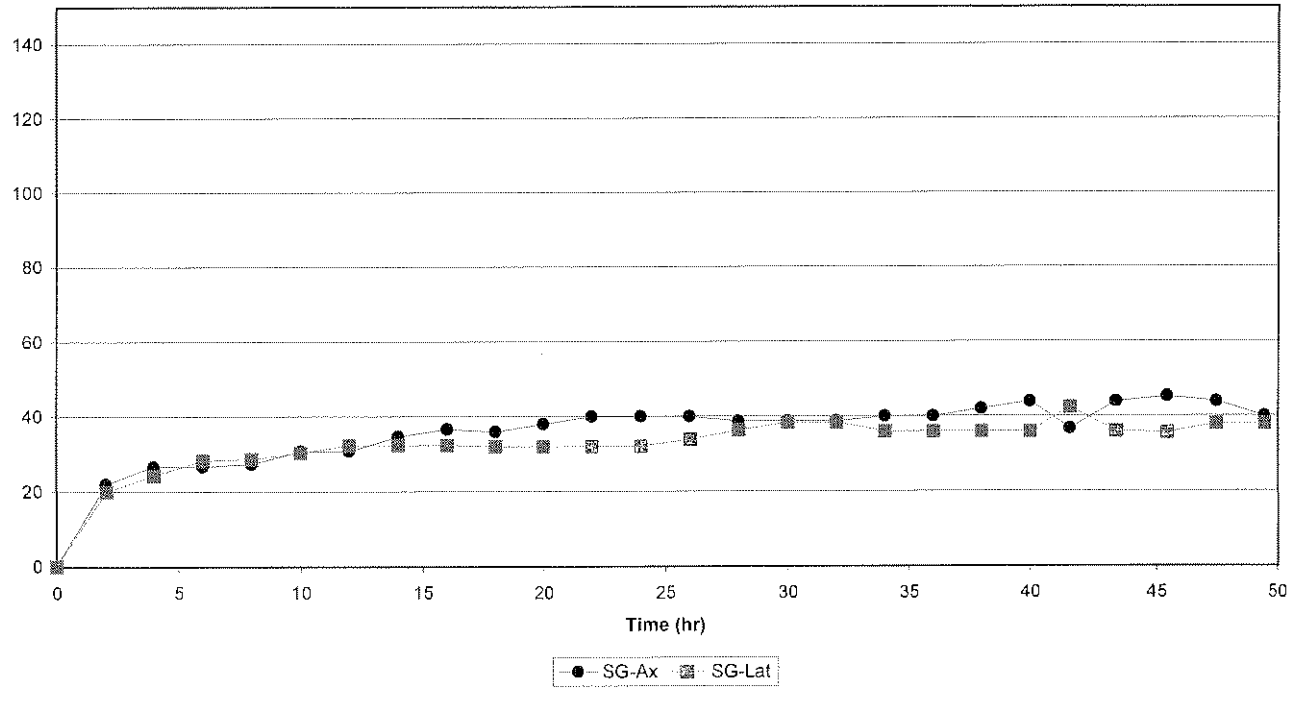

Ventersdorp Lava

Strain vs Time
1640-55 Cycle 3

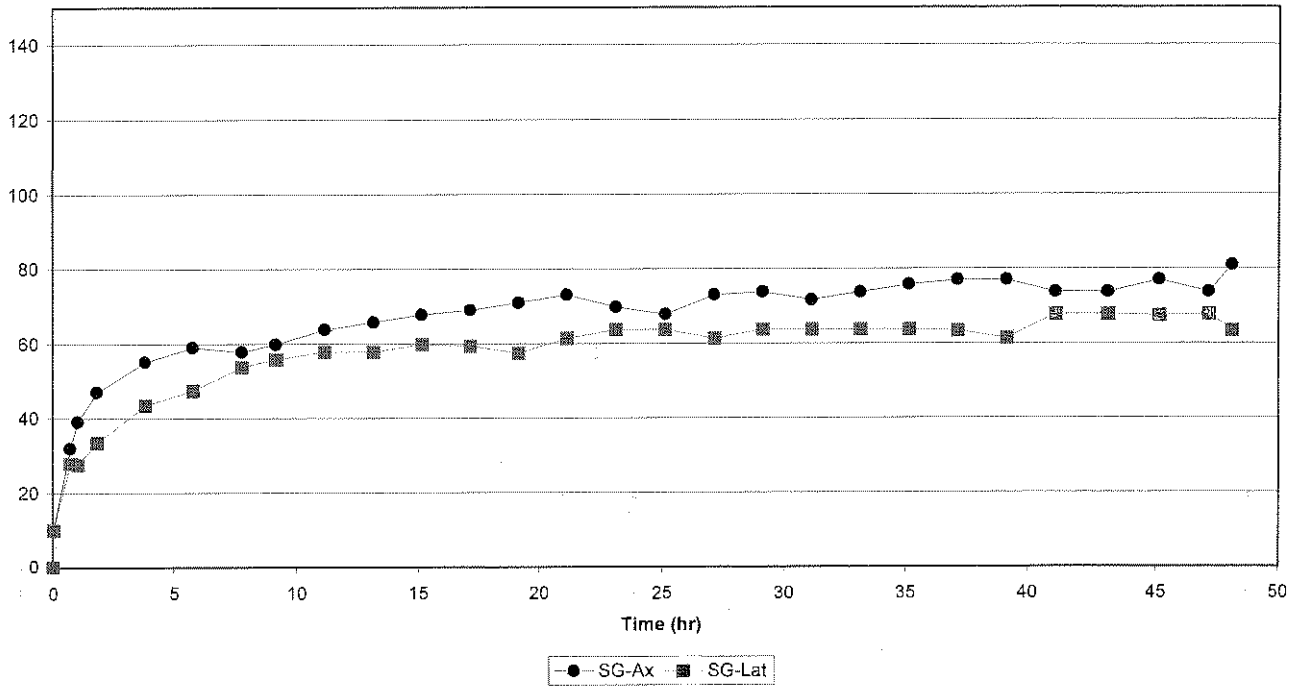

Strain vs Time
1640-55 Cycle 4

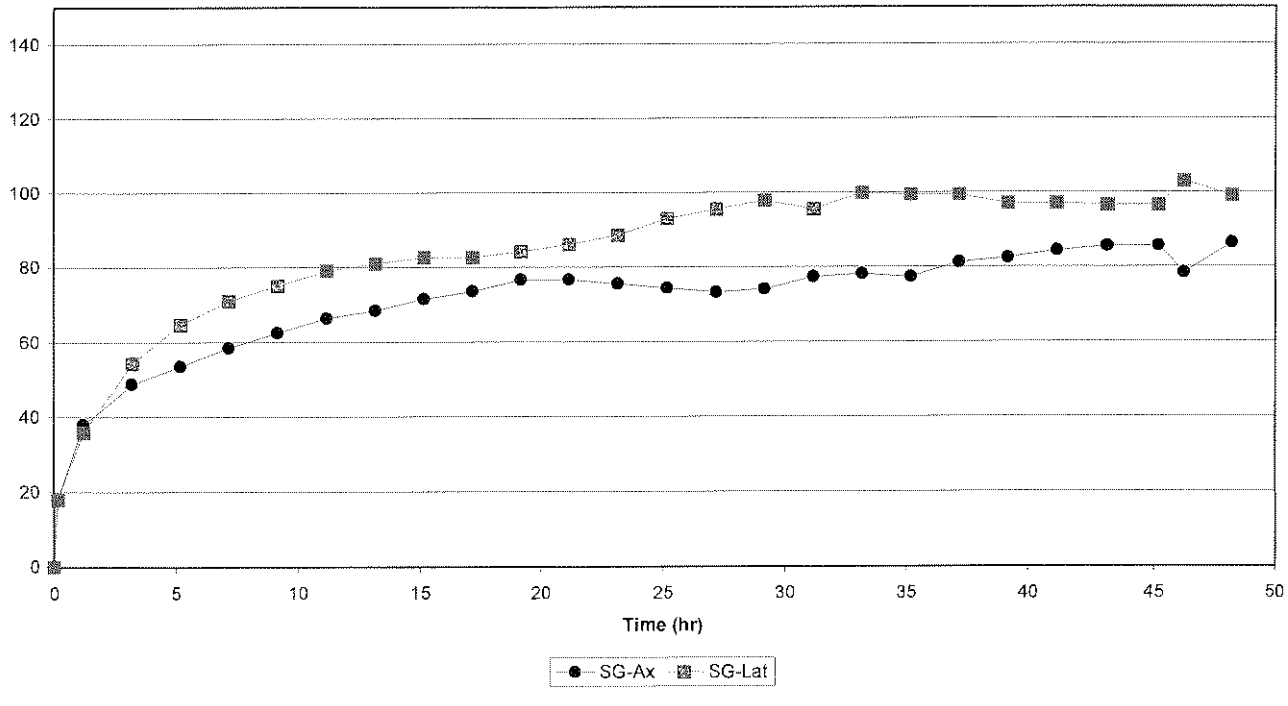

Ventersdorp Lava

Strain vs Time
1640-55 Cycle 5

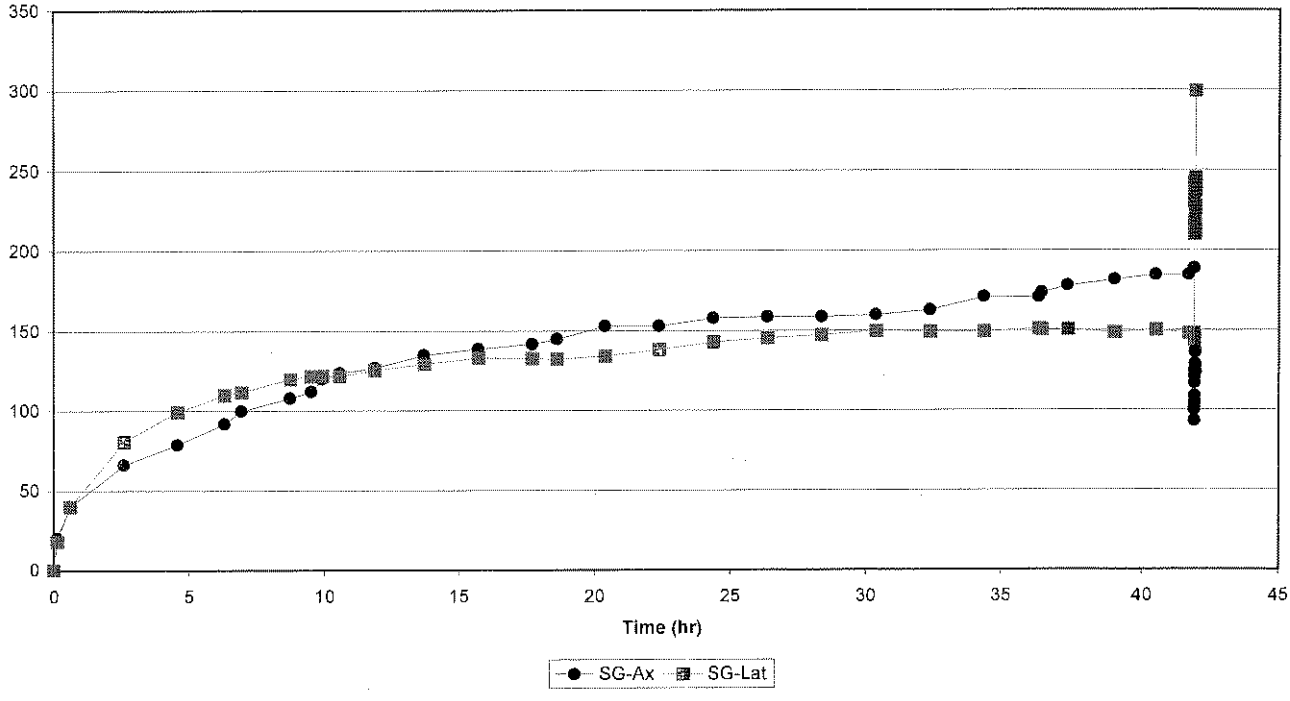

Cumulative Strain vs Stress
1640-55

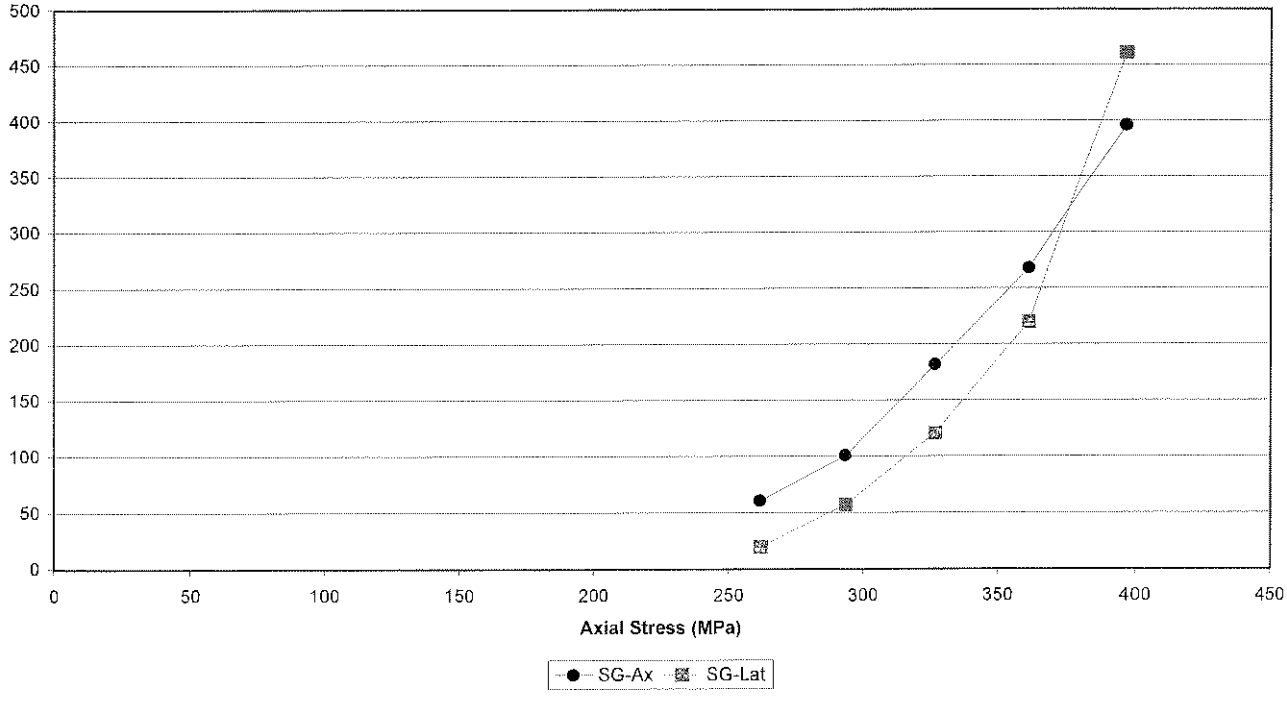

Ventersdorp Lava

Creep rate vs Stress
1640-55

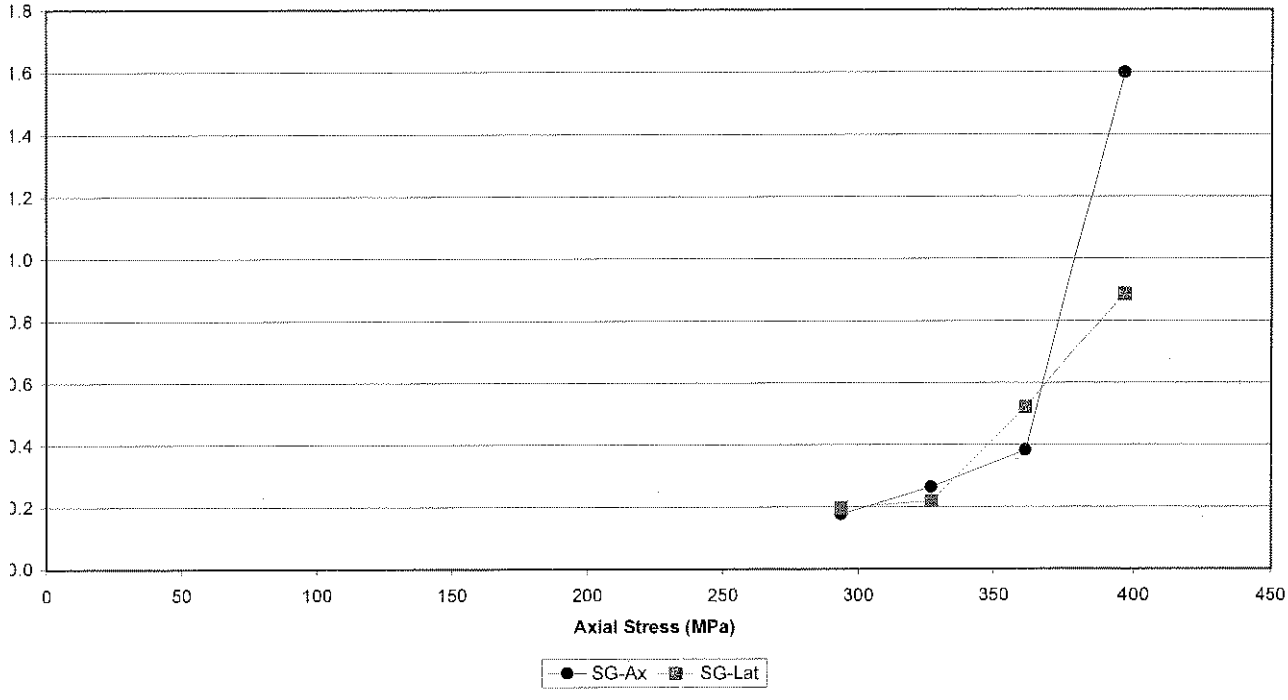

Log Creeprate vs Log Stress
1640-55

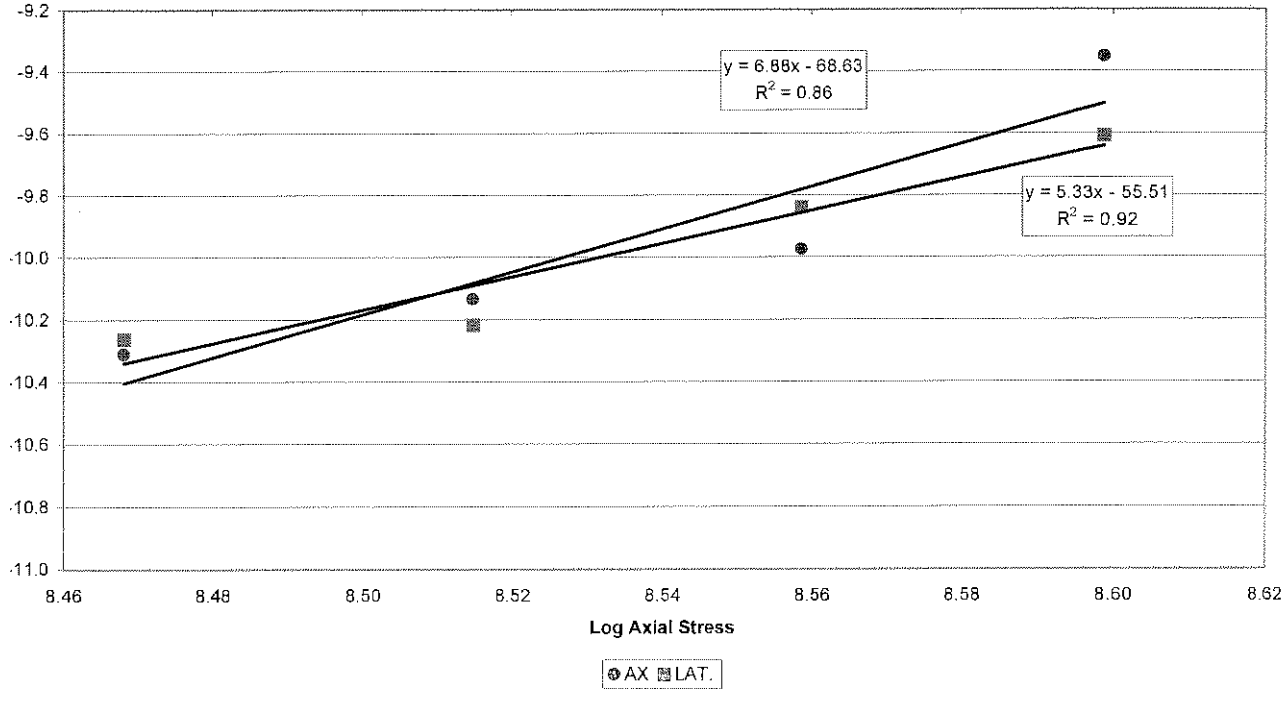

Ventersdorp Lava

Axial Stress vs Strain
1640-63

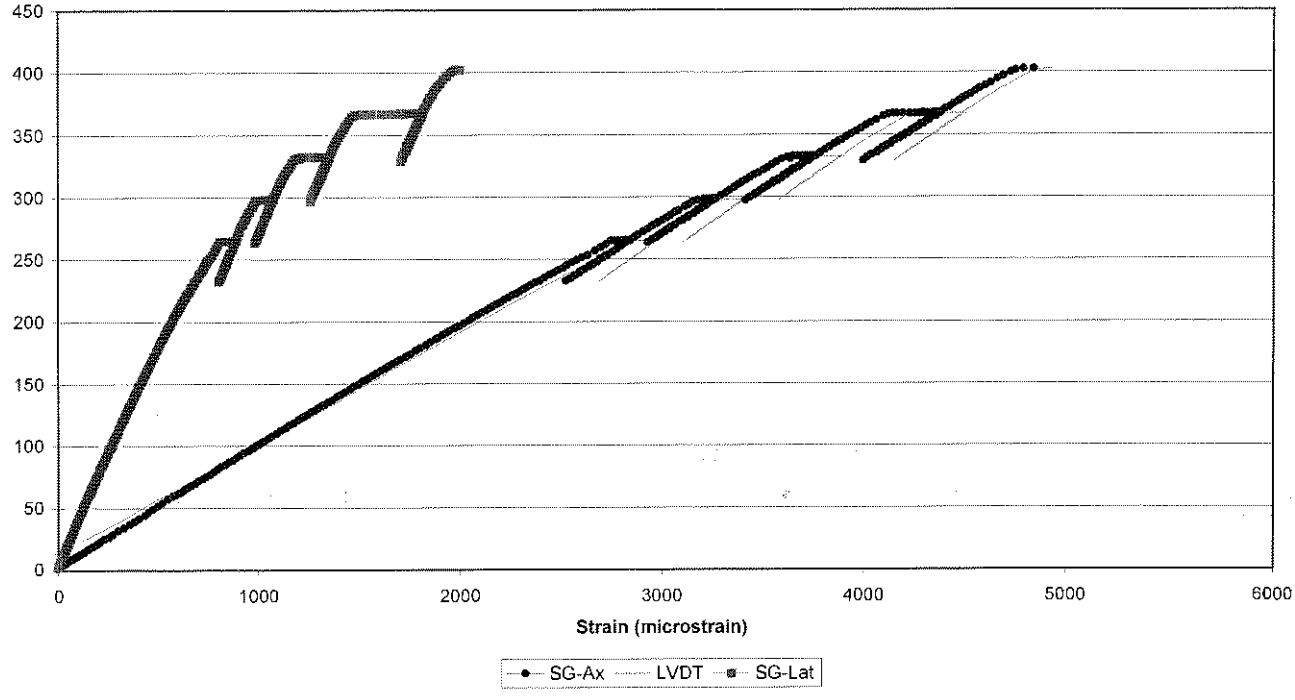

Strain vs Time
1640-63

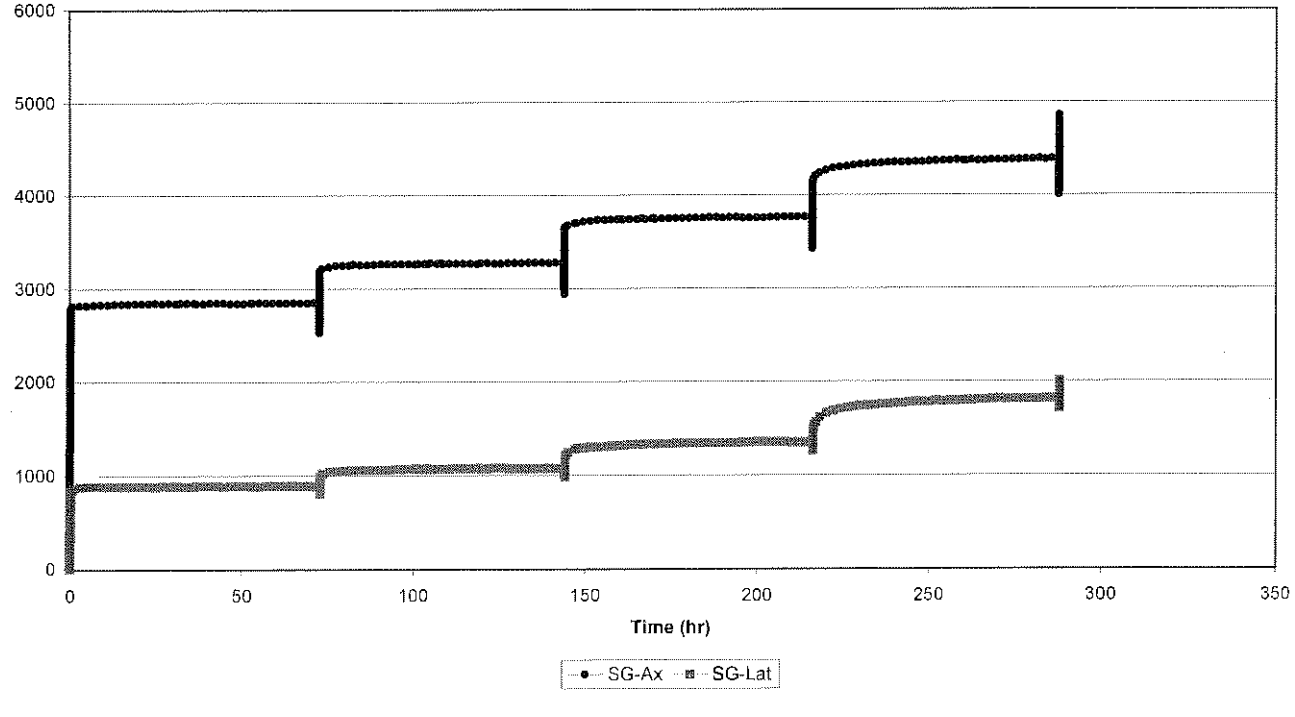

Ventersdorp Lava

Strain vs Time
1640-63 Cycle 1

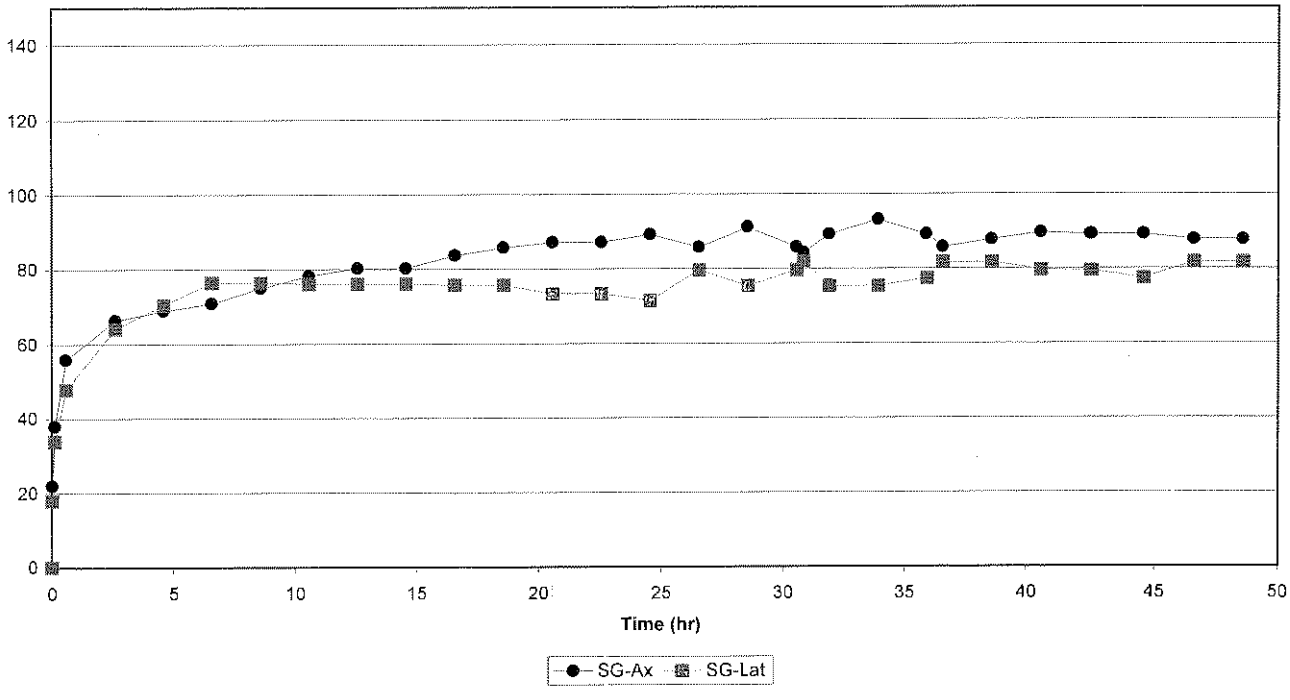

Strain vs Time
1640-63 Cycle 2

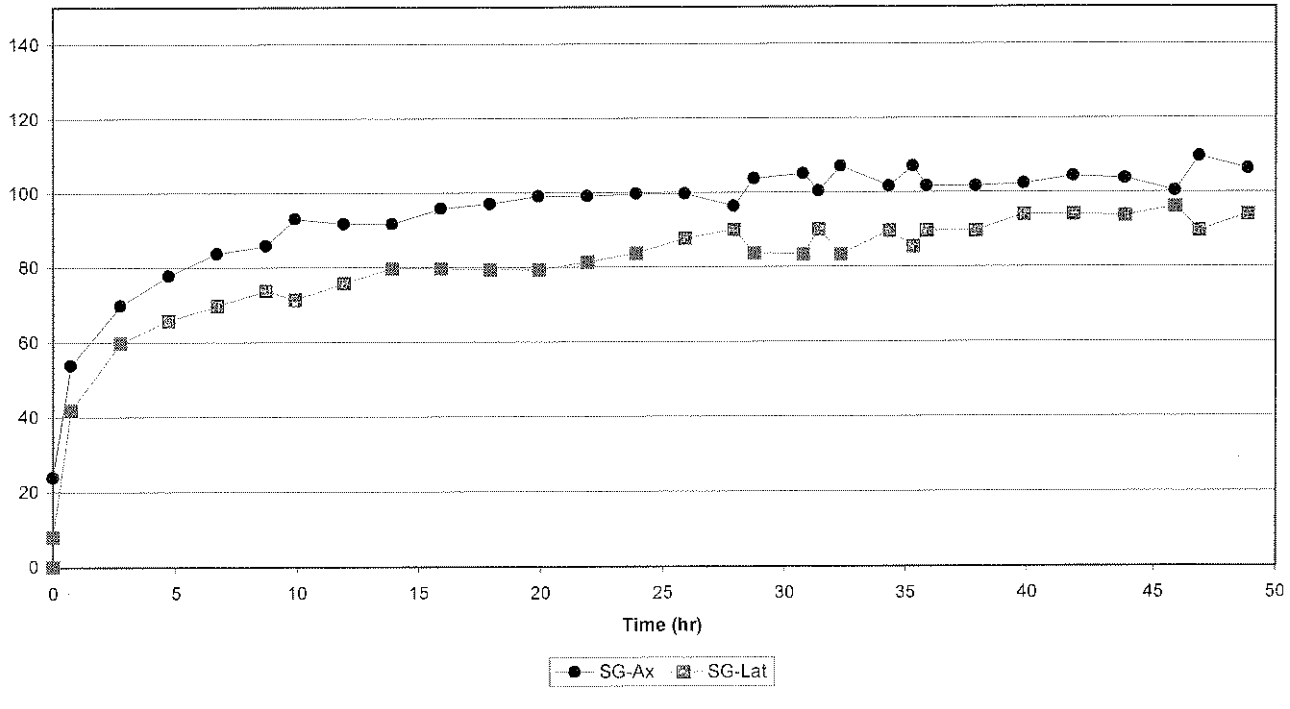

Ventersdorp Lava

Strain vs Time
1640-63 Cycle 3

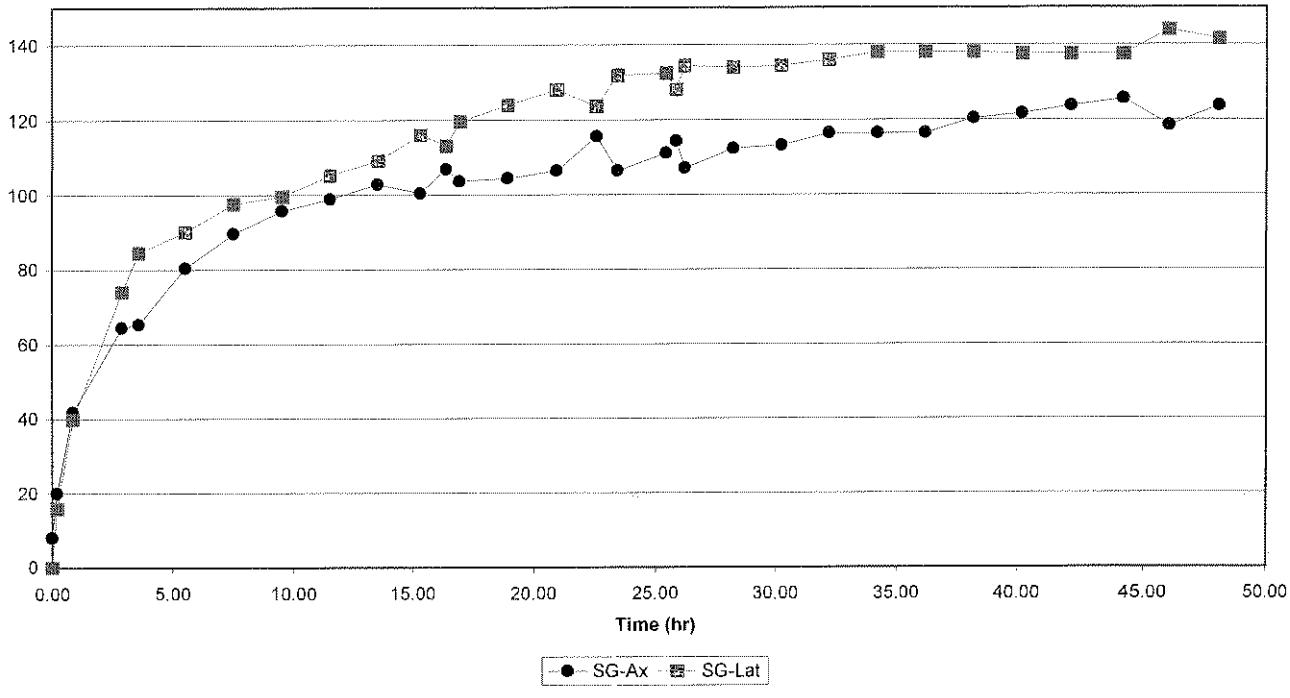

Strain vs Time
1640-63 Cycle 4

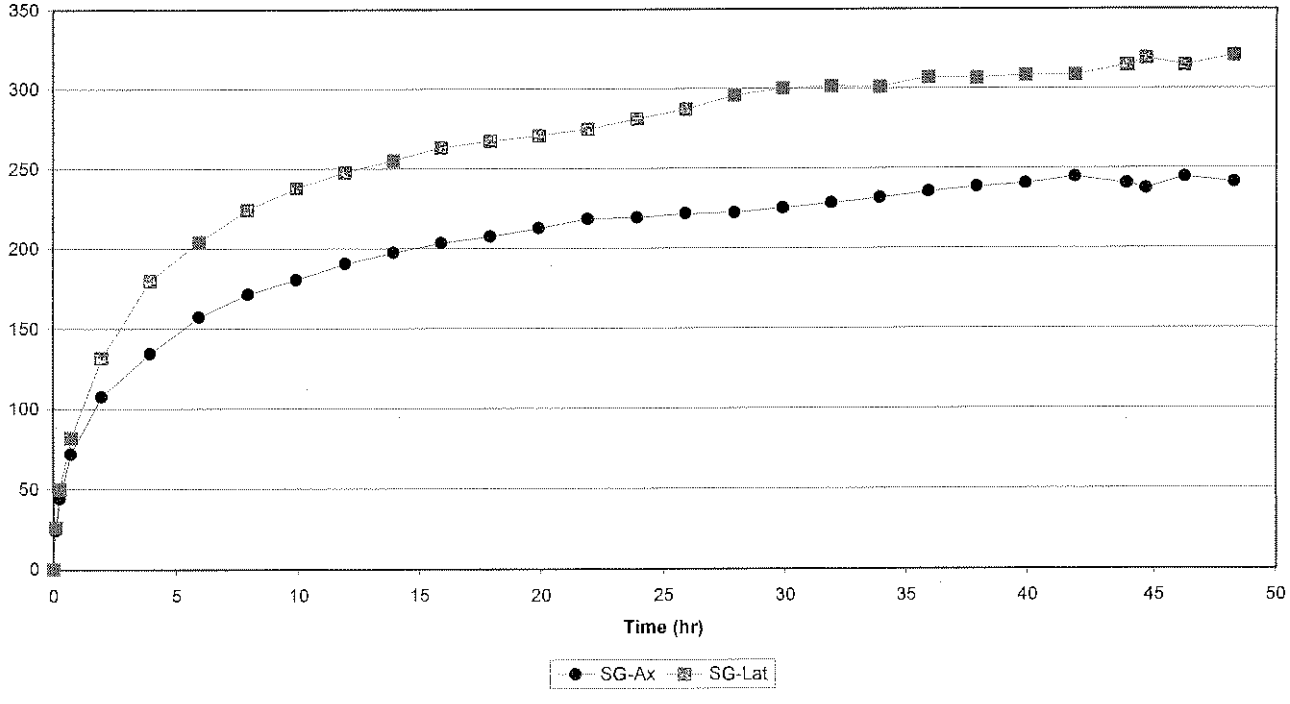

Ventersdorp Lava

Strain vs Time
1640-63 Cycle 5

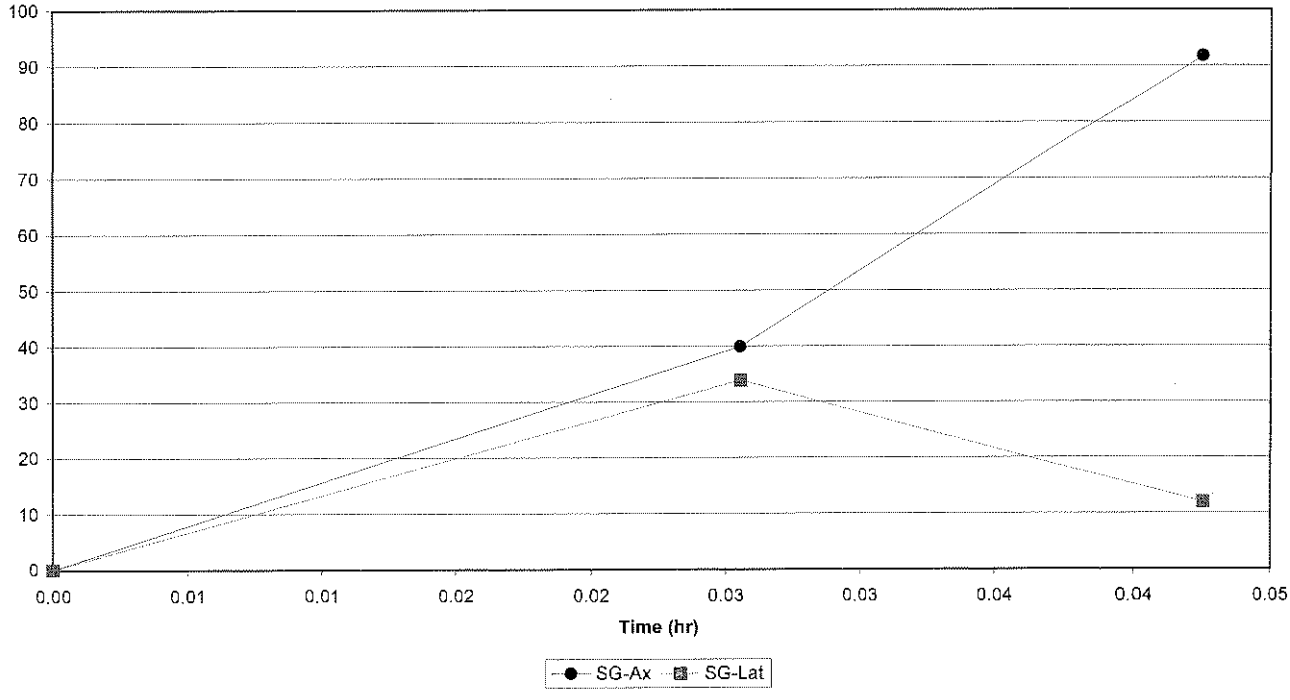

Cumulative Strain vs Stress
1640-63

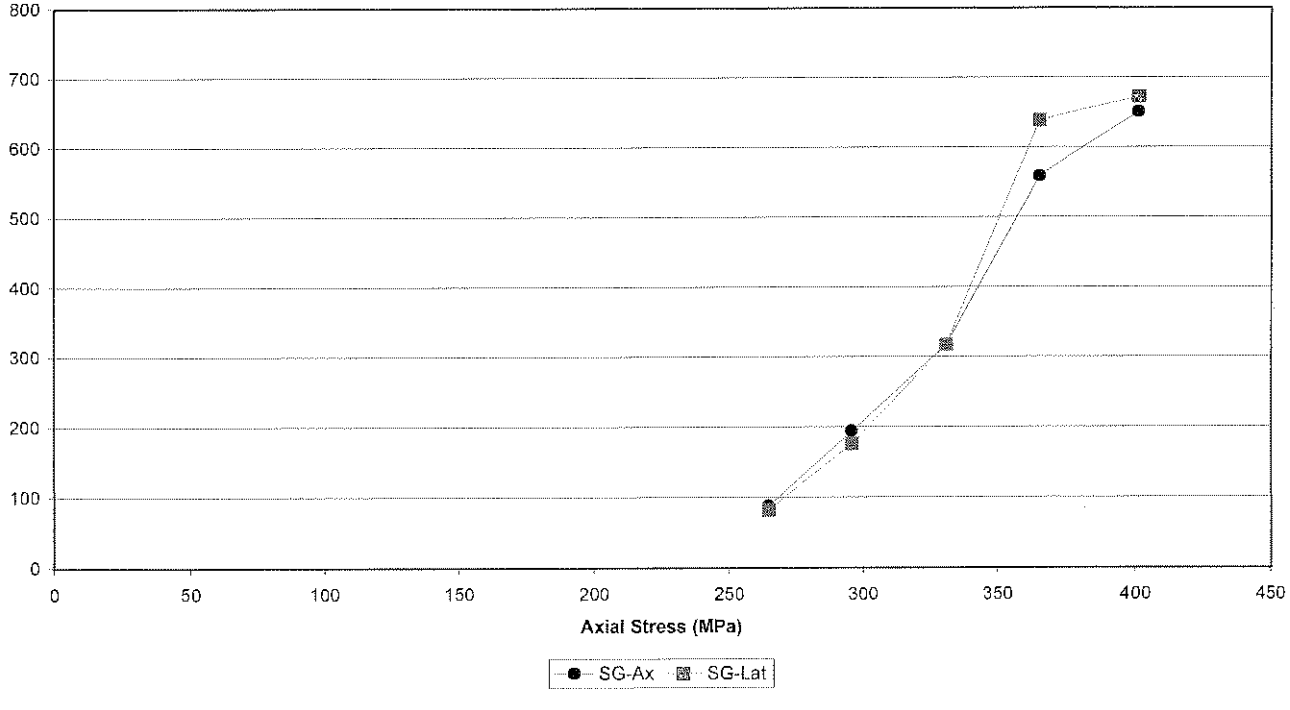

Ventersdorp Lava

Creep rate vs Stress
1640-63

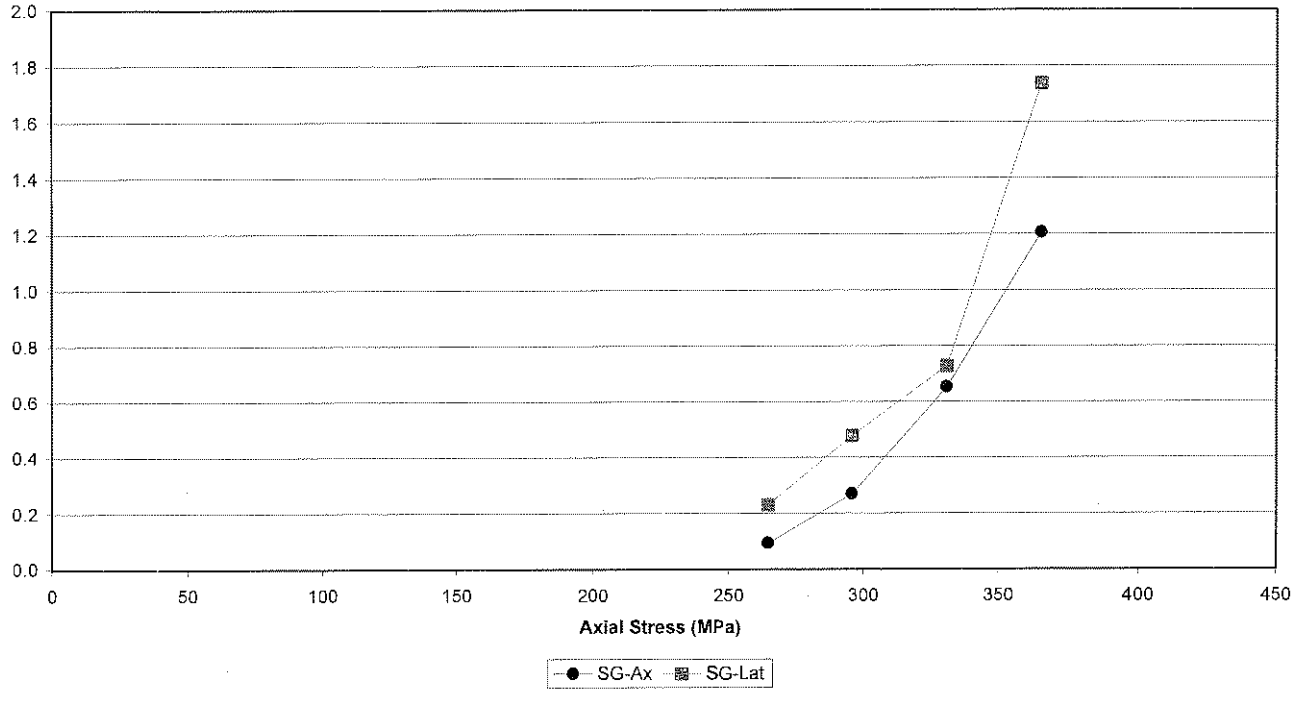

Log Creeprate vs Log Stress
1640-63

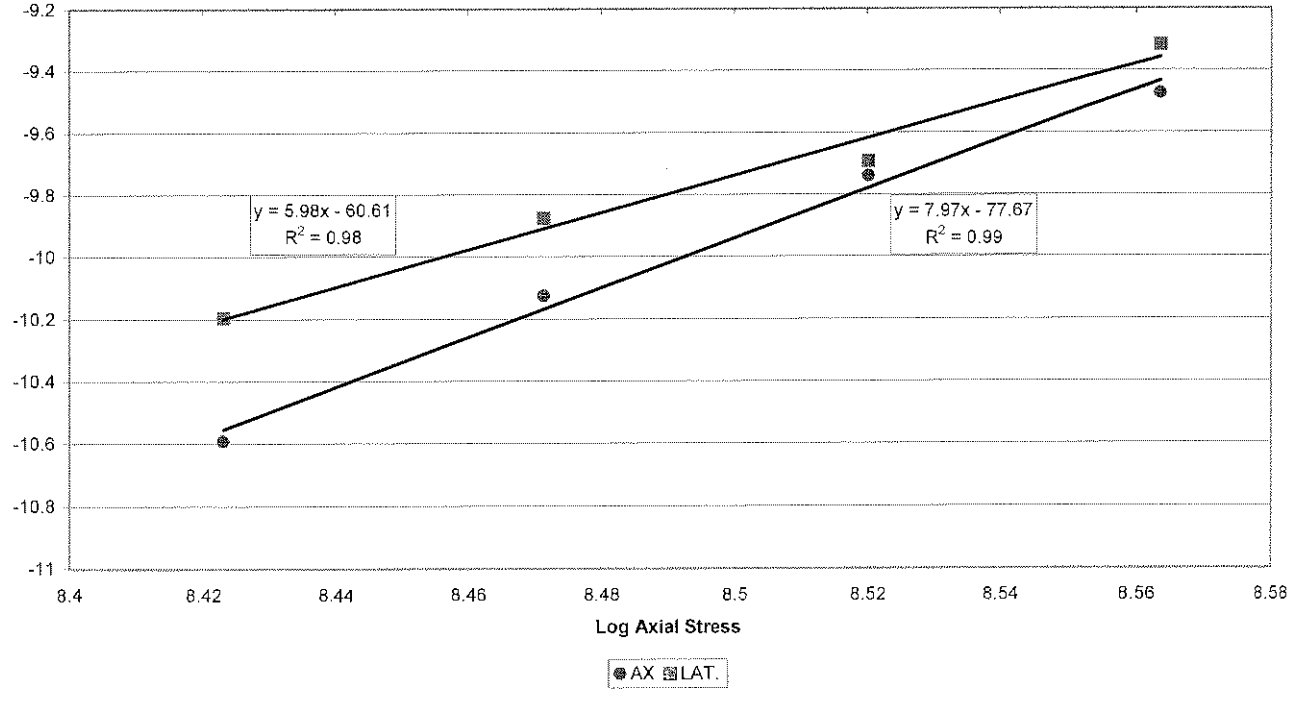

Elsburg Quartzite

Axial Stress vs Strain
2056-116

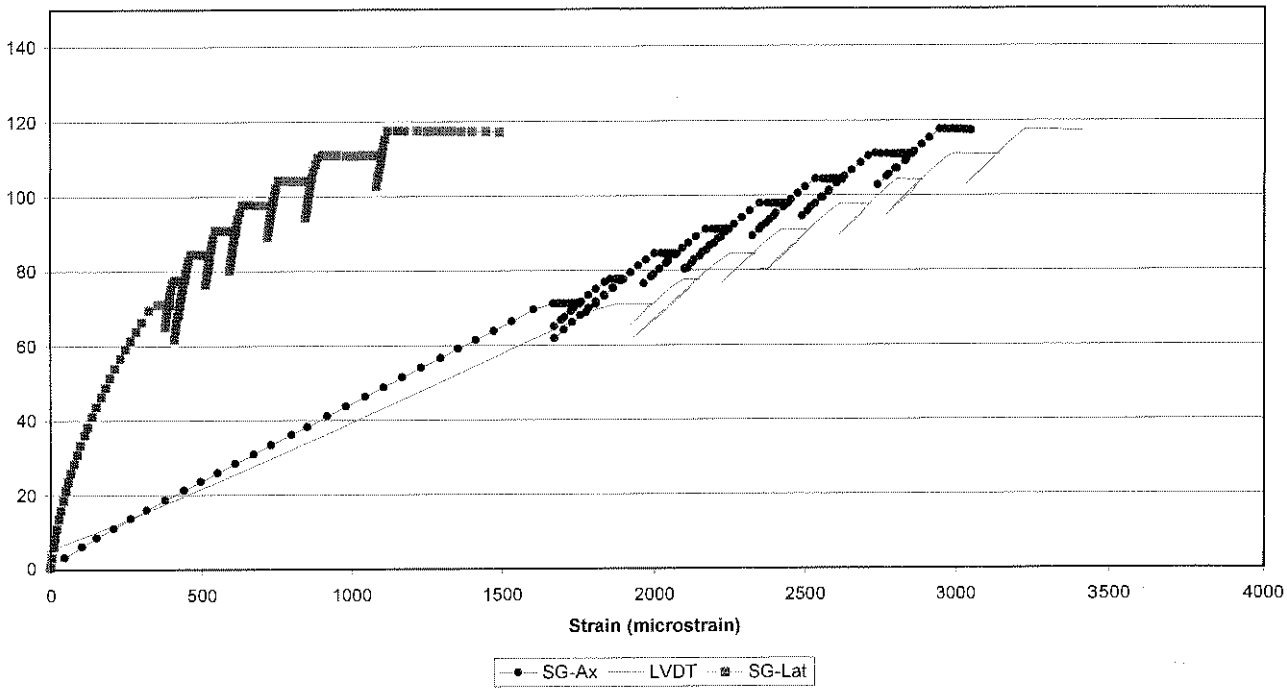

Strain vs Time
2056-116

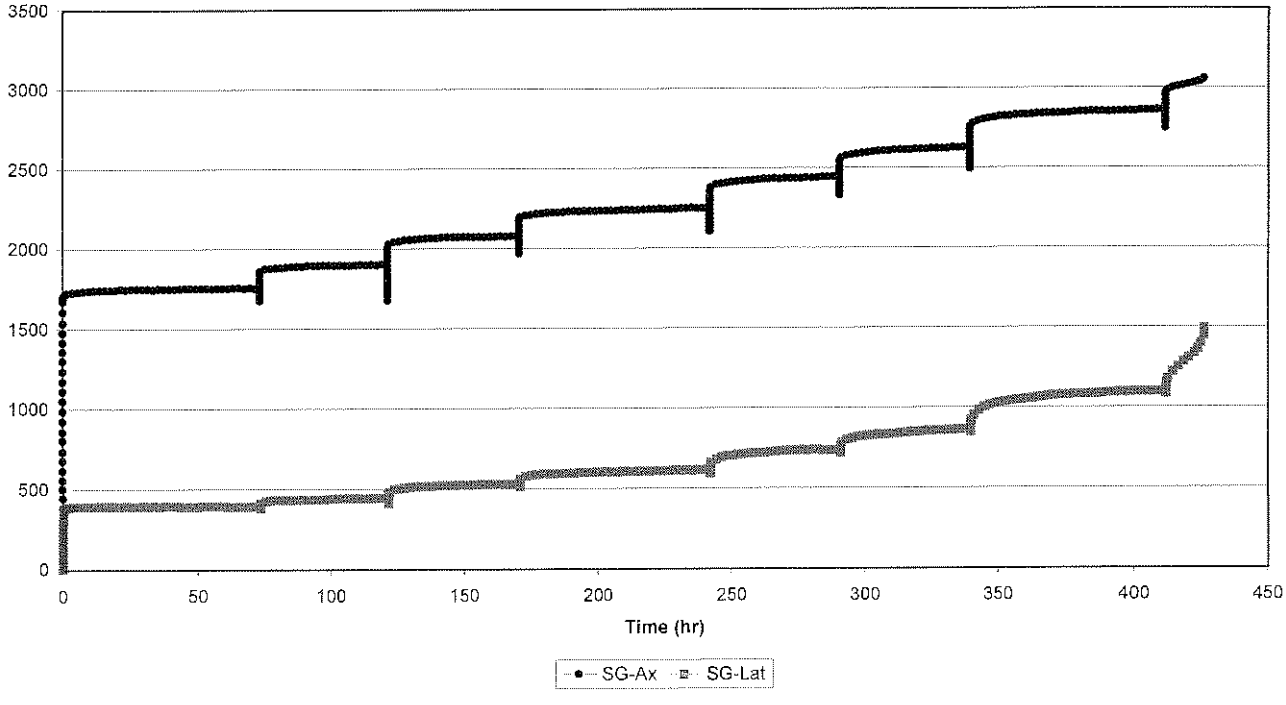

Elsburg Quartzite

Strain vs Time
2056-116 Cycle 1

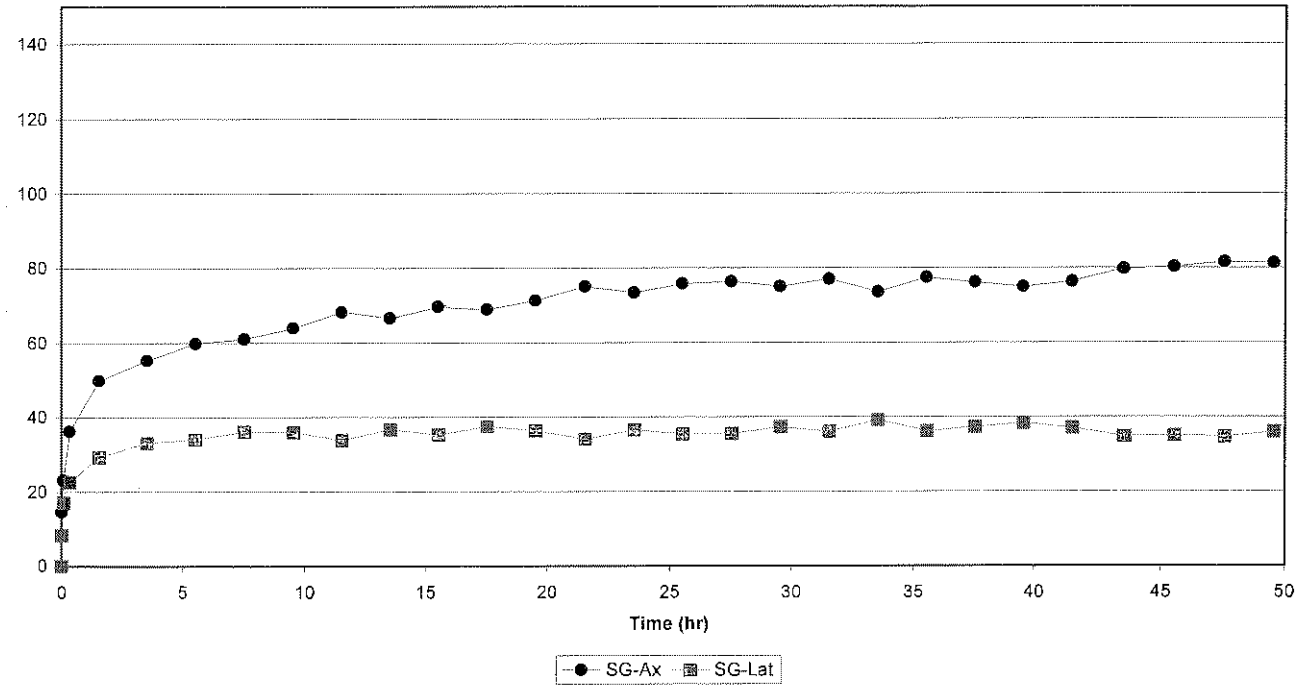

Strain vs Time
2056-116 Cycle 2

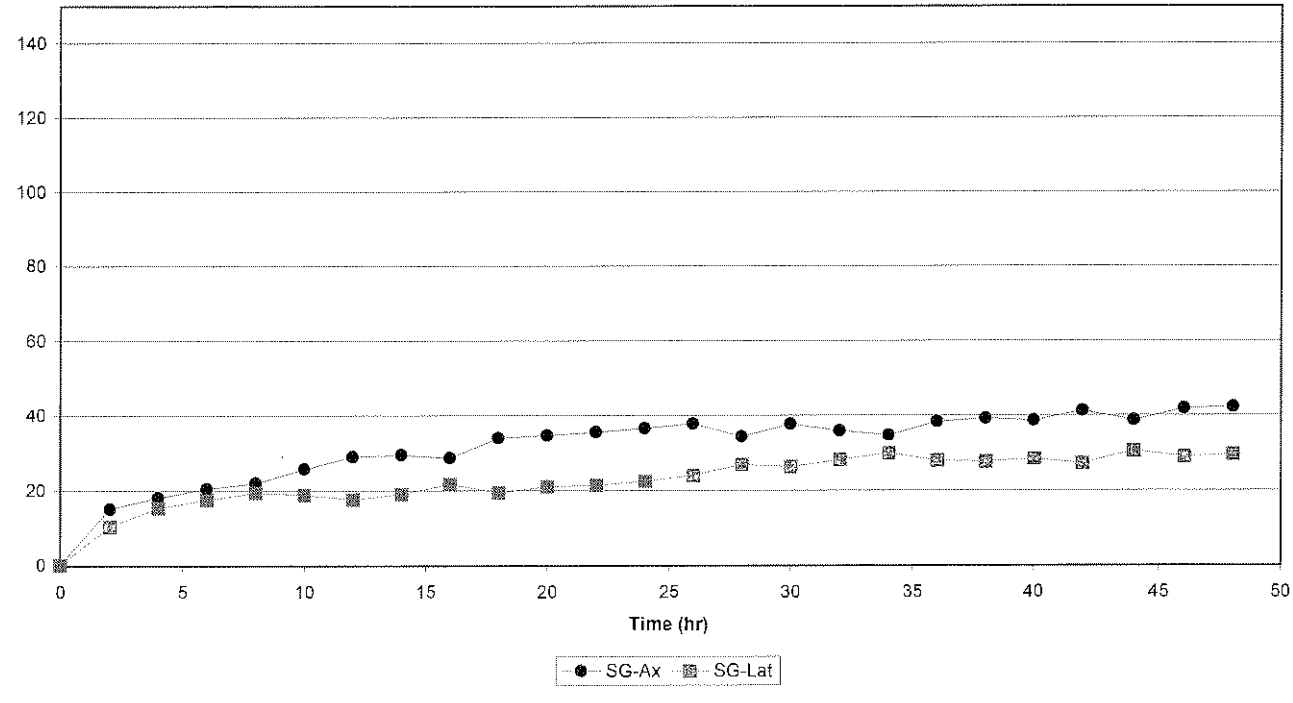

Elsburg Quartzite

Strain vs Time
2056-116 Cycle 3

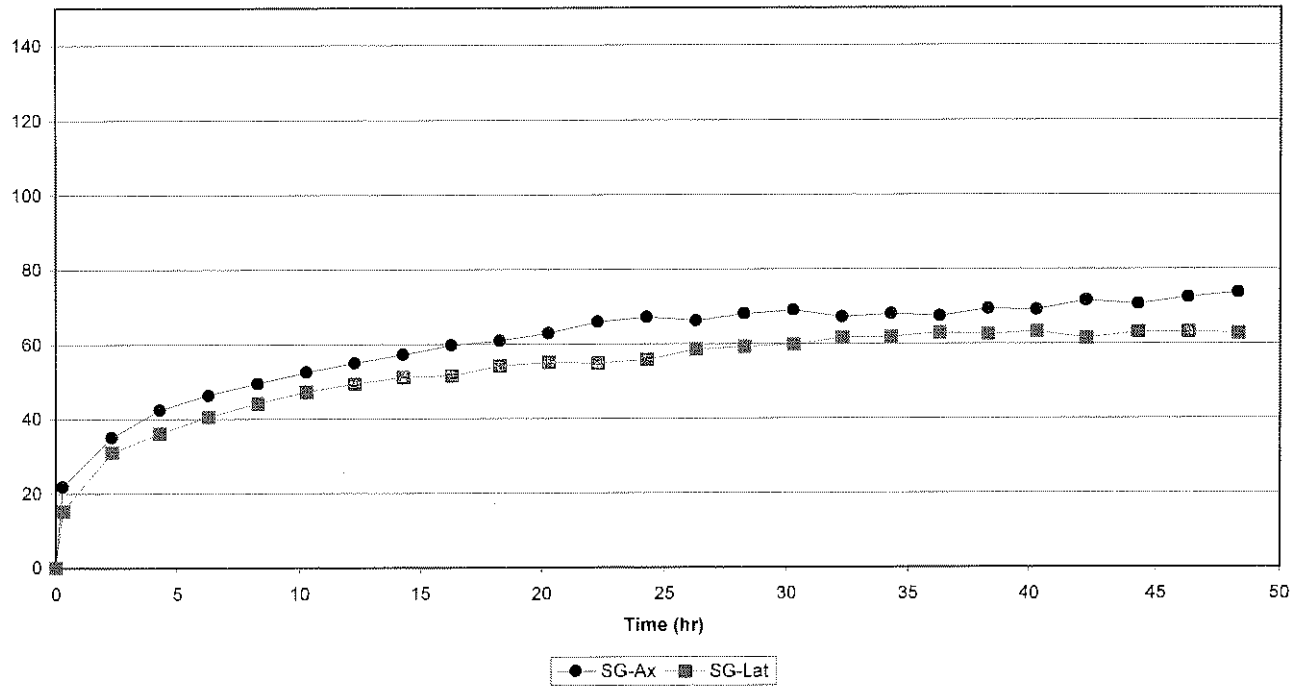

Strain vs Time
2056-116 Cycle 4

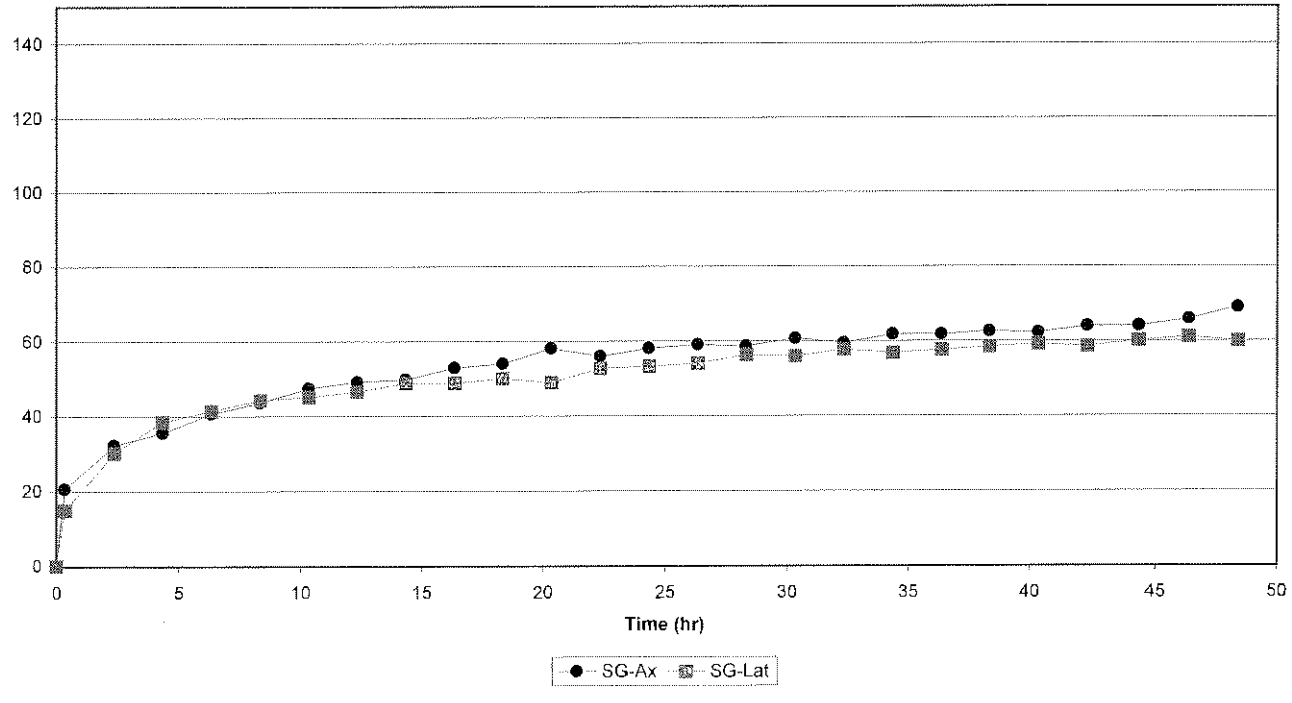

Elsburg Quartzite

Strain vs Time
2056-116 Cycle 5

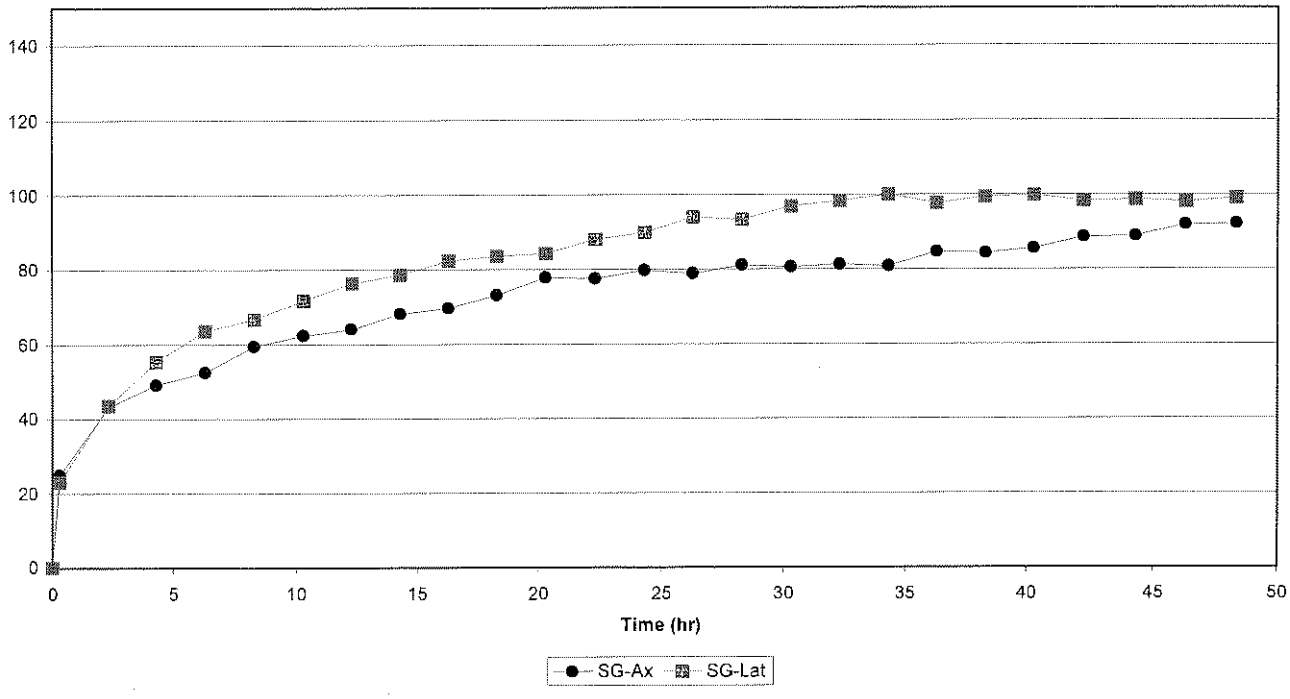

Strain vs Time
2056-116 Cycle 6

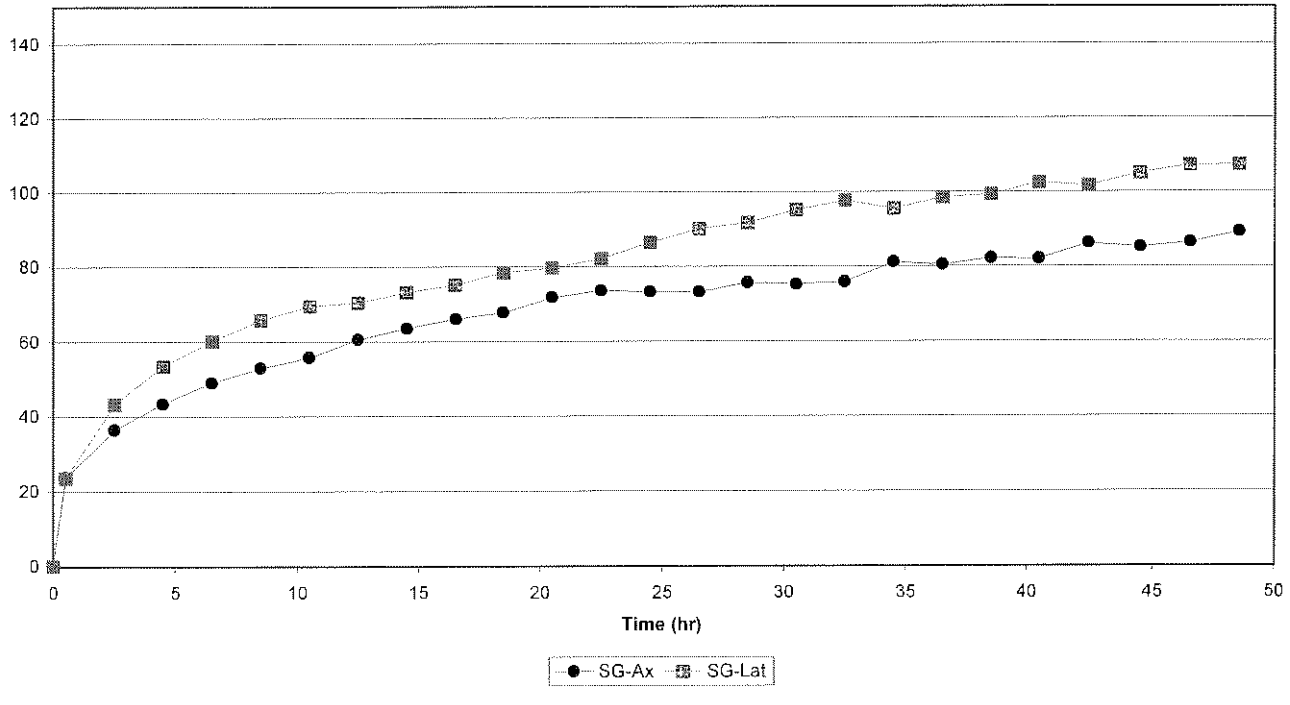

Elsburg Quartzite

Strain vs Time
2056-116 Cycle 7

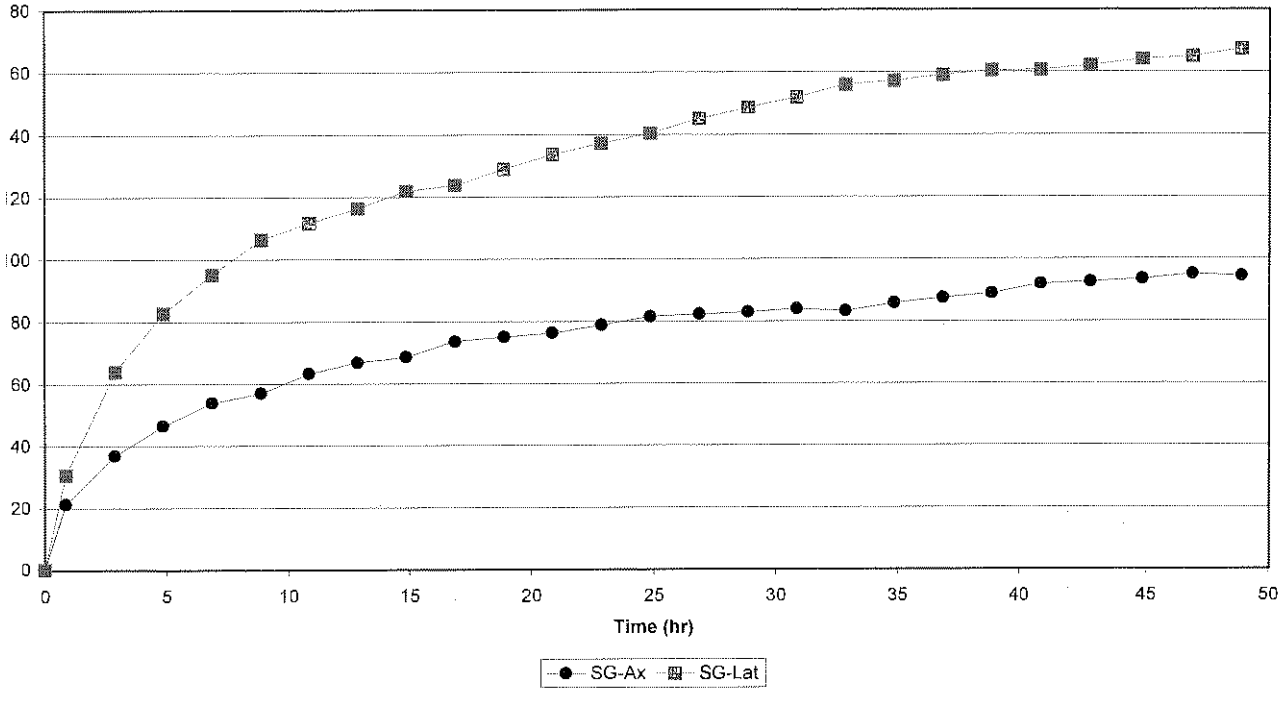

Strain vs Time
2056-116 Cycle 8

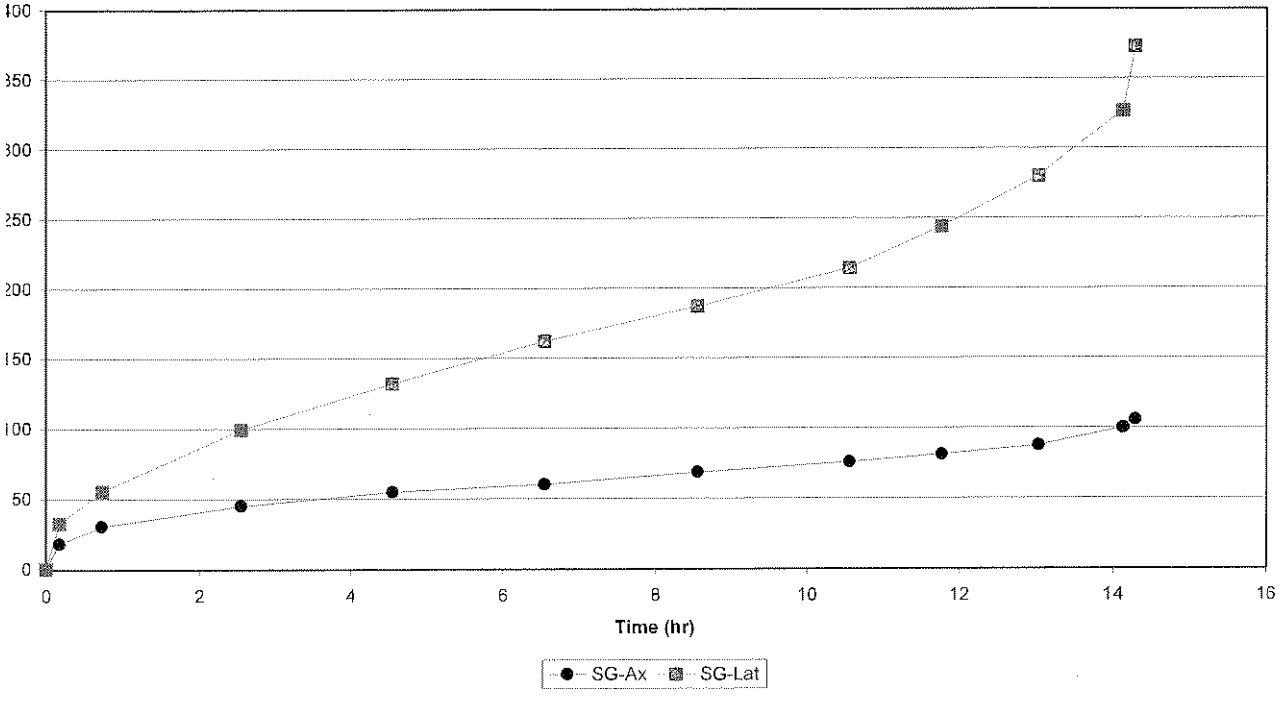

Elsburg Quartzite

Cumulative Strain vs Stress
2056-116

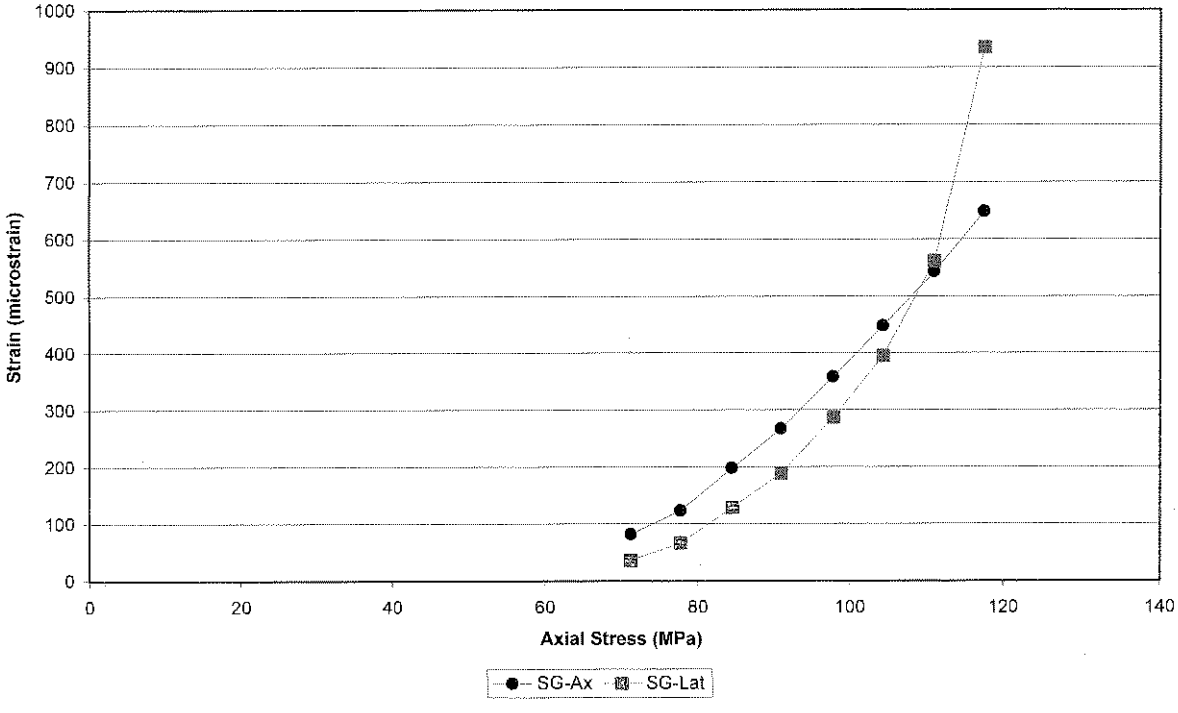

Creep rate vs Stress
2056-116

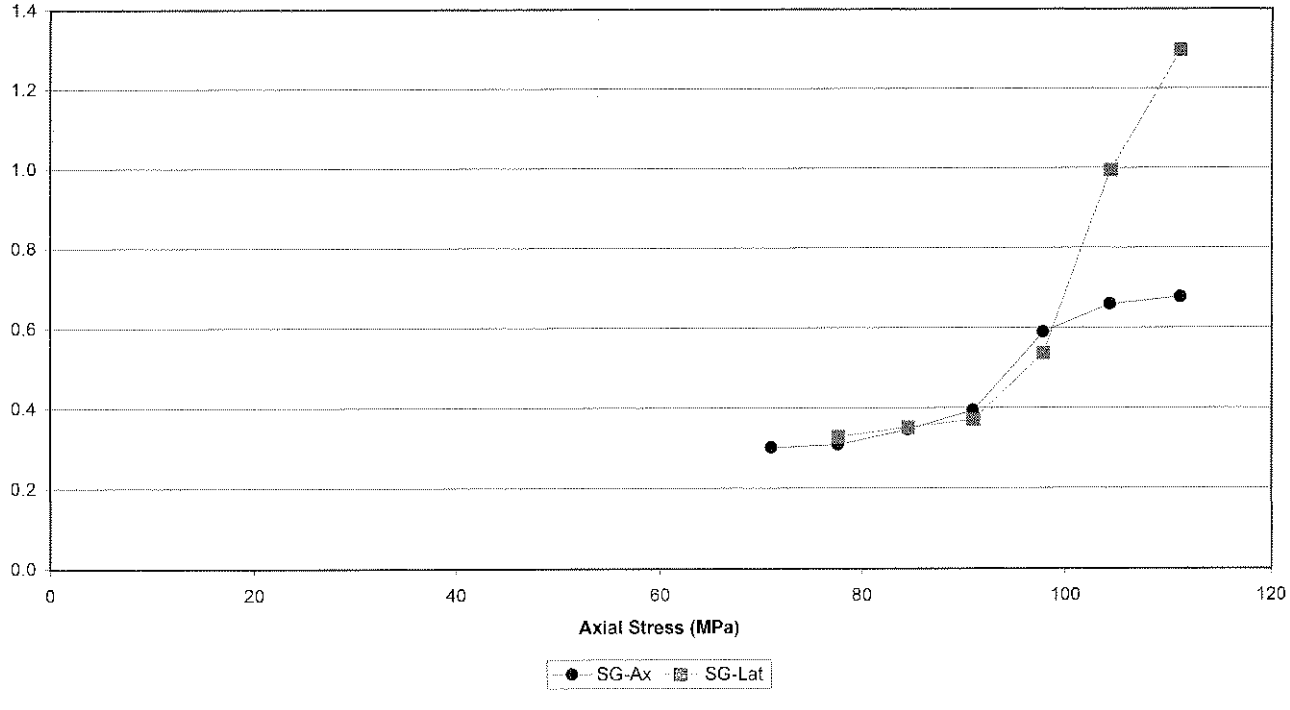

Elsburg Quartzite

Log Creeprate vs Log Stress
2056-116

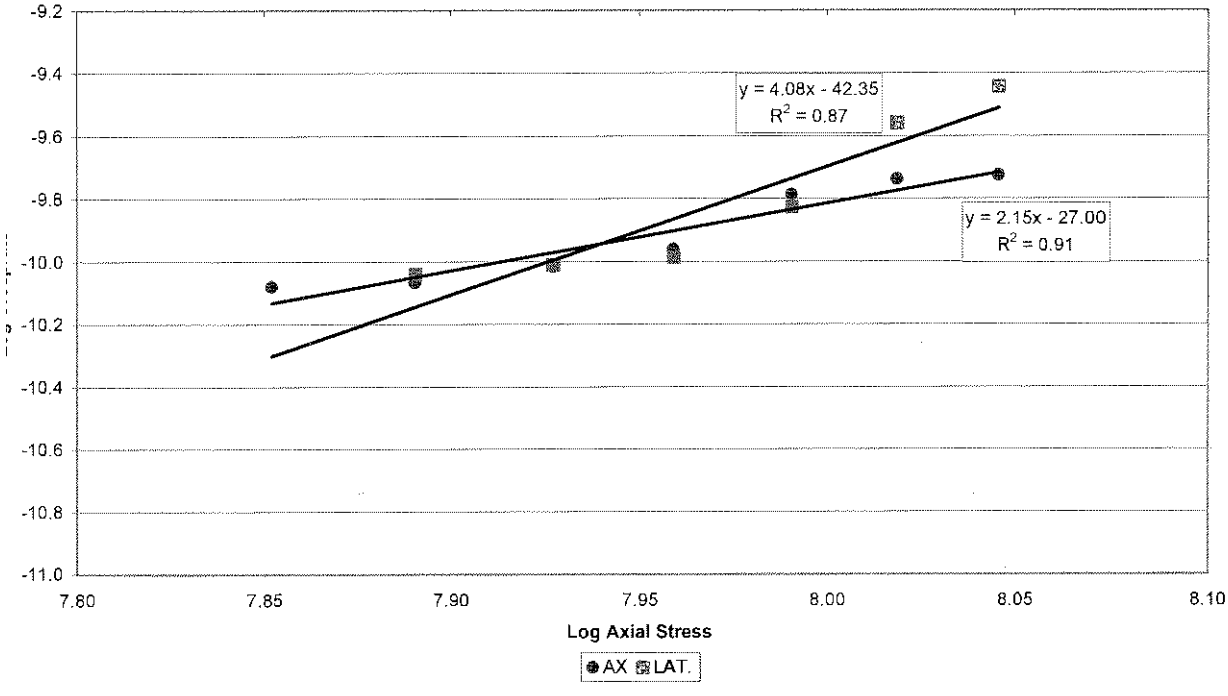

Elsburg Quartzite

Axial Stress vs Strain
2056-117

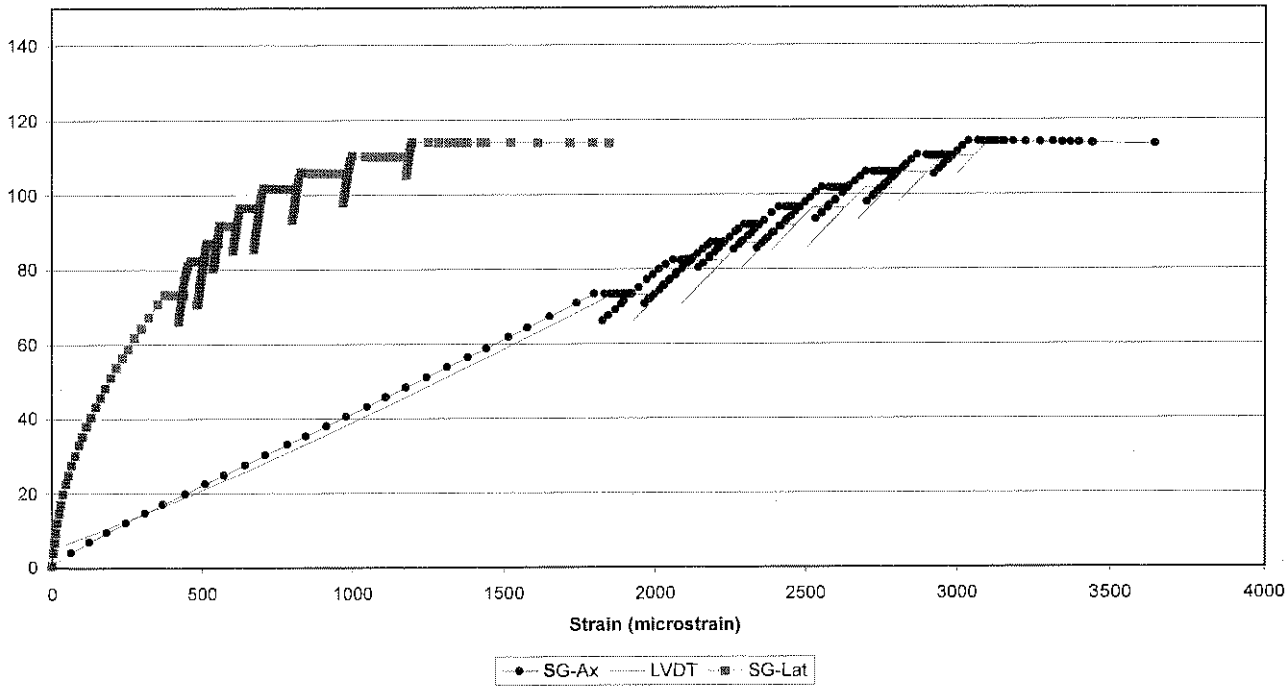

Strain vs Time
2056-117

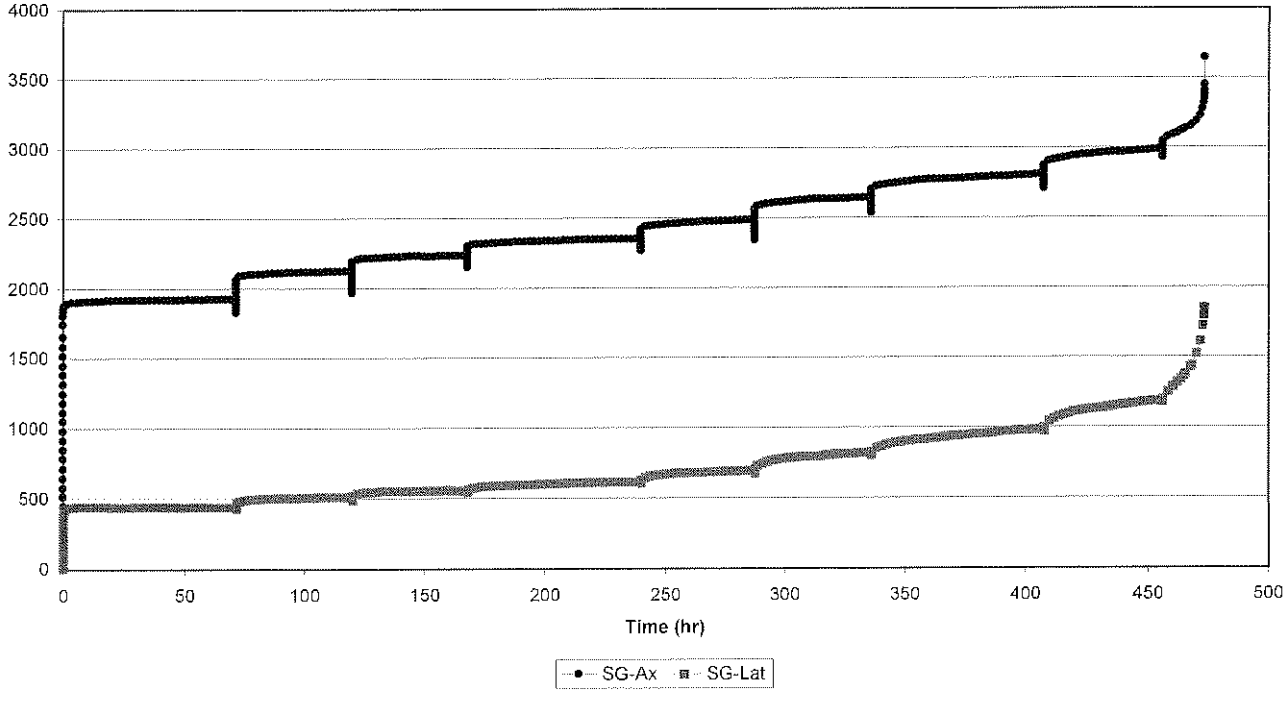

Elsburg Quartzite

Strain vs Time
2056-117 Cycle 1

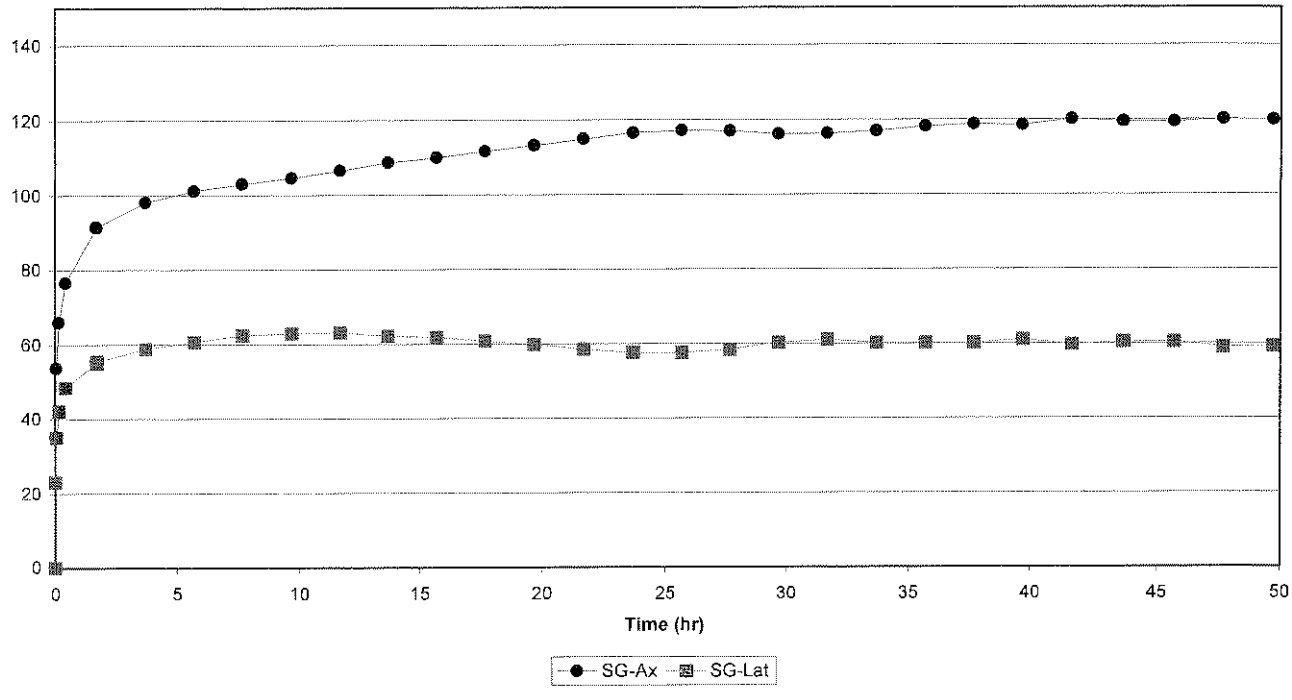

Strain vs Time
2056-117 Cycle 2

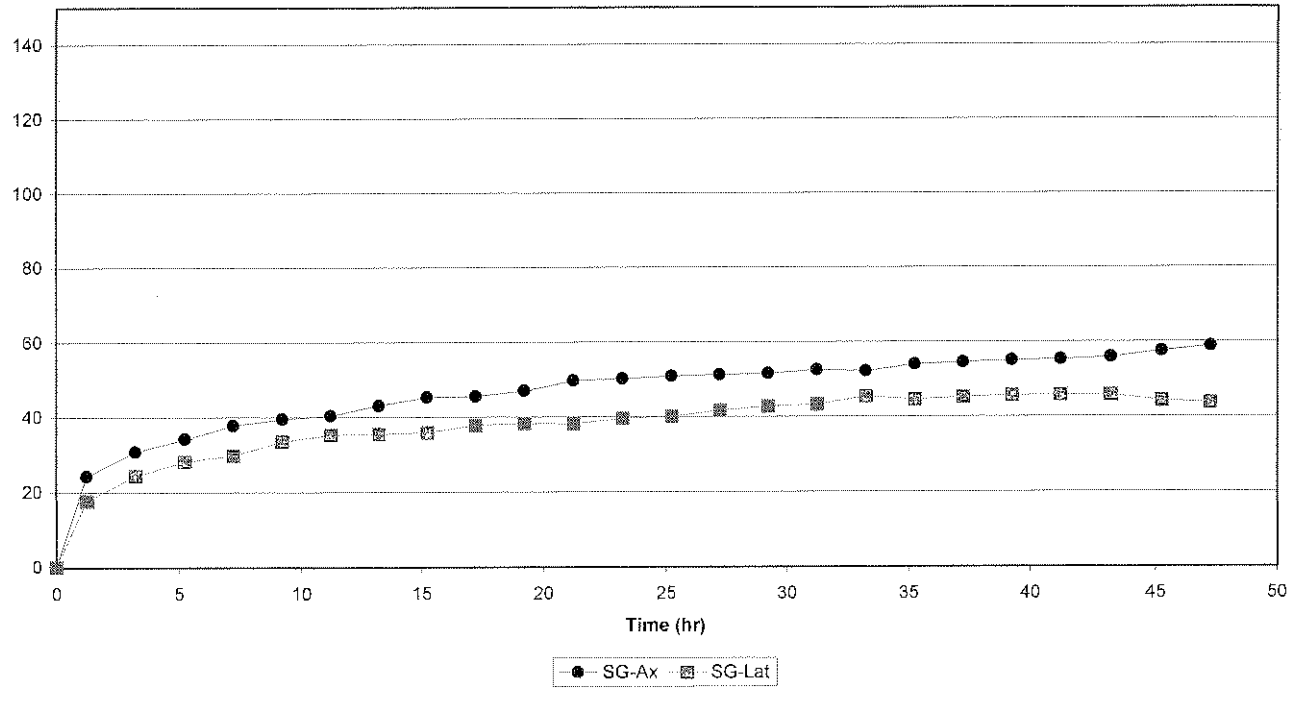

Elsburg Quartzite

Strain vs Time
2056-117 Cycle 3

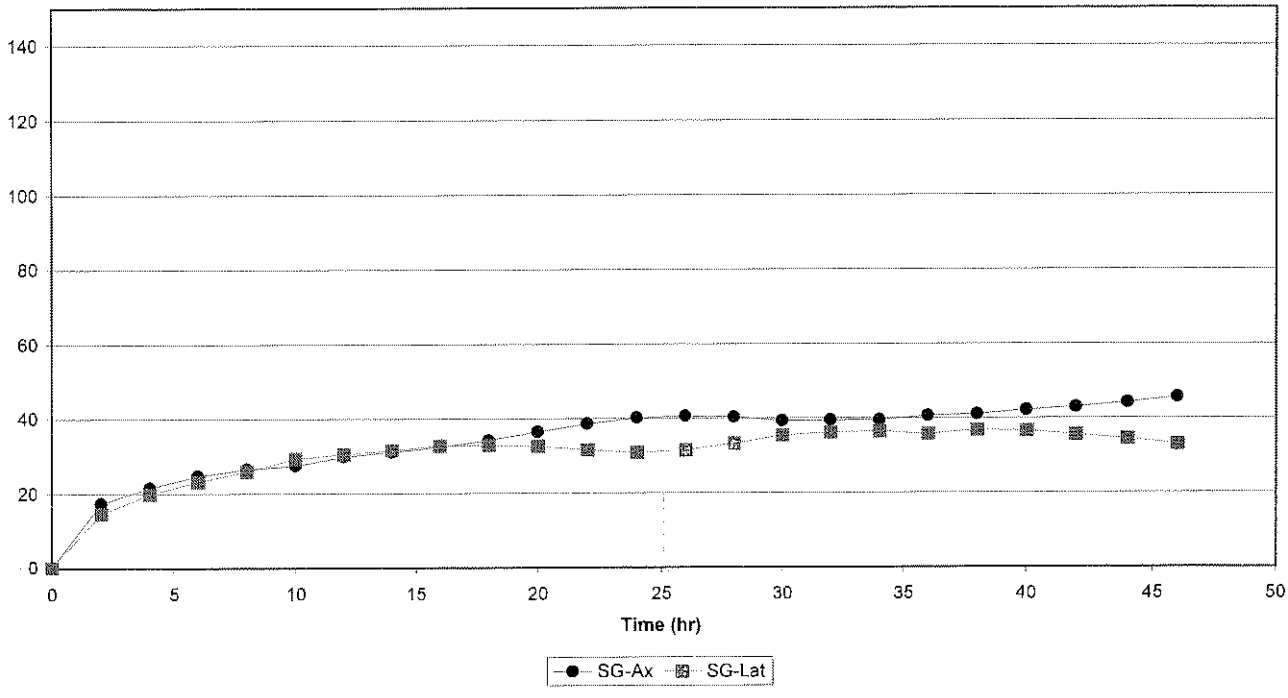

Strain vs Time
2056-117 Cycle 4

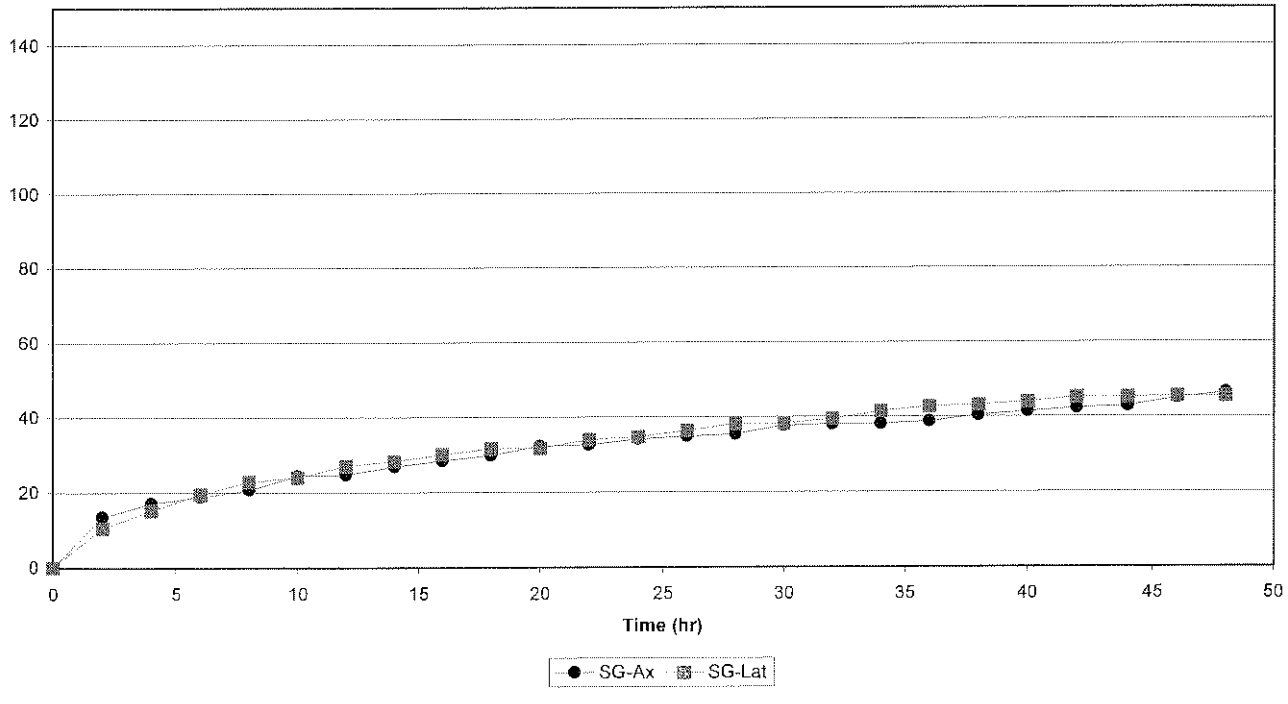

Elsburg Quartzite

Strain vs Time
2056-117 Cycle 5

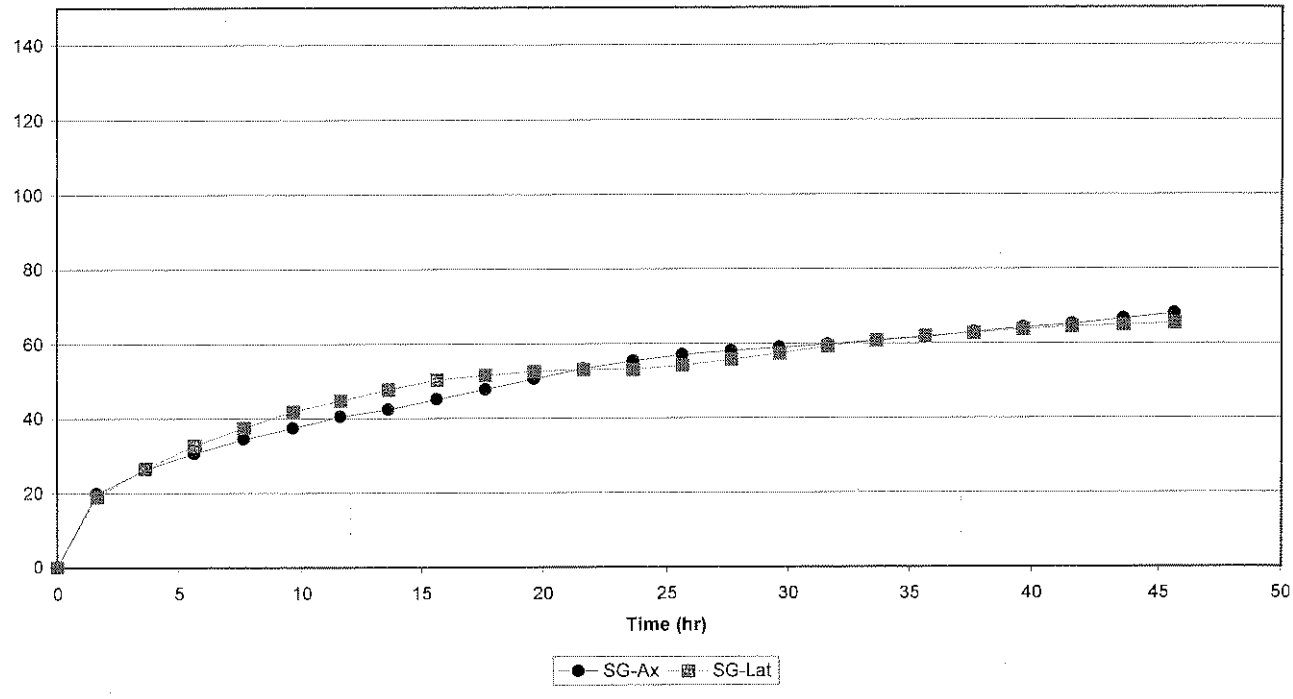

Strain vs Time
2056-117 Cycle 6

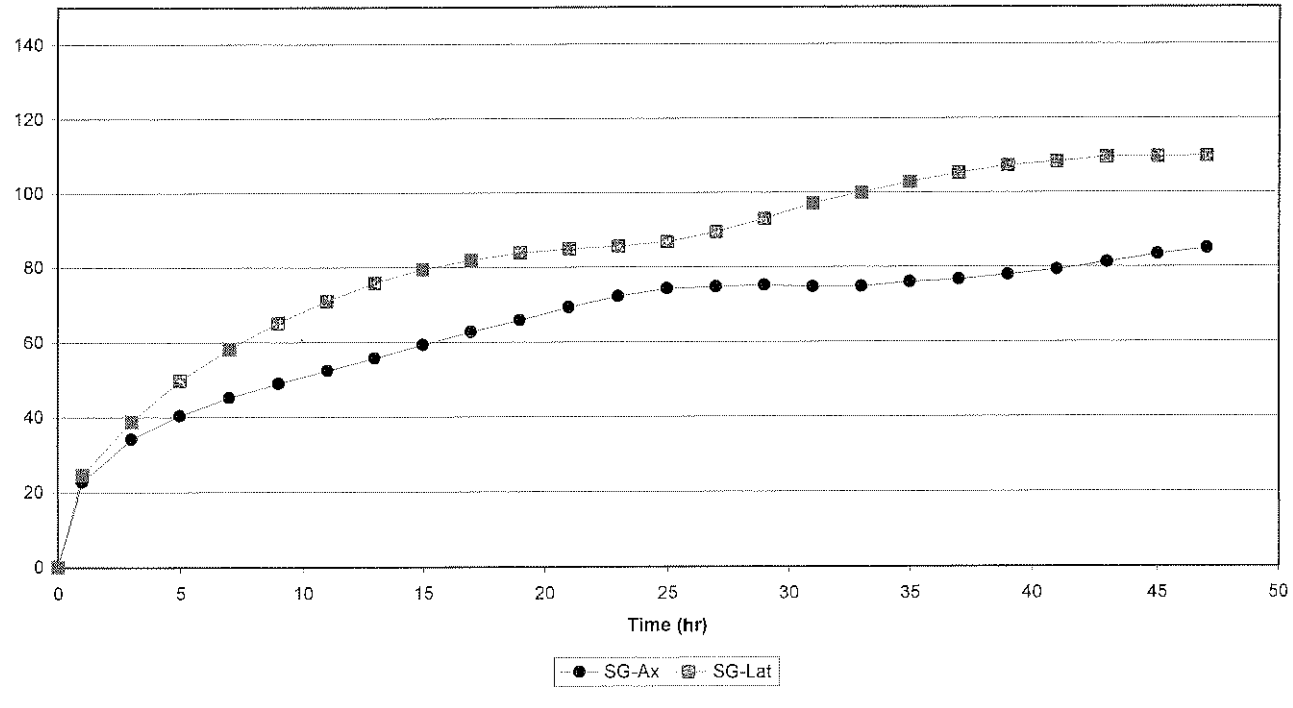

Elsburg Quartzite

Strain vs Time
2056-117 Cycle 7

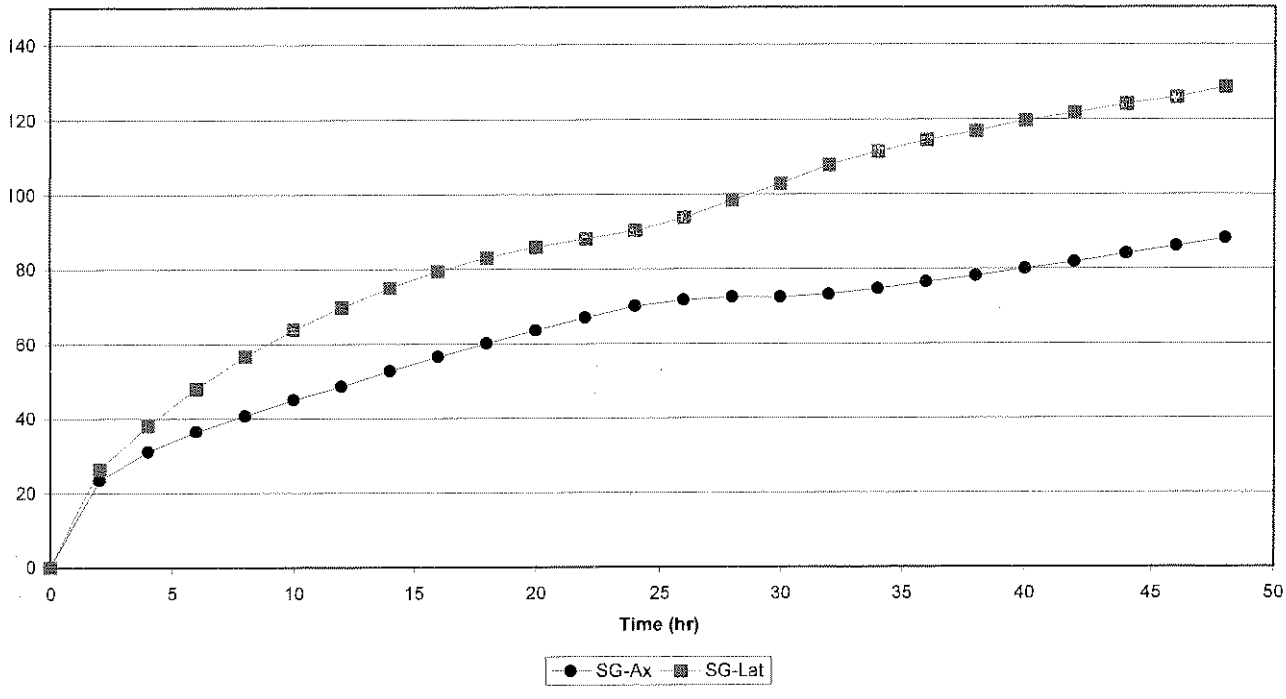

Strain vs Time
2056-117 Cycle 8

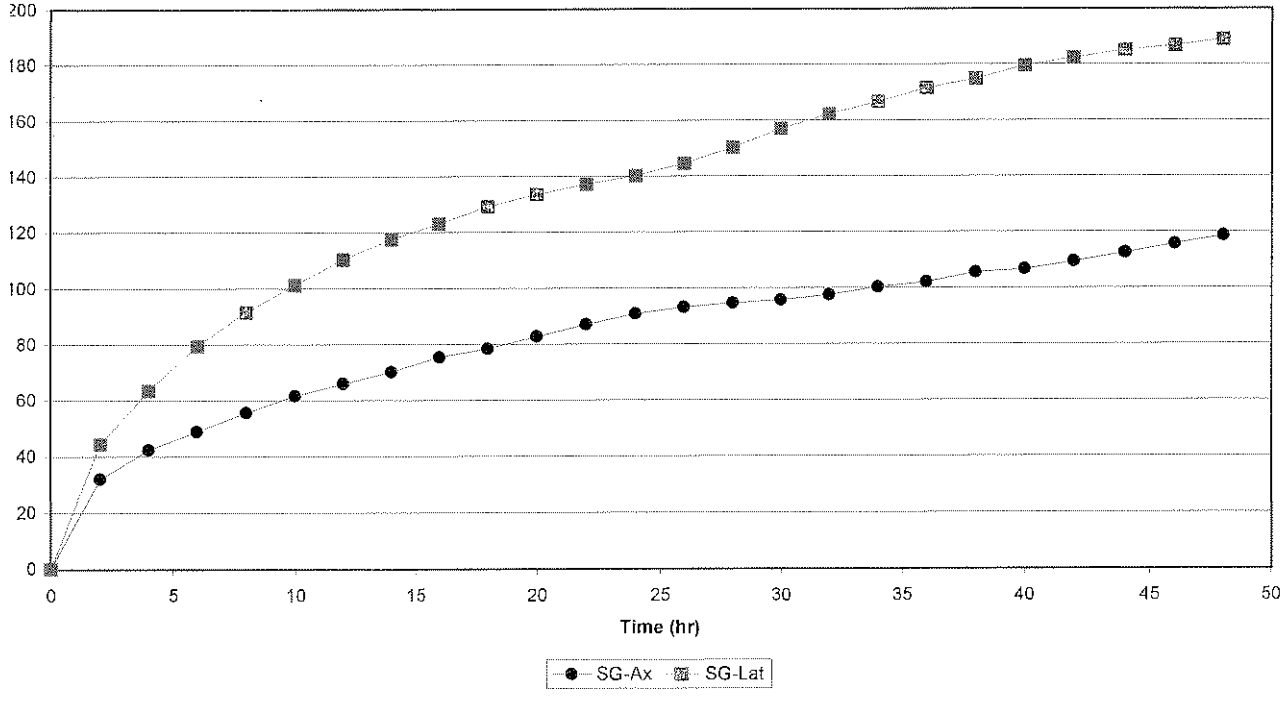

Elsburg Quartzite

Strain vs Time
2056-117 Cycle 9

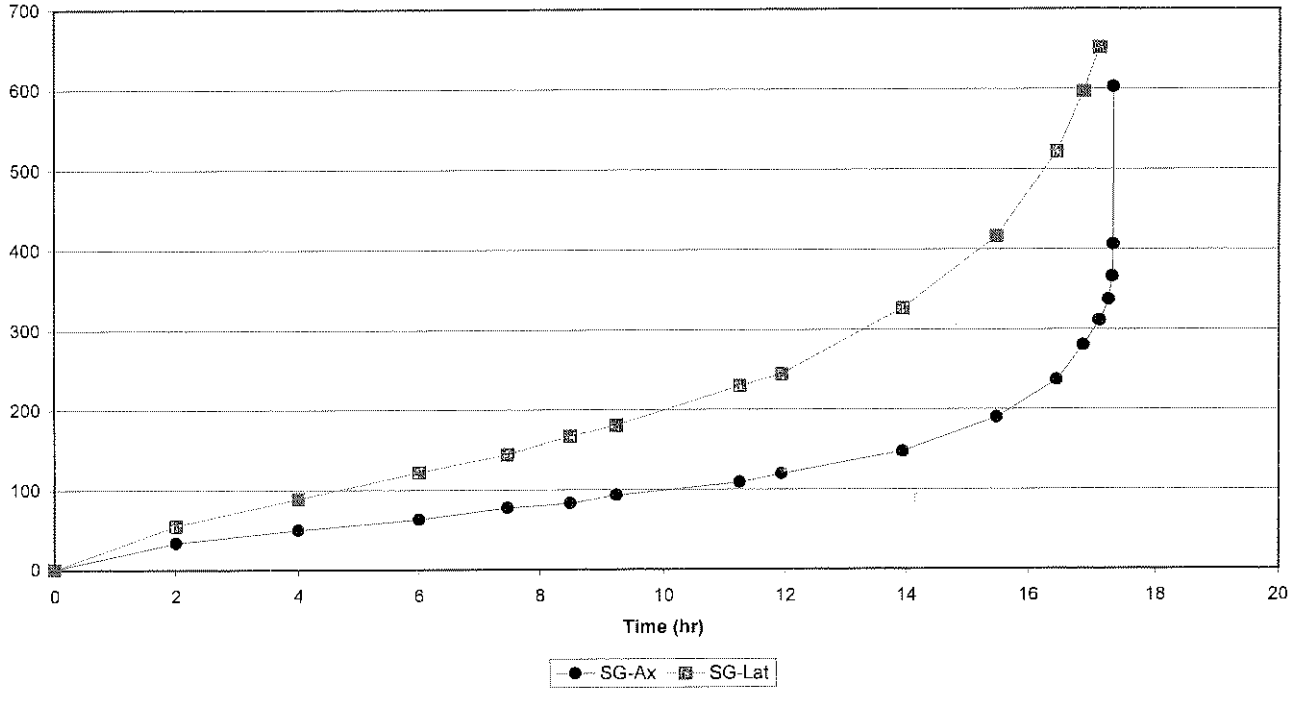

Cumulative Strain vs Stress
2056-117

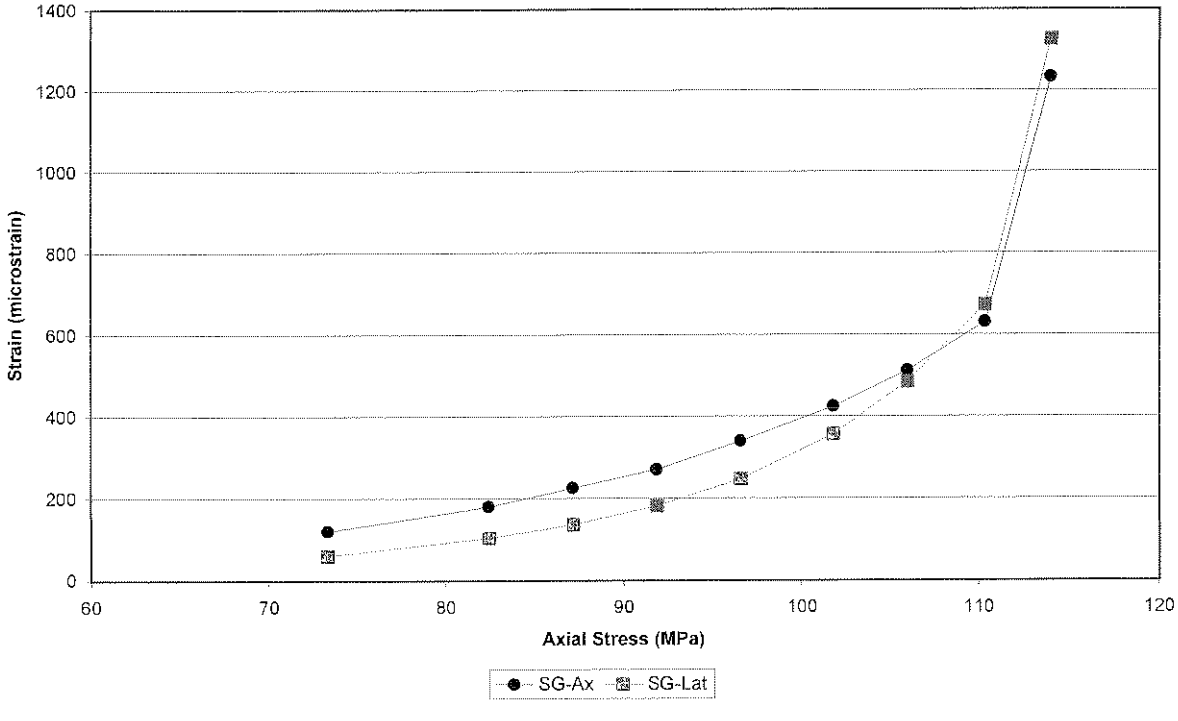

Elsburg Quartzite

Creep rate vs Stress
2056-117

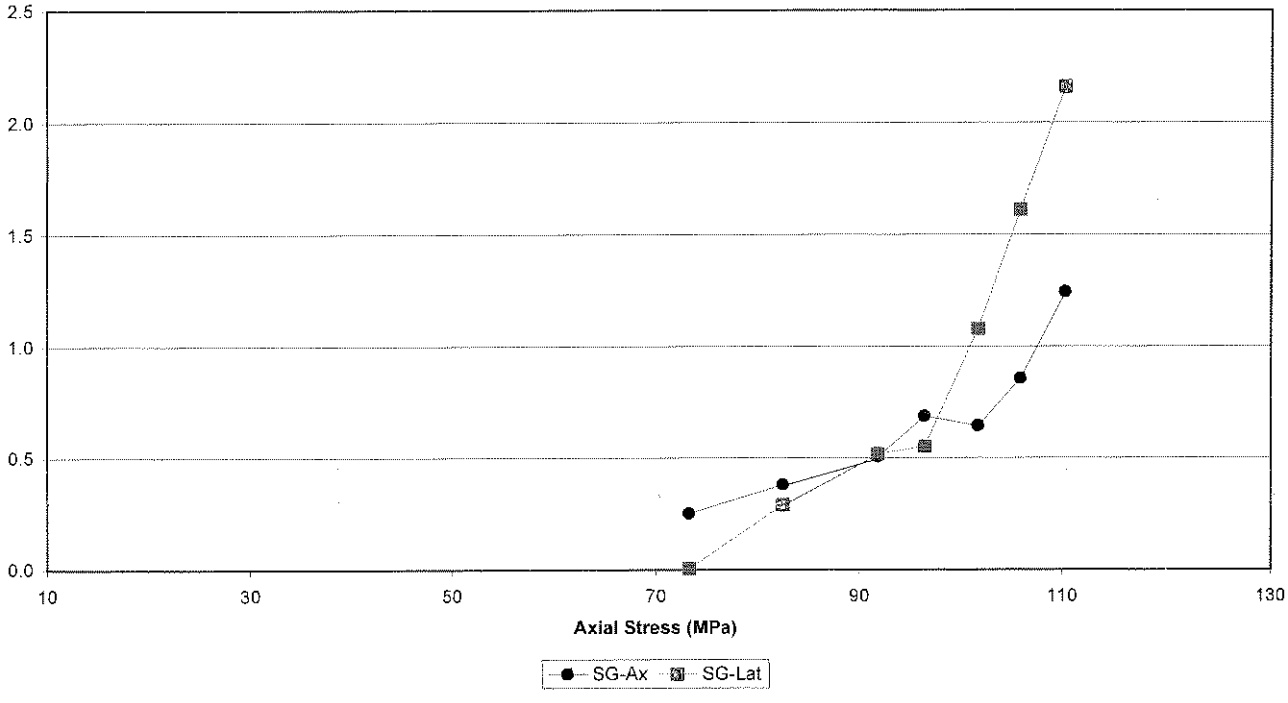

Log Creeprate vs Log Stress
2056-117

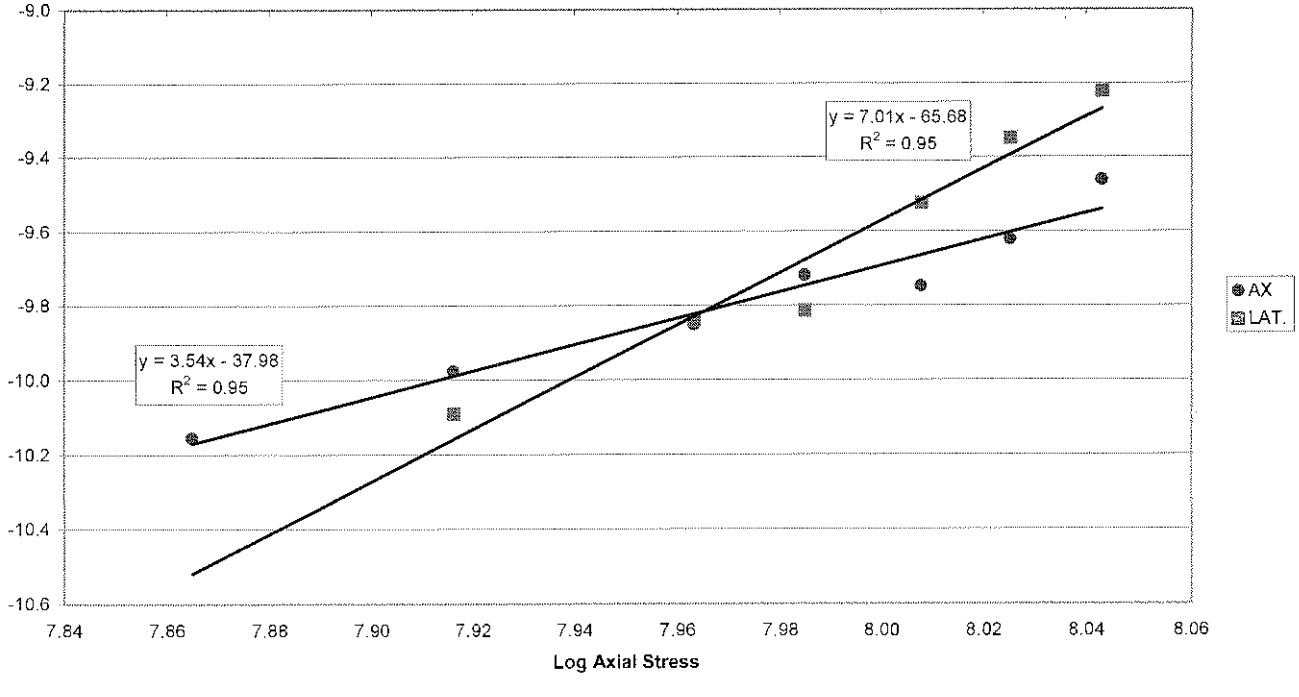

Elsburg Quartzite

Axial Stress vs Strain
2056-118

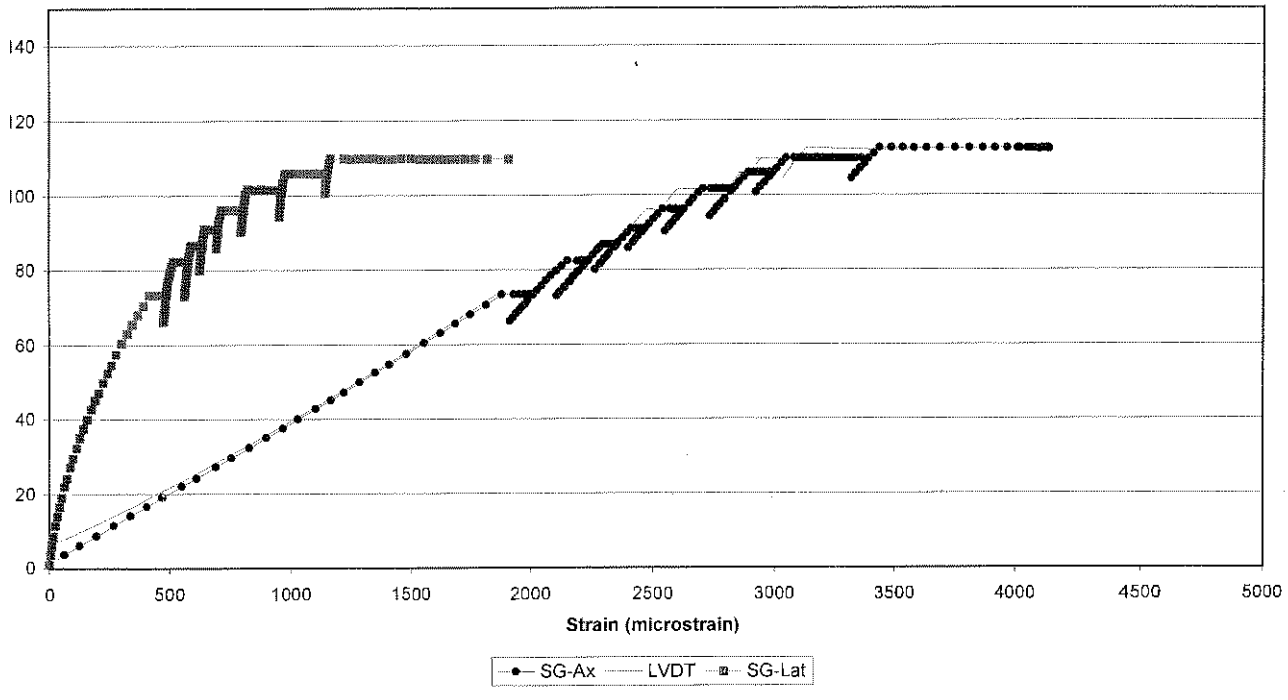

Strain vs Time
2056-118

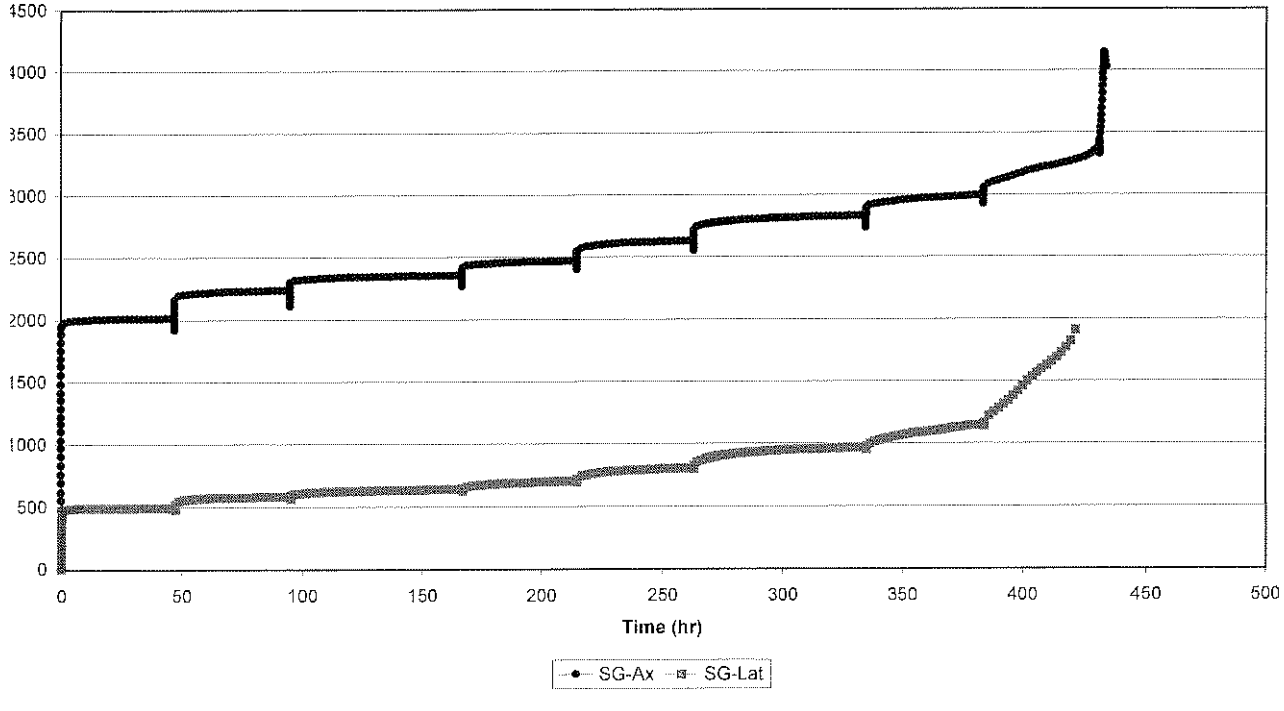

Elsburg Quartzite

Strain vs Time
2056-118 Cycle 1

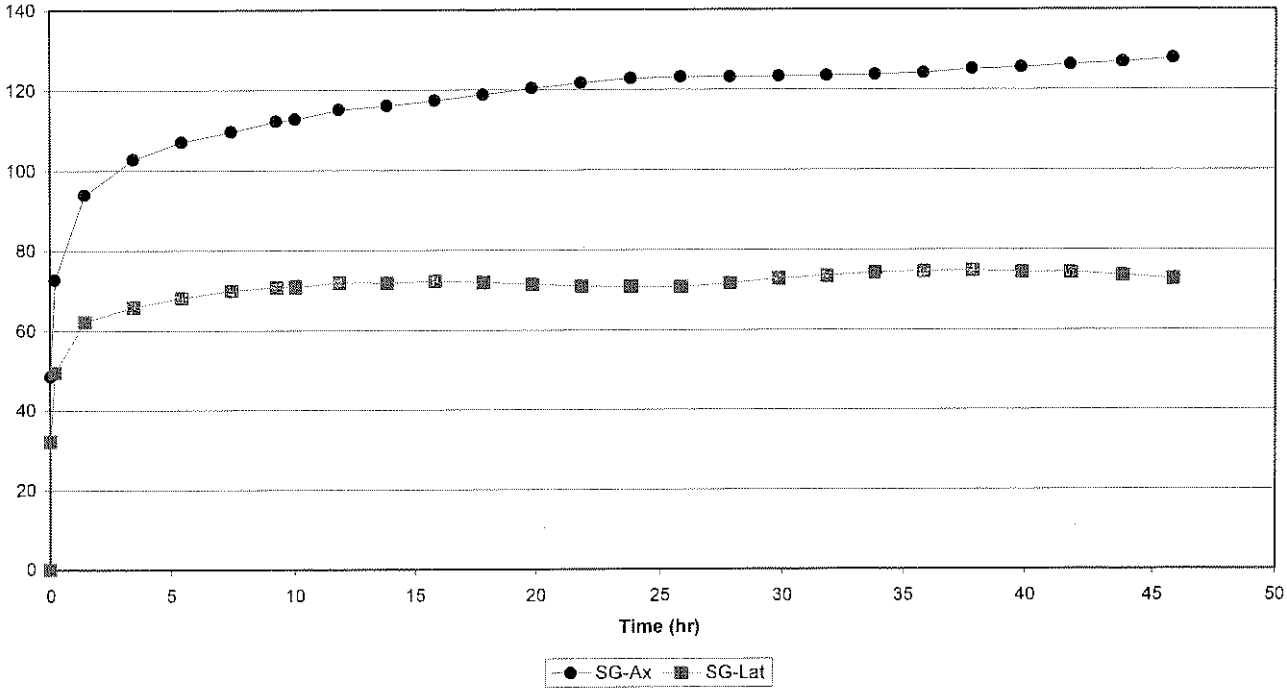

Strain vs Time
2056-118 Cycle 2

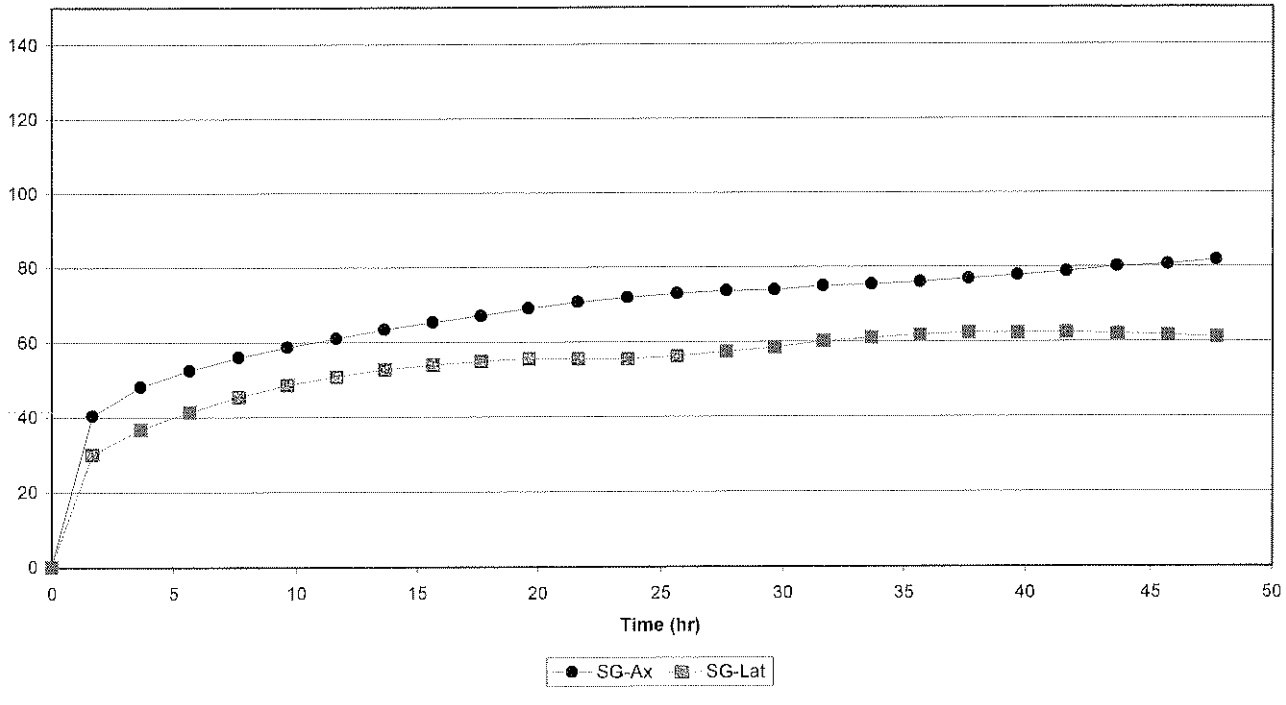

Elsburg Quartzite

Strain vs Time
2056-118 Cycle 3

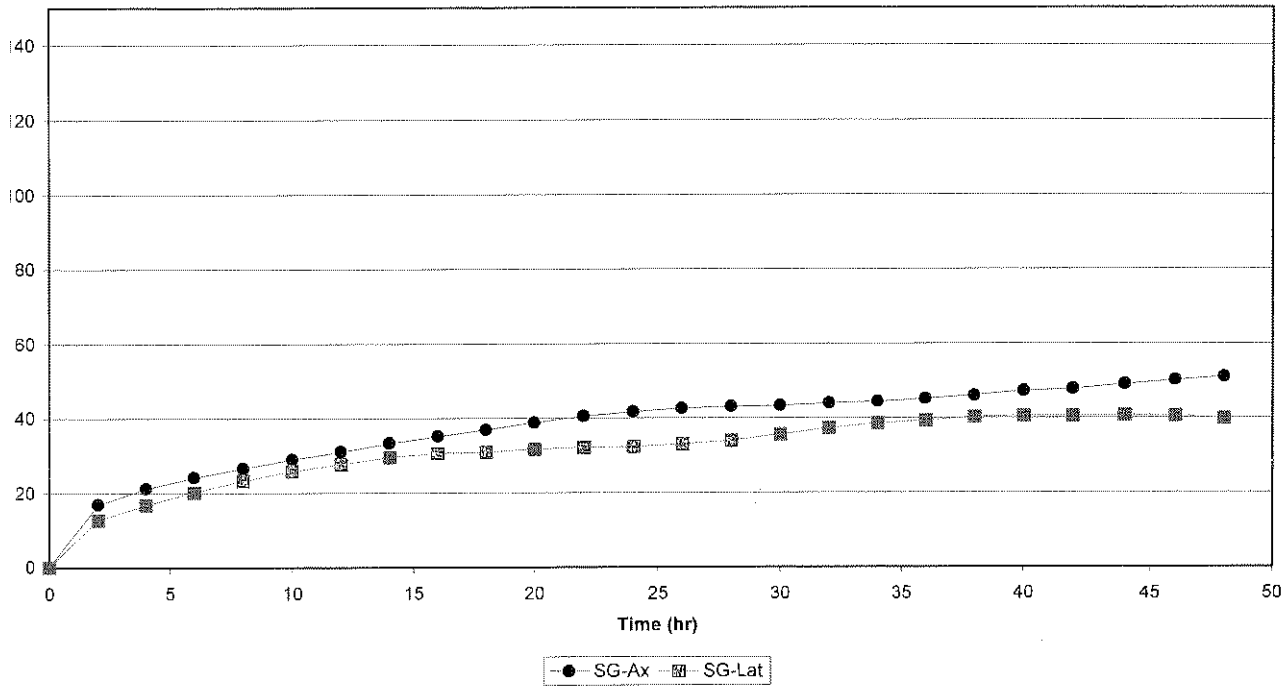

Strain vs Time
2056-118 Cycle 4

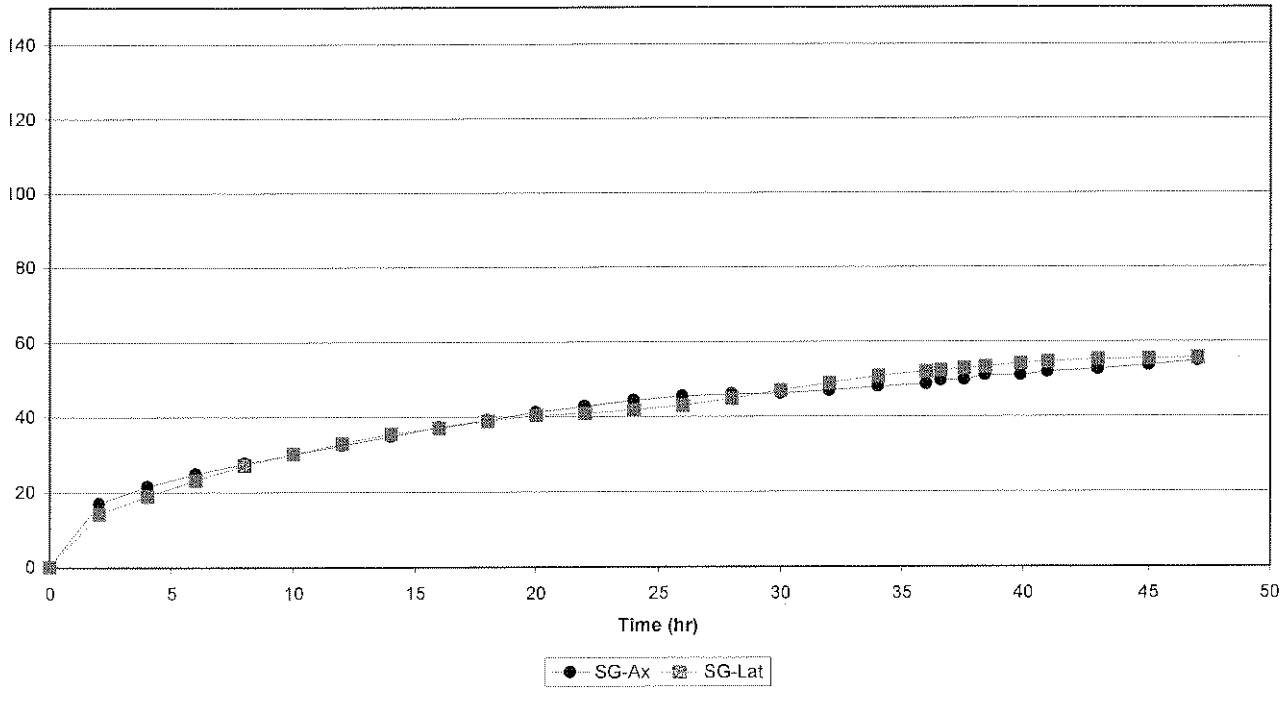

Elsburg Quartzite

Strain vs Time
2056-118 Cycle 5

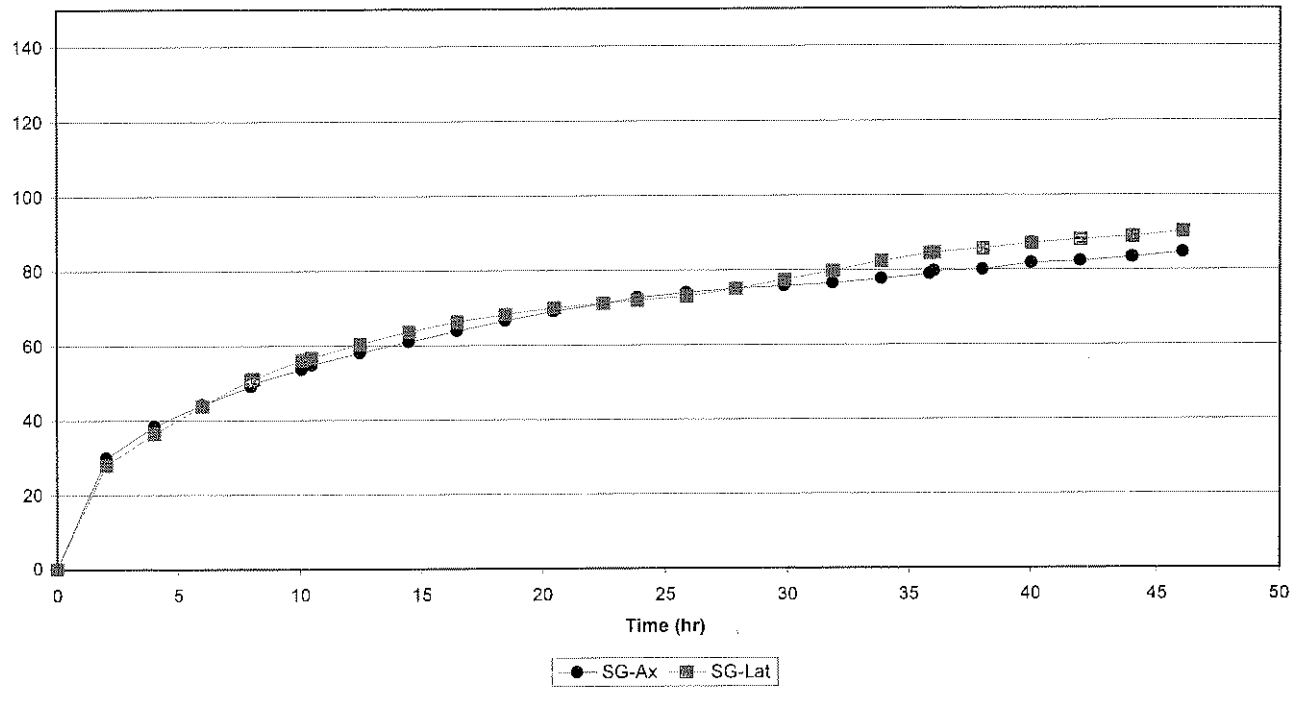

Strain vs Time
2056-118 Cycle 6

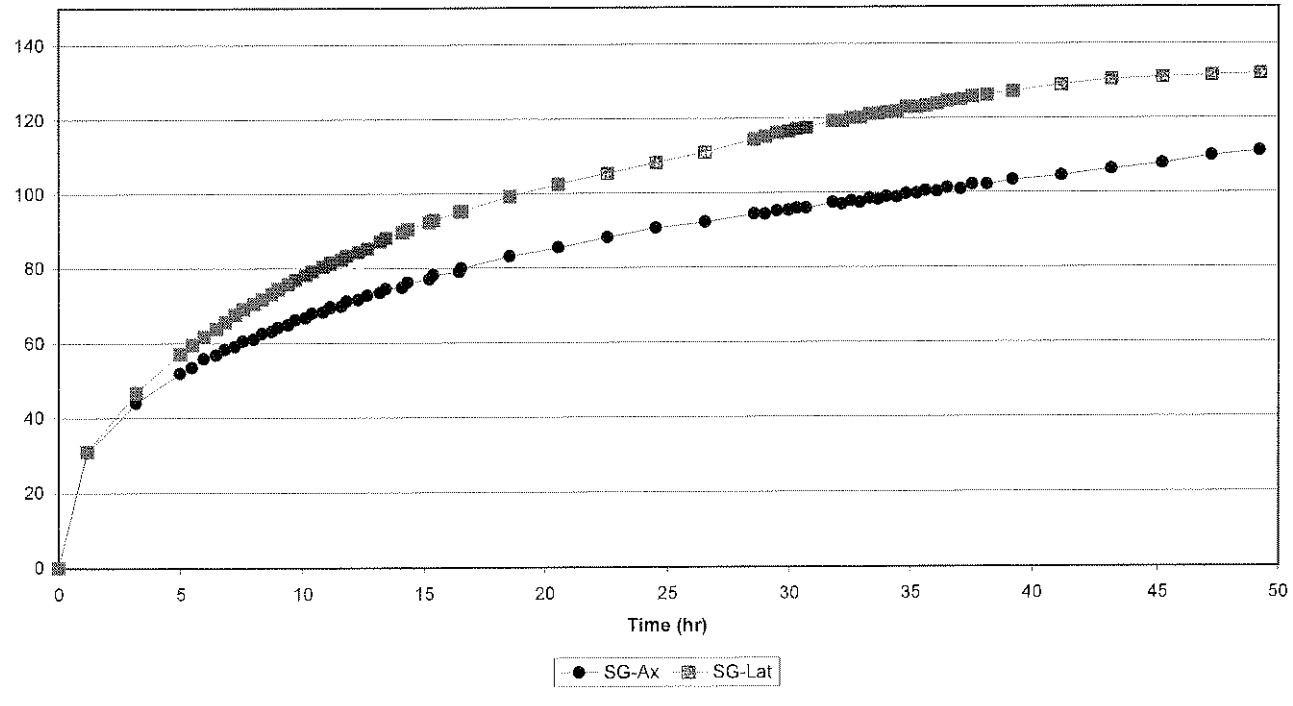

Elsburg Quartzite

Strain vs Time
2056-118 Cycle 7

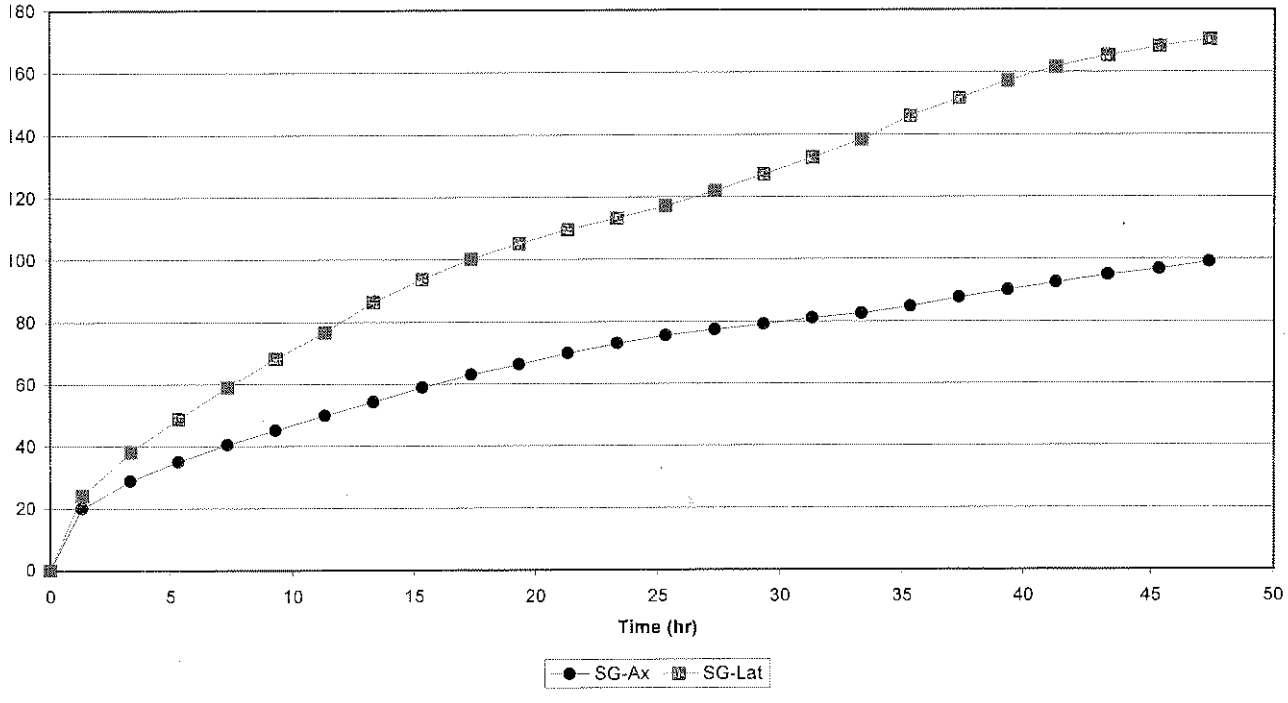

Strain vs Time
2056-118 Cycle 8

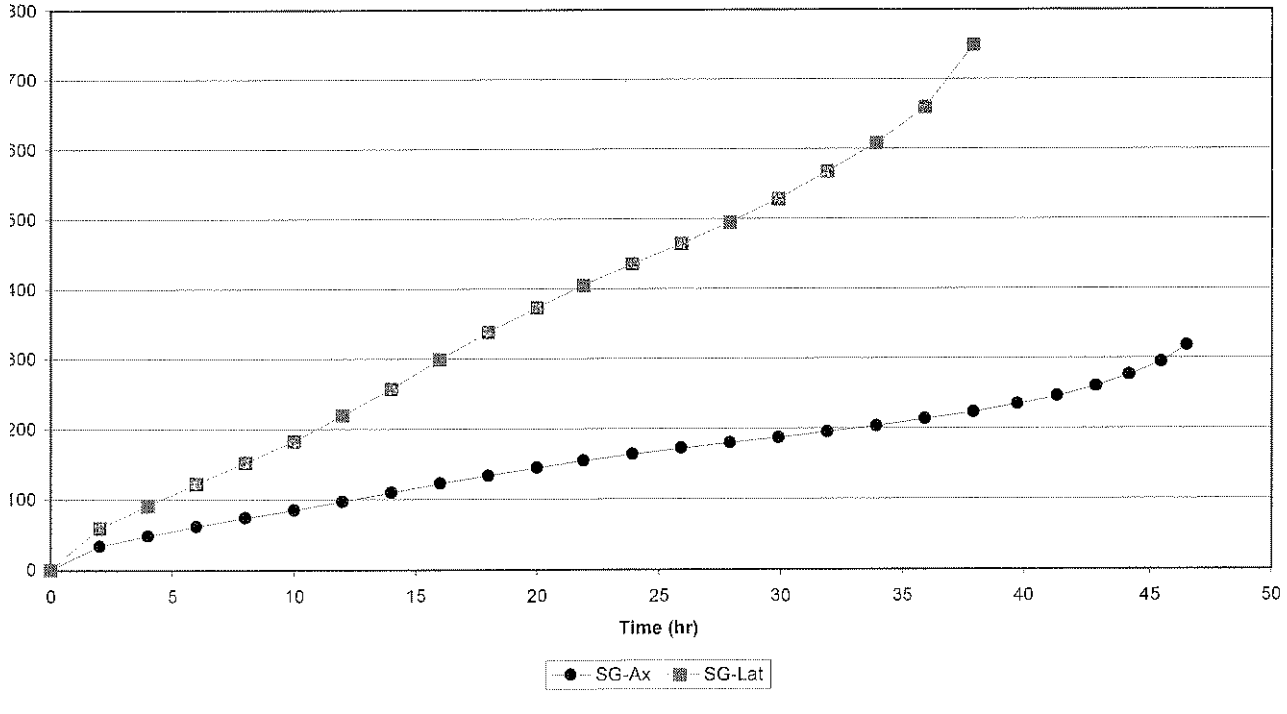

Elsburg Quartzite

Strain vs Time
2056-118 Cycle 9

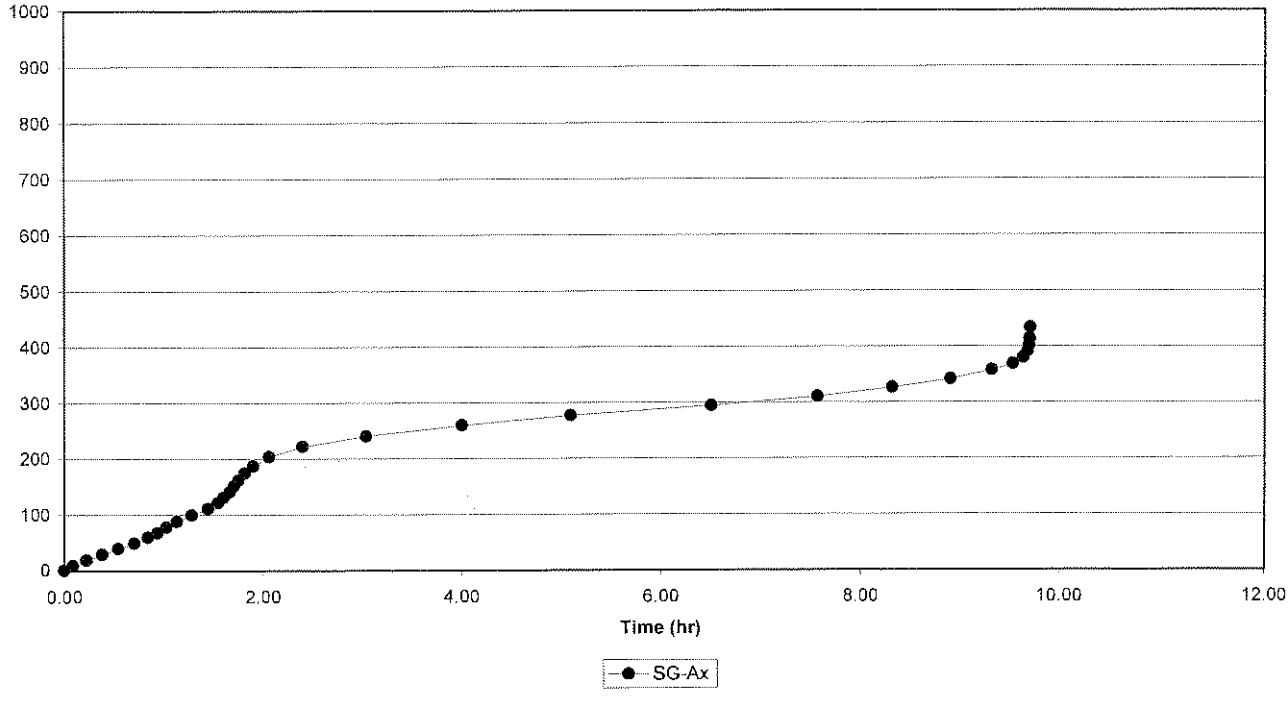

Cumulative Strain vs Stress
2056-118

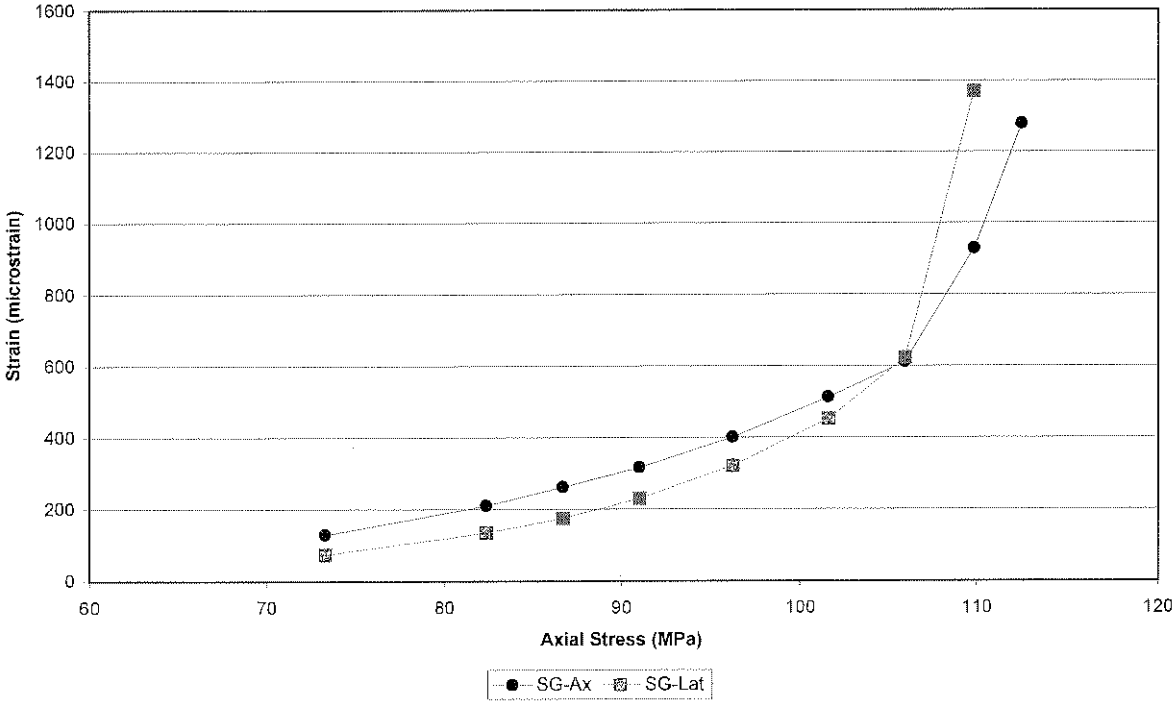

Elsburg Quartzite

Creep rate vs Stress
2056-118

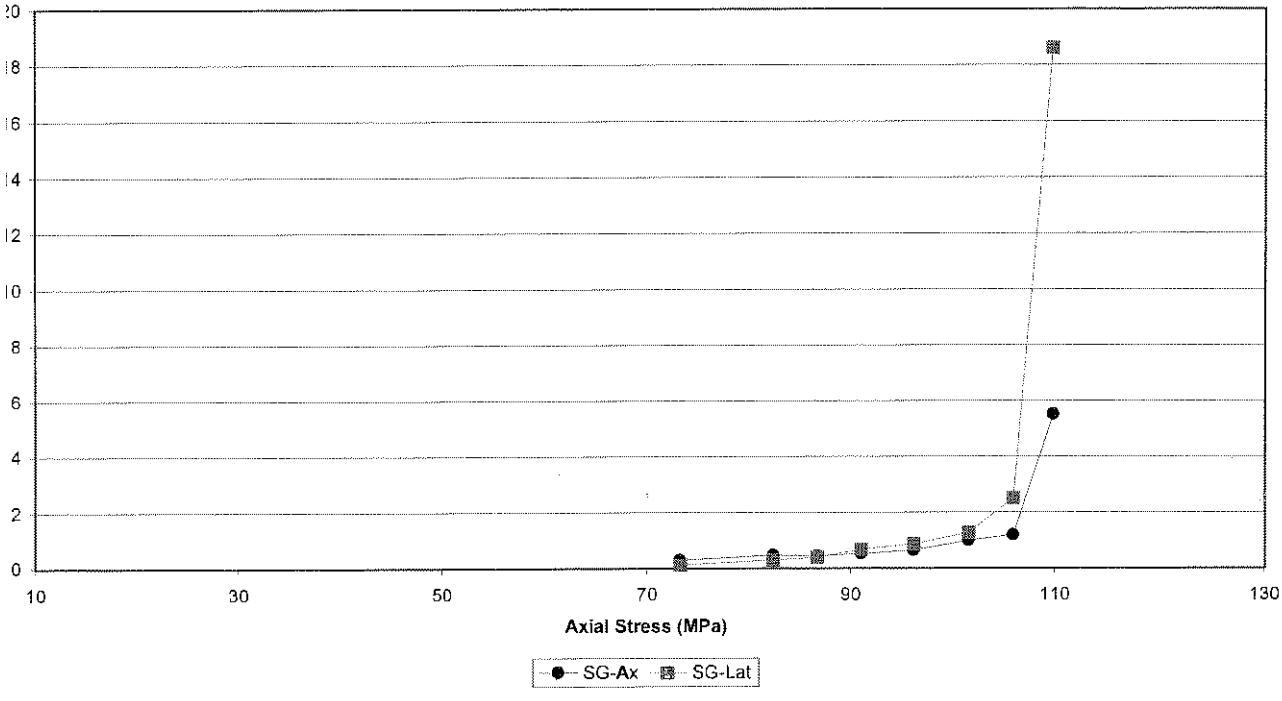

Log Creeprate vs Log Stress
2056-118

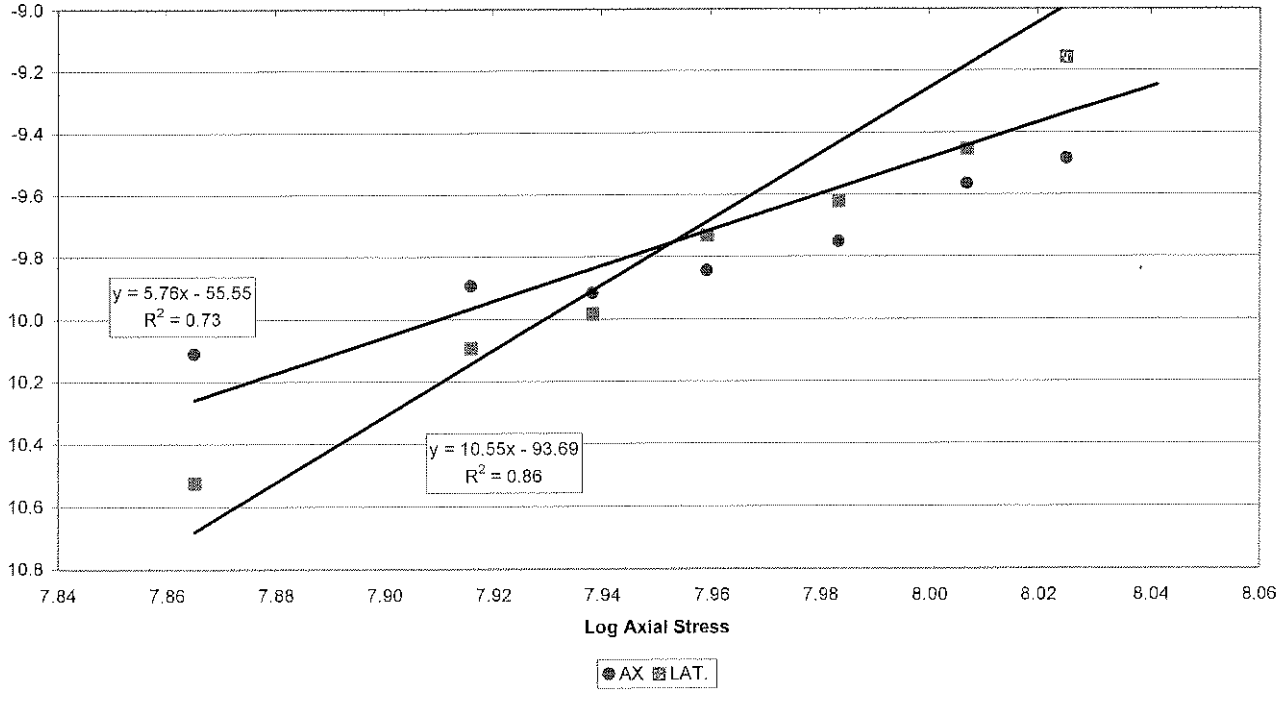

Elsburg Quartzite

Axial Stress vs Strain
2056-121

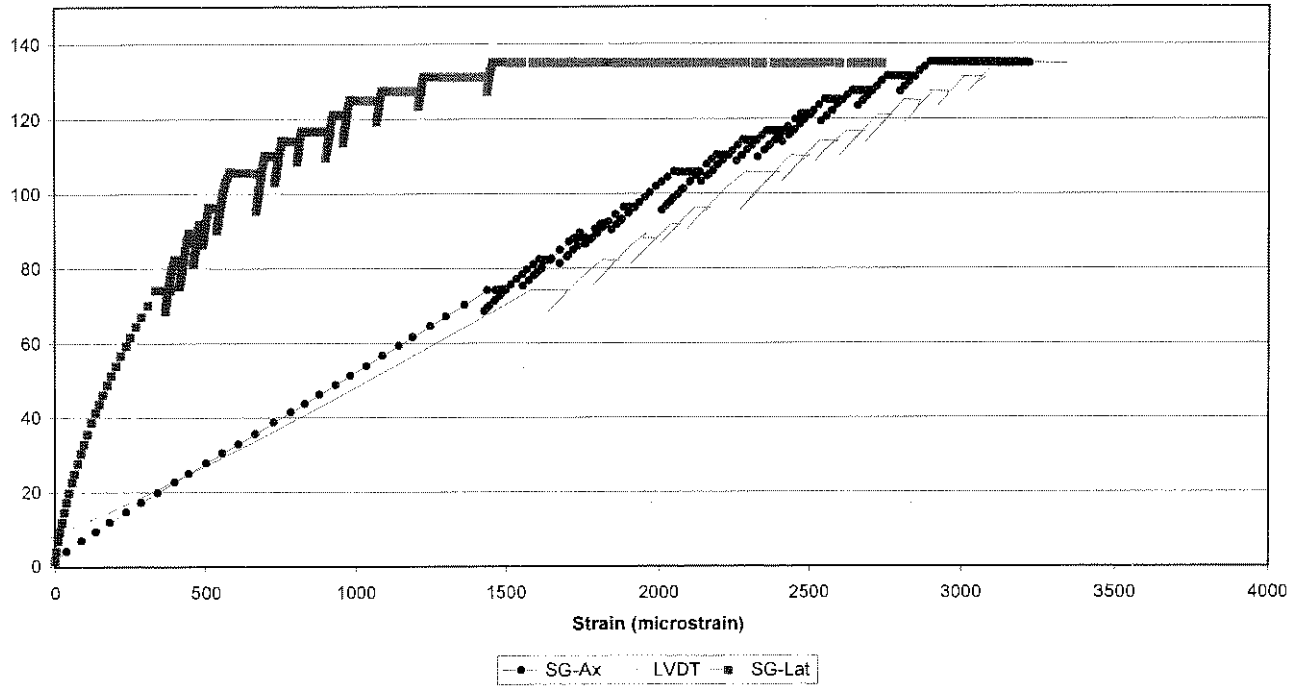

Strain vs Time
2056-121

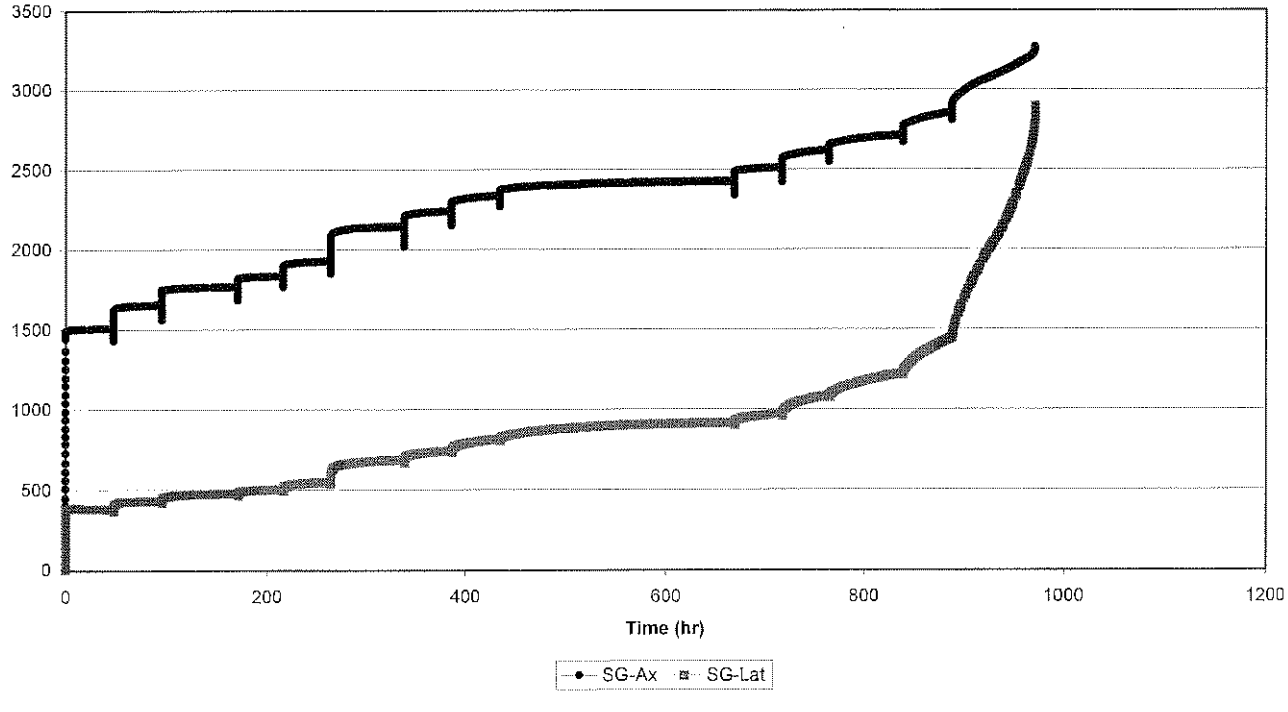

Elsburg Quartzite

Strain vs Time
2056-121 Cycle 1

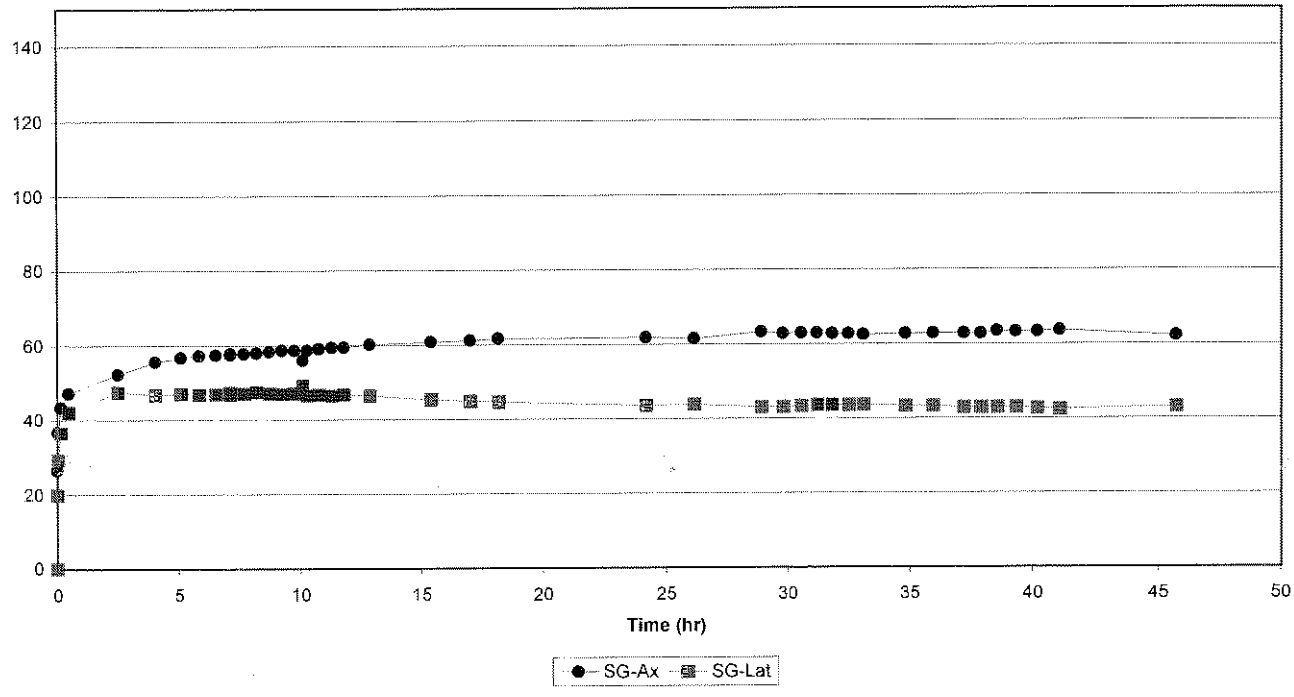

Strain vs Time
2056-121 Cycle 2

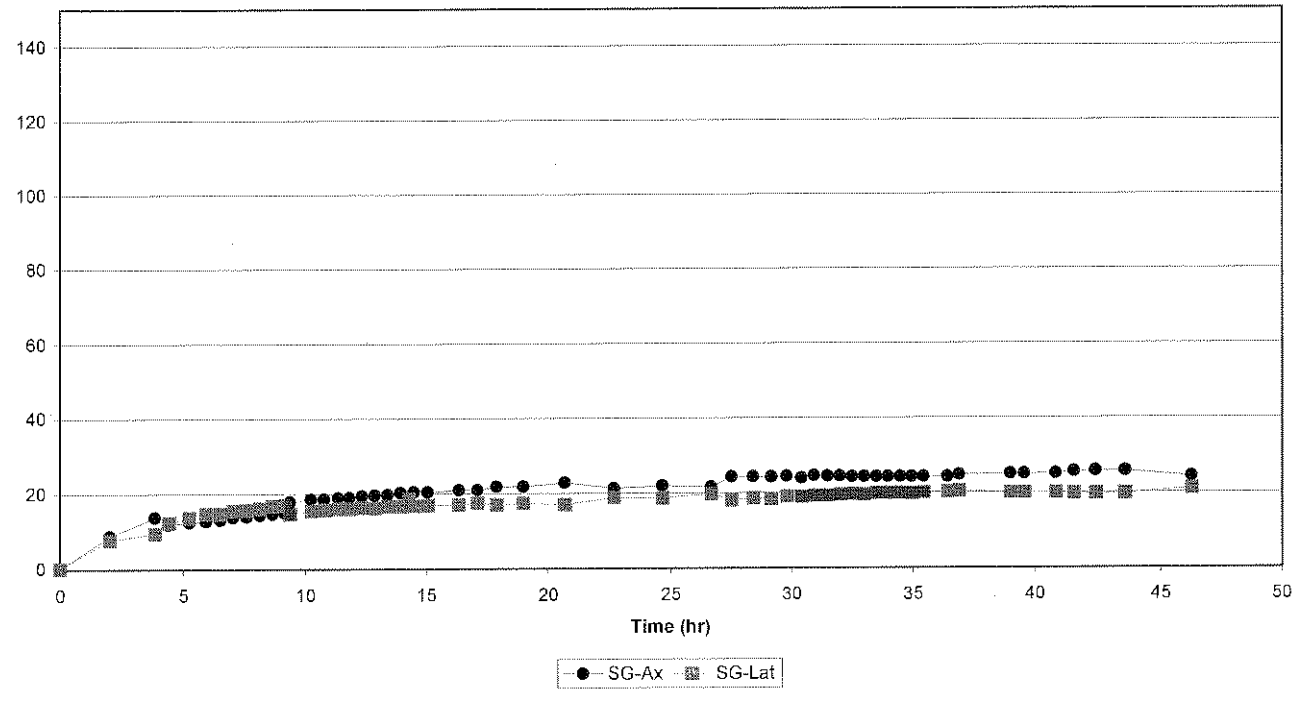

Elsburg Quartzite

Strain vs Time
2056-121 Cycle 3

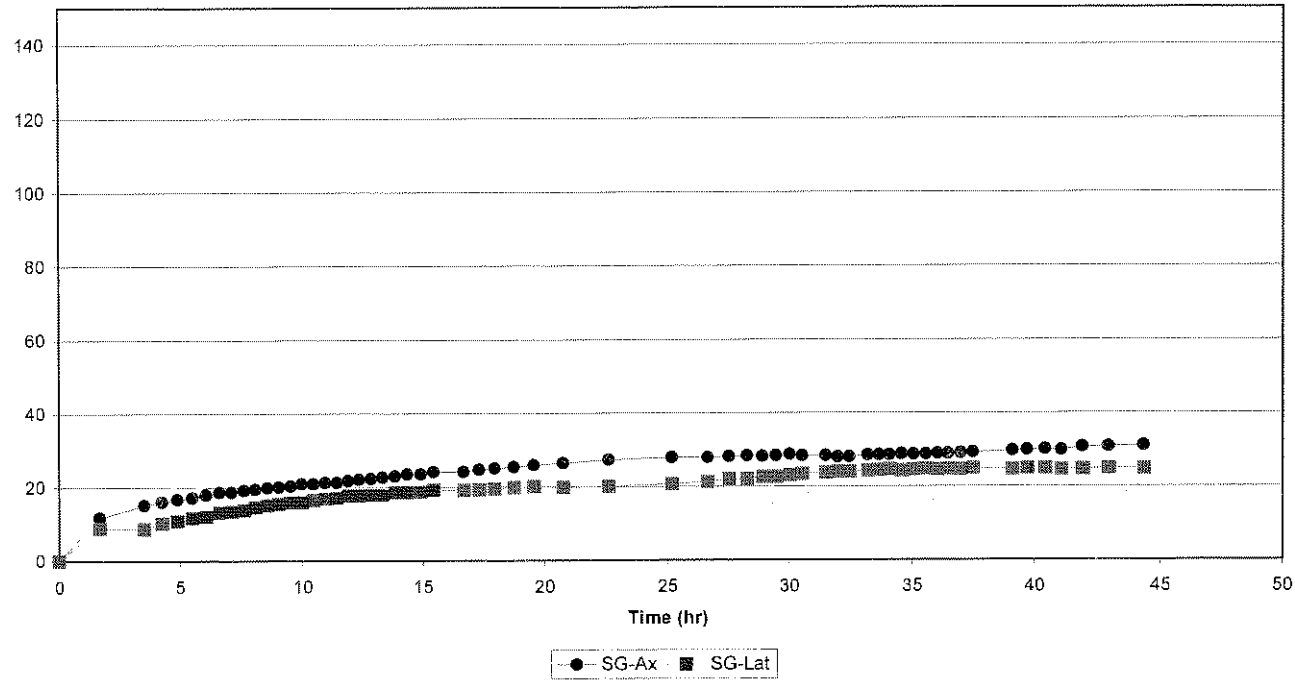

Axial Strain vs Time
2056-121 Cycle 4

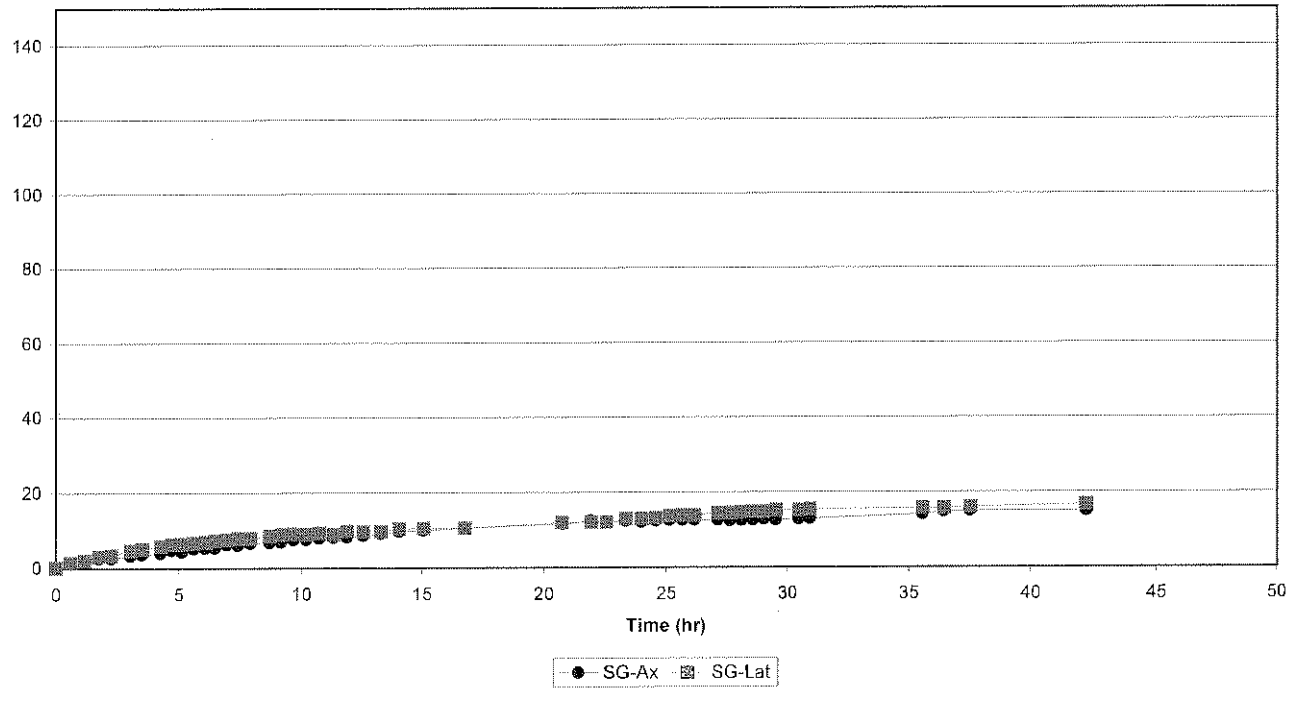

Elsburg Quartzite

Strain vs Time
2056-121 Cycle 5

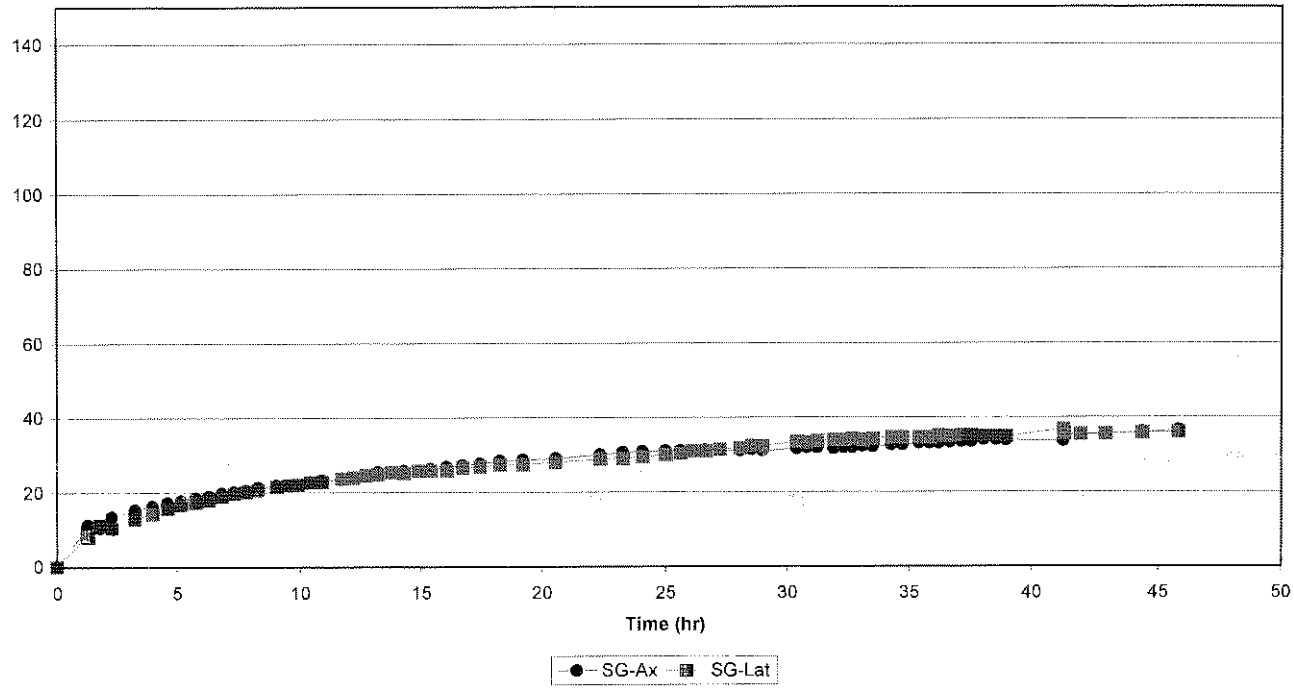

Strain vs Time
2056-121 Cycle 6

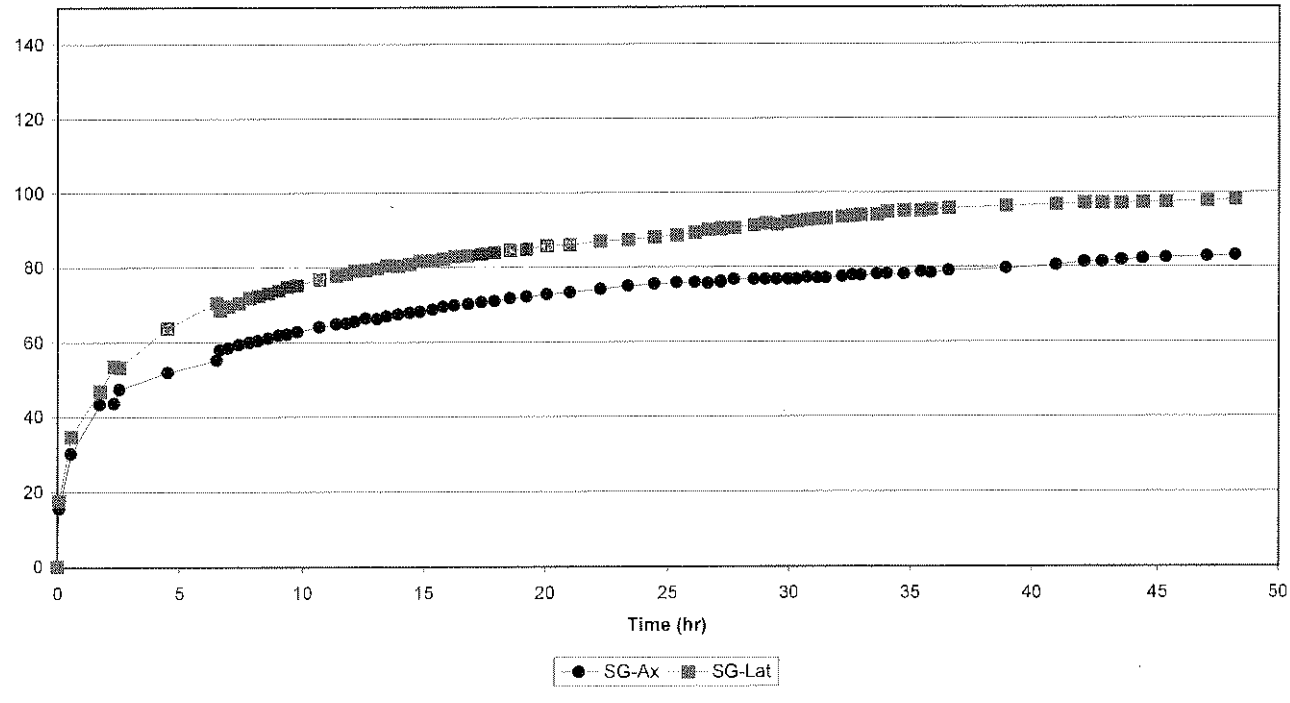

Elsburg Quartzite

Strain vs Time
2056-121 Cycle 7

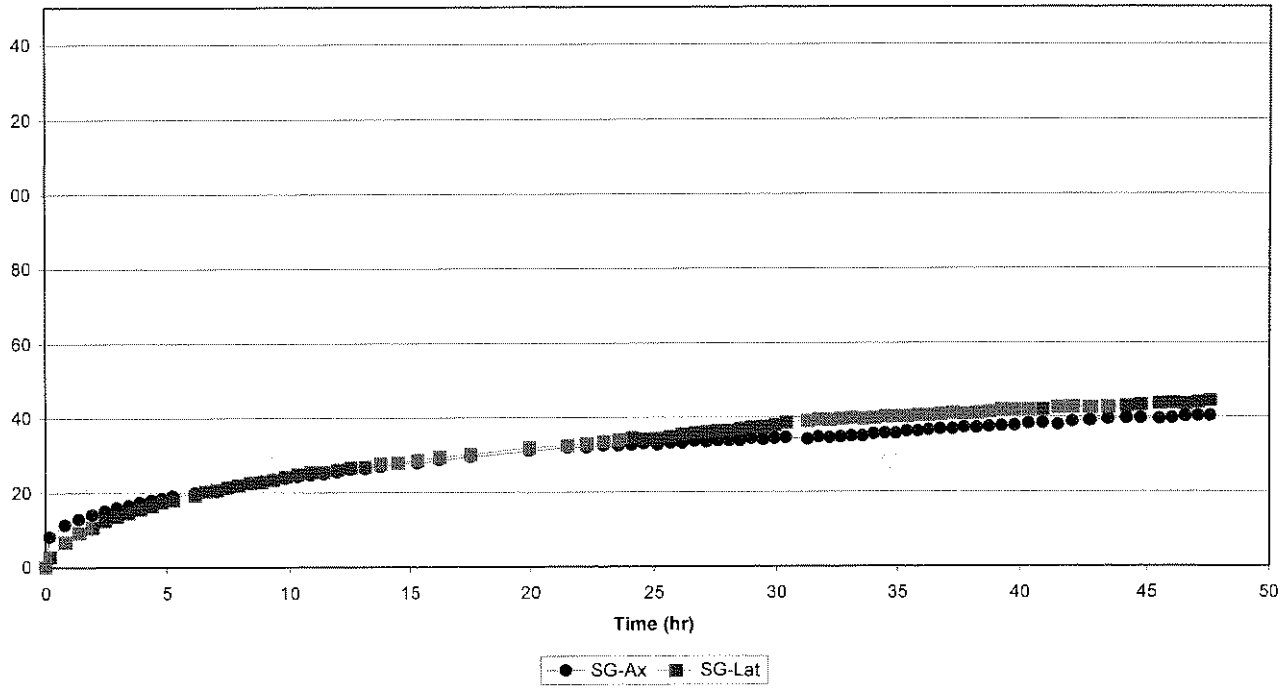

Strain vs Time
2056-121 Cycle 8

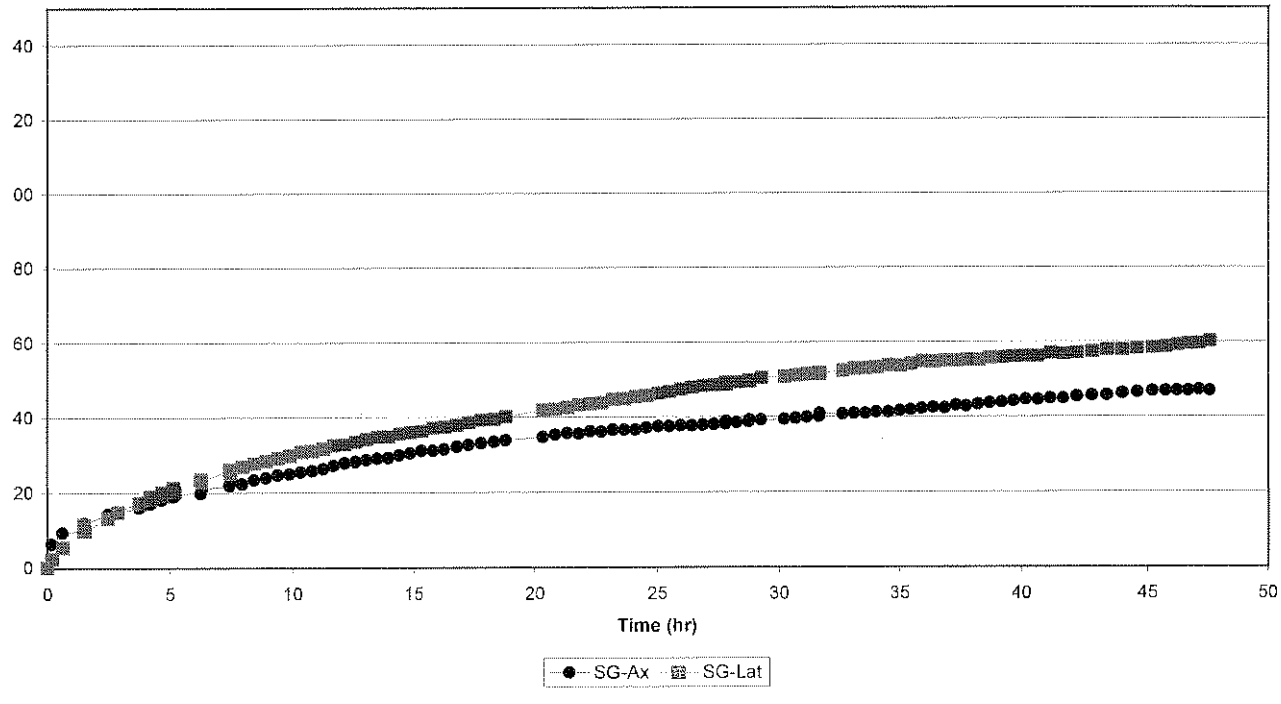

Elsburg Quartzite

Strain vs Time
2056-121 Cycle 9

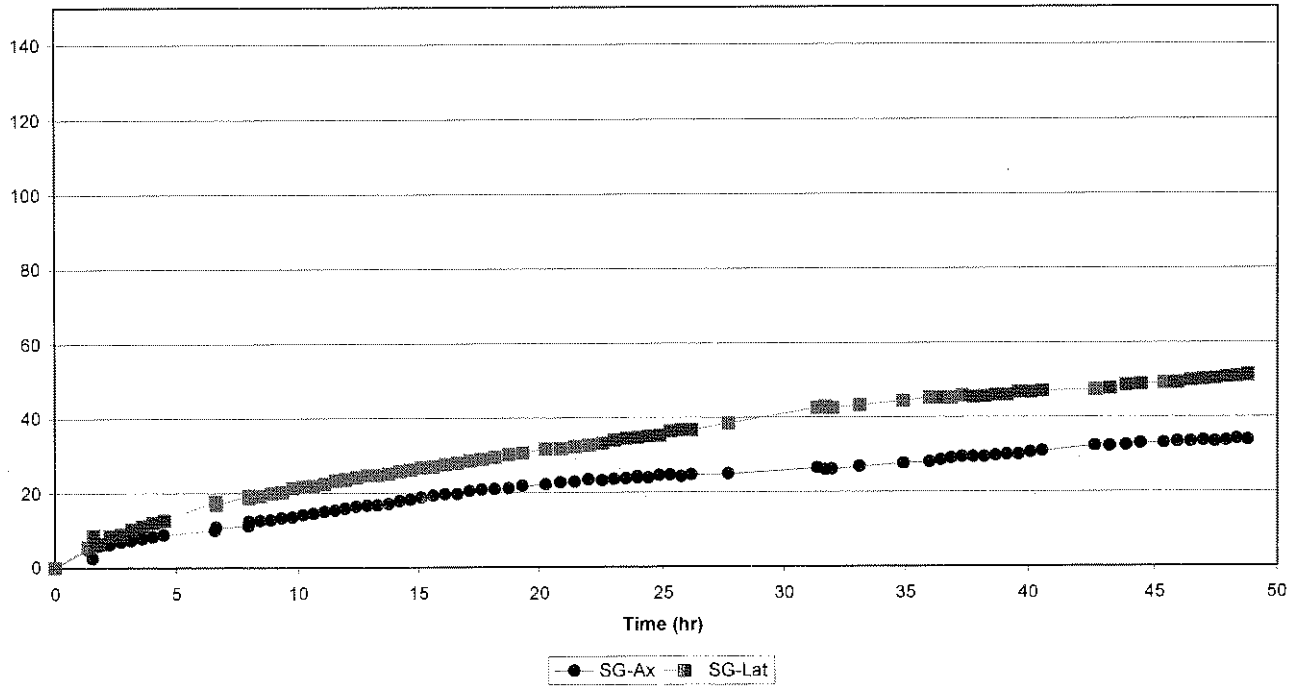

Strain vs Time
2056-121 Cycle 10

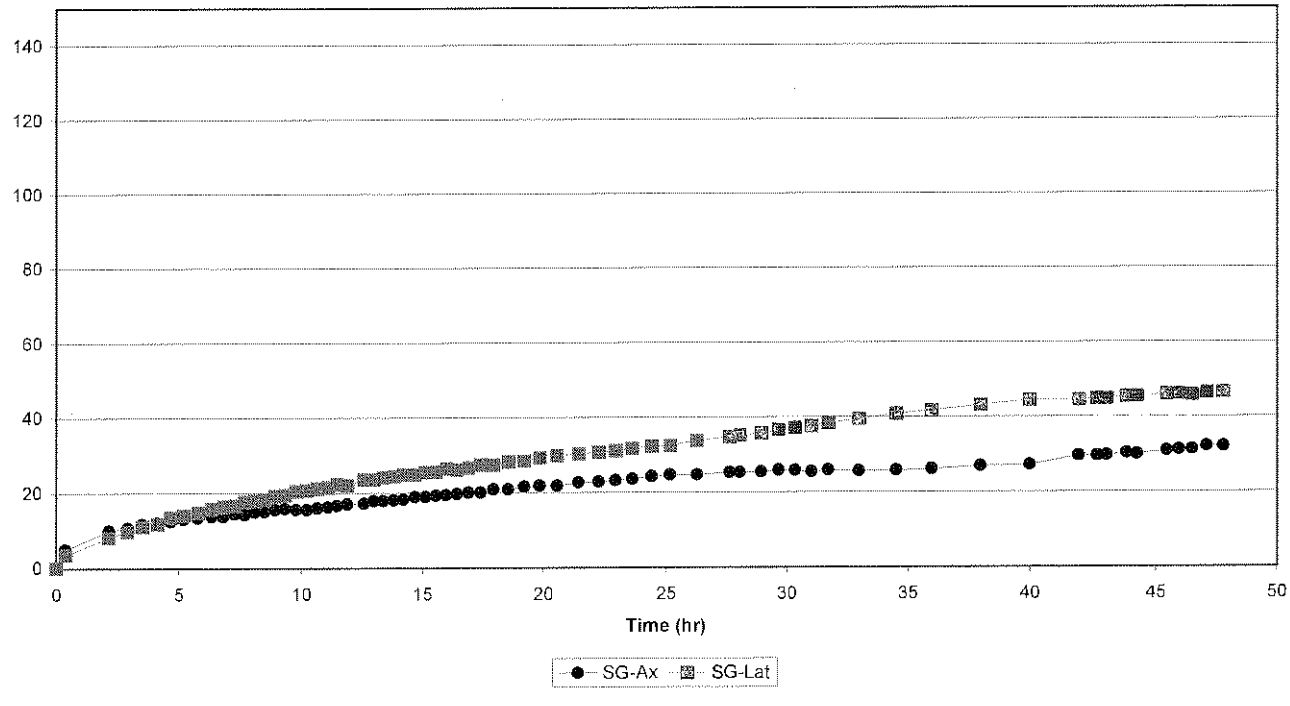

Elsburg Quartzite

Strain vs Time
2056-121 Cycle 11

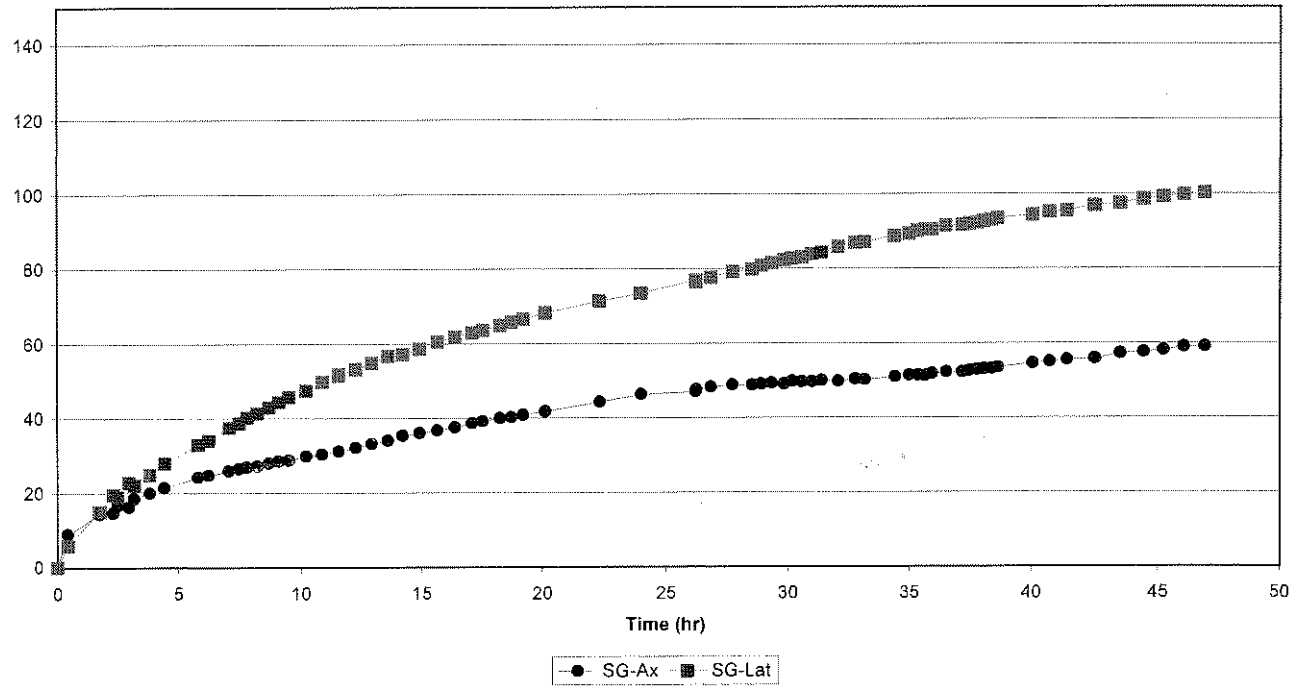

Strain vs Time
2056-121 Cycle 12

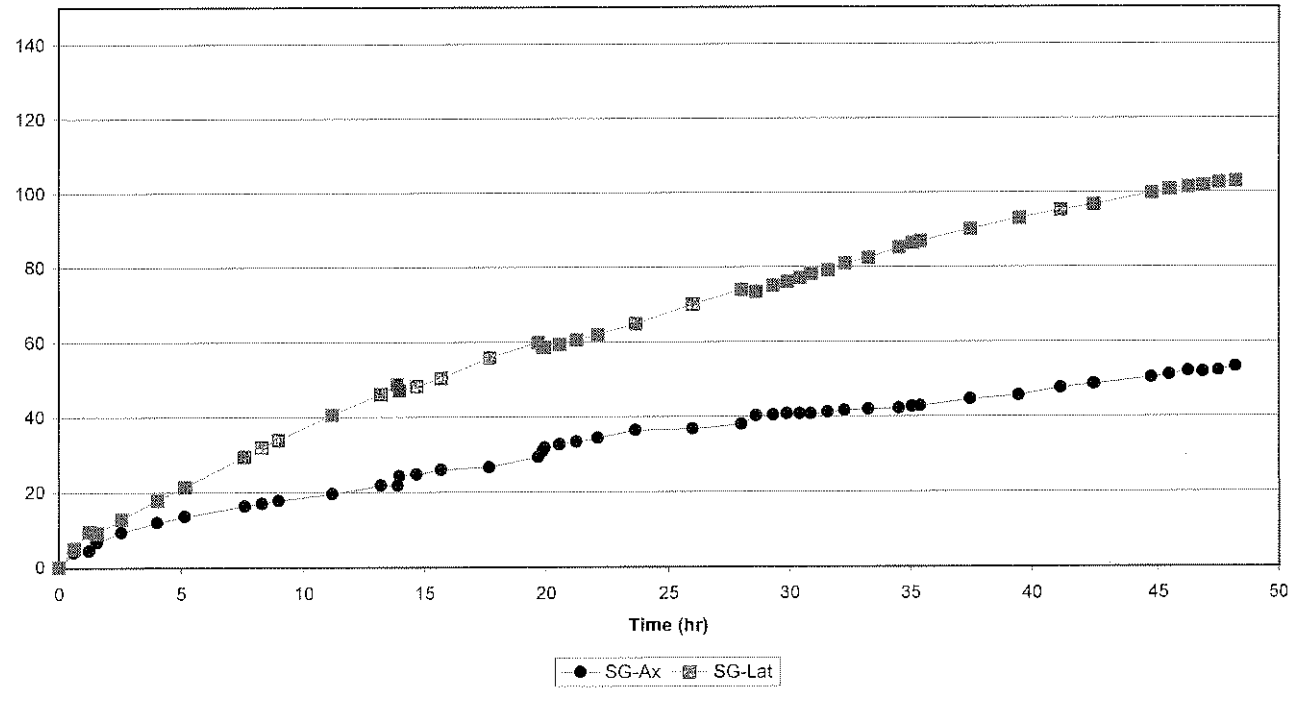

Elsburg Quartzite

Strain vs Time
2056-121 Cycle 13

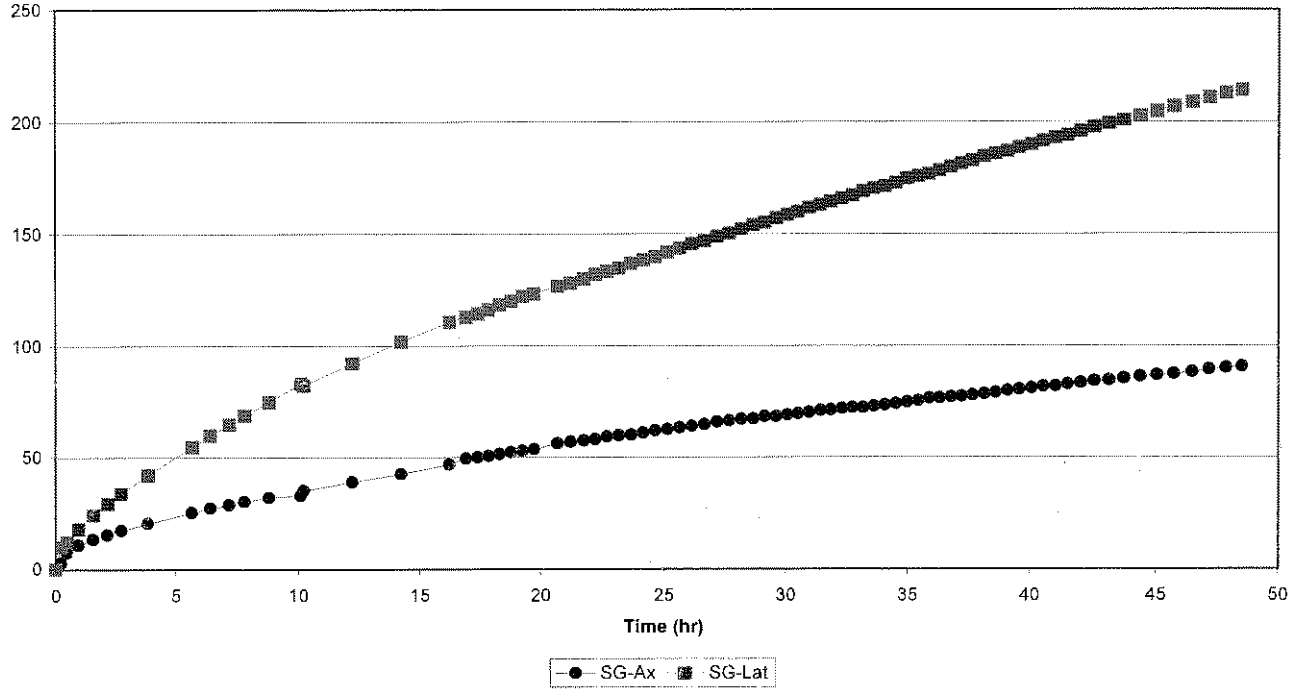

Strain vs Time
2056-121 Cycle 14

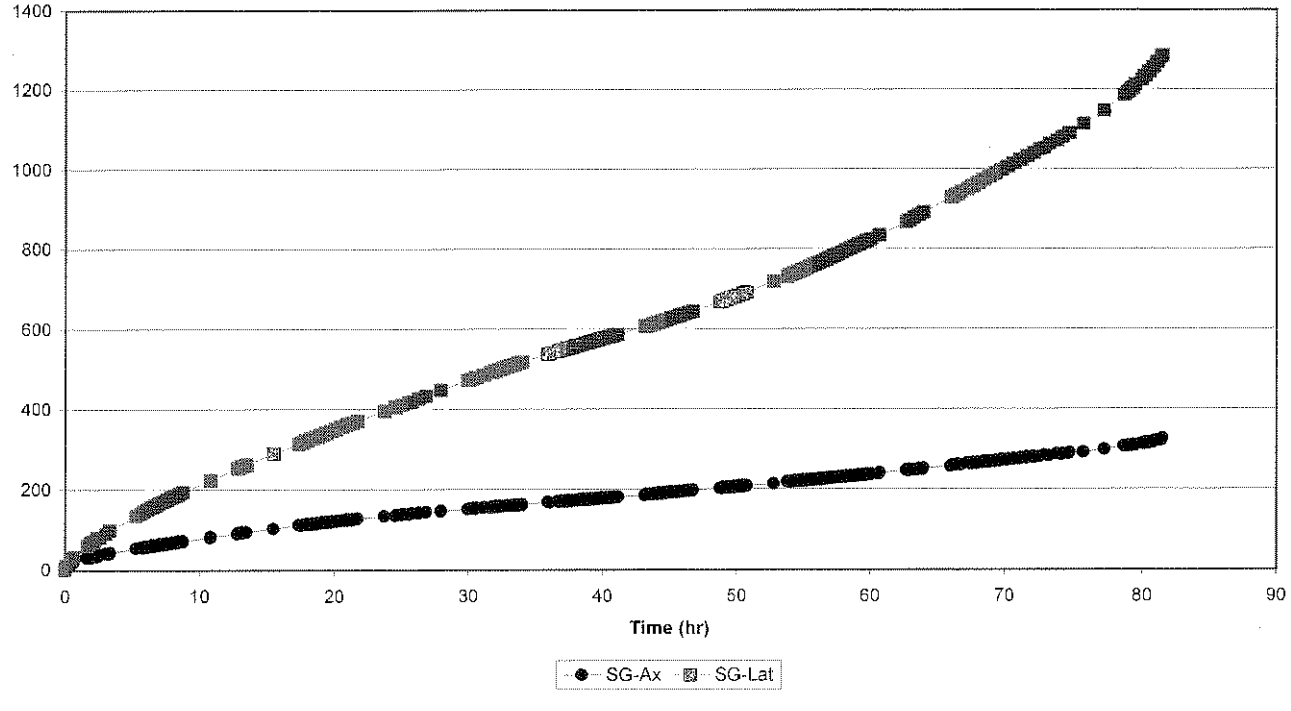

Elsburg Quartzite

Cumulative Strain vs Stress
2056-121

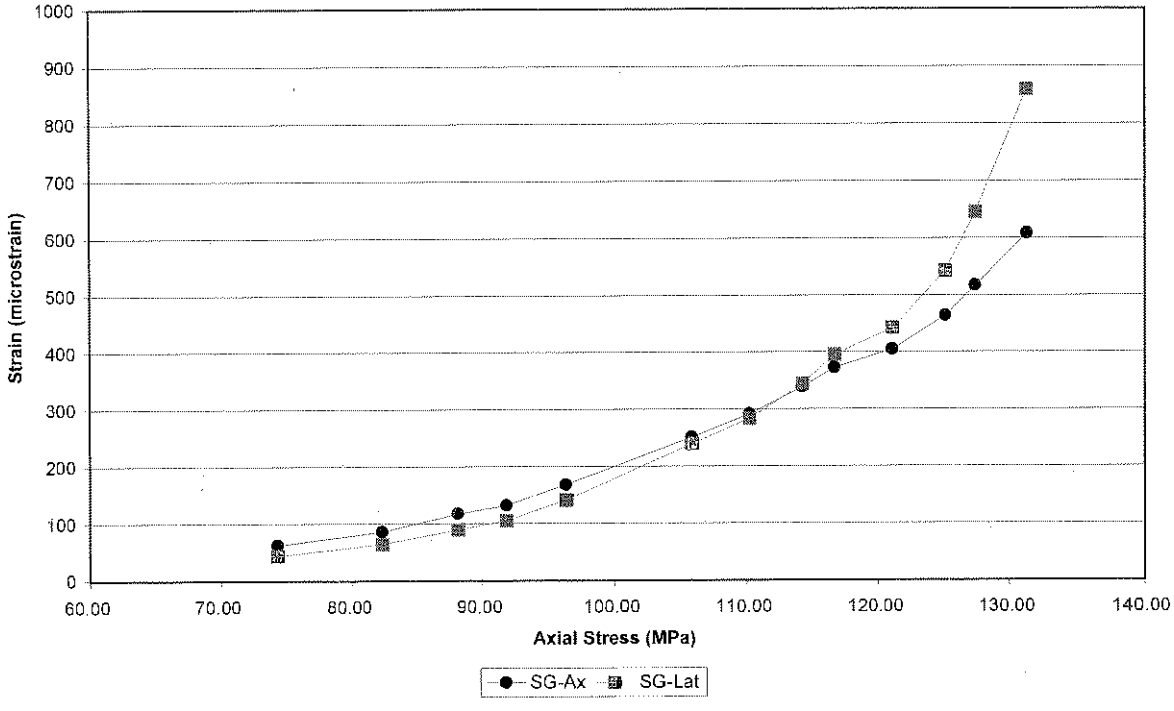

Creep rate vs Stress
2056-121

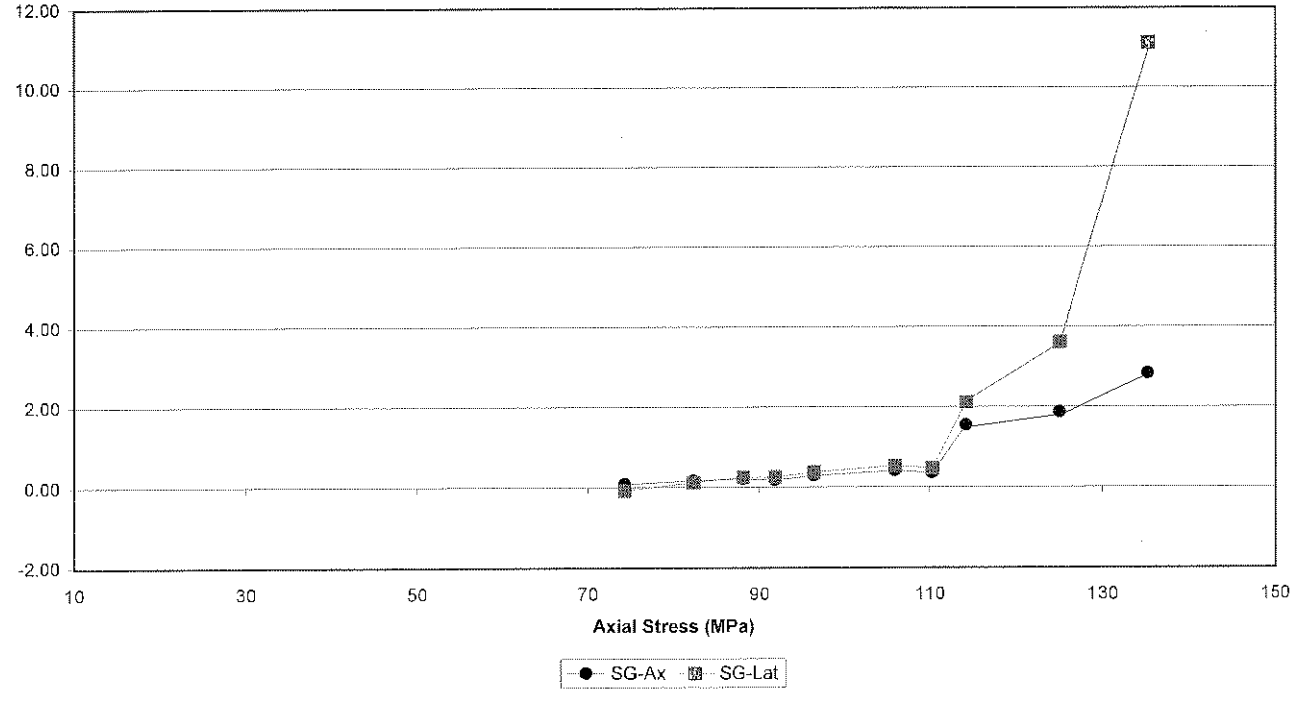

Elsburg Quartzite

Log Creeprate vs Log Stress
2056-121

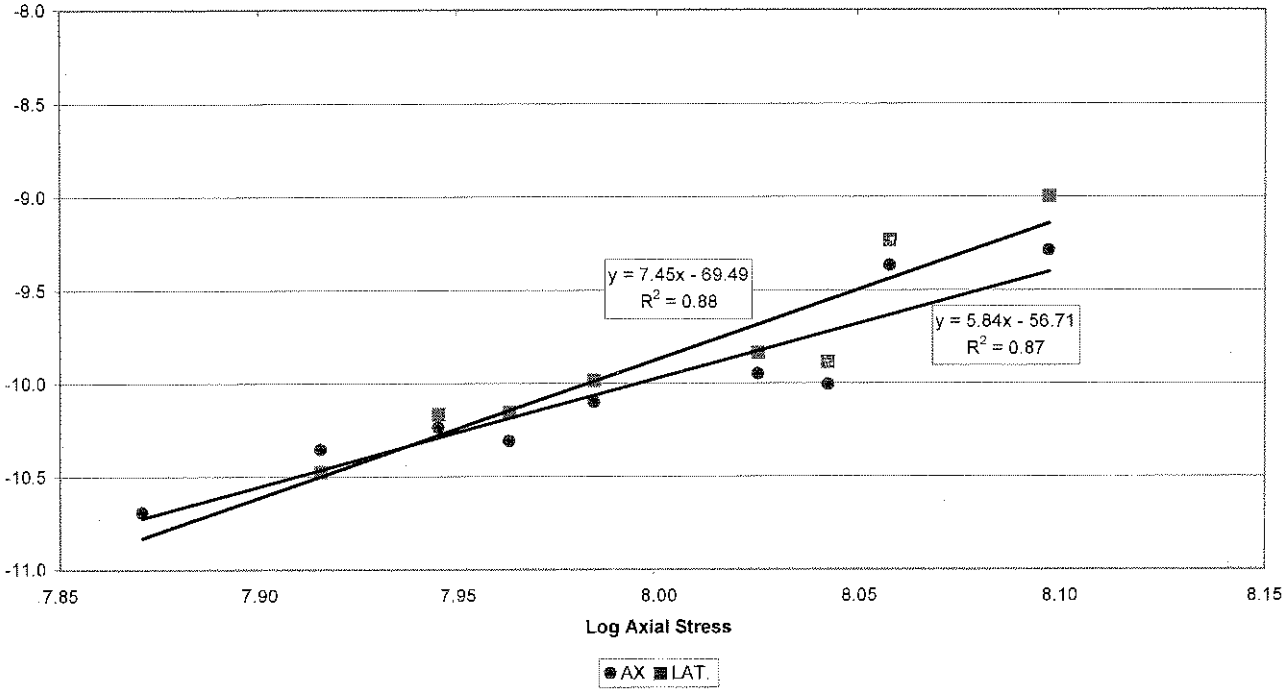

Appendix C

Results of creep shear tests

Creep Shear 2056-143
Crushed Elsburg Quartzite (dry, < 0.5mm, 0.5mm)

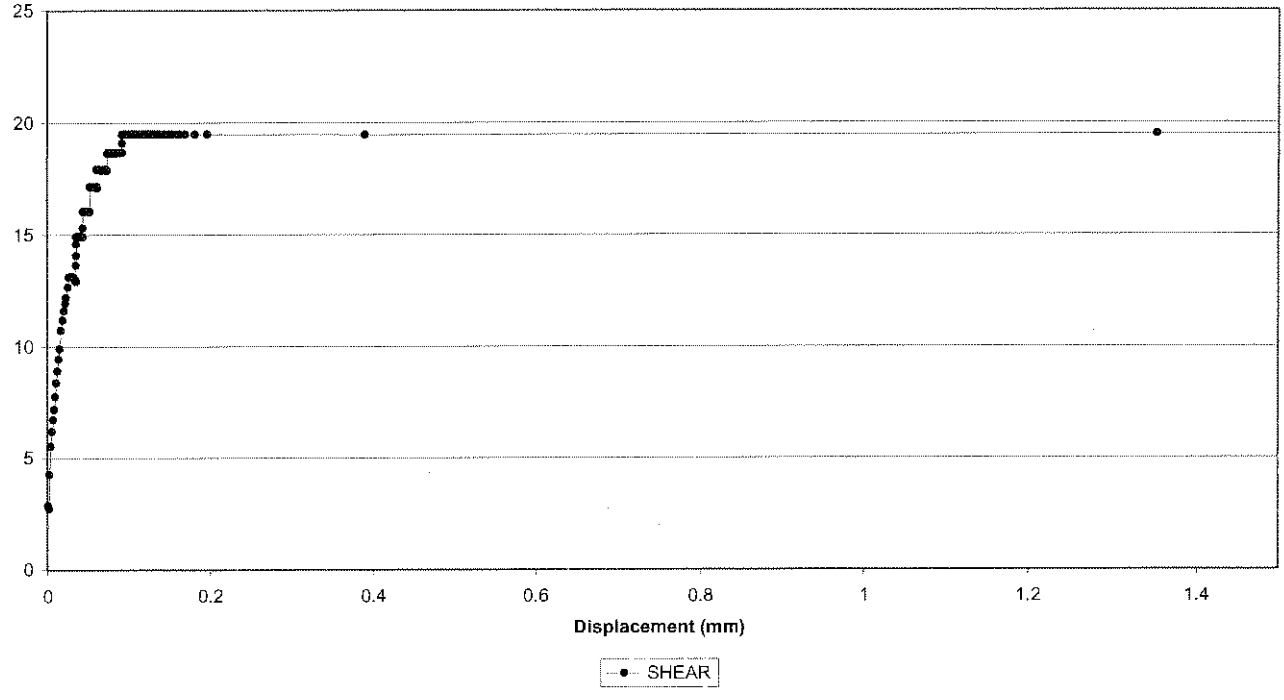

Creep Shear 2056-143
Crushed Elsburg Quartzite (dry, < 0.5mm, 0.5mm)

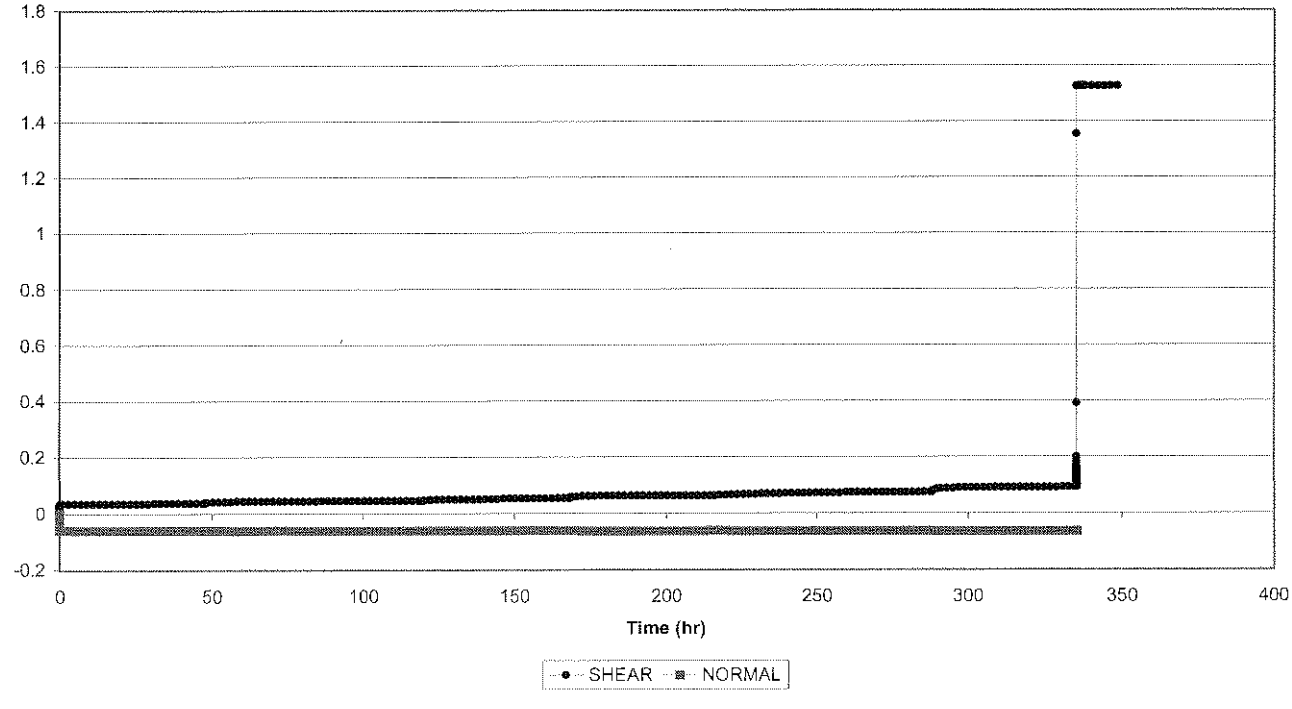

Creep Shear 2056-143, Cycle 1
Crushed Elsburg Quartzite (dry, < 0.5mm, 0.5mm)

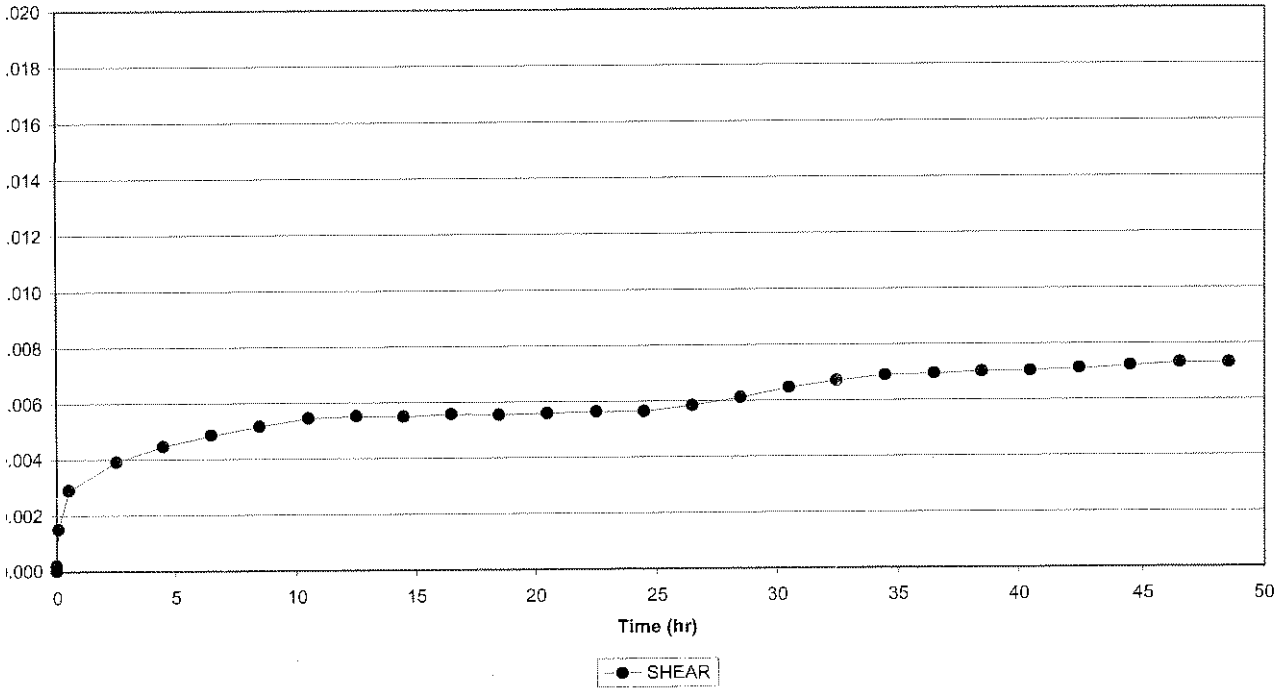

Creep Shear 2056-143, Cycle 2
Crushed Elsburg Quartzite (dry, < 0.5mm, 0.5mm)

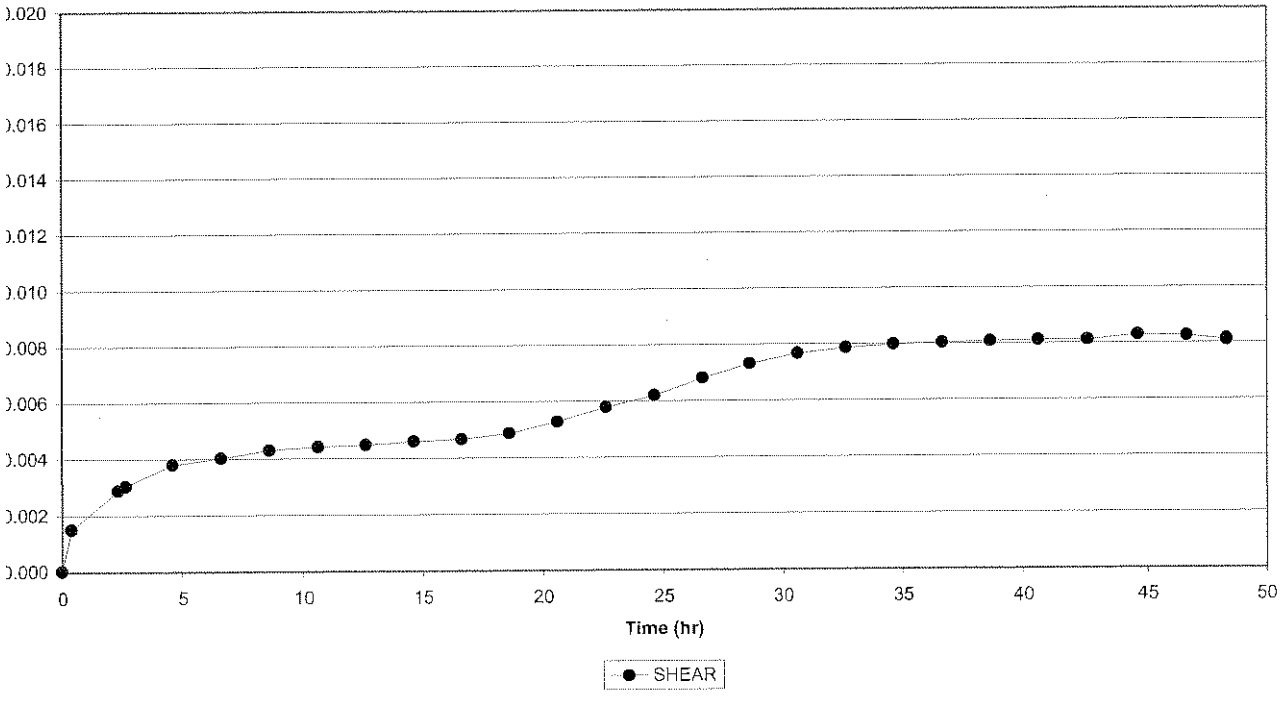

Creep Shear 2056-143, Cycle 3
Crushed Elsburg Quartzite (dry, < 0.5mm, 0.5mm)

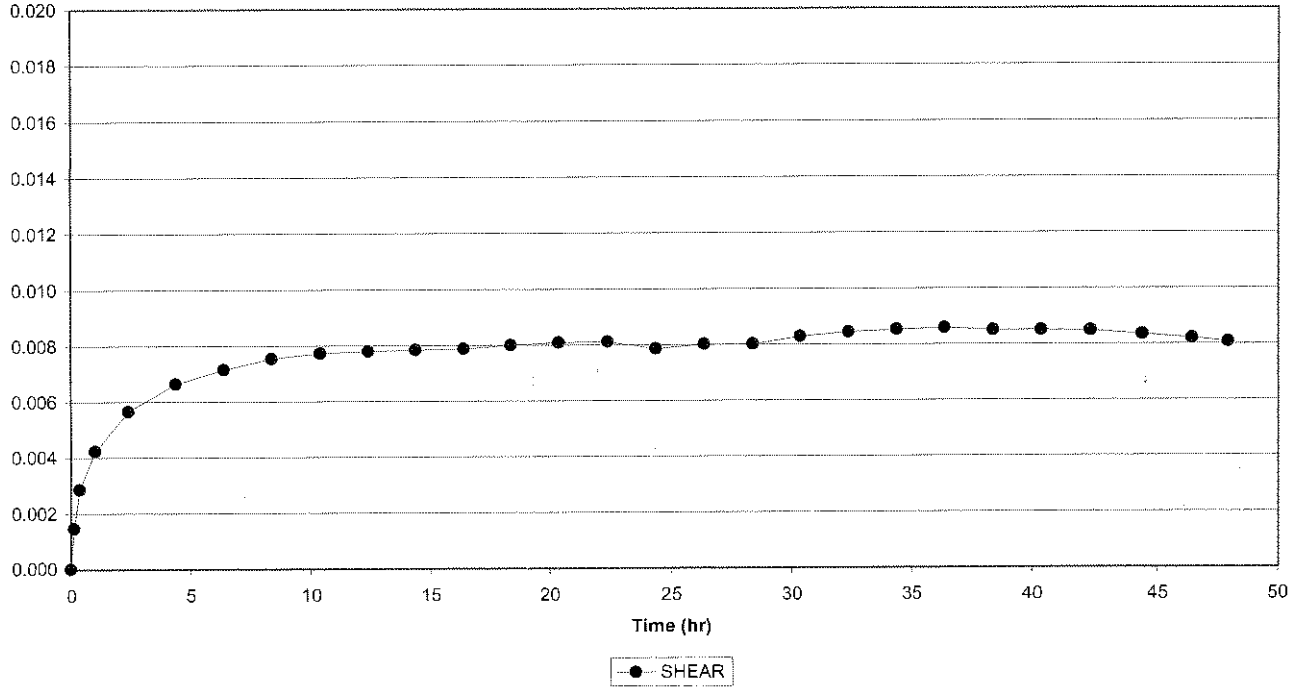

Creep Shear 2056-143, Cycle 4
Crushed Elsburg Quartzite (dry, < 0.5mm, 0.5mm)

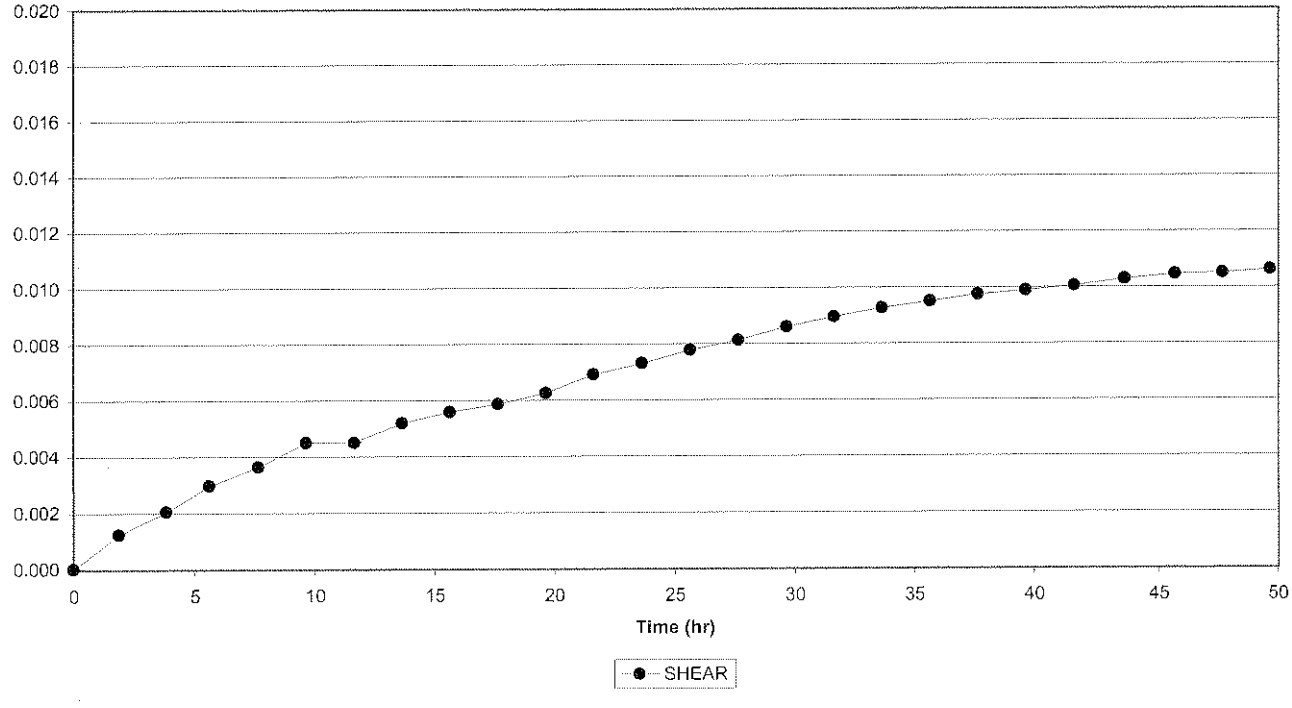

Creep Shear 2056-143, Cycle 5
Crushed Elsburg Quartzite (dry, < 0.5mm, 0.5mm)

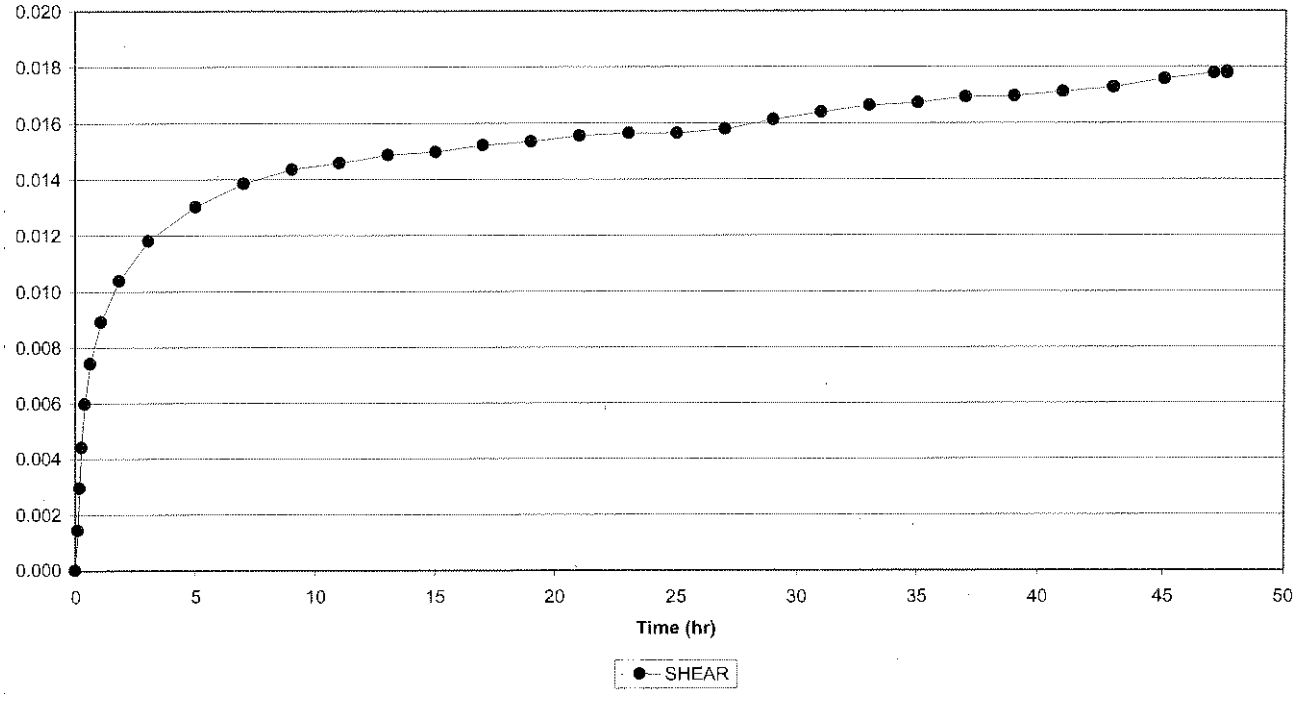

Creep Shear 2056-143, Cycle 5
Crushed Elsburg Quartzite (dry, < 0.5mm, 0.5mm)

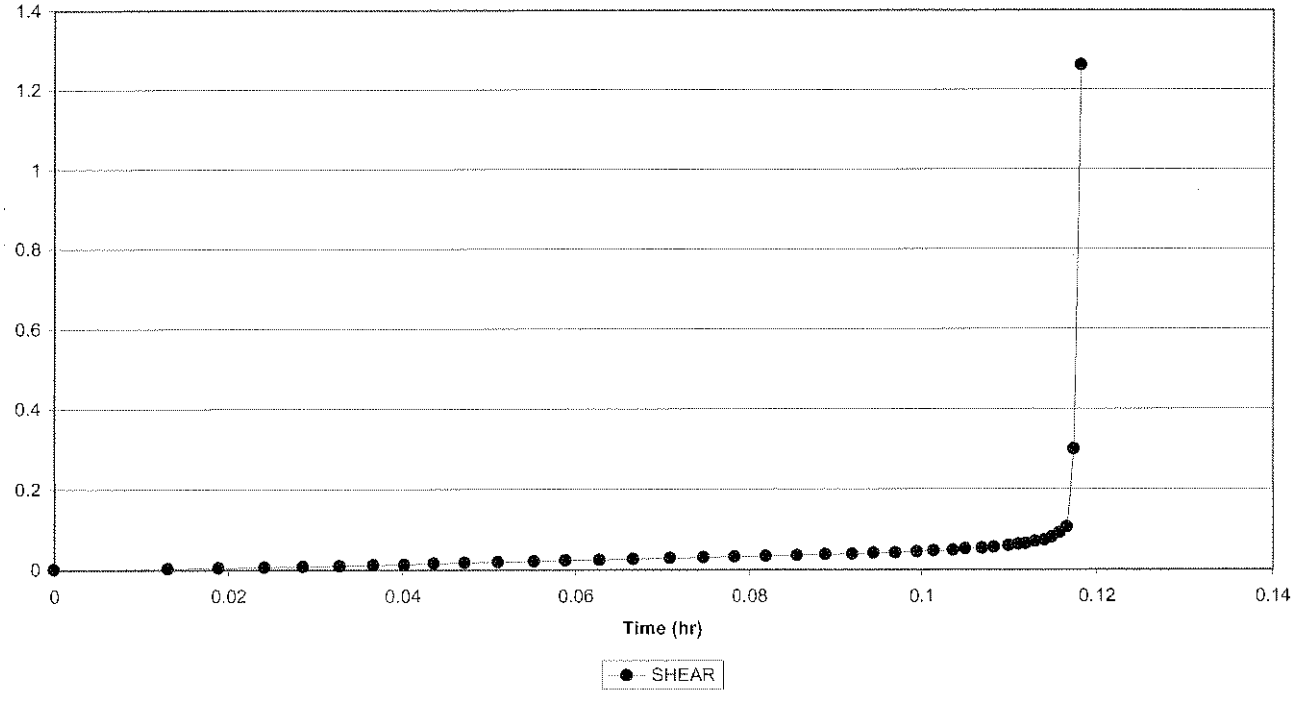

Creep Shear 2056-143
Crushed Elsburg Quartzite (dry, < 0.5mm, 0.5mm)

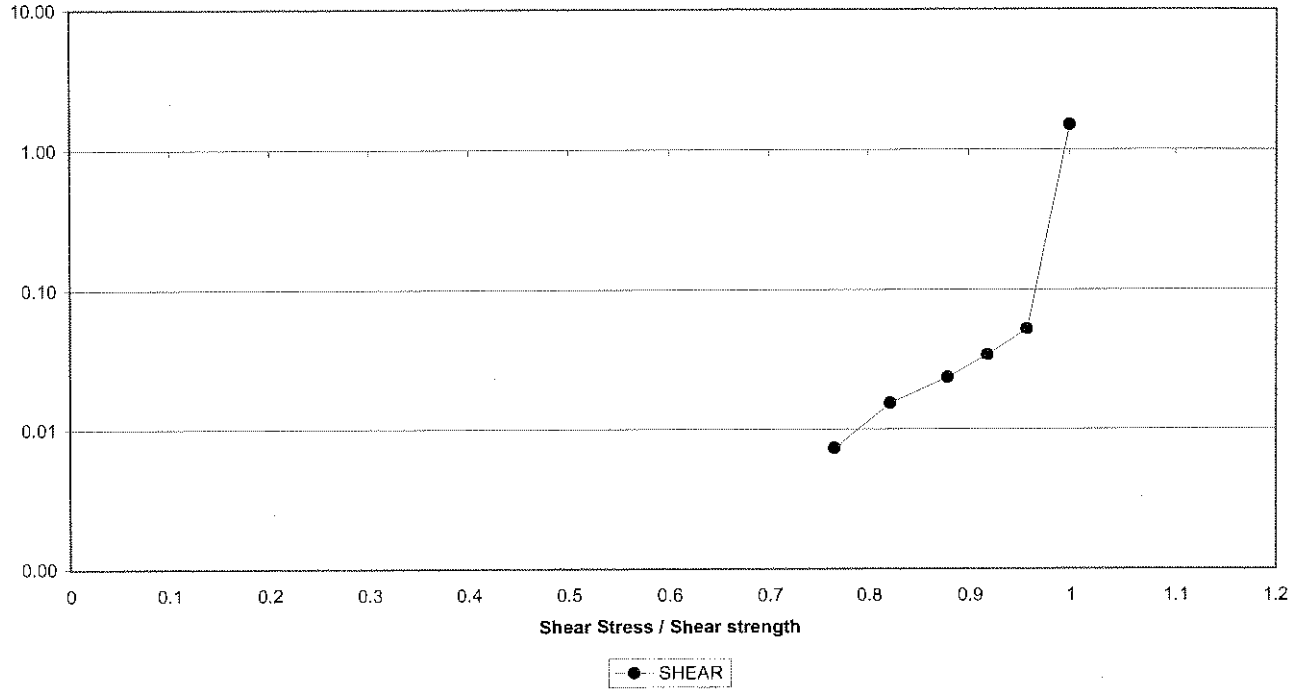

Creep Shear 2056-143
Crushed Elsburg Quartzite (dry, < 0.5mm, 0.5mm)

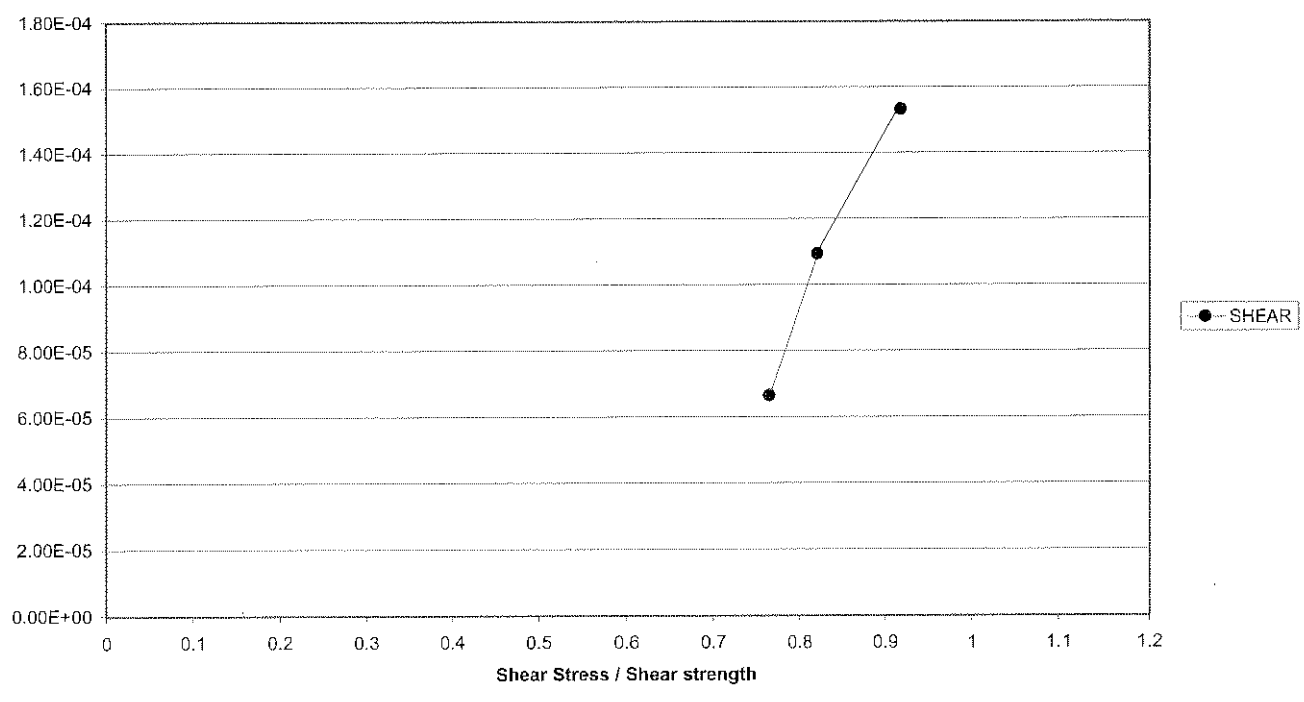

Creep Shear 2056-143
Crushed Elsburg Quartzite (dry, < 0.5mm, 0.5mm)

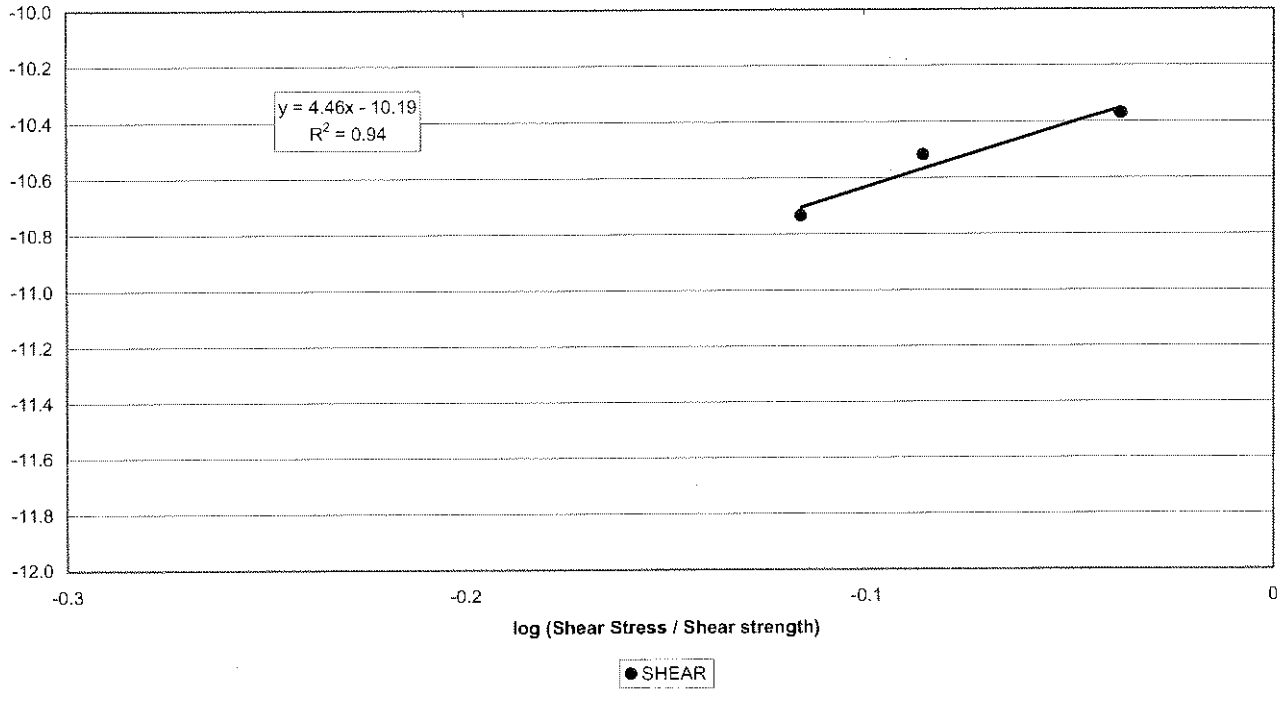

Creep Shear 2056-144
Crushed Elsburg Quartzite (dry, < 0.5mm, 1mm)

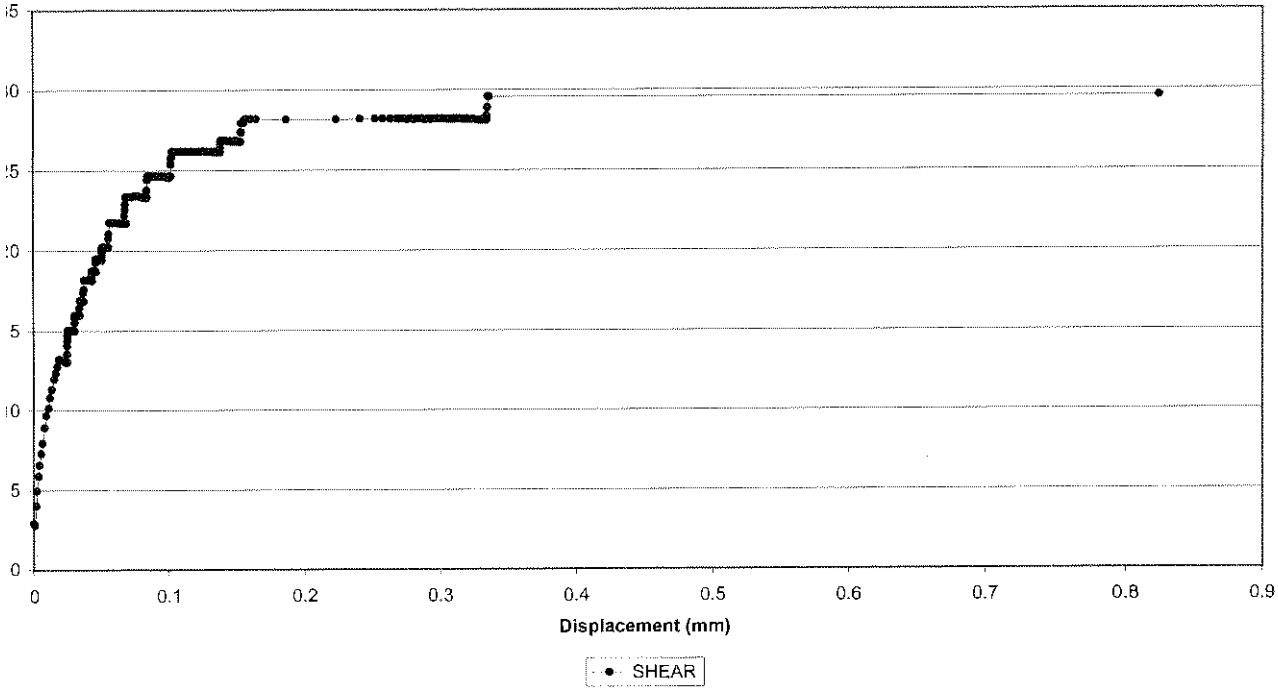

Creep Shear 2056-144
Crushed Elsburg Quartzite (dry, < 0.5mm, 1mm)

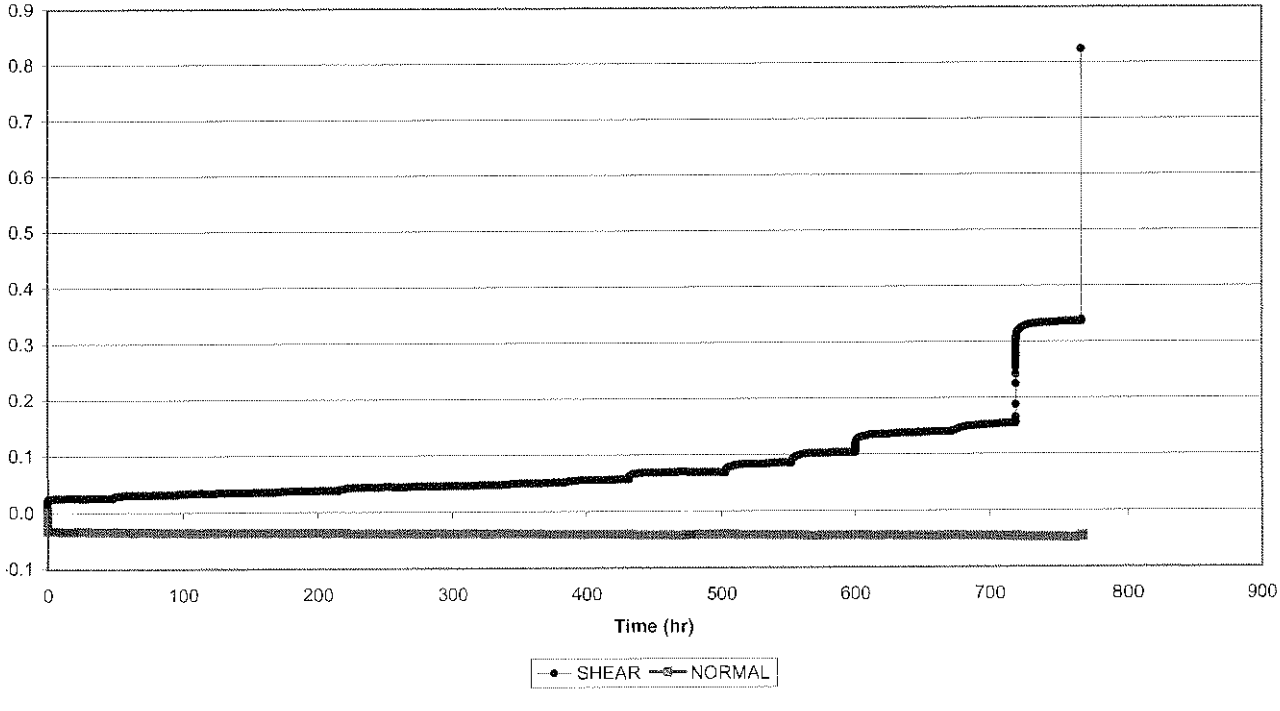

Creep Shear 2056-144, Cycle 1
Crushed Elsburg Quartzite (dry, < 0.5mm, 1mm)

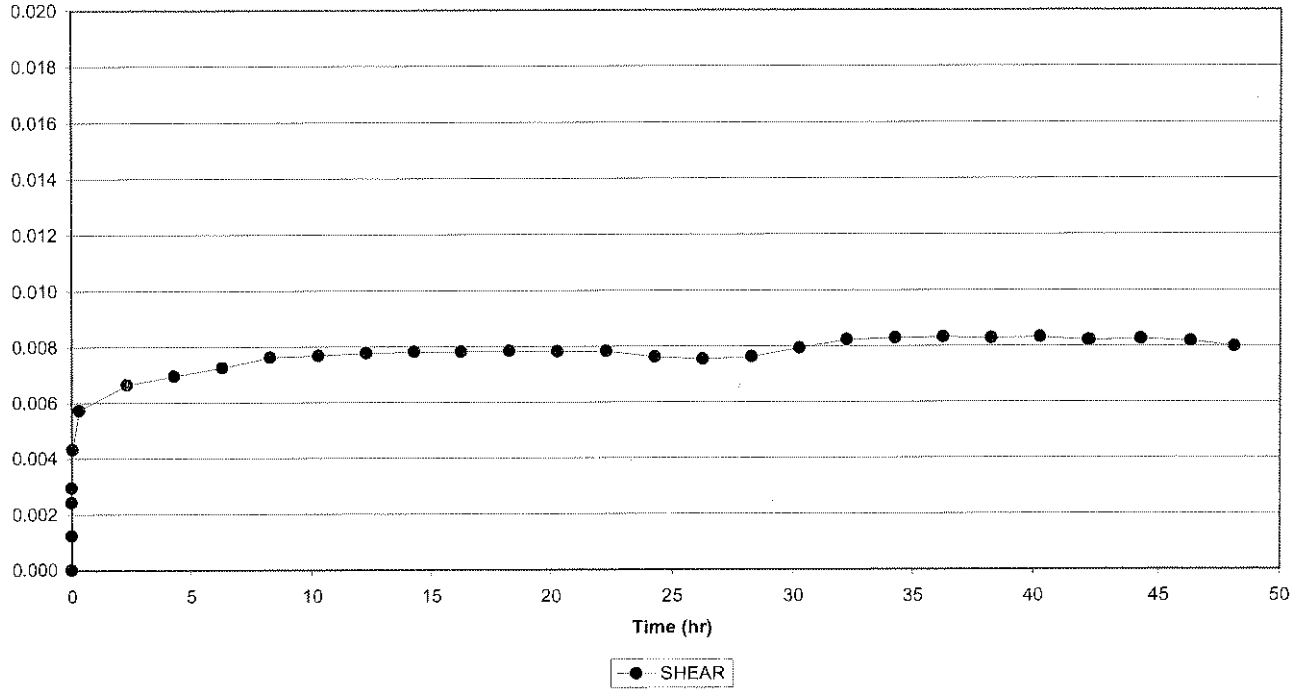

Creep Shear 2056-144, Cycle 2
Crushed Elsburg Quartzite (dry, < 0.5mm, 1mm)

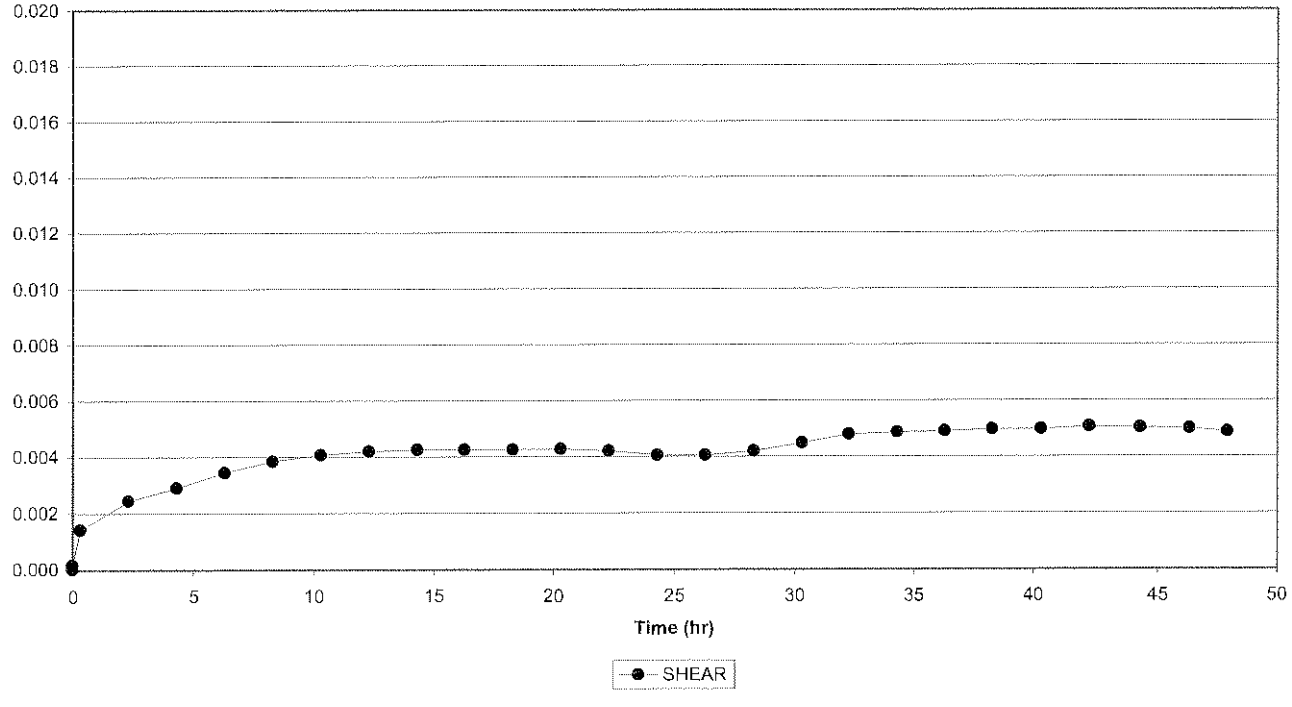

Creep Shear 2056-144, Cycle 8
Crushed Elsburg Quartzite (dry, < 0.5mm, 1mm)

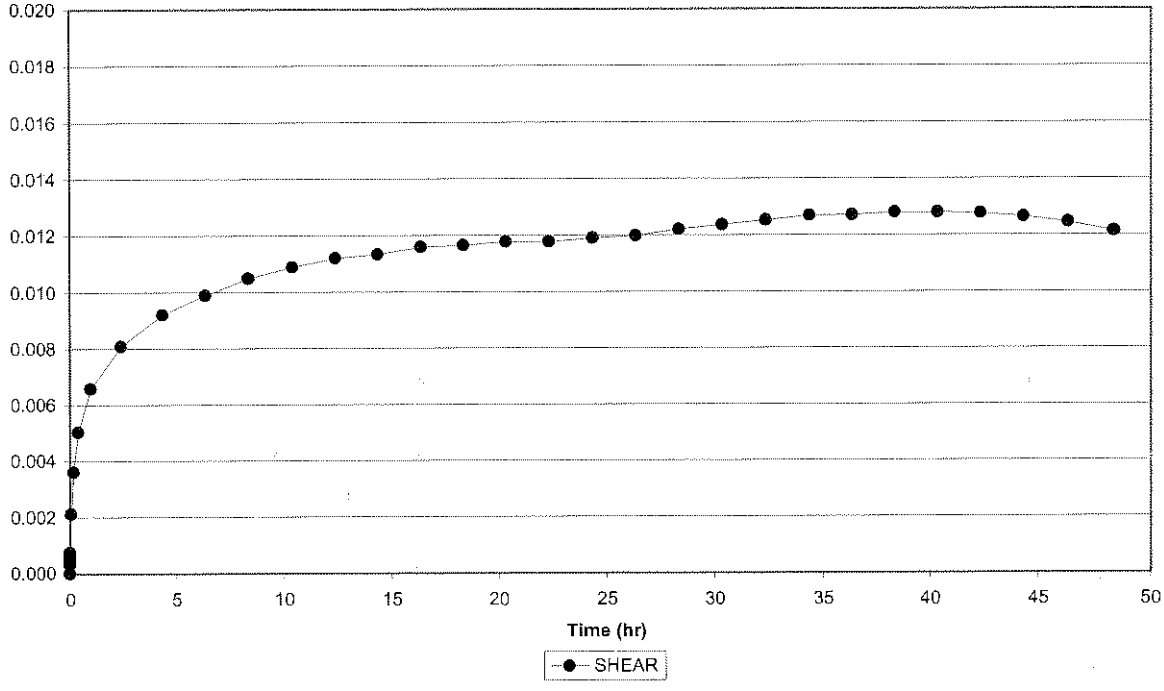

Creep Shear 2056-144, Cycle 9
Crushed Elsburg Quartzite (dry, < 0.5mm, 1mm)

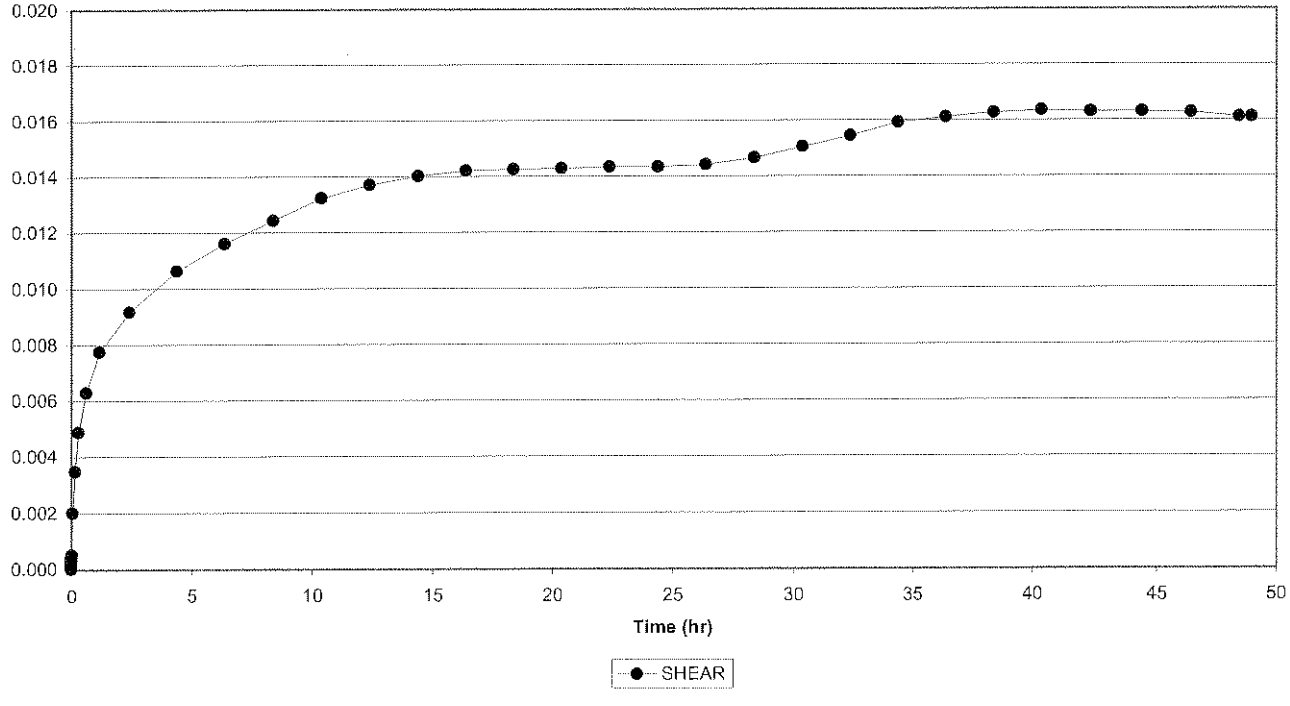

Creep Shear 2056-144, Cycle 10
Crushed Elsburg Quartzite (dry, < 0.5mm, 1mm)

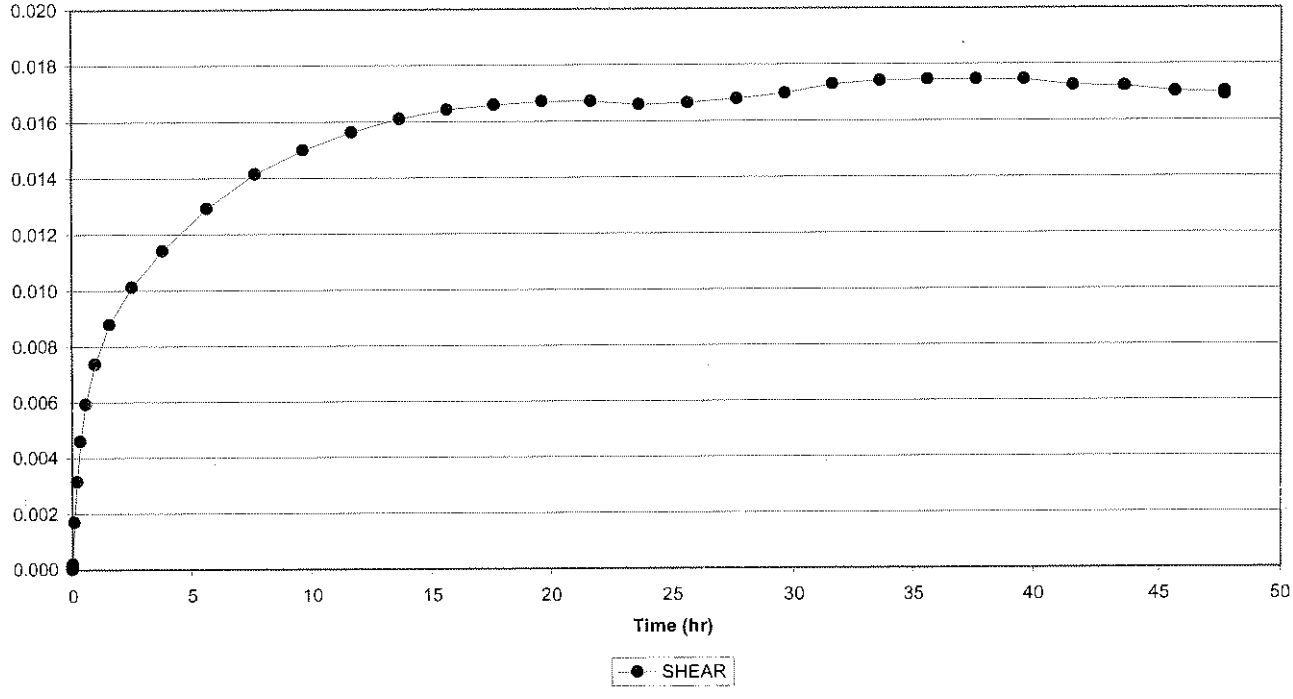

Creep Shear 2056-144, Cycle 11
Crushed Elsburg Quartzite (dry, < 0.5mm, 1mm)

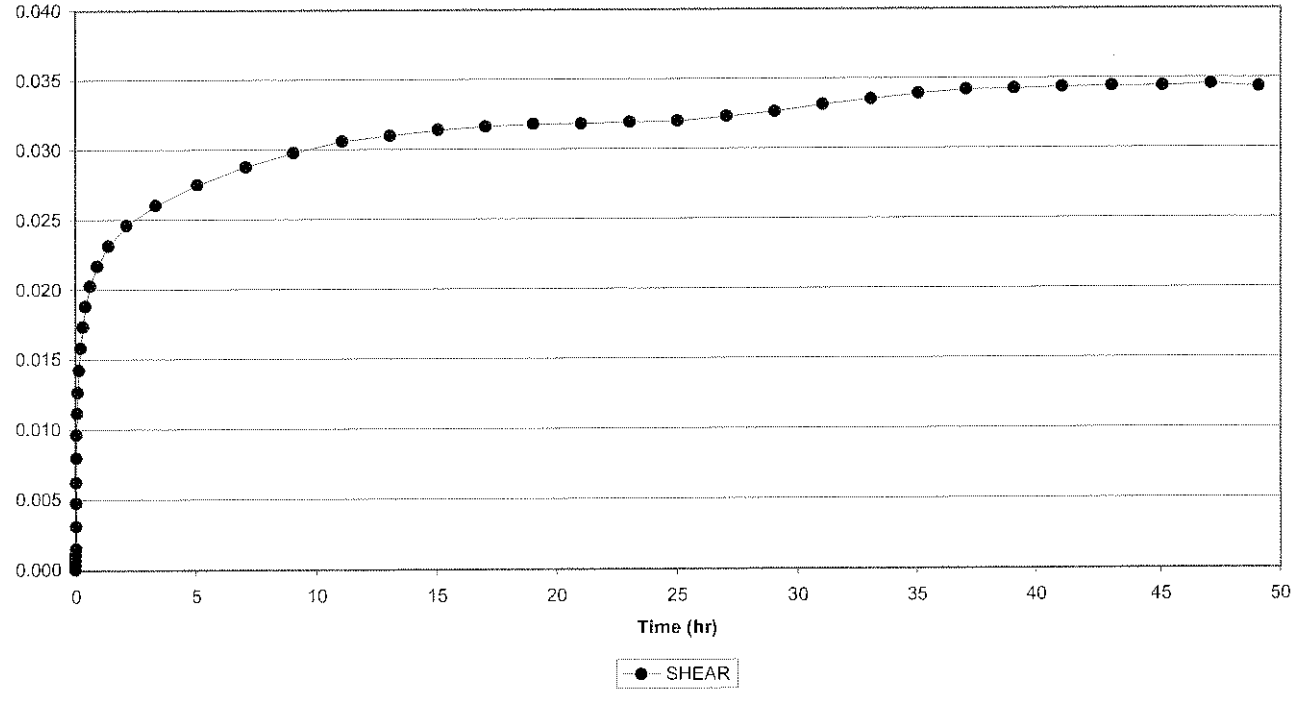

Creep Shear 2056-144, Cycle 12
Crushed Elsburg Quartzite (dry, < 0.5mm, 1mm)

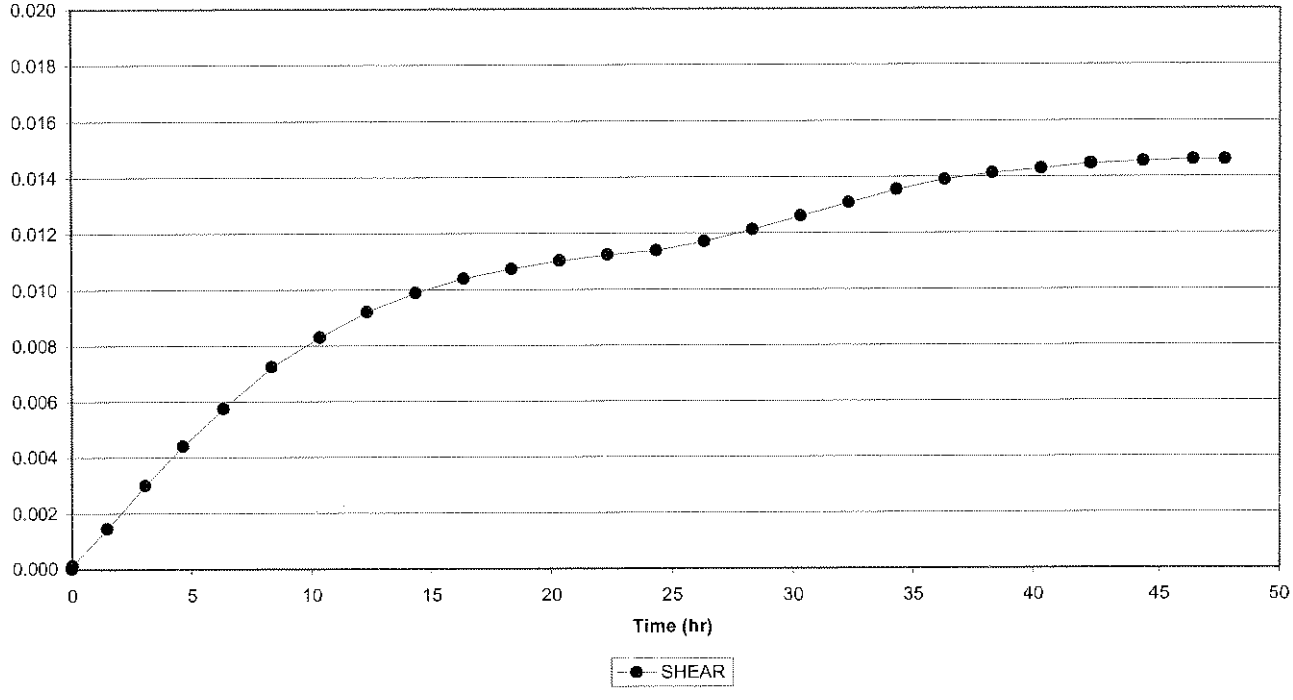

Creep Shear 2056-144, Cycle 13
Crushed Elsburg Quartzite (dry, < 0.5mm, 1mm)

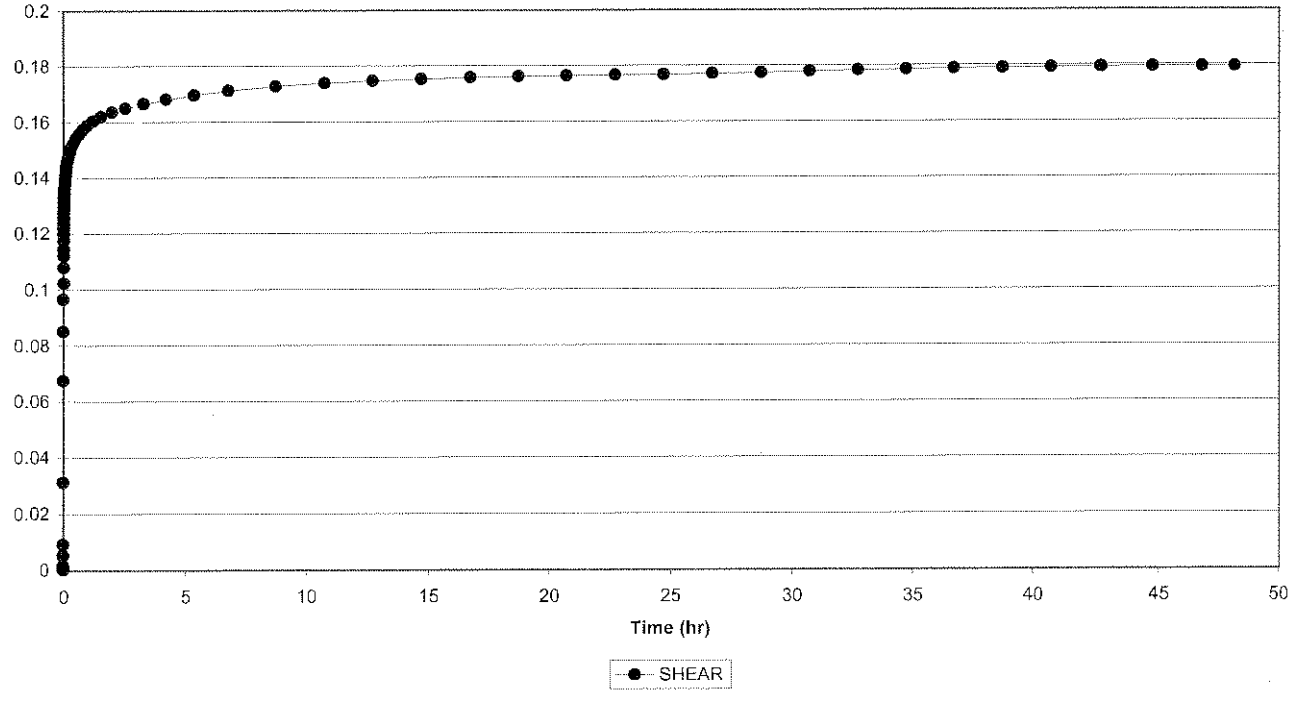

Creep Shear 2056-144, Cycle 14
Crushed Elsburg Quartzite (dry, < 0.5mm, 1mm)

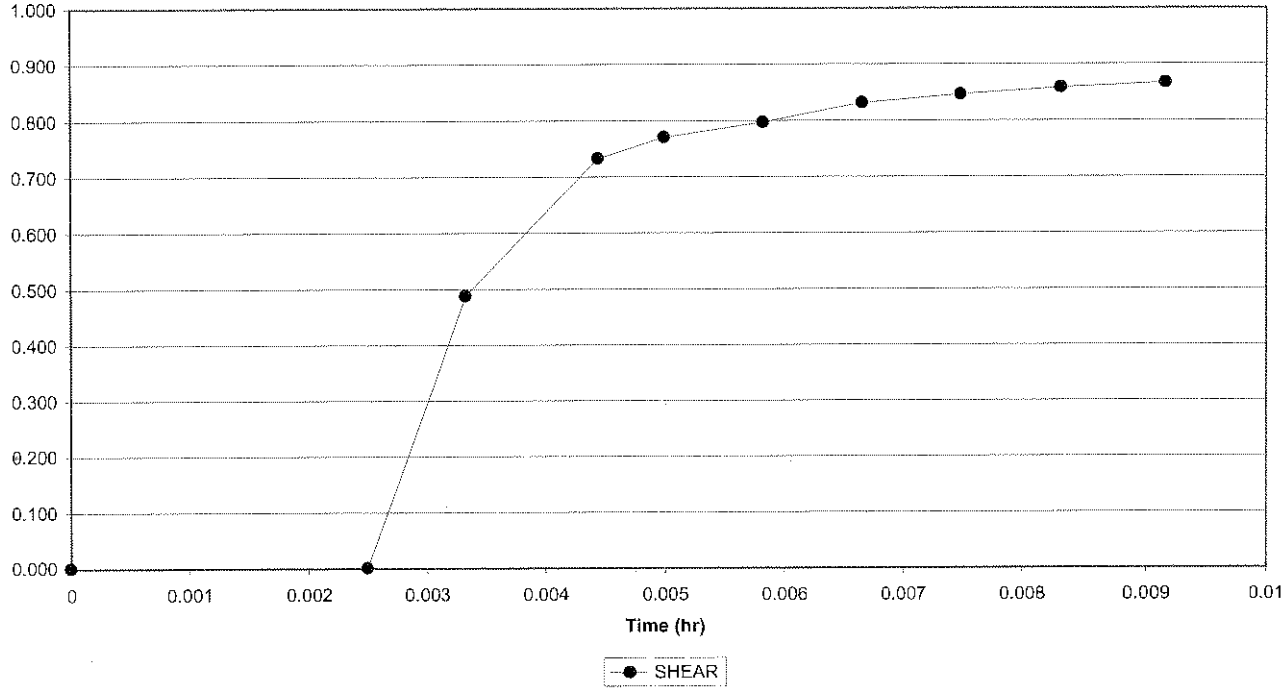

Creep Shear 2056-144
Crushed Elsburg Quartzite (dry, < 0.5mm, 1mm)

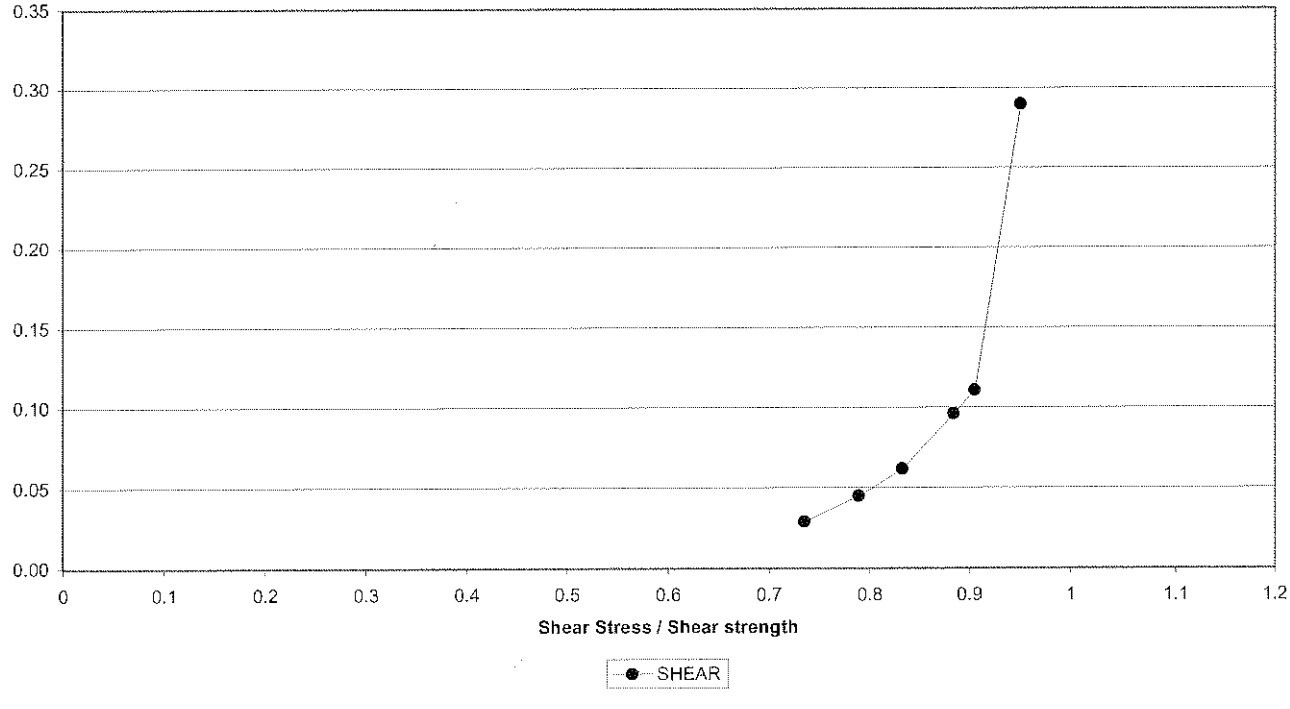

Creep Shear 2056-144
Crushed Elsburg Quartzite (dry, < 0.5mm, 1mm)

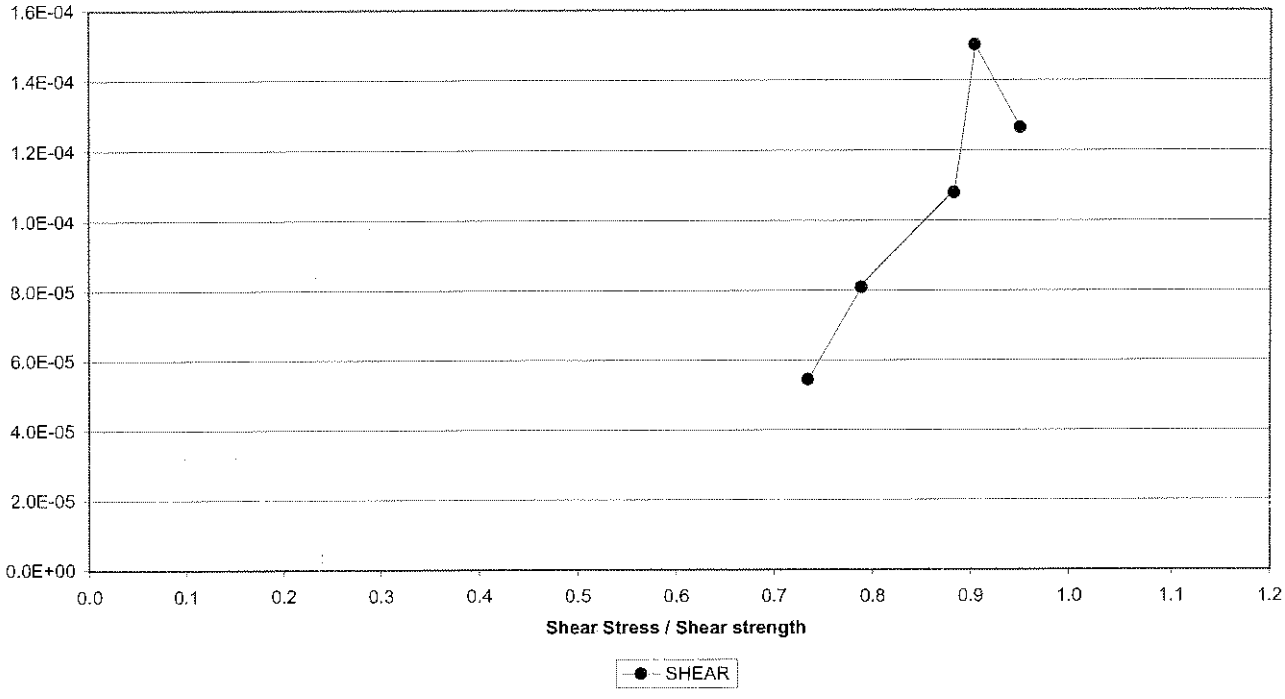

Creep Shear 2056-144
Crushed Elsburg Quartzite (dry, < 0.5mm, 1mm)

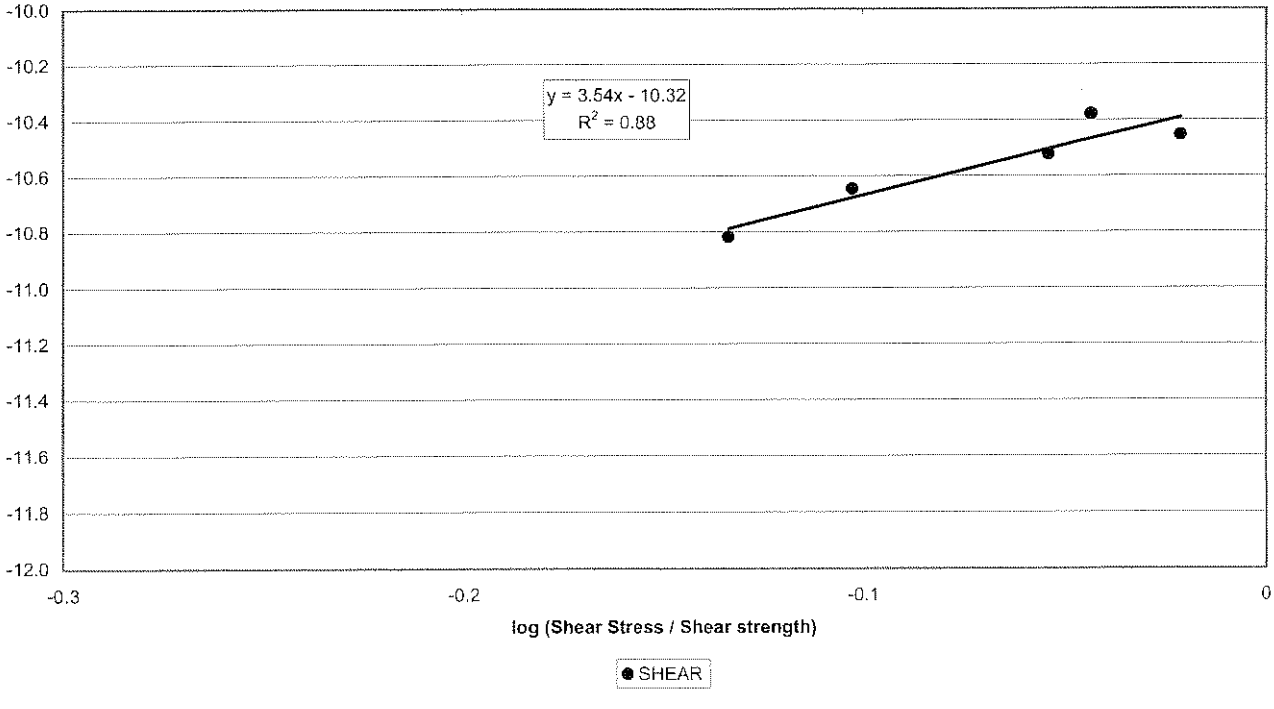

Creep Shear 2056-145
Crushed Elsburg Quartzite (dry, < 0.5mm, 2mm)

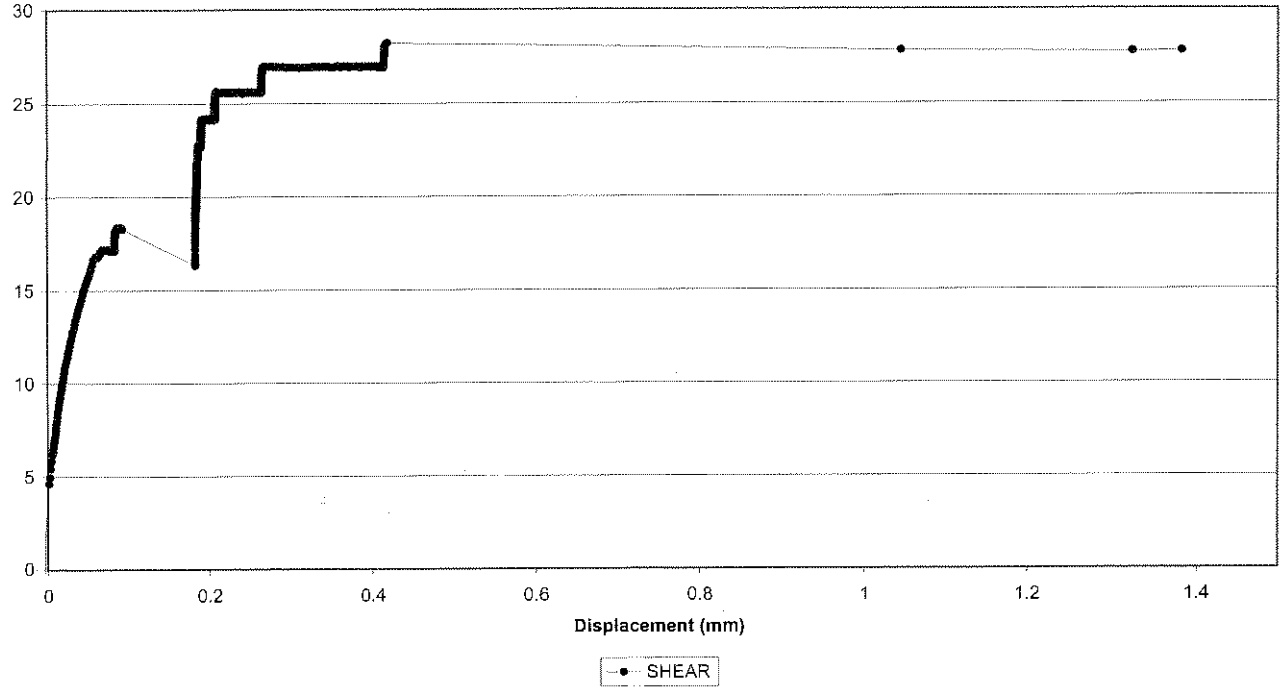

Creep Shear 2056-145
Crushed Elsburg Quartzite (dry, < 0.5mm, 2mm)

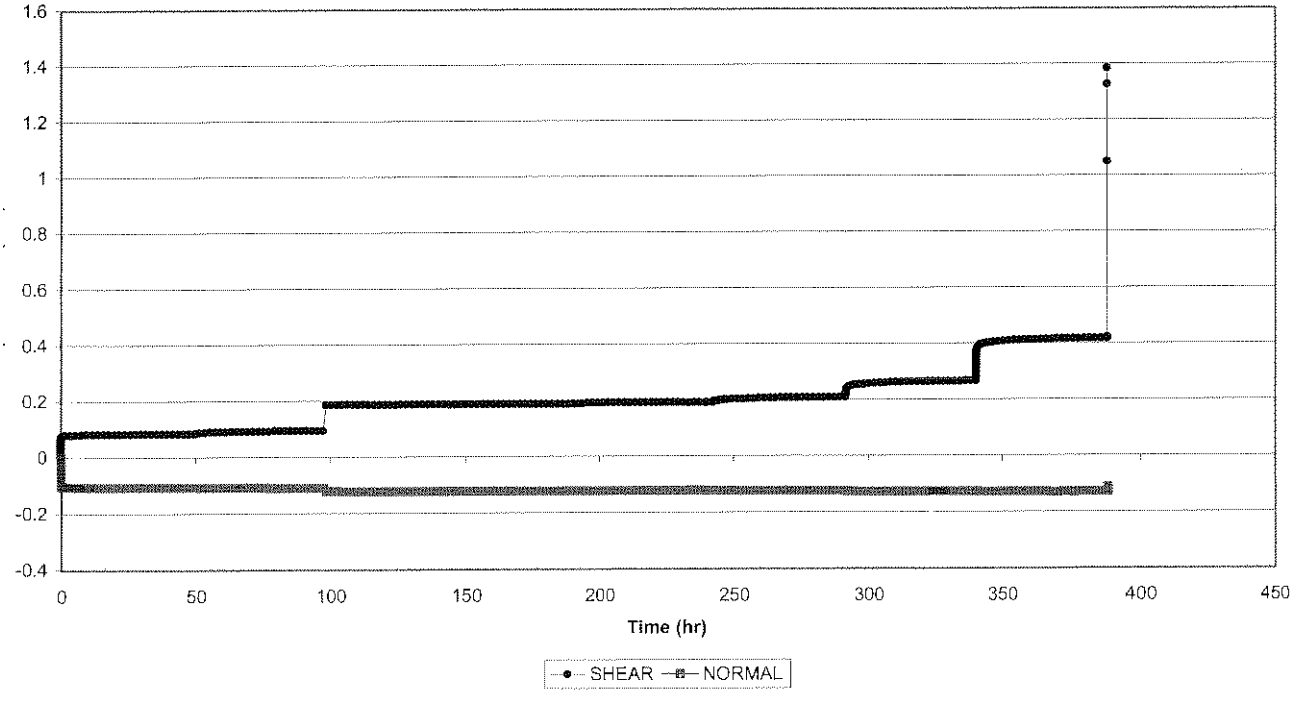

Creep Shear 2056-145, Cycle 1
Crushed Elsburg Quartzite (dry, < 0.5mm, 2mm)

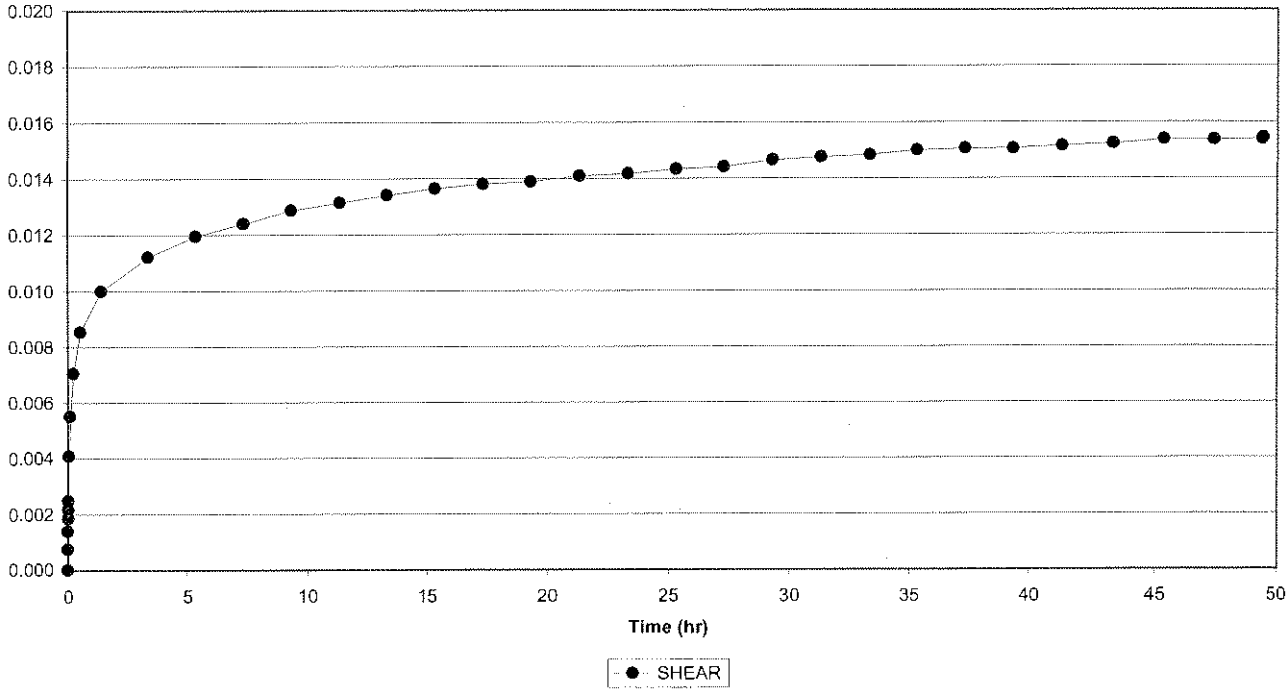

Creep Shear 2056-145, Cycle 2
Crushed Elsburg Quartzite (dry, < 0.5mm, 2mm)

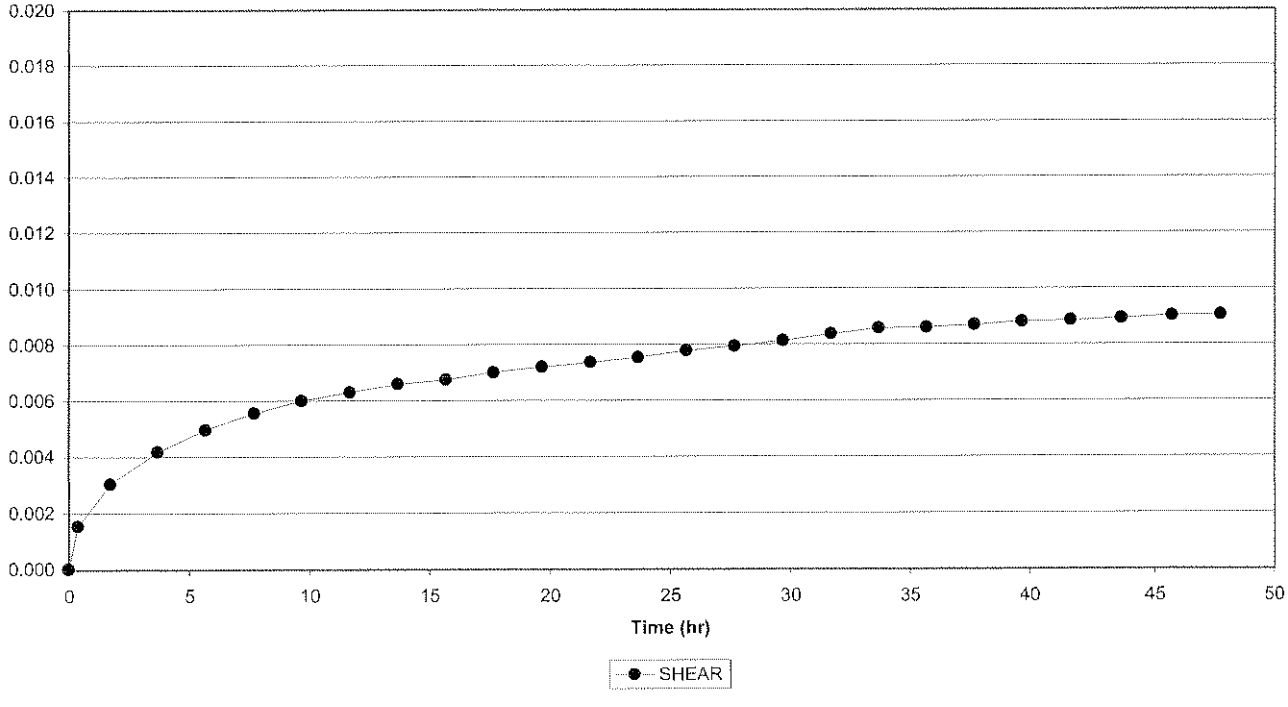

Creep Shear 2056-145, Cycle 3
Crushed Elsburg Quartzite (dry, < 0.5mm, 2mm)

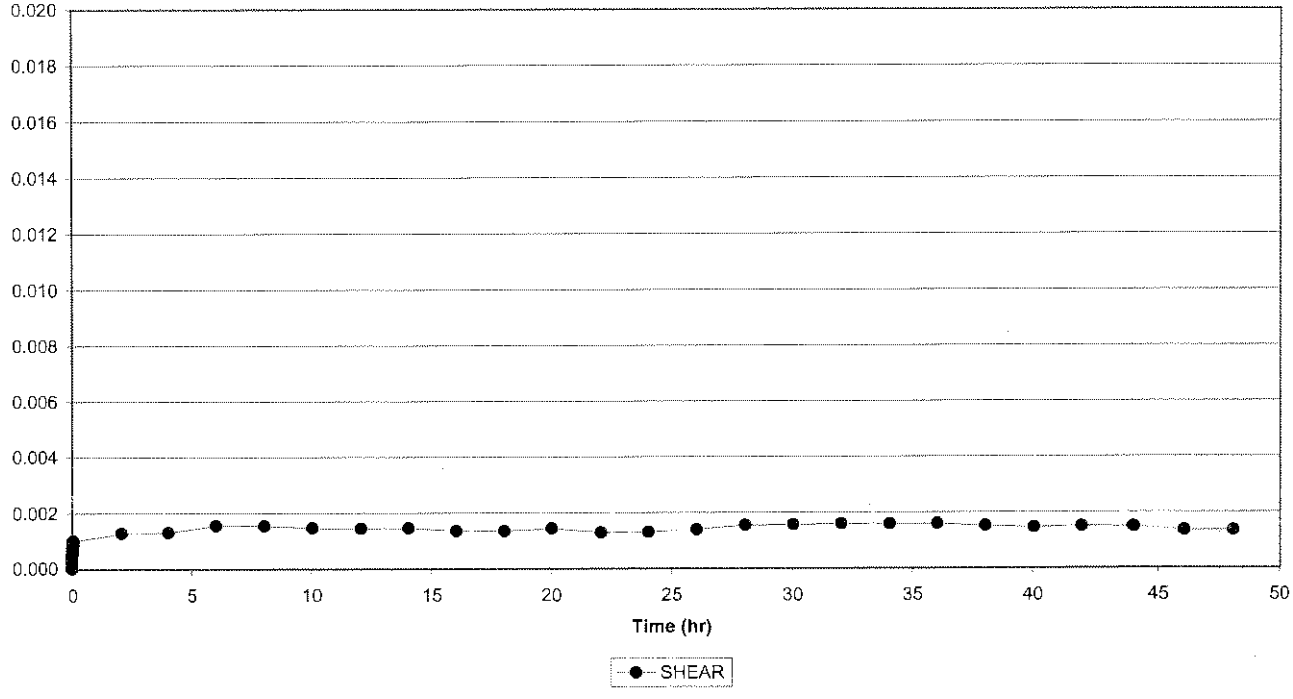

Creep Shear 2056-145, Cycle 4
Crushed Elsburg Quartzite (dry, < 0.5mm, 2mm)

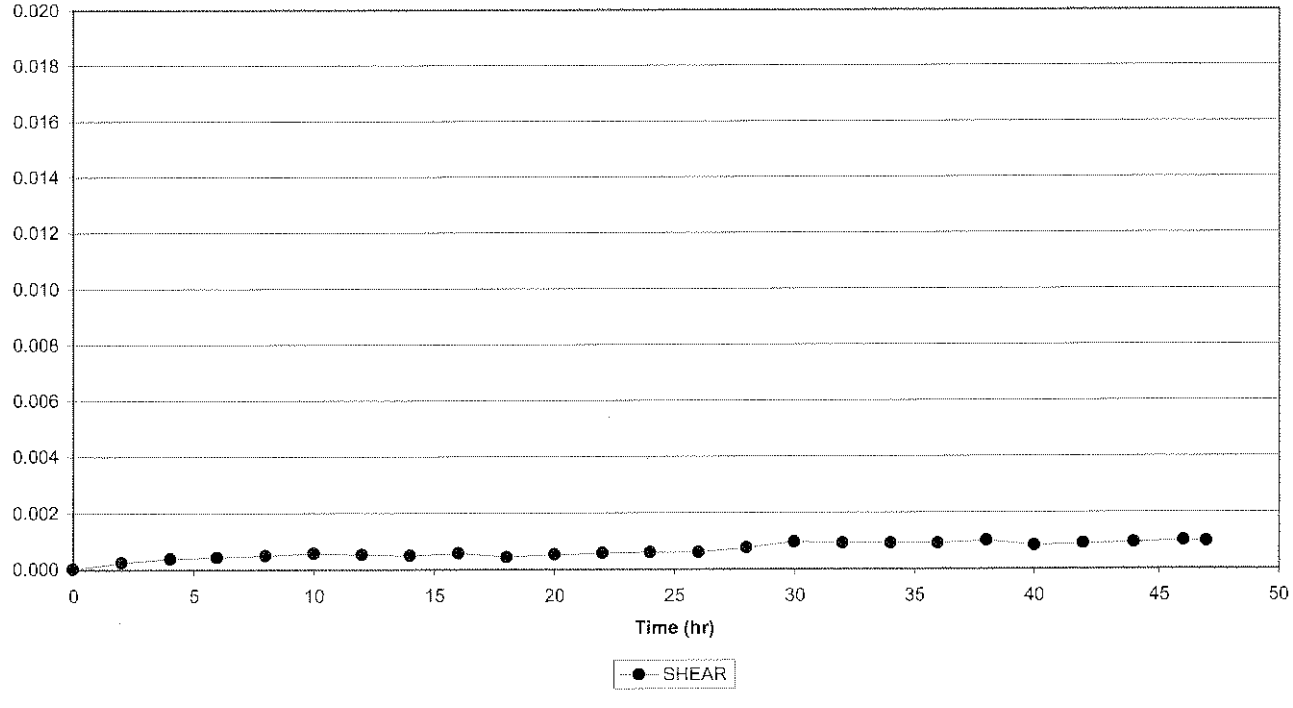

Creep Shear 2056-145, Cycle 5
Crushed Elsburg Quartzite (dry, < 0.5mm, 2mm)

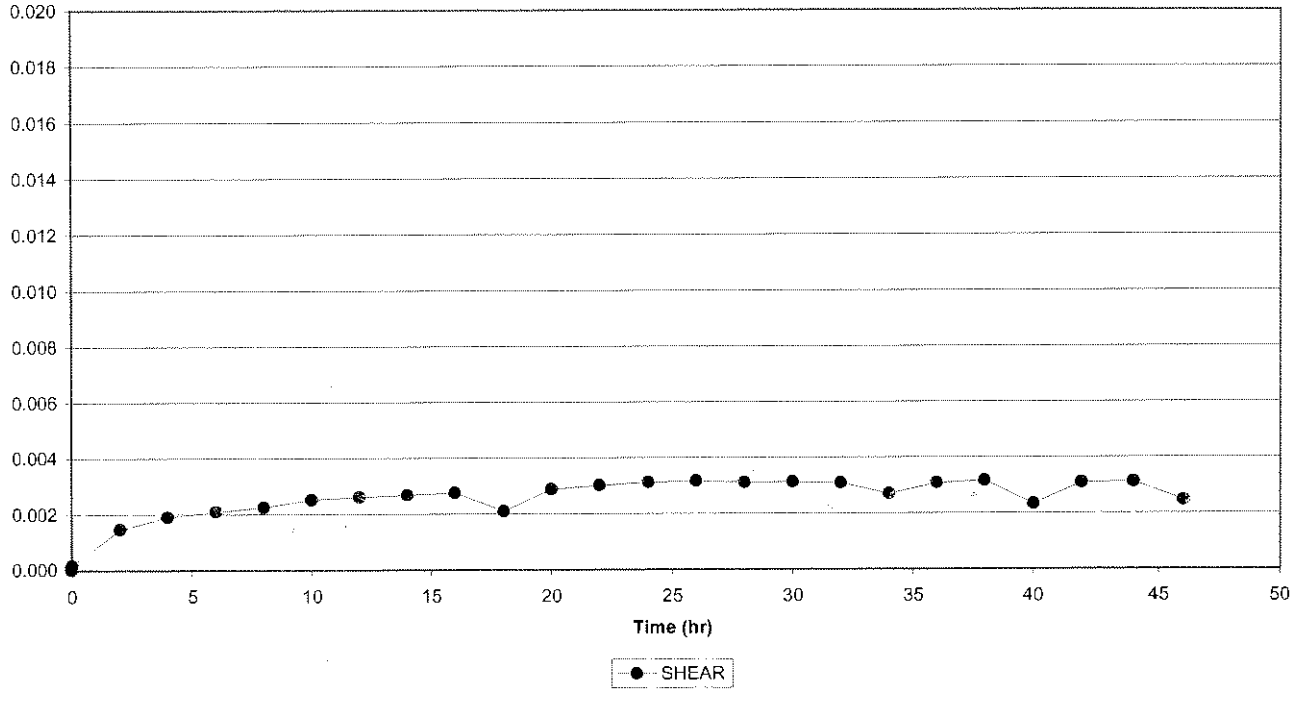

Creep Shear 2056-145, Cycle 6
Crushed Elsburg Quartzite (dry, < 0.5mm, 2mm)

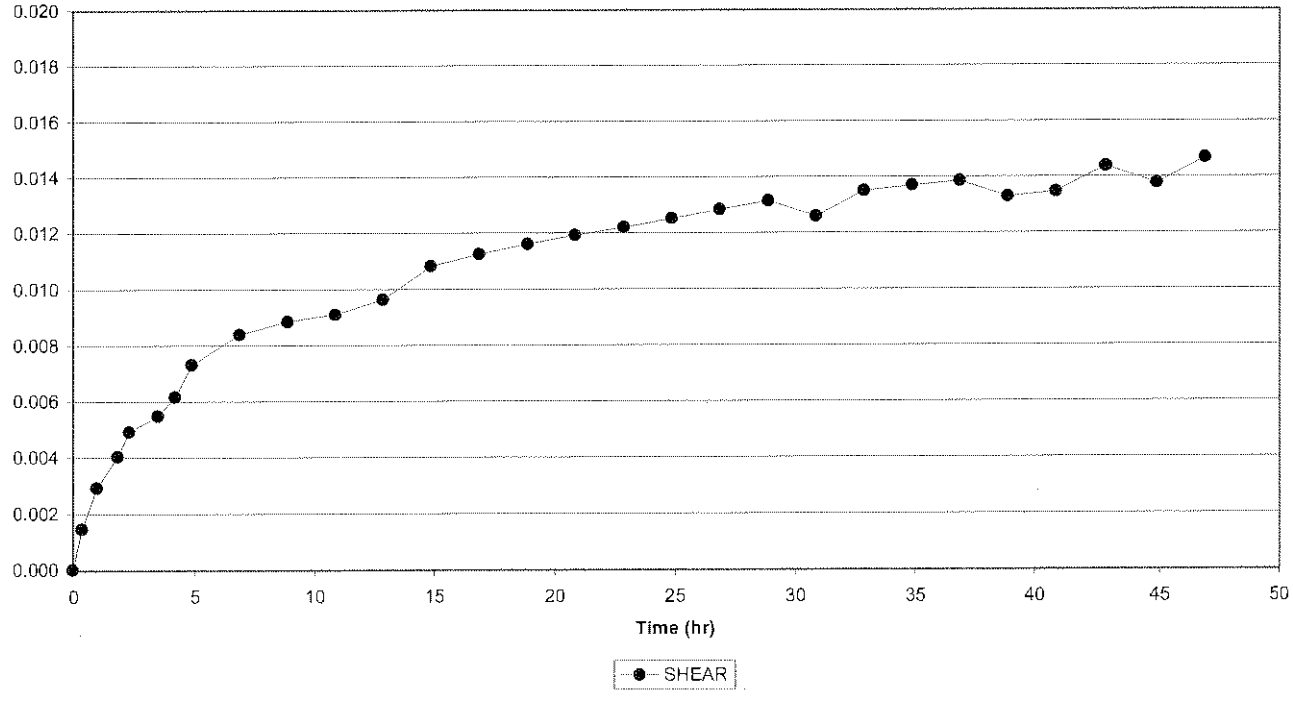

Creep Shear 2056-145, Cycle 7
Crushed Elsburg Quartzite (dry, < 0.5mm, 2mm)

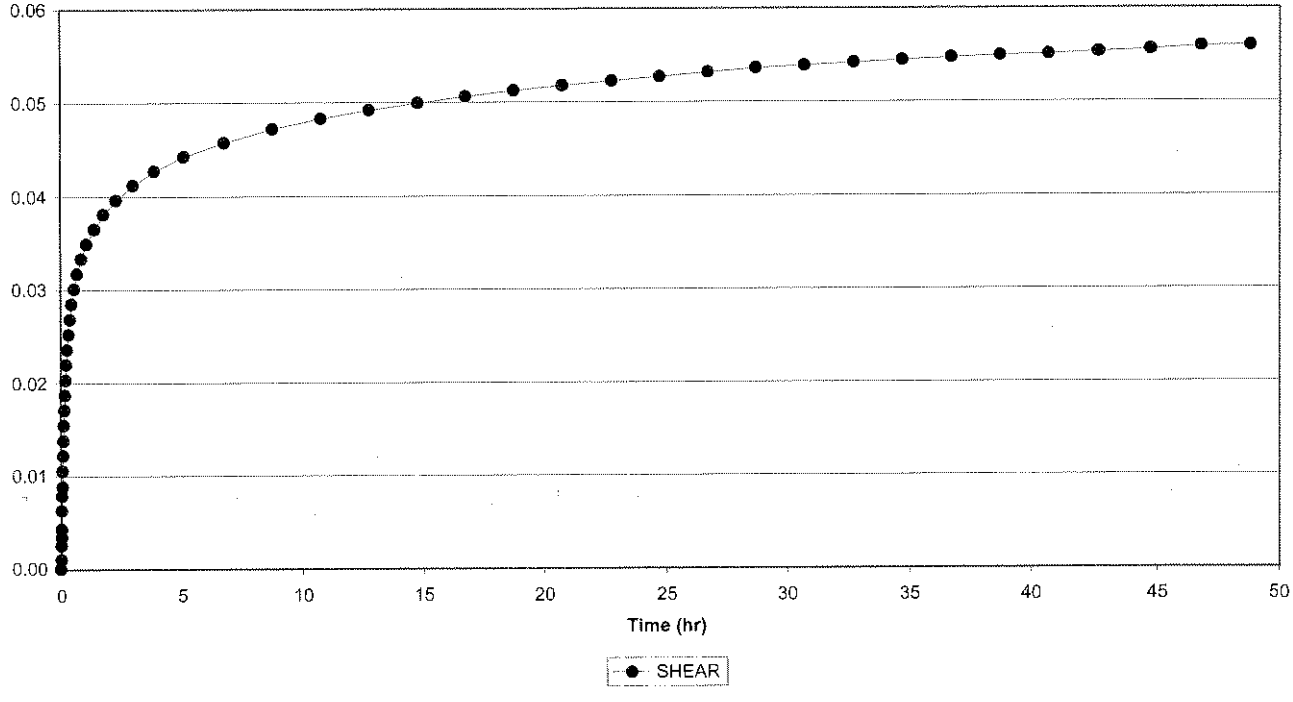

Creep Shear 2056-145, Cycle 8
Crushed Elsburg Quartzite (dry, < 0.5mm, 2mm)

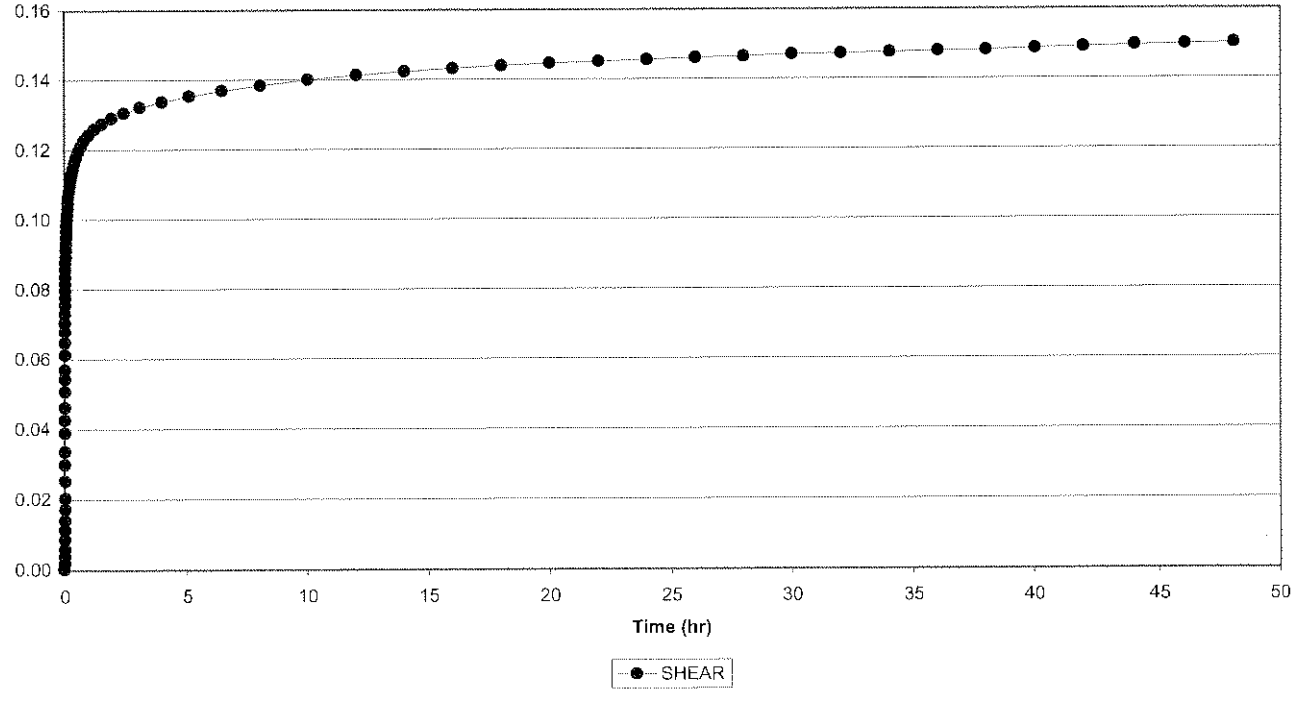

Creep Shear 2056-145, Cycle 9
Crushed Elsburg Quartzite (dry, < 0.5mm, 2mm)

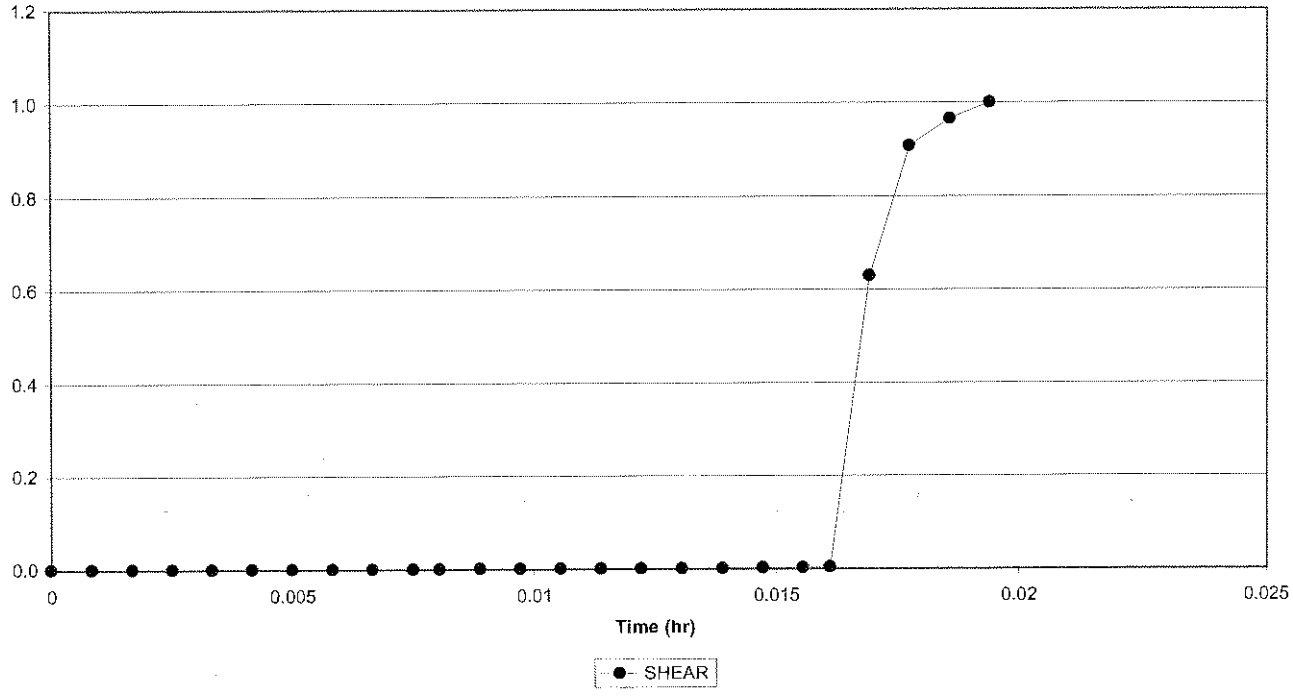

Creep Shear 2056-145
Crushed Elsburg Quartzite (dry, < 0.5mm, 2mm)

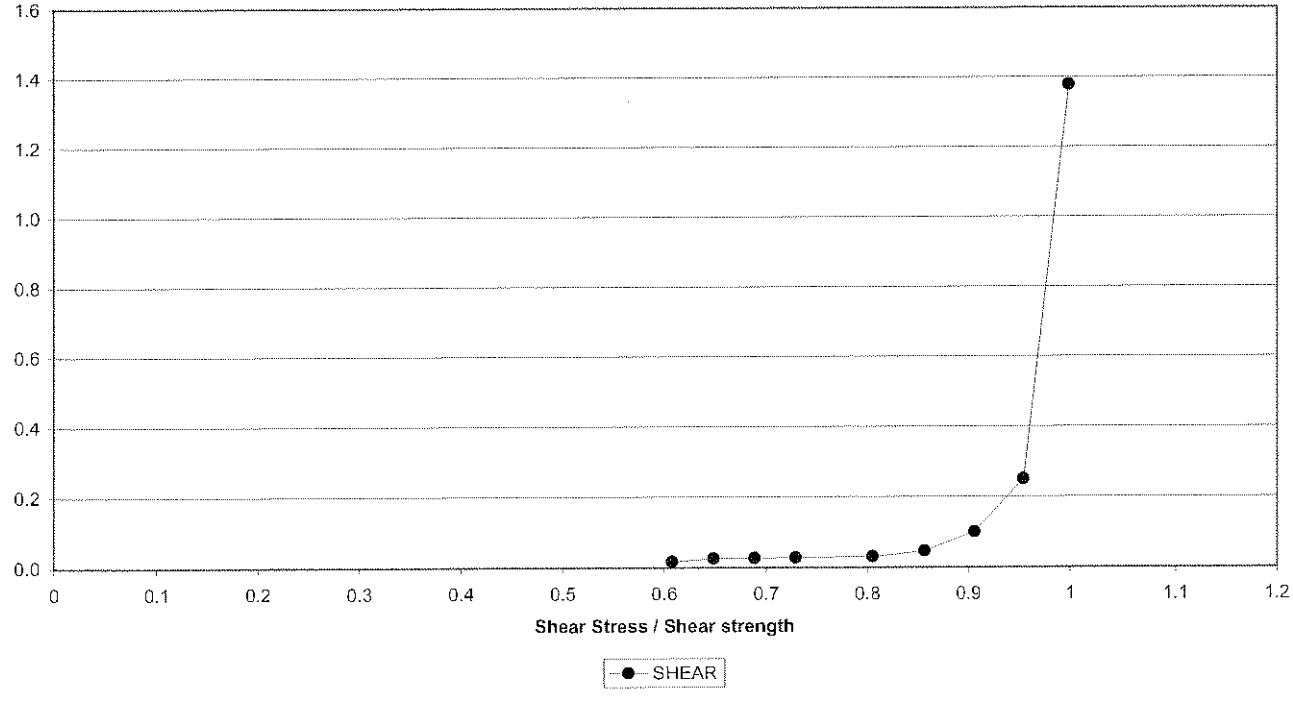

Creep Shear 2056-145
Crushed Elsburg Quartzite (dry, < 0.5mm, 2mm)

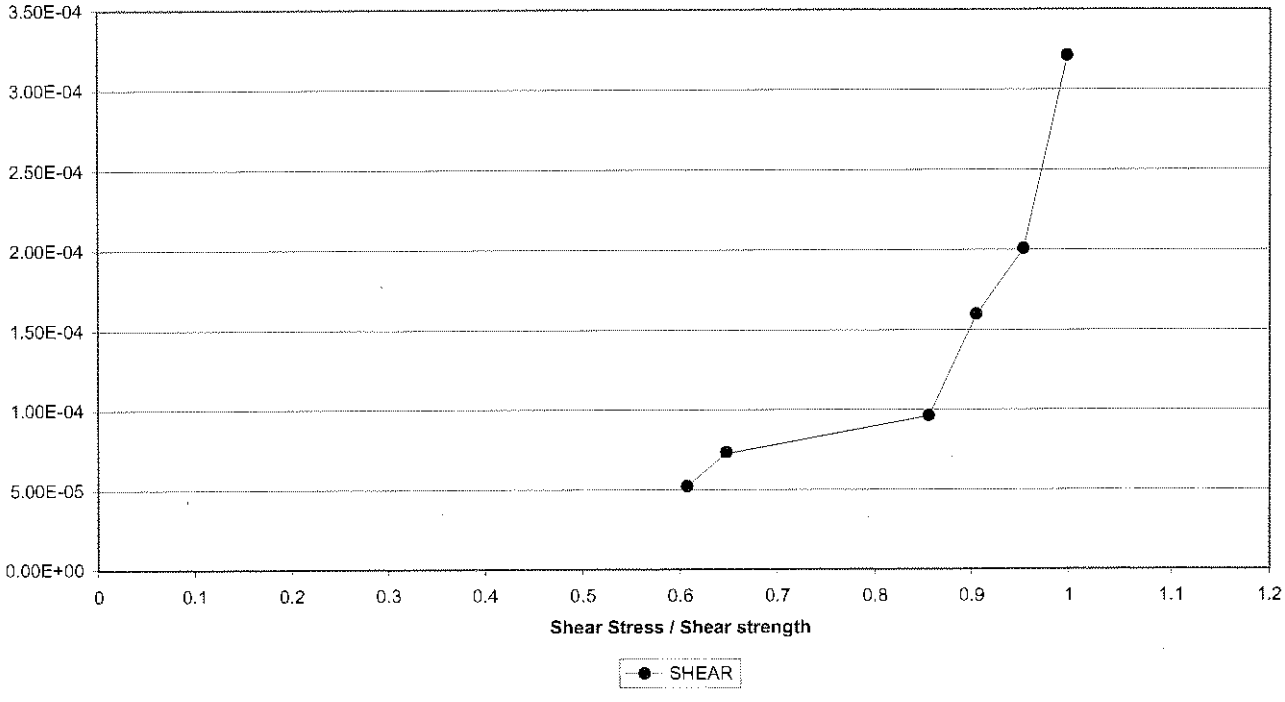

Creep Shear 2056-145
Crushed Elsburg Quartzite (dry, < 0.5mm, 2mm)

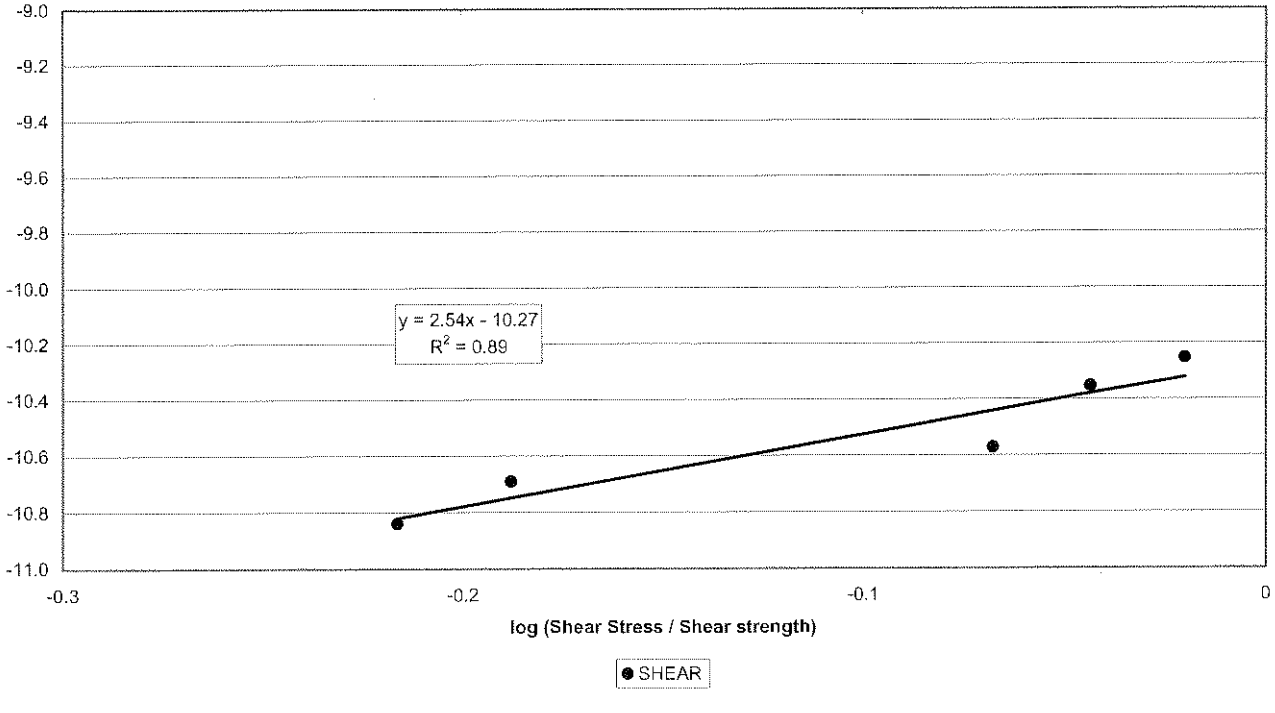

Creep Shear 2056-146
Crushed Elsburg Quartzite (wet, < 0.5mm, 1mm)

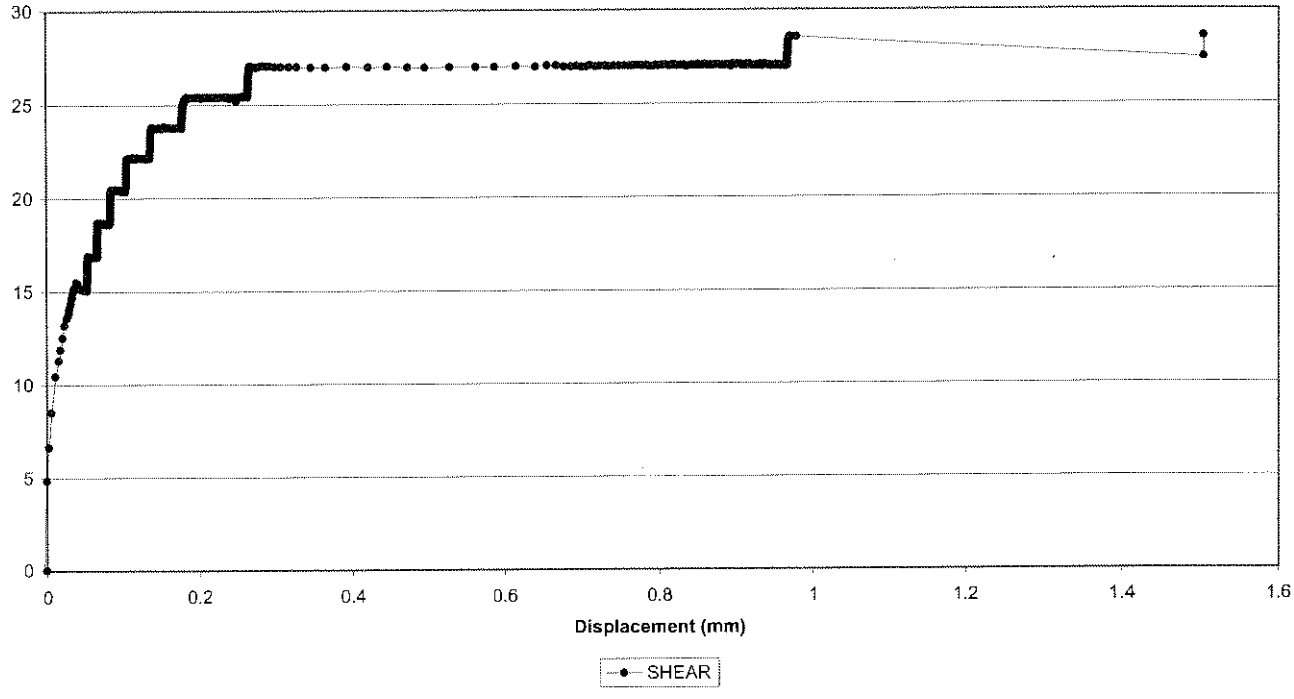

Creep Shear 2056-146
Crushed Elsburg Quartzite (wet, < 0.5mm, 1mm)

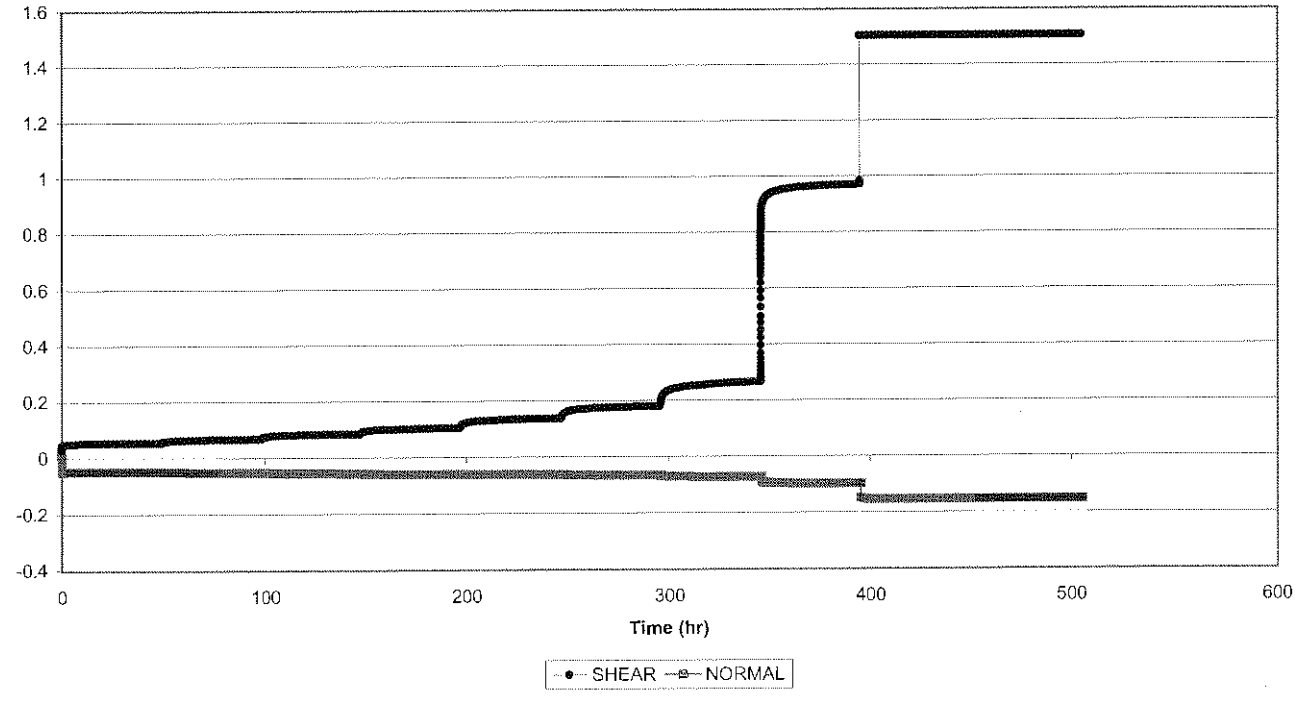

Creep Shear 2056-146, Cycle 1
Crushed Elsburg Quartzite (wet, < 0.5mm, 1mm)

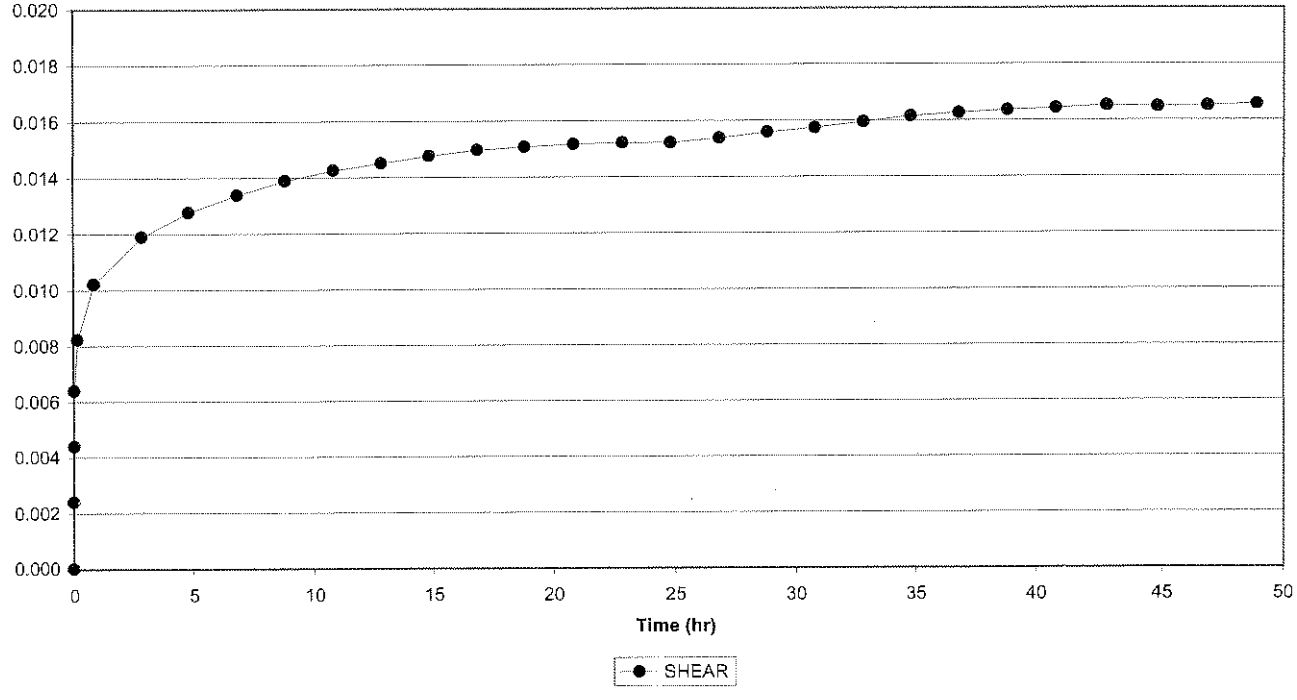

Creep Shear 2056-146, Cycle 2
Crushed Elsburg Quartzite (wet, < 0.5mm, 1mm)

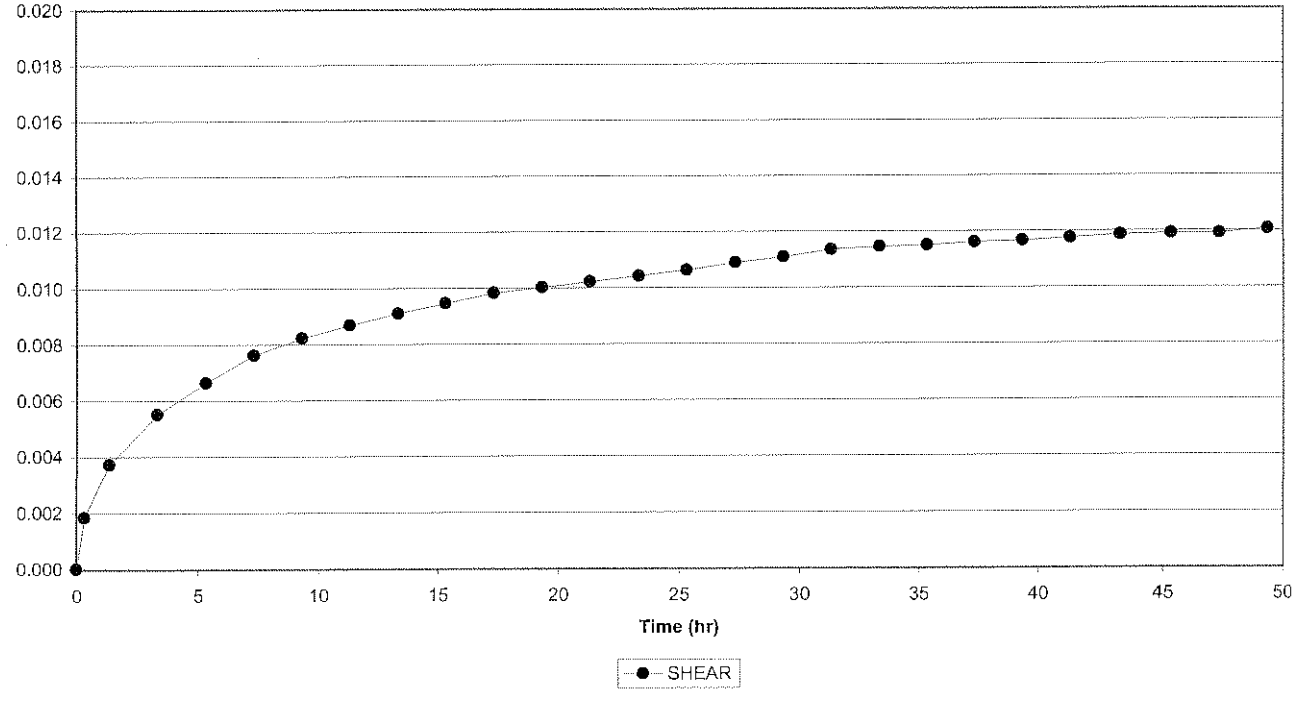

Creep Shear 2056-146, Cycle 3
Crushed Elsburg Quartzite (wet, < 0.5mm, 1mm)

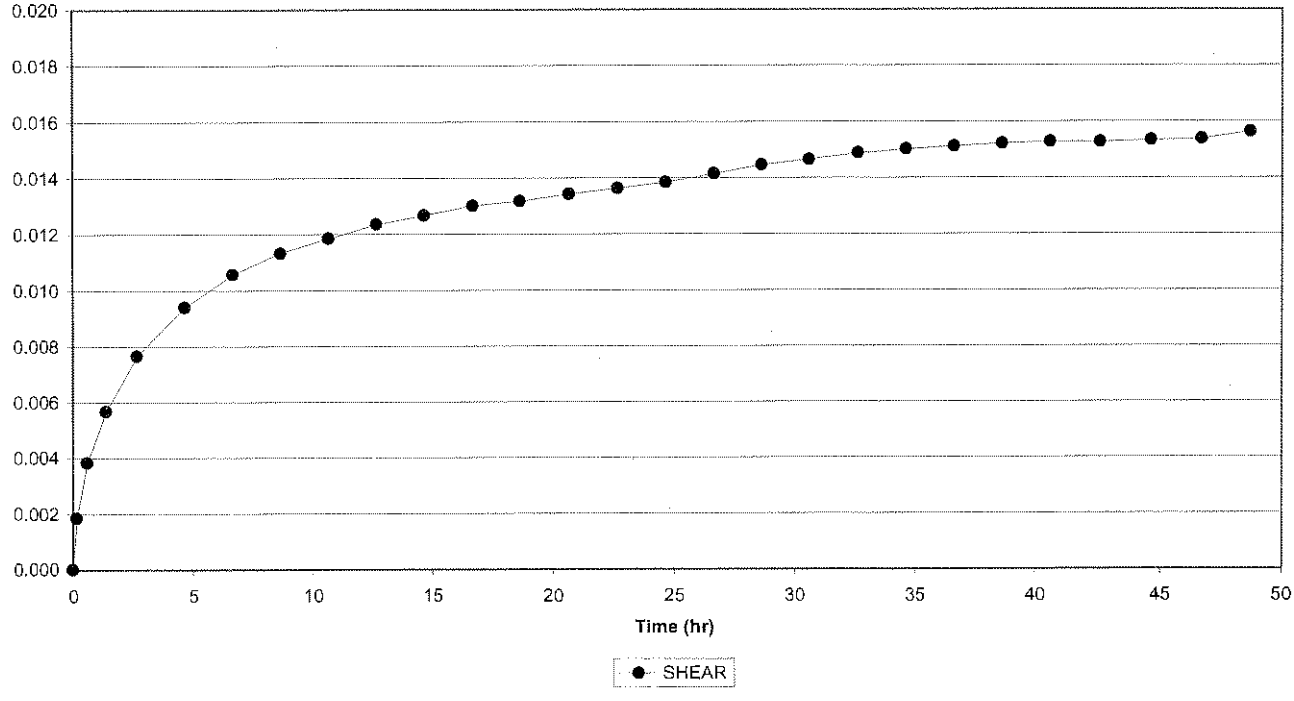

Creep Shear 2056-146, Cycle 4
Crushed Elsburg Quartzite (wet, < 0.5mm, 1mm)

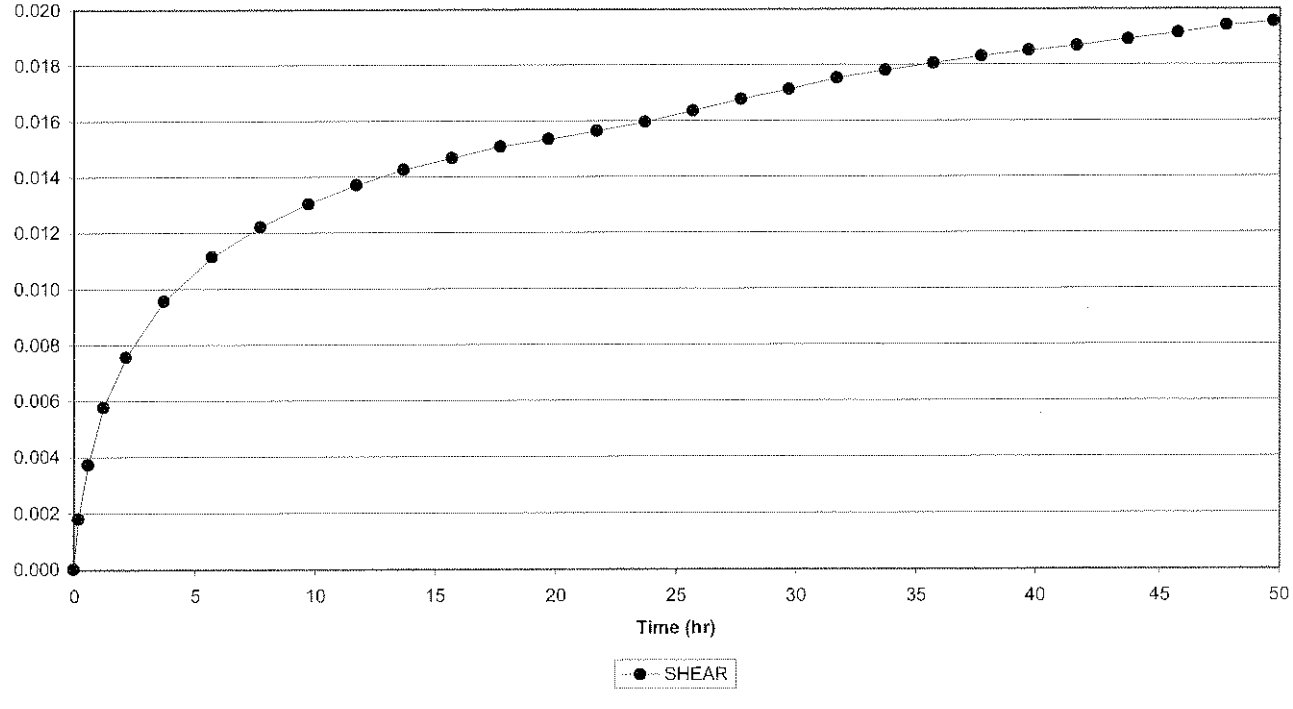

Creep Shear 2056-146, Cycle 5
Crushed Elsburg Quartzite (wet, < 0.5mm, 1mm)

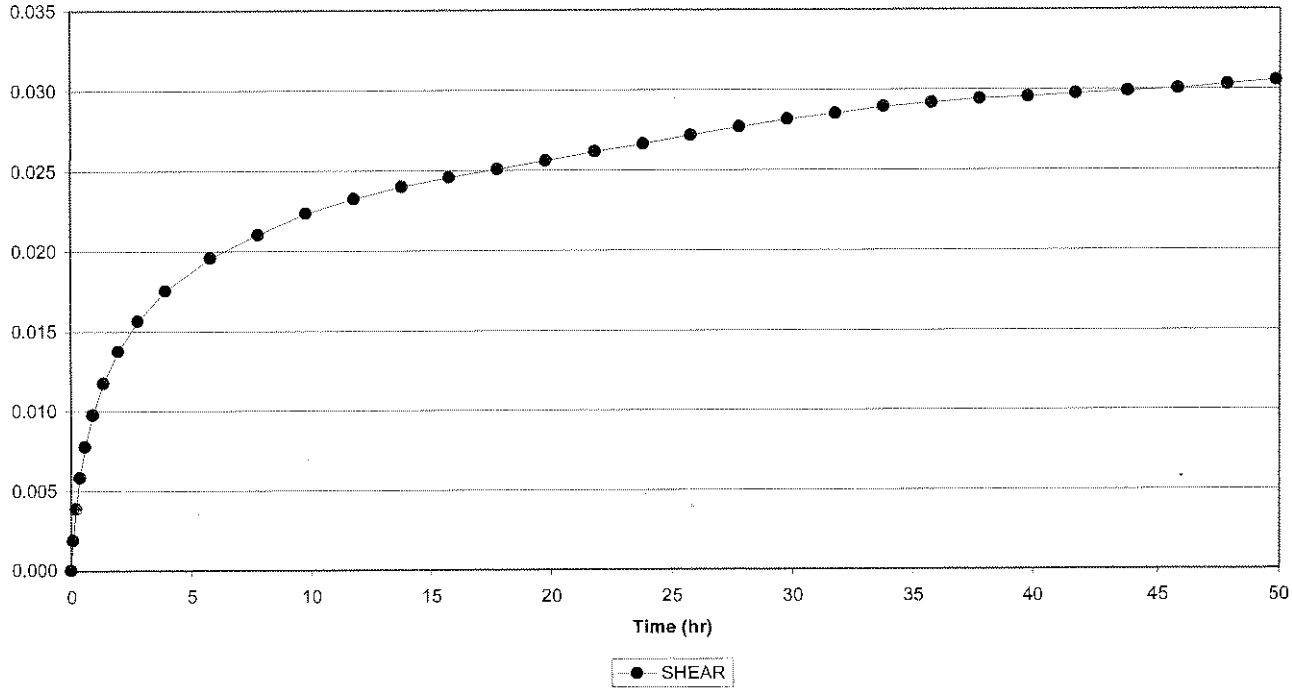

Creep Shear 2056-146, Cycle 6
Crushed Elsburg Quartzite (wet, < 0.5mm, 1mm)

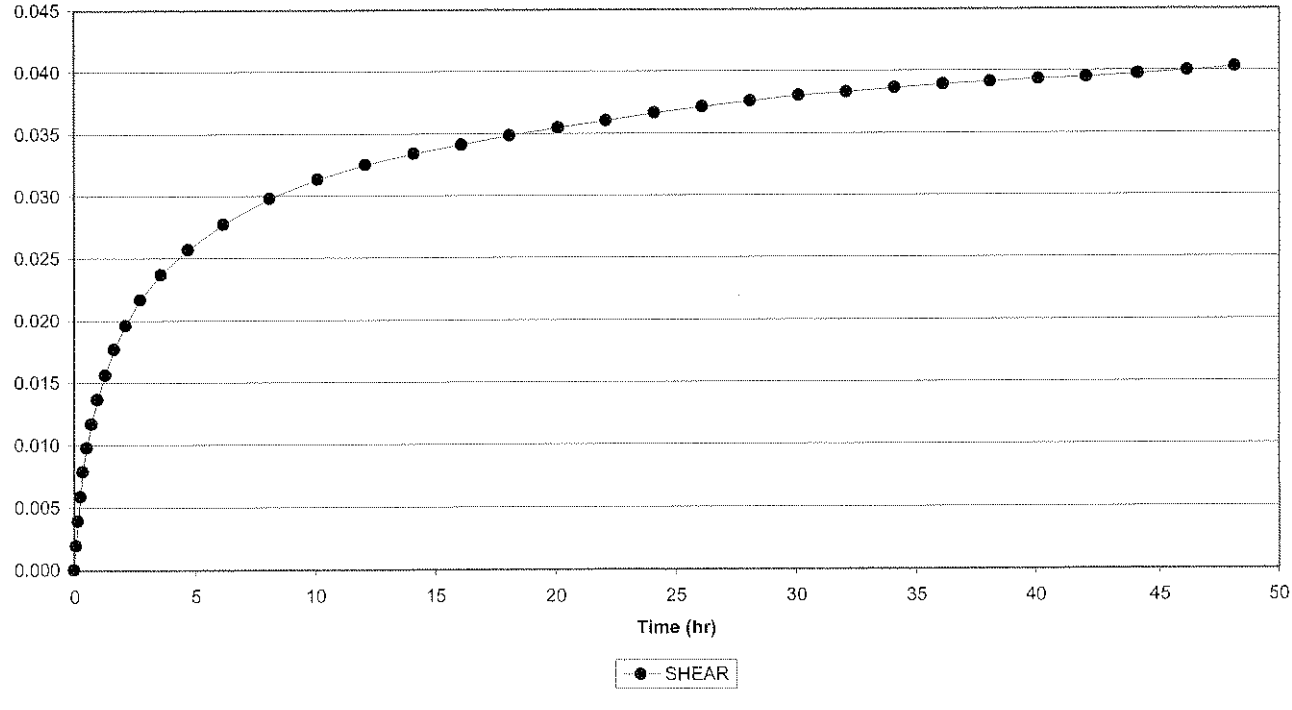

Creep Shear 2056-146, Cycle 7
Crushed Elsburg Quartzite (wet, < 0.5mm, 1mm)

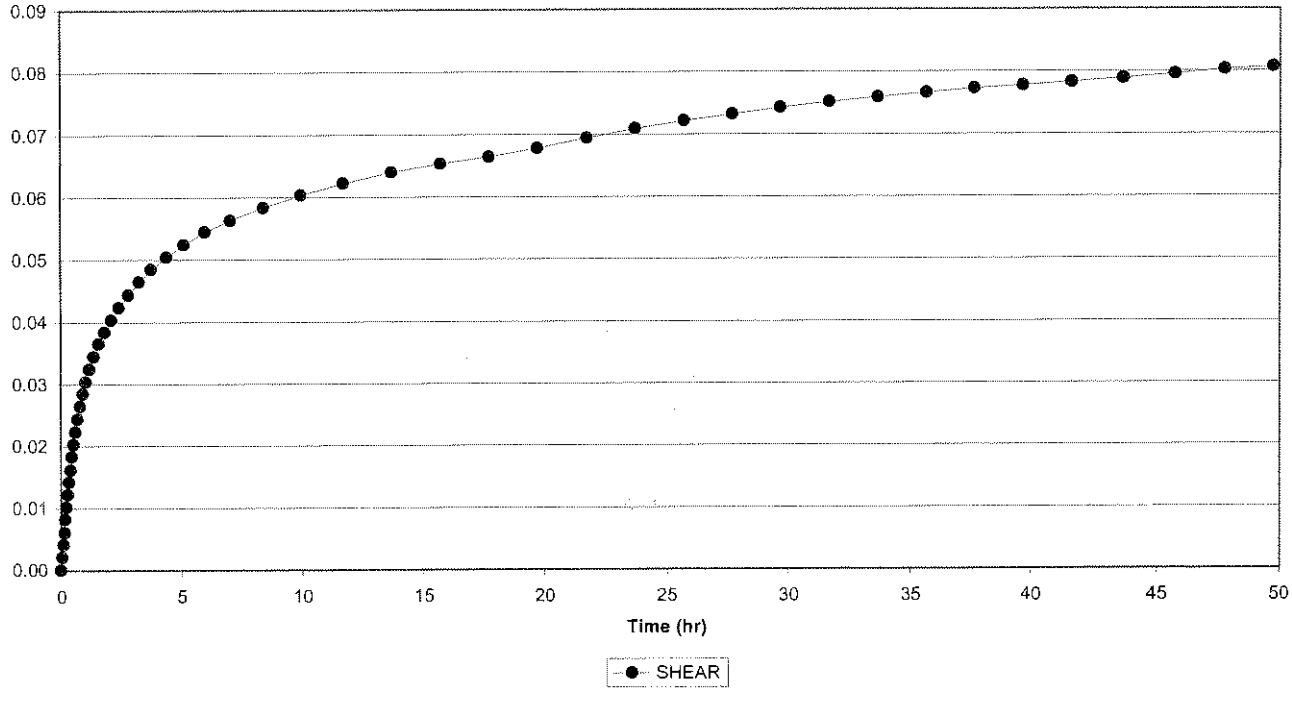

Creep Shear 2056-146, Cycle 8
Crushed Elsburg Quartzite (wet, < 0.5mm, 1mm)

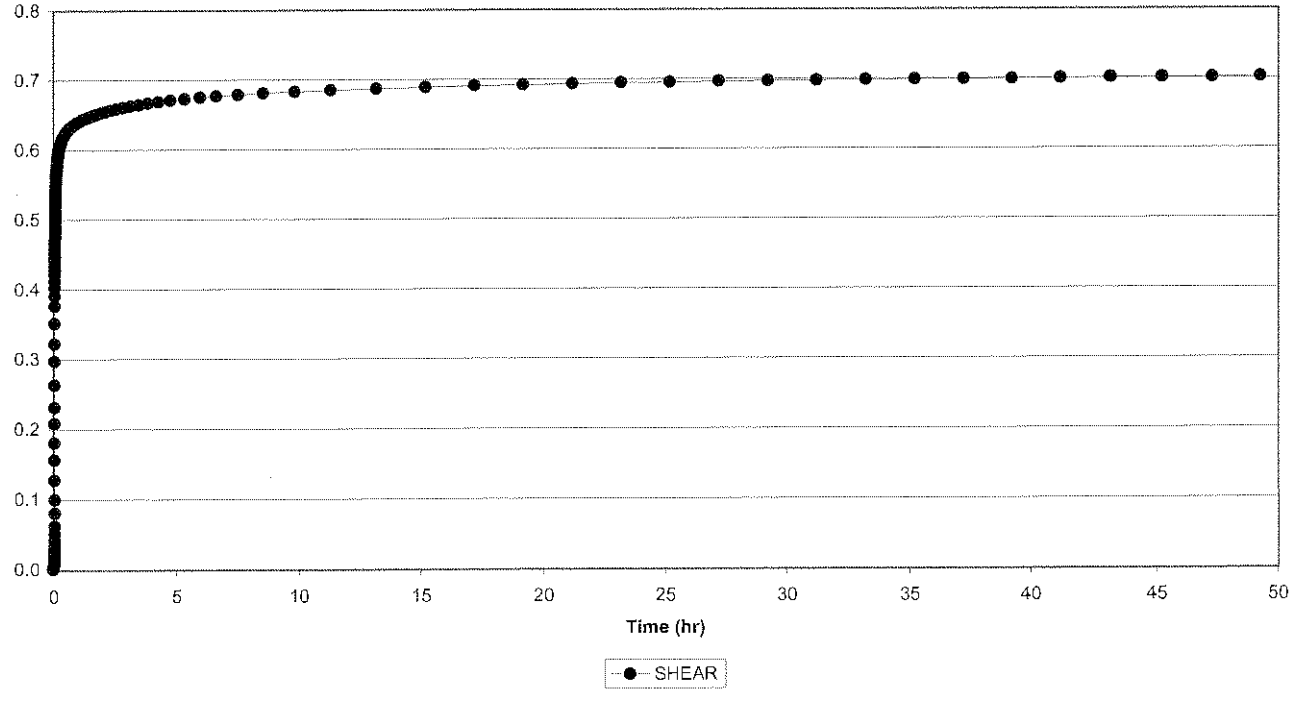

Creep Shear 2056-146, Cycle 9
Crushed Elsburg Quartzite (wet, < 0.5mm, 1mm)

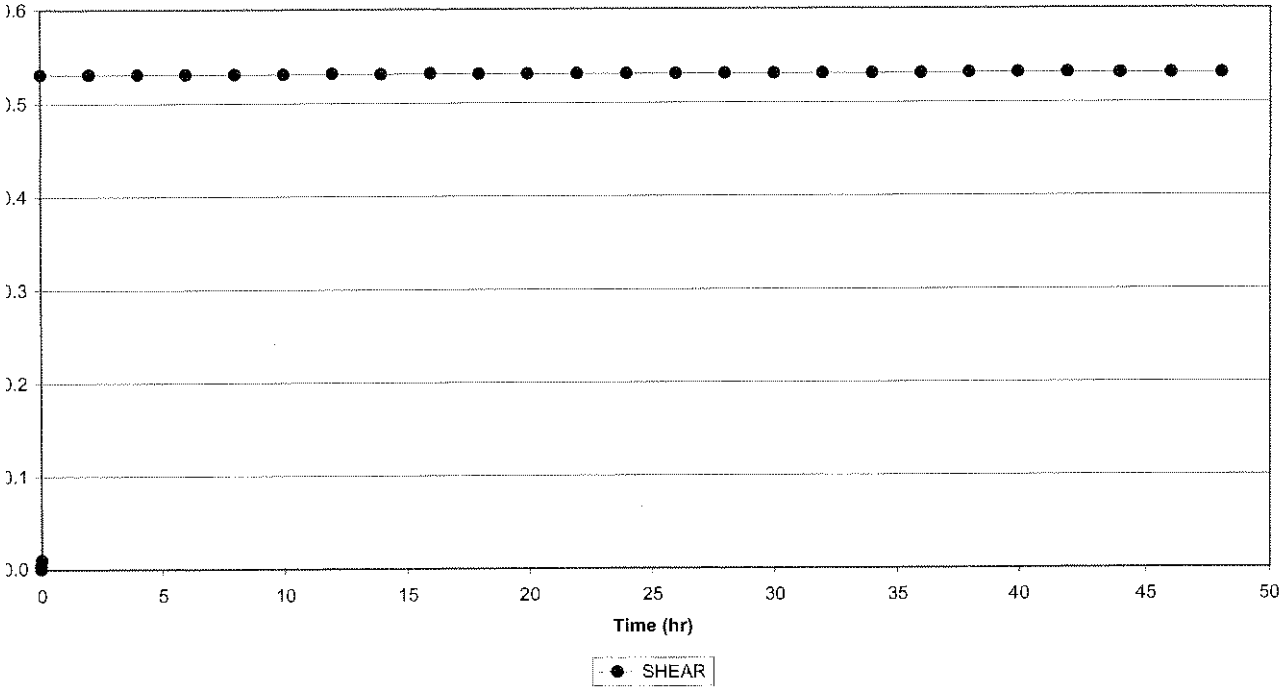

Creep Shear 2056-146
Crushed Elsburg Quartzite (wet, < 0.5mm, 1mm)

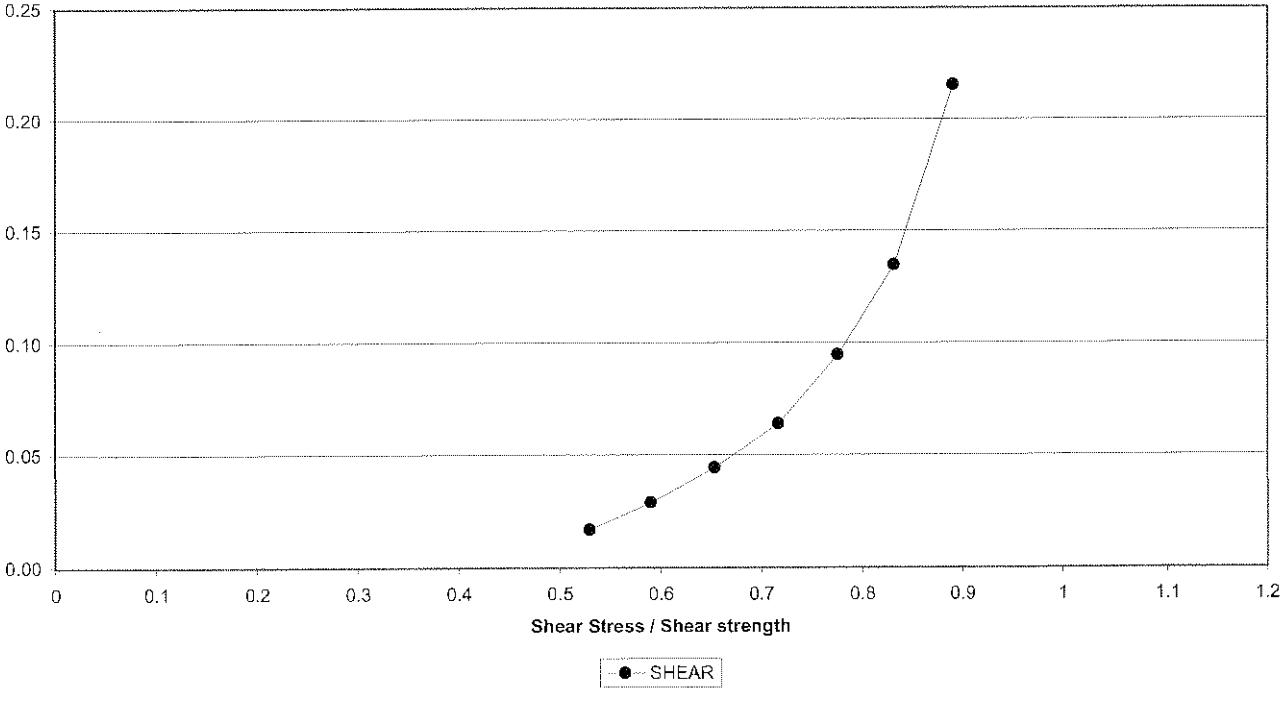

Creep Shear 2056-146
Crushed Elsburg Quartzite (wet, < 0.5mm, 1mm)

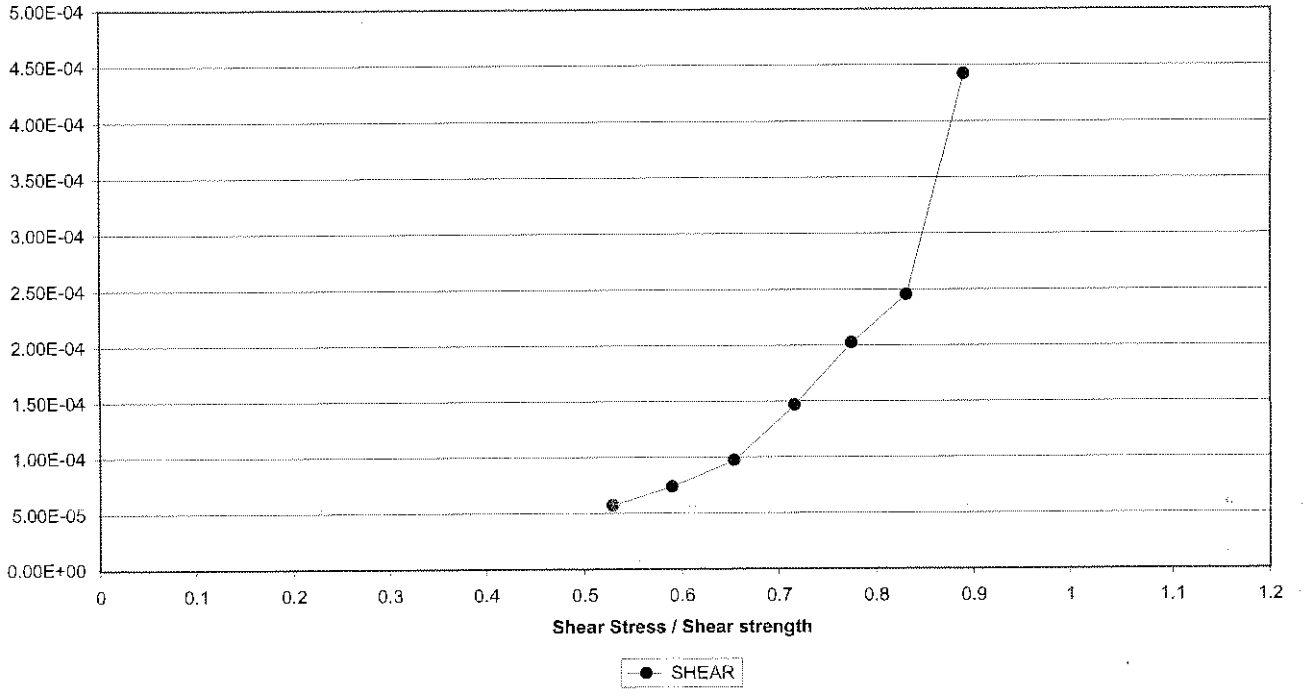

Creep Shear 2056-146
Crushed Elsburg Quartzite (wet, < 0.5mm, 1mm)

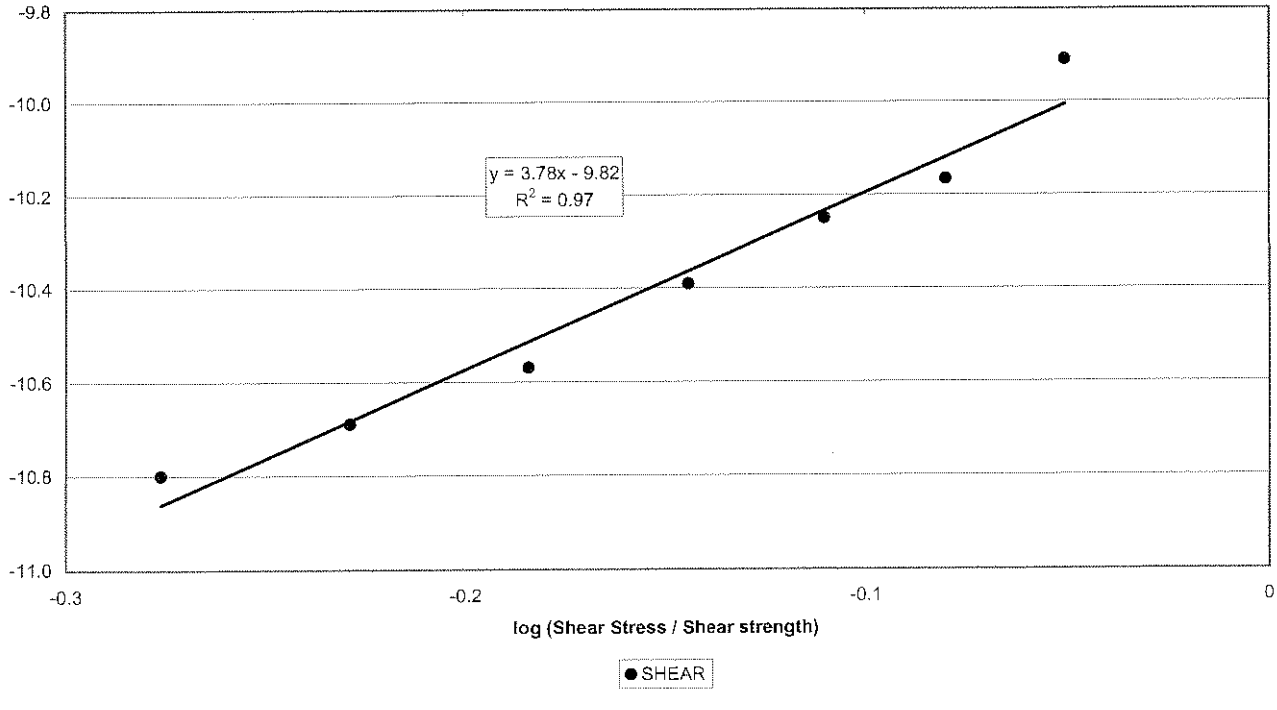

Creep Shear 2056-162
Crushed Ventersdorp Lava (dry, < 0.5mm, 0.5mm)

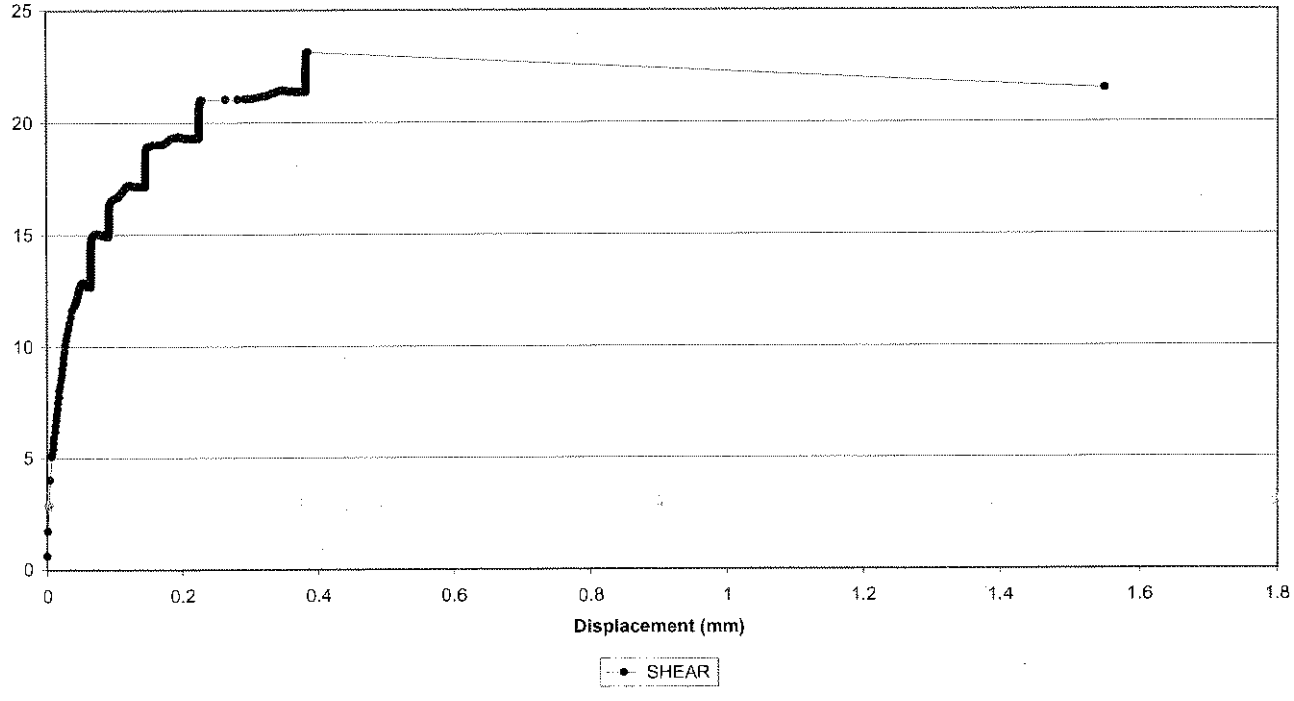

Creep Shear 2056-162
Crushed Ventersdorp Lava (dry, < 0.5mm, 0.5mm)

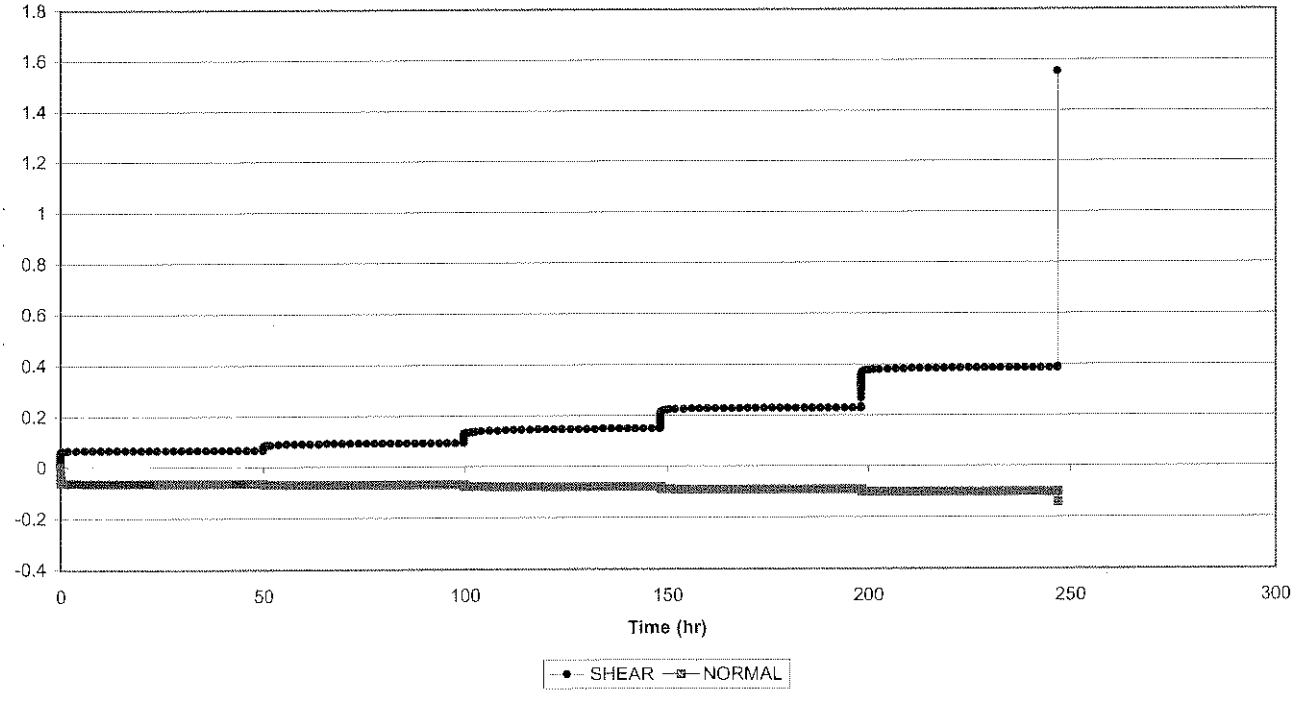

Creep Shear 2056-162, Cycle 1
Crushed Ventersdorp Lava (dry, < 0.5mm, 0.5mm)

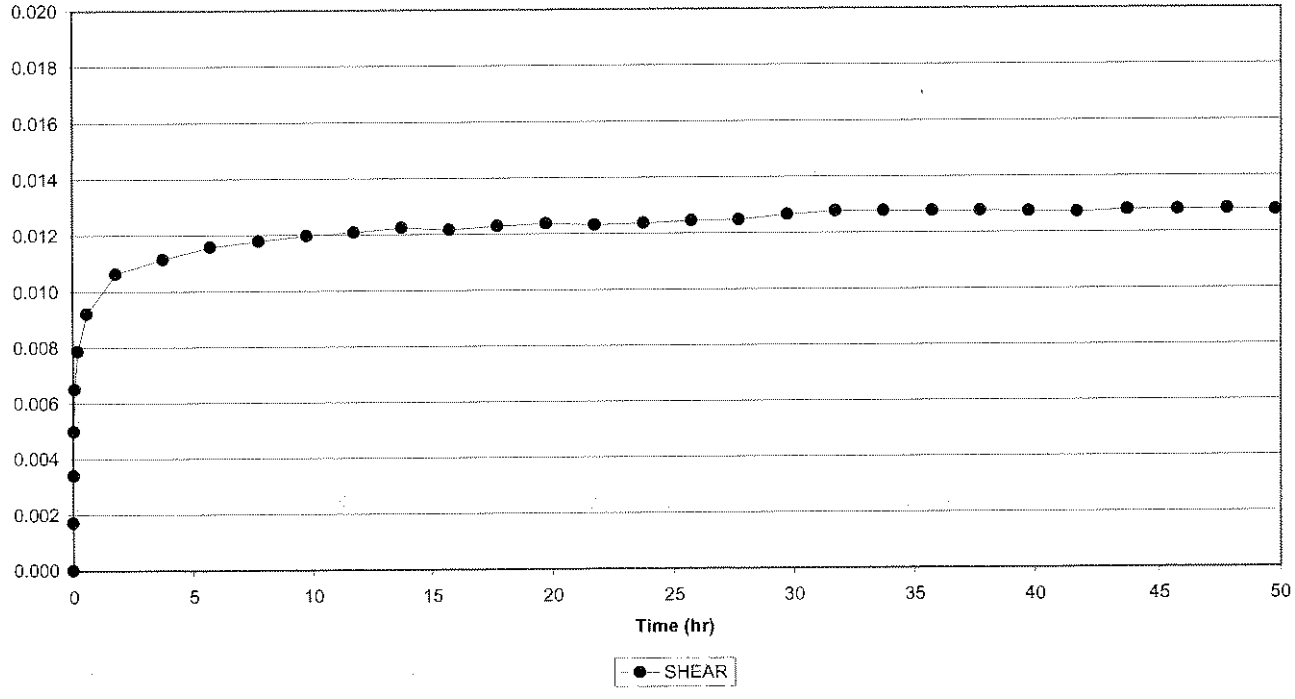

Creep Shear 2056-162, Cycle 2
Crushed Ventersdorp Lava (dry, < 0.5mm, 0.5mm)

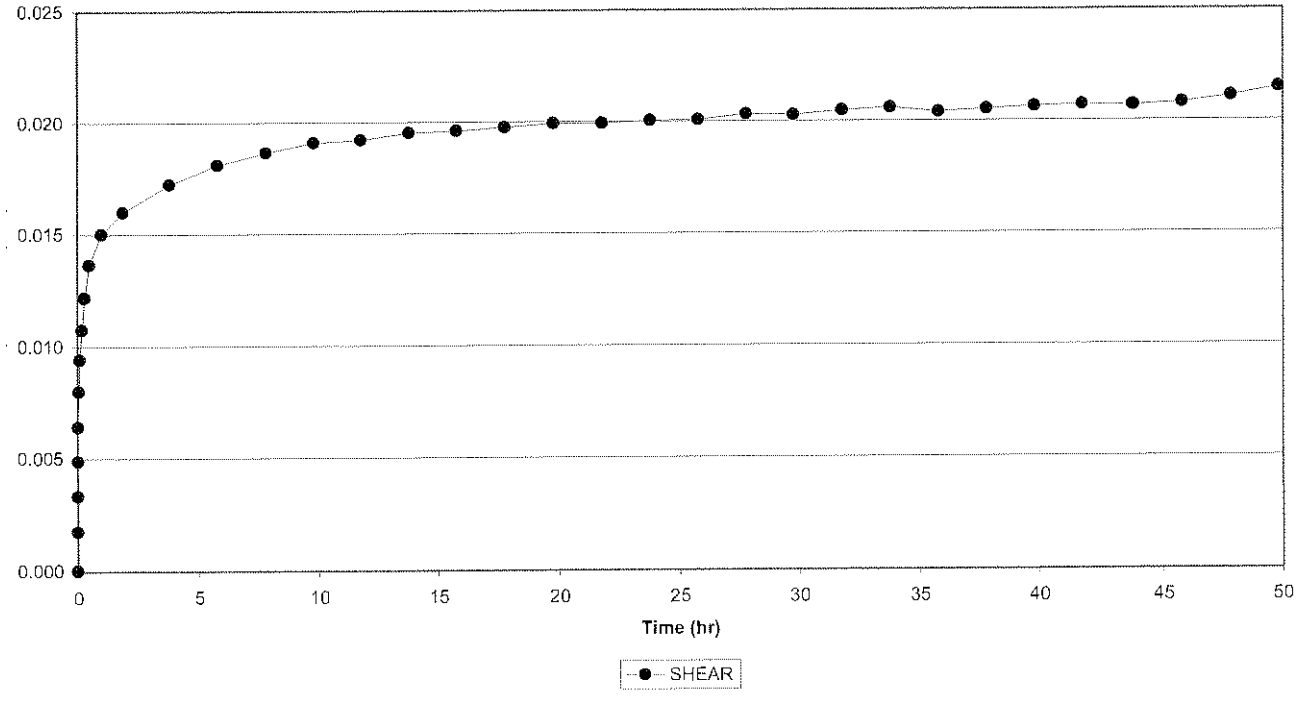

Creep Shear 2056-162, Cycle 3
Crushed Ventersdorp Lava (dry, < 0.5mm, 0.5mm)

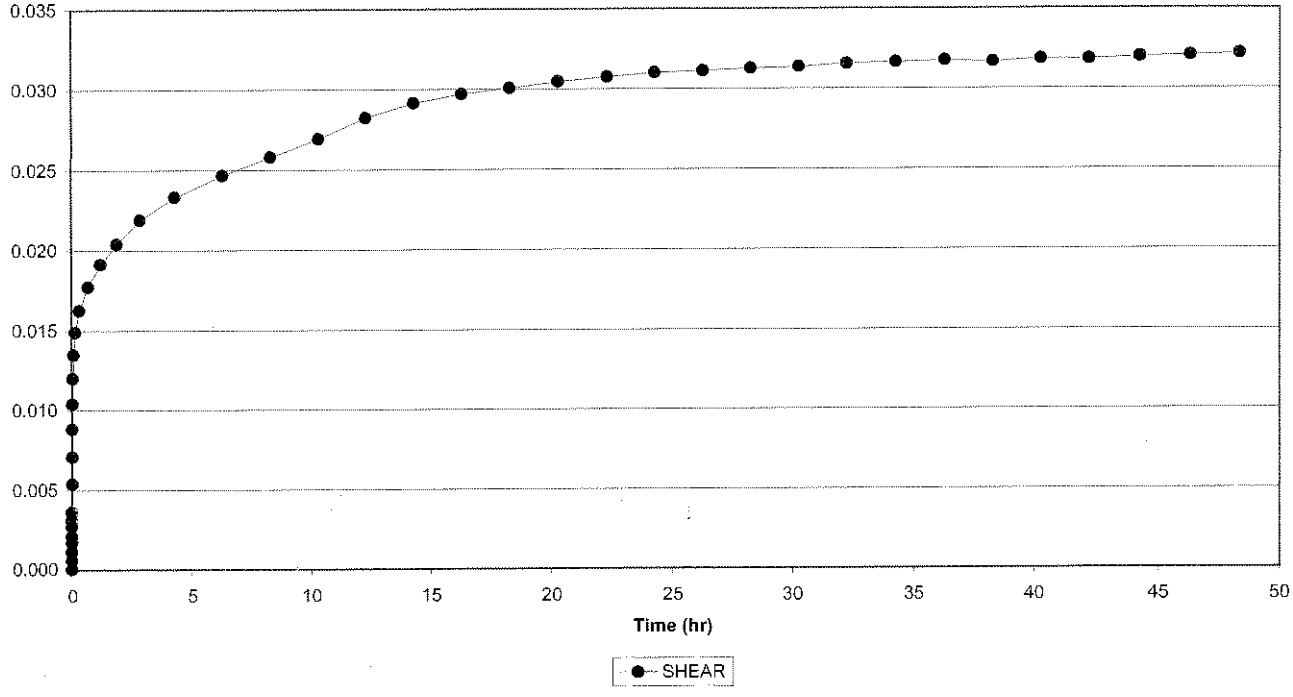

Creep Shear 2056-162, Cycle 4
Crushed Ventersdorp Lava (dry, < 0.5mm, 0.5mm)

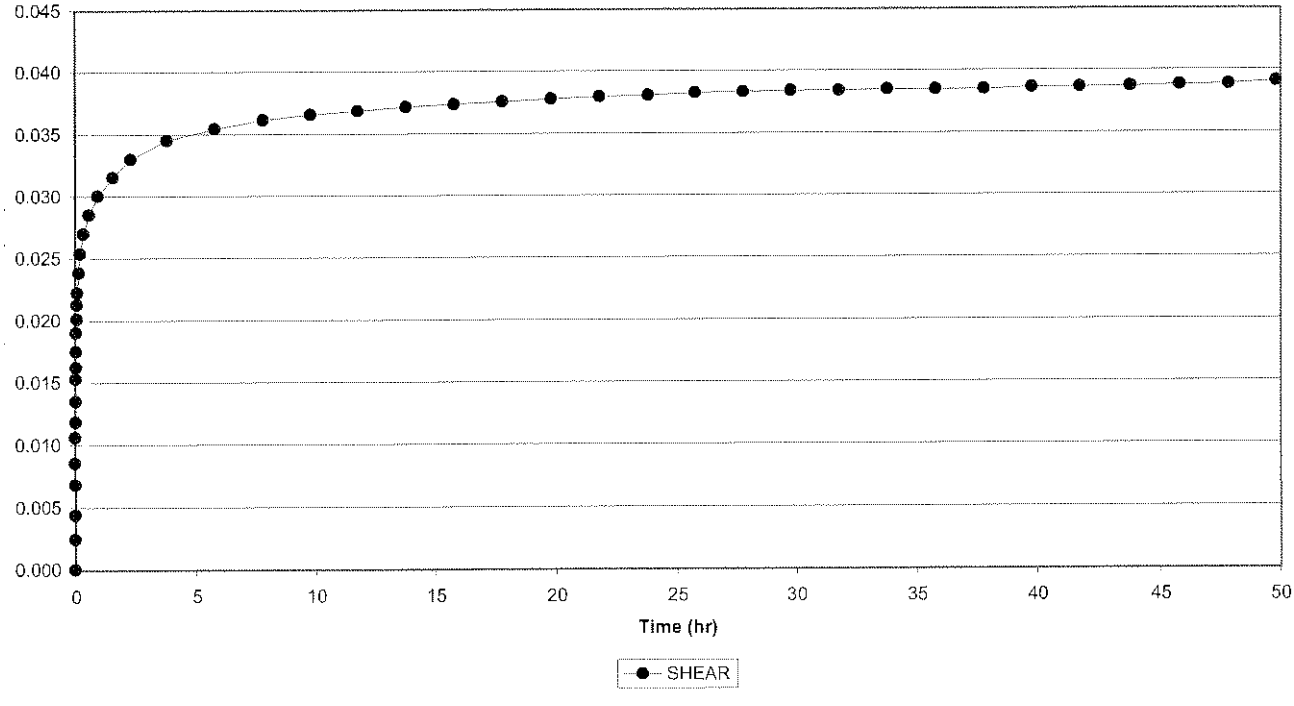

Creep Shear 2056-162, Cycle 5
Crushed Ventersdorp Lava (dry, < 0.5mm, 0.5mm)

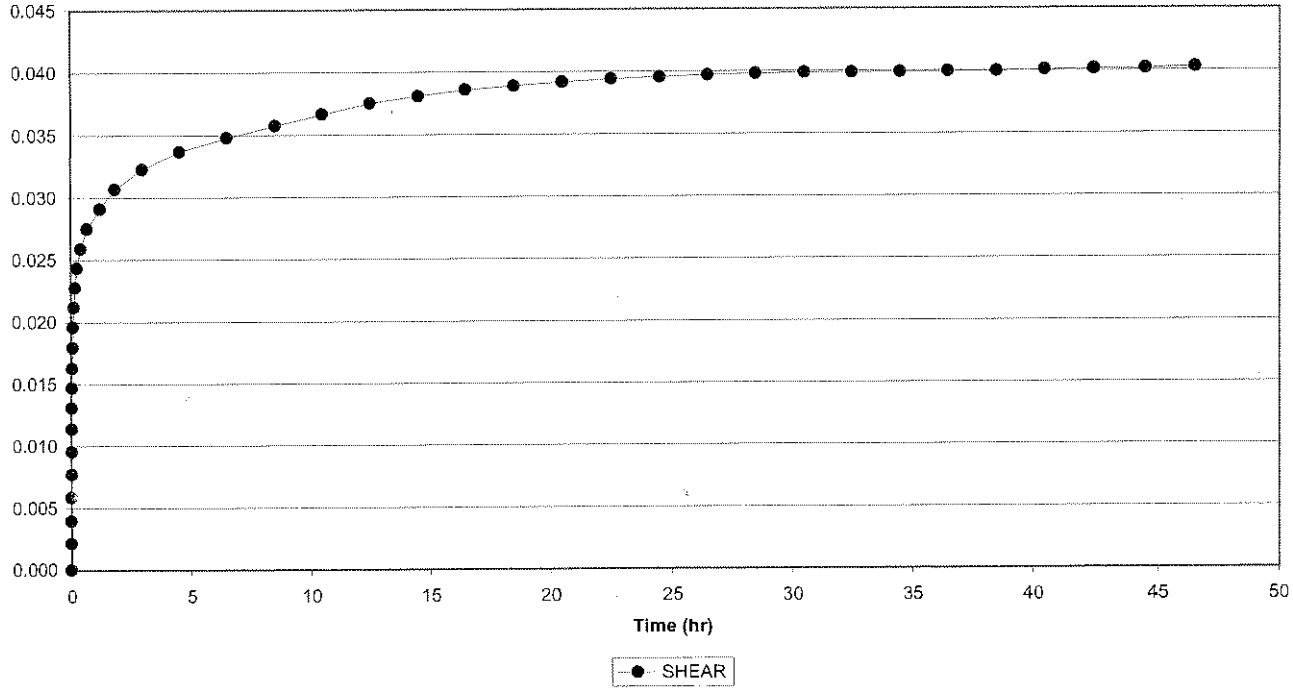

Creep Shear 2056-162
Crushed Ventersdorp Lava (dry, < 0.5mm, 0.5mm)

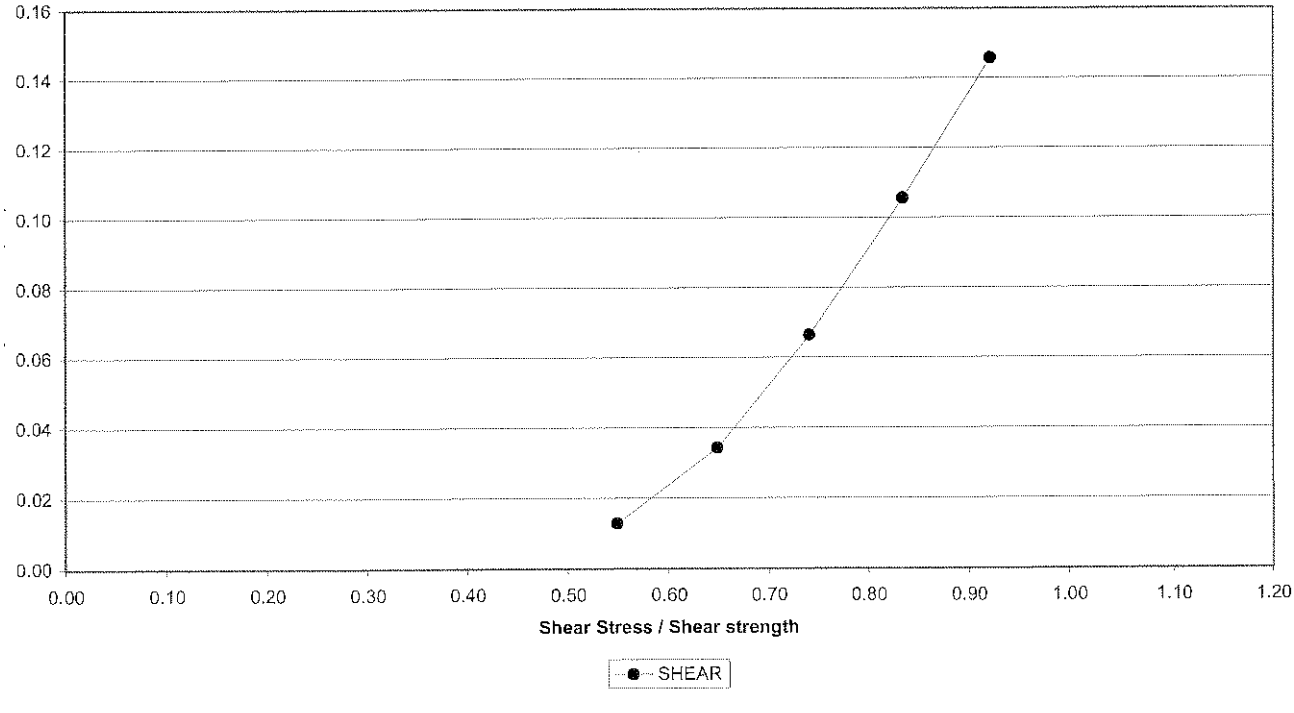

Creep Shear 2056-162
Crushed Ventersdorp Lava (dry, < 0.5mm, 0.5mm)

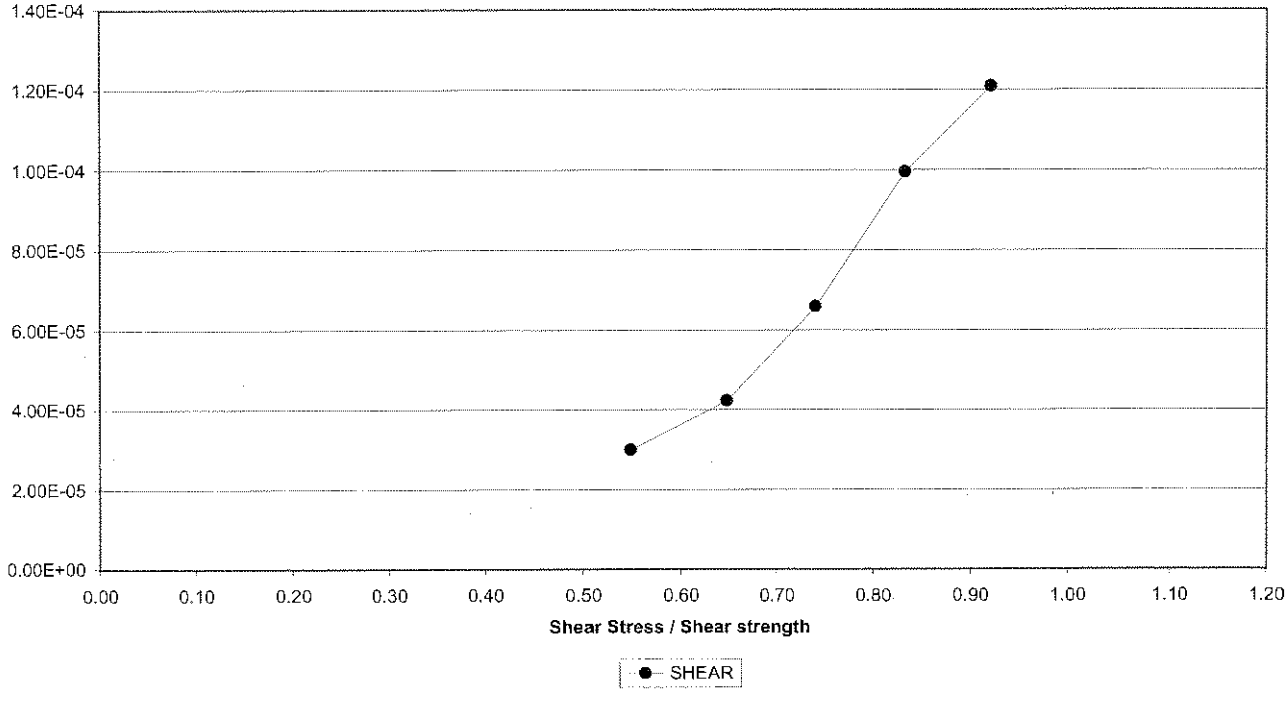

Creep Shear 2056-162
Crushed Ventersdorp Lava (dry, < 0.5mm, 0.5mm)

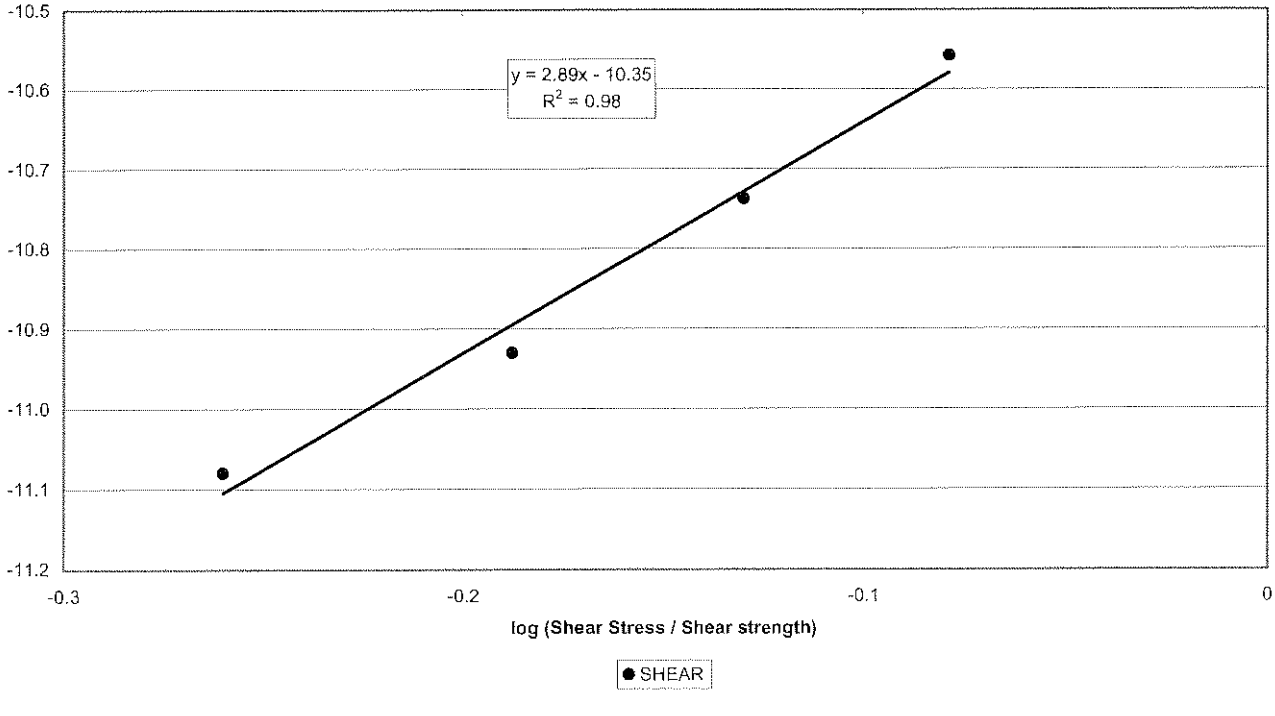

Creep Shear 2056-148
Crushed Ventersdorp Lava (dry, < 0.5mm, 1mm)

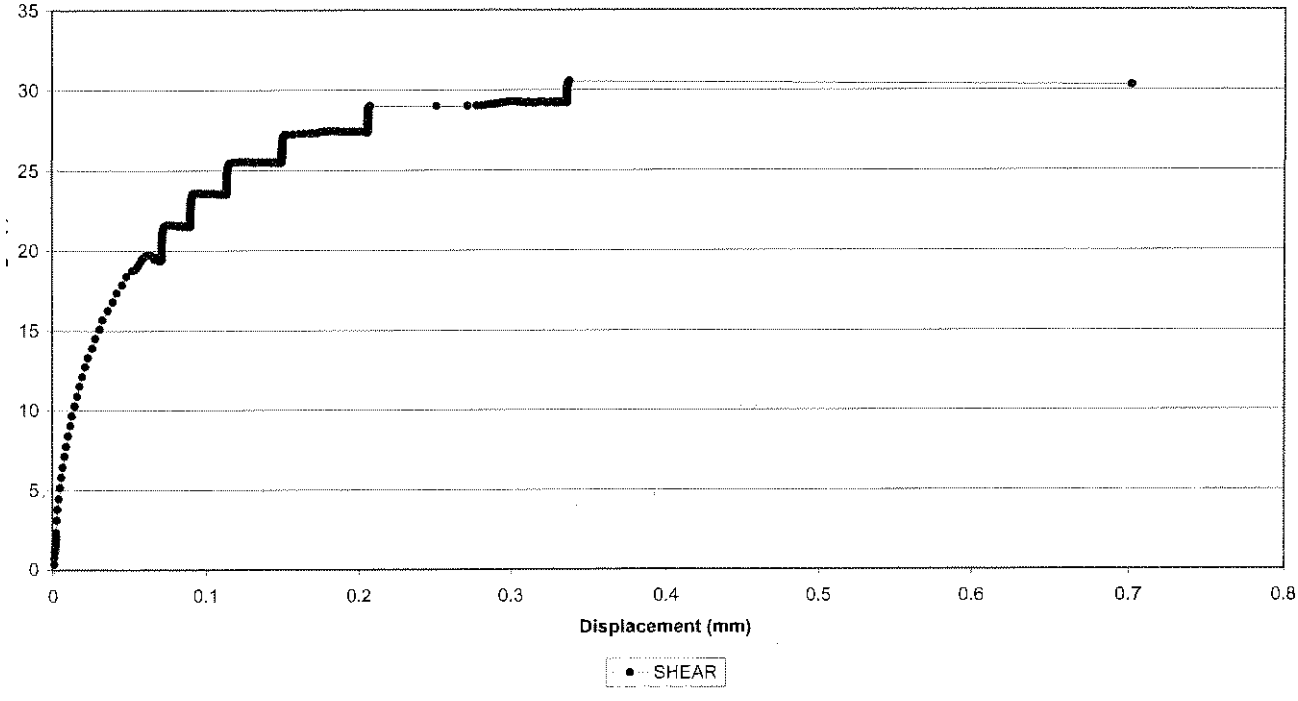

Creep Shear 2056-148
Crushed Ventersdorp Lava (dry, < 0.5mm, 1mm)

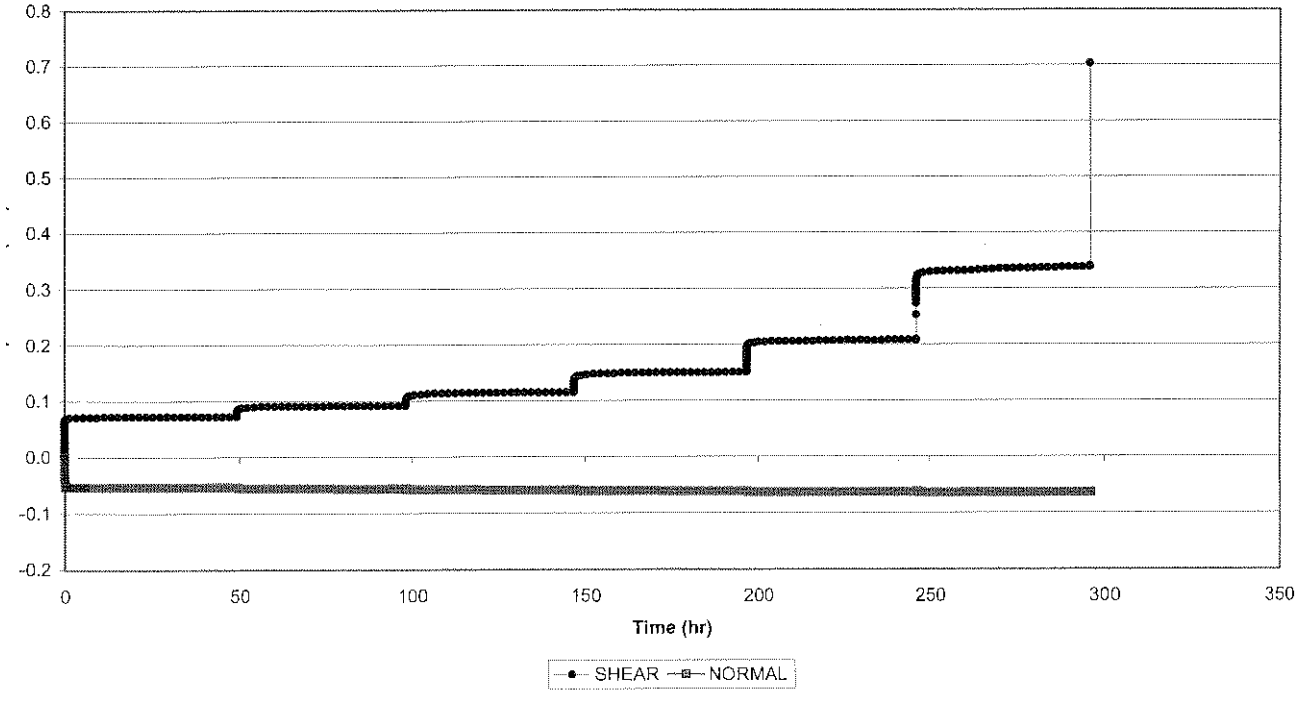

Creep Shear 2056-148, Cycle 1
Crushed Ventersdorp Lava (dry, < 0.5mm, 1mm)

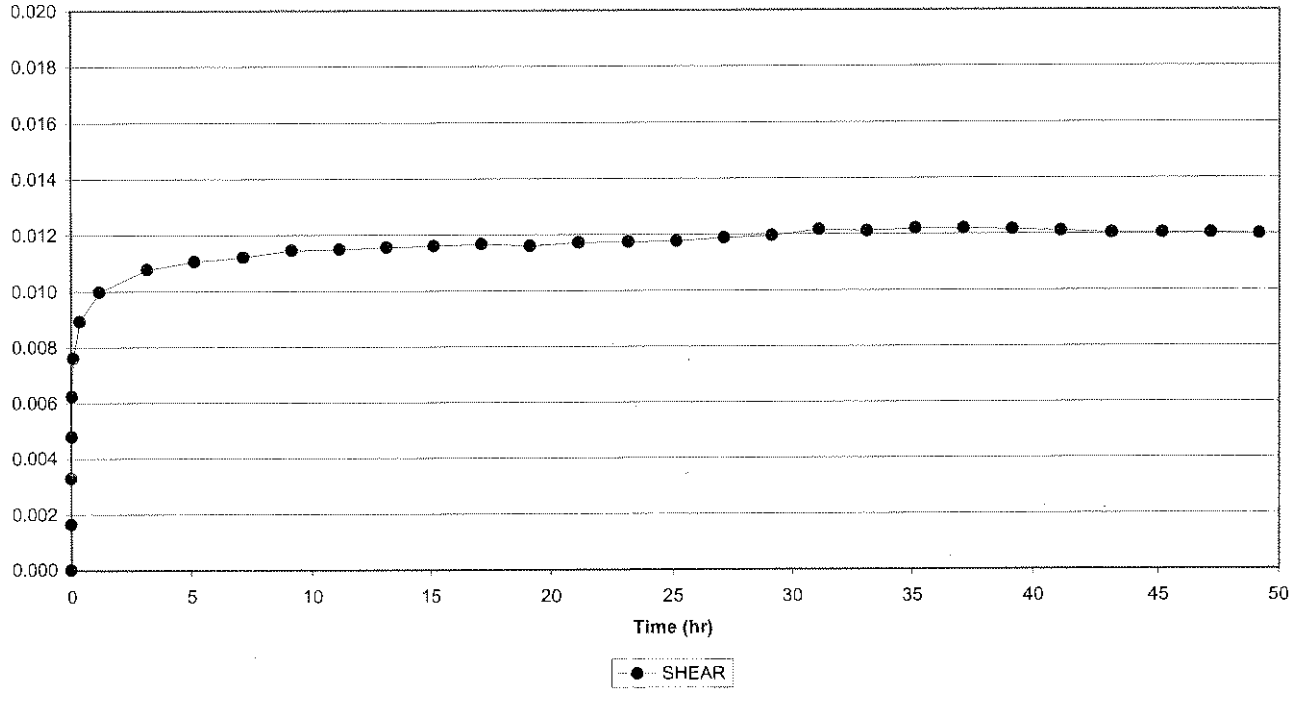

Creep Shear 2056-148, Cycle 2
Crushed Ventersdorp Lava (dry, < 0.5mm, 1mm)

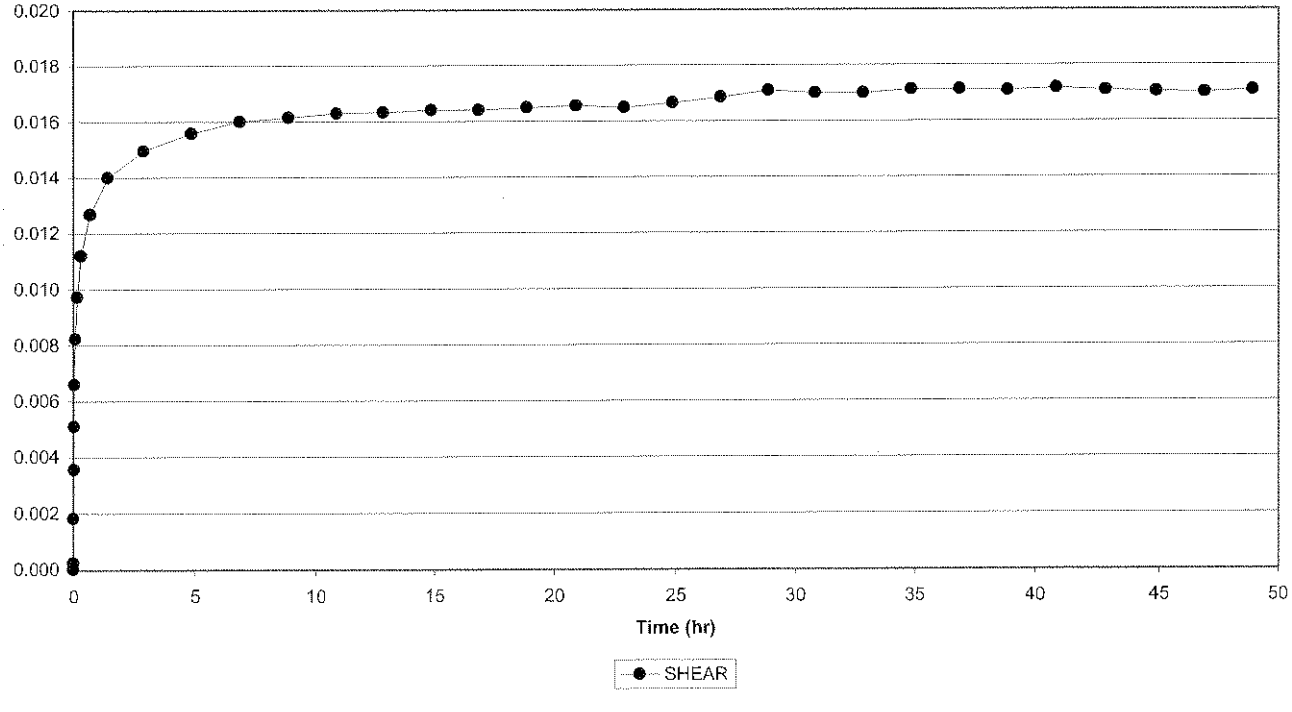

Creep Shear 2056-148, Cycle 3
Crushed Ventersdorp Lava (dry, < 0.5mm, 1mm)

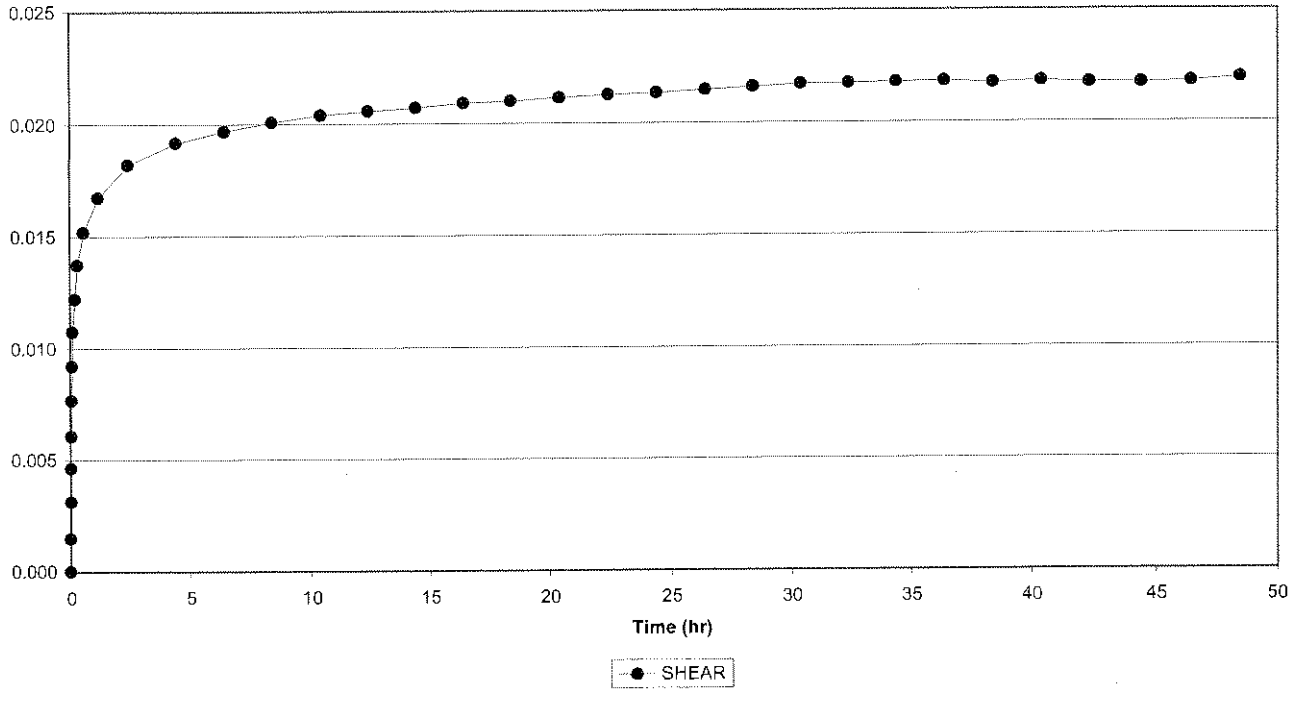

Creep Shear 2056-148, Cycle 4
Crushed Ventersdorp Lava (dry, < 0.5mm, 1mm)

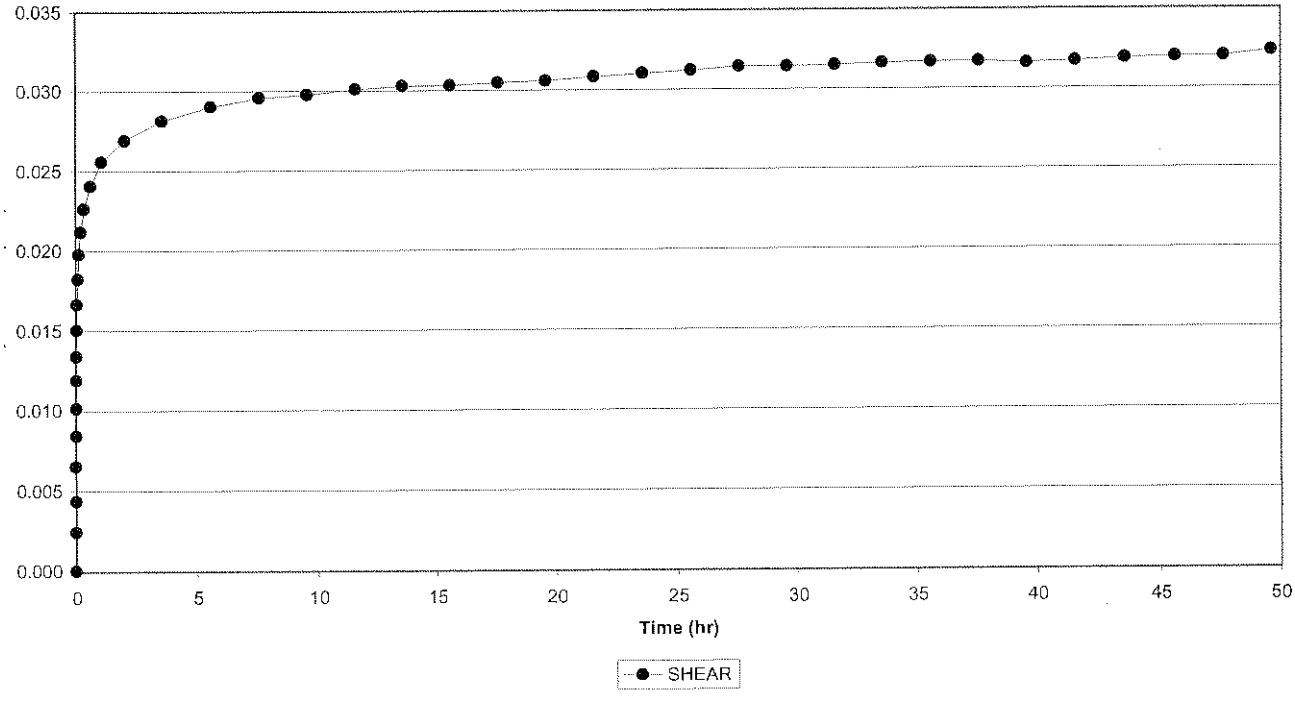

Creep Shear 2056-148, Cycle 5
Crushed Ventersdorp Lava (dry, < 0.5mm, 1mm)

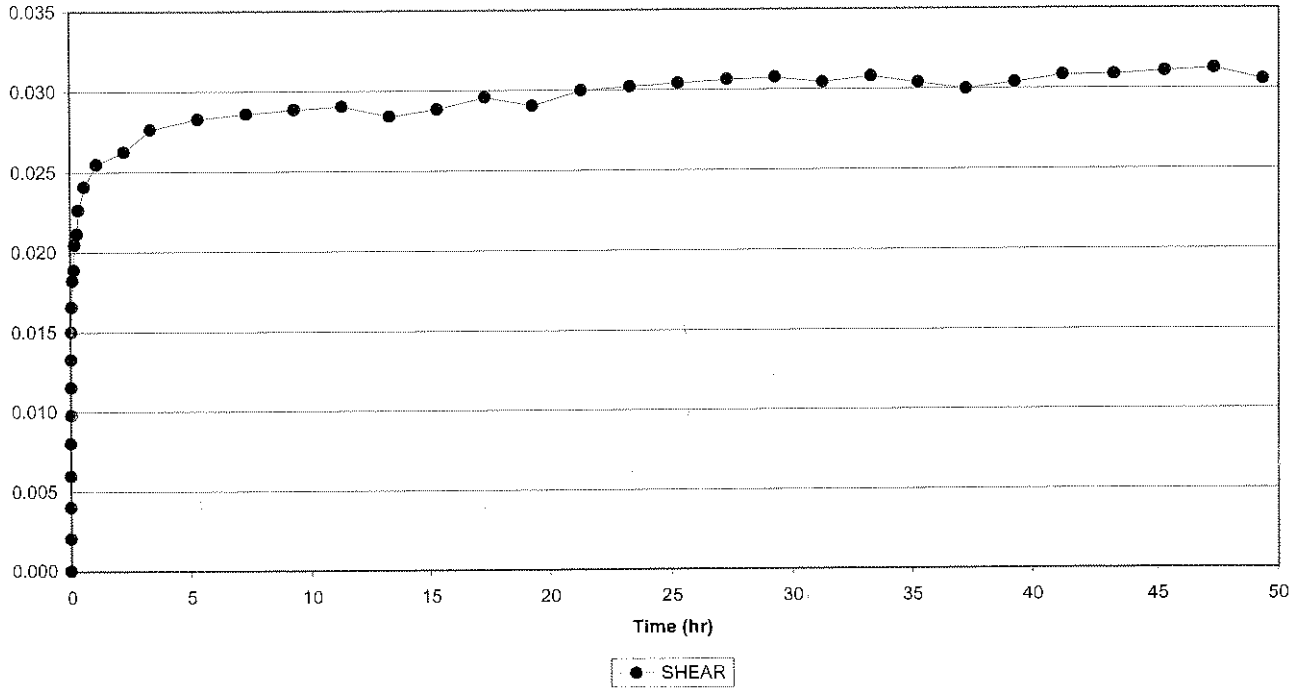

Creep Shear 2056-148, Cycle 6
Crushed Ventersdorp Lava (dry, < 0.5mm, 1mm)

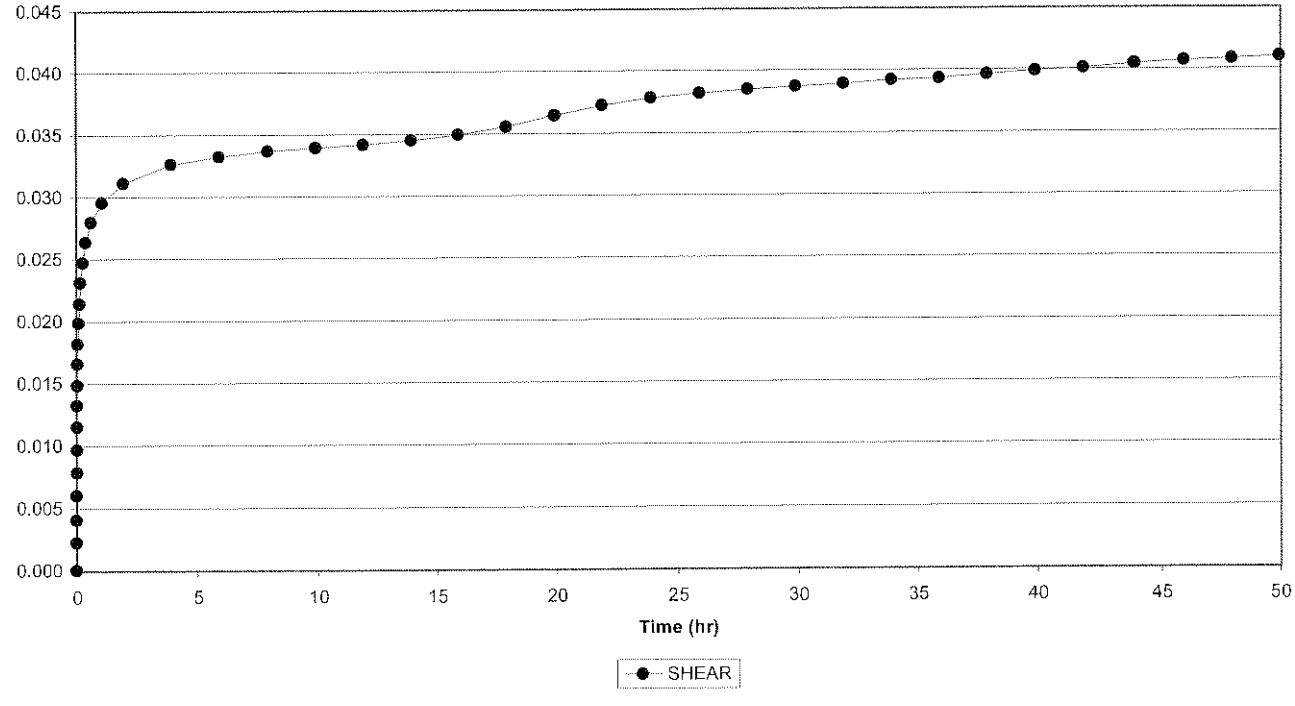

Creep Shear 2056-148
Crushed Ventersdorp Lava (dry, < 0.5mm, 1mm)

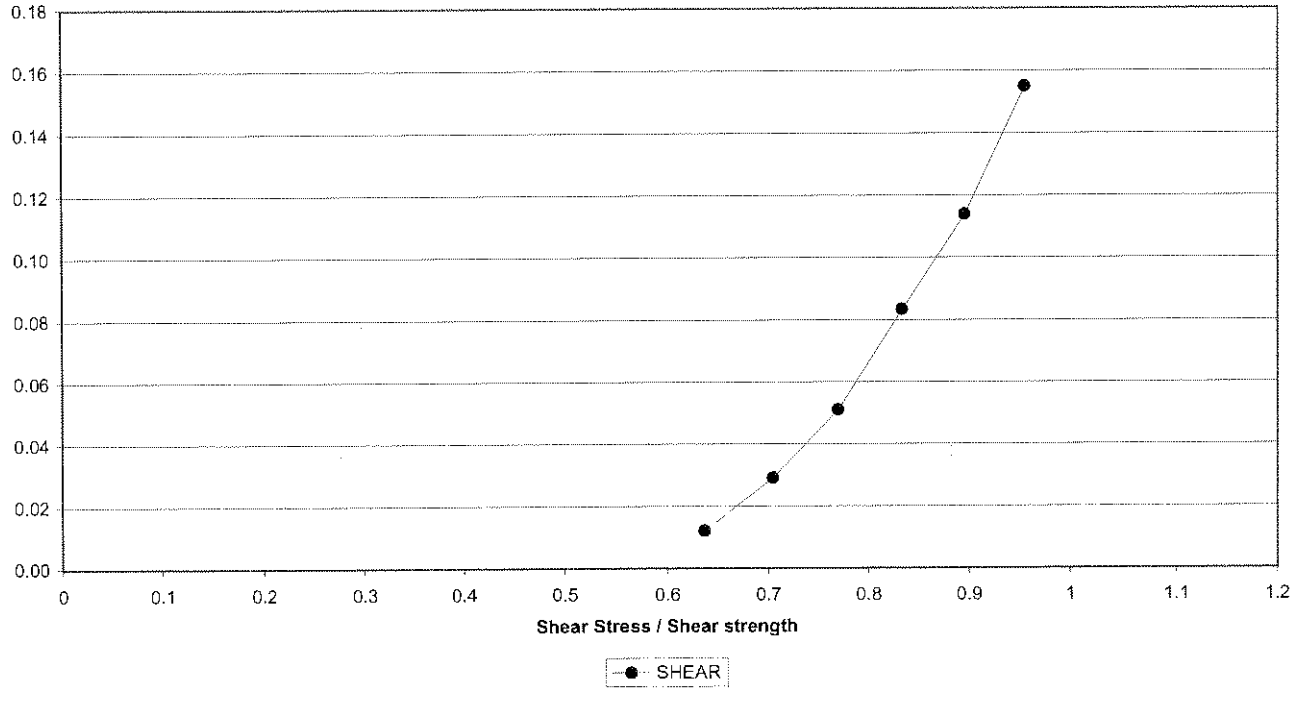

Creep Shear 2056-148
Crushed Ventersdorp Lava (dry, < 0.5mm, 1mm)

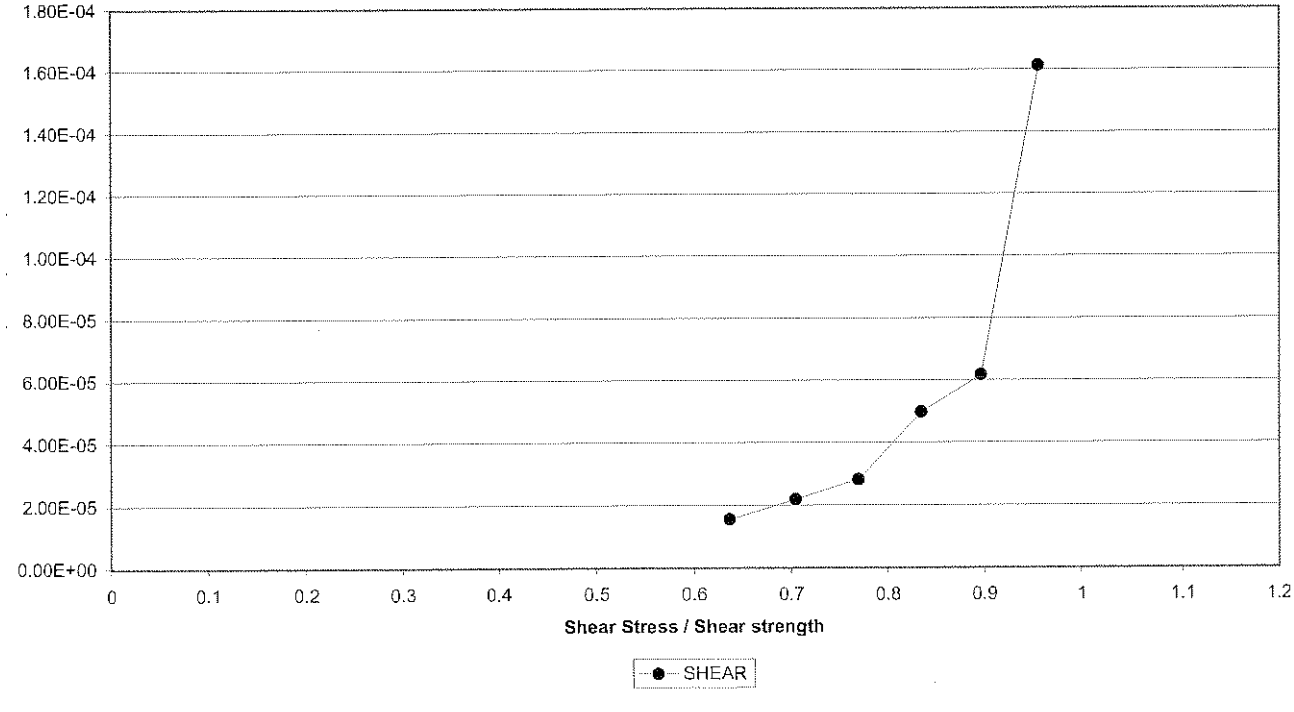

Creep Shear 2056-148
Crushed Ventersdorp Lava (dry, < 0.5mm, 1mm)

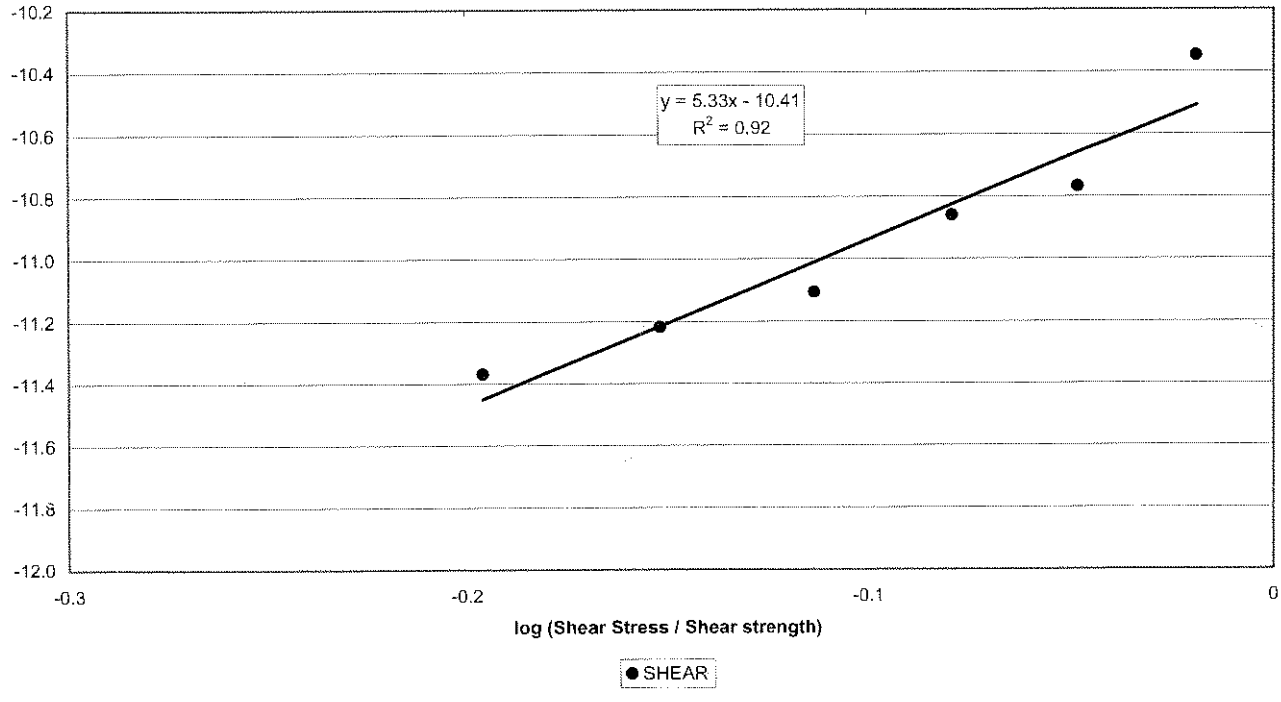

Creep Shear 2056-149
Crushed Ventersdorp Lava (dry, < 0.5mm, 2mm)

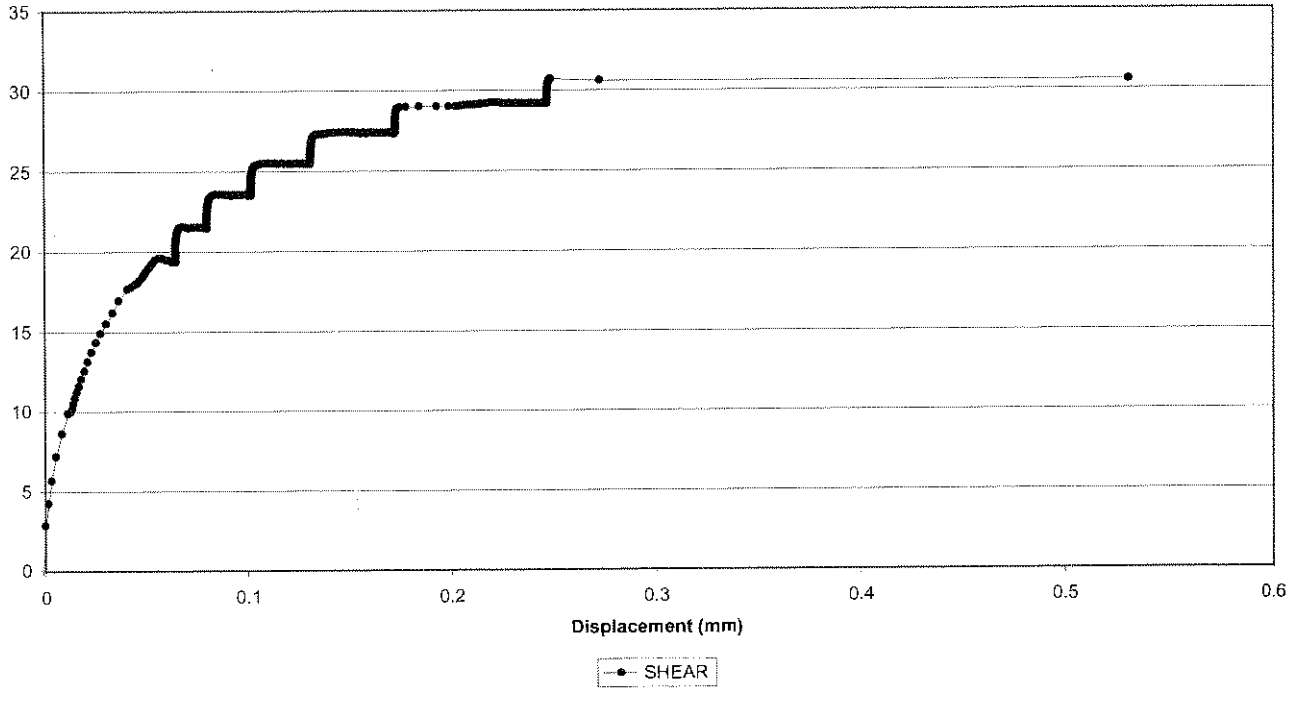

Creep Shear 2056-149
Crushed Ventersdorp Lava (dry, < 0.5mm, 2mm)

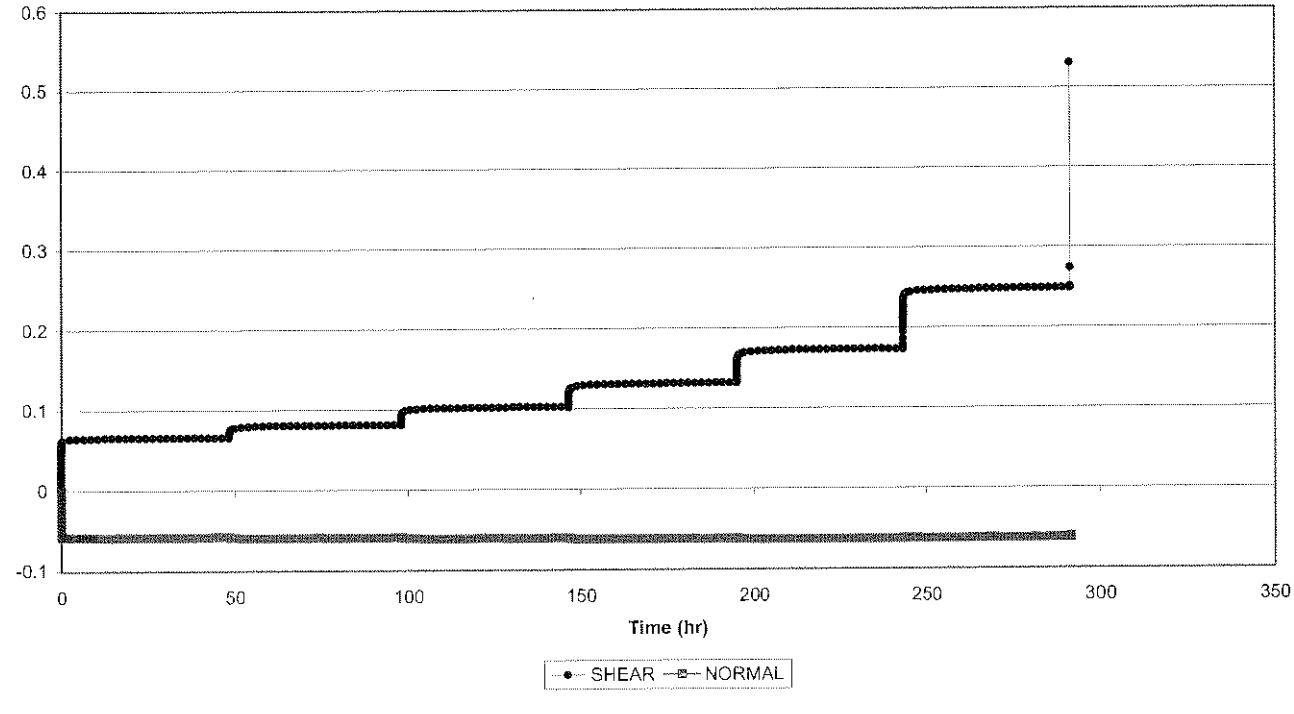

Creep Shear 2056-149, Cycle 1
Crushed Ventersdorp Lava (dry, < 0.5mm, 2mm)

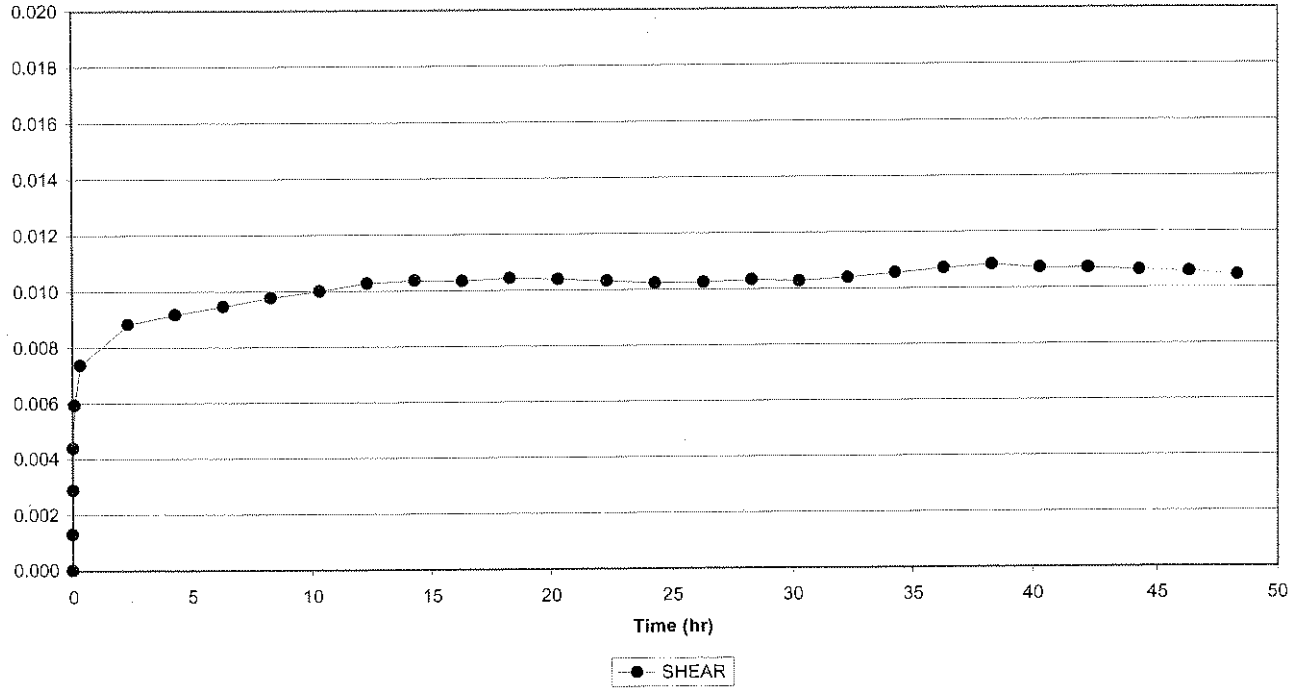

Creep Shear 2056-149, Cycle 2
Crushed Ventersdorp Lava (dry, < 0.5mm, 2mm)

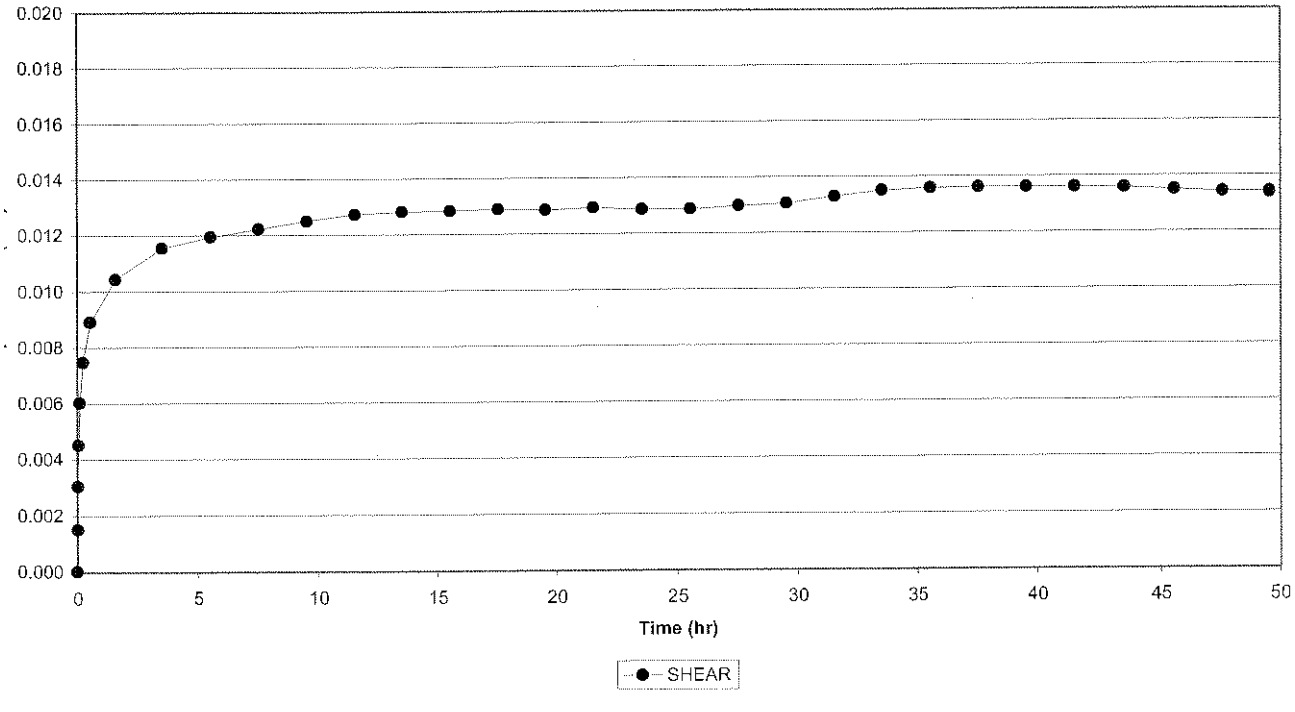

Creep Shear 2056-149, Cycle 3
Crushed Ventersdorp Lava (dry, < 0.5mm, 2mm)

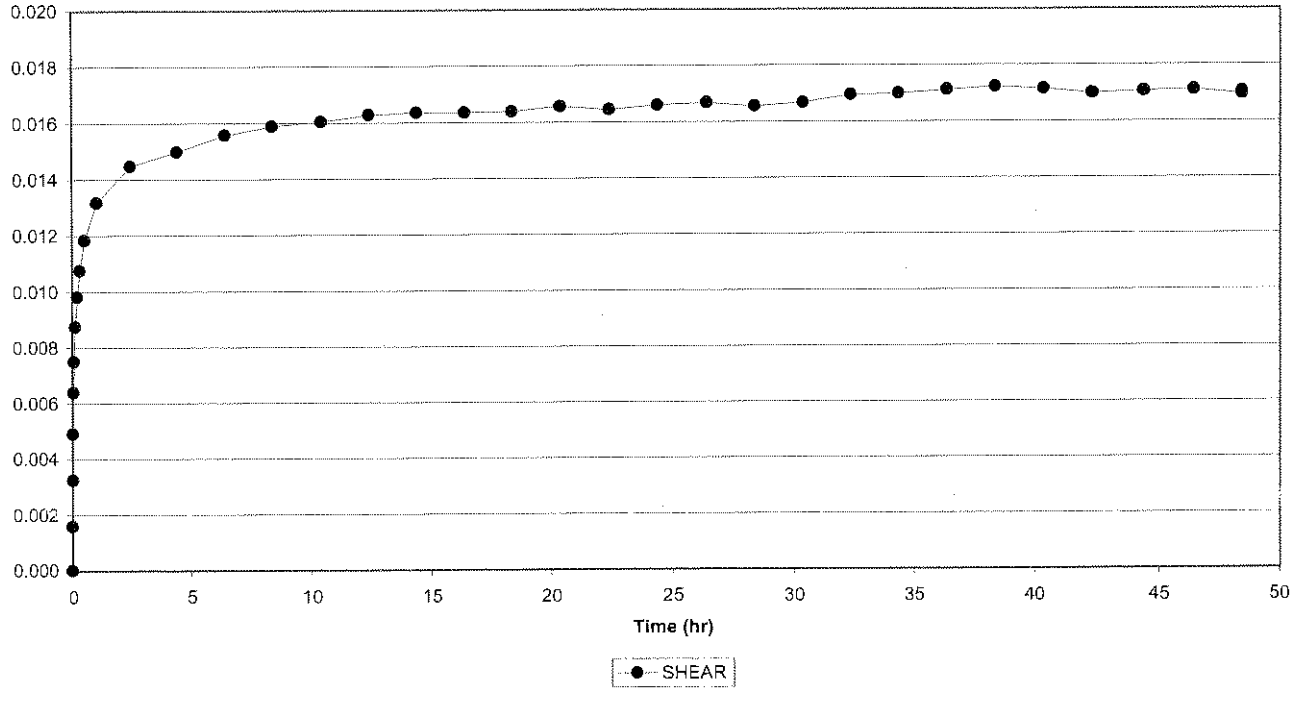

Creep Shear 2056-149, Cycle 4
Crushed Ventersdorp Lava (dry, < 0.5mm, 2mm)

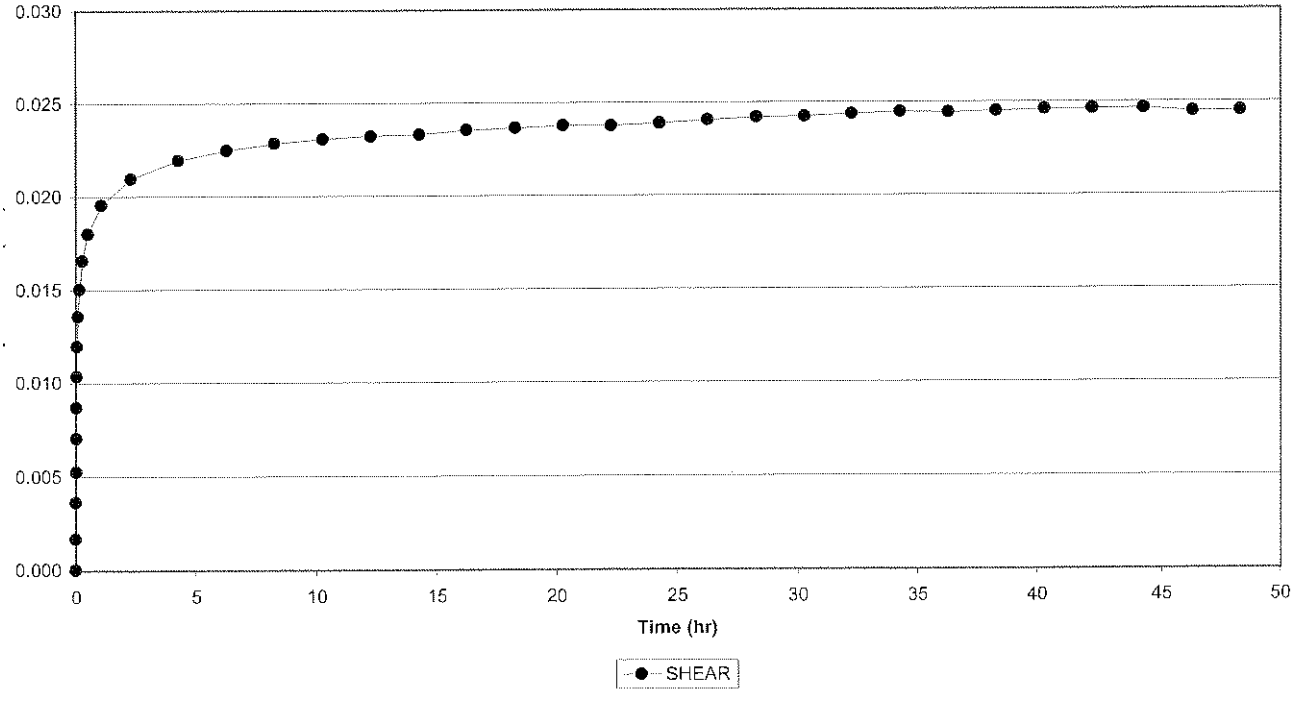

Creep Shear 2056-149, Cycle 5
Crushed Ventersdorp Lava (dry, < 0.5mm, 2mm)

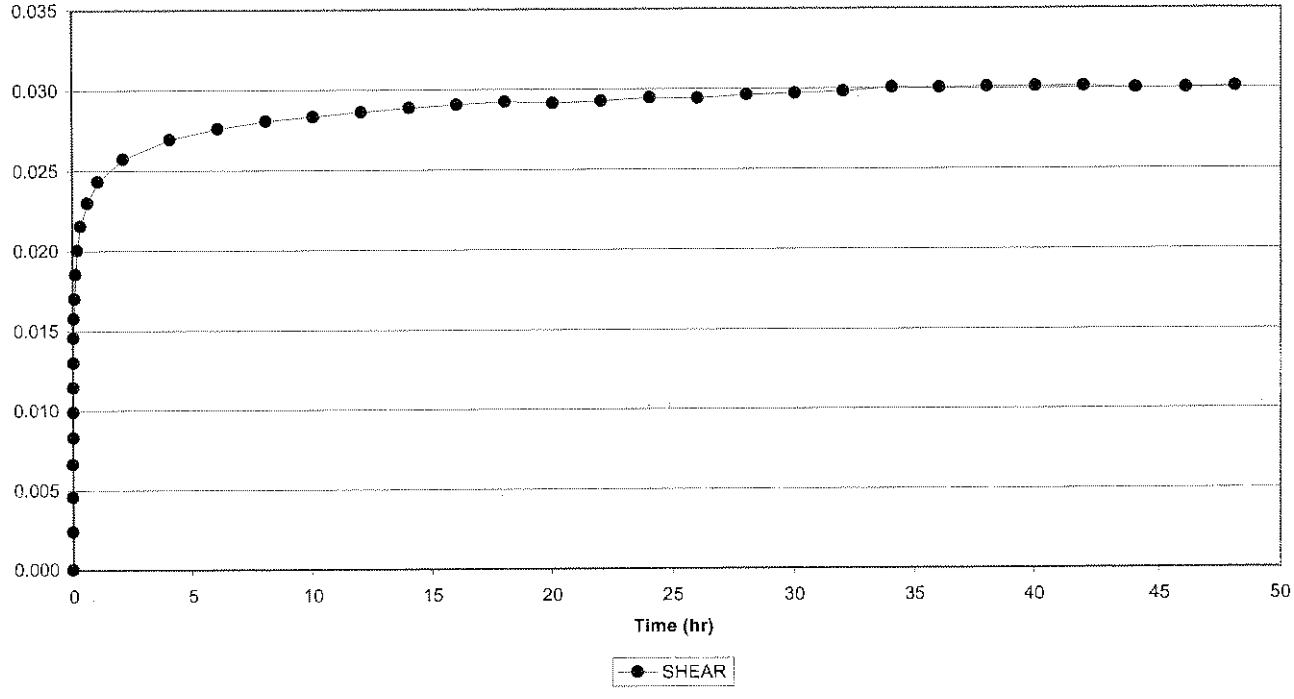

Creep Shear 2056-149, Cycle 6
Crushed Ventersdorp Lava (dry, < 0.5mm, 2mm)

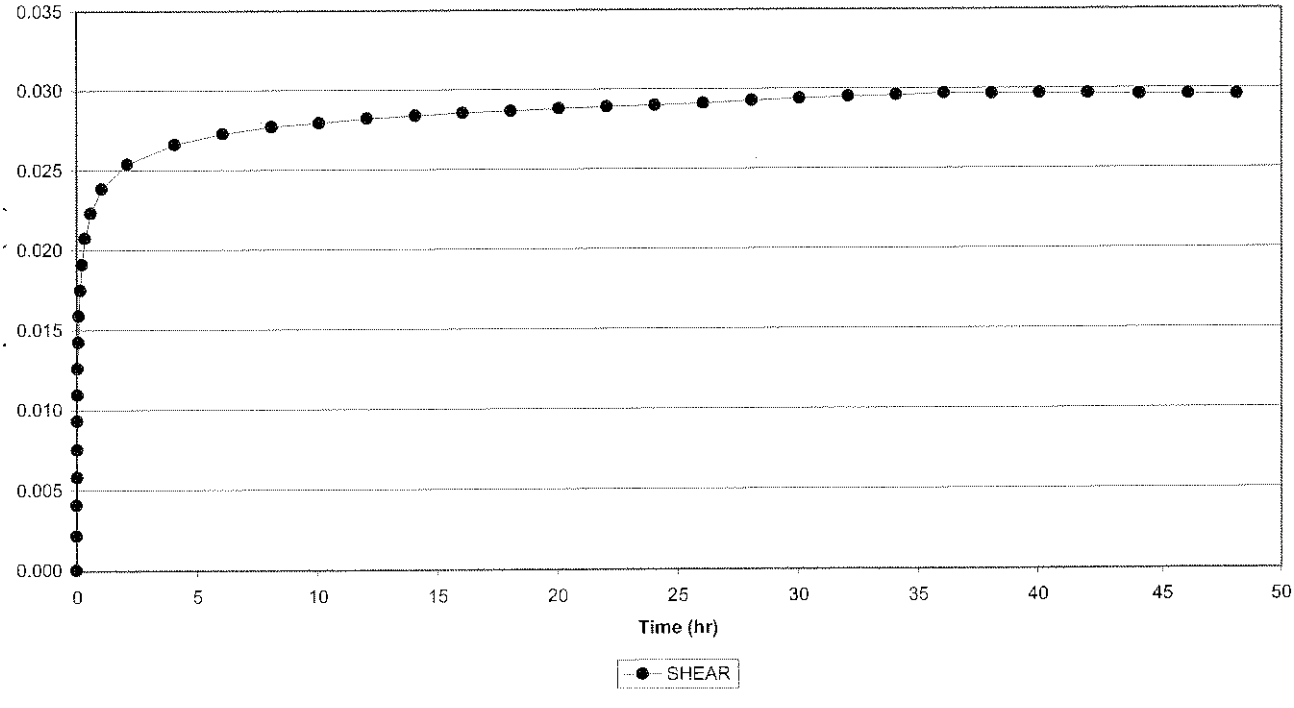

Creep Shear 2056-149
Crushed Ventersdorp Lava (dry, < 0.5mm, 2mm)

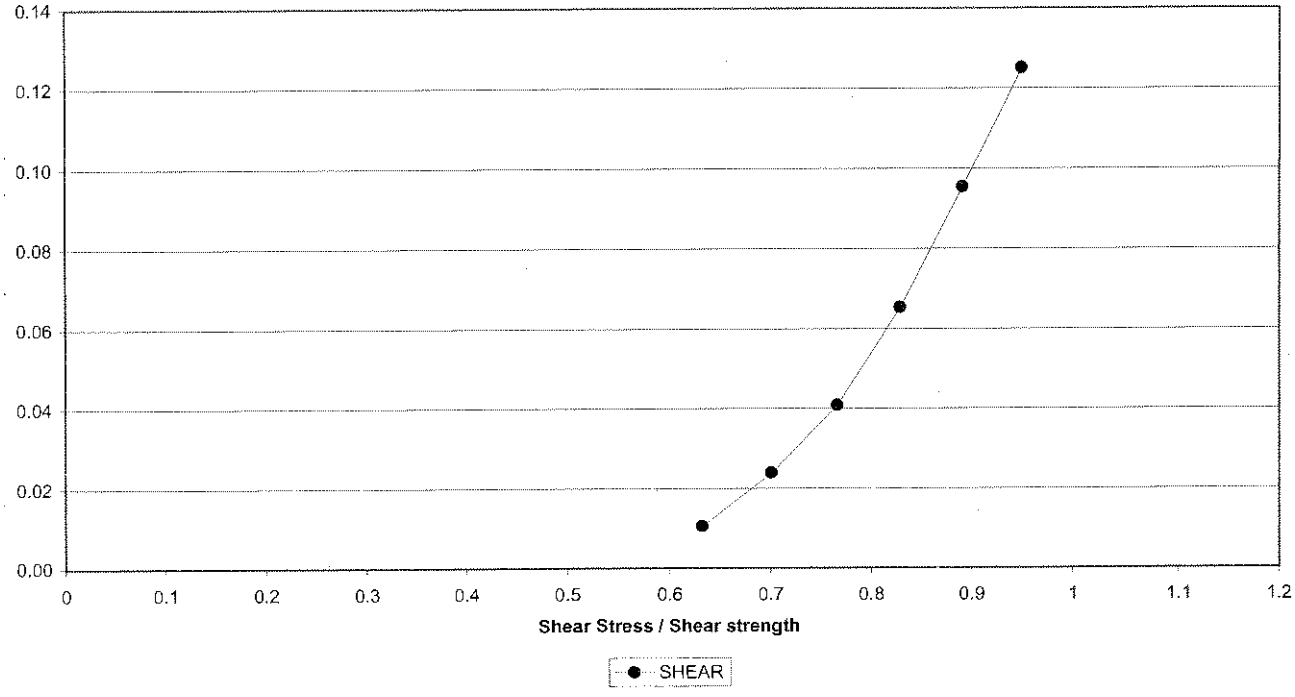

Creep Shear 2056-149
Crushed Ventersdorp Lava (dry, < 0.5mm, 2mm)

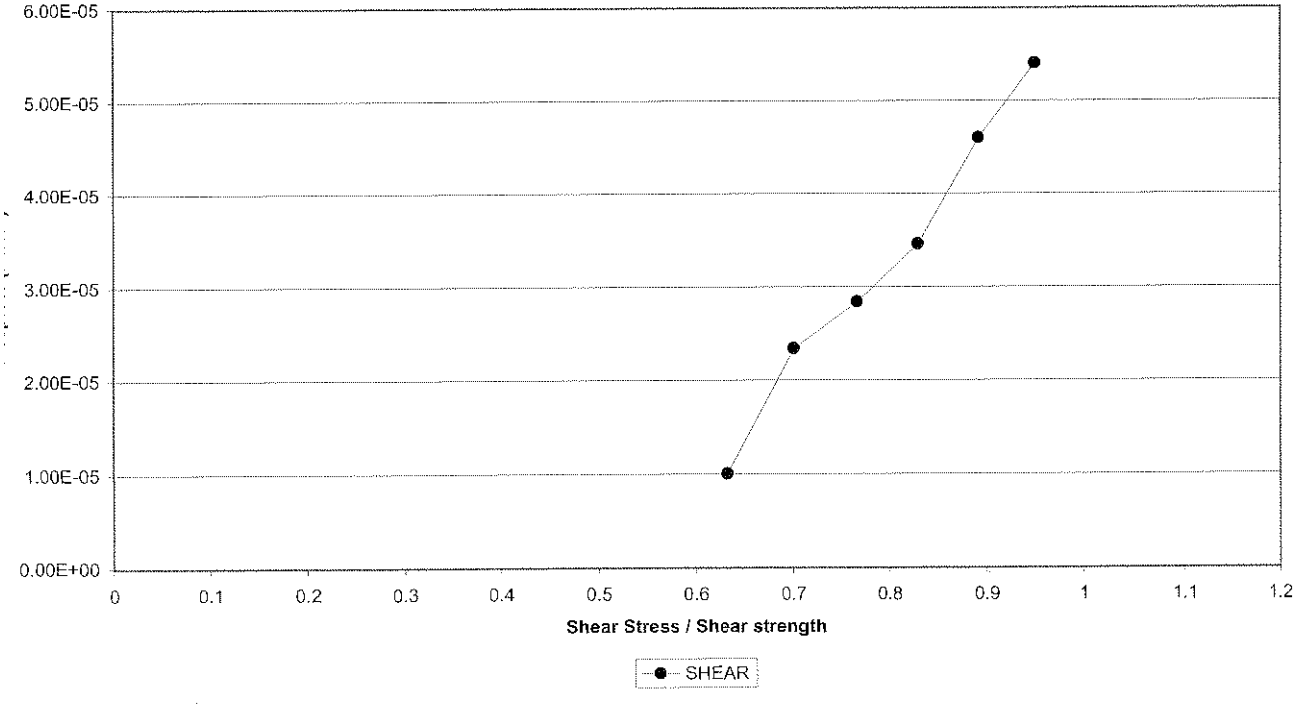

Creep Shear 2056-149
Crushed Ventersdorp Lava (dry, < 0.5mm, 2mm)

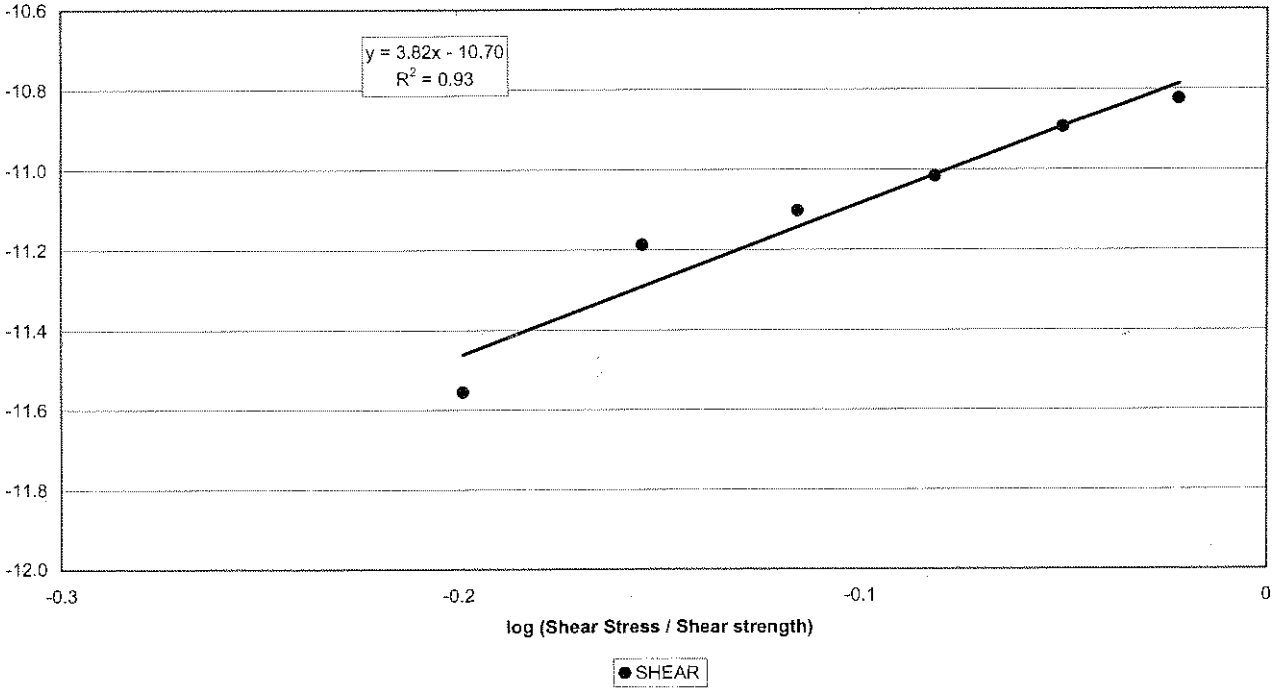

Creep Shear 2056-150
Crushed Ventersdorp Lava (wet, < 0.5mm, 1mm)

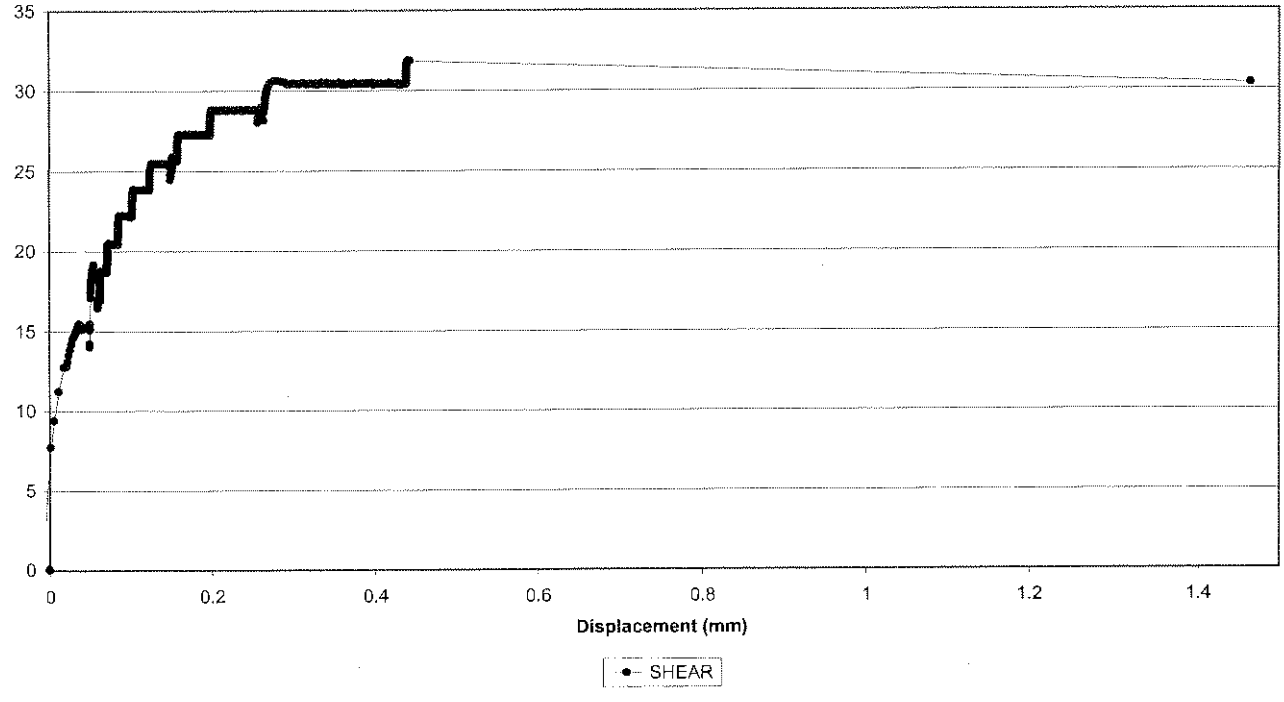

Creep Shear 2056-150
Crushed Ventersdorp Lava (wet, < 0.5mm, 1mm)

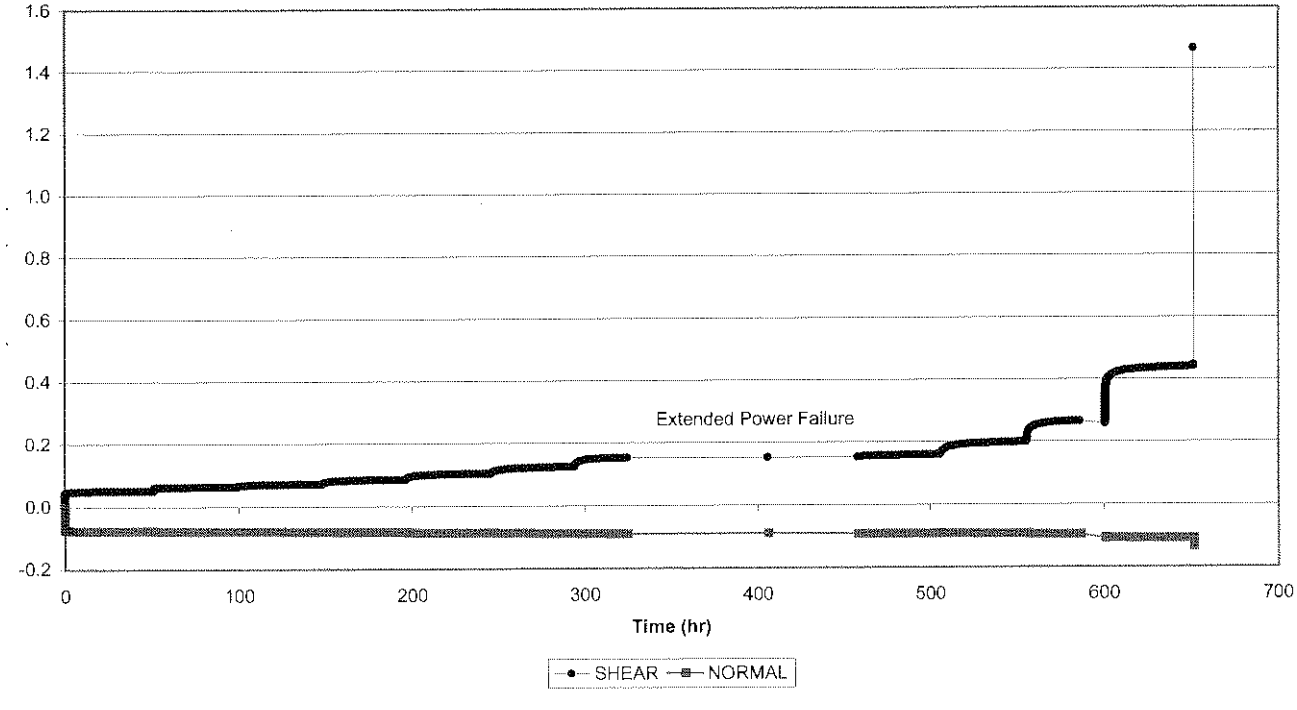

Creep Shear 2056-150, Cycle 1
Crushed Ventersdorp Lava (wet, < 0.5mm, 1mm)

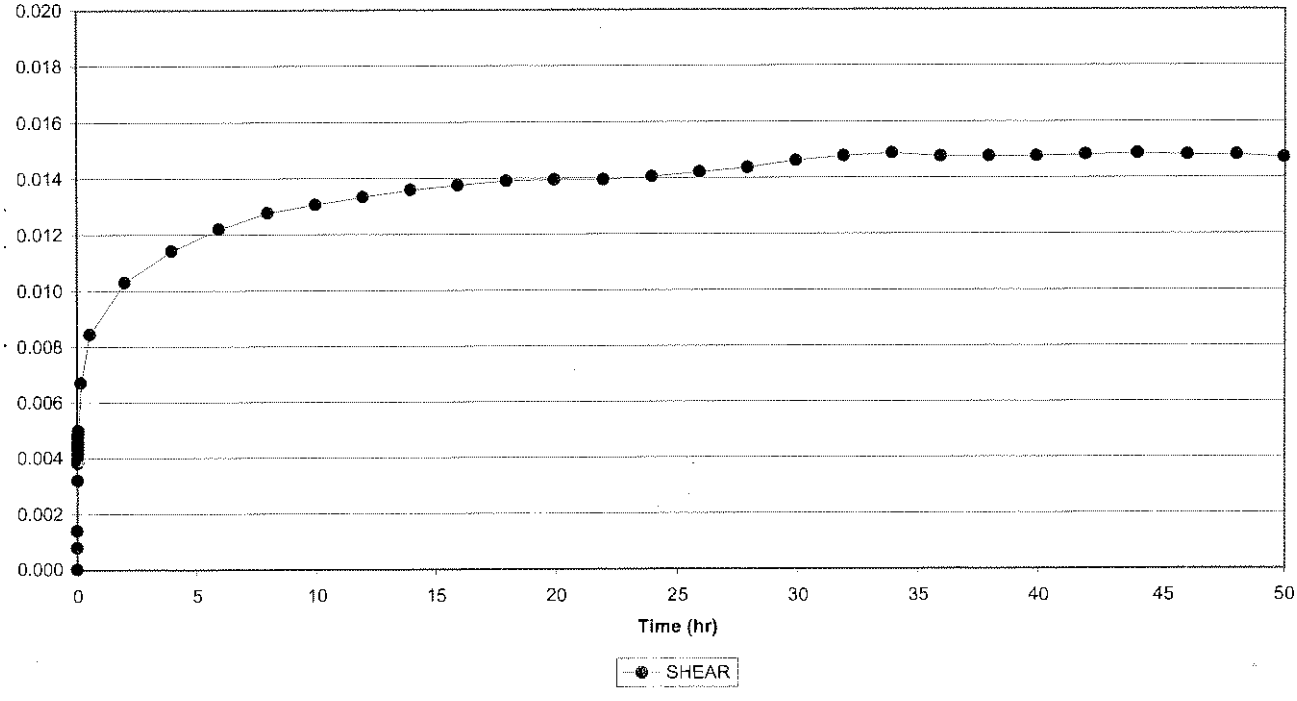

Creep Shear 2056-150, Cycle 2
Crushed Ventersdorp Lava (wet, < 0.5mm, 1mm)

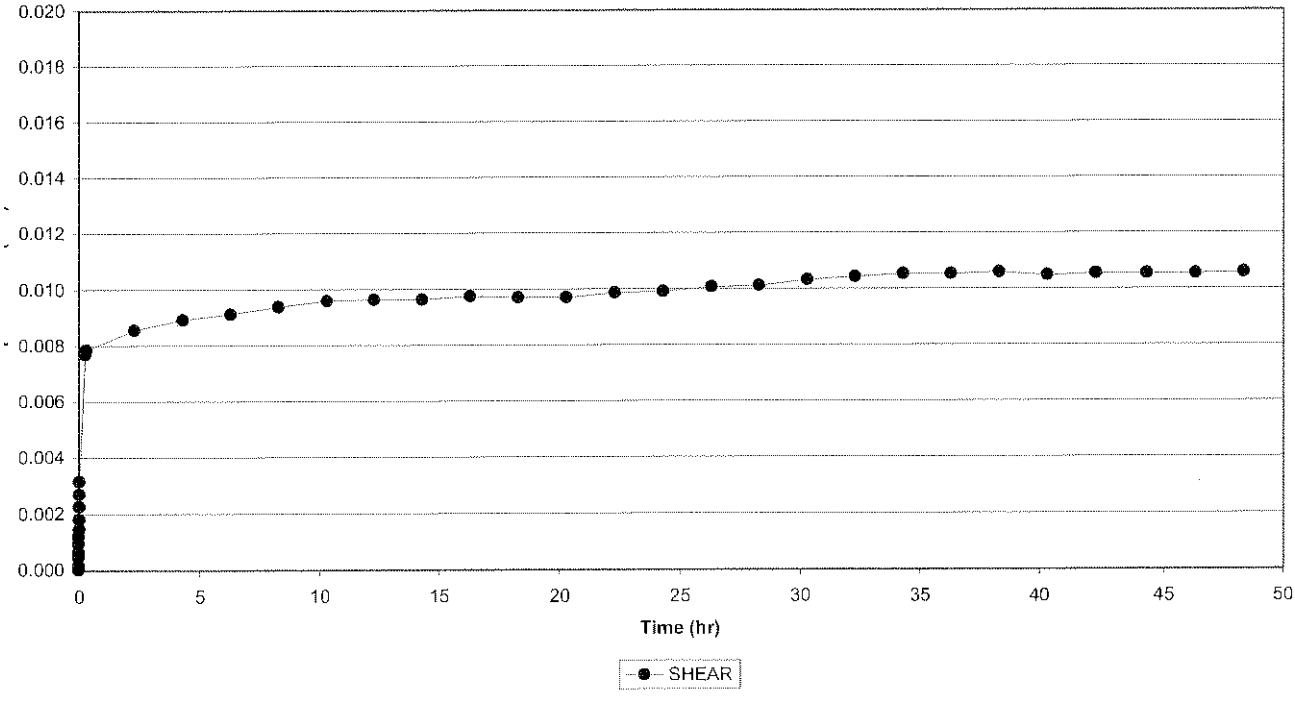

Creep Shear 2056-150, Cycle 3
Crushed Ventersdorp Lava (wet, < 0.5mm, 1mm)

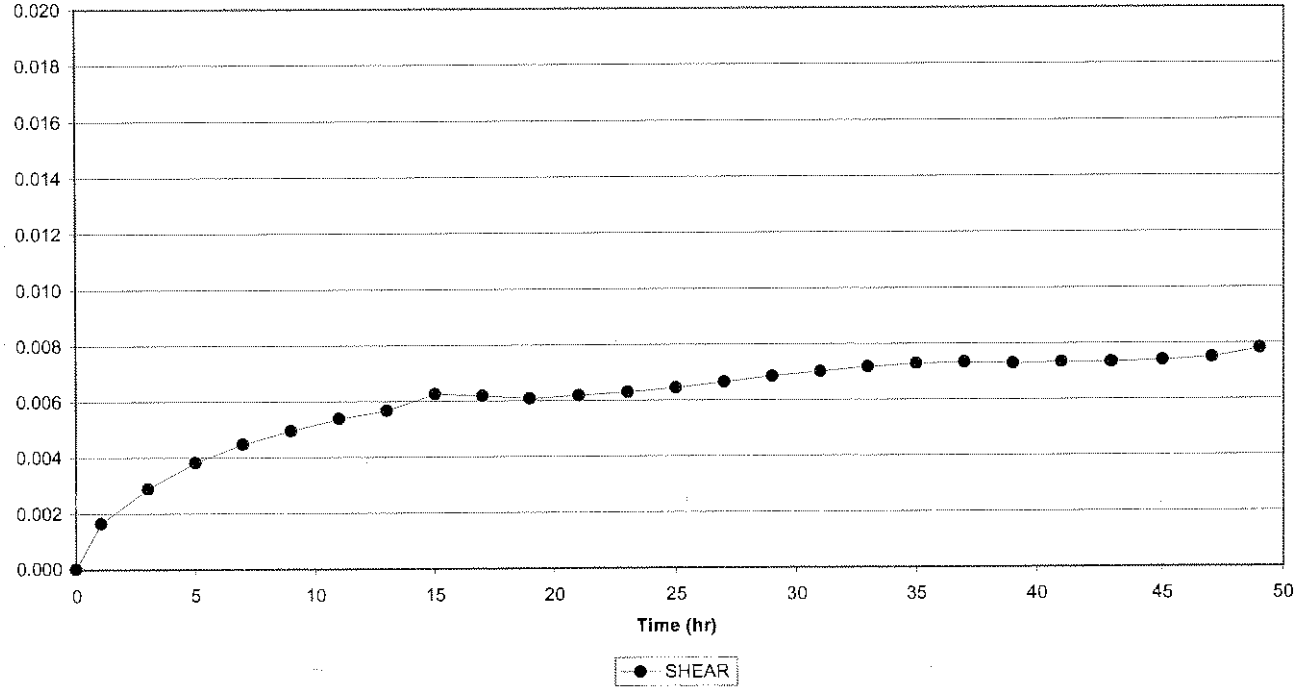

Creep Shear 2056-150, Cycle 4
Crushed Ventersdorp Lava (wet, < 0.5mm, 1mm)

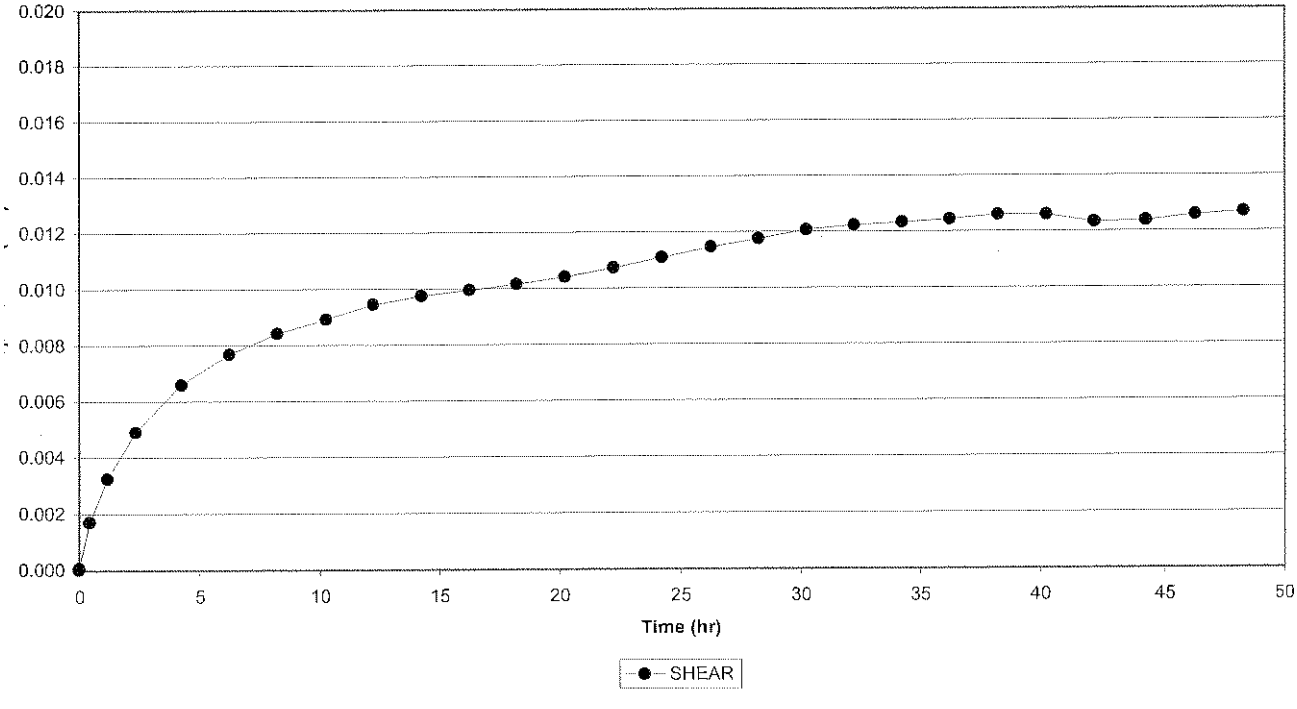

Creep Shear 2056-150, Cycle 5
Crushed Ventersdorp Lava (wet, < 0.5mm, 1mm)

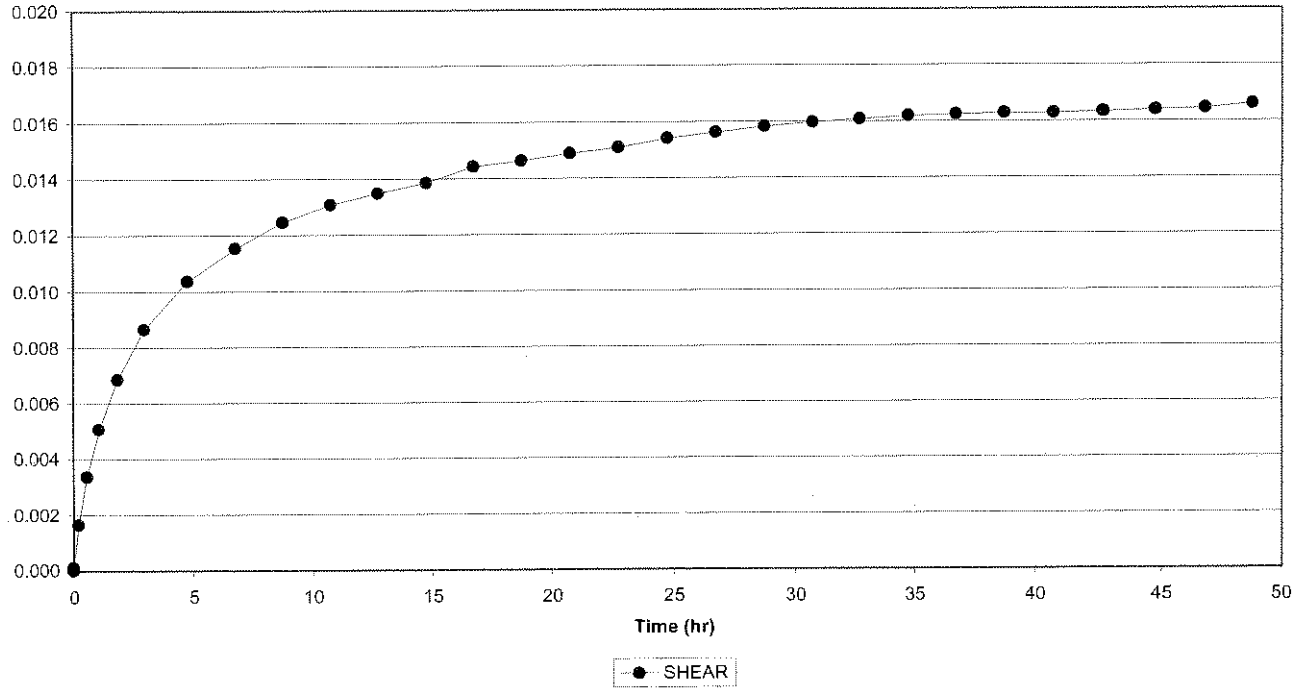

Creep Shear 2056-150, Cycle 6
Crushed Ventersdorp Lava (wet, < 0.5mm, 1mm)

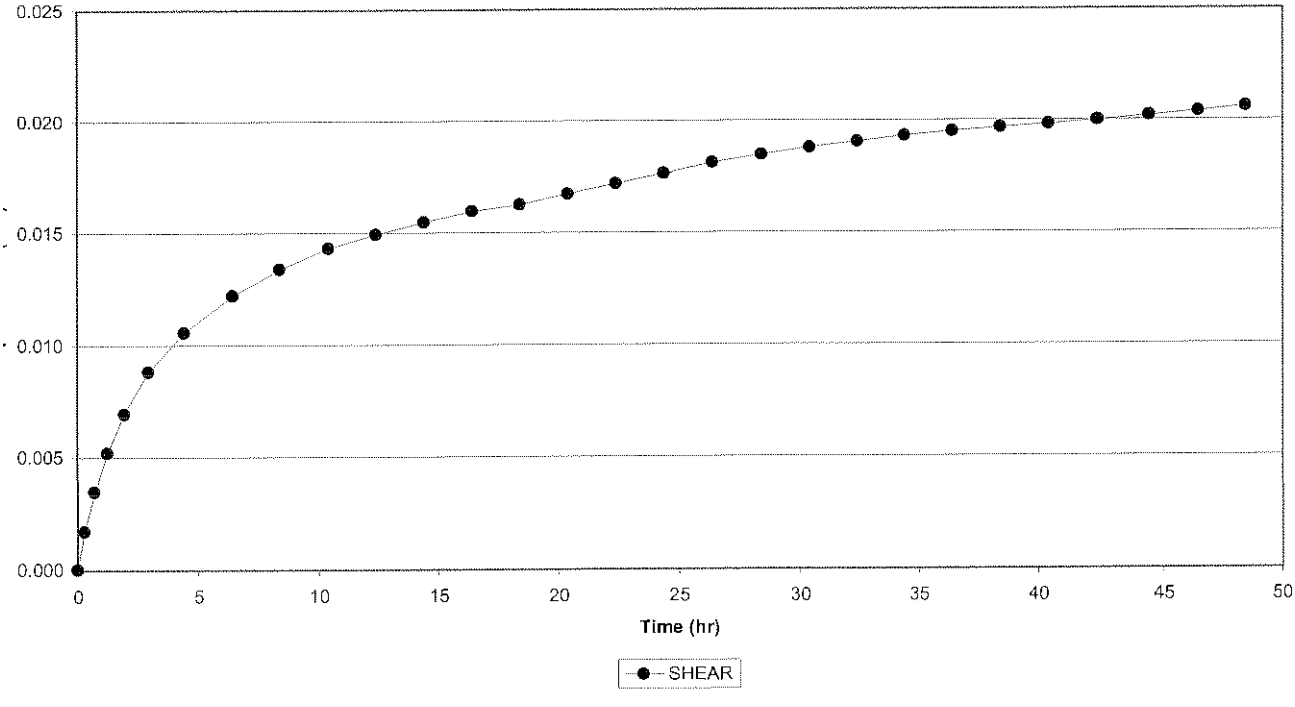

Creep Shear 2056-150, Cycle 7
Crushed Ventersdorp Lava (wet, < 0.5mm, 1mm)

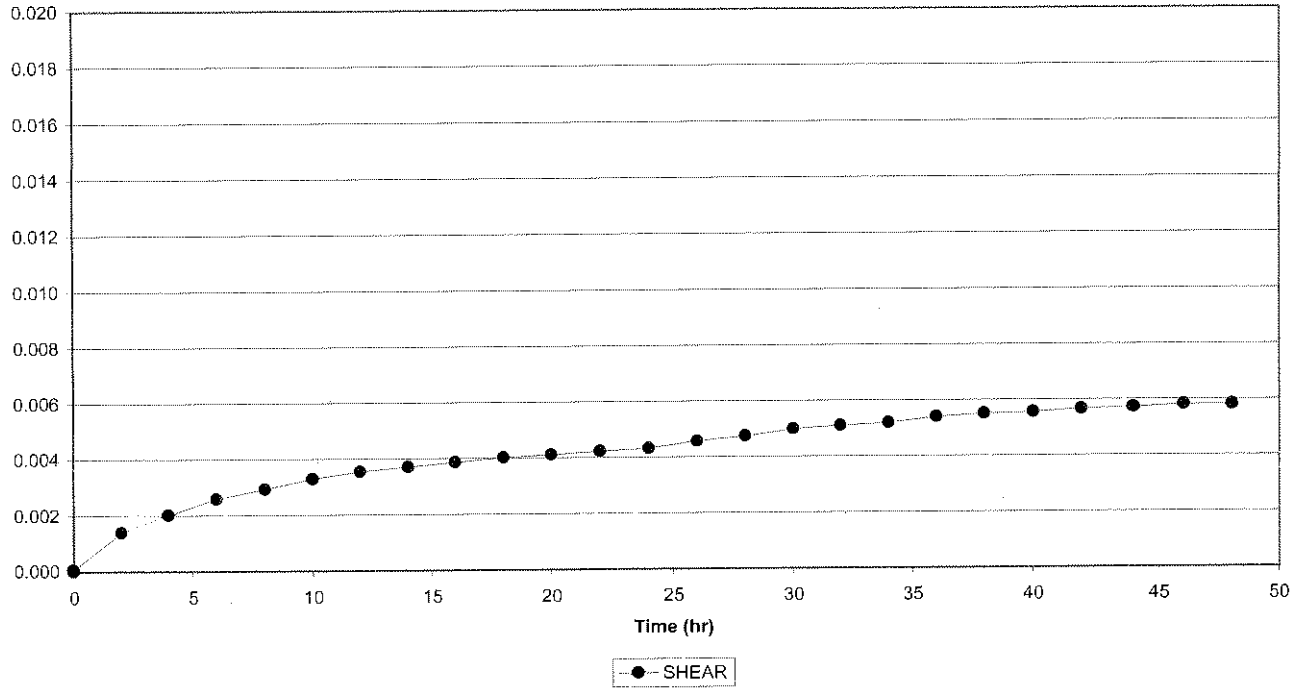

Creep Shear 2056-150, Cycle 8
Crushed Ventersdorp Lava (wet, < 0.5mm, 1mm)

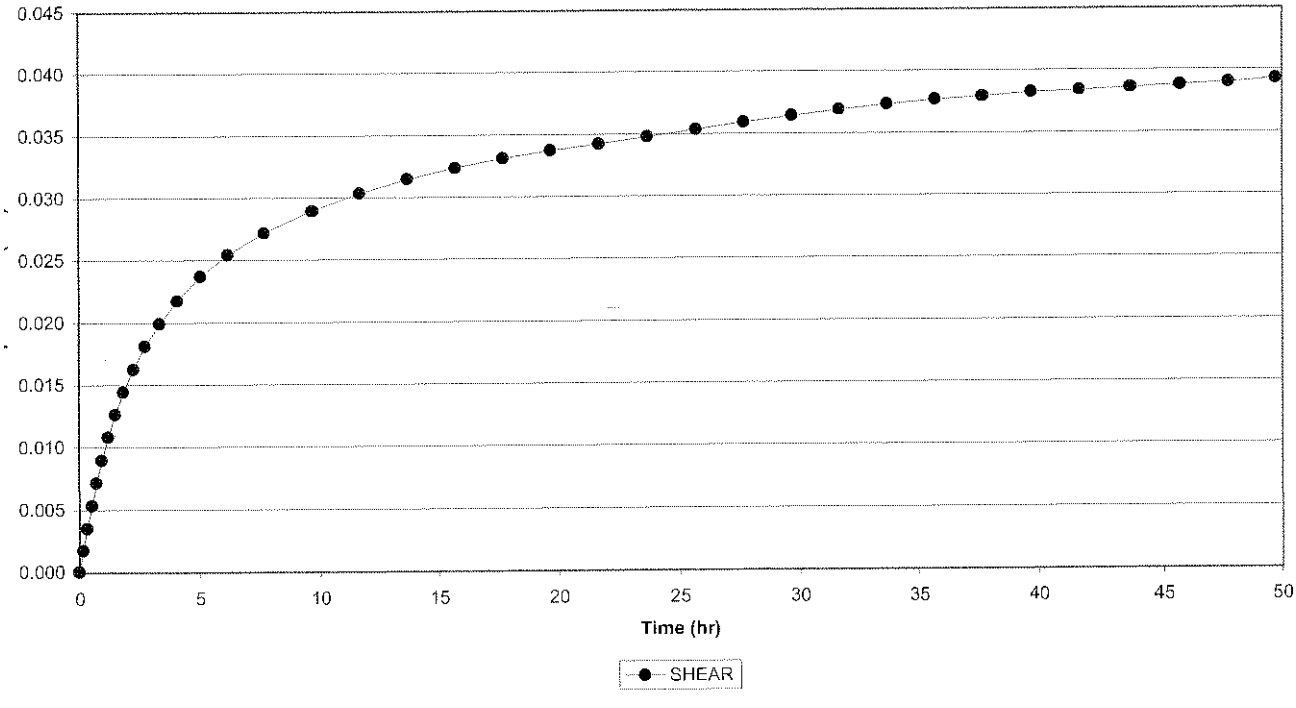

Creep Shear 2056-150, Cycle 9
Crushed Ventersdorp Lava (wet, < 0.5mm, 1mm)

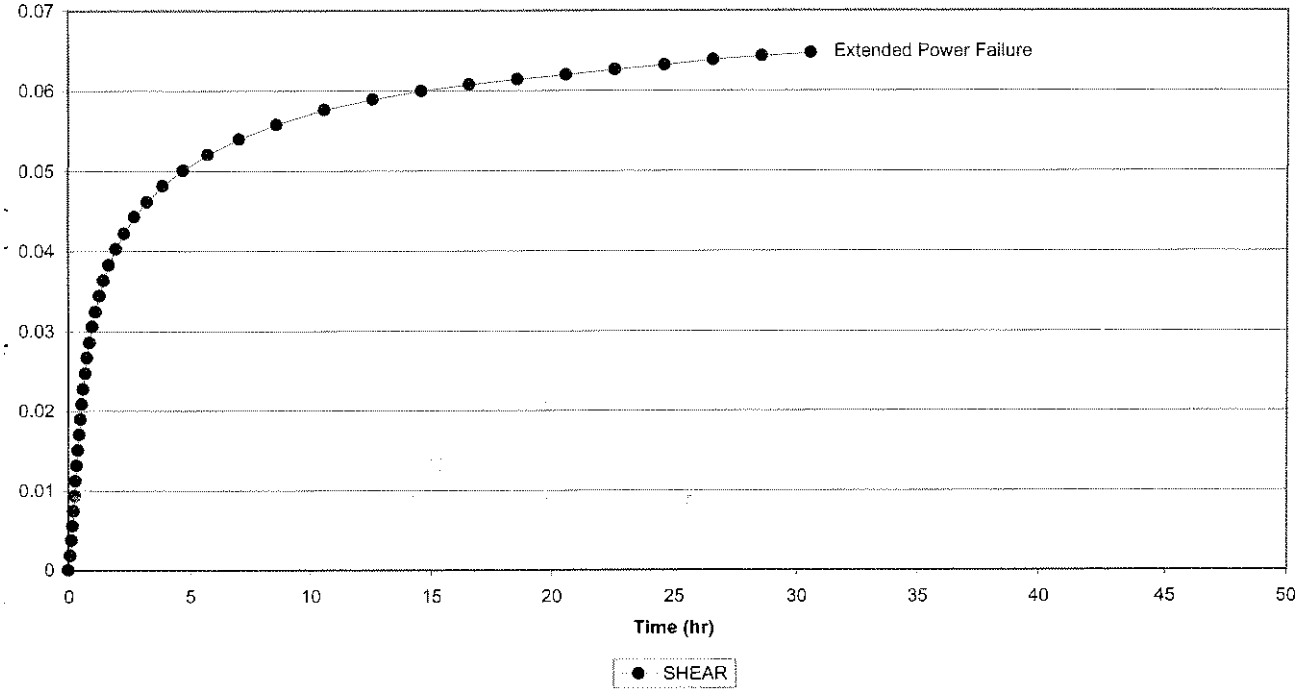

Creep Shear 2056-150, Cycle 10
Crushed Ventersdorp Lava (wet, < 0.5mm, 1mm)

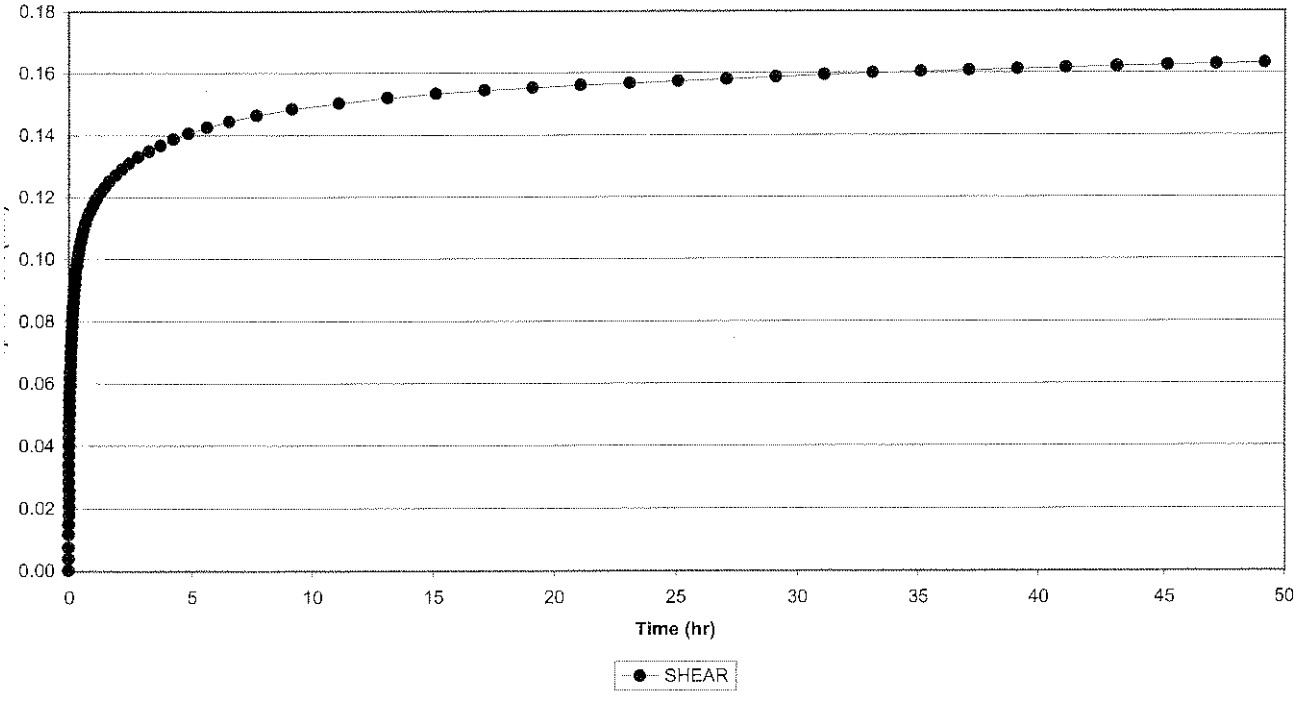

Creep Shear 2056-150
Crushed Ventersdorp Lava (wet, < 0.5mm, 1mm)

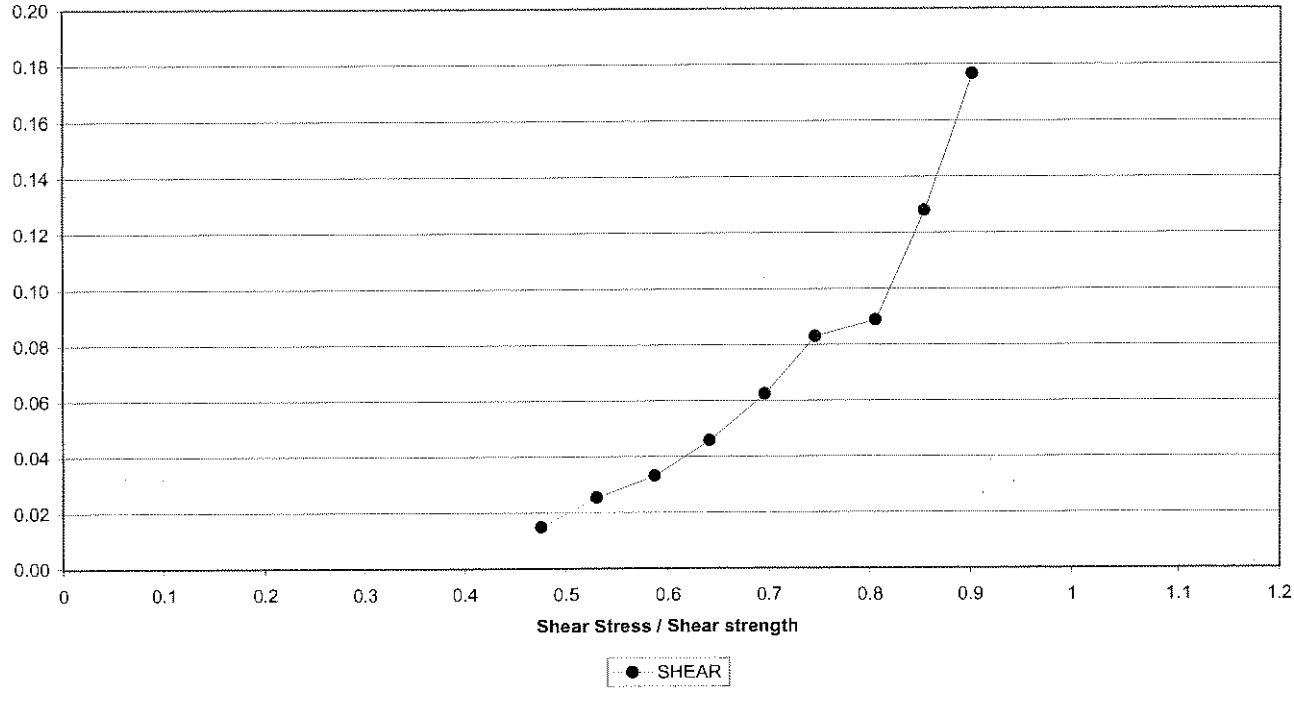

Creep Shear 2056-150
Crushed Ventersdorp Lava (wet, < 0.5mm, 1mm)

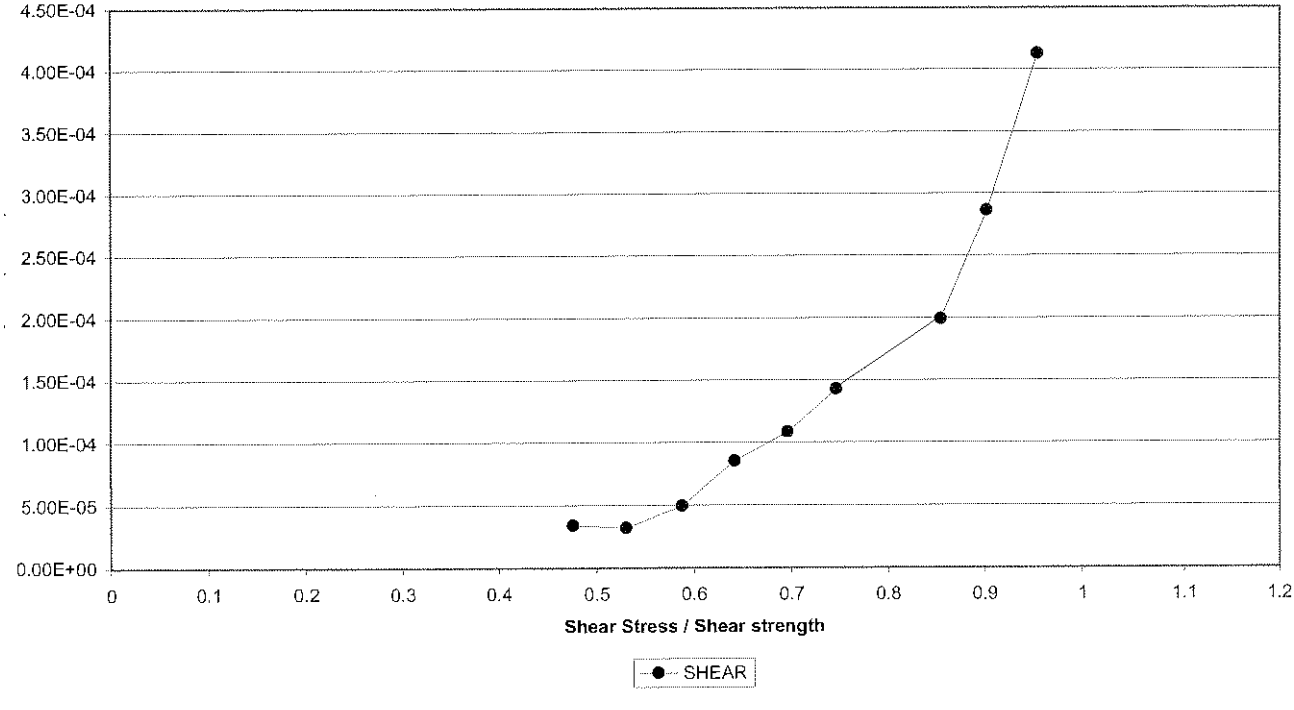

Creep Shear 2056-150
Crushed Ventersdorp Lava (wet, < 0.5mm, 1mm)

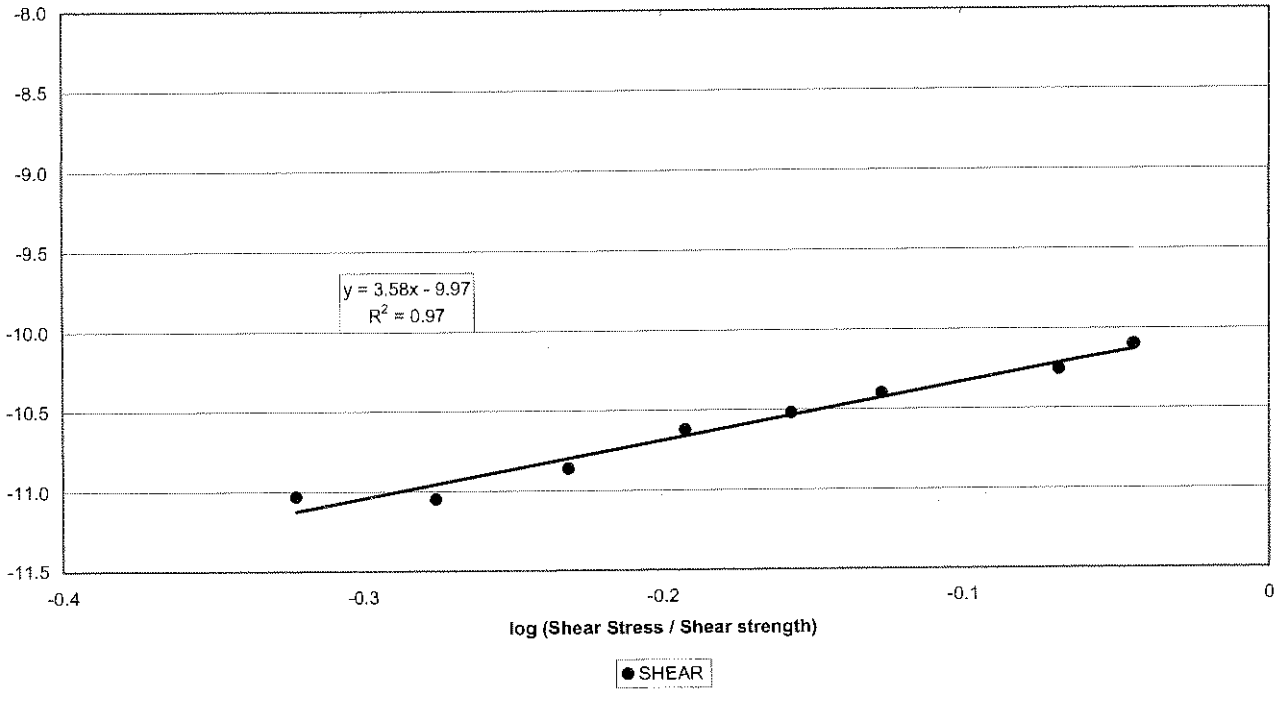

Creep Shear 2056-239
Natural gouge (dry, < 0.5mm, 0.5mm)

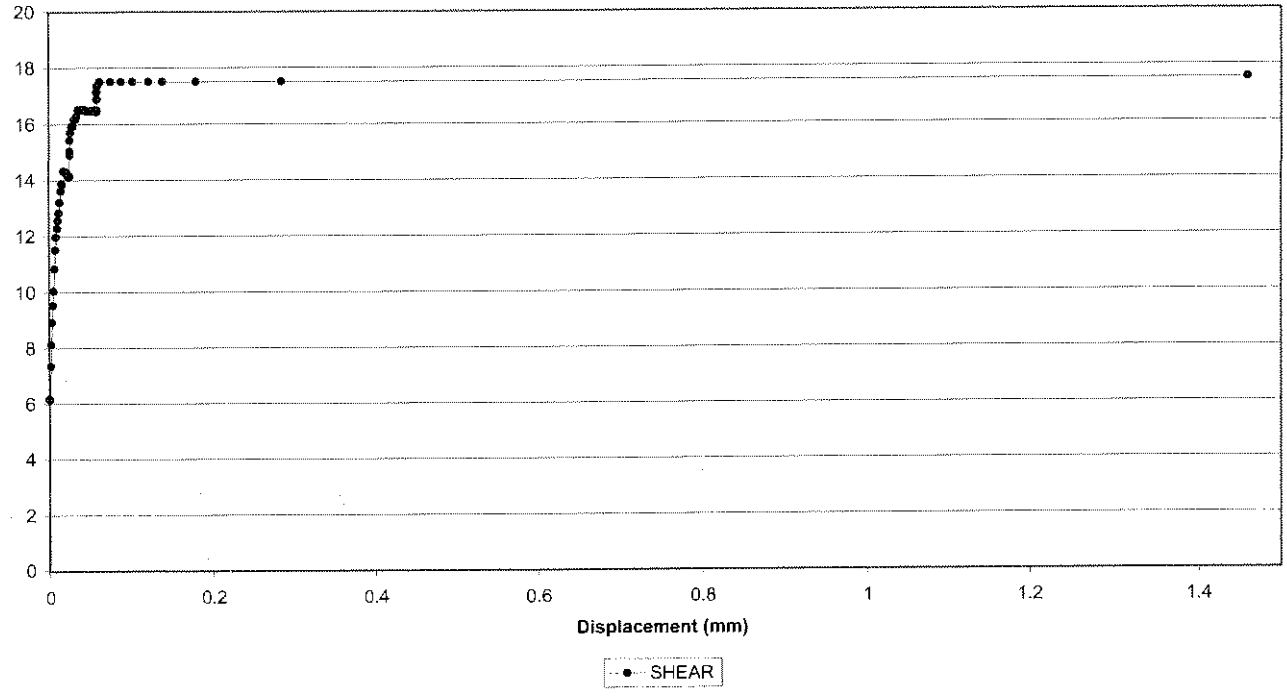

Creep Shear 2056-239
Natural gouge (dry, < 0.5mm, 0.5mm)

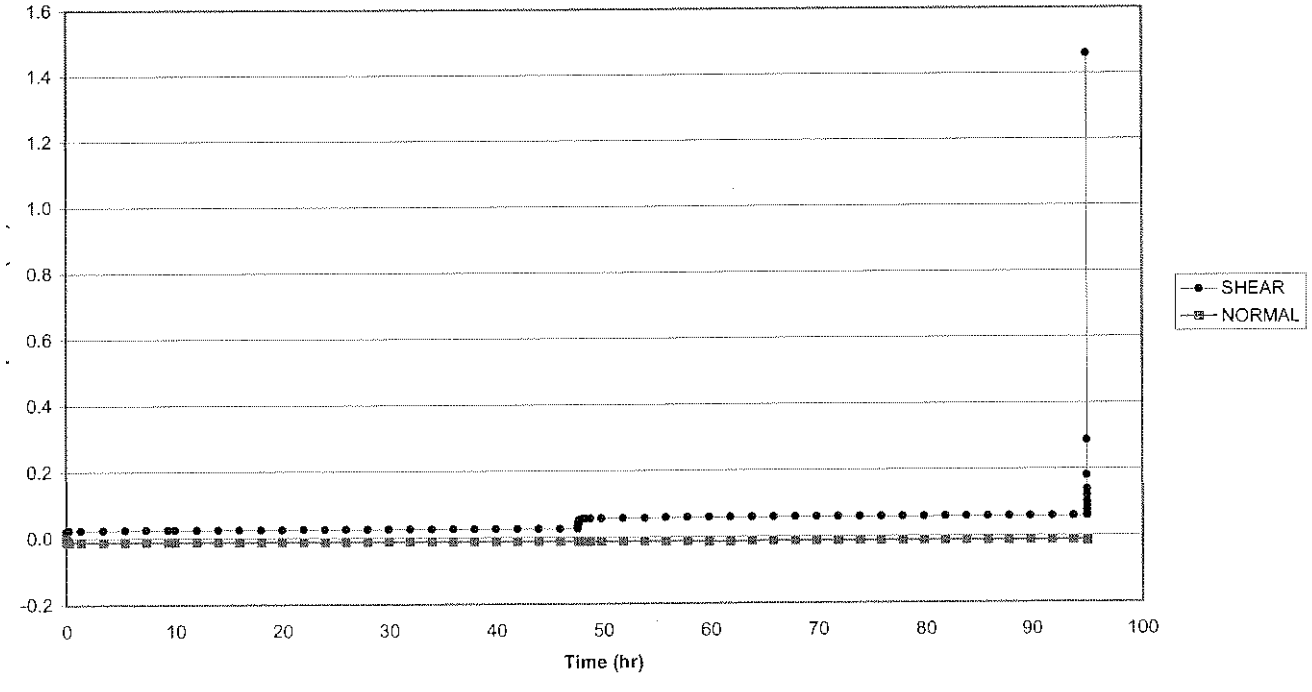

Creep Shear 2056-239, Cycle 1
Natural gouge (dry, < 0.5mm, 0.5mm)

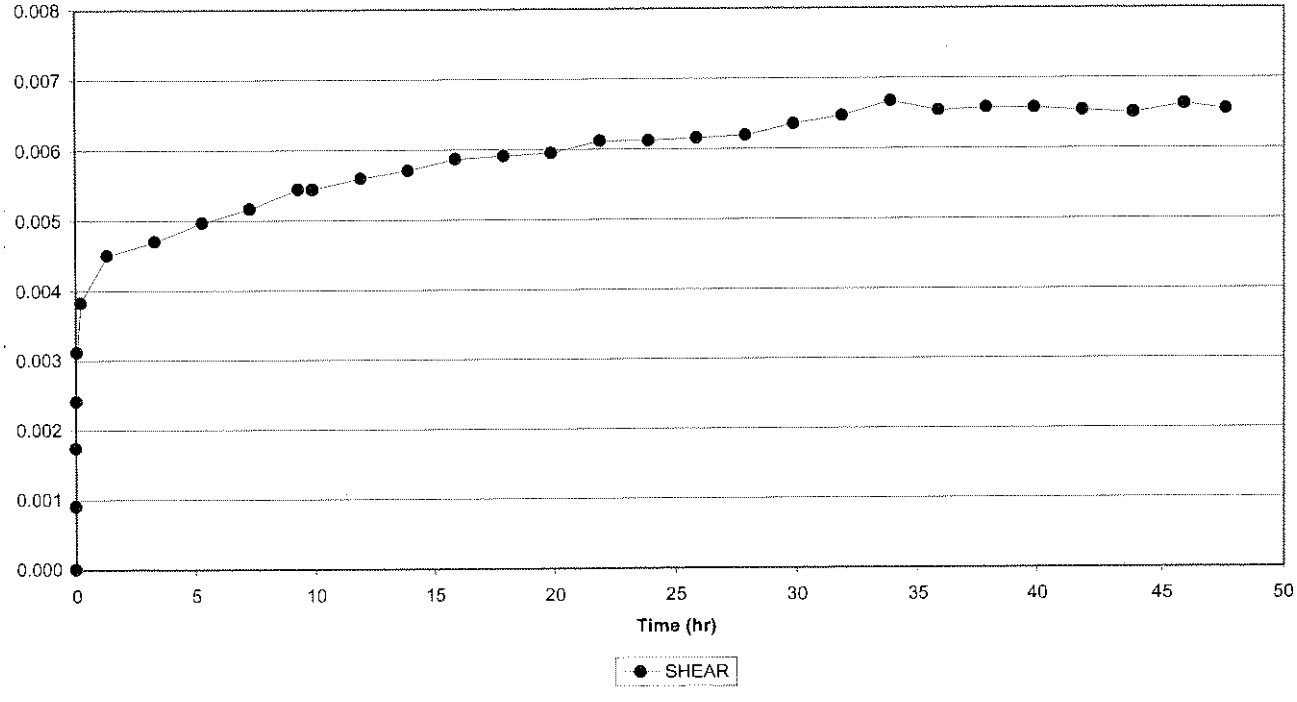

Creep Shear 2056-239, Cycle 2
Natural gouge (dry, < 0.5mm, 0.5mm)

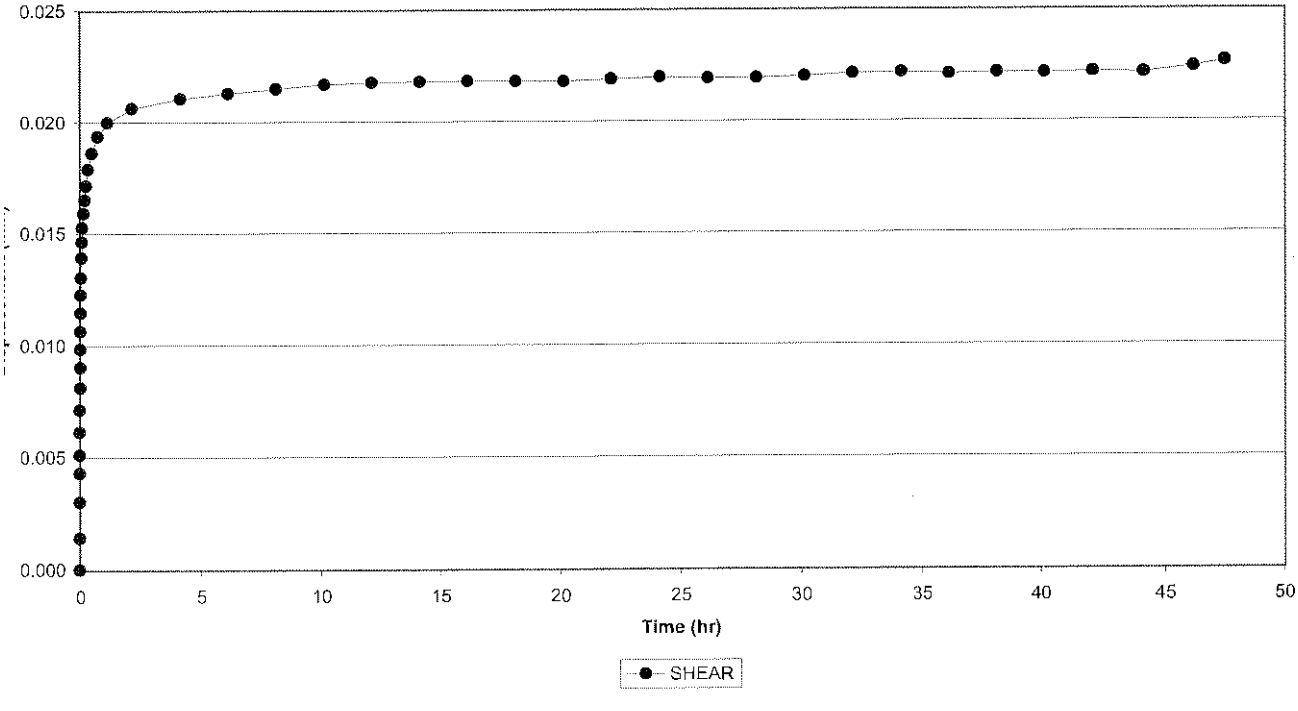

Creep Shear 2056-239, Cycle 3
Natural gouge (dry, < 0.5mm, 0.5mm)

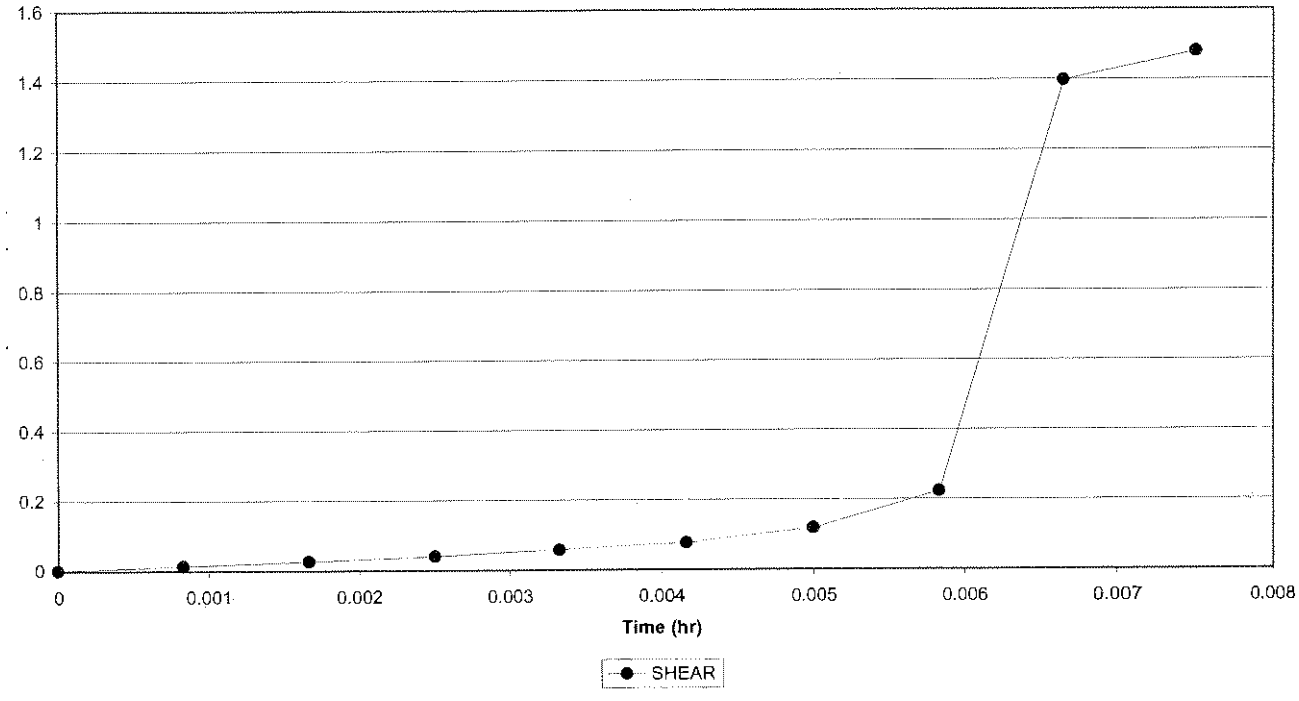

Creep Shear 2056-239
Natural gouge (dry, < 0.5mm, 0.5mm)

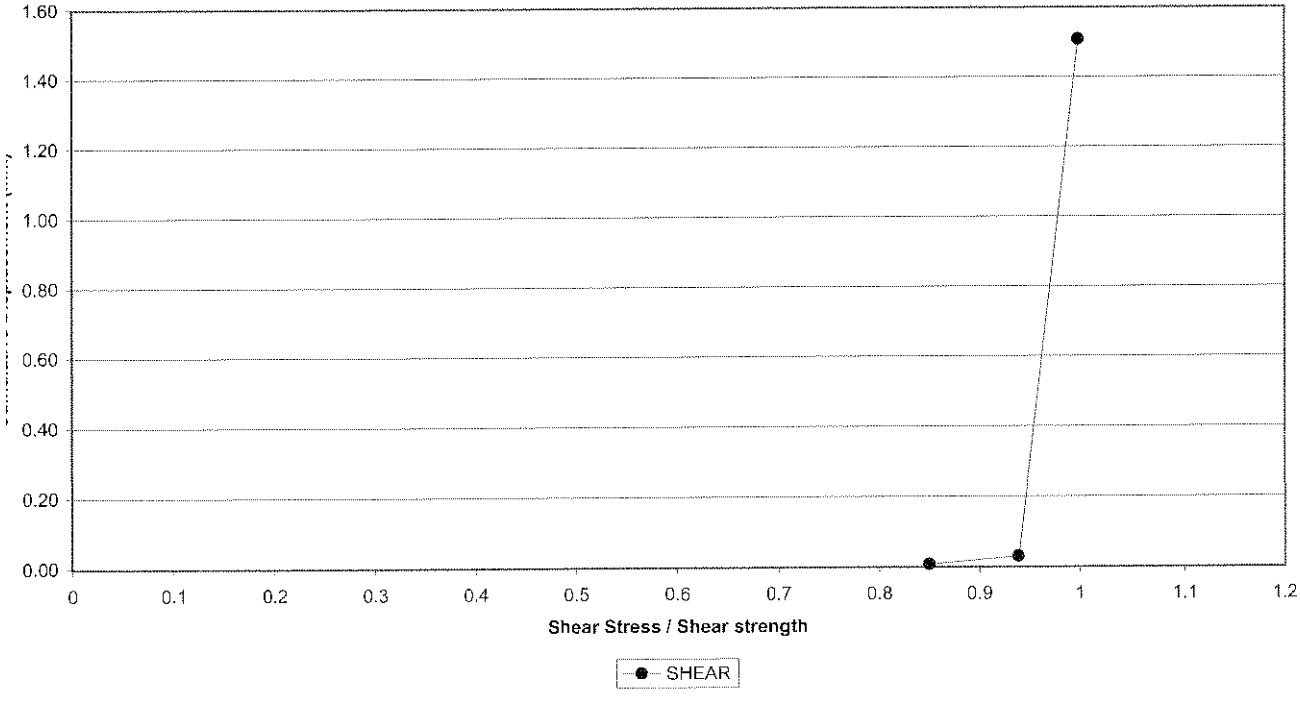

Creep Shear 2056-239
Natural gouge (dry, < 0.5mm, 0.5mm)

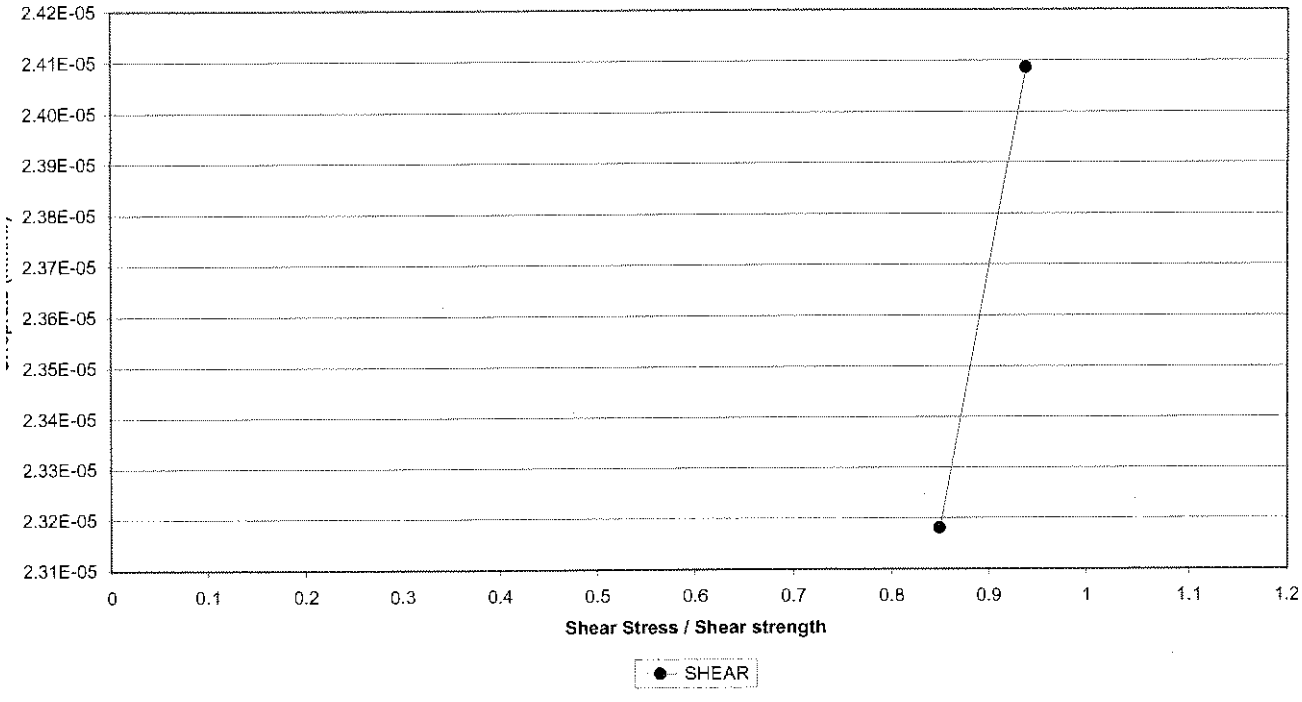

Creep Shear 2056-239
Natural gouge (dry, < 0.5mm, 0.5mm)

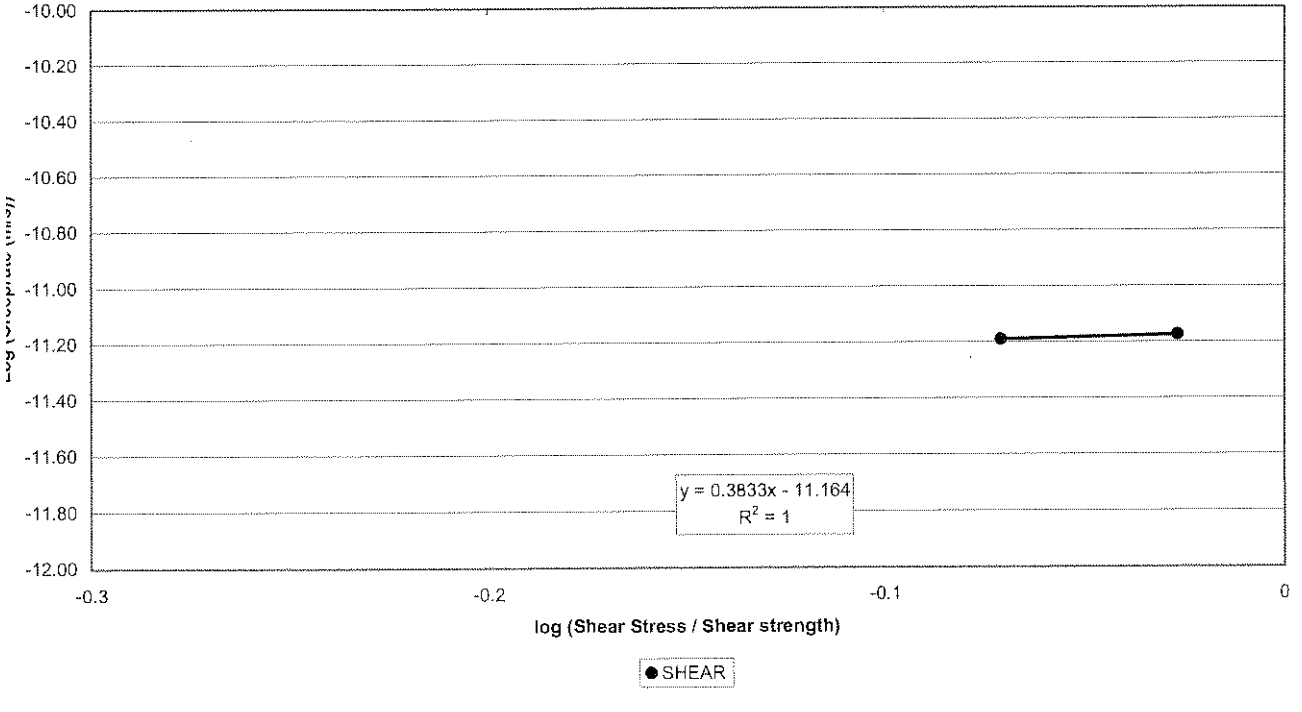

Creep Shear 2056-238
Natural gouge (dry, < 0.5mm, 1mm)

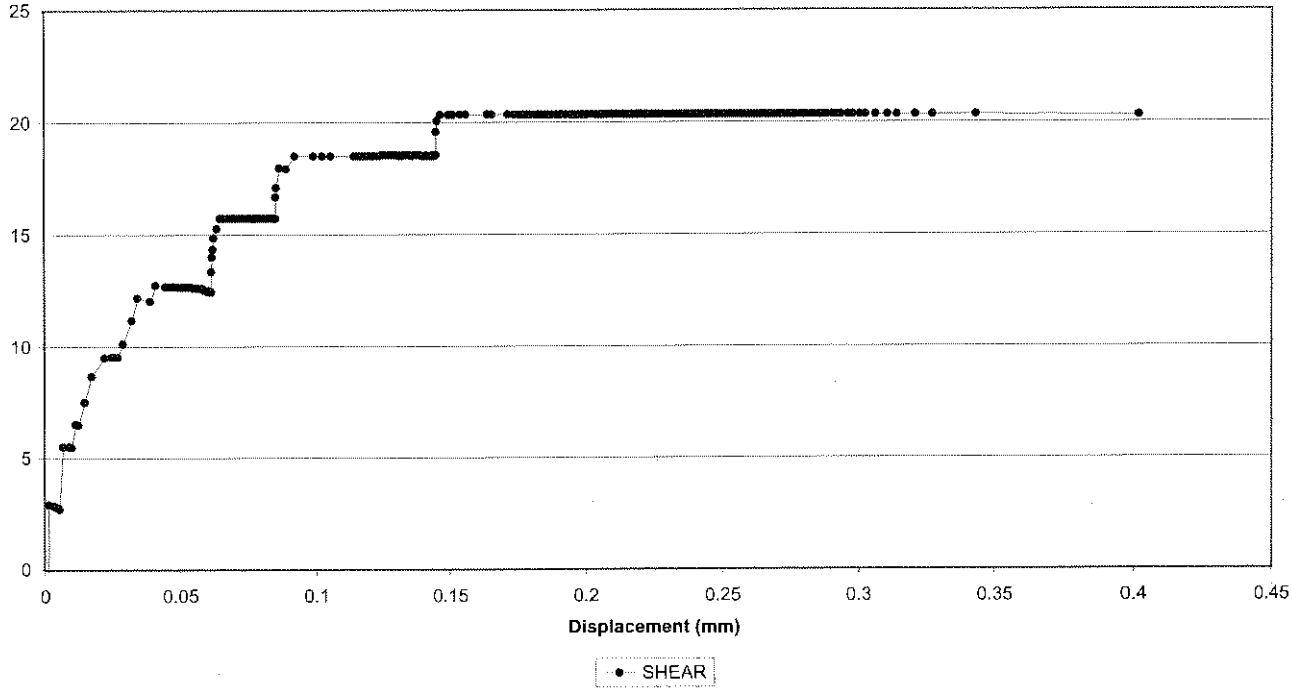

Creep Shear 2056-238
Natural gouge (dry, < 0.5mm, 1mm)

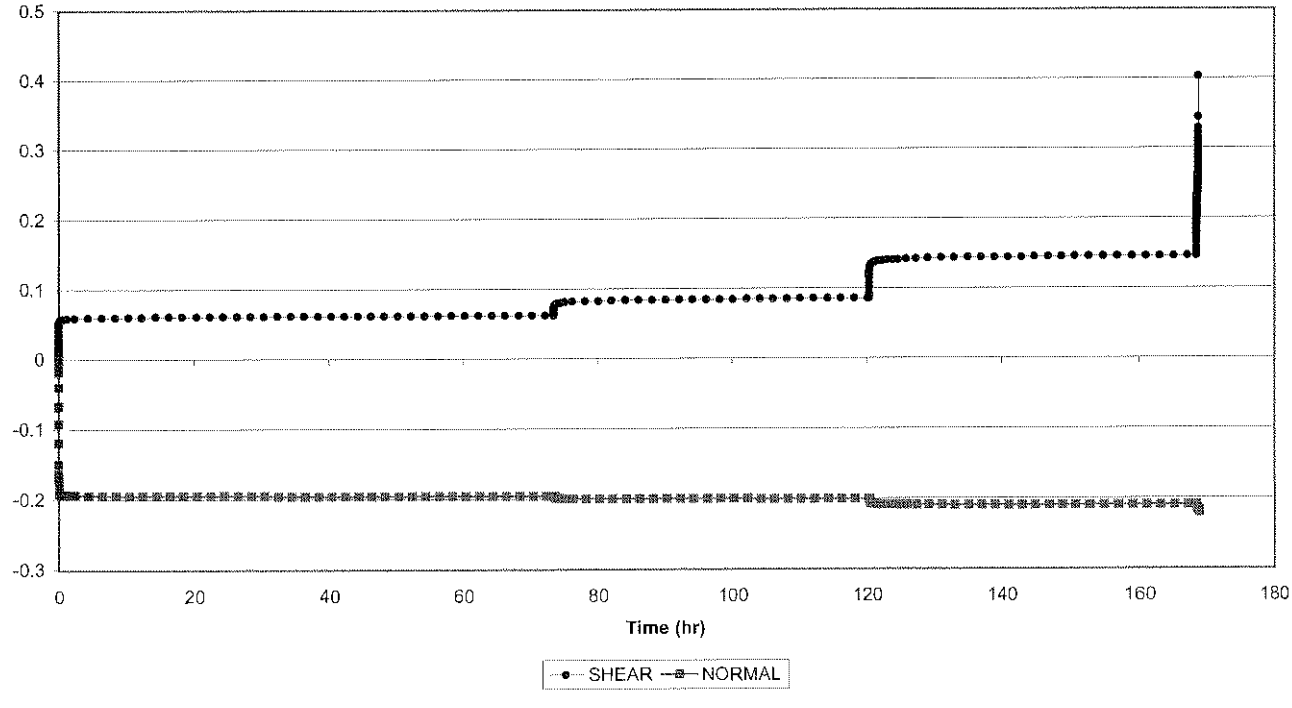

Creep Shear 2056-238, Cycle 1
Natural gouge (dry, < 0.5mm, 1mm)

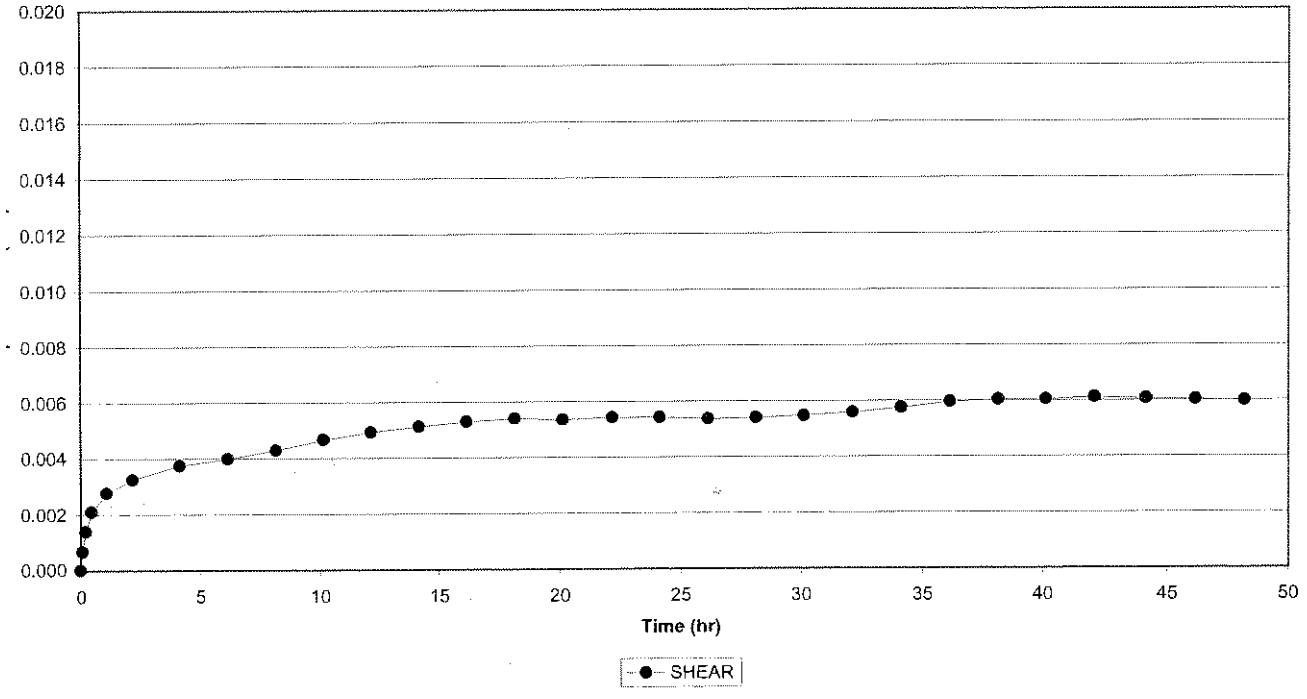

Creep Shear 2056-238, Cycle 2
Natural gouge (dry, < 0.5mm, 1mm)

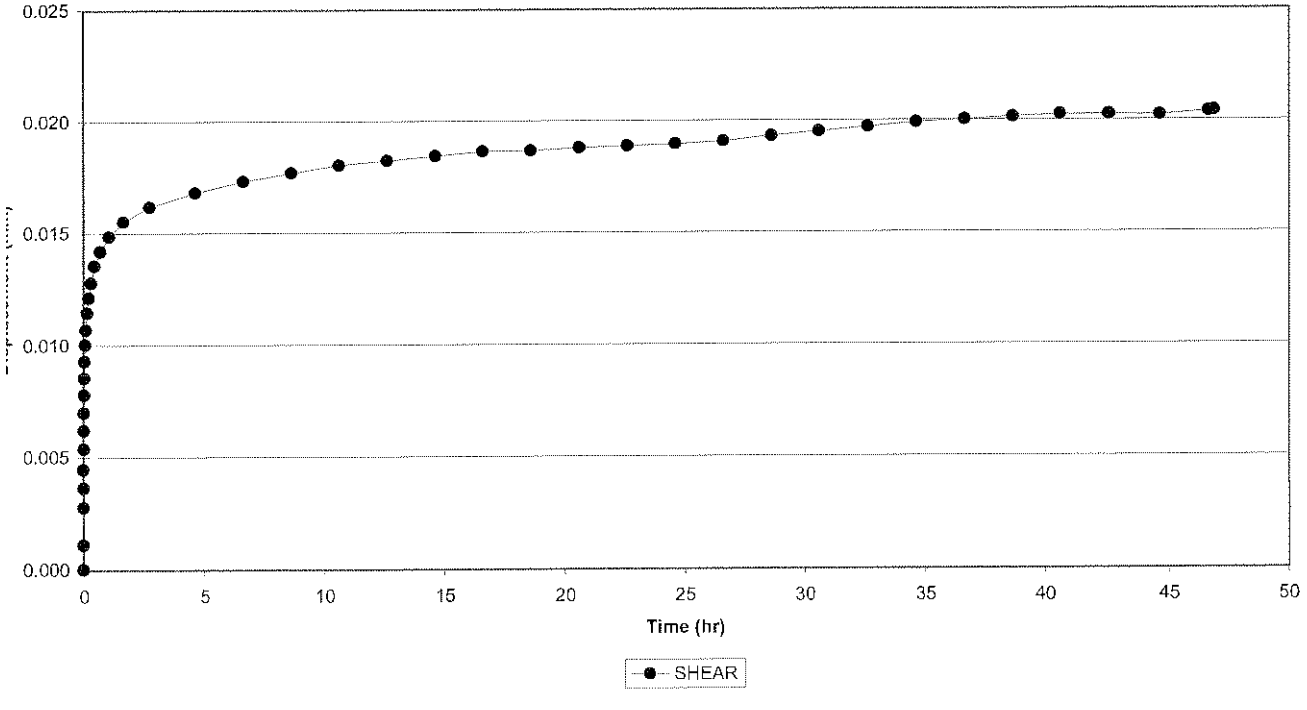

Creep Shear 2056-238, Cycle 3
Natural gouge (dry, < 0.5mm, 1mm)

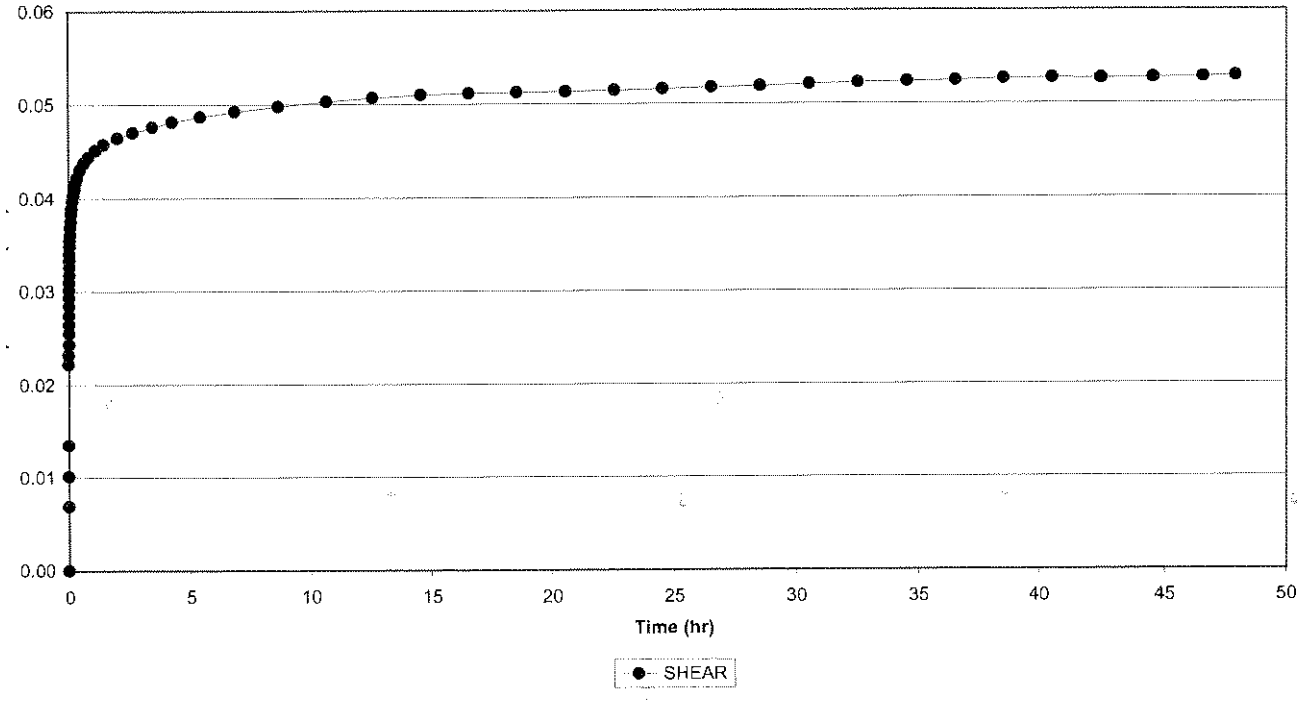

Creep Shear 2056-238, Cycle 4
Natural gouge (dry, < 0.5mm, 1mm)

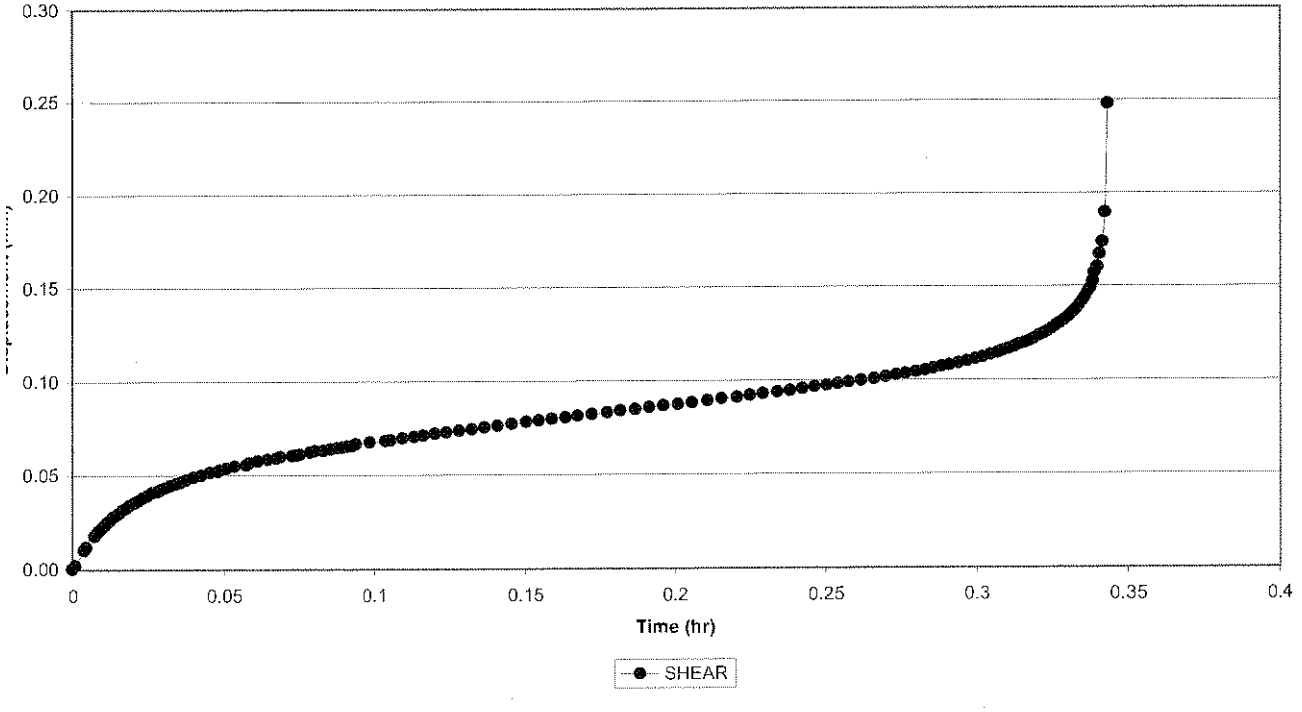

Creep Shear 2056-238
Natural gouge (dry, < 0.5mm, 1mm)

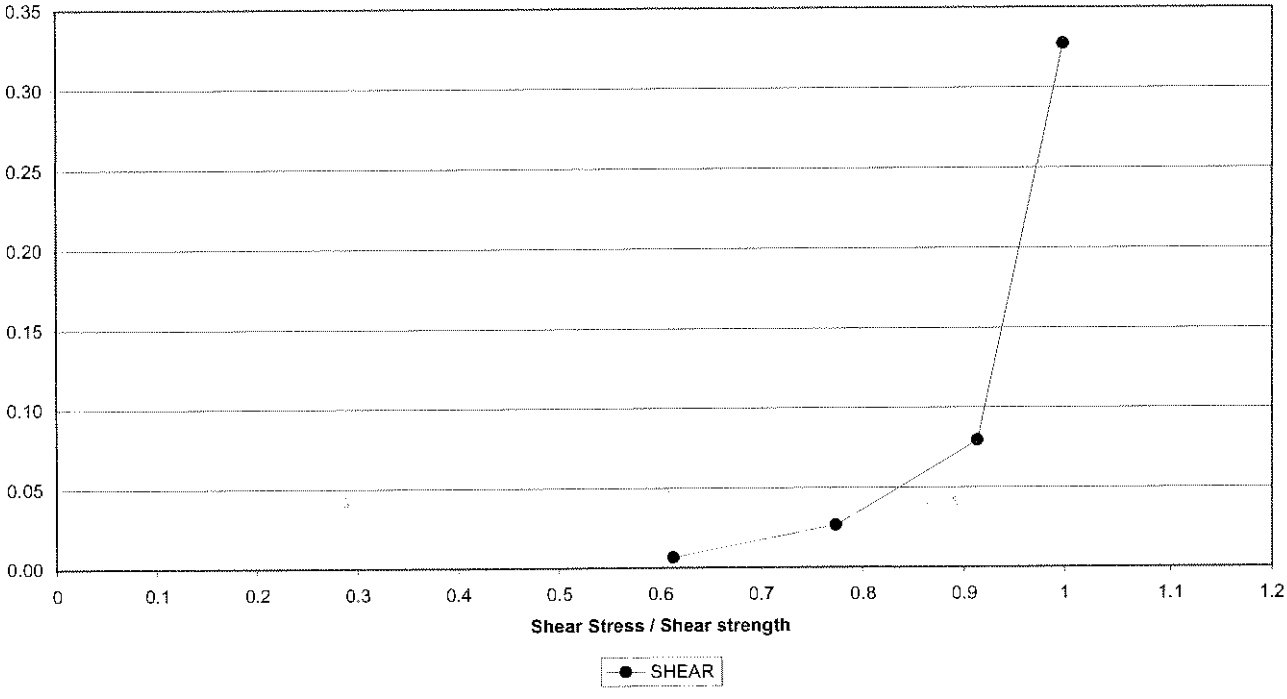

Creep Shear 2056-238
Natural gouge (dry, < 0.5mm, 1mm)

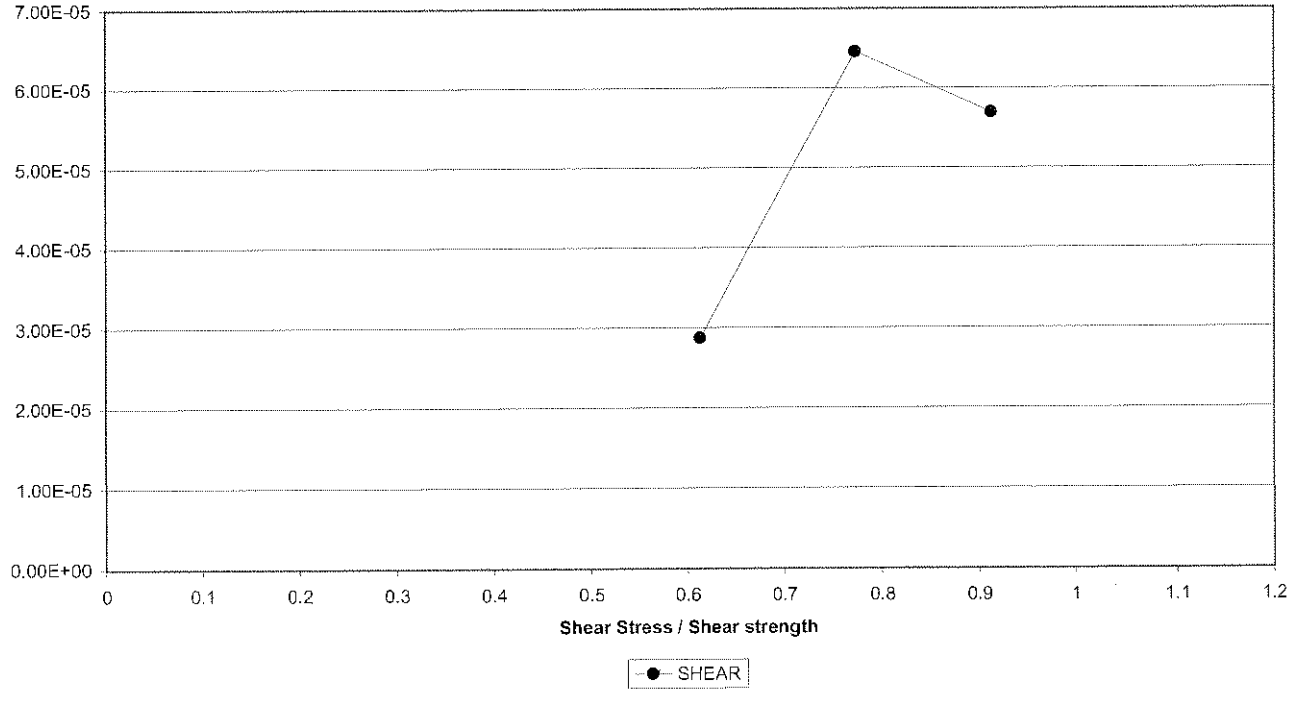

Creep Shear 2056-238
Natural gouge (dry, < 0.5mm, 1mm)

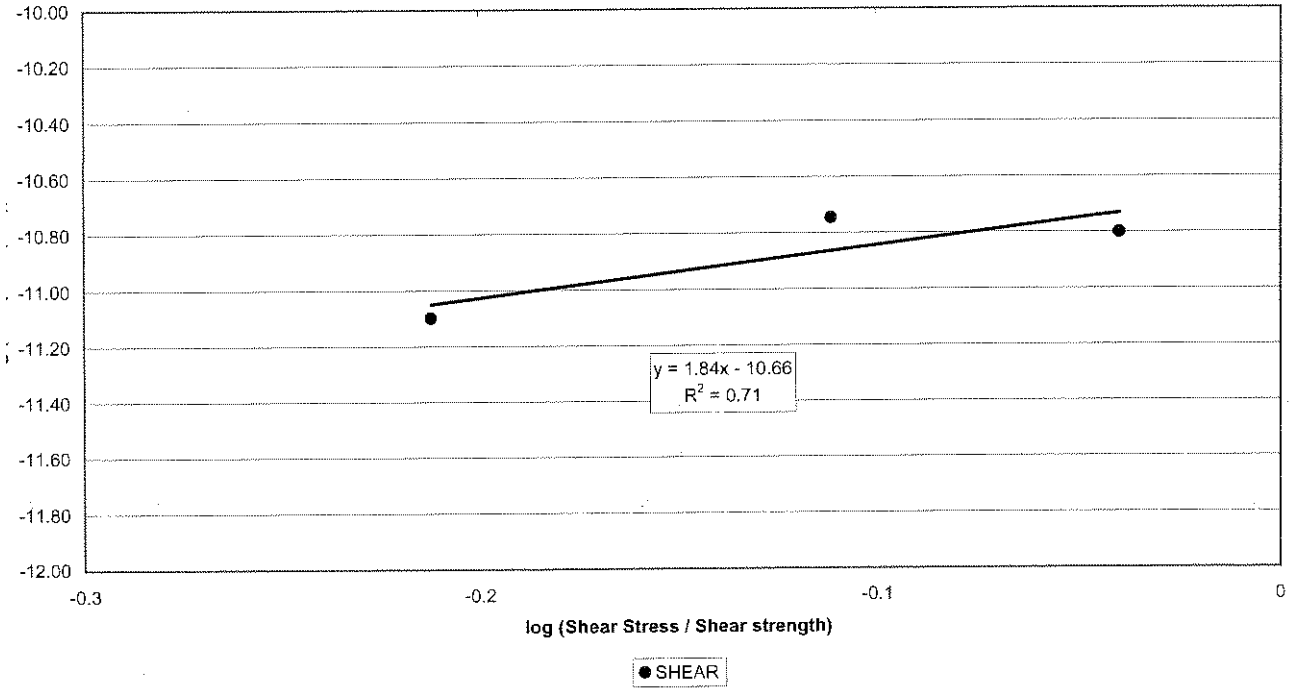

Creep Shear 2056-240
Natural gouge (dry, < 0.5mm, 2mm)

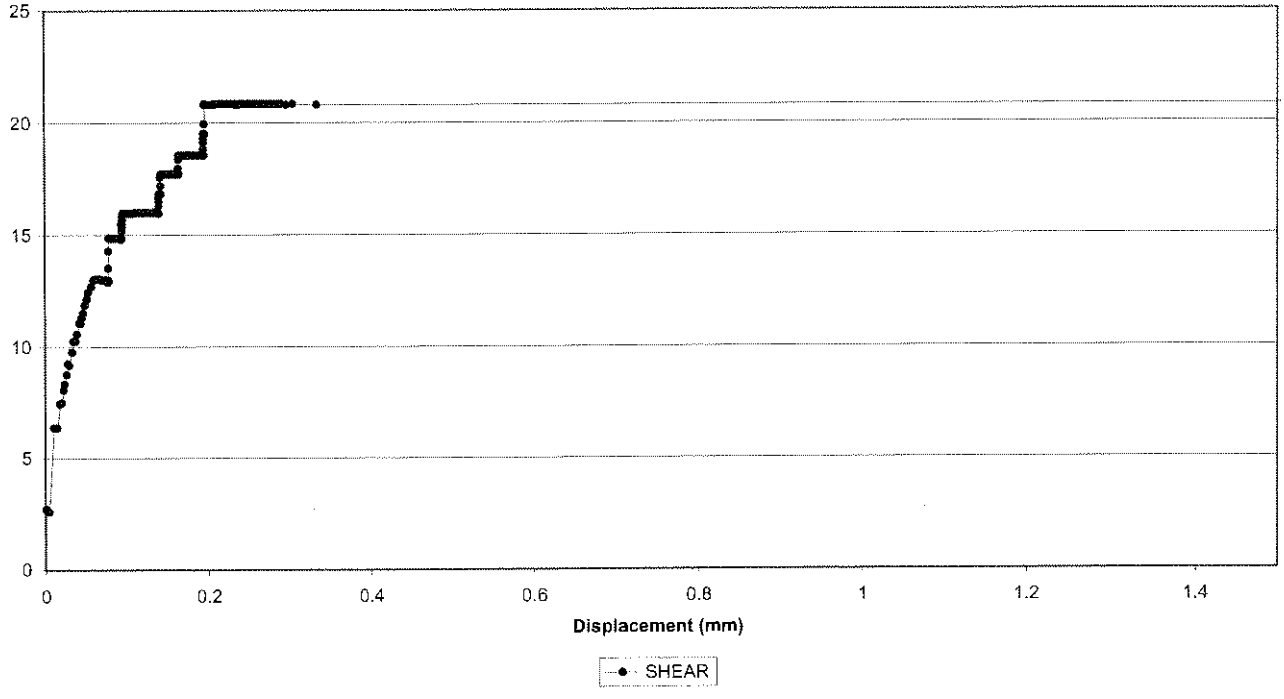

Creep Shear 2056-240
Natural gouge (dry, < 0.5mm, 2mm)

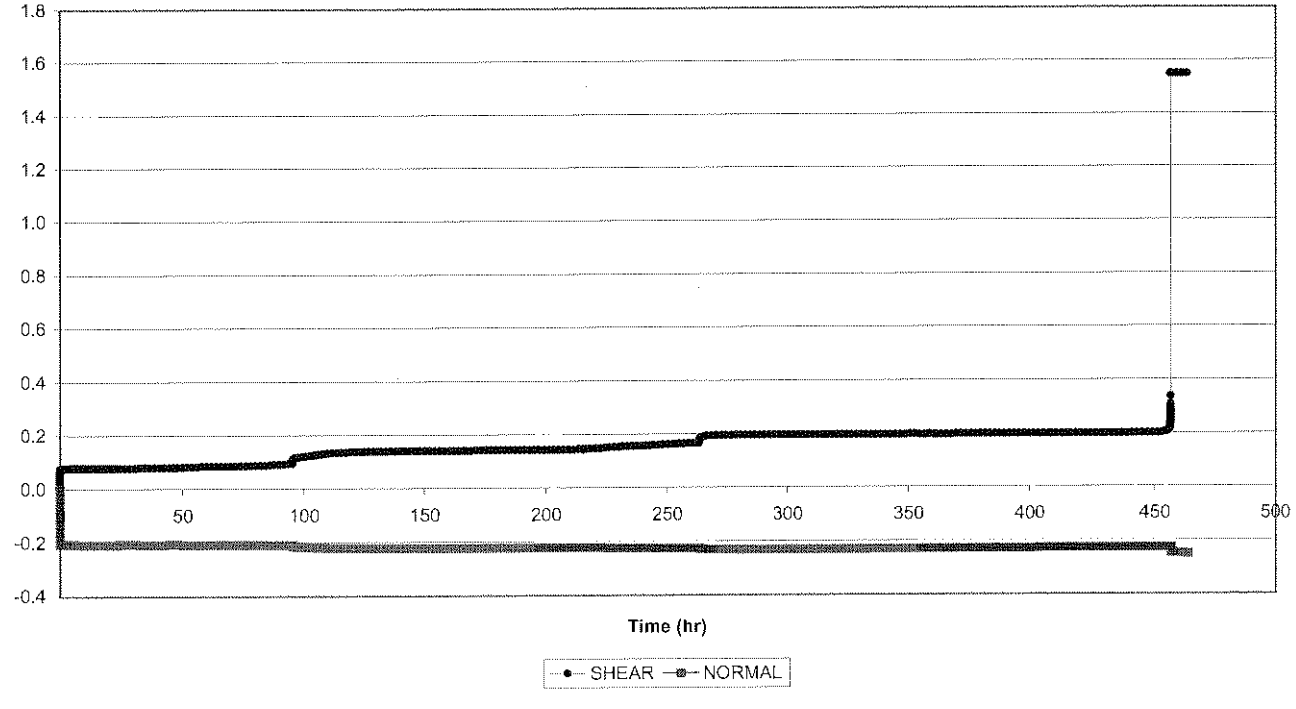

Creep Shear 2056-240, Cycle 1
Natural gouge (dry, < 0.5mm, 2mm)

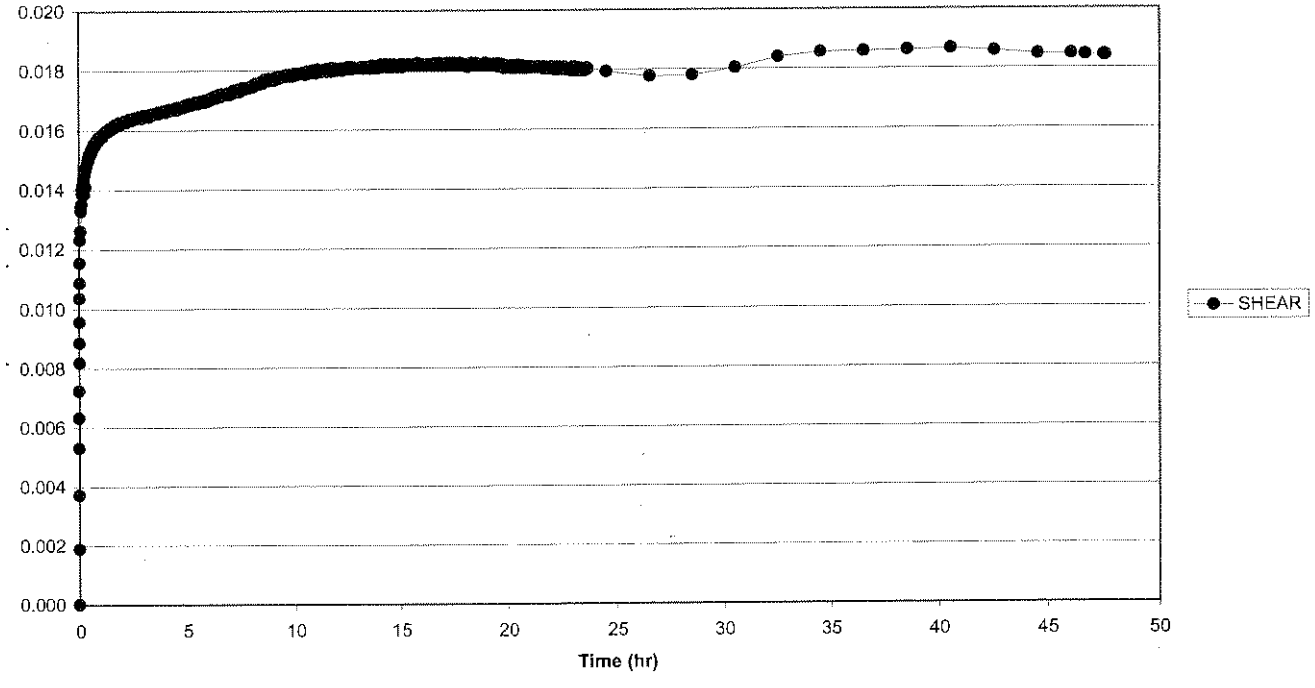

Creep Shear 2056-240, Cycle 2
Natural gouge (dry, < 0.5mm, 2mm)

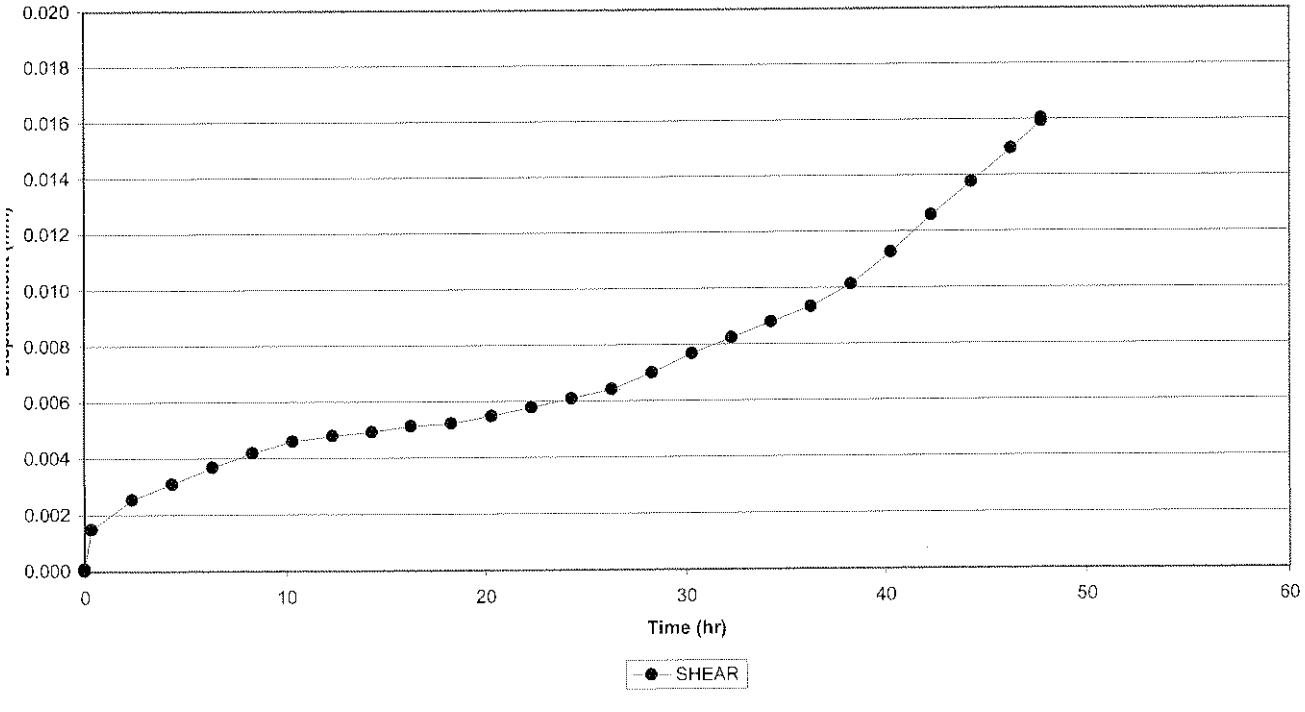

Creep Shear 2056-240, Cycle 3
Natural gouge (dry, < 0.5mm, 2mm)

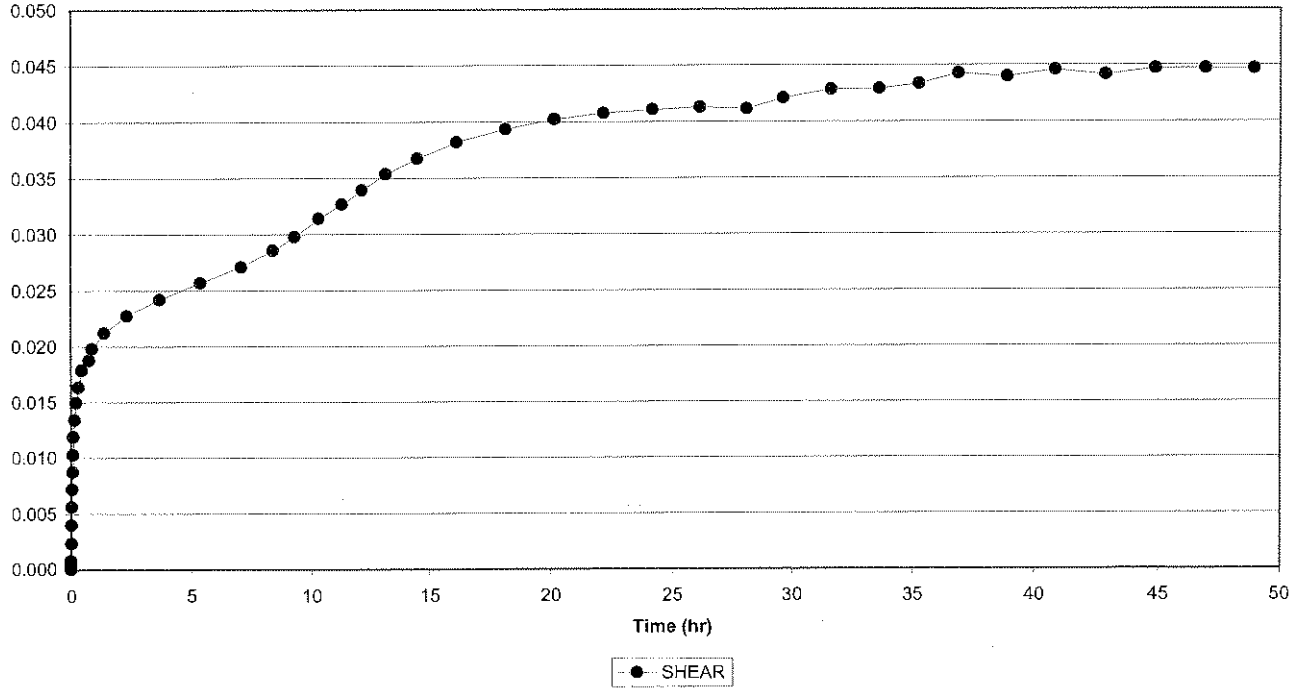

Creep Shear 2056-240, Cycle 4
Natural gouge (dry, < 0.5mm, 2mm)

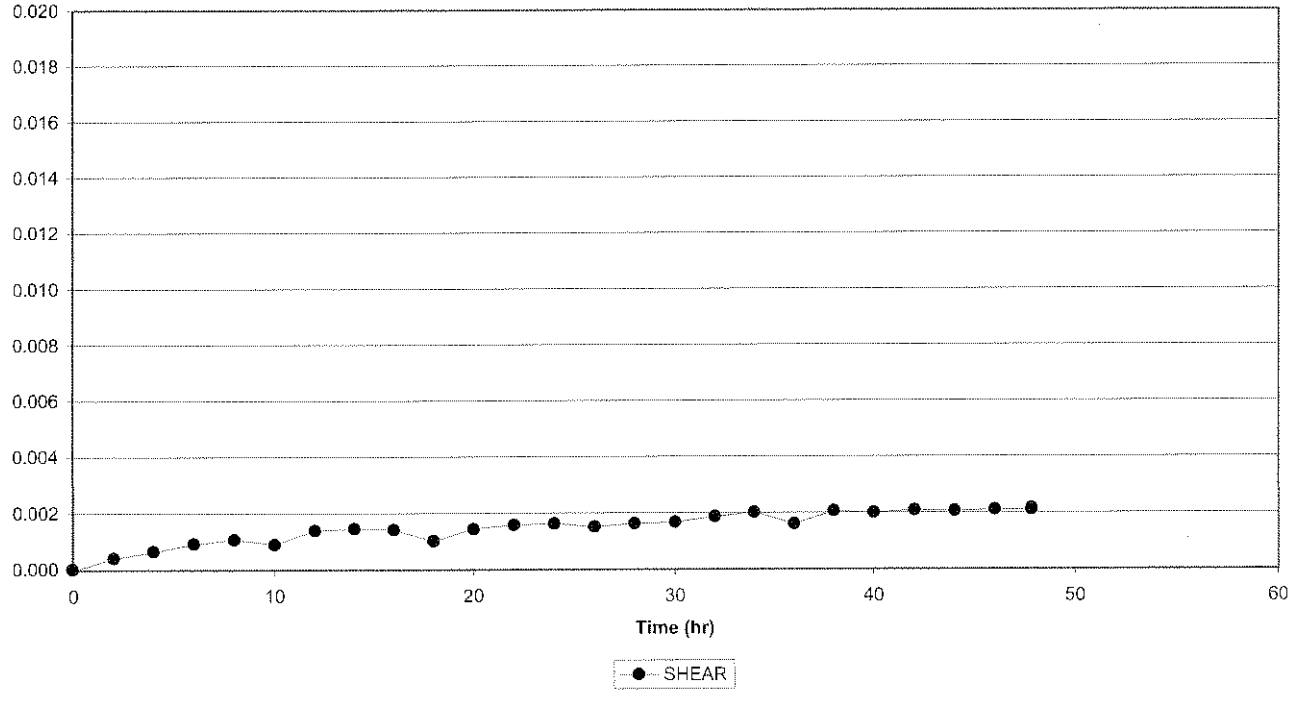

Creep Shear 2056-240, Cycle 5
Natural gouge (dry, < 0.5mm, 2mm)

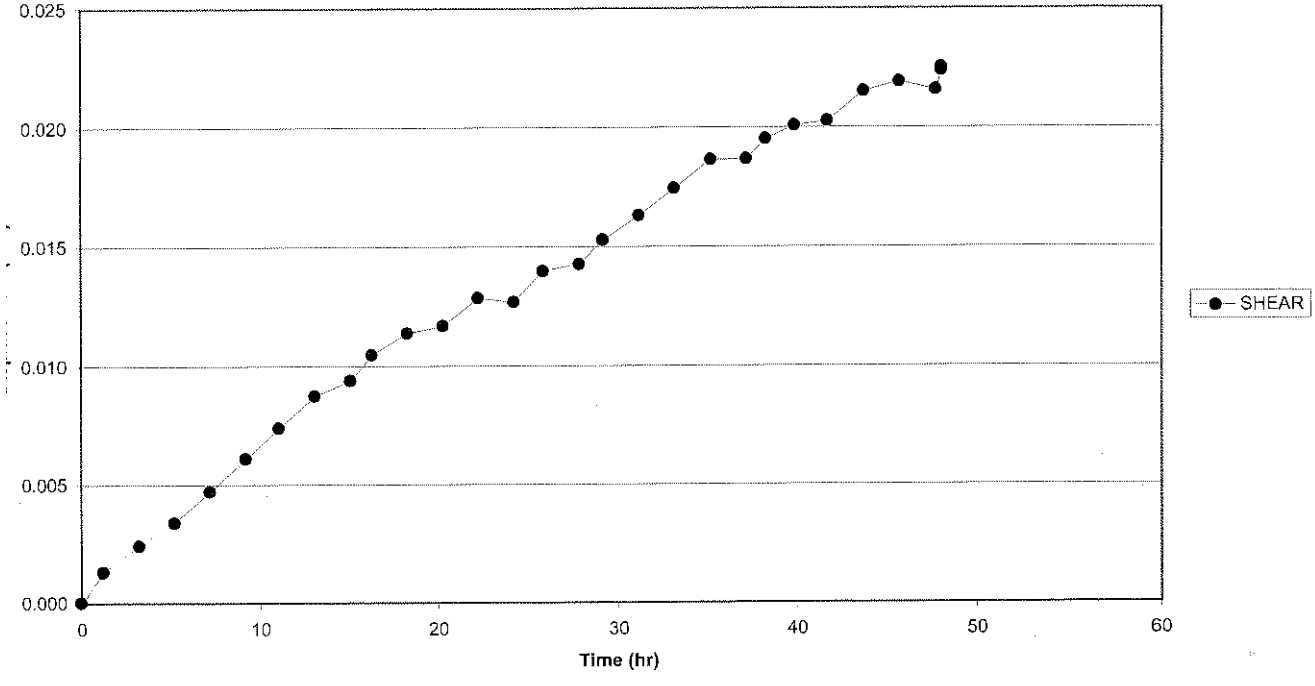

Creep Shear 2056-240, Cycle 6
Natural gouge (dry, < 0.5mm, 2mm)

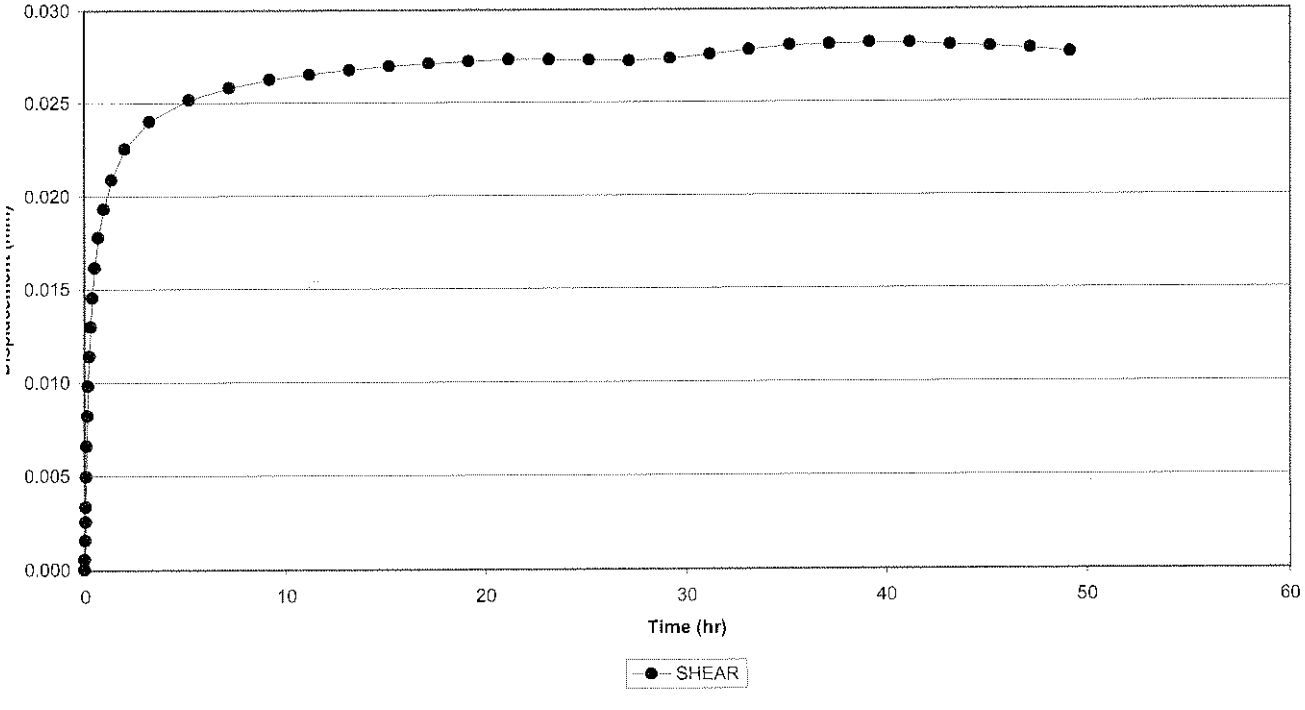

Creep Shear 2056-240, Cycle 7
Natural gouge (dry, < 0.5mm, 2mm)

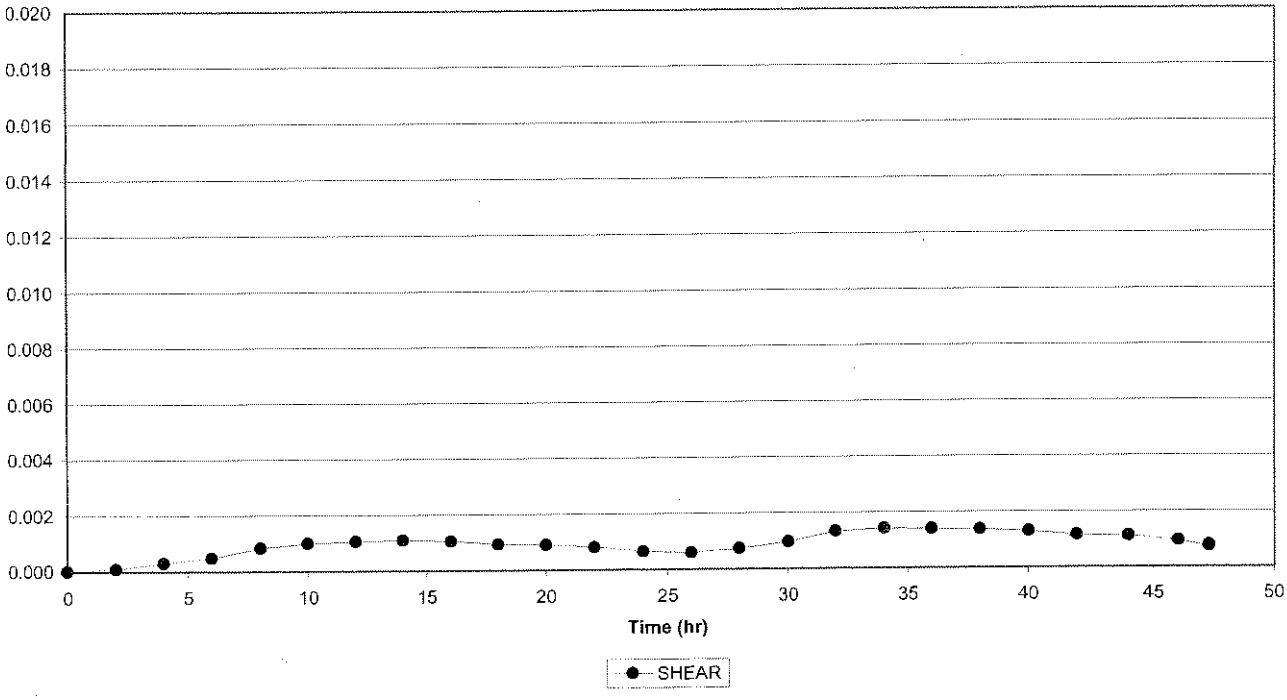

Creep Shear 2056-240, Cycle 7
Natural gouge (dry, < 0.5mm, 2mm)

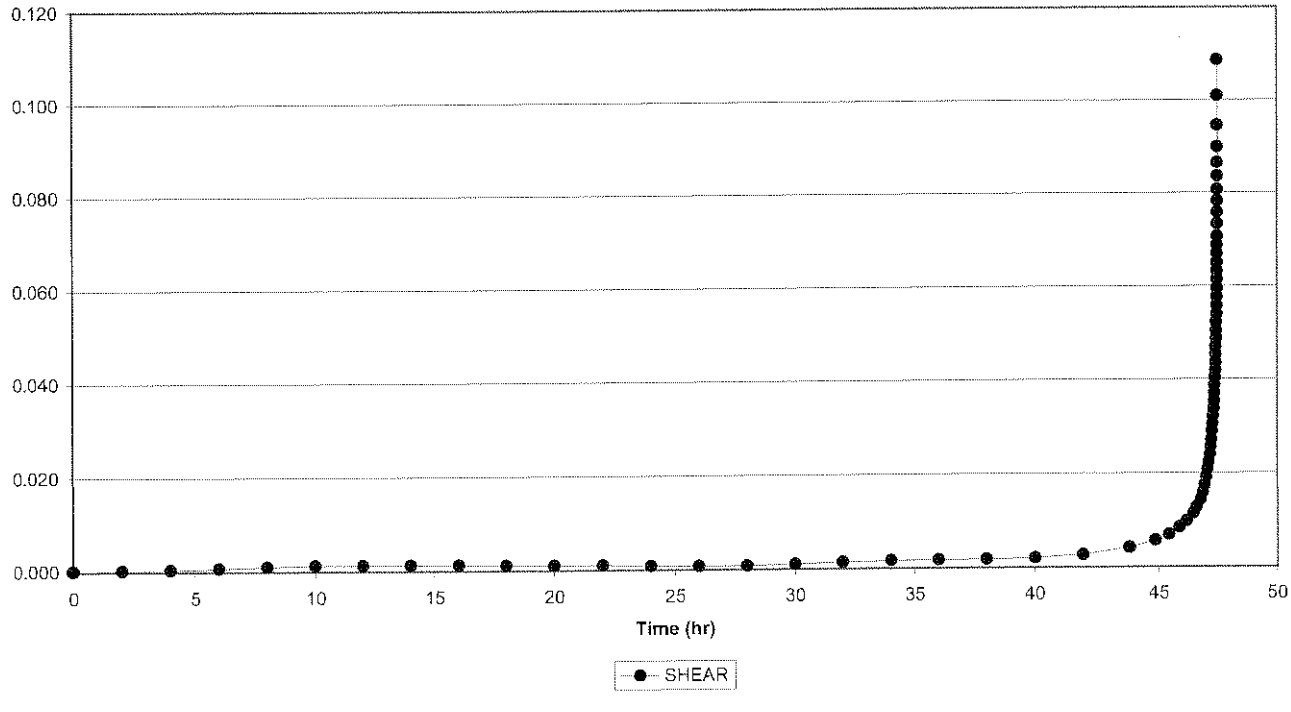

Creep Shear 2056-240
Natural gouge (dry, < 0.5mm, 2mm)

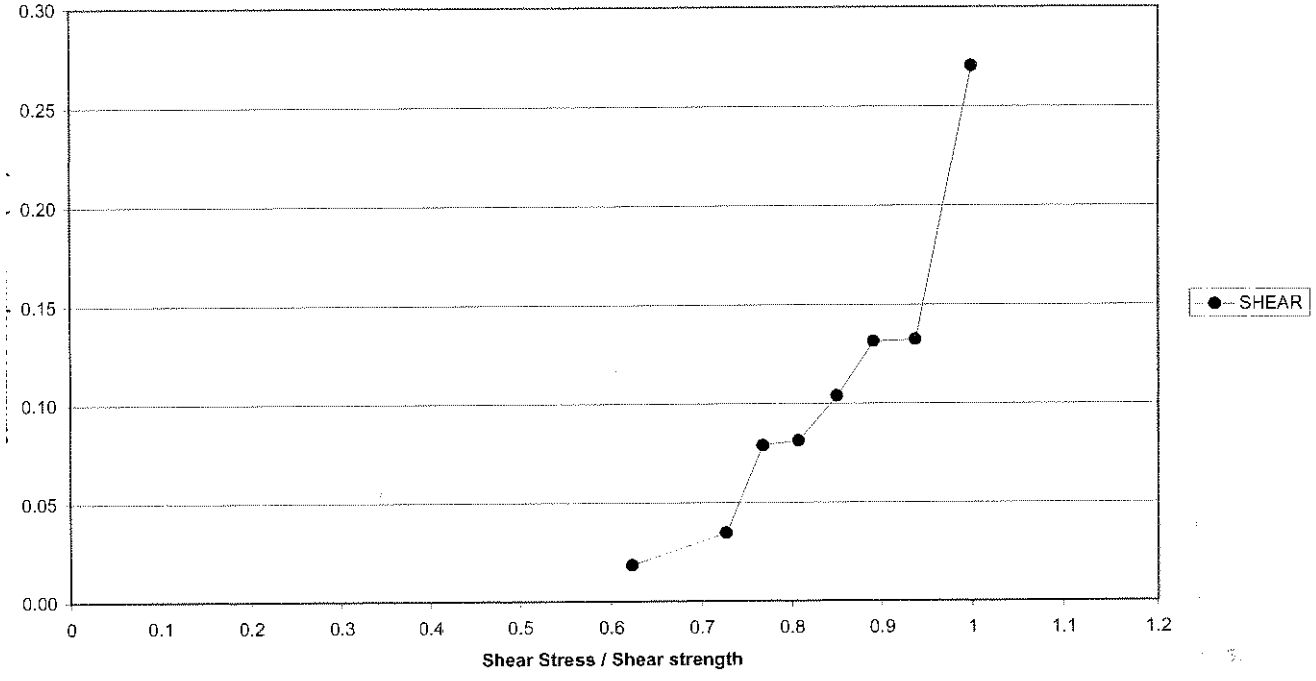

Creep Shear 2056-240
Natural gouge (dry, < 0.5mm, 2mm)

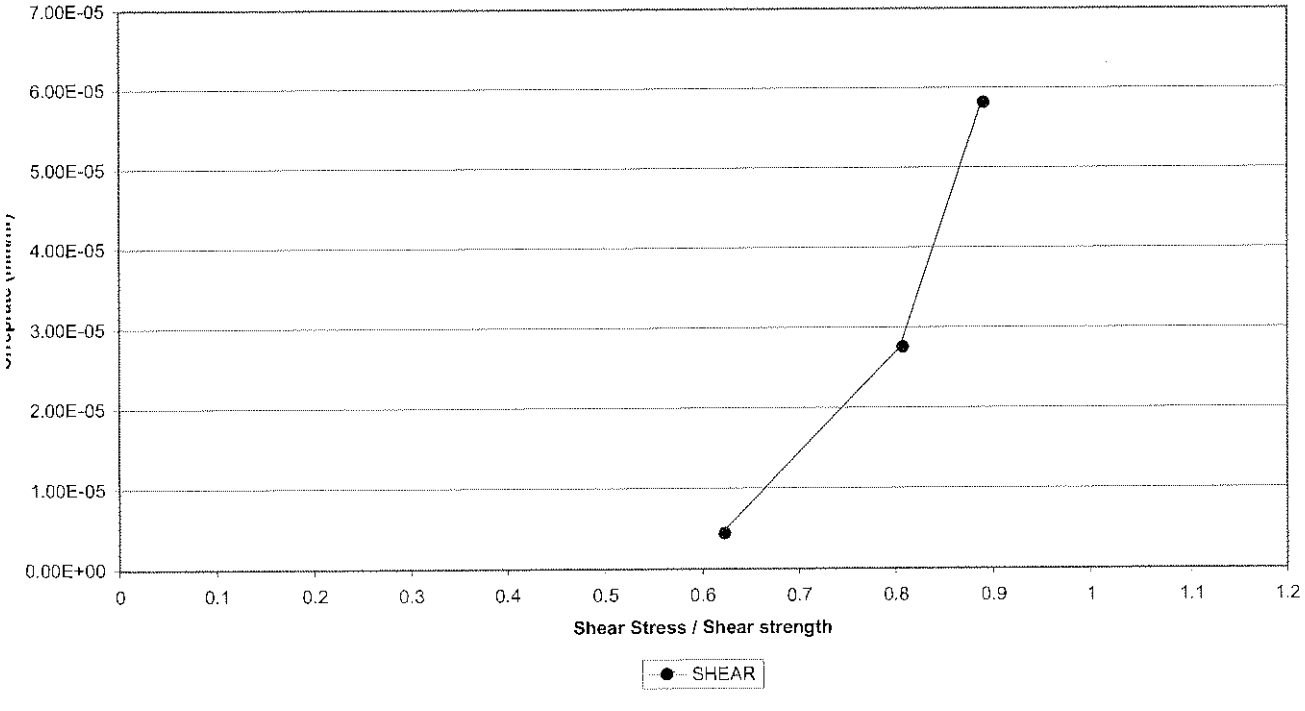

Creep Shear 2056-240
Natural gouge (dry, < 0.5mm, 2mm)

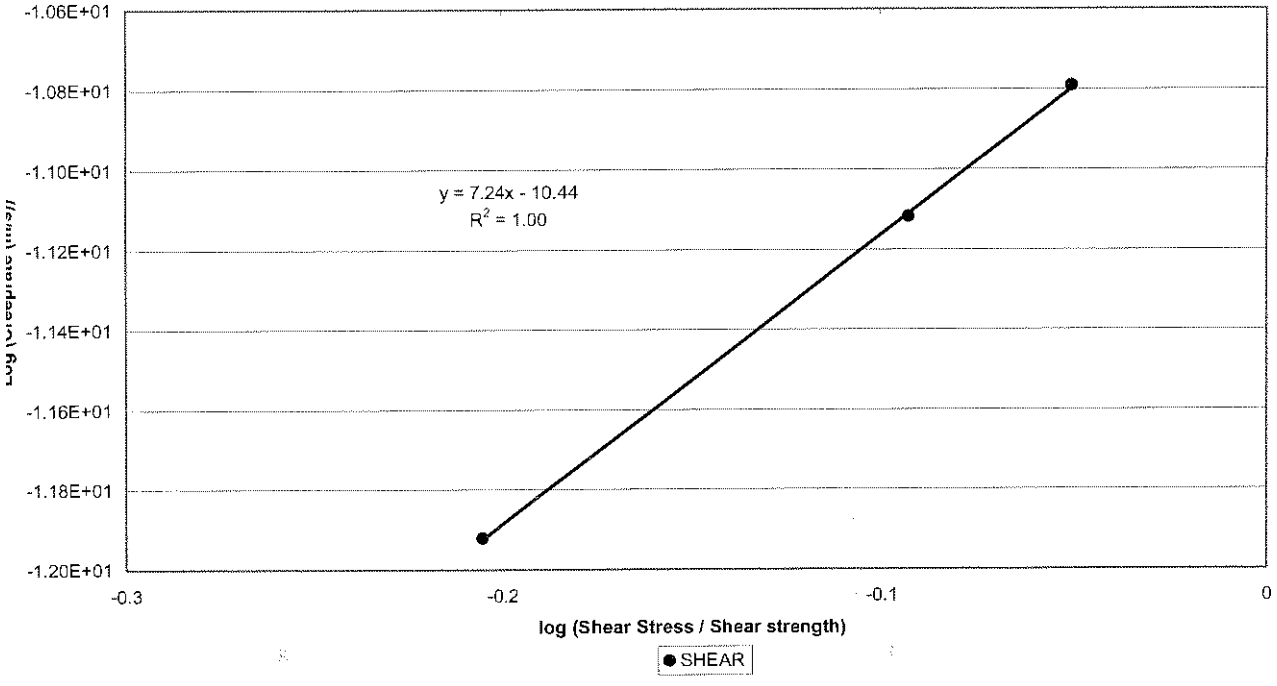

Creep Shear 2056-241
Natural gouge (wet, < 0.5mm, 1mm)

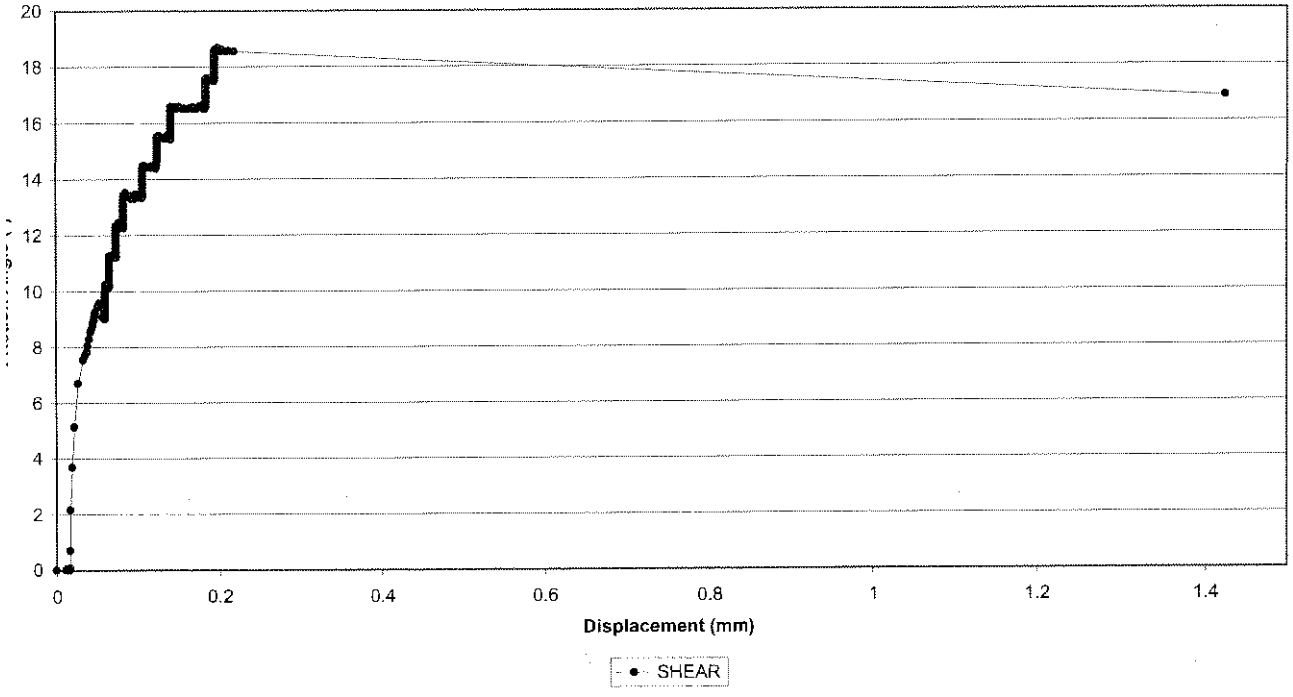

Creep Shear 2056-241
Natural gouge (wet, < 0.5mm, 1mm)

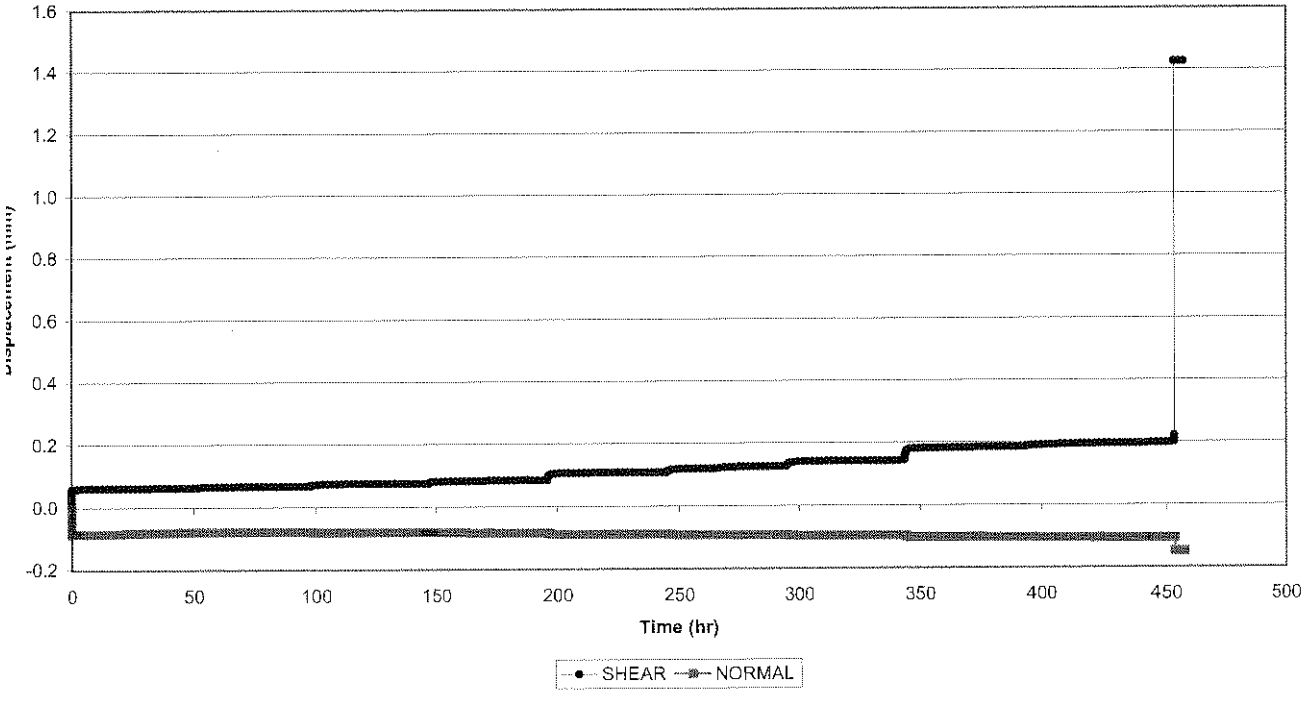

Creep Shear 2056-241, Cycle 1
Natural gouge (wet, < 0.5mm, 1mm)

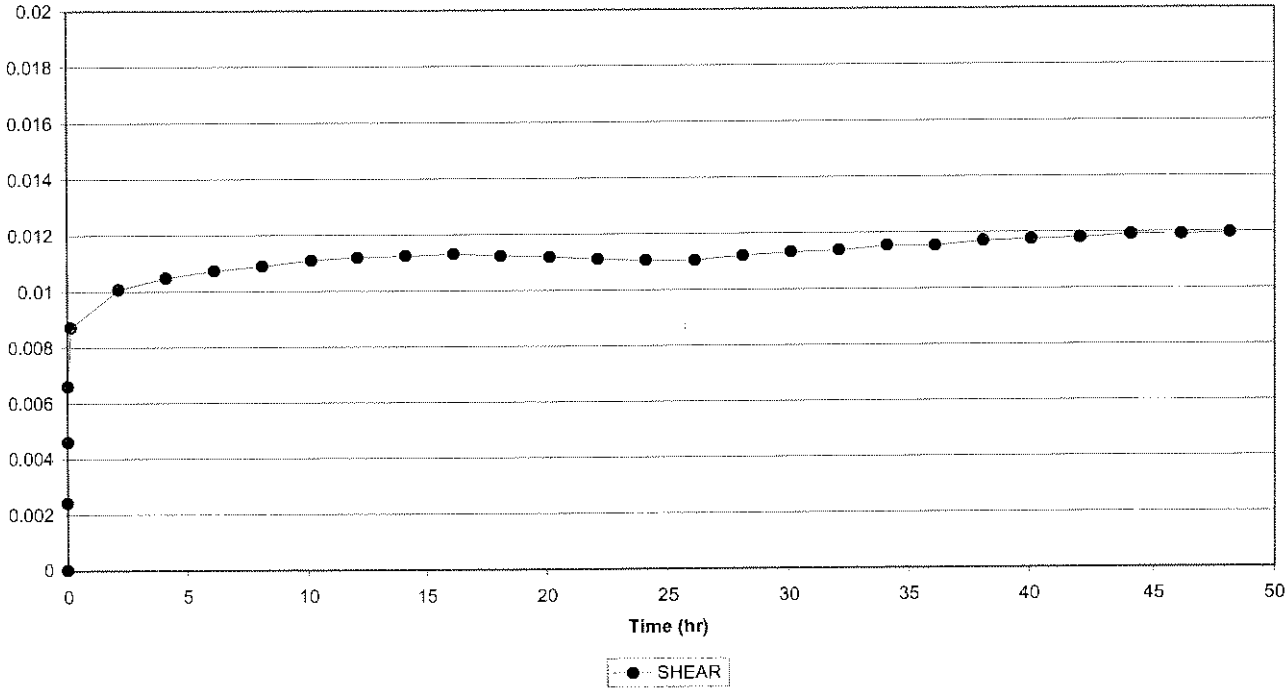

Creep Shear 2056-241, Cycle 2
Natural gouge (wet, < 0.5mm, 1mm)

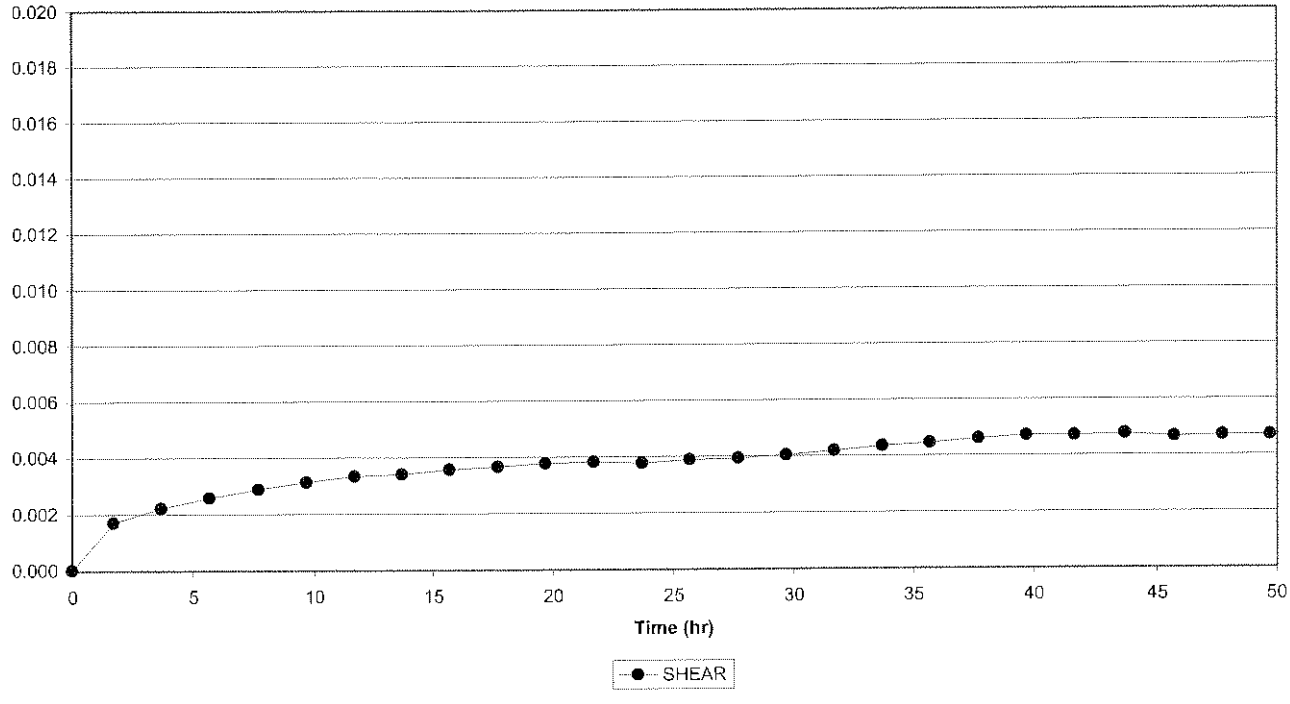

Creep Shear 2056-241, Cycle 3
Natural gouge (wet, < 0.5mm, 1mm)

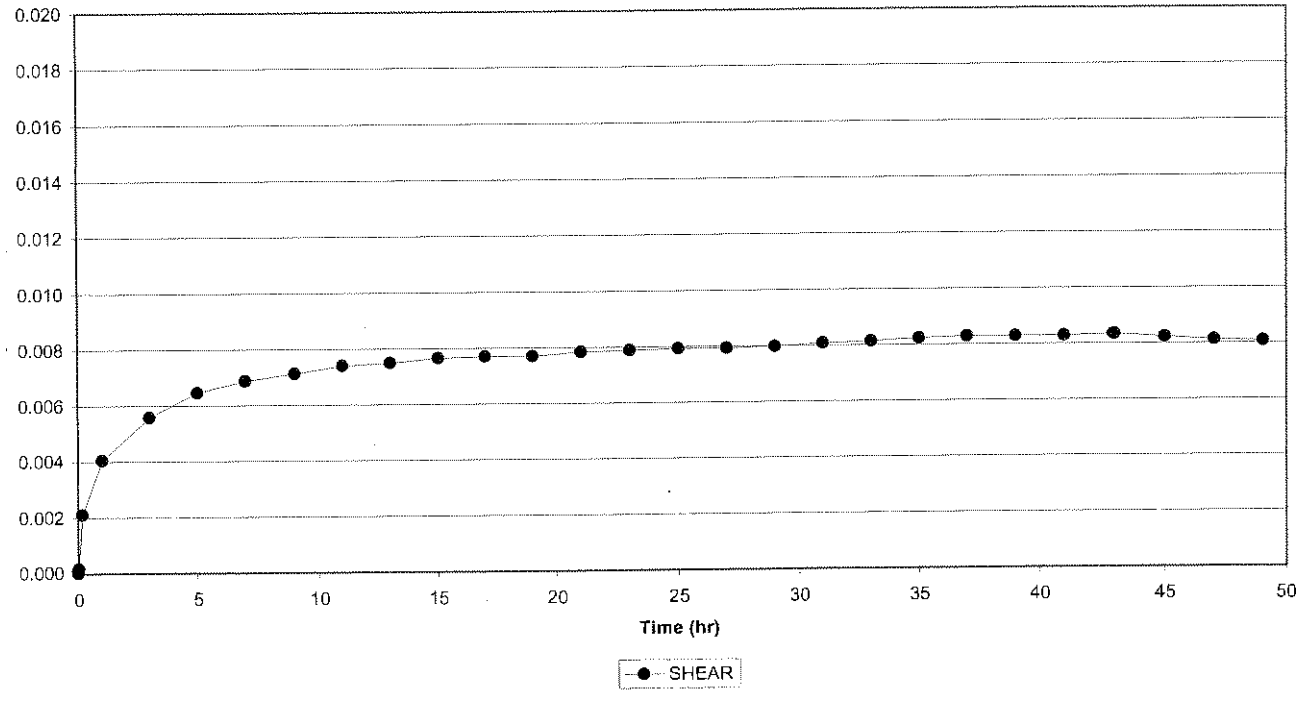

Creep Shear 2056-241, Cycle 4
Natural gouge (wet, < 0.5mm, 1mm)

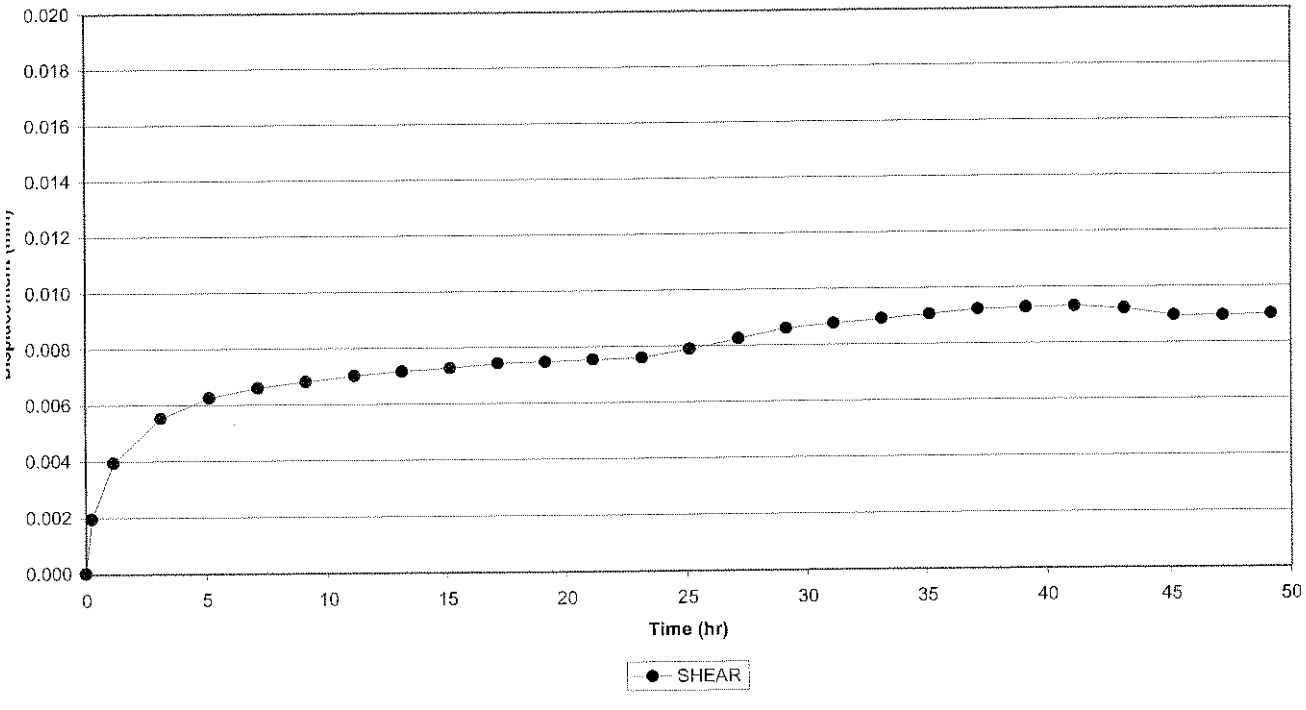

Creep Shear 2056-241, Cycle 5
Natural gouge (wet, < 0.5mm, 1mm)

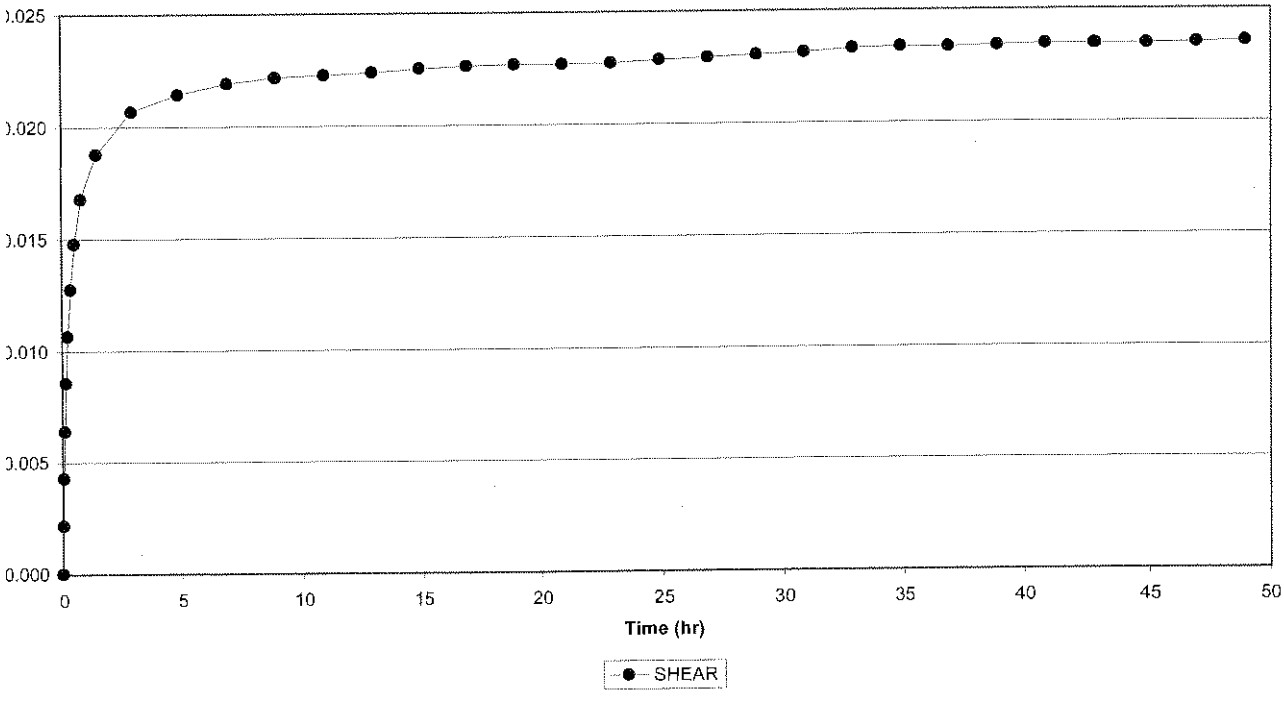

Creep Shear 2056-241, Cycle 6
Natural gouge (wet, < 0.5mm, 1mm)

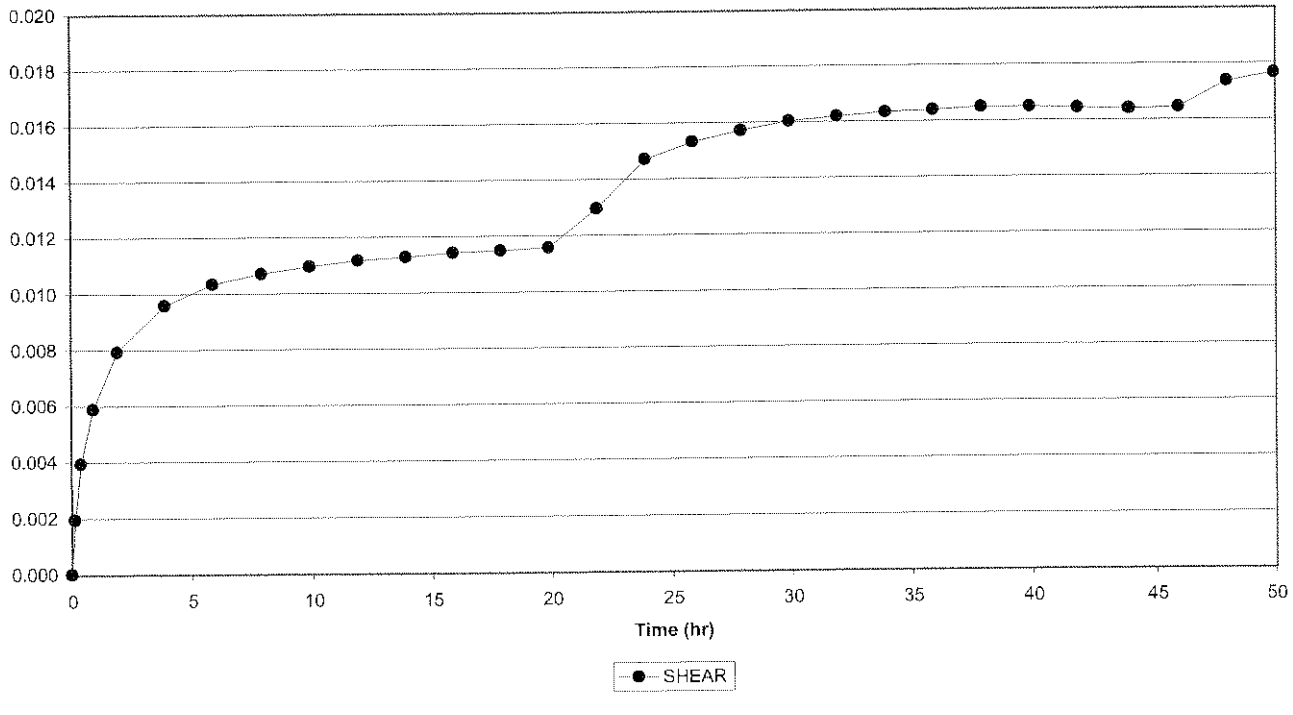

Creep Shear 2056-241, Cycle 7
Natural gouge (wet, < 0.5mm, 1mm)

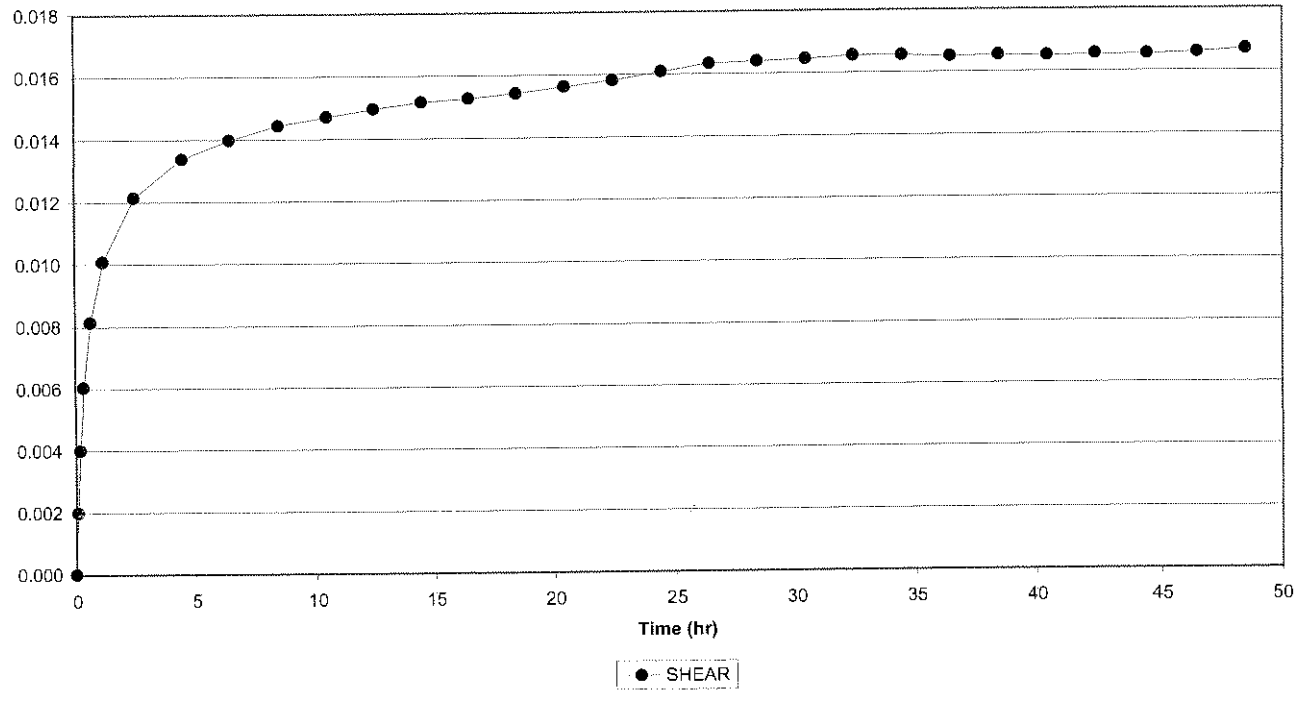

Creep Shear 2056-241, Cycle 8
Natural gouge (wet, < 0.5mm, 1mm)

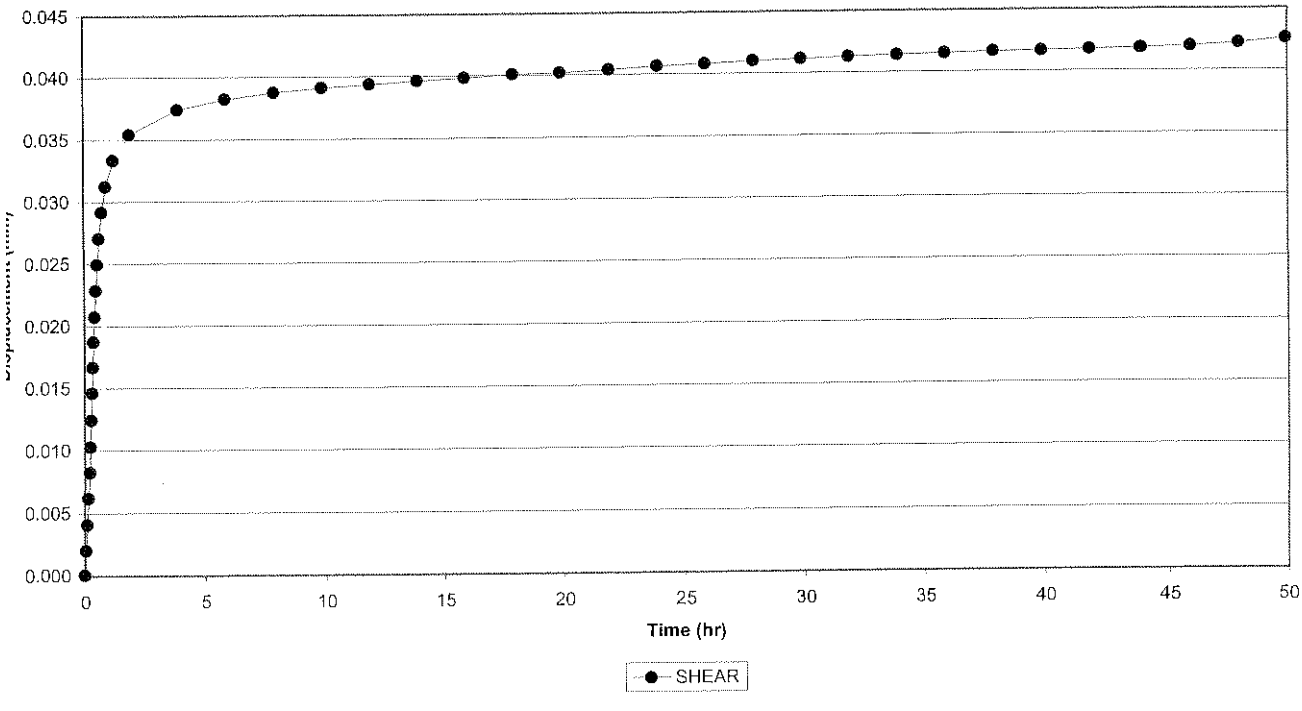

Creep Shear 2056-241, Cycle 9
Natural gouge (wet, < 0.5mm, 1mm)

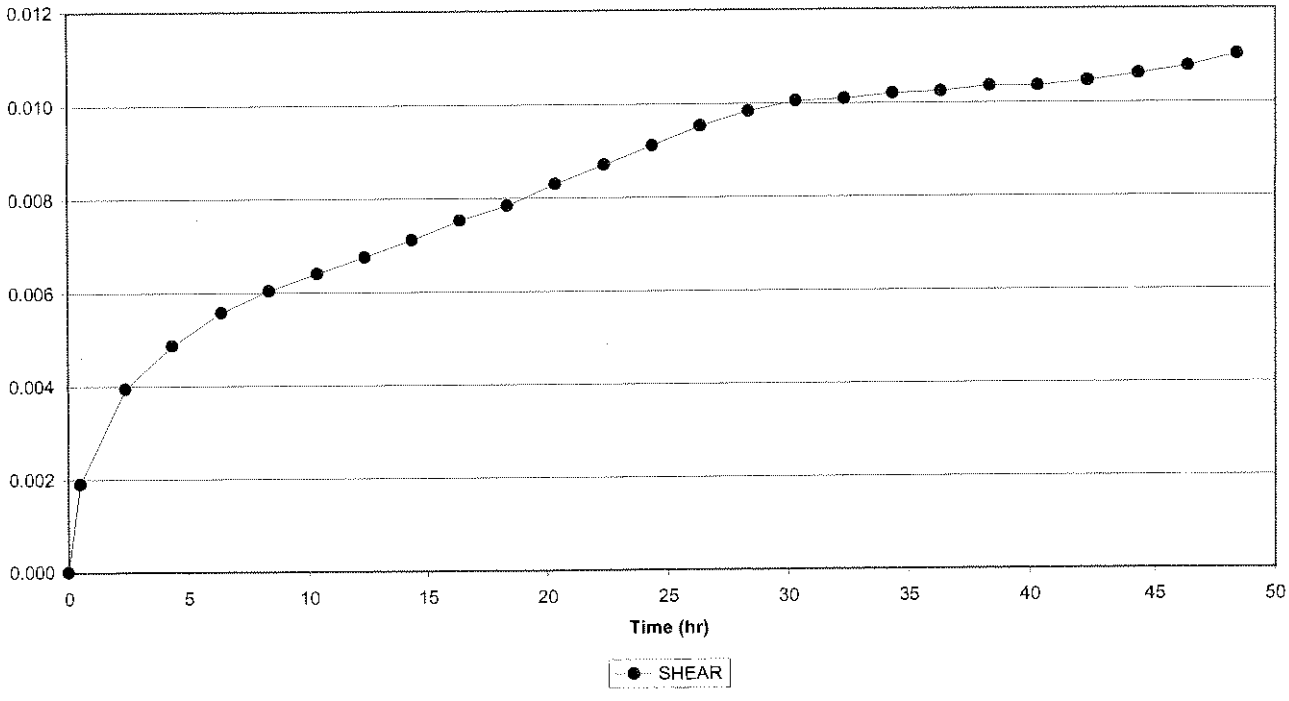

Creep Shear 2056-241, Cycle 10
Natural gouge (wet, < 0.5mm, 1mm)

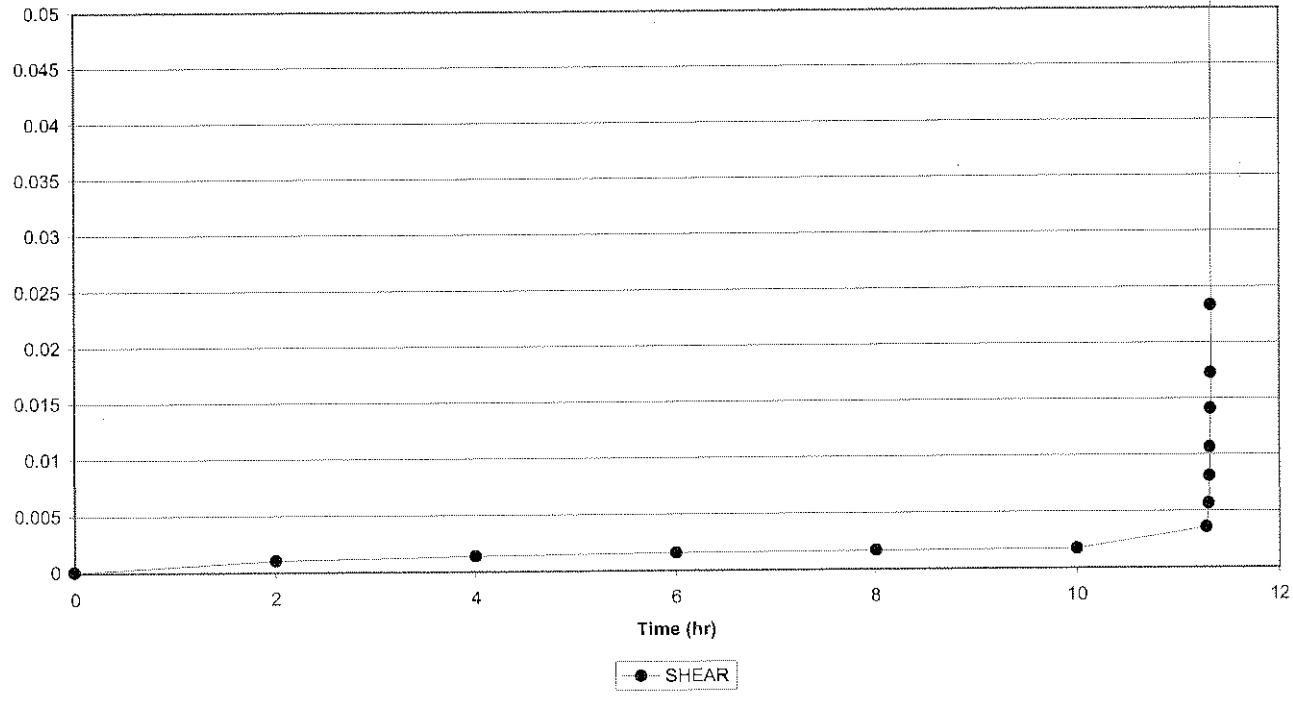

Creep Shear 2056-241
Natural gouge (wet, < 0.5mm, 1mm)

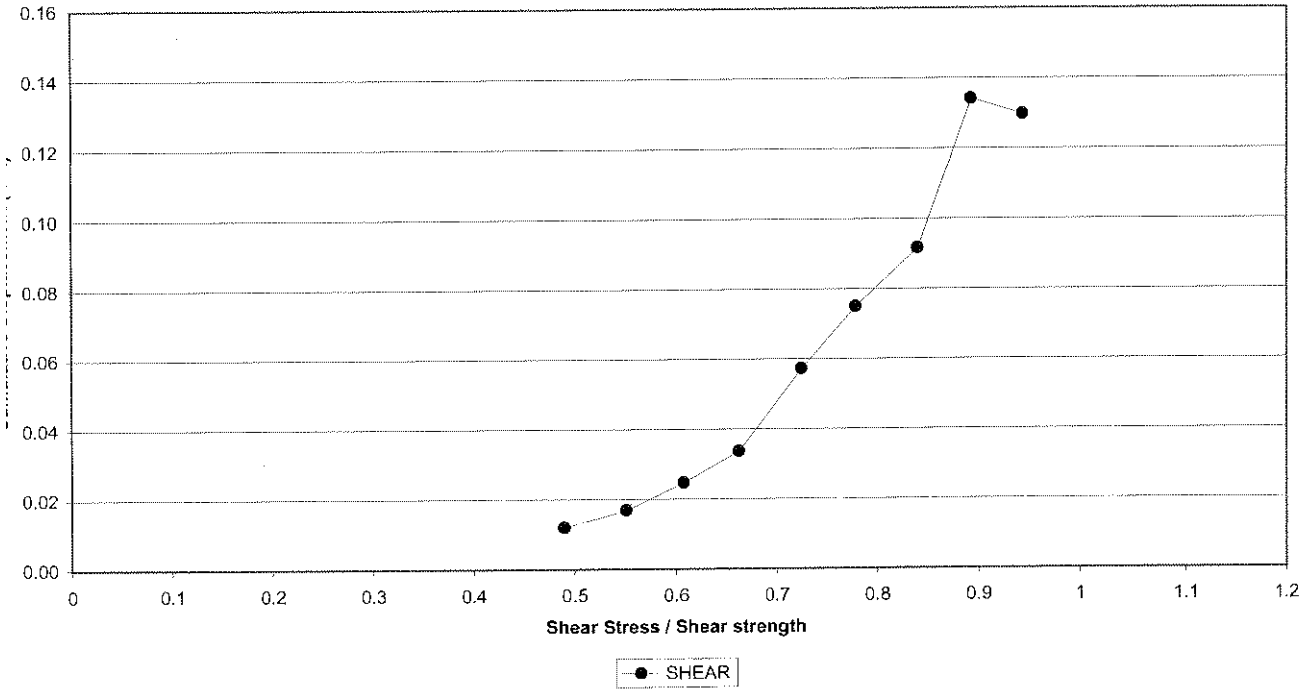

Creep Shear 2056-241
Natural gouge (wet, < 0.5mm, 1mm)

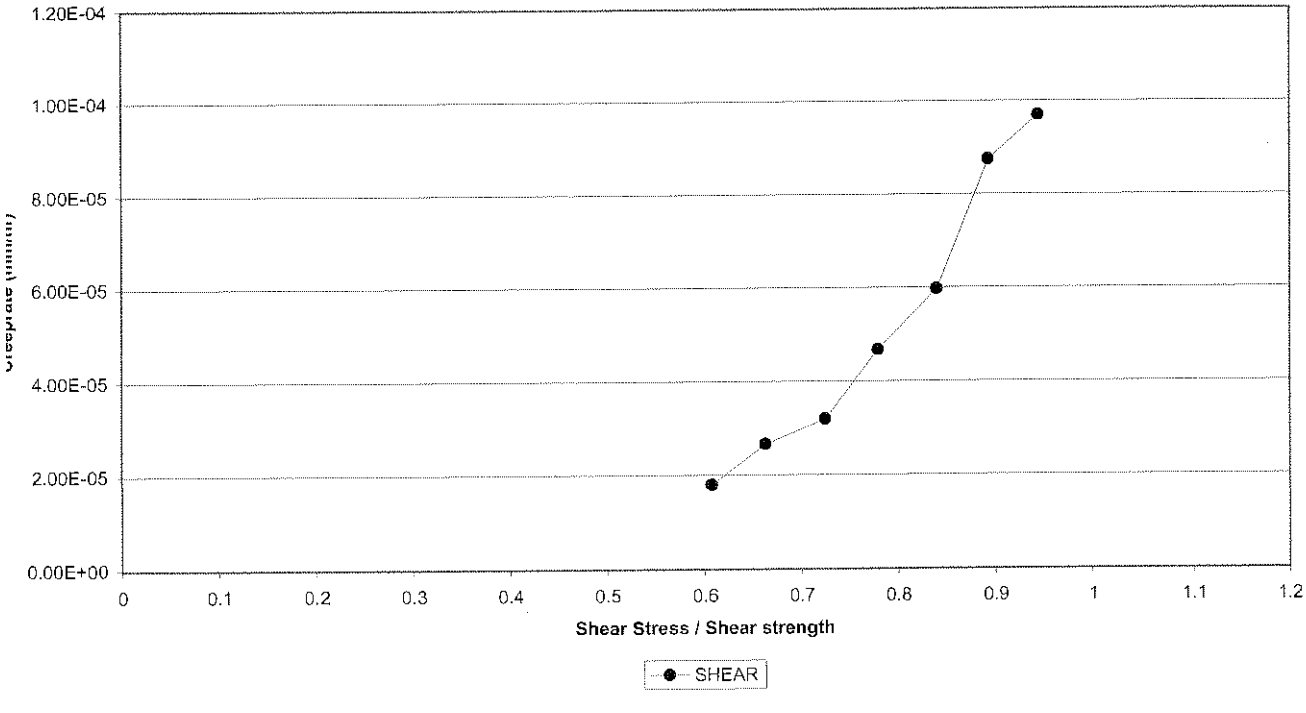

Creep Shear 2056-241
Natural gouge (wet, < 0.5mm, 1mm)

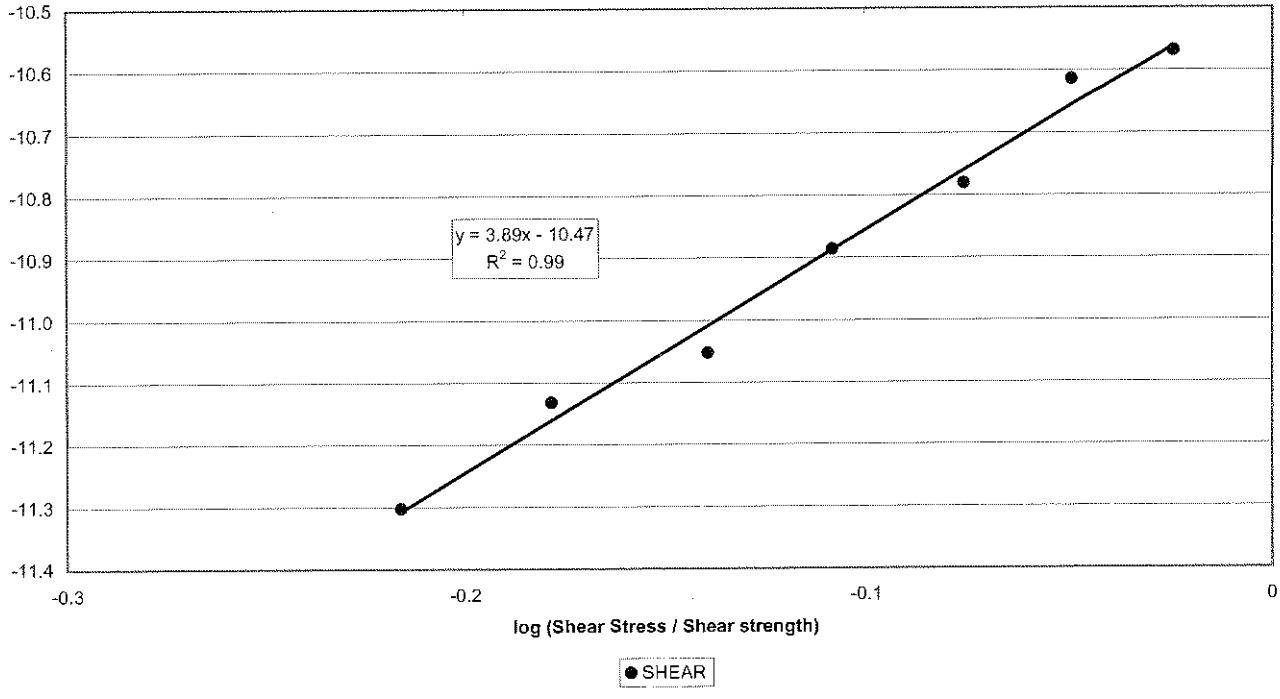

Creep Shear 2056-161
Crushed Elsburg Quartzite (dry, < 0.5mm, 0.5mm)

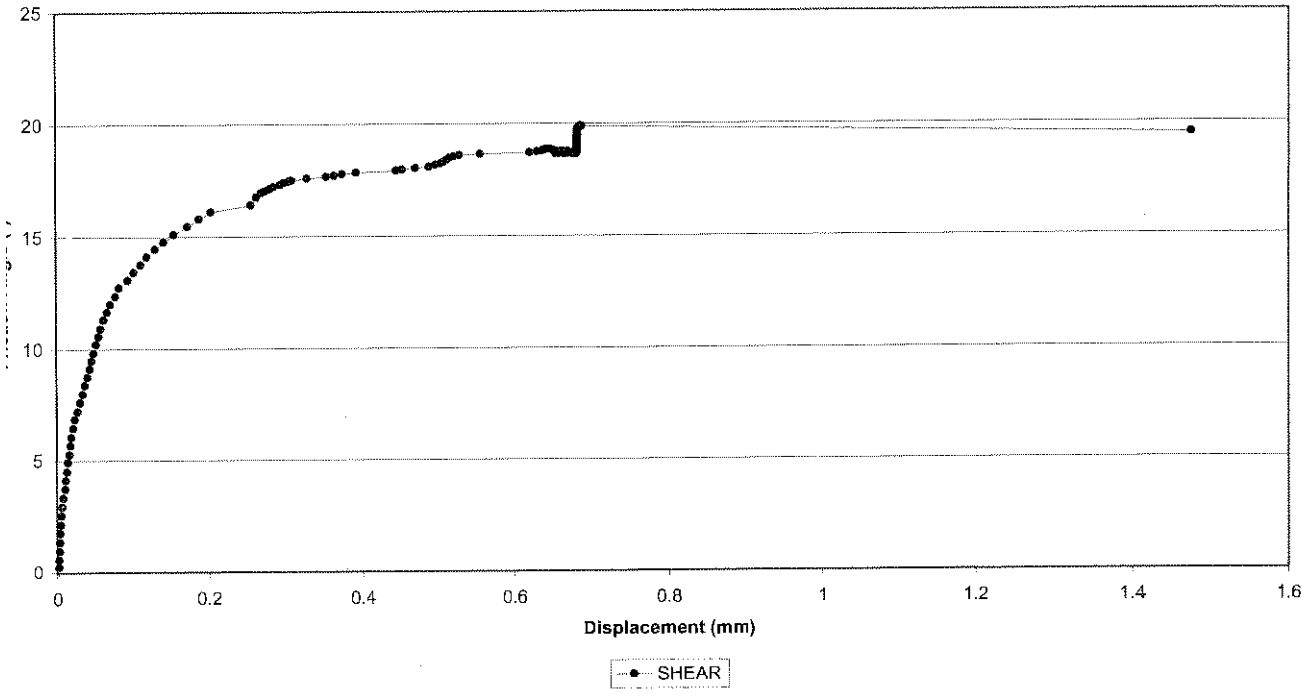

Creep Shear 2056-161
Crushed Elsburg Quartzite (dry, < 0.5mm, 0.5mm)

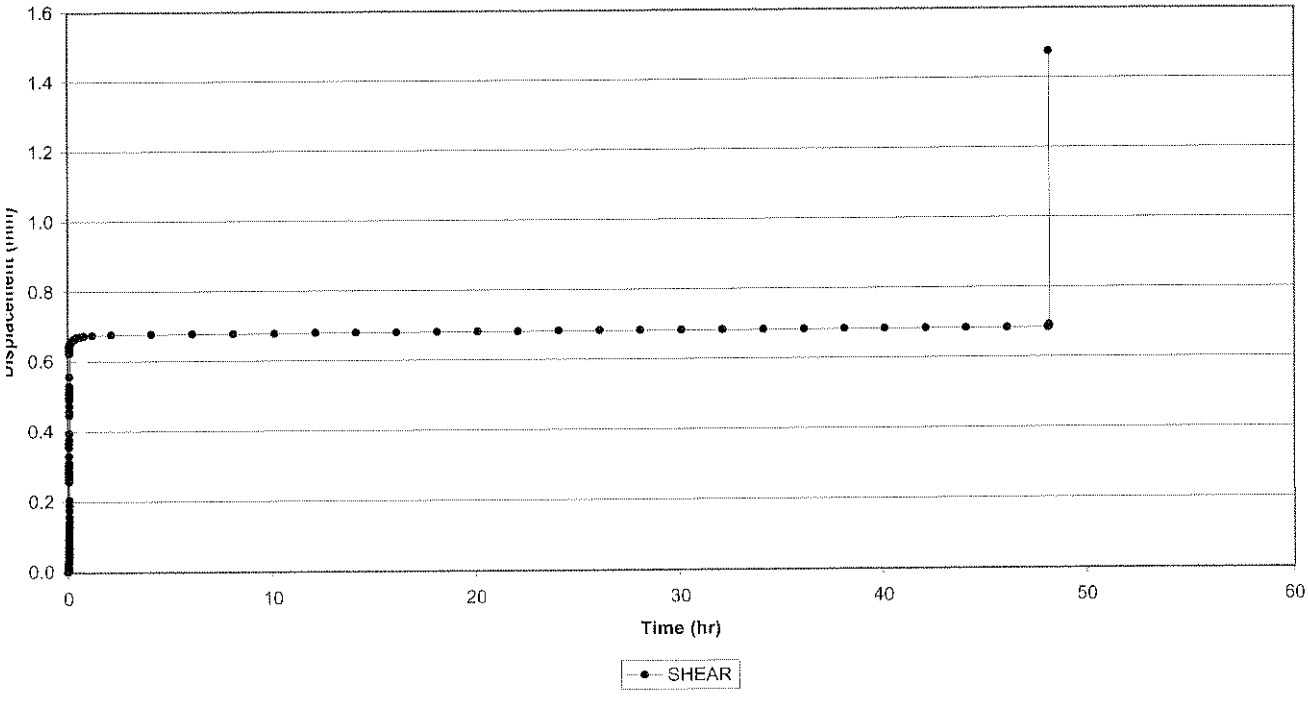

Creep Shear 2056-161, Cycle 1
Crushed Elsburg Quartzite (dry, < 0.5mm, 0.5mm)

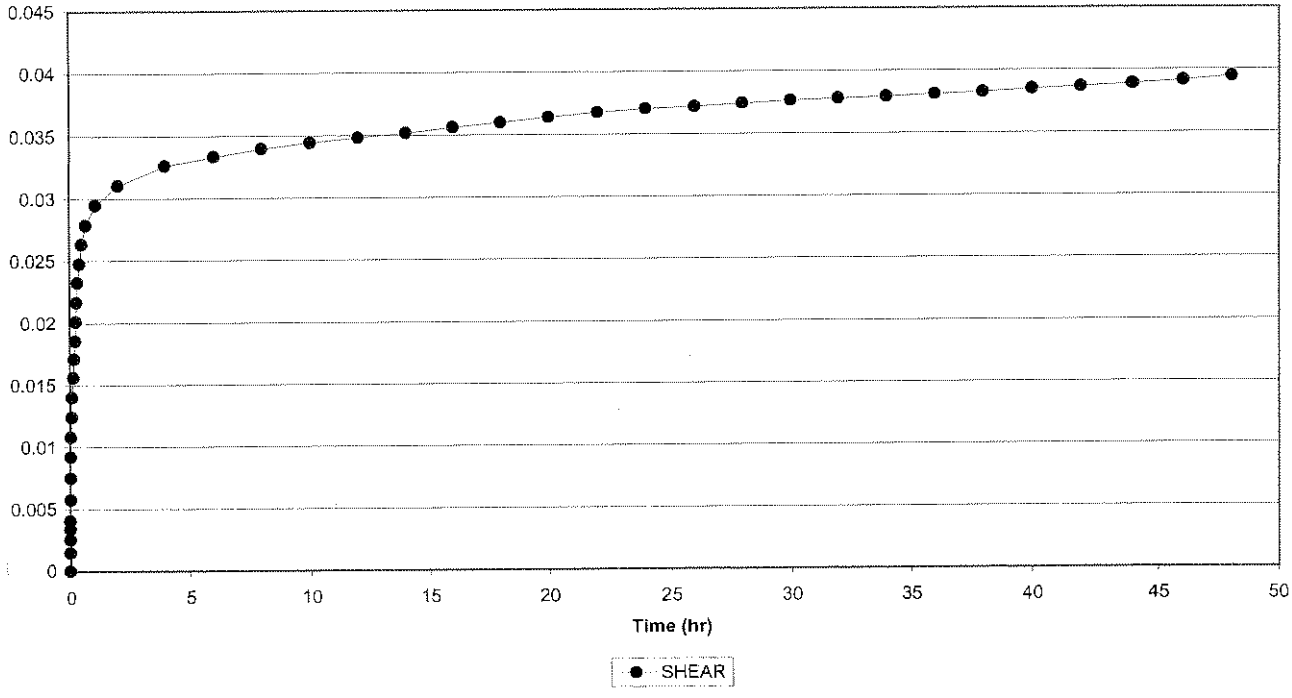

Appendix D

Results of triaxial post failure relaxation tests

UNIVERSITEIT VAN PRETORIA
UNIVERSITY OF PRETORIA
YUNIBESITHI YA PRETORIA

CSIR MININGTEK

Elsburg Quartzite

Triaxial compressive strength test with axial and lateral deformation measurements (MTS Machine)

Specimen No: 2056-TCM-104

Strength:	472.0 MPa	Modulus:	65.6 GPa
Confinement:	40.0 MPa	Poisson's Ratio:	0.24

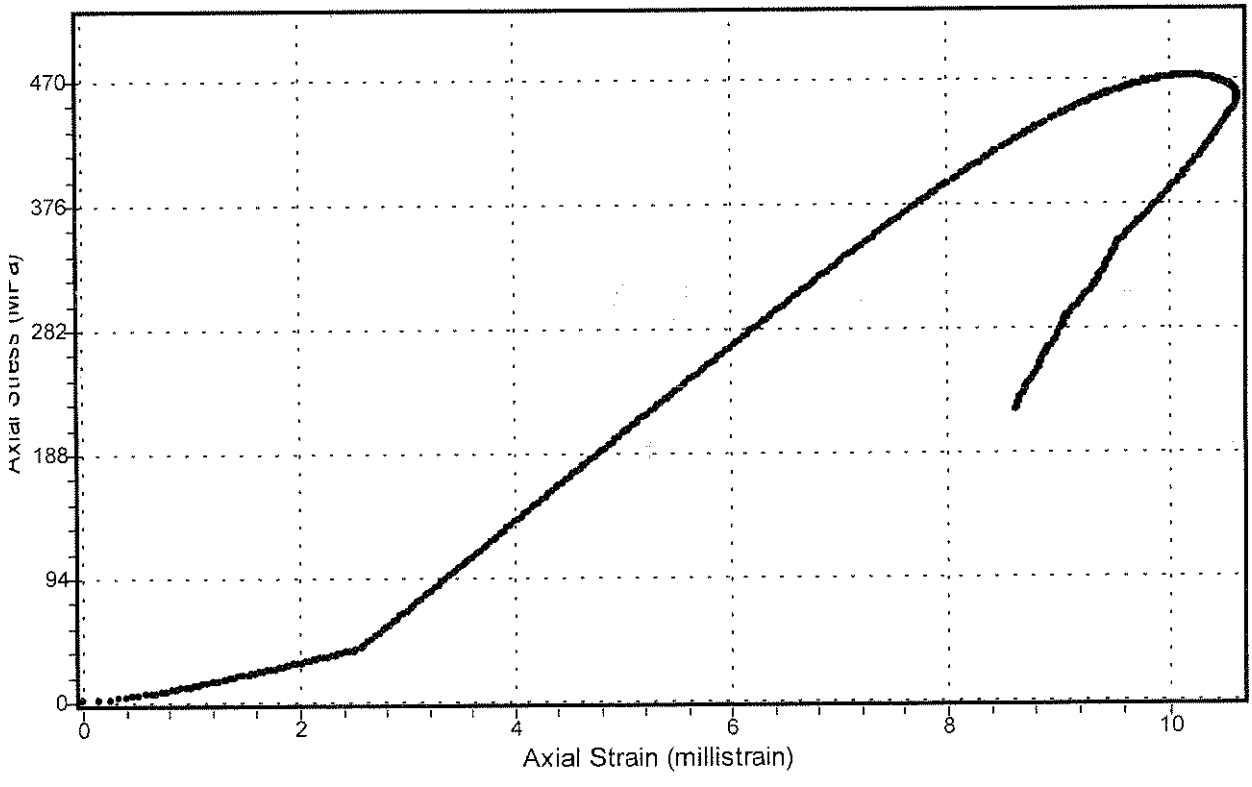

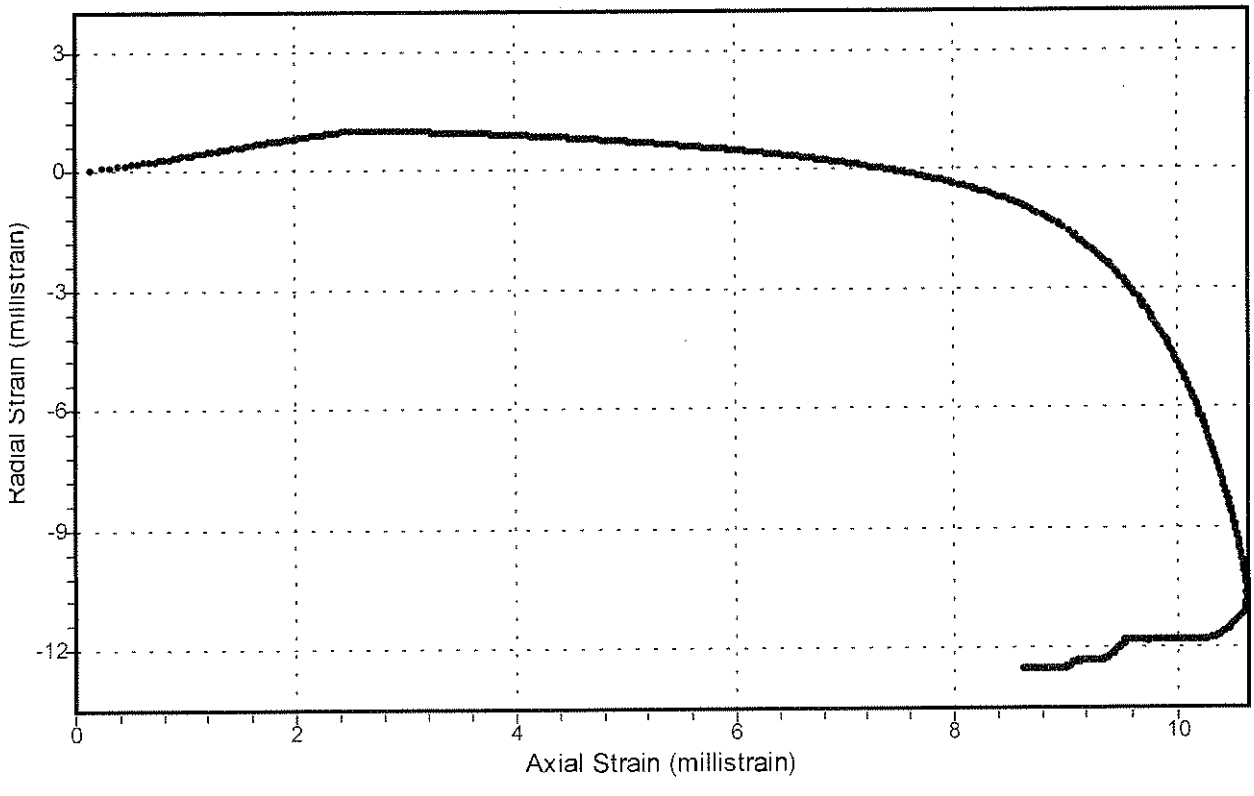

2001-08-27 18:19:07

UNIVERSITEIT VAN PRETORIA
UNIVERSITY OF PRETORIA
YUNIBESITHI YA PRETORIA

CSIR MININGTEK

Elsburg Quartzite

Triaxial time dependant behaviour

Specimen No: 2056-104td Confinement: 40.0 MPa

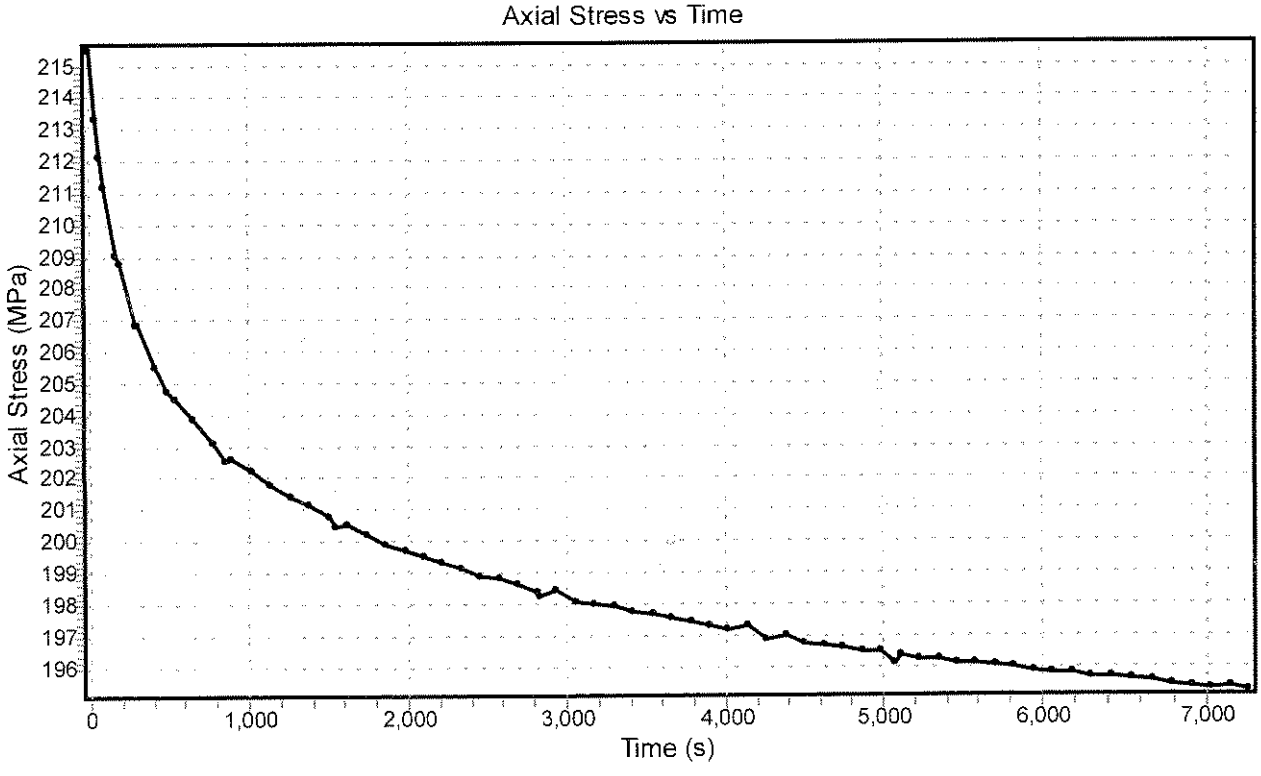

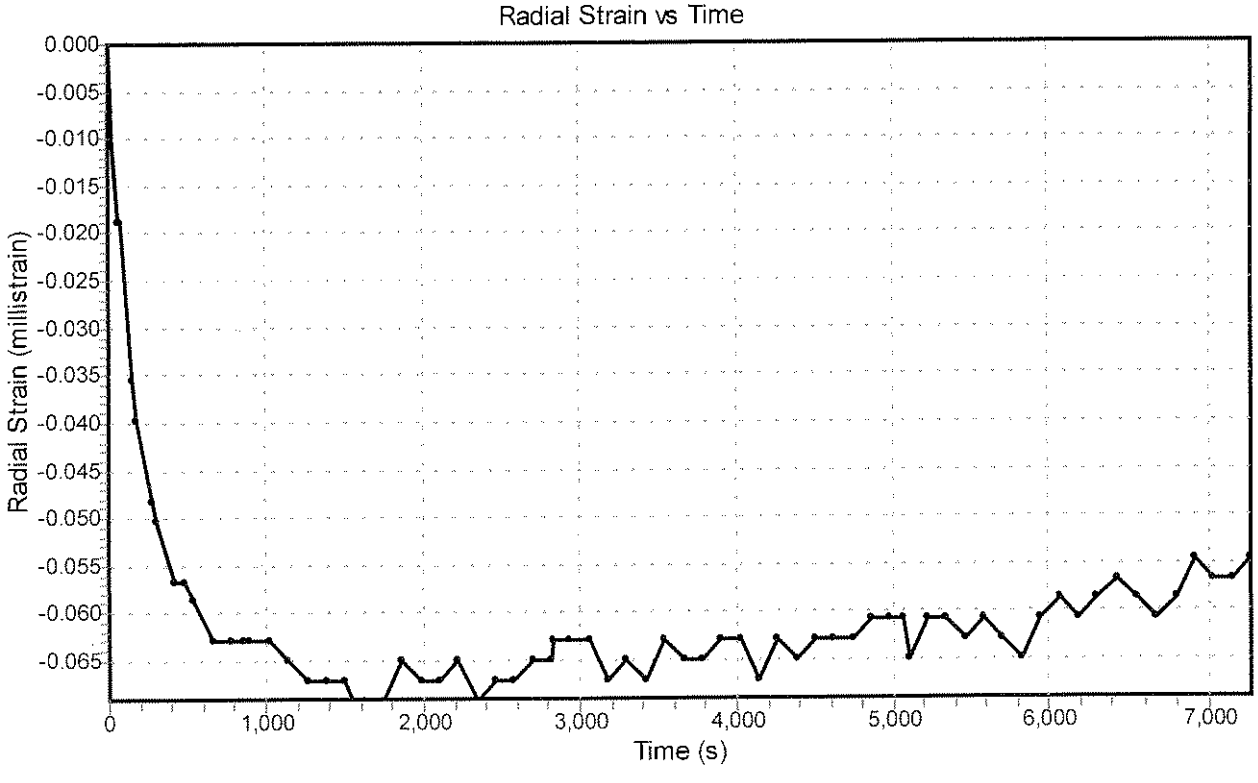

2001-08-27 18:56:02

UNIVERSITEIT VAN PRETORIA
UNIVERSITY OF PRETORIA
YUNIBESITHI YA PRETORIA

CSIR MININGTEK

Elsburg Quartzite

Triaxial compressive strength test with axial and lateral deformation measurements (MTS Machine)

Specimen No: 2056-TCM-105

Strength:	478.8 MPa	Modulus:	62.6 GPa
Confinement:	40.0 MPa	Poisson's Ratio:	0.23

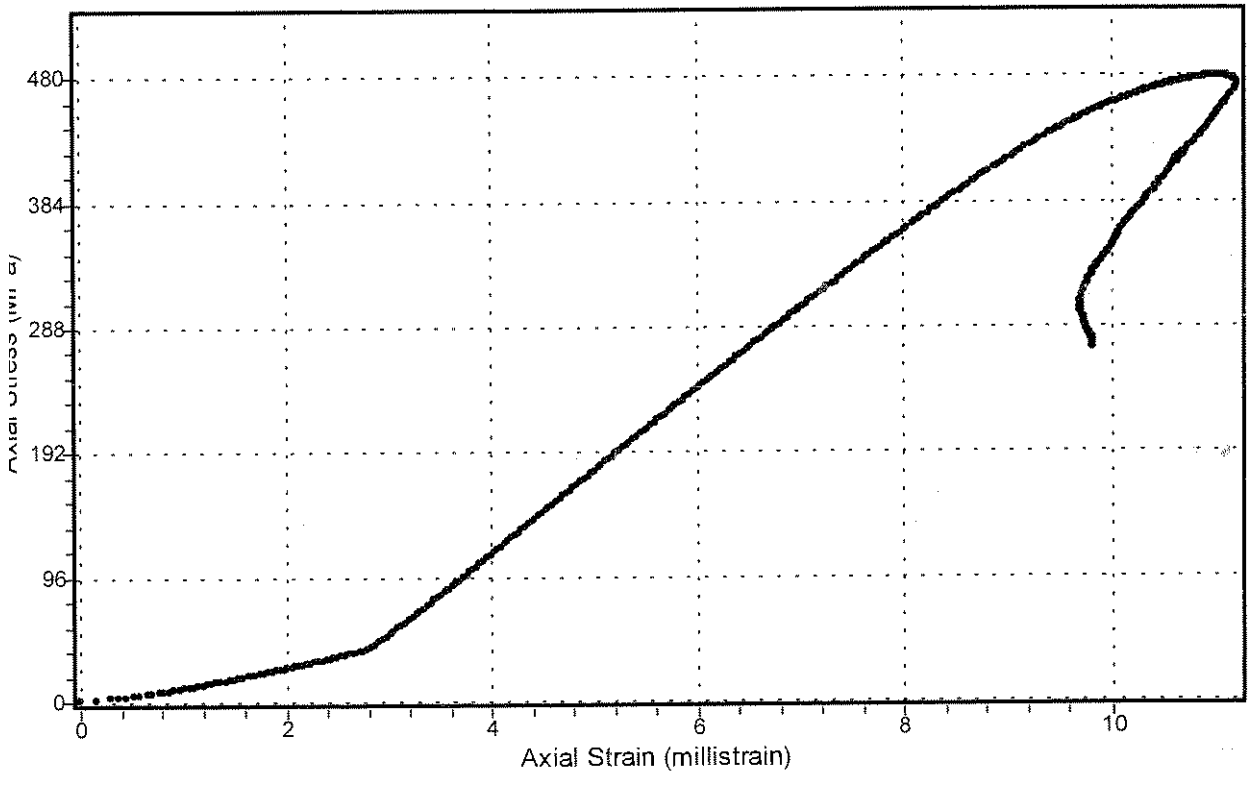

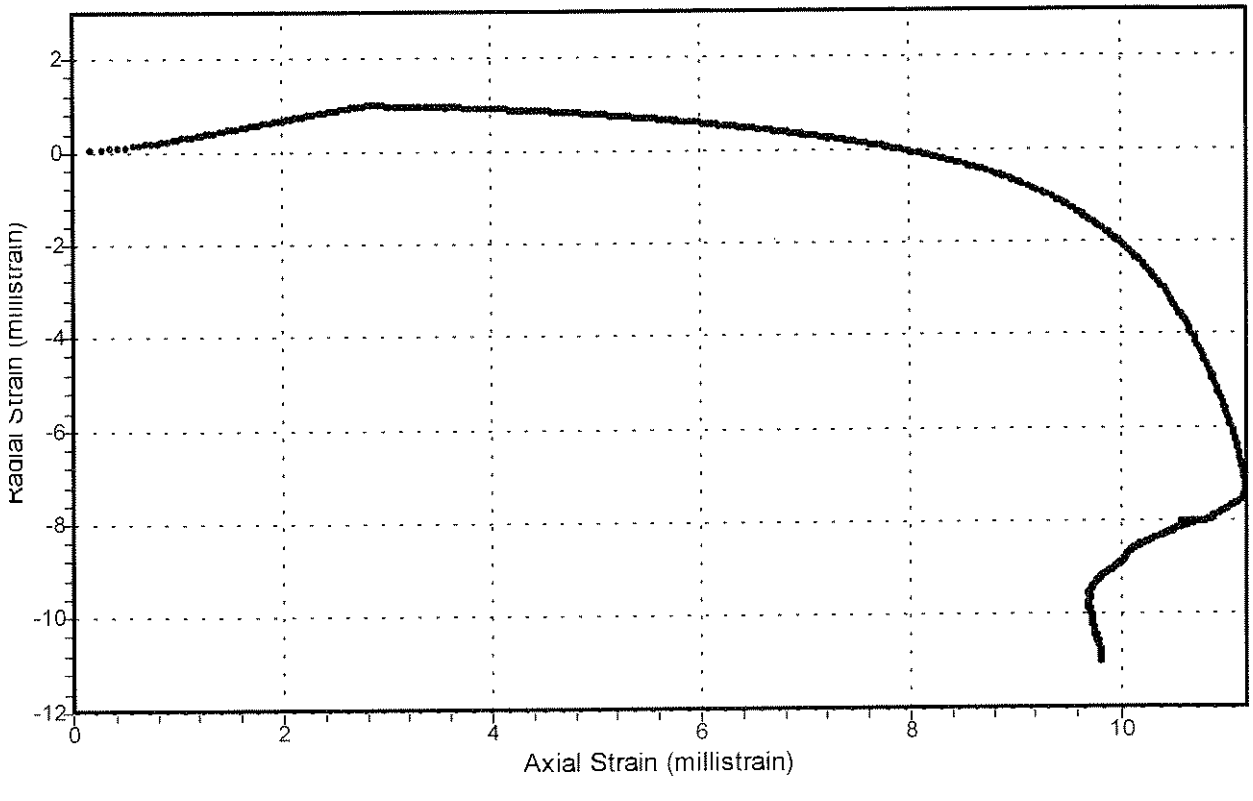

2001-08-27 18:20:13

Elsburg Quartzite

Triaxial time dependant behaviour

Specimen No: 2056-105td Confinement: 40.0 MPa

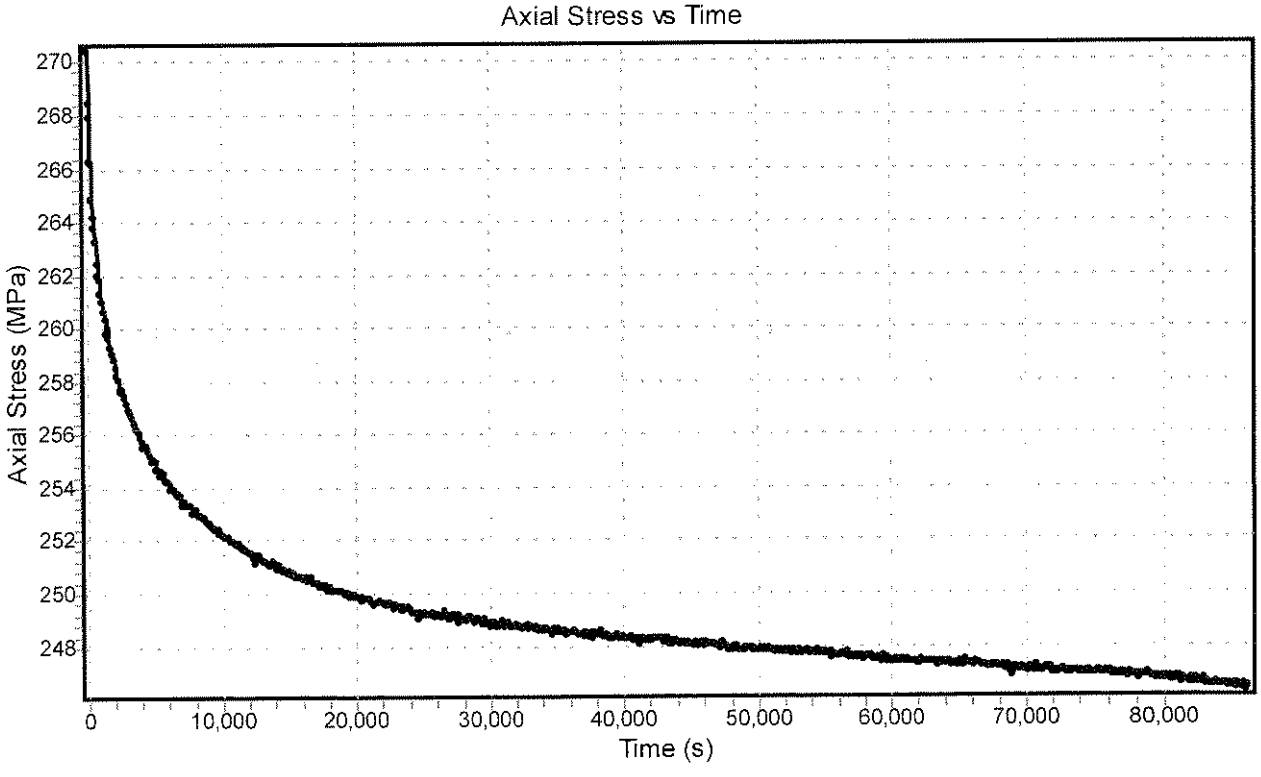

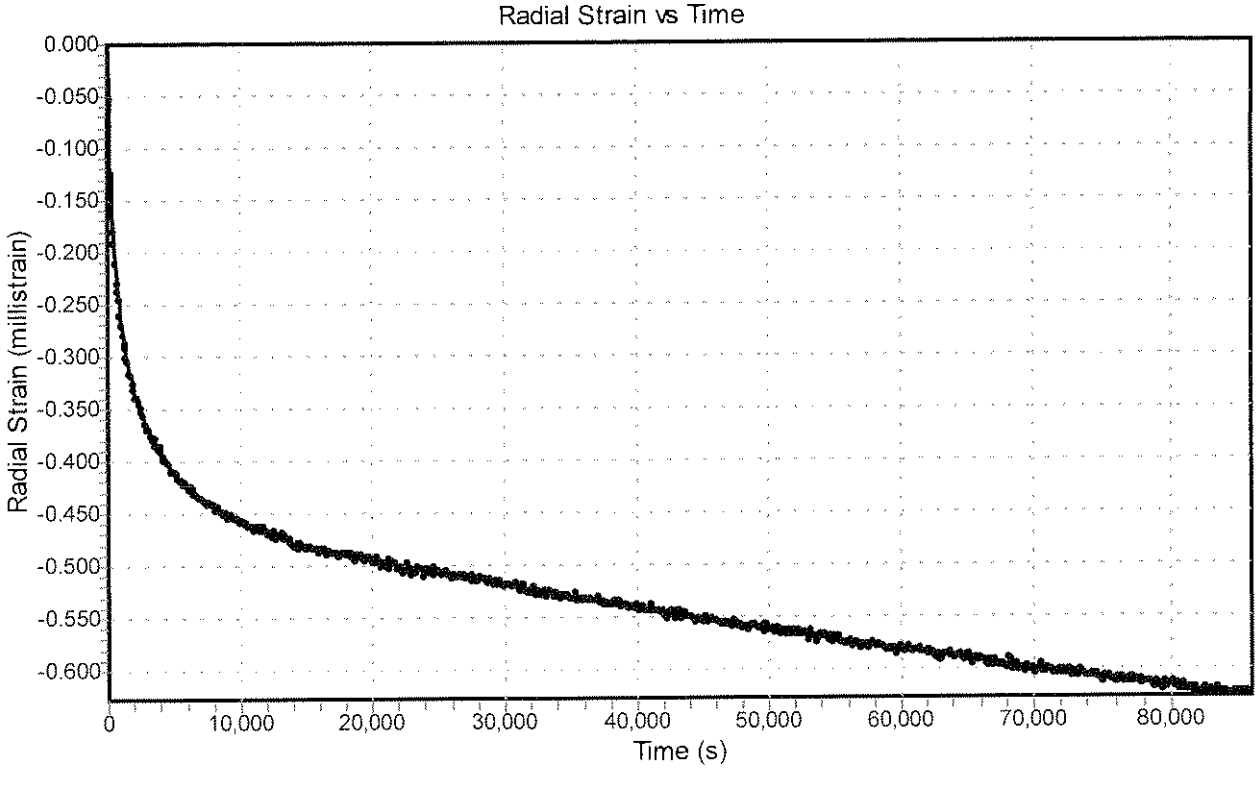

2001-08-27 18:56:58

UNIVERSITEIT VAN PRETORIA
UNIVERSITY OF PRETORIA
YUNIBESITHI YA PRETORIA

CSIR MININGTEK

Elsburg Quartzite

Triaxial compressive strength test with axial and lateral deformation measurements (MTS Machine)

Specimen No: 2056-TCM-106

Strength:	323.7 MPa	Modulus:	50.3 GPa
Confinement:	40.0 MPa	Poisson's Ratio:	0.28

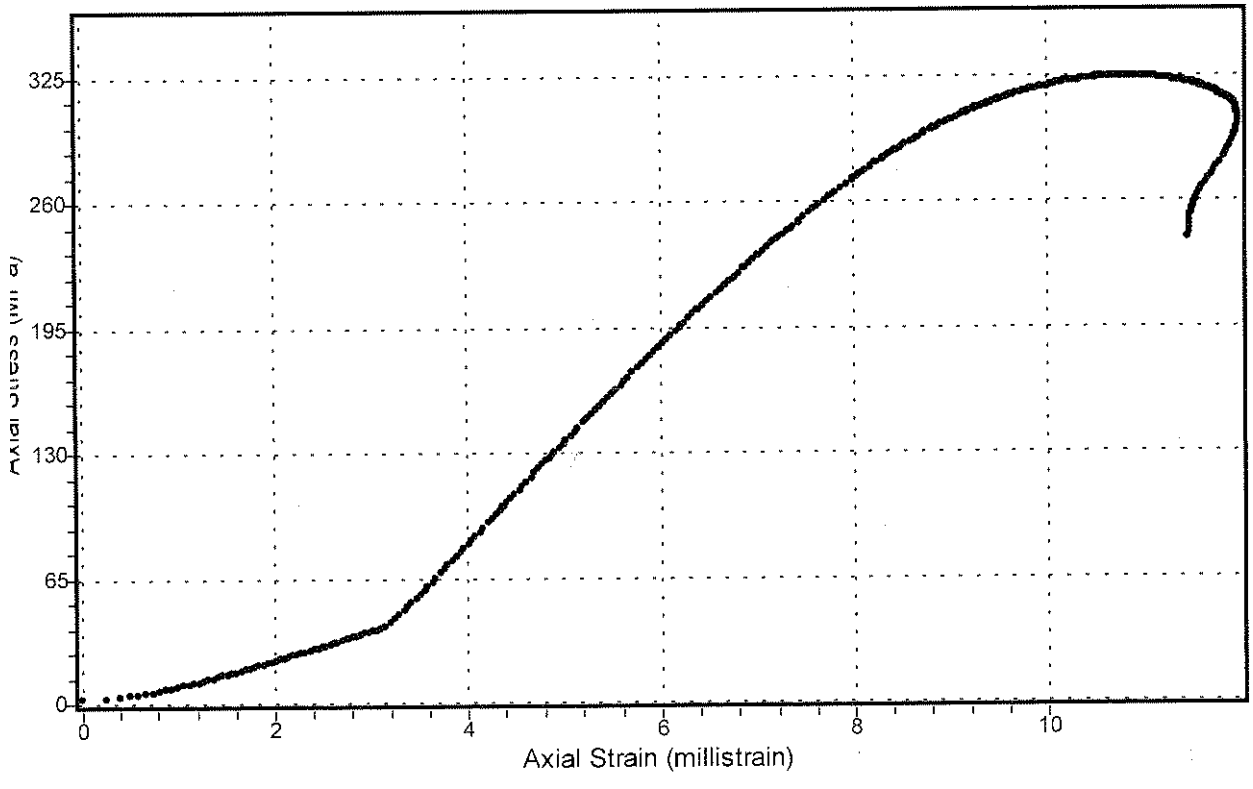

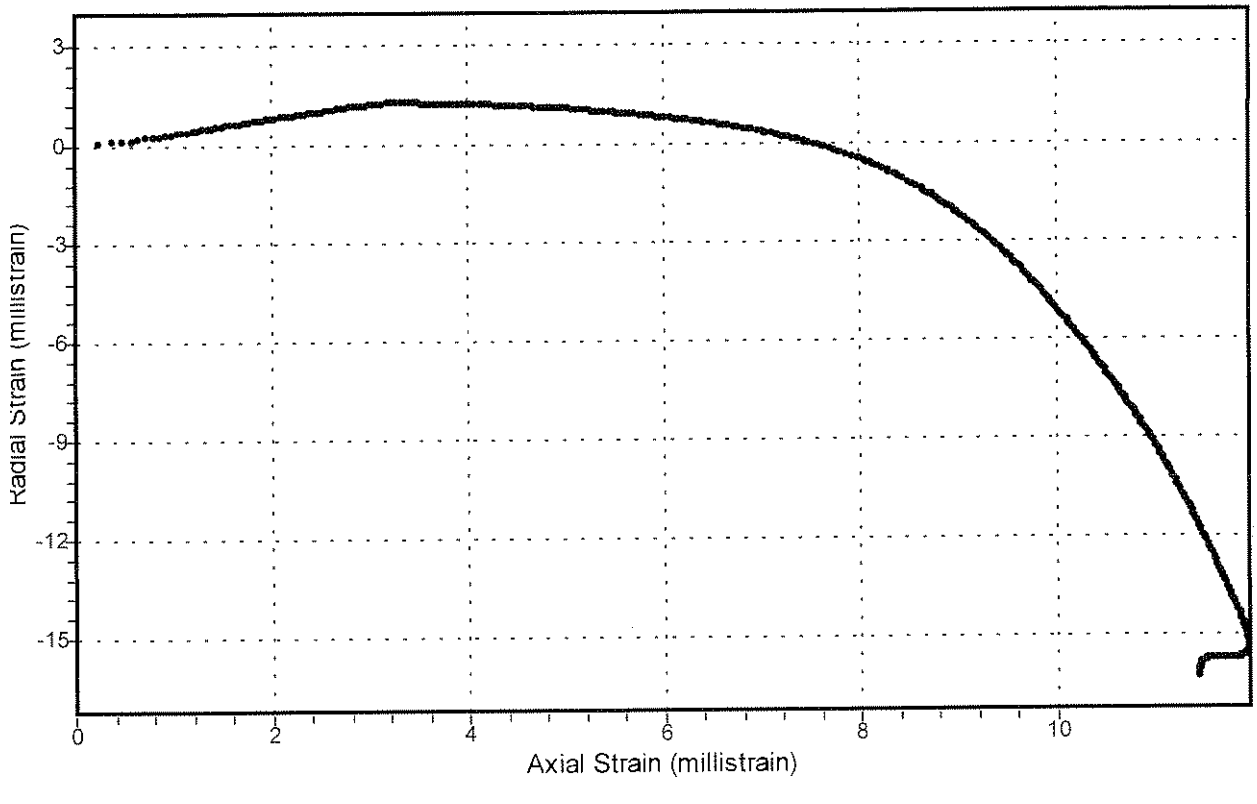

2001-08-27 18:21:36

UNIVERSITEIT VAN PRETORIA
UNIVERSITY OF PRETORIA
YUNIBESITHI YA PRETORIA

CSIR MININGTEK

Elsburg Quartzite

Triaxial time dependant behaviour

Specimen No: 2056-106td Confinement: 40.0 MPa

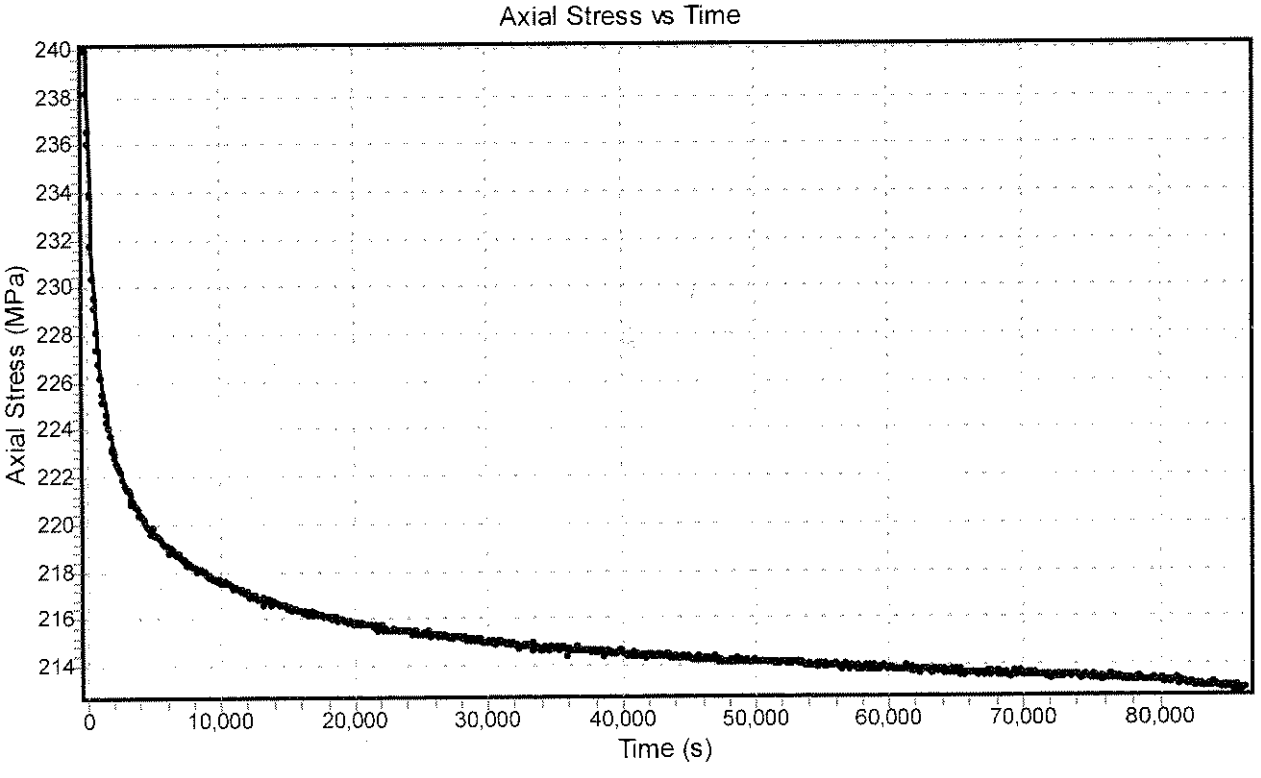

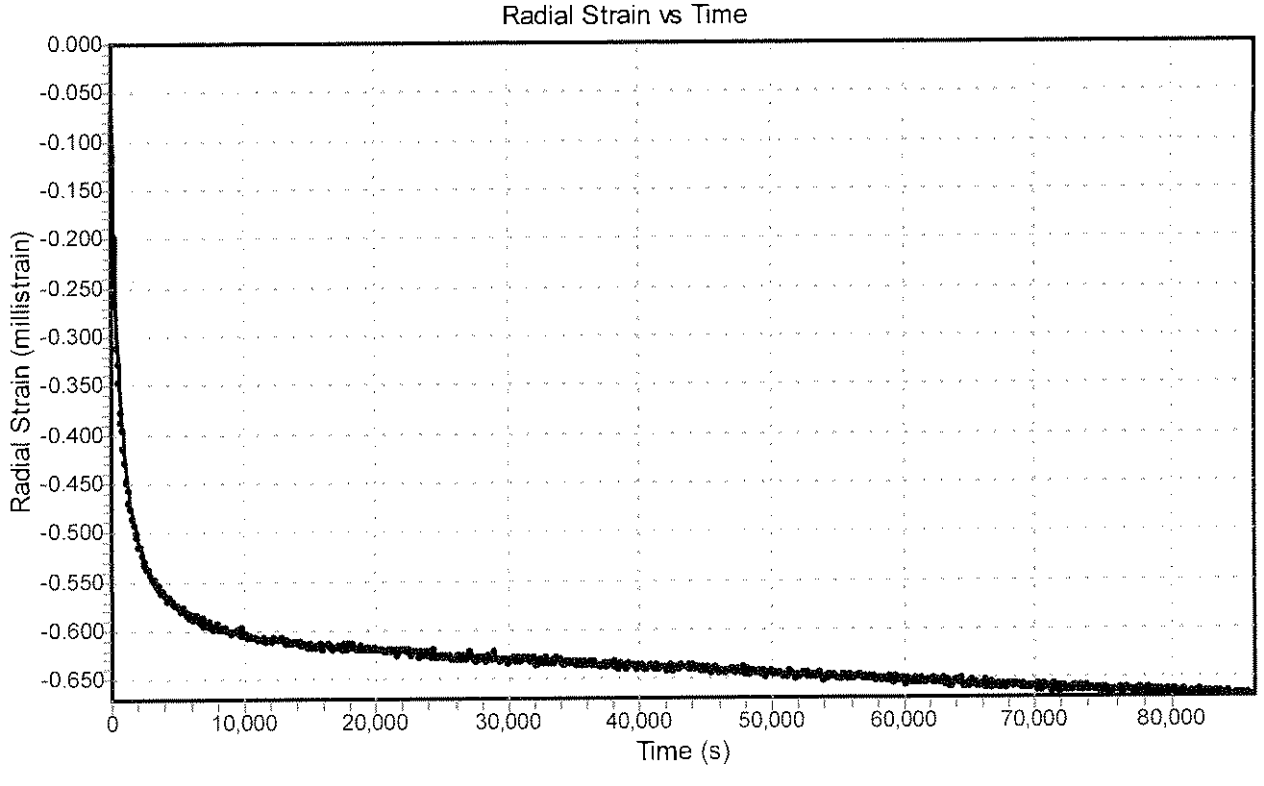

2001-08-27 19:04:49

UNIVERSITEIT VAN PRETORIA
UNIVERSITY OF PRETORIA
YUNIBESITHI YA PRETORIA

CSIR MININGTEK

Elsburg Quartzite

Triaxial compressive strength test with axial and lateral deformation measurements (MTS Machine)

Specimen No: 2056-TCM-108

Strength:	420.3 MPa	Modulus:	67.8 GPa
Confinement:	40.0 MPa	Poisson's Ratio:	0.26

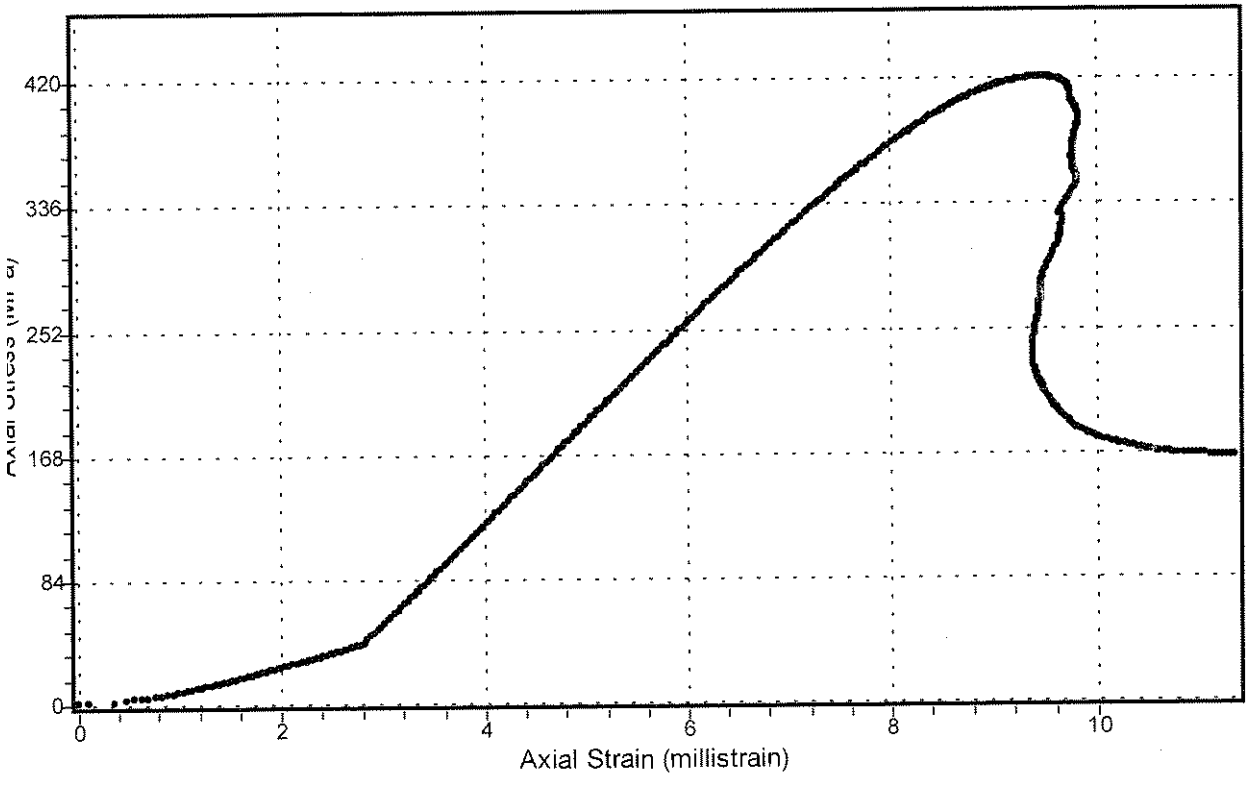

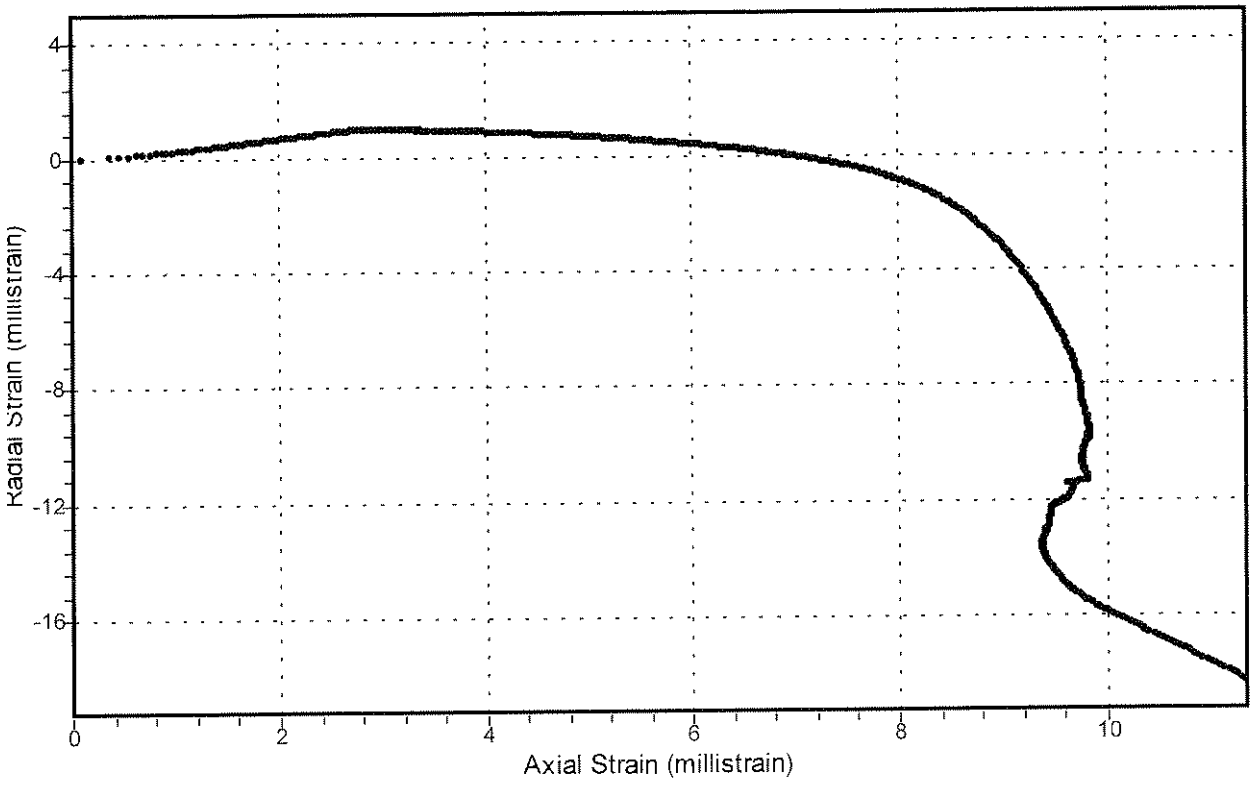

2001-08-27 18:26:27

UNIVERSITEIT VAN PRETORIA
UNIVERSITY OF PRETORIA
YUNIBESITHI YA PRETORIA

CSIR MININGTEK

Elsburg Quartzite

Triaxial time dependant behaviour

Specimen No: 2056-108td Confinement: 40.0 MPa

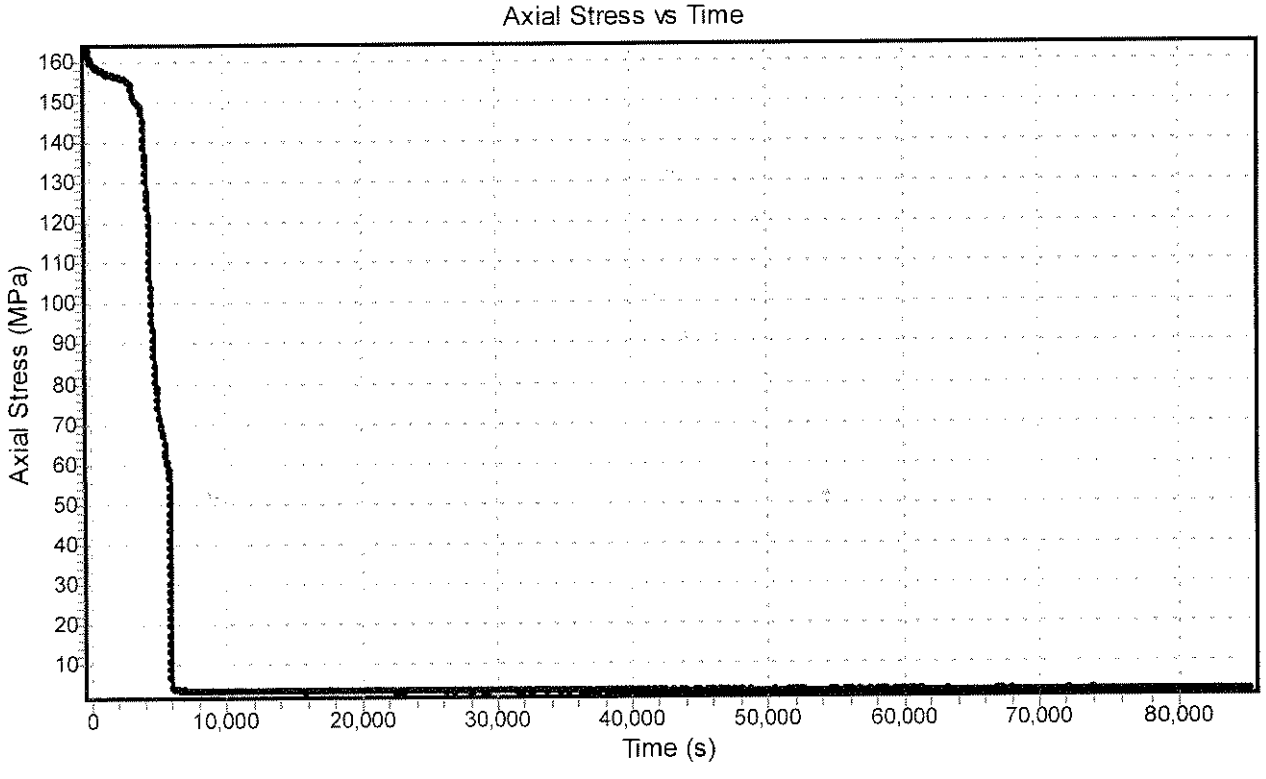

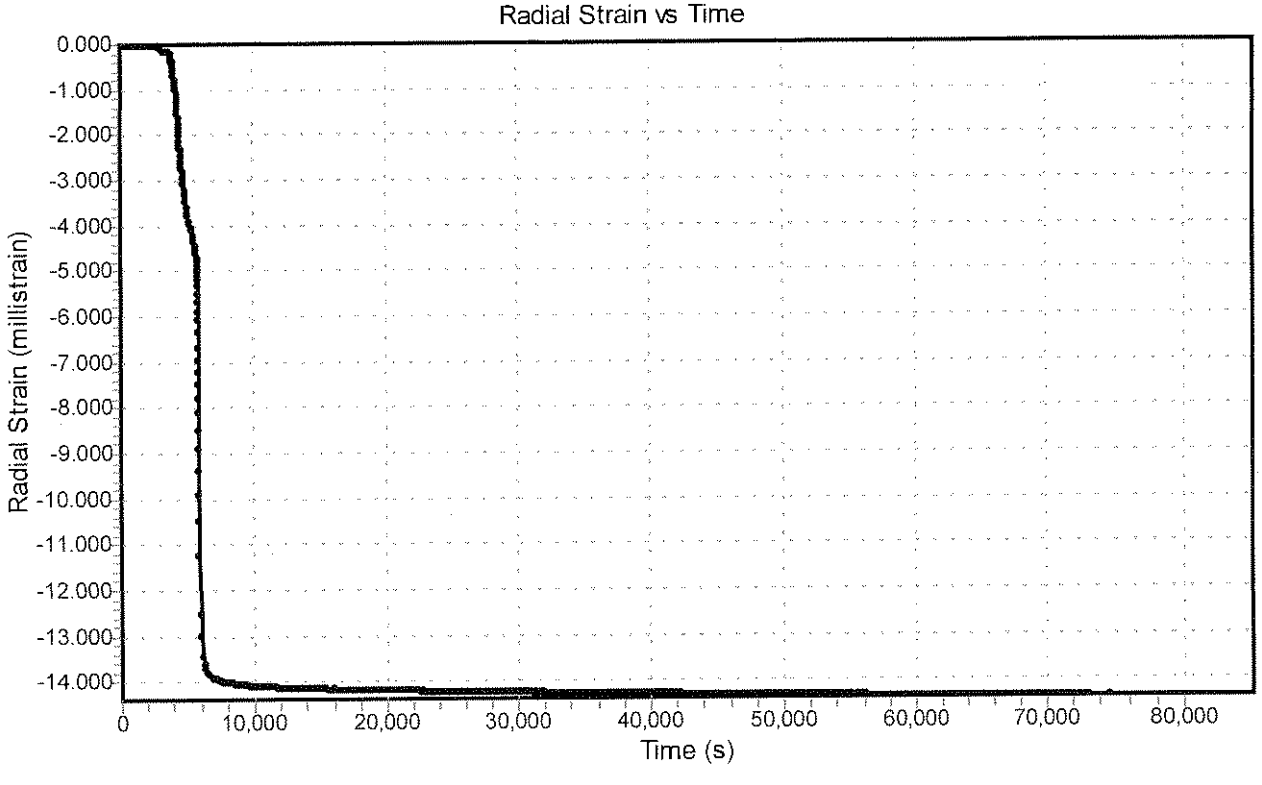

2001-08-27 19:06:20

UNIVERSITEIT VAN PRETORIA
UNIVERSITY OF PRETORIA
YUNIBESITHI YA PRETORIA

CSIR MININGTEK

Elsburg Quartzite

Triaxial compressive strength test with axial and lateral deformation measurements (MTS Machine)

Specimen No: 2056-TCM-112

Strength:	416.4 MPa	Modulus:	62.2 GPa
Confinement:	40.0 MPa	Poisson's Ratio:	0.24

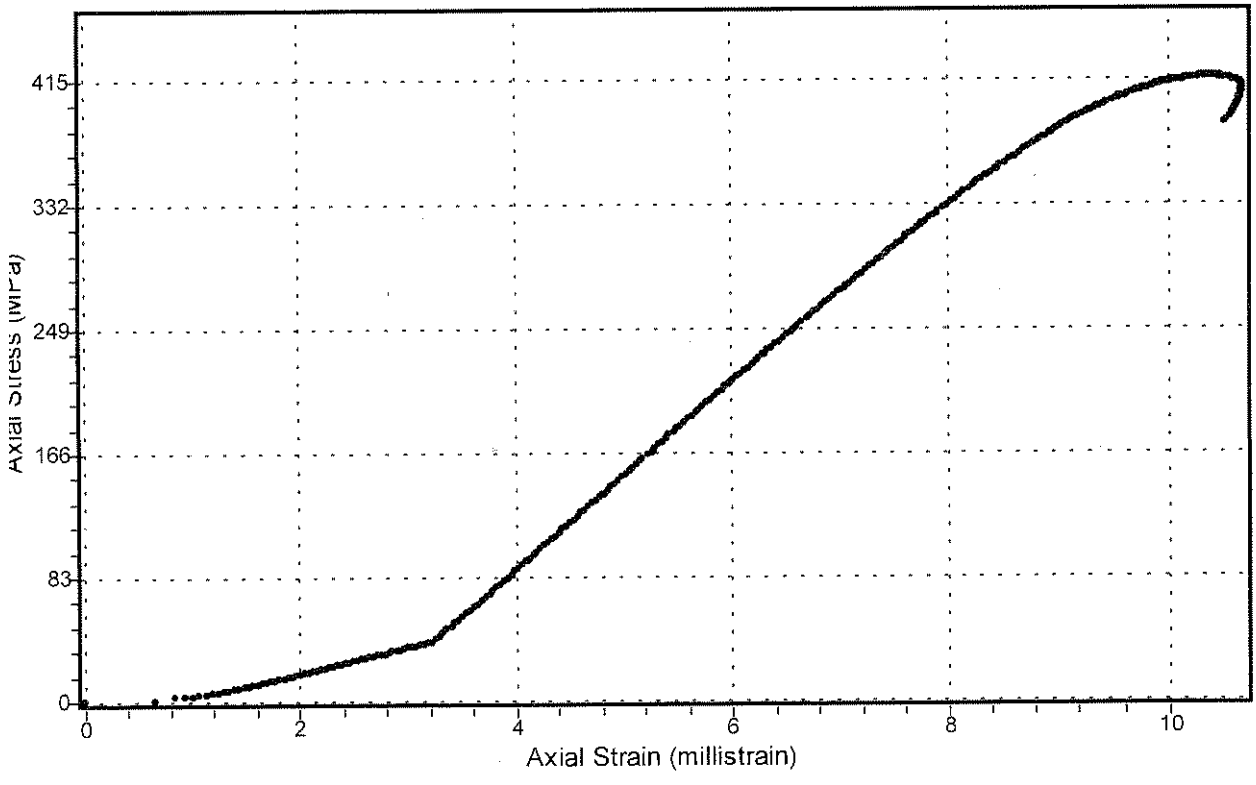

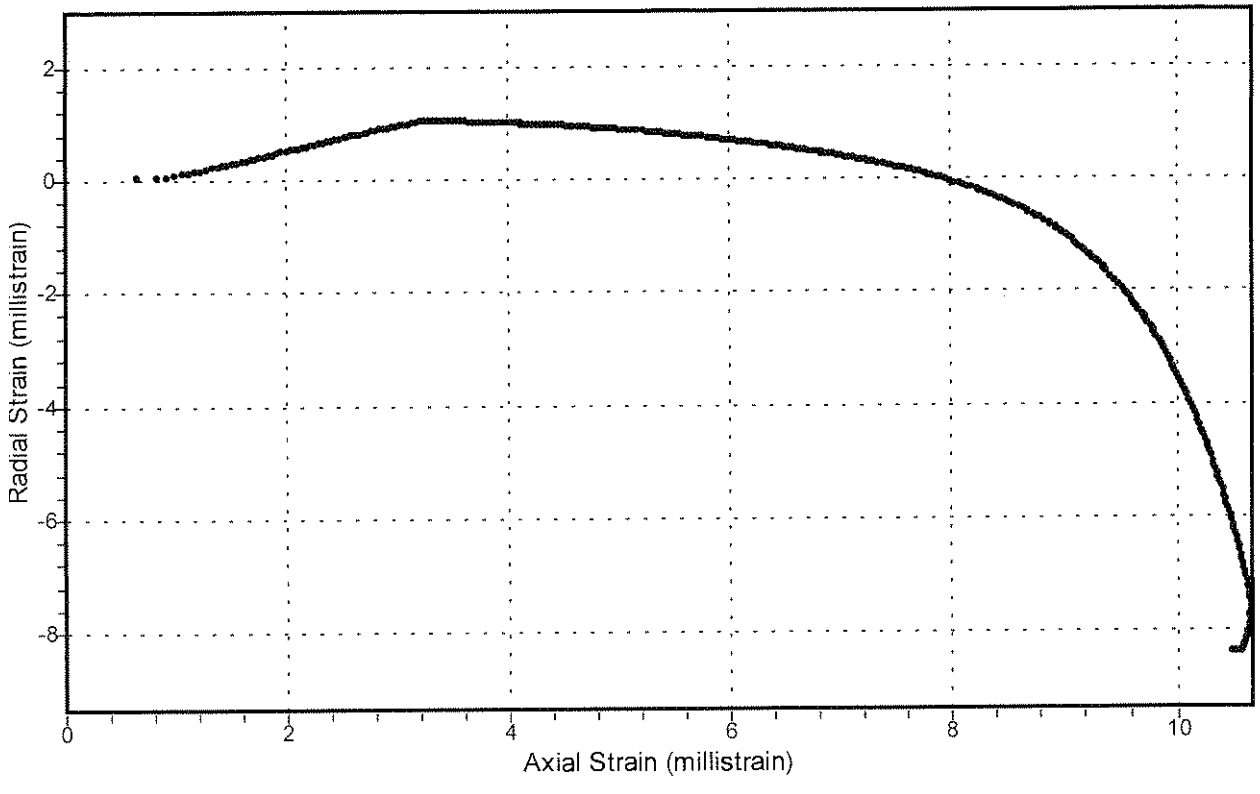

2001-08-27 18:17:36

Elsburg Quartzite

Triaxial time dependant behaviour

Specimen No: 2056-112td Confinement: 40.0 MPa

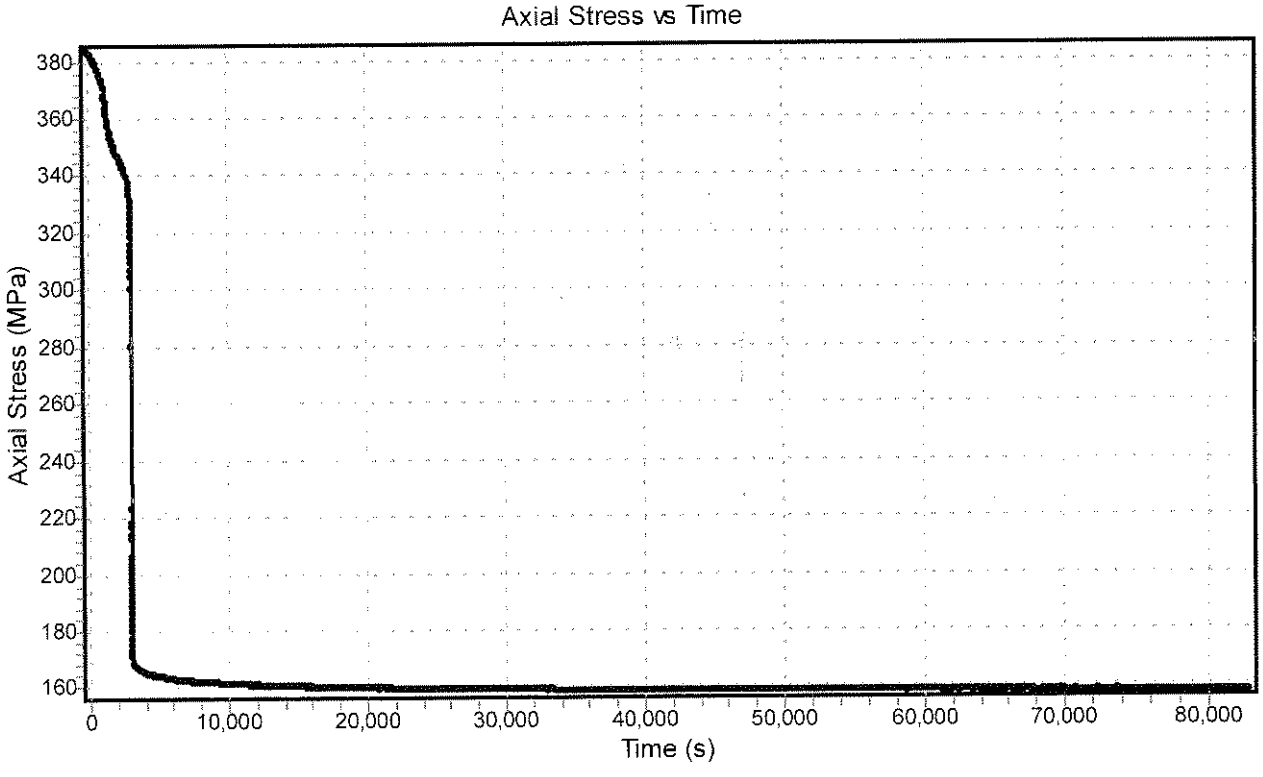

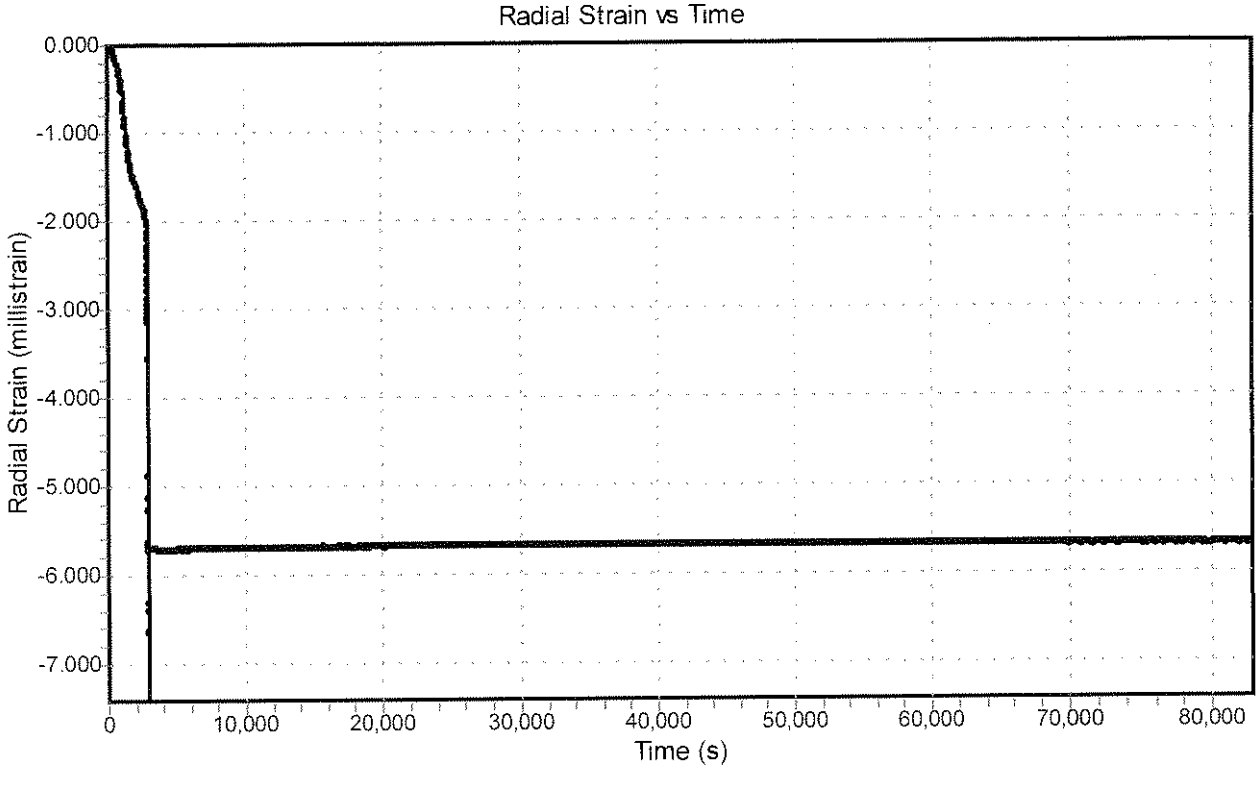

2001-08-27 19:07:50

UNIVERSITEIT VAN PRETORIA
UNIVERSITY OF PRETORIA
YUNIBESITHI YA PRETORIA

CSIR MINERGTEK

Ventersdorp Lava

Triaxial compressive strength test with axial and lateral deformation measurements (MTS Machine)

Specimen No: 2056-TCM-123

Strength:	809.3 MPa	Modulus:	80.7 GPa
Confinement:	40.0 MPa	Poisson's Ratio:	0.31

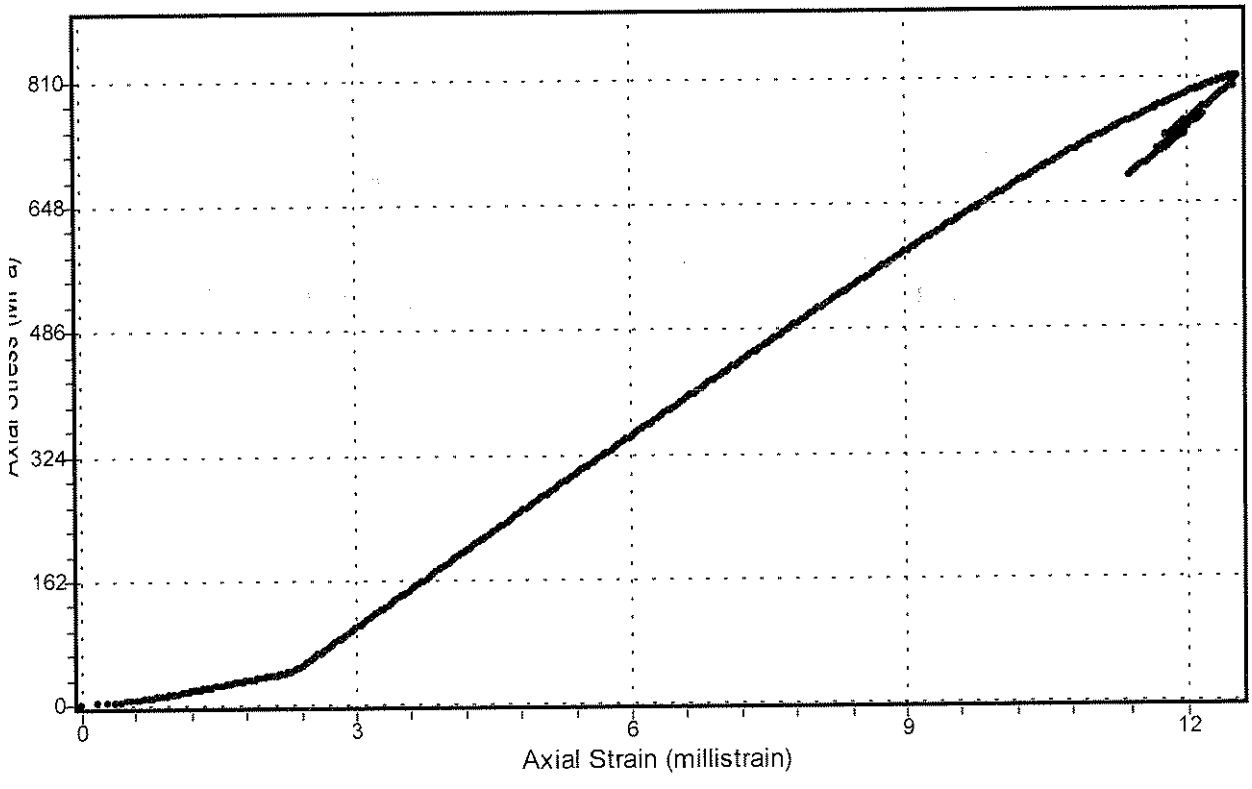

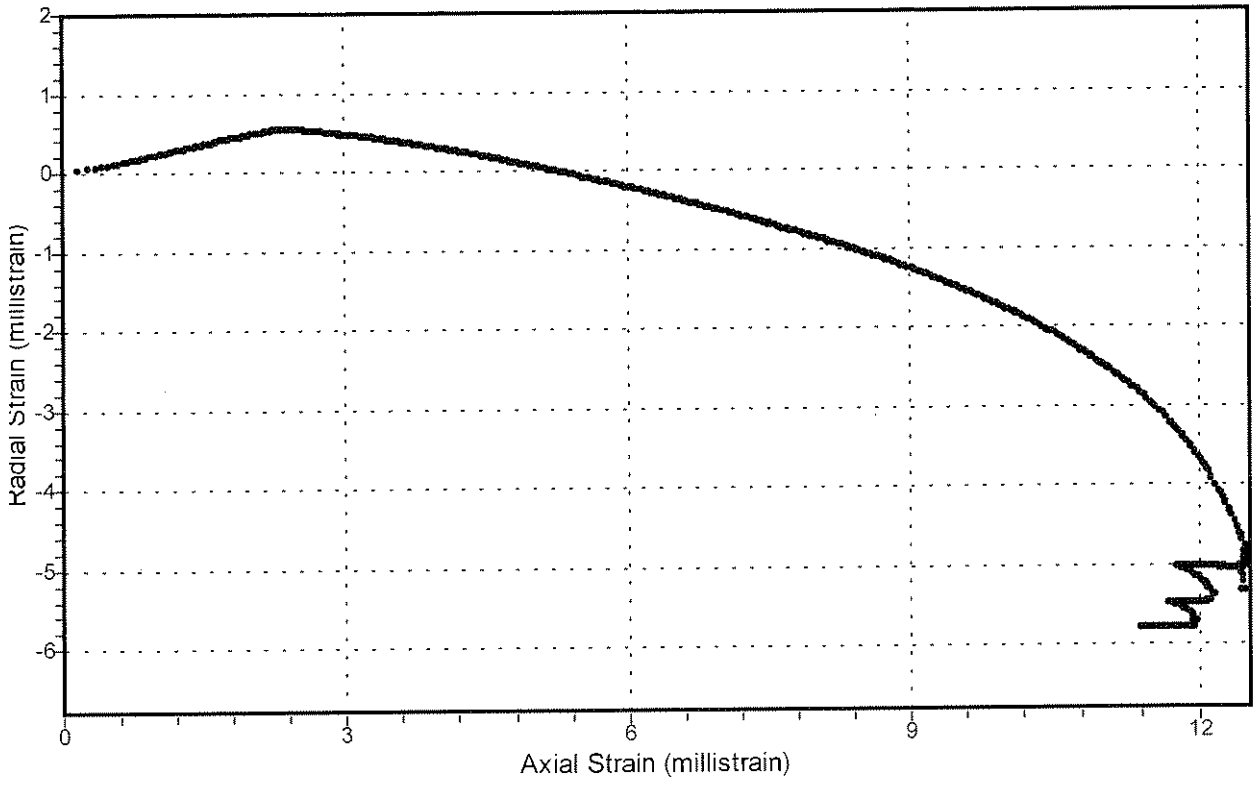

2001-08-27 18:29:44

Ventersdorp Lava

Triaxial time dependant behaviour

Specimen No: 2056-123td Confinement: 40.0 MPa

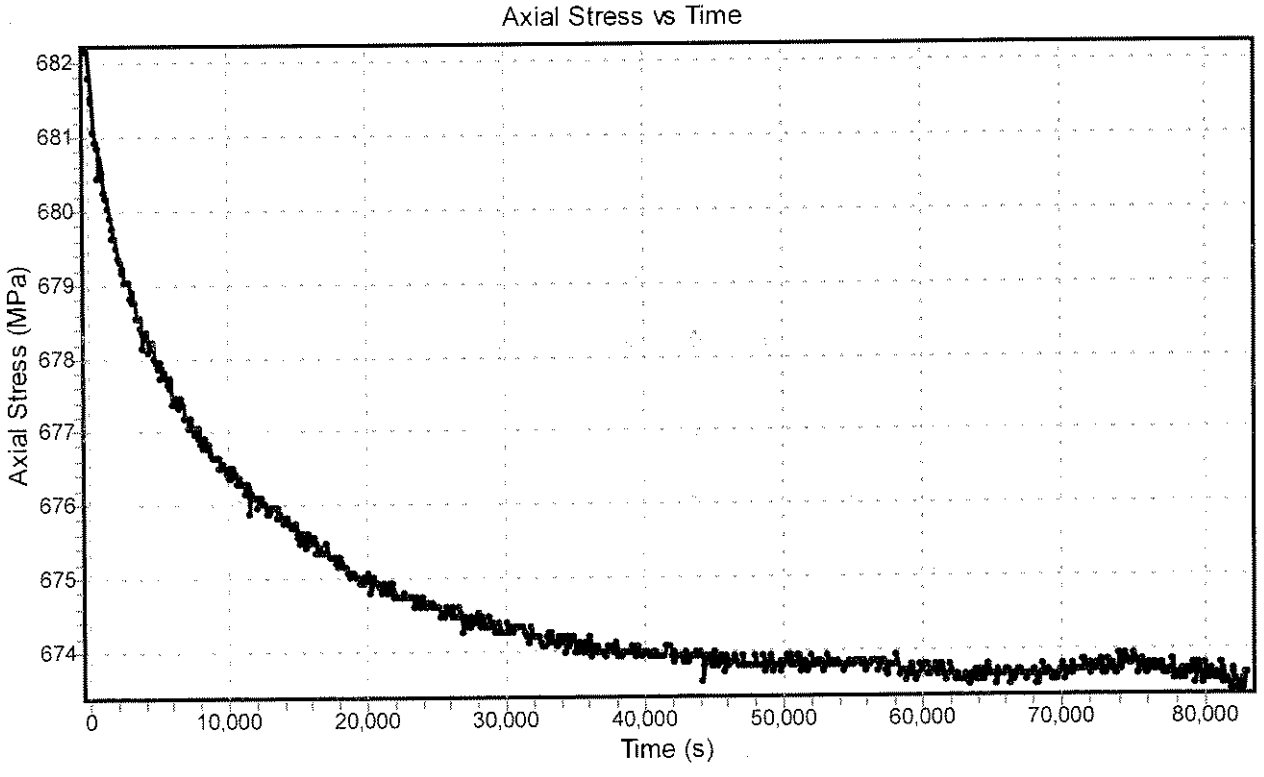

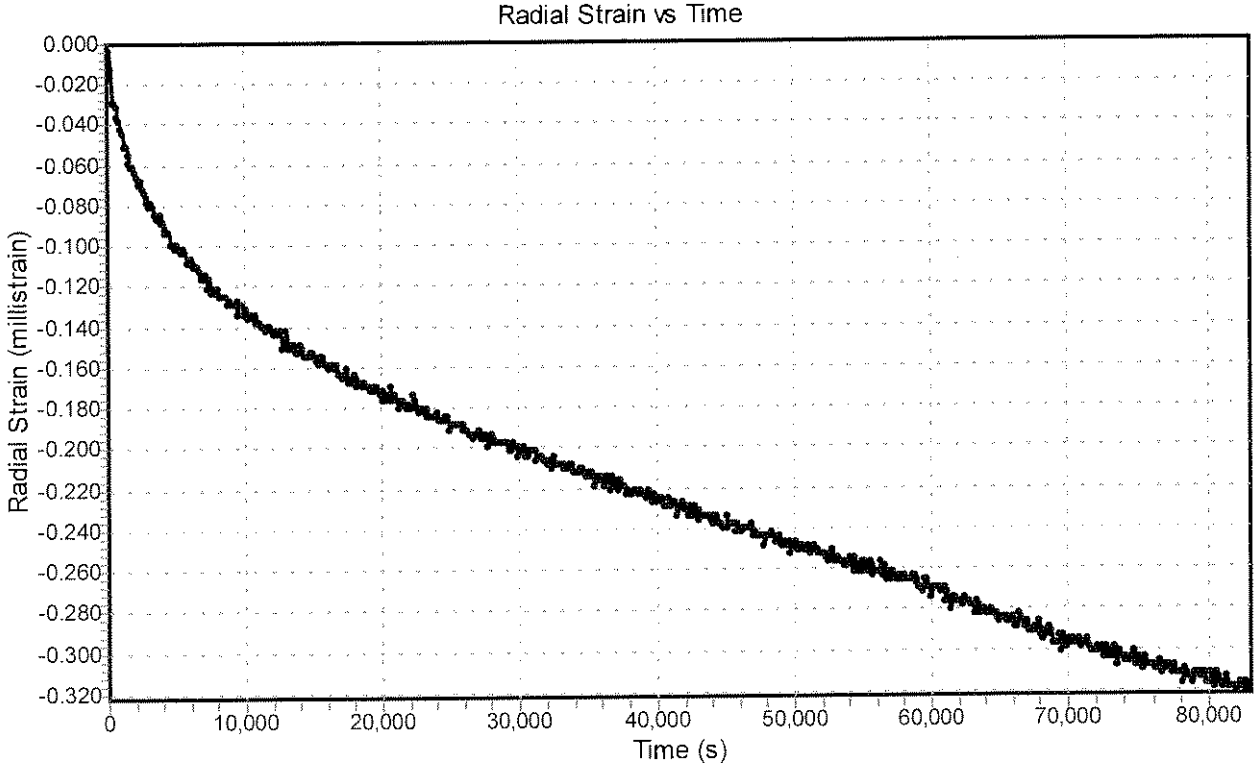

2001-08-27 19:08:51

UNIVERSITEIT VAN PRETORIA
UNIVERSITY OF PRETORIA
YUNIBESITHI YA PRETORIA

CSIR MININGTEK

Ventersdorp Lava

Triaxial compressive strength test with axial and lateral deformation measurements (MTS Machine)

Specimen No: 2056-TCM-124

Strength:	778.0 MPa	Modulus:	81.2 GPa
Confinement:	40.0 MPa	Poisson's Ratio:	0.31

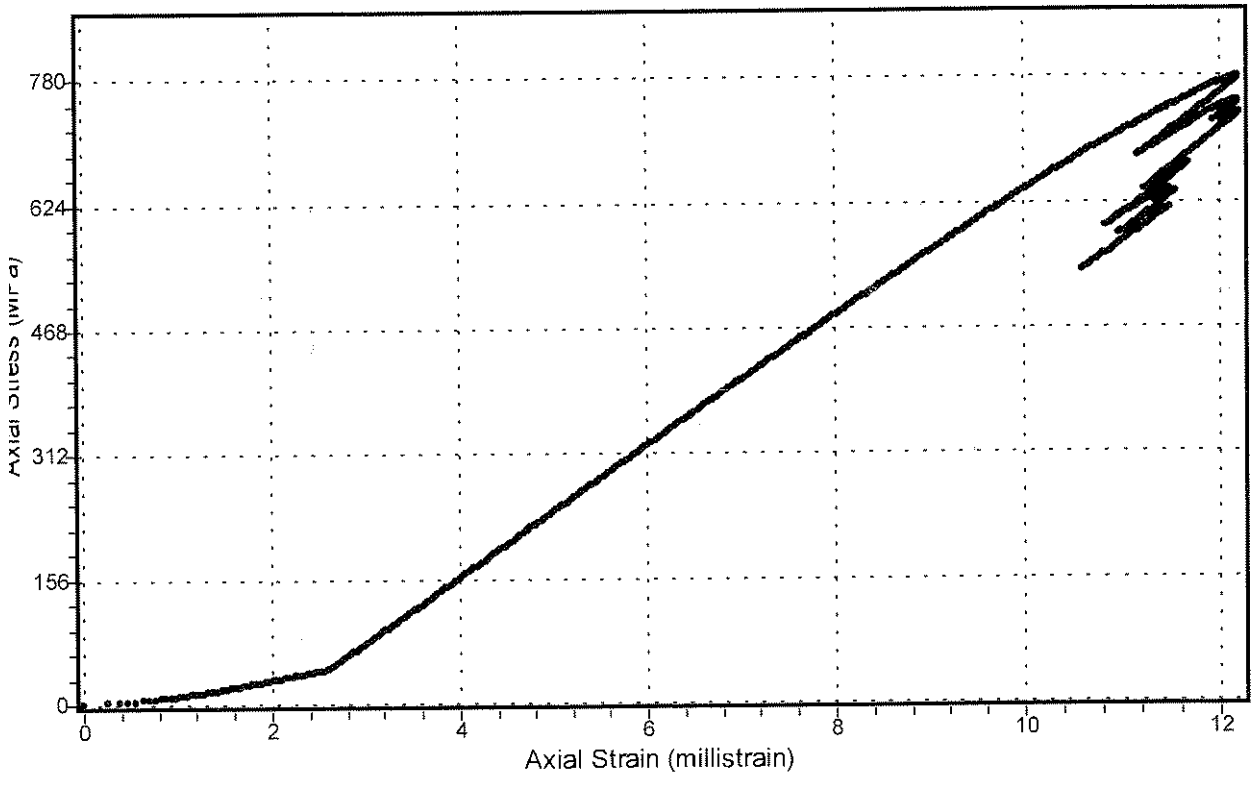

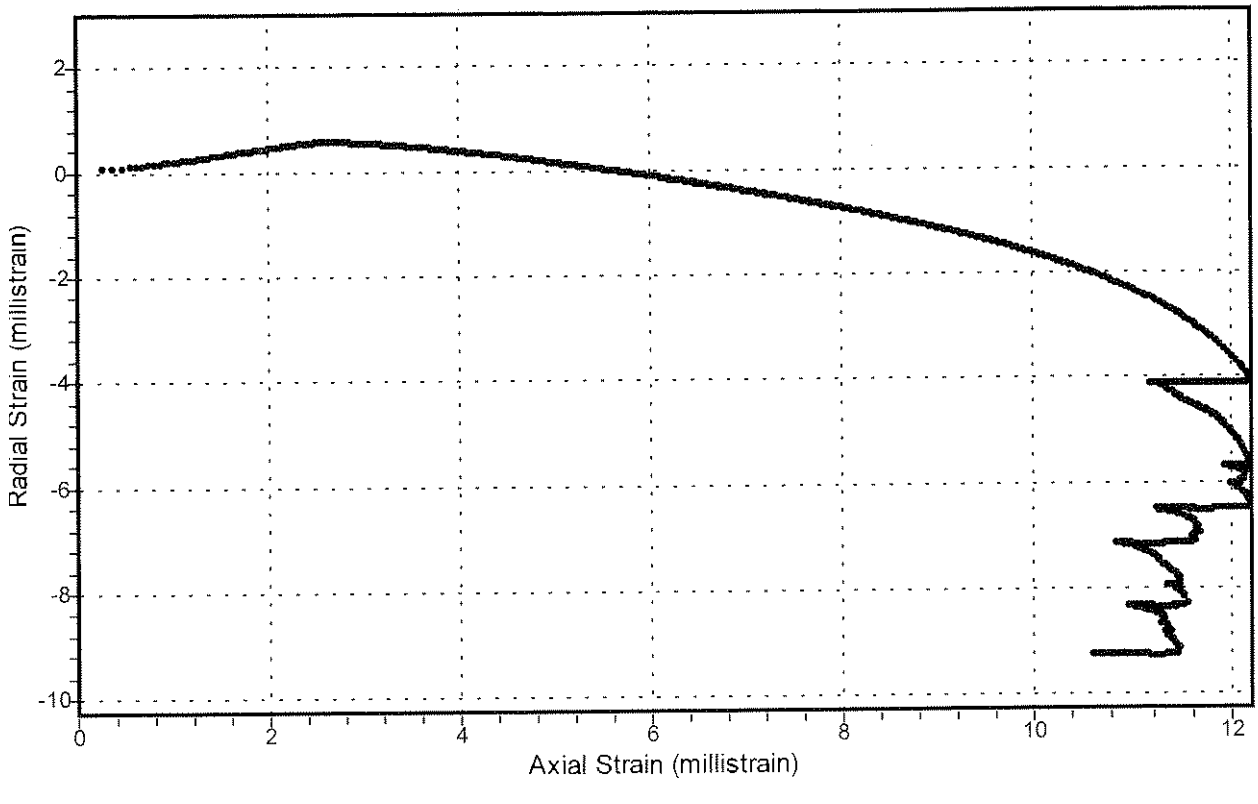

2001-08-27 18:31:35

Ventersdorp Lava

Triaxial time dependant behaviour

Specimen No: 2056-124td Confinement: 40.0 MPa

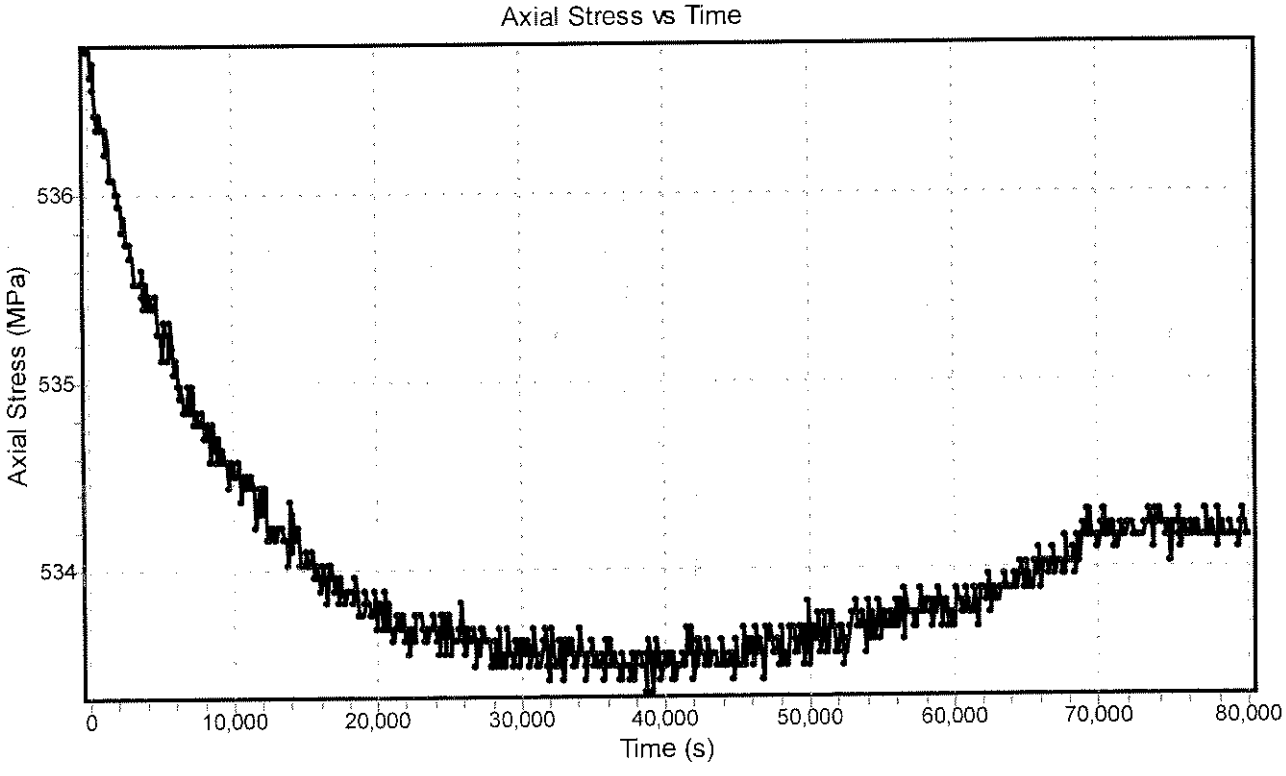

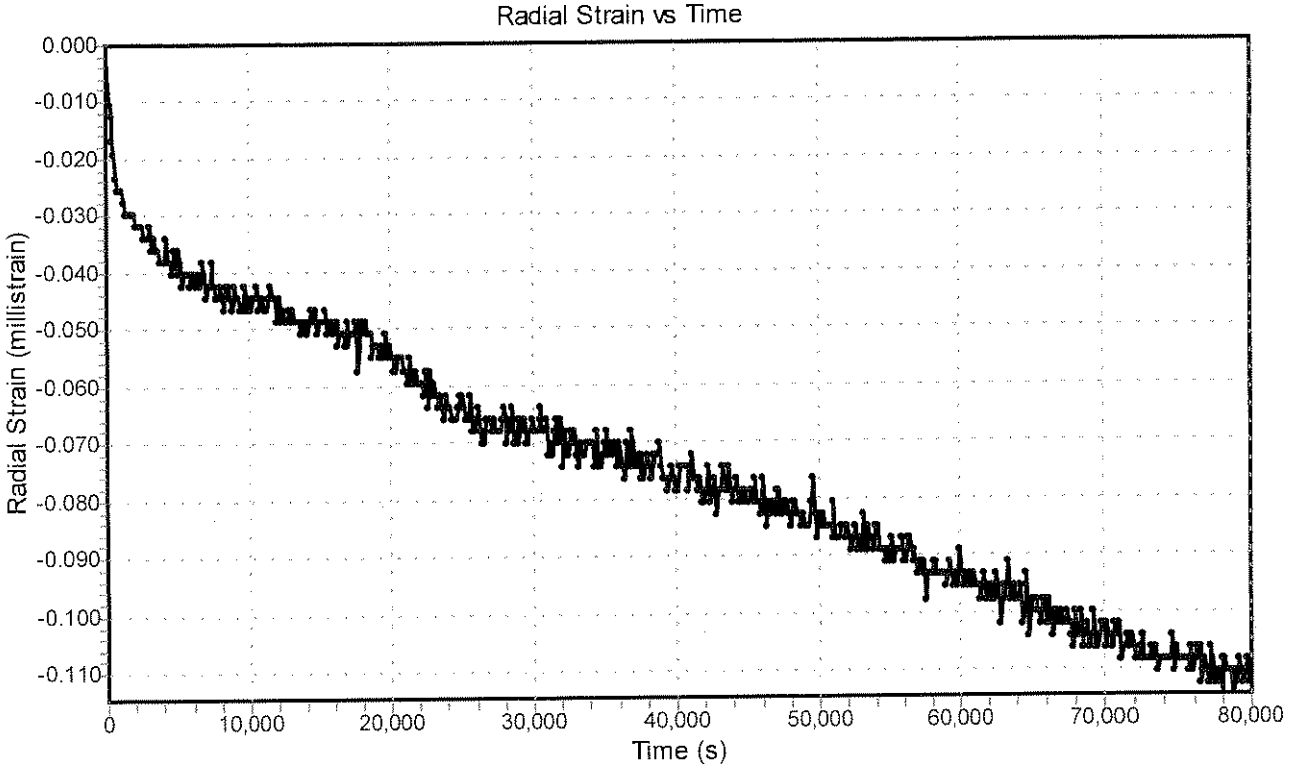

2001-08-27 19:10:09

UNIVERSITEIT VAN PRETORIA
UNIVERSITY OF PRETORIA
YUNIBESITHI YA PRETORIA

CSIR MININGTEK

Ventersdorp Lava

Triaxial compressive strength test with axial and lateral deformation measurements (MTS Machine)

Specimen No: 2056-TCM-126

Strength:	745.8 MPa	Modulus:	77.5 GPa
Confinement:	40.0 MPa	Poisson's Ratio:	0.29

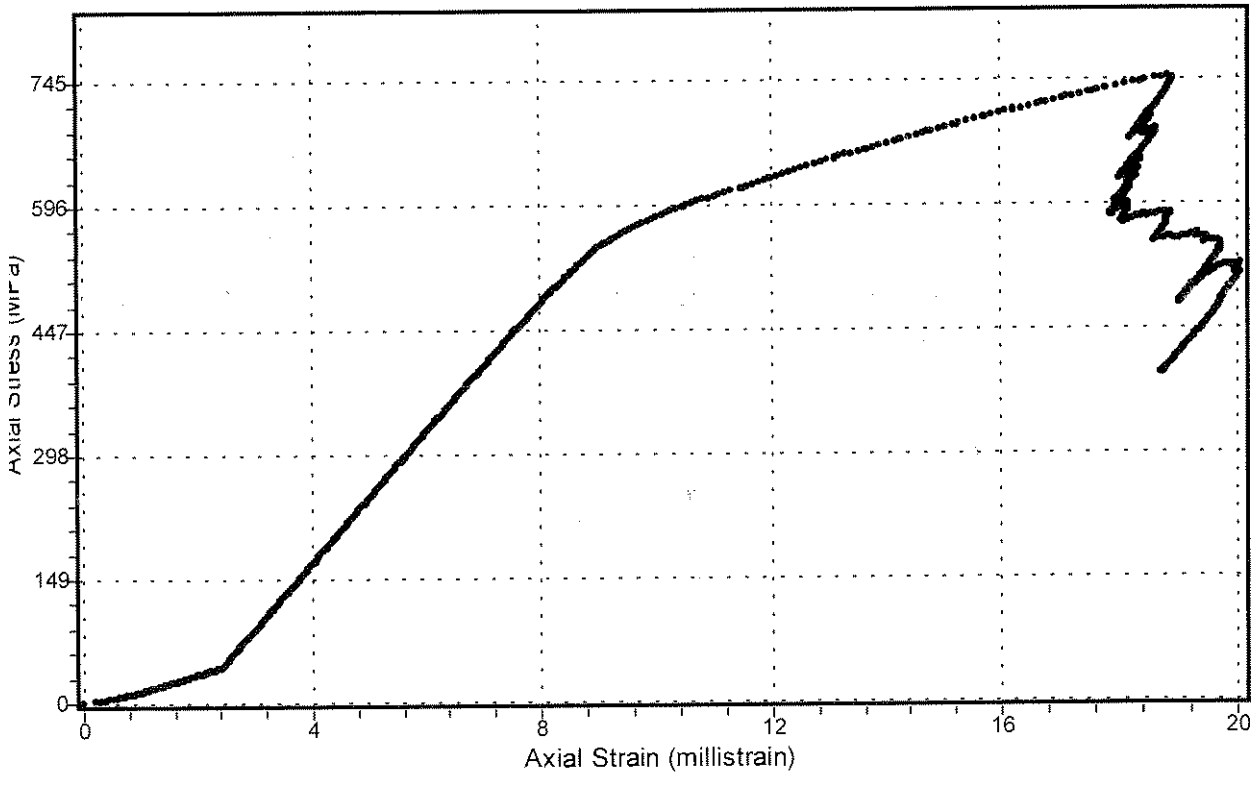

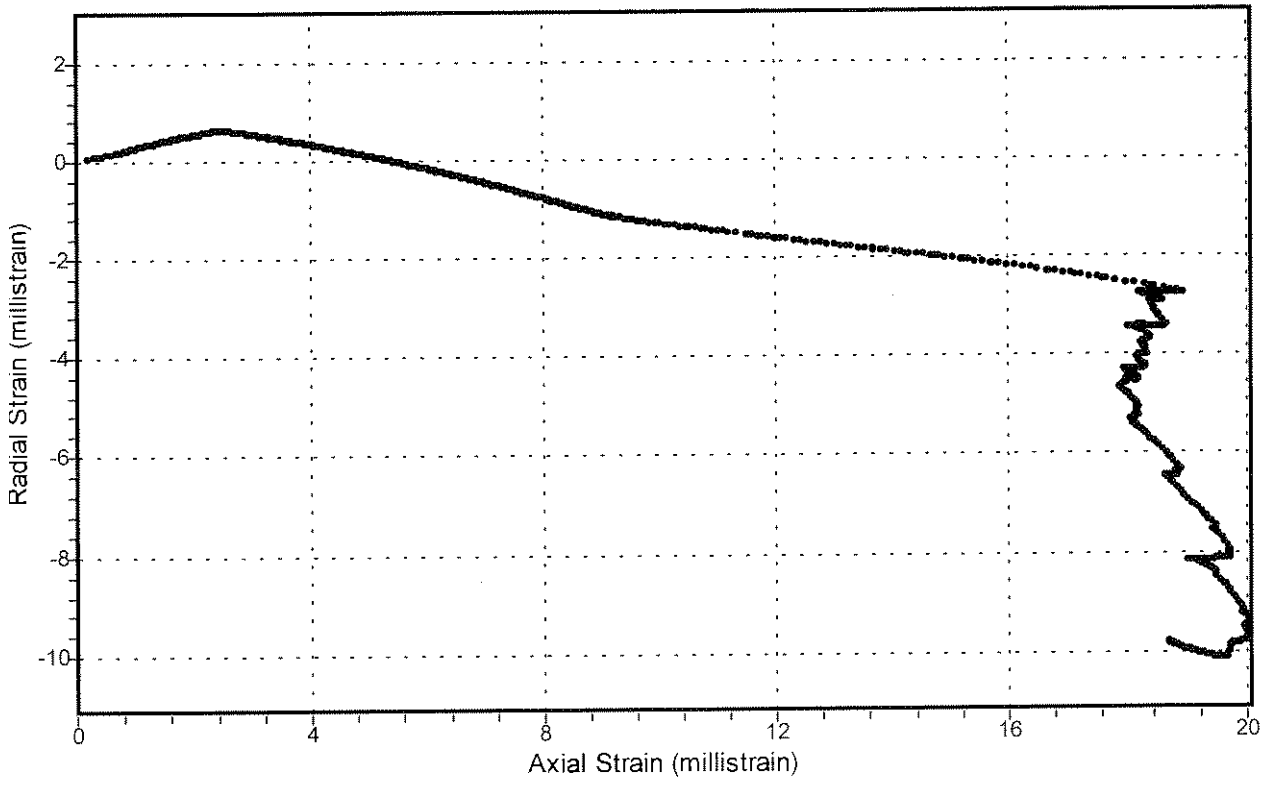

2001-08-27 18:33:56

Ventersdorp Lava

Triaxial time dependant behaviour

Specimen No: 2056-126td Confinement: 40.0 MPa

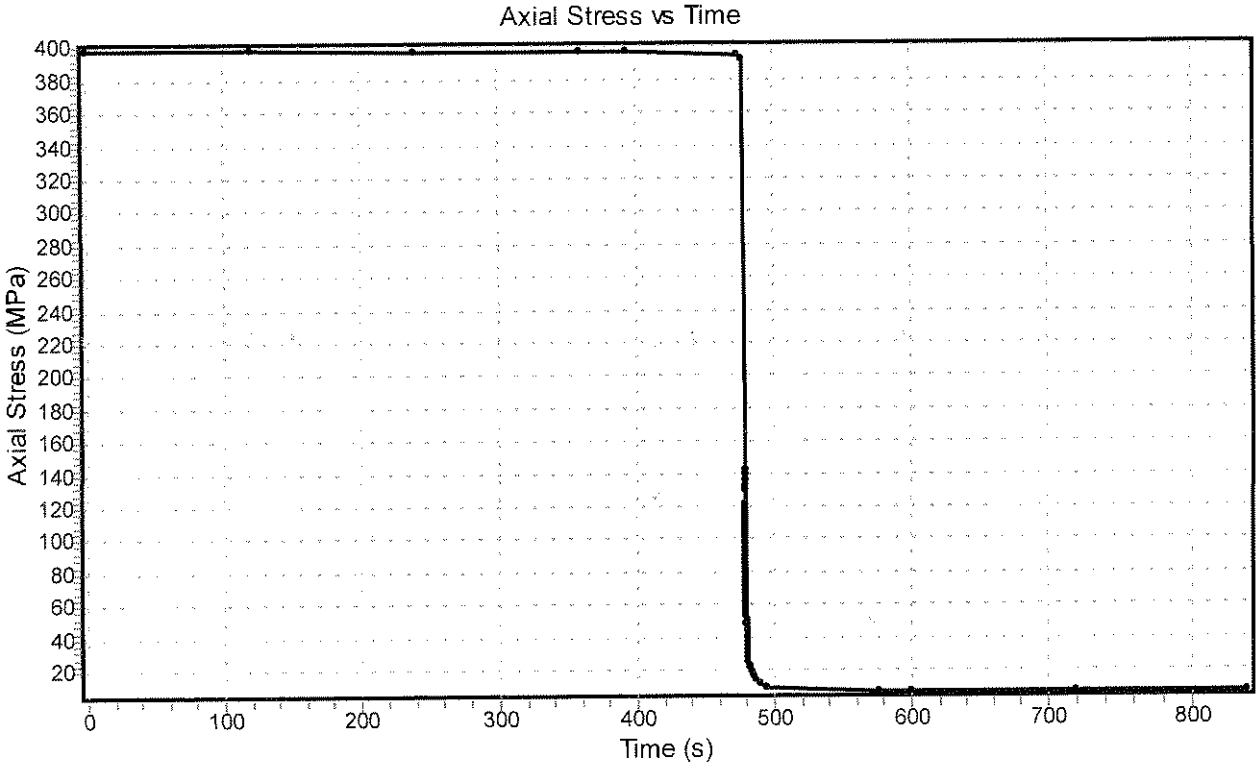

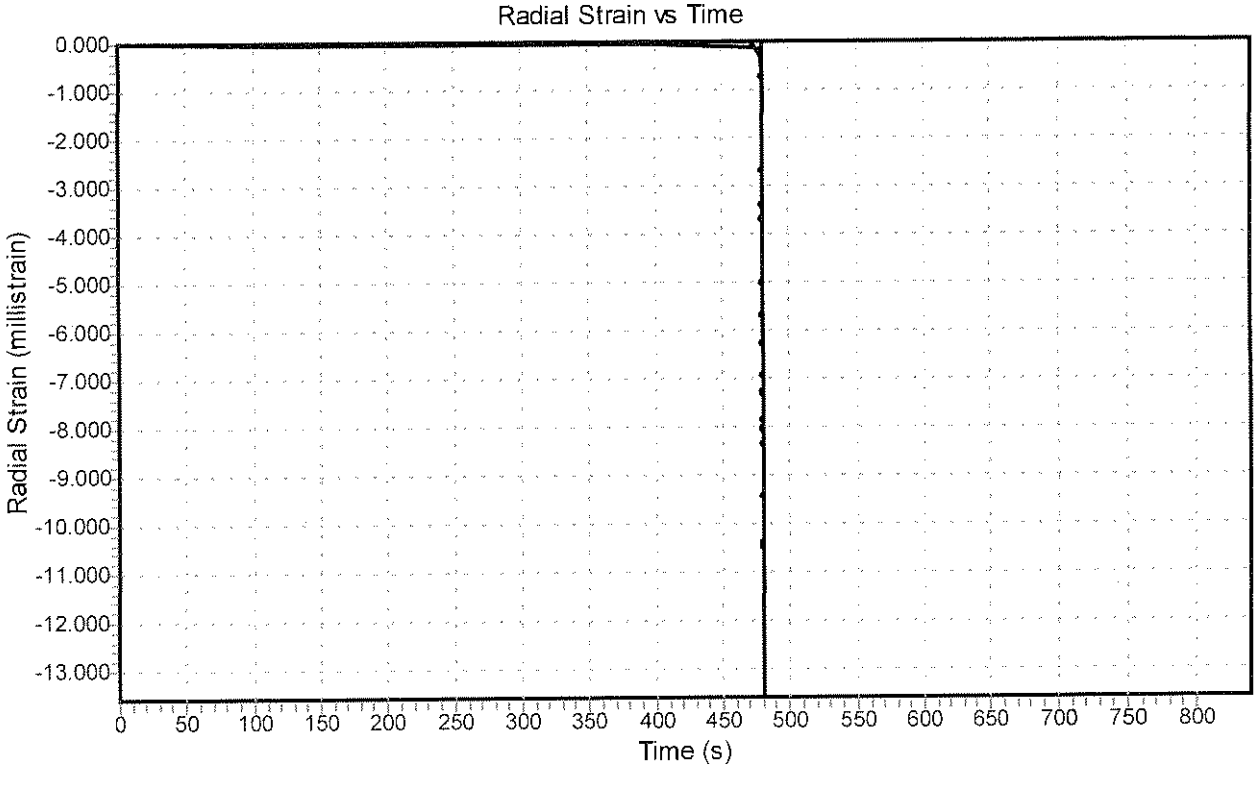

2001-08-27 19:13:41

UNIVERSITEIT VAN PRETORIA
UNIVERSITY OF PRETORIA
YUNIBESITHI YA PRETORIA

CSIR MININGTEK

Elsburg Quartzite

Triaxial compressive strength test with axial and lateral deformation measurements (MTS Machine)

Specimen No: 2056-TCM-155

Strength:	385.6 MPa	Modulus:	54.2 GPa
Confinement:	40.0 MPa	Poisson's Ratio:	0.30

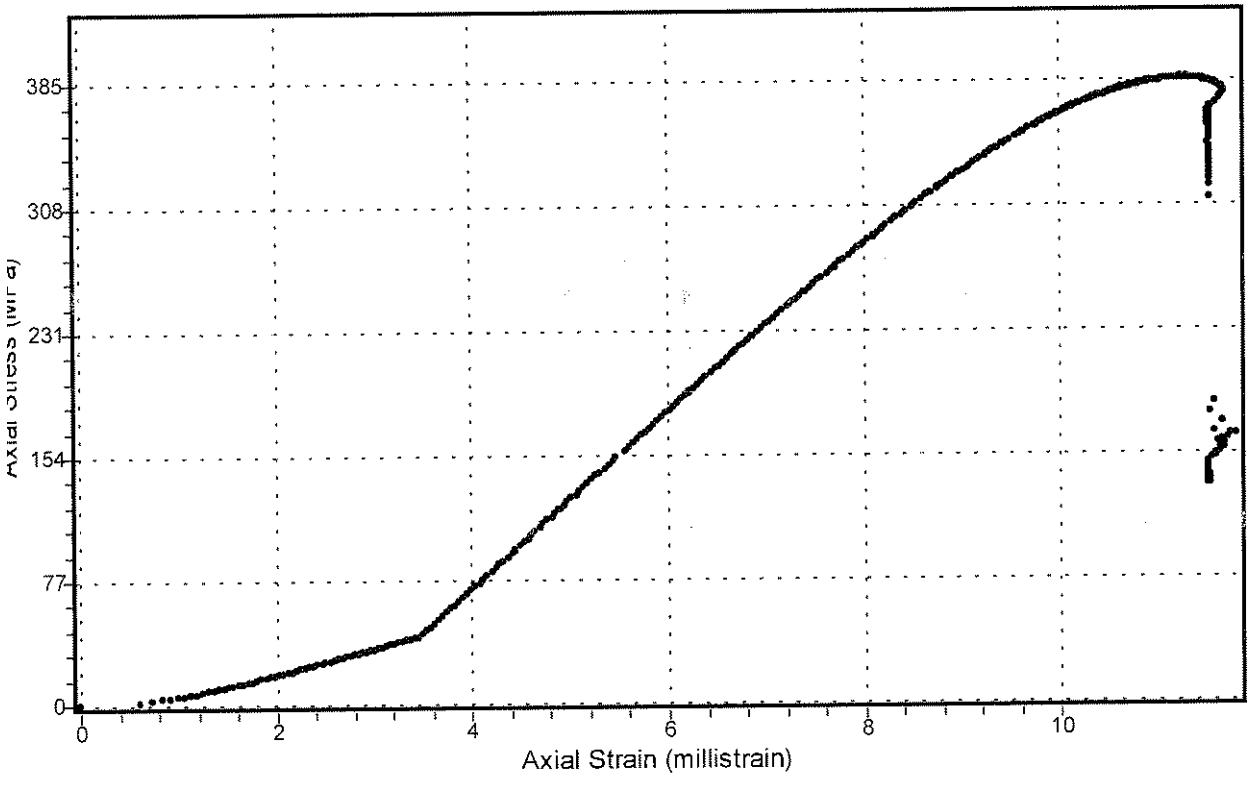

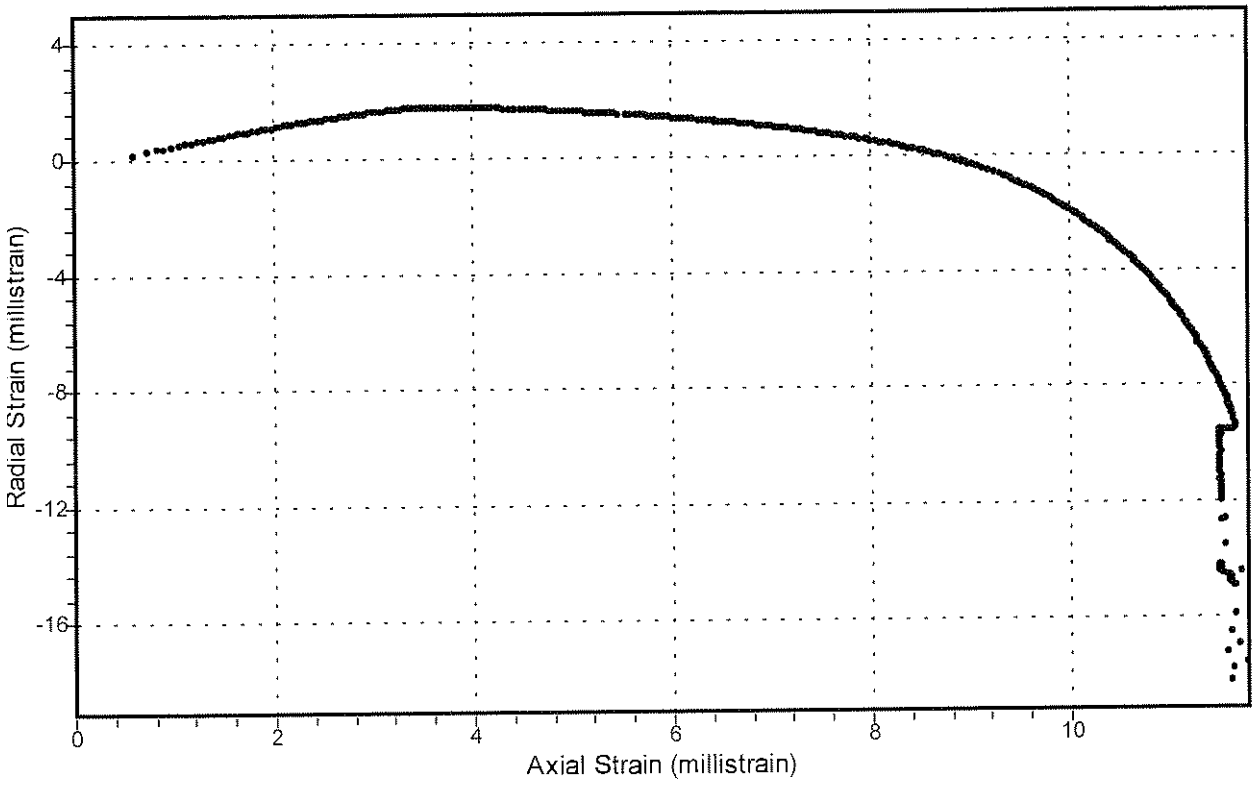

2001-08-27 18:35:33

Elsburg Quartzite

Triaxial time dependant behaviour

Specimen No: 2056-155td Confinement: 40.0 MPa

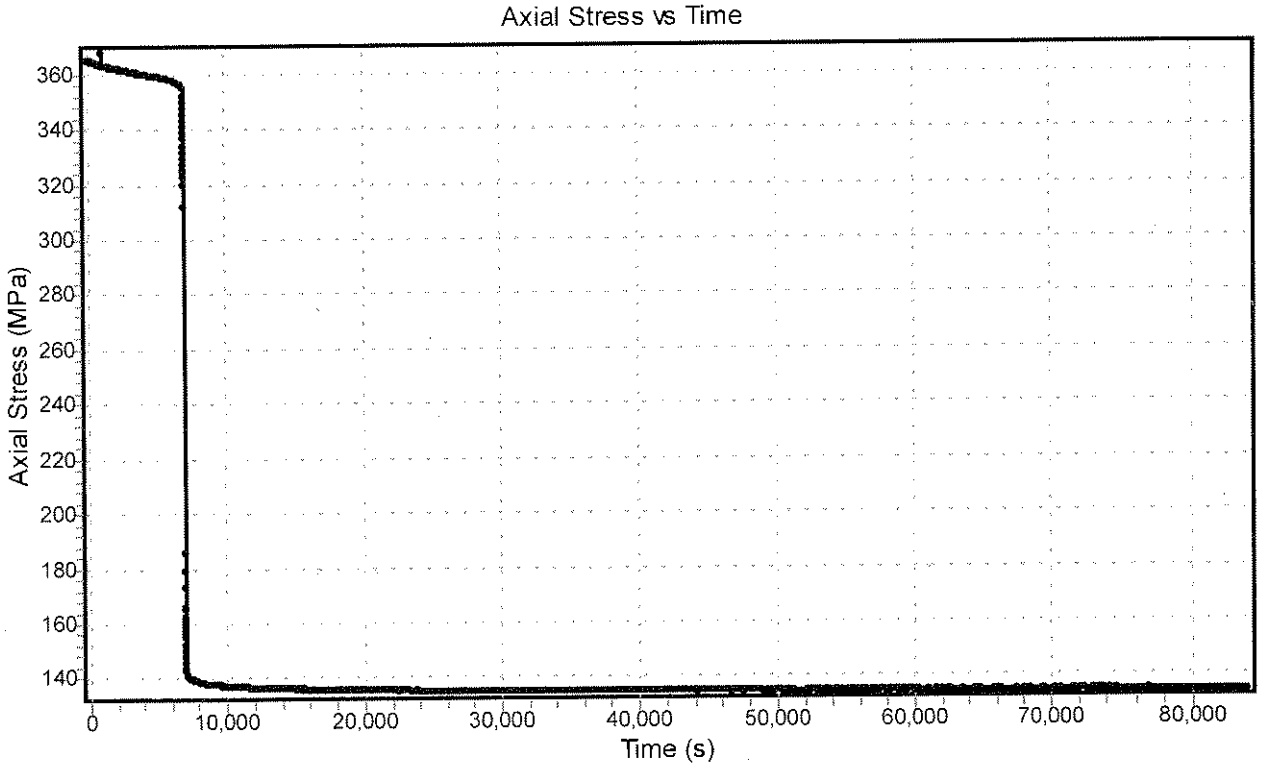

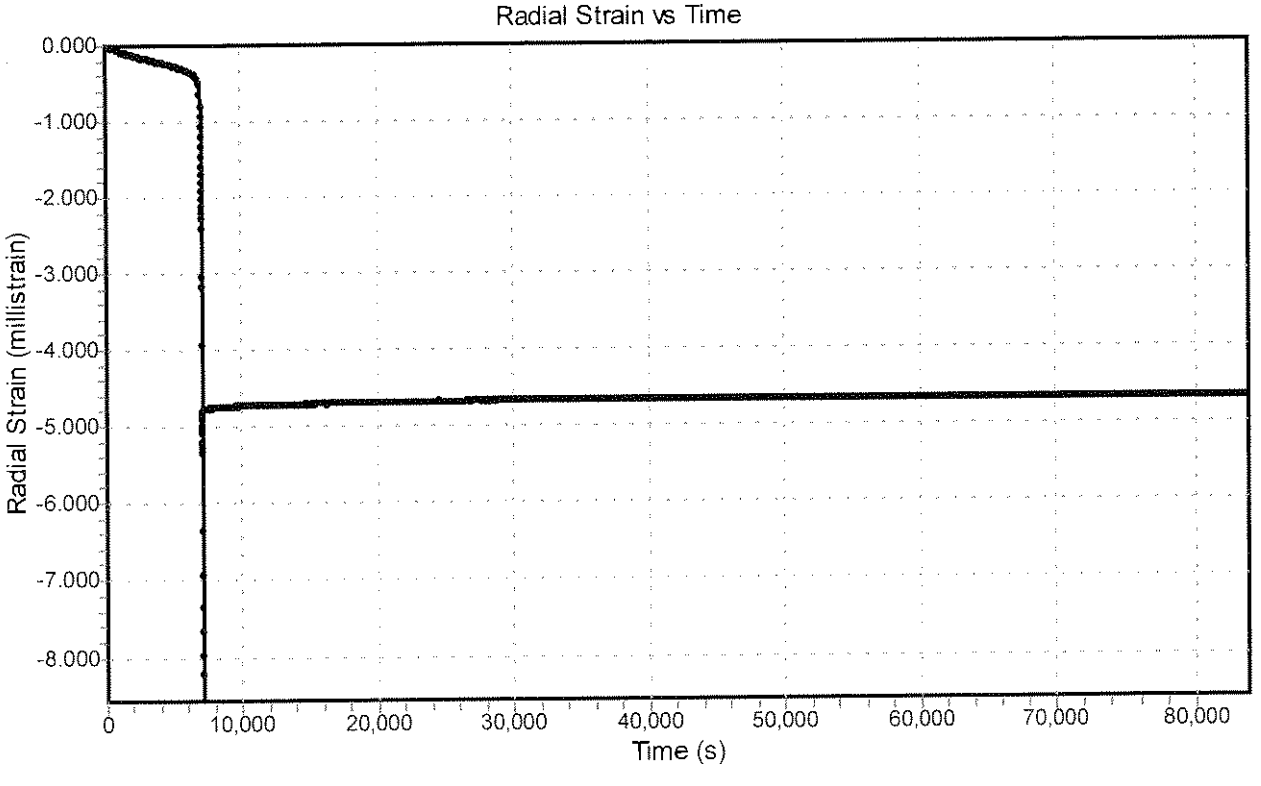

2001-08-27 19:24:22

UNIVERSITEIT VAN PRETORIA
UNIVERSITY OF PRETORIA
YUNIBESITHI YA PRETORIA

CSIR MININGTEK

Elsburg Quartzite

Triaxial compressive strength test with axial and lateral deformation measurements (MTS Machine)

Specimen No: 2056-TCM-157

Strength:	310.6 MPa	Modulus:	45.6 GPa
Confinement:	40.0 MPa	Poisson's Ratio:	0.27

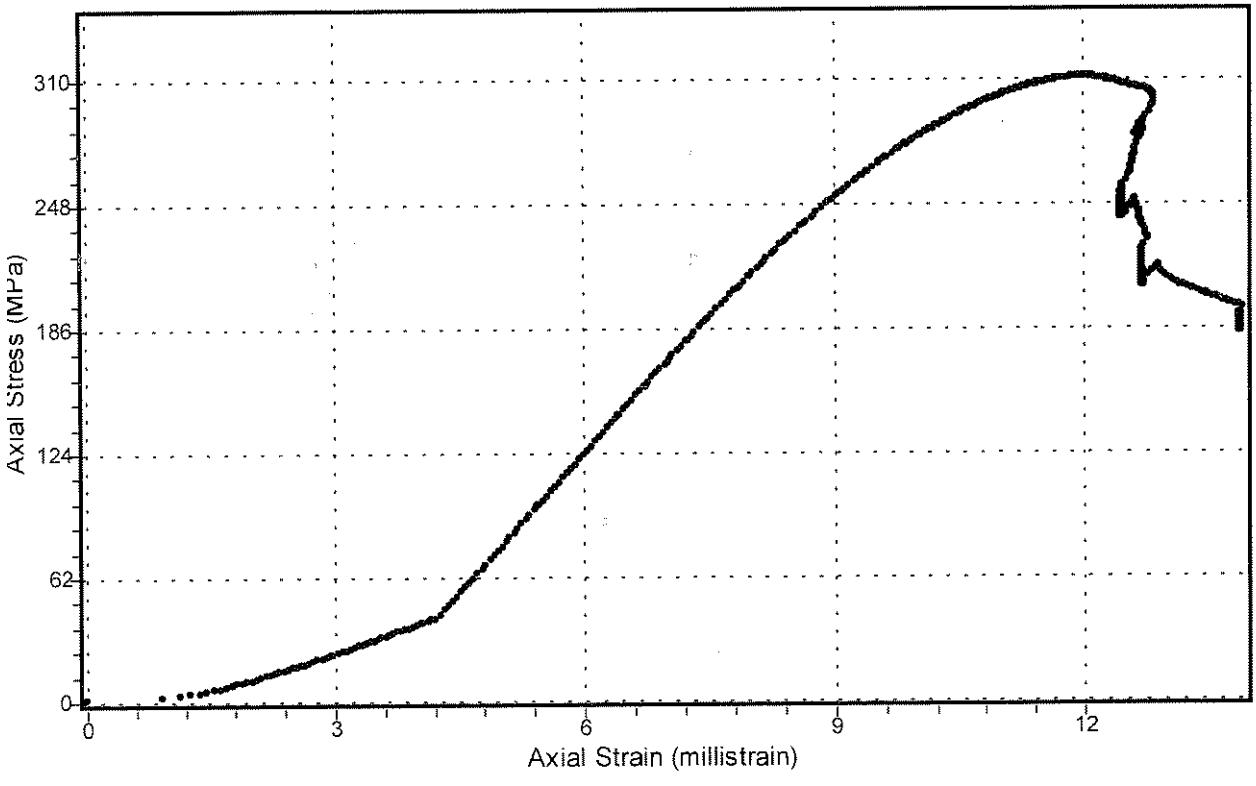

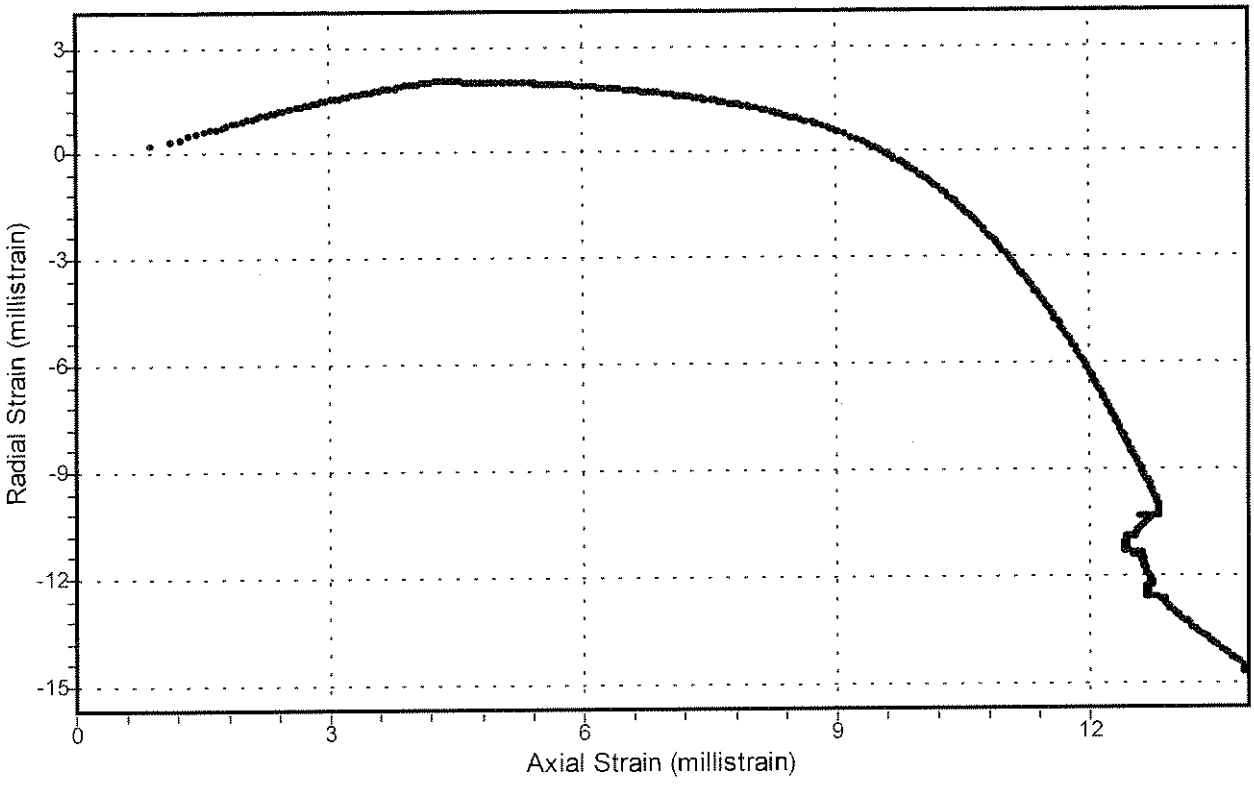

2001-08-27 18:47:08

Elsburg Quartzite

Triaxial time dependant behaviour

Specimen No: 2056-157td-1 Confinement: 40.0 MPa

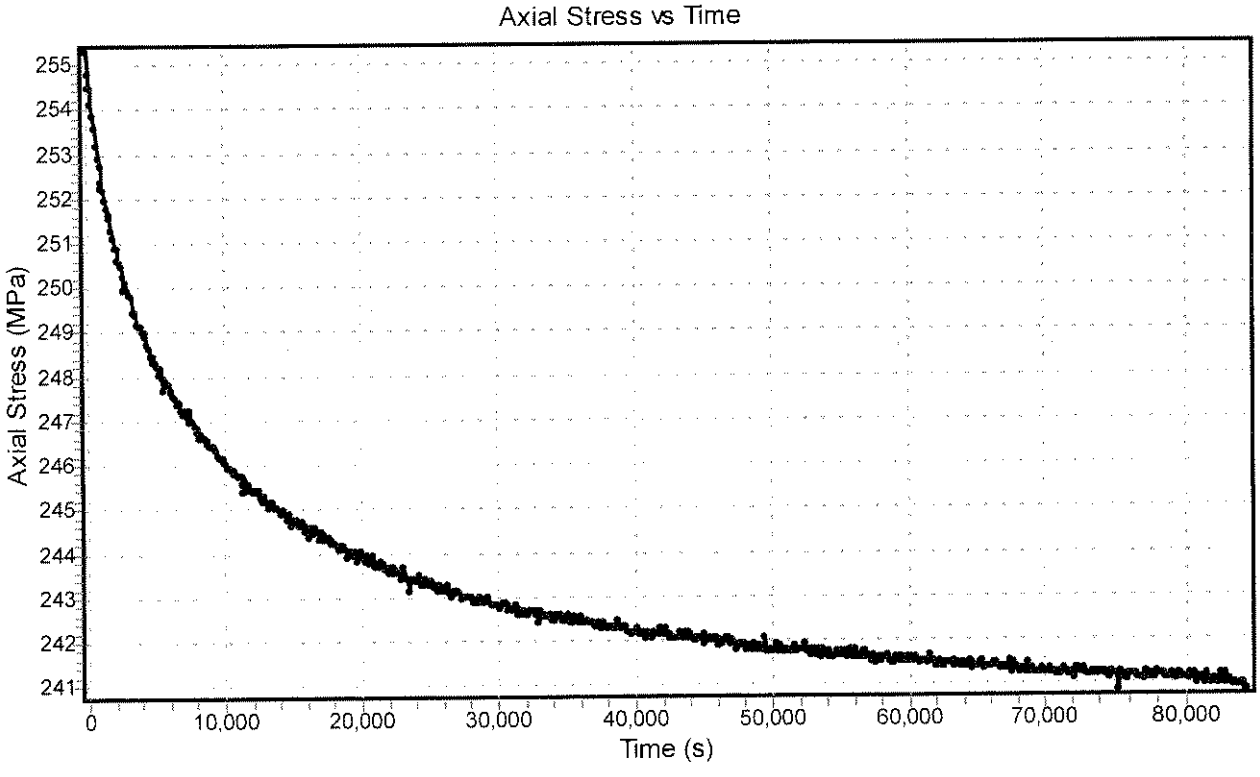

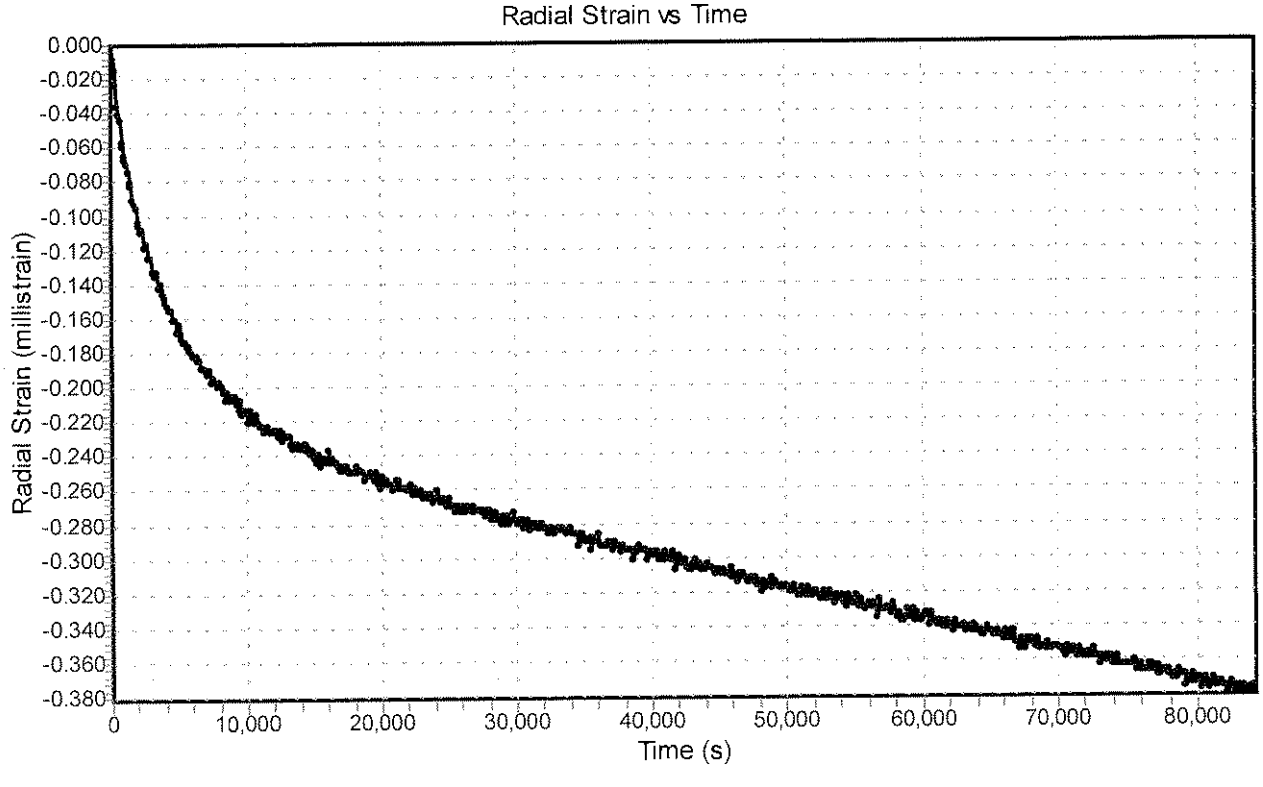

2001-08-27 19:16:33

Elsburg Quartzite

Triaxial time dependant behaviour

Specimen No: 2056-157td-2 Confinement: 40.0 MPa

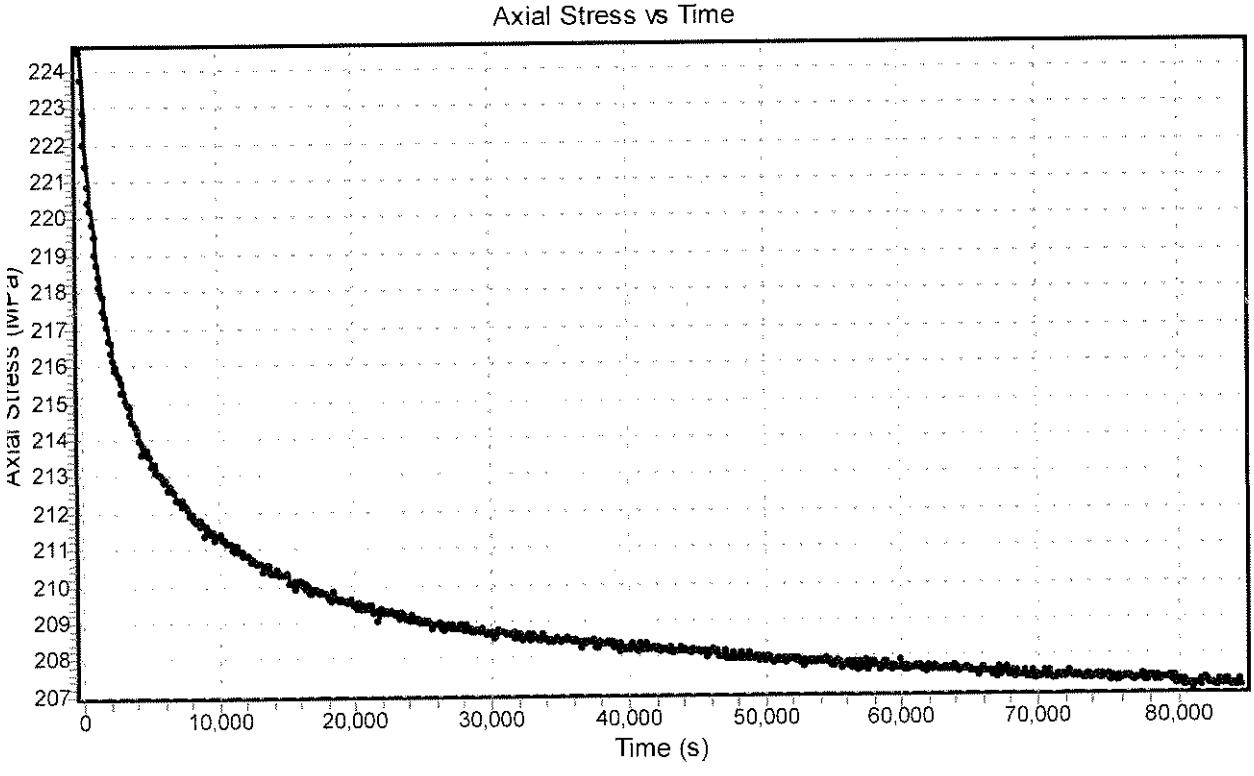

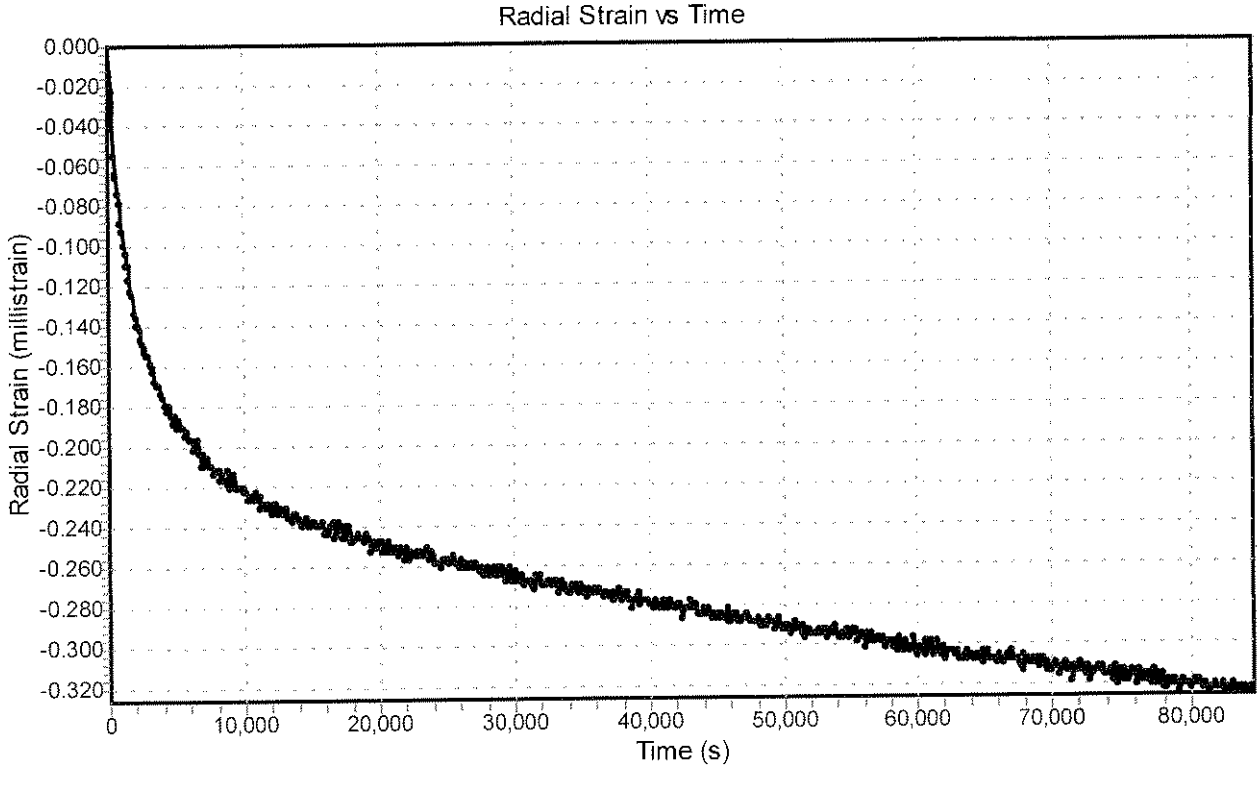

2001-08-27 19:18:40

Elsburg Quartzite

Triaxial time dependant behaviour

Specimen No: 2056-157td-3 Confinement: 40.0 MPa

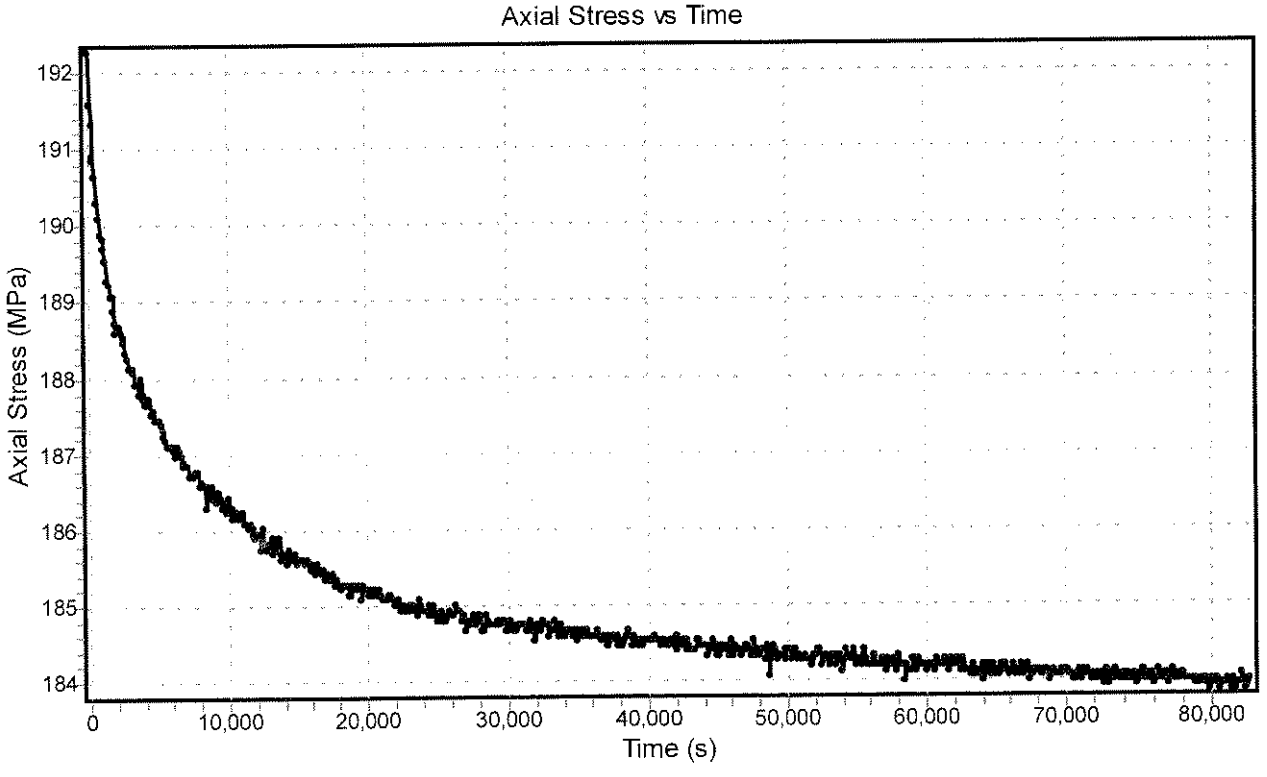

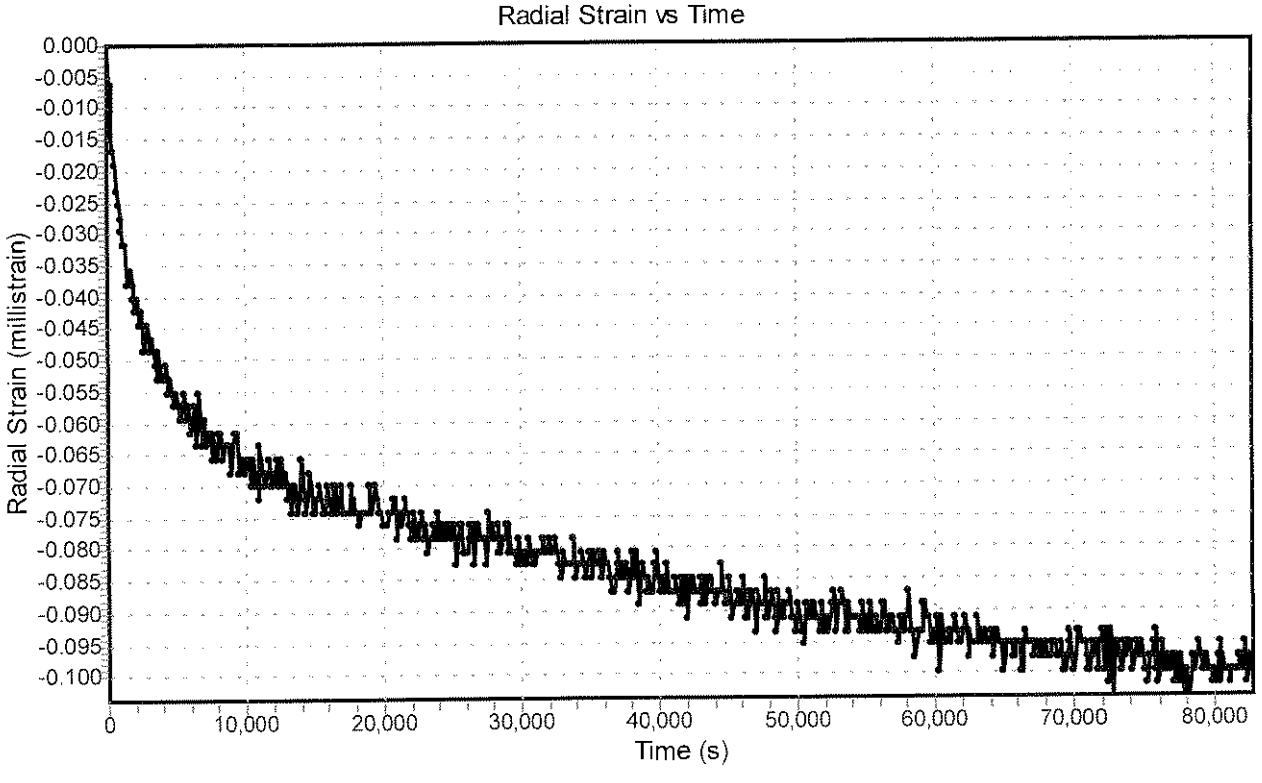

2001-08-27 19:19:58

Appendix E

MTS Teststar II procedures for triaxial post-failure relaxation tests (multiple relaxation steps)

TestWare-SX

Procedure Name = KD-TXCPM Default Procedure
File Specification = C:\TS2\790.60\KD-TXCPM.000
Software Version = 3.1A
Printout Date = 05-21-2001 11:03:53 AM

Data File Options
File Format = Excel Text File
Log Events = Yes
Include Procedure Description = No

Recovery Options
Autosave disabled.

Specimen Pre-test Information : Step
Step Done Trigger 1 = Specimen Pre-test Information

Specimen Pre-test Information : Data Input
Start Trigger = Step Start
End Trigger = <none>
Window = Pre-test Specimen Data Input
Utilization = Process Parameterization and Execution
Test Type = Triaxial
Specific Test = Single Failure
Test Title = Triaxial Single Failure Test

Hydrostat & Load ramp : Step
Step Done Trigger 1 = Hold

Query Start of Test : Operator Event
Start Trigger = Step Start
End Trigger = <none>
Button ID = Button 1
Single Shot = Yes
Button Label = Start
Description = Press to start the test for this specimen.
Grab Focus = Yes

Data Collection Hydrostat : Data Acquisition
Start Trigger = Query Start of Test
End Trigger = Hydrostatic Pressure Ramp
Mode = Level Crossing
Buffer Type = Continuous
Master Channel = Time
Slave Channel 1 = Axial LVDT
Slave Channel 2 = InVessel Load
Slave Channel 3 = Axial Strain
Slave Channel 4 = Circ. Disp
Slave Channel 5 = Conf. Pressure
Slave Channel 6 = Axial def (mm)
Data Header = Hydrostat
Level Increment = 5 (Sec)
Buffer Size = 4096

Load vs. Displacement Plot : Run-time Plotting
Start Trigger = Query Start of Test
End Trigger = <none>
Title = Load vs Displacement
X Axis = Y
Channel = InVessel Load
Scaling = Linear

Minimum = 0.000000 kN
Maximum = 1.000000 kN
Y Axis = X
Channel 1 = Axial LVDT
Color = Red
Style = Solid
Channel 2 = Axial def (mm)
Color = Blue
Style = Solid
Channel 3 = Circ. Disp
Color = Black
Style = Solid
Scaling = Linear
Minimum = 0.000000 mm
Maximum = 1.000000 mm
X Axis Level Cross = Not Enabled
Y Axis Level Cross = Not Enabled
Reduce Rate on Decimation = Not Enabled

Sigma 1 vs Sigma 3 Plot : Run-time Plotting
Start Trigger = Query Start of Test
End Trigger = Hydrostatic Pressure Ramp
Title = Sigma 1 vs Sigma 3
X Axis = X
Channel = Conf. Pressure
Scaling = Linear
Minimum = 0.000000 MPa
Maximum = 1.000000 MPa
Y Axis = Y
Channel 1 = Sigma 1
Color = Red
Style = Solid
Channel 2 = <none>
Color = Blue
Style = Solid
Channel 3 = <none>
Color = Black
Style = Solid
Scaling = Linear
Minimum = 0.000000 MPa
Maximum = 1.000000 MPa
X Axis Level Cross = Not Enabled
Y Axis Level Cross = Not Enabled
Reduce Rate on Decimation = Not Enabled

Hydrostatic Pressure Ramp : Monotonic Command
Start Trigger = Query Start of Test
End Trigger = <none>
Segment Shape = Ramp
Time = 5 Min
Axial
Control Mode = Load SG
End level = 55 (kN)
Confining
Control Mode = Conf.Pressure SG
End level = 40 MPa

Hold : Hold Command
Start Trigger = Hydrostatic Pressure Ramp
End Trigger = <none>
Hold Time = 5 (Sec)
Axial
Control Mode = Load SG

Data Load : Data Acquisition
Start Trigger = Hold
End Trigger = <none>
Mode = Level Crossing
Buffer Type = Continuous
Master Channel = InVessel Load
Slave Channel 1 = Time
Slave Channel 2 = Axial LVDT
Slave Channel 3 = Axial Strain
Slave Channel 4 = Circ. Disp
Slave Channel 5 = Conf. Pressure
Slave Channel 6 = Axial def (mm)
Data Header = Data Load
Level Increment = 3 (kN)
Buffer Size = 10000

data circ. disp : Data Acquisition
Start Trigger = Hold
End Trigger = <none>
Mode = Level Crossing
Buffer Type = Continuous
Master Channel = Circ. Disp
Slave Channel 1 = Time
Slave Channel 2 = Axial LVDT
Slave Channel 3 = InVessel Load
Slave Channel 4 = Axial Strain
Slave Channel 5 = Conf. Pressure
Slave Channel 6 = Axial def (mm)
Data Header = data circ. disp
Level Increment = 0.01 (mm)
Buffer Size = 6000

Operator Terminate the Test : Operator Event
Start Trigger = Query Start of Test
End Trigger = <none>
Button ID = Button 3
Single Shot = Yes
Button Label = Terminate
Description = Press to terminate the test for this specimen.
Grab Focus = Yes

testing 1 : Step
Step Done Trigger 1 = hold Axial LVDT
Step Done Trigger 2 = end creep (op ev)

Load vs. Displacement Plot : Run-time Plotting
Start Trigger = Step Start
End Trigger = Creep (op. event)
Title = Load vs Displacement
X Axis = Y
Channel = InVessel Load
Scaling = Linear
Minimum = 0.000000 kN
Maximum = 1.000000 kN
Y Axis = X
Channel 1 = Axial LVDT
Color = Red
Style = Solid
Channel 2 = Axial def (mm)
Color = Blue
Style = Solid

Channel 3 = Circ. Disp
Color = Black
Style = Solid
Scaling = Linear
Minimum = 0.000000 mm
Maximum = 1.000000 mm
X Axis Level Cross = Not Enabled
Y Axis Level Cross = Not Enabled
Reduce Rate on Decimation = Not Enabled

Circ. Disp. Ramp 1 : Run-time Rate Control
Start Trigger = Step Start
End Trigger = Creep (op. event)
Segment Shape = Ramp
Axial
Control Mode = Circ. Disp SG
Rate Type = 0.010000 mm/Min
Minimum Rate = 0.000100 mm/Min
Maximum Rate = 1.000000 mm/Min
Endlevel = 7.5 (mm)

Data Load : Data Acquisition
Start Trigger = Step Start
End Trigger = Creep (op. event)
Mode = Level Crossing
Buffer Type = Continuous
Master Channel = InVessel Load
Slave Channel 1 = Time
Slave Channel 2 = Axial LVDT
Slave Channel 3 = Axial Strain
Slave Channel 4 = Circ. Disp
Slave Channel 5 = Conf. Pressure
Slave Channel 6 = Axial def (mm)
Data Header = Data Load
Level Increment = 3 (kN)
Buffer Size = 10000

data circ. disp : Data Acquisition
Start Trigger = Step Start
End Trigger = Creep (op. event)
Mode = Level Crossing
Buffer Type = Continuous
Master Channel = Circ. Disp
Slave Channel 1 = Time
Slave Channel 2 = Axial LVDT
Slave Channel 3 = InVessel Load
Slave Channel 4 = Axial Strain
Slave Channel 5 = Conf. Pressure
Slave Channel 6 = Axial def (mm)
Data Header = data circ. disp
Level Increment = 0.01 (mm)
Buffer Size = 6000

Creep (op. event) : Operator Event
Start Trigger = Step Start
End Trigger = <none>
Button ID = Button 1
Single Shot = Yes
Button Label = Creep
Description =
Grab Focus = Yes

hold Axial LVDT : Hold Command

```
    Start Trigger    = Creep (op. event)
    End Trigger      = end creep (op ev)
    Hold Time        = 50 Hr
    Axial
       Control Mode     = Axial LVDT SG
    Confining
       Control Mode     = Conf.Pressure SG

end creep (op ev) : Operator Event
    Start Trigger    = Creep (op. event)
    End Trigger      = <none>
    Button ID        = Button 2
    Single Shot      = Yes
    Button Label     = End Creep
    Description      =
    Grab Focus       = Yes

Load-time plot : Run-time Plotting
    Start Trigger    = Creep (op. event)
    End Trigger      = end creep (op ev)
    Title            = Load vs Time
    X Axis           = X
       Channel       = Time
       Scaling       = Linear
       Minimum       = 0.000000 Sec
       Maximum       = 1.000000 Sec
    Y Axis           = Y
       Channel 1     = InVessel Load
          Color      = Red
          Style      = Solid
       Channel 2     = <none>
          Color      = Blue
          Style      = Solid
       Channel 3     = <none>
          Color      = Black
          Style      = Solid
       Scaling       = Linear
       Minimum       = 0.000000 kN
       Maximum       = 1.000000 kN
    X Axis Level Cross          = Not Enabled
    Y Axis Level Cross          = Not Enabled
    Reduce Rate on Decimation   = Enabled

creep data time : Data Acquisition
    Start Trigger    = Creep (op. event)
    End Trigger      = end creep (op ev)
    Mode             = Level Crossing
    Buffer Type      = Continuous
    Master Channel   = Time
    Slave Channel 1  = Axial LVDT
    Slave Channel 2  = InVessel Load
    Slave Channel 3  = Axial Strain
    Slave Channel 4  = Circ. Disp
    Slave Channel 5  = Conf. Pressure
    Slave Channel 6  = Axial def (mm)
    Data Header      = Creep Data Timed
    Level Increment  = 2 Min
    Buffer Size      = 8000

creep data Load : Data Acquisition
    Start Trigger    = Creep (op. event)
    End Trigger      = end creep (op ev)
    Mode             = Level Crossing
```

Buffer Type = Continuous
Master Channel = InVessel Load
Slave Channel 1 = Time
Slave Channel 2 = Axial LVDT
Slave Channel 3 = Axial Strain
Slave Channel 4 = Circ. Disp
Slave Channel 5 = Conf. Pressure
Slave Channel 6 = Axial def (mm)
Data Header = creep data Load
Level Increment = 3 (kN)
Buffer Size = 8000

testing 2 : Step
Step Done Trigger 1 = hold Axial LVDT
Step Done Trigger 2 = end creep (op ev)

Load vs. Displacement Plot : Run-time Plotting
Start Trigger = Step Start
End Trigger = Creep (op. event)
Title = Load vs Displacement
X Axis = Y
Channel = InVessel Load
Scaling = Linear
Minimum = 0.000000 kN
Maximum = 1.000000 kN
Y Axis = X
Channel 1 = Axial LVDT
Color = Red
Style = Solid
Channel 2 = Axial def (mm)
Color = Blue
Style = Solid
Channel 3 = Circ. Disp
Color = Black
Style = Solid
Scaling = Linear
Minimum = 0.000000 mm
Maximum = 1.000000 mm
X Axis Level Cross = Not Enabled
Y Axis Level Cross = Not Enabled
Reduce Rate on Decimation = Not Enabled

Circ. Disp. Ramp 1 : Run-time Rate Control
Start Trigger = Step Start
End Trigger = Creep (op. event)
Segment Shape = Ramp
Axial
Control Mode = Circ. Disp SG
Rate Type = 0.001000 mm/Min
Minimum Rate = 0.000100 mm/Min
Maximum Rate = 1.000000 mm/Min
Endlevel = 7.5 (mm)

Data Load : Data Acquisition
Start Trigger = Step Start
End Trigger = Creep (op. event)
Mode = Level Crossing
Buffer Type = Continuous
Master Channel = InVessel Load
Slave Channel 1 = Time
Slave Channel 2 = Axial LVDT
Slave Channel 3 = Axial Strain

```
    Slave Channel 4  = Circ. Disp
    Slave Channel 5  = Conf. Pressure
    Slave Channel 6  = Axial def (mm)
    Data Header      = Data Load
    Level Increment  = 3 ( kN )
    Buffer Size      = 10000

data circ. disp : Data Acquisition
    Start Trigger    = Step Start
    End Trigger      = Creep (op. event)
    Mode             = Level Crossing
    Buffer Type      = Continuous
    Master Channel   = Circ. Disp
    Slave Channel 1  = Time
    Slave Channel 2  = Axial LVDT
    Slave Channel 3  = InVessel Load
    Slave Channel 4  = Axial Strain
    Slave Channel 5  = Conf. Pressure
    Slave Channel 6  = Axial def (mm)
    Data Header      = data circ. disp
    Level Increment  = 0.01 ( mm )
    Buffer Size      = 6000

Creep (op. event) : Operator Event
    Start Trigger    = Step Start
    End Trigger      = <none>
    Button ID        = Button 1
    Single Shot      = Yes
    Button Label     = Creep
    Description      =
    Grab Focus       = Yes

hold Axial LVDT : Hold Command
    Start Trigger    = Creep (op. event)
    End Trigger      = end creep (op ev)
    Hold Time        = 50 Hr
    Axial
        Control Mode     = Axial LVDT SG
    Confining
        Control Mode     = Conf.Pressure SG

end creep (op ev) : Operator Event
    Start Trigger    = Creep (op. event)
    End Trigger      = <none>
    Button ID        = Button 2
    Single Shot      = Yes
    Button Label     = End Creep
    Description      =
    Grab Focus       = Yes

Load-time plot : Run-time Plotting
    Start Trigger    = Creep (op. event)
    End Trigger      = end creep (op ev)
    Title            = Load vs Time
    X Axis           = X
        Channel      = Time
        Scaling      = Linear
        Minimum      = 0.000000 Sec
        Maximum      = 1.000000 Sec
    Y Axis           = Y
        Channel 1    = InVessel Load
            Color    = Red
            Style    = Solid
```

```
        Channel 2  = <none>
            Color  = Blue
            Style  = Solid
        Channel 3  = <none>
            Color  = Black
            Style  = Solid
        Scaling    = Linear
        Minimum    = 0.000000 kN
        Maximum    = 1.000000 kN
    X Axis Level Cross          = Not Enabled
    Y Axis Level Cross          = Not Enabled
    Reduce Rate on Decimation   = Enabled

creep data time : Data Acquisition
    Start Trigger   = Creep (op. event)
    End Trigger     = end creep (op ev)
    Mode            = Level Crossing
    Buffer Type     = Continuous
    Master Channel  = Time
    Slave Channel 1 = Axial LVDT
    Slave Channel 2 = InVessel Load
    Slave Channel 3 = Axial Strain
    Slave Channel 4 = Circ. Disp
    Slave Channel 5 = Conf. Pressure
    Slave Channel 6 = Axial def (mm)
    Data Header     = Creep Data Timed
    Level Increment = 2 Min
    Buffer Size     = 8000

creep data Load : Data Acquisition
    Start Trigger   = Creep (op. event)
    End Trigger     = end creep (op ev)
    Mode            = Level Crossing
    Buffer Type     = Continuous
    Master Channel  = InVessel Load
    Slave Channel 1 = Time
    Slave Channel 2 = Axial LVDT
    Slave Channel 3 = Axial Strain
    Slave Channel 4 = Circ. Disp
    Slave Channel 5 = Conf. Pressure
    Slave Channel 6 = Axial def (mm)
    Data Header     = creep data Load
    Level Increment = 3 ( kN )
    Buffer Size     = 8000


testing 3 : Step
    Step Done Trigger 1 = hold Axial LVDT
    Step Done Trigger 2 = end creep (op ev)

    Load vs. Displacement Plot : Run-time Plotting
        Start Trigger   = Step Start
        End Trigger     = Creep (op. event)
        Title           = Load vs Displacement
        X Axis          = Y
            Channel     = InVessel Load
            Scaling     = Linear
            Minimum     = 0.000000 kN
            Maximum     = 1.000000 kN
        Y Axis          = X
            Channel 1   = Axial LVDT
                Color   = Red
                Style   = Solid
```

Channel 2 = Axial def (mm)
Color = Blue
Style = Solid
Channel 3 = Circ. Disp
Color = Black
Style = Solid
Scaling = Linear
Minimum = 0.000000 mm
Maximum = 1.000000 mm
X Axis Level Cross = Not Enabled
Y Axis Level Cross = Not Enabled
Reduce Rate on Decimation = Not Enabled

Circ. Disp. Ramp 1 : Run-time Rate Control
Start Trigger = Step Start
End Trigger = Creep (op. event)
Segment Shape = Ramp
Axial
Control Mode = Circ. Disp SG
Rate Type = 0.001000 mm/Min
Minimum Rate = 0.000100 mm/Min
Maximum Rate = 1.000000 mm/Min
Endlevel = 7.5 (mm)

Data Load : Data Acquisition
Start Trigger = Step Start
End Trigger = Creep (op. event)
Mode = Level Crossing
Buffer Type = Continuous
Master Channel = InVessel Load
Slave Channel 1 = Time
Slave Channel 2 = Axial LVDT
Slave Channel 3 = Axial Strain
Slave Channel 4 = Circ. Disp
Slave Channel 5 = Conf. Pressure
Slave Channel 6 = Axial def (mm)
Data Header = Data Load
Level Increment = 3 (kN)
Buffer Size = 10000

data circ. disp : Data Acquisition
Start Trigger = Step Start
End Trigger = Creep (op. event)
Mode = Level Crossing
Buffer Type = Continuous
Master Channel = Circ. Disp
Slave Channel 1 = Time
Slave Channel 2 = Axial LVDT
Slave Channel 3 = InVessel Load
Slave Channel 4 = Axial Strain
Slave Channel 5 = Conf. Pressure
Slave Channel 6 = Axial def (mm)
Data Header = data circ. disp
Level Increment = 0.01 (mm)
Buffer Size = 6000

Creep (op. event) : Operator Event
Start Trigger = Step Start
End Trigger = <none>
Button ID = Button 1
Single Shot = Yes
Button Label = Creep
Description =

```
    Grab Focus      = Yes

hold Axial LVDT : Hold Command
    Start Trigger   = Creep (op. event)
    End Trigger     = end creep (op ev)
    Hold Time       = 50 Hr
    Axial
        Control Mode    = Axial LVDT SG
    Confining
        Control Mode    = Conf.Pressure SG

end creep (op ev) : Operator Event
    Start Trigger   = Creep (op. event)
    End Trigger     = <none>
    Button ID       = Button 2
    Single Shot     = Yes
    Button Label    = End Creep
    Description     =
    Grab Focus      = Yes

Load-time plot : Run-time Plotting
    Start Trigger   = Creep (op. event)
    End Trigger     = end creep (op ev)
    Title           = Load vs Time
    X Axis          = X
        Channel     = Time
        Scaling     = Linear
        Minimum     = 0.000000 Sec
        Maximum     = 1.000000 Sec
    Y Axis          = Y
        Channel 1   = InVessel Load
            Color   = Red
            Style   = Solid
        Channel 2   = <none>
            Color   = Blue
            Style   = Solid
        Channel 3   = <none>
            Color   = Black
            Style   = Solid
        Scaling     = Linear
        Minimum     = 0.000000 kN
        Maximum     = 1.000000 kN
    X Axis Level Cross          = Not Enabled
    Y Axis Level Cross          = Not Enabled
    Reduce Rate on Decimation   = Enabled

creep data time : Data Acquisition
    Start Trigger   = Creep (op. event)
    End Trigger     = end creep (op ev)
    Mode            = Level Crossing
    Buffer Type     = Continuous
    Master Channel  = Time
    Slave Channel 1 = Axial LVDT
    Slave Channel 2 = InVessel Load
    Slave Channel 3 = Axial Strain
    Slave Channel 4 = Circ. Disp
    Slave Channel 5 = Conf. Pressure
    Slave Channel 6 = Axial def (mm)
    Data Header     = Creep Data Timed
    Level Increment = 2 Min
    Buffer Size     = 8000

creep data Load : Data Acquisition
```

Start Trigger = Creep (op. event)
End Trigger = end creep (op ev)
Mode = Level Crossing
Buffer Type = Continuous
Master Channel = InVessel Load
Slave Channel 1 = Time
Slave Channel 2 = Axial LVDT
Slave Channel 3 = Axial Strain
Slave Channel 4 = Circ. Disp
Slave Channel 5 = Conf. Pressure
Slave Channel 6 = Axial def (mm)
Data Header = creep data Load
Level Increment = 3 (kN)
Buffer Size = 8000

Release Load From Specimen : Step
Step Done Trigger 1 = Stop hydraulics

Switch to Stroke Control : Hold Command
Start Trigger = Step Start
End Trigger = <none>
Hold Time = 0.05 (Sec)
Axial
Control Mode = Axial LVDT SG

Release confiment and load : Monotonic Command
Start Trigger = Switch to Stroke Control
End Trigger = <none>
Segment Shape = Ramp
Time = 2 Min
Axial
Control Mode = Load SG
End level = 1 (kN)
Confining
Control Mode = Conf.Pressure SG
End level = 0 MPa

Stop hydraulics : Program Control
Start Trigger = Release confiment and load
End Trigger = <none>
Action = HPS Off
Message = Hydraulics off
Send To:
Screen = No
LUC Display = Yes
Data File = No

Specimen Post-test Information : Step
Step Done Trigger 1 = Post-test Specimen Information

Post-test Specimen Information : Data Input
Start Trigger = Step Start
End Trigger = <none>
Window = Post-test Specimen Data Input
Utilization = Process Parameterization and Execution